THE QUEST FOR THE FUNDAMENTAL CONSTANTS IN COSMOLOGY

XXIVth Rencontre de Moriond
Les Arcs, Savoie, France - March 5-12, 1989

**THE QUEST FOR THE FUNDAMENTAL
CONSTANTS IN COSMOLOGY**
Series : Moriond Astrophysics Meetings

Proceedings of the XXIVth RENCONTRE DE MORIOND

Series : Moriond Astrophysics Meetings

Les Arcs, Savoie, France

March 5-12, 1989

THE QUEST FOR THE FUNDAMENTAL CONSTANTS IN COSMOLOGY

edited by
J. AUDOUZE
and
J. TRAN THANH VAN

Editions Frontières

The Astrophysics Session of the Twenty-fourth Rencontre de Moriond

THE QUEST FOR THE FUNDAMENTAL
CONSTANTS IN COSMOLOGY

was organized by :

Audouze J.
Tran Thanh Van J.

with the active collaboration of :

Cesarsky C.
Crane P.
Gaisser T.
Hegyi D.
Kunth D.
Norman C.
Truran J.

AVANT-PROPOS

Ce livre rassemble les contributions de la neuvième rencontre d'Astrophysique de Moriond consacrée à la détermination des constantes cosmologiques et qui s'est tenue en mars 1989. Ces constantes sont celles qui décrivent la dynamique de l'Univers dans son ensemble (constante de Hubble et paramètre de décélération), la température du bruit de fond cosmologique (et ses fluctuations), le paramètre cosmologique qui est une autre façon d'exprimer la densité de l'Univers et son caractère ouvert ou fermé et la constante cosmologique introduite après coup par A. Einstein dans les équations de la Relativité Générale.

Comme cet atelier d'astrophysique s'est déroulé en même temps que l'atelier de physique des particules, une part importante de cette rencontre a été consacrée à la détection éventuelle et aux caractéristiques des particules non baryoniques qui doivent normalement peupler l'Univers.

Comme les livres précédents de cette série, ces comptes-rendus reflètent l'interaction forte qui existe entre la cosmologie (et plus généralement l'astrophysique) et la physique des particules. Beaucoup de chercheurs actifs et d'équipes travaillant dans ces deux domaines aiment se rencontrer et bénéficier de l'atmosphère amicale et porteuse d'inspiration aux Arcs par Jean Tran Thanh Van et son équipe.

Qu'il me soit permis de remercier les membres du Comité Scientifique pour leurs avis, les auteurs pour leurs contributions, le CNRS et surtout le PICS n°18 pour leur aide financière.

Enfin je souhaite exprimer toute ma gratitude à Marie-Christine Pelletan qui a assuré une grande partie du travail éditorial.

Jean AUDOUZE

FOREWORD

This book assembles the contributions of the ninth Moriond Astrophysics meeting devoted to the determination of the cosmological constants and which has been held in march 1989. These constants are those describing the dynamics of the Universe as a whole (Hubble constant and deceleration parameter), the temperature of the microwave background and the fluctuations of this quantity, the cosmological parameter which is related to the value of the density of the Universe of its closed or open character, and the cosmological constant which has been introduced by A. Einstein after the establishment of General Relativity.

Since this astrophysics workshop takes place together with the elementary particle workshop, a large fraction of this meeting has also been devoted to the detection and characteristics of non baryonic particles which are likely to populate the Universe.

Like the previous books of this series these proceedings clearly show the strong interaction between cosmology (and more generally astrophysics) and particle physics. Many productive researchers and teams working in these two fields like to meet in the most friendly and inspiring atmosphere created at Les Arcs thanks to Jean Tran Thanh Van and his team.

Let me thank the members of the scientific committee for their advice, the authors for their contributions, CNRS and especially PICS n°18 for their support.

Last but not least a large fraction the edition work has been undertaken by Marie-Christine Pelletan whom I thank very warmly.

Jean AUDOUZE

CONTENTS

IV. THE COSMOLOGICAL CONSTANT

V. DETECTION, MASS AND LIFE TIME OF NON BARYONIC PARTICLES

Joint session with particle physicists.

VI. GENERAL DISCUSSION

I. DETERMINATION OF THE HUBBLE CONSTANT

THE HUBBLE CONSTANT

Lucienne Gouguenheim, Lucette Bottinelli, Pascal Fouqué,
Observatoire de Paris, 92195 MEUDON Cedex , France
Georges Paturel,
Observatoire de Lyon, 69230 SAINT-GENIS-LAVAL, France
Pekka Teerikorpi
University of Turku Observatory, TURKU, Finland

ABSTRACT

The value of the Hubble constant H_0 relies on velocity and distances determinations either of field or cluster galaxies. Emphasis is put on the effects of statistical biases which affect the calibrating relations, such as the Tully-Fisher one. The Malmquist bias, which applies for field galaxies, and the cluster incompleteness bias lead to an overestimation of the value of H_0.

The possible effect of a "local velocity anomaly" is tested from an enlarged sample of unbiased field data. Recent studies of the Virgo cluster are reviewed. Both cluster and field data lead to a value of the Hubble constant in the range 68-75 km s^{-1} Mpc^{-1}.

INTRODUCTION.

An accurate determination of the extragalactic distance scale is needed in order to obtain a good determination of the Hubble constant. However it must be kept in mind that it leads also to informations on deviations from a uniform Hubble flow. The accuracy needed is twofold: it concerns firstly a good linearity of the distance scale, particularly important for studying the velocity field, and secondly a good calibration which gives the accuracy on H_0. At the time being, the various estimates of H_0 are in the range 50-100 km s^{-1} Mpc^{-1}. It has been widely assumed that the distance determinations suffered mostly from an uncertainty on the zero point and that possible non-linearities were small enough so that the individual distance determinations allow a good study of the kinematics of the nearby universe. There is, however, a growing evidence of the importance of statistical biases (Bottinelli et al., 1988; Sandage, 1987, 1988).

The extragalactic distance scale is built on two main steps, the so-called primary and secondary distance indicators. The primary calibration relies on individual stars which are well studied in our Galaxy and recognized in nearby ones. It is assumed that similar stars, whose similarity is recognized from directly observable parameters, have the same intrinsic luminosity wherever they are observed. The calibration of the intrinsic luminosity relies on stellar distances within our Galaxy. These primary indicators have generally sound physical basis, related to our good knowledge of stellar properties and evolution, but they fail at large distances, except for the supernovae, when individual stars are no more observable.

A second kind of indicators is thus needed: they involve global properties of galaxies. They are calibrated from the properties of the previous sample whose distances have been obtained from primary calibration. Their physical basis are not so well understood, due to the limited knowledge of galaxies evolution, but they have a larger range, up to 100 Mpc.

PRIMARY CALIBRATION.

An extensive review has been made recently by Van den Bergh (1989) . We give here a summary of the properties of those which seems to be the best primary indicators.

(1) The **RR Lyrae** variable stars are a good indicator, but due to their low luminosity they are observable only in the Magellanic Clouds and M31 (Pritchett and Van den Bergh, 1987a).They provide essentially a good check of the other indicators.

(2) The **novae** are observable at larger distances, up to the Virgo cluster (Pritchett and Van den Bergh, 1987b) and the theoretical understanding of their phenomenon is well improved. However, they show a large range in their observed properties.

(3) The **supernovae** have the greatest potential, because they are observable at very large distances. In practice, there remains much difficulties considering both their theoretical understanding and the calibration of their absolute magnitudes. There are two different approaches. The first one involves the application of the Baade-Wesselink method to type II supernovae. The main problem relies on the deviation from the black body radiation. The second approach relies on type I supernovae taken as standard candles. The criterion must be restricted to early type galaxies in order to avoid difficult extinction problems. However, their origin is still under debate and it appears that a significant fraction of them are of a peculiar nature, with different luminosity characteristics.

(4) The luminosity function of **planetary nebulae** has been shown by Jacoby et al. (1988) to be universal with a sharp bright-end cutoff near M([OIII] , λ=5007) = -4.48. This seems to provide a good estimate of distance.

(5) The **cepheid** variable stars are the most promising of the primary indicators: (i) they are rather luminous, (ii) the period-luminosity-colour relation is on secure theoretical basis and (iii) considerable improvements are coming from near IR photometry.

Much of the uncertainty in broad-band optical studies relies on the difficulty to account for the effects of interstellar extinction and chemical composition variations among cepheids in different galaxies. There are three main advantages in the near IR compared to the visible. The effects of absorption and reddening are much lowered: the attenuation of starlight in the H-band is lower than in the B-band by a factor of 6. UBV magnitudes and colours are relatively sensible to chemical composition variations, due to the importance of stellar absorption lines in the blue part of the spectrum; these effects are drastically reduced at shorter wavelengths, where the density of metallic absorption lines is low. Temperature differences across the instability strip give rise to a finite magnitude width in the (P,L) relation, at constant P. A three parameter (P,L,C) relation is thus needed to characterize the properties of an individual cepheid. It is not easy in the blue to disentangle this effect from differential extinction. Because the monochromatic flux is less sensitive to the temperature at longer wavelength, the width of the (P,L) relation at H is only one third of the width at B. In addition, the amplitude of the light curve of an individual cepheid, which is due primarily to temperature variations, is reduced in the IR: thus, random IR observations are competitive with time-averaged B-band photometry.

Recent determinations of distances of nearby galaxies are listed in Table 1.

SECONDARY CALIBRATION.

The following relations are examples of secondary calibrators:

$$- M = a \log V_m + b \qquad (1)$$
$$- M = a \log \sigma_v + b \qquad (2)$$
$$- M = a \wedge_c + b \qquad (3)$$

They give the absolute magnitude M of a galaxy as a function of the maximum circular velocity V_m in disk galaxies [Tully-Fisher relation (1)], of the internal velocity dispersion, σ_v in bulge galaxies [Faber-Jackson relation (2)] or the luminosity index $\wedge_c$ [de Vaucouleurs relation (3)], which applies for disk galaxies. The first two relations are the expression of a mass-luminosity relation and all of them have the general shape:

$$- M = a p + b \qquad (4)$$

where p is a directly observable parameter.

An improved version of relation (2) has been developed by Lynden-Bell et al. (1988) who find a stronger correlation between the velocity dispersion σ_v and the parameter D_n which is defined as the diameter enclosing an area with a mean surface brightness above some fiducial level.

It is generally considered that the Tully-Fisher (1977), hereafter TF, relation is the most accurate with a dispersion of 0.4 - 0.5 mag. at given $p = \log V_m$, and the following discussion will concentrate on it.

THE TULLY-FISHER RELATION.

The maximum circular velocity V_m is deduced from the width of the 21-cm line of neutral hydrogen, observed in a galaxy seen as a point source by the radiotelescope, after correcting for inclination effects. Non-circular motions must also be taken into account, because

Table 1

Distance moduli of primary calibrators

1	2	3	4	5	6
Local Group:					
LMC	18.45	18.5	18.5	18.3	18.7
SMC	18.80	18.85	18.8	18.6	19.1
M31	24.3	24.2	24.2	24.1	24.25
M33	24.5	24.4	24.2	23.9	24.65
NGC6822	23.47	23.4			23.77
IC1613	24.28	24.1			24.29
Sculptor Group:					
NGC55	25.7		26.1	26.6	26.44
NGC247		26.1	26.8	27.2	26.44
NGC253		27.5	27.5	27.2	26.44
NGC300	25.7	26.0	26.1	26.4	26.44
NGC7793		27.5	27.5	27.7	26.44
M81 Group:					
NGC2403	27.8	27.8	27.5		27.31
NGC4236		27.8	27.8		27.31
IC2574		27.8	27.8		27.31
NGC 3031	27.8	28.7	27.8	27.31	29.16
M101 Group:					
M101		29.2	28.7		29.16
NGC5204		29.2	28.7		29.16
NGC5585		29.2	28.7		29.16

column 2: Van den Bergh, 1989
column 3: Tammann, 1986
column 4: Fouqué et al, 1989
column 5: de Vaucouleurs, 1986
column 6: Rowan-Robinson, 1985

they tend to widen the 21-cm line. Bottinelli et al.(1983) have applied a linear summation of the random motions, described by a gaussian function with $\sigma_x = \sigma_y = 1.5\ \sigma_z = 10$ - 15 km s^{-1} (the z-axis being perpendicular to the disk); the rotation components V_m have been then deduced from the different 21-cm line width measured respectively at 20, 40 and 50% of maximum intensity. They show a good agreement with the directly measured ones from rotation curves. Lewis (1984) has found $\sigma_x = \sigma_y = \sigma_z = 12$ km s^{-1} and Tully and Fouqué (1985) have confirmed the validity of a linear summation for non-dwarf galaxies.

Not applying this correction leads to a steeper slope of the TF relation and should add some extra noise to the distance determinations; however no systematic effect is expected if all the line widths, including those of the calibrators, are corrected in the same way.

Two main systems of magnitudes have been used: the $B_T{}^o$ system of de Vaucouleurs et al. (1976) and the $H_{.5}$ system of Aaronson et al. (1979). The $B_T{}^o$ magnitudes have the advantage of being total, but they are sensitive to extinction effects; on the contrary, the $H_{.5}$ magnitudes are not sensitive to extinction effects, but they are measured within an aperture which is one third of the **blue** photometric diameter a_{25}. This has two consequences: first, they do not measure the same fraction of the total light, depending on the bulge to disk ratio, and second they involve B-band diameters, which are subject to light extinction.

The calibration of the TF relation needs the determination of 2 parameters: the slope a, using either local calibrators, or cluster data, or kinematic distances, and the zero point, b, which is determined from local calibrators and is thus affected by the uncertainty of the primary calibration.

The value of the slope depends on the system of magnitude and also, to a smaller extent, as discussed above, to the system of line withs, corrected or not for non-circular motions. It is in the range 5-6 at B (Bottinelli et al., 1983) and 10-12 at H (Aaronson et al., 1979, 1983).

The variation of the slope with the magnitude wavelength can be easily understood, keeping in mind that the TF relation relies on a total mass to total luminosity relation. B-band and H-band magnitudes do not measure the same fraction of the total luminosity for blue or red galaxies. The bluest are expected to have the smallest log V_m, and thus M_B - M_H is expected to increase with log V_m; this effect is reinforced by the limited aperture of the $H_{.5}$ magnitude system: the luminosity of the blue, late type galaxies, with small log V_m and small bulge to disk ratio is more underestimated than the luminosity of red, large log V_m and large bulge to disk ratio early type galaxies. For both these reasons, one expects a systematic increase of M_B - M_H with log V_m.

The steeper slope in the red reflects thus more widely on M_H than on M_B the errors on log V_m (including both line widths and inclination measurements). This point has been controverted from arguments related to the observed dispersion of the TF relation; this dispersion, in fact, is not easy to determine, owing to the statistical problems discussed below.

A possible type effect has also been discussed: either the slope a or the zero point b, or possibly both of them could be functions of a second parameter, the morphological type. For example, Giraud (1985) shows a segregation between late type Scd-Sd galaxies and early type Sab-Sb ones, when plotting the Hubble parameter H vs. the recession velocity; at a given velocity, the late type galaxies have systematically larger values of H than the early type ones. He suggests to introduce a shift of 0.5 magnitudes in the zero point of the TF relation between Scd-Sd and Sab-Sb galaxies. This effect is curiously not present among the H-band data, which could be (wrongly) interpreted as an argument favouring this last system. These so-called "type effects" are in fact related to the Malmquist bias, as discussed below.

POSSIBLE INTERPRETATION OF THE TF RELATIONSHIP.

The general idea is that the TF relation comes from a total mass to bolometric luminosity relation among galaxies; this interpretation holds if the maximum rotational velocity is a good indicator of the total mass.

Interesting results have been obtained by Lafon (1976) who has developed dynamical models of self-consistent thin disks, from microscopic distribution functions with no energy truncature. His main results are the following:

(1) flat rotation curves are quite usual,

(2) these flat rotation curves neither request nor exclude any galactic halo, massive or not,

(3) the rotation curves depend on two parameters, the total mass of the galaxy and the kinematic temperatures of the internal parts,

(4) the maximum rotational velocity is essentially sensitive to the total mass of the system.

MALMQUIST BIAS IN TF RELATION.

The bias arising when determining distances from a magnitude linited sample using relation (4) has been studied by Teerikorpi (1984). Its main properties can be understood from fig. 1.

We consider first a class of galaxies characterized by the same value of $p = \log V_m$. Through the TF relation their mean absolute magnitude M_p is known $(-M_p = a\,p + b)$ and the individual magnitudes are distributed around M_p. We assume this distribution to be gaussian, with dispersion σ_{M_p}. If the sample is cut at the apparent limiting magnitude m_l, it results an absolute limiting magnitude at distance d, $M_l(d) = m_l - 5 \log d - 25$. When d increases, $M_l(d)$ becomes brighter, the mean absolute magnitude $<M>$ of the sample selected becomes more luminous and the bias $\Delta M_d = -(<M> - M_p)$ increases.

For a larger m_l the limiting absolute magnitude is less luminous and the bias is smaller.

If 2 different samples of galaxies, characterized by p and p'<p are considered, it is also easily seen that the bias is stronger for the p' class, which is the less luminous. Thus:

- at given m_l and given p, the bias increases with the distance
- at given m_l and distance, the bias is stronger for smaller p
- at given p and distance, the bias is smaller for larger m_l.

The shapes of the bias curves are shown in fig.2

- For a given class of galaxies (p), the bias is negligible up to a threshold and then it increases with distance

- The threshold depends on p: it is larger for larger p

- When considering a sample of galaxies with all p, it results a cloud of points, distributed around the various curves and the remaining plateau is the smallest one. As a consequence, the bias is not conspicuous.

In order to overcome these problems, Bottinelli et al. (1986) have introduced the concept of **normalized distance:**

$$d' = d \times dex\{-0.2a(2.7 - \log V_m)\}$$

where d is the kinematic distance, which is an unbiased estimate of the distance. At same d', all galaxies with different p suffer from the same amount of bias, provided that all these
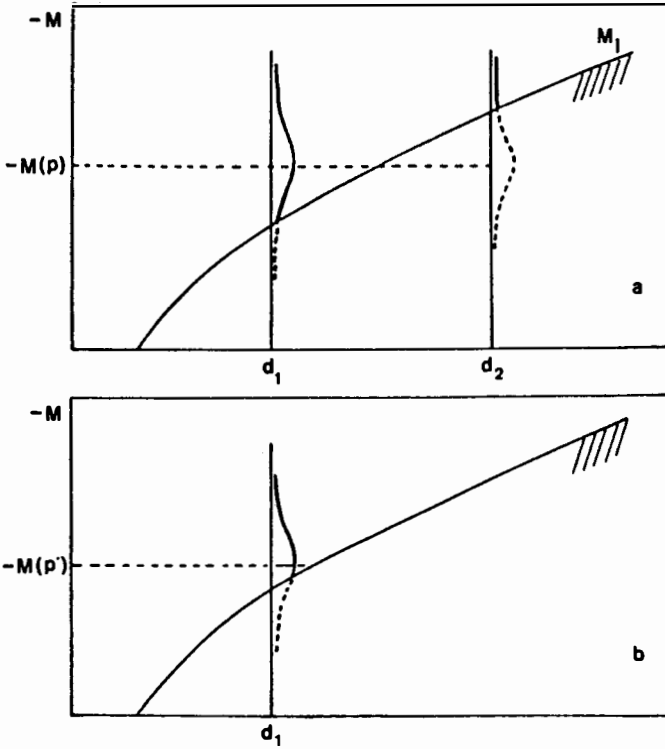
Figure 1: (a) only the galaxies more luminous than the absolute limiting magnitude M_l, i.e. above the limiting curve, are observed: the more distant the galaxy, the more severe the cutoff. For a given value of p, the luminosity function is more severely cut at larger distance; (b) for a class of lower luminosity galaxies, characterized by p'<p, the bias, at the same distance, is larger.
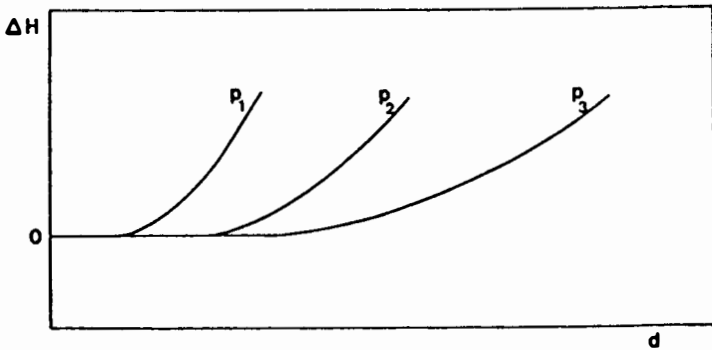
Figure2: 3 bias curves, obtained for 3 different values of the parameter p, with $p_1<p_2<p_3$,are represented; the other parameters, m_l and σ_{Mp} are the same.

subsamples are characterizd by same m_l and $\sigma_{M\rho}$. All the plateau data are also selected.

This method has been applied to B-band TF distances, with line widths corrected for non-circular motions [Bottinelli et al. (1986a)] and to H-band TF relation with non-corrected line widths [Bottinelli et al. (1988a)]. The main results are the following:

       - both samples are affected by a strong bias

       - the plateau data give a mean value of the Hubble constant, in de Vaucouleurs local scale, $H_0 = (72 \pm 3)$ km s^{-1} Mpc^{-1} in both B-band and H-band, which is significantly different from the values of H_0 previously determined from similar samples (de Vaucouleurs et al., 1981; Aaronson et al., 1979).

The "type effect" mentioned above is actually expected from the bias, because late type galaxies are, on the mean, less luminous than early type ones and thus expected to suffer from a larger bias (Bottinelli et al., 1986b). Moreover, this so-called type effect is not conspicuous in H-band data; it should however not be concluded that this has something to do with a better quality of the H-band data. This comes essentially from the constitution of the samples where the limiting magnitude is larger for low luminosity galaxies (small p). Thus the two different effects, of m_l and p respectively, on the resulting bias compensate each other.

Some authors [Tammann, (1986); Giraud, (1986)] have considered the bias arising in the whole sample (including all p) without any normalization; it has been seen previously that the bias is much difficult to put in evidence and that the unbiased data are not so easily recognized. Moreover, Giraud has tried to compute the expected bias; he comes to the conclusion that there remains an intrinsinc increase of H with kinematic distance after correcting the bias, which should explain only one third of the effect. In fact this method is a step backward in comparison to the method using the normalized distance and relies on a strong assumption concerning the luminosity function. The separate curves of fig. 2 indicate how galaxies in different log V_m intervals populate the diagram. In order to calculate the average dependence of the biased H on d one must know how crowded each curve is by galaxies. The expected bias depends on the mean absolute magnitude and σ_M of the global luminosity function of galaxies, which is assumed to be gaussian. When dealing with a subsample of galaxies with same value of log V_m, the mean unbiased absolute magnitude of the sample is known from the TF relation. It is not the case here, where it is determined from apparent magnitudes and (biased !) distances. Moreover the choice of the limiting magnitude, on which the bias is strongly dependent, has not been discussed. For all these reasons, it is difficult to give any credit to the conclusions.

Tully (1988) has suggested that the low value of H_0 obtained from the plateau data is affected by a kinematic effect that he calls the "local velocity anomaly", according to which the Coma-Sculptor cloud should be retarded in its expansion and the Leo spur should be falling toward the Coma-Sculptor cloud. The majority of the 41 plateau data in Bottinelli et al. (1988b) sample (with limiting B magnitude 12.0) being members of these two clouds, the value $H_0 = 72 \pm 3$ obtained from these data should be, according to Tully, underestimated. The best way to check this hypothesis is to increase the sample. A preliminary result, obtained from an enlarged sample, with a larger limiting magnitude, is displayed in fig. 3 where the new plateau data are shown in a log H_0 vs. V_0 plot. There is no evidence at all from this plot for a segregation in H between the galaxies belonging or not to the Leo spur or the Coma-Sculptor cloud. We conclude thus that there is no observational evidence, obtained from unbiased distances, favouring the hypothesis of a "local velocity anomaly".
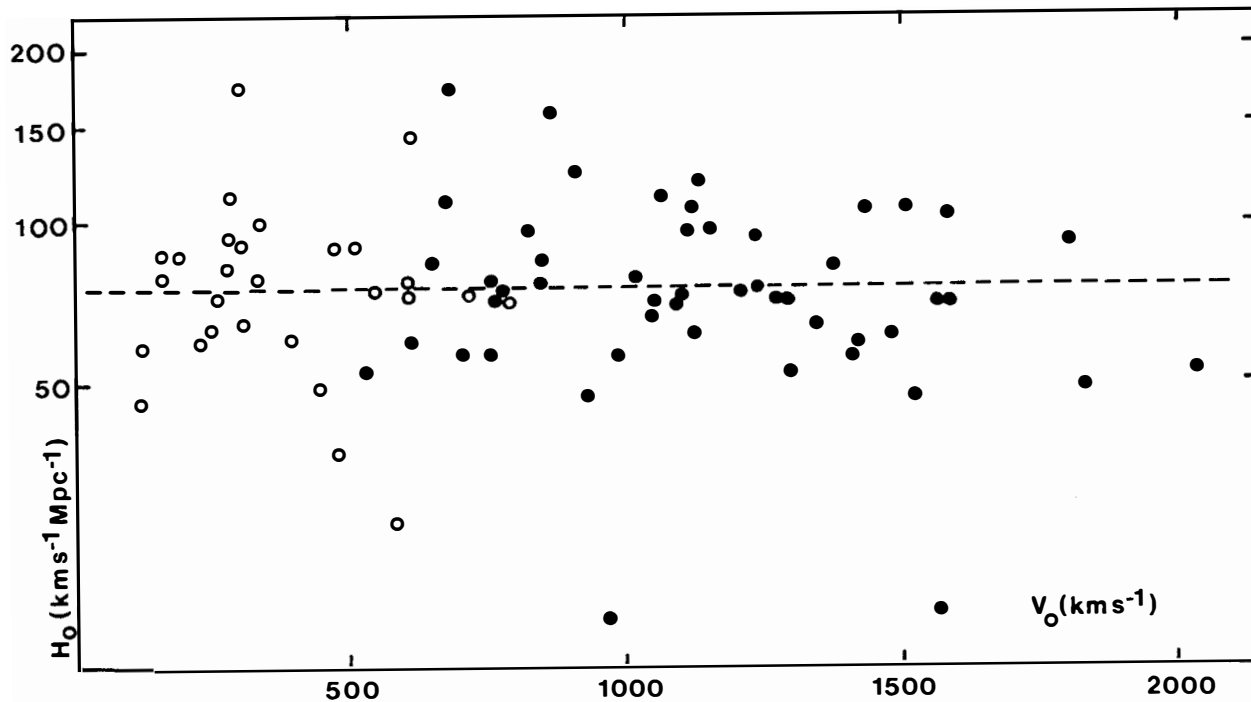
Figure 3: the logaritm of the Hubble parameter is plotted against the systemic velocity V_O for an unbiased sample of galaxies. The galaxies belonging either to the Coma-Sculptor cloud or to the Leo spur (open dots) do not differ from the others (black dots). The dashed line corresponds to $H_O = 75$ km s^{-1} Mpc^{-1}

The main **conclusions** are thus the following:

(1) the bias is the predominant effect. It is much more important than the compared accuracies of B_T^o or $H_{-.5}$ magnitudes or the effects of non circular motions.

(2) the bias does not depend only or predominantly on the observed dispersion of the relation but also strongly on the limiting magnitude of the sample. It results that, contrary to a common statement, when comparing different distance criteria, the best one is not necessarily characterized by the smallest scatter and the bias at a given distance is not necessarily stronger for a criterion with larger dispersion

(3) Is the determination of $H_O = 72 \pm 3$ in de Vaucouleurs primary calibration only local (because of possible local motions) or global ? There are two ways for answering this question. The first one, as it was explained above, is to increase the sample, thus m_l and the plateau threshold. The second relies on cluster data.

CLUSTER INCOMPLETENESS BIAS

Contrary to a general statement, a bias is also expected within a cluster. The bias arising when determining distances from a magnitude limited sample of galaxies within a cluster using relation (4) has been studied by Teerikorpi (1987). It is illustrated in fig. 4. The bias expected at small p is larger because the luminosity function of galaxies with same value of p is more severely cut. A bias decreasing with increasing p and negligeable at large p (plateau region) is thus expected.

The bias arising in a sample of 10 clusters with velocities ranging from 4000 to 11000 km s^{-1} plus Virgo cluster has been studied both in B-band and in H-band (Bottinelli et al.,1987, 1988a). A normalized log V_m taking into account the clusters distances and limiting magnitudes has been used in order to put all the cluster data together. The data (fig. 5) show clearly the trend expected. The plateau data in B-band lead to $H_O = 73 \pm 4$ in de Vaucouleurs primary calibration, adopting an infall velocity of 220 km s^{-1} for the Local group. This result is in remarkable agreement with the value obtained from the field sample.

The limiting magnitude of the $H_{-.5}$ sample is bright, leading to a very small number of plateau data. Using a sample of 19 galaxies including biased data near the threshold and an iterative method for computing the bias, a similar value of H_O is obtained, in the range 70 - 75.

DISTANCE TO THE VIRGO CLUSTER.

The Virgo cluster of galaxies deserves a special attention, because a rather complete sample of spirals is now available. It gives thus the opportunity of (i) determining an unbiased estimate of its distance and (ii) studying in more details the behaviour of the bias and also the possibility of using the "inverse regression" (all the errors on p), $p = a' M + b'$, for determining distances.

The nature of these two regression deserves some discussion, since the topics has generated some confusion. The "true" relation, the one that must be used in a theory explaining the TF relationship, is a mean regression, where the errors on both axis parameters are taken into account. The direct relation has a shallower slope, because of the errors on log V_m, and the inverse regression has a steeper slope, because of the errors on the magnitudes. From one sample to the other, the "true" slope does not change, while the direct and inverse slope change according to the changes in the dispersion of the parameters.
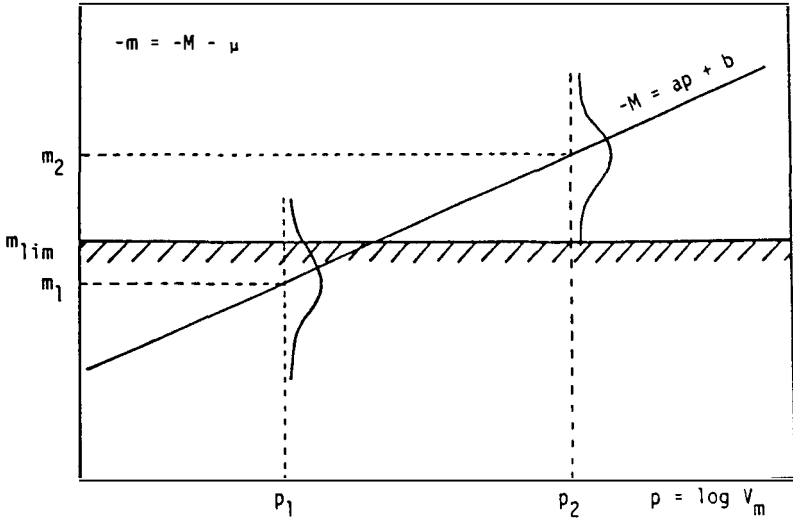
Figure 4: apparent magnitude vs. $p = \log V_m$ diagram in a cluster having a distance modulus μ and observed up to the limiting magnitude m_l (hatched line). The straight line stands for the TF relation. It can be seen that the luminosity function is more severely cut at p_1 than at p_2 ($p_1 < p_2$).
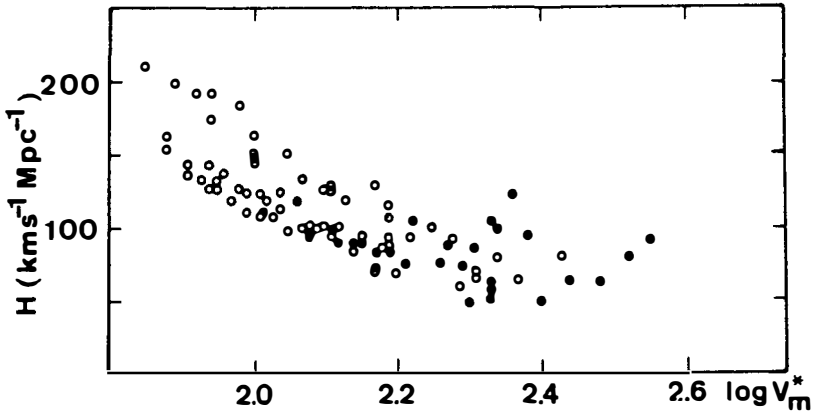
Figure 5: H vs. normalized $\log V_m$ for 10 clusters. The Virgo cluster points (*) have been added, adopting an infall velocity of the Local Group equal to 220 km s^{-1}.

A large number of studies have been devoted to the Virgo cluster (see for example Richter, 1985; Kraan-Korteweg et al., 1988; Pierce and Tully, 1988; Tammann, 1988). Fouqué et al. (1989) have applied the B-band TF relation to an almost complete sample of 139 spiral galaxies. Their study has given the following results.

The direct regression, with all the errors on magnitudes, the one that must be used to measure distances (Bottinelli et al., 1986a; Lynden-Bell et al., 1988) gives:

$$- M = (5.5 \pm 0.5) \log V_m + 8.0 \pm 0.01 \qquad (5a)$$
$$- B_T = (5.5 \pm 0.3) \log V_m - 23.40 \pm 0.06 \qquad (5b)$$

respectively for the calibrators (using the data of Table 1) (5a) and the Virgo cluster (5b).

The inverse regression (all the errors on linewidths) leads to mean distances independent of the limiting magnitude of the sample (Schechter, 1980; Teerikorpi, 1982), if the coverage in $\log V_m$ is complete (Teerikorpi, 1984). It has a slope 6.1 ± 0.5 for the calibrators and 7.8 ± 0.4 for the Virgo data.

The important effect brought to light is that the slope of the direct regression obtained from Virgo and from the calibrators is the same, within the errors; this is not the case for the inverse regression. This result is due to the uncertainties of the data. The slope of the direct regression is modified by the uncertainties on $\log V_m$, whereas that of the inverse regression is modified by the uncertainties on the magnitudes. The explanation for the above effect is that the errors on $\log V_m$ for the Virgo galaxies have not increased when compared to the corresponding errors for the calibrators, but the magnitudes are less accurate for the Virgo galaxies than for the calibrators.

The distance moduli obtained from the direct regression, $\mu_D = 31.40 \pm 0.13$ and from the inverse one, $\mu_I = 31.45 \pm 0.20$ are in good agreement. This agreement is due to the completeness of the sample. Restricting to bright galaxies leads to a smaller μ_D , whereas restricting to large $\log V_m$ leads to a smaller μ_I as can be seen in figure 6.

The determination of Pierce and Tully (1988) based on the inverse relation is smaller by about 0.45 magnitude; the difference is entirely due to different calibrations. Pierce and Tully use only 3 calibrators (M31, M33 and NGC 2403); adopting their parameters for these 3 galaxies and keeping the other calibrators leads Fouqué et al. to modify the zero-point of their TF relation by 0.07 mag. This result illustrates that not only good distances but also good parameters are necessary for the calibrators and that the use of the largest number of calibrators available reduces the accidental errors in the derived distance moduli. Moreover, nothing guarantees that a single calibrator has the average magnitude for its $\log V_m$ in the gaussian luminosity function.

The determination of the Hubble constant from this distance modulus depends on the cosmological velocity of the cluster which is uncertain because of the uncertainties on (i) the mean heliocentric velocity of the cluster and (ii) the infall velocity of the Local Group towards the Virgo cluster; adopting a cosmological velocity of 1330 ± 100 km s^{-1}, leads to $H_0 = 68 \pm 8$ km s^{-1} Mpc^{-1}, in good agreement with the result obtained from field galaxies.
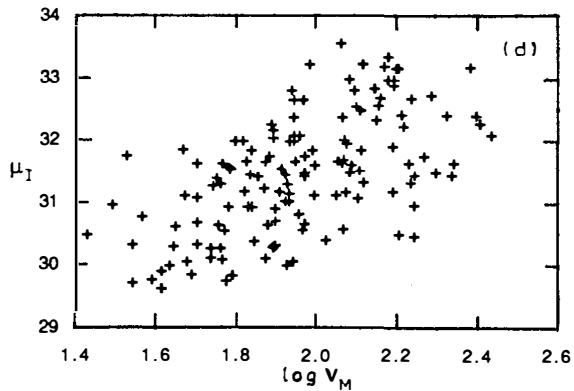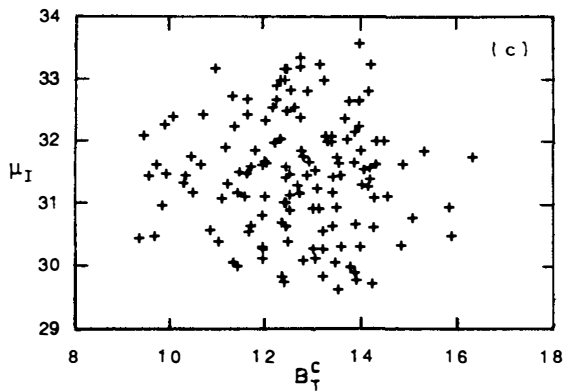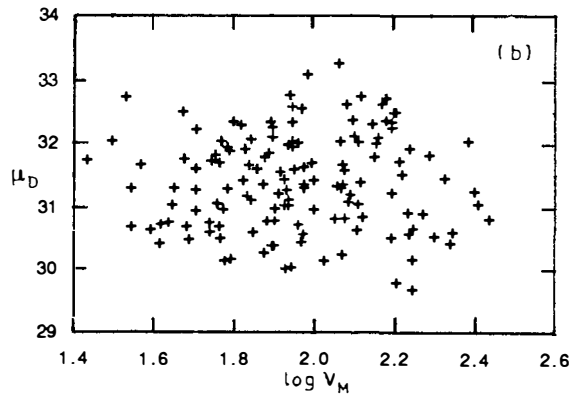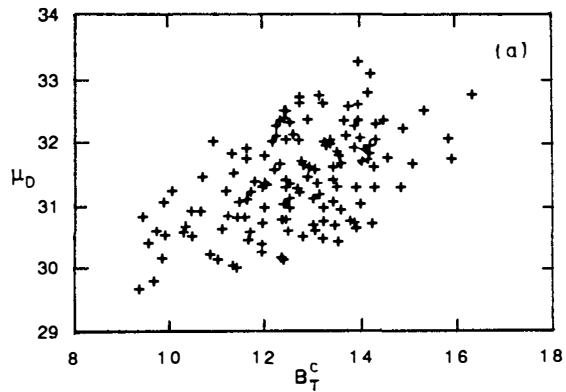
Figure 6: The direct distance modulus, μ_D, and the inverse one, μ_I, are plotted against the apparent magnitude (a and c) and against log V_m (b and d) (from Fouqué et al., 1989)

CONCLUSIONS

(1) The effect of the Malmquist bias and the cluster population incompleteness bias have been strongly underestimated or even ignored (Bottinelli et al., 1988b). What we need before all, are large samples, which are complete up to a large limiting magnitude from which a large number of unbiased distances can be extracted. Under this respect, the B_T^o system is presently the best one.

(2) As a general comment, any physical property obtained statistically from a biased sample must be considered with great caution. Such examples are the "type effect" in TF relation (in fact, a differential Malmquist bias), the particular physical properties of galaxies in clusters which should account for a different slope of the TF relation (the cluster population incompleteness bias predicts a shallower slope) or the kinematics studies performed with biased distances (the local velocity anomaly, predicted from biased distances is not confirmed).

(3) The inverse TF relation can be used to determine the distance of **cluster** galaxies, even in the case of a magnitude limitation, provided that (i) the coverage in log V_m is good and (ii) the slope of this regression can be determined within the given cluster. The inverse relation gives a correct **mean** distance modulus when the individual distances are calculated with the inverse slope derived from the data. Nevertheless, these individual distance moduli are biased, because the inverse slope is not the same as the direct one, which must be used to evaluate distances. Therefore, this method cannot be applied to **field** galaxies.

(4) The use of a very small number of calibrators with good distance determinations may lead to large errors.

(5) Both field and cluster data lead to a value of the Hubble constant in the range 68 - 75 km s^{-1} Mpc^{-1}. This value depends essentially on the primary calibration. Future improvement are expected from space observations of cepheids in nearby galaxies, with the HST and from the calibration of the period-luminosity relation of cepheids from better galactic cepheids distances with HIPPARCOS.

REFERENCES.

Aaronson, M., Huchra, J., Mould, J. 1979, Ap. J. **229**, 1

Aaronson, M., Mould, J. 1983, Ap. J. **265**, 17

Bottinelli, L., Gouguenheim, L., Paturel, G., de Vaucouleurs, G. 1983, A. A. **118**, 4

Bottinelli, L., Gouguenheim, L., Paturel, G., Teerikorpi, P. 1986a, A. A. **166**, 157

Bottinelli, L., Gouguenheim, L., Paturel, G., Teerikorpi, P. 1986b, A. A. **156**, 393

Bottinelli, L., Fouqué, P., Gouguenheim, L., Paturel, G., Teerikorpi, P. 1987, A. A. **181**, 1

Bottinelli, L., Gouguenheim, L., Teerikorpi, P. 1988a, A. A. **196**, 17

Bottinelli, L., Gouguenheim, L., Paturel, G., Teerikorpi, P. 1988b, Ap. J. **328**, 4

De Vaucouleurs, G. 1986, in "Galaxy Distances and Deviations from Universal Expansion", Reidel Publish. C° p.1

De Vaucouleurs, G., de Vaucouleurs, A., Corwin, H. 1976, Second Reference Catalogue of Bright Galaxies, University of Texas Press, Austin, Tx. (RC2)

De Vaucouleurs, G., Peters, W.L., Bottinelli, L., Gouguenheim, L., Paturel, G. 1981, Ap. J. **248**, 408

Fouqué, P., Bottinelli, L., Gouguenheim, L., Paturel, G. 1989, Ap. J. submitted

Giraud, E. 1985, A. A. **153**, 125

Giraud, E. 1986, A. A. **174**, 23

Jacoby, G.,H., Ciardullo, R.,Ford, H.C., 1988, in "The Extragalactic Distance Scale", Astronomical Society of the Pacific Conference Series **4**, 142

Kraan-Korteweg, R.C., Cameron, L.M., Tammann, G.A. 1988, Ap. J. **331**, 620

Lafon, J.P. 1976, A. A. **46**, 461

Lewis, B.M. 1984,Ap. J. **285**, 483

Lynden-Bell, D., Faber, S.M., Burstein, D., Davies, R.L. Dressler, A., Terlevitch, R.,Wegner, G. 1988, Ap. J. **326**, 1

Pierce, M.J., Tully, R.B. 1988, Ap. J. **330**, 579

Pritchett, C.J., van den Bergh, S. 1987a, Ap. J. **316**, 517

Pritchett, C.J., van den Bergh, S. 1987b, Ap. J. **318**, 507

Richter, O.,G. 1985, in "ESO Workshop on the Vitgo Cluster of Galaxies" ed. O.G. Richter and B. Binggeli, Garching European Southern Observatory, p. 409

Rowan-Robinson, M. 1985, "The Cosmological Distance Scale", W.H. Freeman and C°

Sandage, A. 1987, Ap. J. **331**, 605

Sandage, A. 1988, Annual Review Astron. Astrophys. p.561

Schechter, P.L. 1980, A. J. **85**, 801

Tammann, G.A. 1986, I.A.U. Symp. **124**,151

Tammann, G.A. 1988, in "The Extragalactic Distance Scale", Astronomical Society of the Pacific Conference Series **4**, 282

Teerikorpi, P. 1982, A. A. **109**, 314

Teerikorpi, P. 1984, A. A. **141**, 407

Teerikorpi, P. 1987, A. A. **173**, 39

Tully, R.B. 1988, in "The Extragalactic Distance Scale", Astronomical Society of the Pacific Conference Series **4**, 318

Tully, R.B., Fisher, J.R. 1977, A.A. **54**, 661

Tully, R.B., Fouqué, P. 1985, Ap. J. Suppl. Ser. **58**, 67

Van den Bergh S. 1989, Astron. Astrophys. Rev., in press

II. THE MICROWAVE BACKGROUND

COSMOLOGICAL PARAMETERS DERIVED FROM

THE COSMIC MICROWAVE BACKGROUND RADIATION

R. B. Partridge

Haverford College
Haverford, Pa 19041, U.S.A.

ABSTRACT

Recent observational results on the spectrum and isotropy of the cosmic microwave background are reviewed. Seven different cosmological parameters emerge from these studies.

Introduction

Let me begin by making the claim that studies of the cosmic microwave background radiation (CBR) in fact yield seven different values of cosmological significance. (Any temptation to compare this talk to the story of the tailor who slew "seven at one blow"--seven flies, that is--should be avoided.) The seven fundamental parameters I refer to are the thermodynamic temperature of the CBR, written here T_0; the dipole moment of the radiation, T_1; the quadrupole moment, T_2; the large-scale polarization, T_p; and the limits on anisotropy of the CBR on three different angular scales. In this paper, I will review the most recent observational results on all seven of these parameters. Since the anisotropy measurements are closest to my own work, I will emphasize them. The most exciting recent result in CBR studies, however, is a measurement of the submillimeter spectrum of the background and that is where I will begin.

The temperature of the CBR, T_0. In general, measurements of the thermodynamic temperature of the CBR at wavelengths longer than a few millimeters are in good agreement with a value of $T_0 = 2.75 \pm 0.03$ K (note the 1% accuracy, rare in cosmology). Many of the recent measurements are the results of an international collaboration between several Italian institutions and the University of California, Berkeley, in which Haverford initially also participated (Smoot et al, 1985; Partridge, 1985; Smoot et al, 1988). Two of the most recent measurements, by the Berkeley, group, are of particular interest: measurements at 3 cm and 3.3 mm have produced values 1-2 σ below the general average (the values are $T_0 = 2.61 \pm 0.06$ and 2.60 ± 0.09, respectively). In contrast, the single most precise measurement in the centimeter range is somewhat high at $T_0 = 2.783 \pm 0.025$ K (Johnson and Wilkinson, 1987). As we shall see, the discrepancy, while not overwhelming, may be important.

Supplementing these direct radiometric measurements are determinations of T_0 based on the excitation of interstellar molecules, particularly CN. These measurements of T_0 are very precise and have the added advantage of being free of the many possible sources of systematic error which may crop up in observations made beneath all or part of the earth's atmosphere. There are, of course, sources of systematic and statistical error present in the CN measurements as well; these and the most recent, exquisite results at $\lambda = 2.64$ and 1.32 mm are described below by Phil Crane.

Reference	λ, cm	(a) T_{atm}, K	T_0, K
Howell and Shakeshaft (1967) " "	73.5 49.2	1.3 (c) 1.95 (c) }	3.7 ± 1.2
Stankevich et al (1970) " "	73 47	n.a. n.a. }	3.0 ± 0.5
Sironi et al (1988)	50	1.17 (c)	2.98 ± 0.55
Pelyushenko and Stankevich (1969) " " " "	30 20.9 15	}	2.5 ± 0.3
Levin et al (1988)	21.3	0.83 (c)	2.11 ± 0.38
Penzias and Wilson (1967)	21.2	2.3	3.2 ± 1.0
Howell and Shakeshaft (1966)	20.7	2.2 (c)	2.8 ± 0.6
Otoshi and Stelzried (1975)	13	2.3	2.66 ± 0.26
Sironi and Bonelli (1986)	12		2.79 ± 0.15
De Amici et al (1988)	8.2	0.87	2.59 ± 0.13
Penzias and Wilson (1965)	7.35	3.4	3.5 ± 1.0
Mandolesi et al (1986)	6.3		2.70 ± 0.07
Roll and Wilkinson (1967)	3.2	3.0	3.0 ± 0.5
Stokes et al (1967)	3.2	1.3	$2.69^{+0.16}_{-0.21}$
Kogut et al (1988)	3.0	1.2	2.61 ± 0.06
Stokes et al (1967)	1.58	~ 4	$2.78^{+0.12}_{-0.17}$
Welch et al (1967)	1.58	~ 4	2.0 ± 0.8
Johnson and Wilkinson (1987)	1.2	~ 0	2.783 ± 0.025
Ewing et al (1967)	0.92	~ 5	3.16 ± 0.26
De Amici et al (1985)	0.91		2.81 ± 0.12
Wilkinson (1967)	0.86	6–7	$2.56^{+0.17}_{-0.22}$
Puzanov et al	0.82	16–19	2.9 ± 0.7
Kislyakov et al (1971)	0.36	~ 15	2.4 ± 0.7
Boynton et al (1968)	0.33	11–12	$2.46^{+0.40}_{-0.44}$
Millea et al (1971)	0.33	12	2.61 ± 0.25
Boynton and Stokes (1974)	0.33	1.2	$2.48^{+0.50}_{-0.54}$
Bersanelli et al (1989)	0.33	14–16	2.60 ± 0.09

Table 1   Results of all direct measurements of T_0 at λ > 3 mm.   For references, see Partridge, 1989.

(a) In this column, (c) is used to indicate calculated rather than directly measured values. Note that the measurements were made at many different altitudes; that explains some of the apparent discrepancies in T_{atm}.

Table 1, copied from Partridge (1989) presents all the measurements at wavelengths $\lambda > 3$ mm that I am aware of (mostly ground-based radiometric results). An unweighted average of all these results and the CN values at 2.64 mm gives $T_0 = 2.757 \pm 0.058$. I have also averaged the 11 measurements with the highest precision in the range 13 cm $> \lambda > 2$ mm. The result is 2.714 ± 0.023 K, lower because of the greater weight of the new Berkeley measurements at 3 and 0.33 cm (Kogut et al, 1988 and Bersanelli et al, 1989). The reduced χ^2 is 2.43, making it clear that these measurements are not internally consistent. The largest contributions to the χ^2 come from the new 3 cm measurement of Kogut et al (1988) and the Johnson and Wilkinson (1987) measurement at 1.2 cm, both referred to above.

The real excitment is in the short wavelength, Wien region of a 2-3 K spectrum. On the same day as supernova 1987A, a Japanese sounding rocket carried aloft an experiment to measure the submillimeter spectrum of the cosmic background radiation. The instrument was a collaborative effort by Paul Richards and his group at Berkeley and Toshio Matsumoto and his group at Nagoya (see Matsumoto et al, 1988). Cooled optics were employed to reduce systematic offsets; only data free of residual atmospheric emission were used in the final analysis. The sensitivity of the bolometric detectors was high enough to ensure ~ 1% measurements in the few minutes the instrument was above the atmosphere. Table 2 and Figure 1 show the results. At λ ~ 1 mm, $T_0 = 2.799 \pm 0.018$, in good agreement with both the cyanogen results and the measurement by Johnson and Wilkinson. The shortest wavelength bands employed by Matsumoto and his colleagues

Center wavelength, mm	Bandwidth $\Delta\lambda/\lambda$	T_0, K
1.16	30%	2.799 ± 0.018
0.71	21%	2.955 ± 0.017
0.48	19%	3.175 ± 0.027

Table 2. Matsumoto et al's (1988) rocket measurements of the CBR, expressed in thermodynamic temperature.

were dominated by thermal emission from dust in our own Galaxy. It is worth noting that the Berkeley-Nagoya results in these bands are in good

agreement with projections based on IRAS measurements of dust emission made at slightly shorter wavelengths (fig. 1). We thus have some confidence that the shortest and longest wavelength channels were working properly and were correctly calibrated.
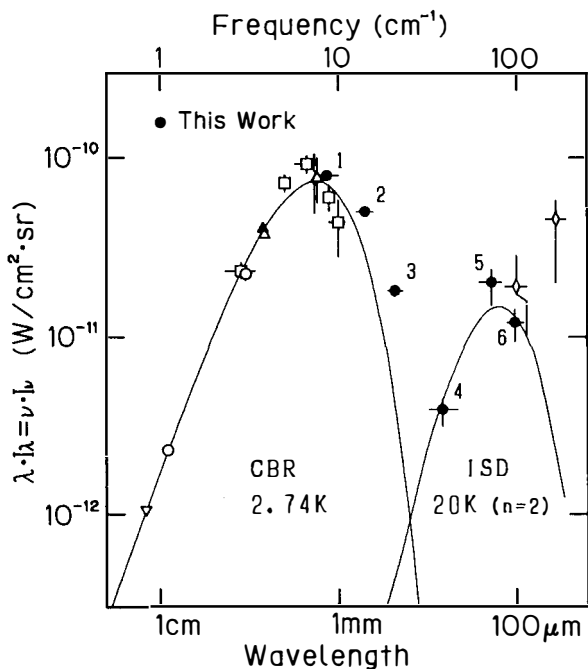
1. Taken from Matsumoto et al (1988)--"this work." The open symbols show CN and ground-based measurements.

The results at two intermediate wavelengths of 0.7 and 0.48 mm show an upward trend in T_0 as the wavelength drops--the submillimeter excess. The composite spectrum from 75 cm to 0.48 mm is not well fit by a blackbody at any temperature, or even by a graybody spectrum. Indeed, a small industry has grown up around explanations of this submillimeter excess. The most developed models involve photo-decays of exotic particles at high redshift (see Hayakawa et al, 1987; Fukugita, 1988); inverse Compton scattering of CBR photons by hot electrons (see Hayakawa et al, 1987; Lacey and Field, 1988) and thermal emission by dust in high redshift galaxies (e.g., Negroponte et al, 1981; Bond, Carr and Hogan, 1986). All of these models have problems, particularly with energetics (Lacey and Field, 1988; and

Adams et al, 1989). Some, in my view, have problems with the spectral measurements themselves. In particular, the close agreement between the CN values reported by Crane in this volume and the Johnson and Wilkinson measurement at 5 times longer wavelength presents problems for the inverse Compton model. Likewise, the sharp increase in temperature with falling wavelength is hard to match to a dust emission spectrum unless the emissivity of the dust is strongly dependent on wavelength and both the temperature of the dust and the redshift of emission are narrowly delineated (a range of temperatures or redshifts would smear out the spectrum).

Given both the importance of Matsumoto's result and the difficulty in finding convincing theoretical models for it, it is fair to ask how certain we are of the experimental results themselves. Is the submillimeter excess really there? There is, as some of you will know, a history of "false starts" in rocket observations of the CBR (Shivanandan et al, 1968; Woody and Richards, 1979); but the Berkeley-Nagoya experiment seems to me to be more sensitive, better designed and "cleaner" than past efforts. More to the point, the group will fly a similar payload (with slightly different filter bands) this summer (1989). In addition, if all goes well, the COBE satellite should quickly pin down the spectrum across the entire millimeter and far infrared band soon after its summer 1989 launch by NASA. Thus it is unsafe as well as unnecessary for me to speculate now on the reality of the submillimeter excess!

T_1, the dipole moment. The only reliably detected anisotropy in the CBR is its dipole moment. The amplitude, $T_1/T_0 = (1.20 \pm 0.03) \times 10^{-3}$, is known to a few percent accuracy, and the direction to an accuracy of about 1°, that is about the angle subtended by one's thumb held at arm's length. The consistency in the directions obtained by the various groups in this field (see Table 3) is particularly encouraging since widely different wavelengths were used. If there had been any appreciable contamination from the Galaxy, I would have expected a wavelength-dependent bias since Galactic millimeter wave emission depends strongly on wavelength.

The dipole moment in the CBR is universally ascribed to the Doppler shift resulting from the motion of the observer. In Table 3 are shown the results of the measurements corrected only for the motion of the earth about the sun; the implied velocity of ~ 300 Km/sec is thus heliocentric. The microwave results have usually been converted to a velocity of the center of mass of the local group by vector subtraction of the sun's velocity relative to the local group. This latter figure is

conventionally taken to be 300 Km/sec towards $\ell = 90°$, $b = 0°$ (or $\alpha = 21^h$, $\delta = + 50°$). In fact the solar motion relative to the center of mass of the local group is much less precisely known than the CBR dipole velocity. Indeed, Yahil et al (1977) find $\ell = 105°$ and $b = - 7°$ a better fit. Hence it might be prudent for theorists to calculate heliocentric velocities directly.

T_2, the quadrupole moment. The best available limits are set by the Soviet space experiment (Table 3). The value I cite is less model-dependent than a slightly more stringent upper limit given by Klypin et al (1987)--T_2/T_0 < 2×10^{-5}. Improving on this limit will require careful subtraction of Galactic emission (Boughn et al, 1989); COBE's multi-wavelength observations should help. Even the currently available limits place interesting constraints on anisotropic expansion between $z \approx$ 1000 and now, and on some models for the origin of large-scale structure.

T_p, large-scale polarization. As shown by Negroponte and Silk (1980) and Basko and Polnarev (1980), large-scale linear polarization of the CBR will be produced if the expansion of the Universe was anisotropic just at the epoch of last scattering. T_p thus measures anisotropy at a specific moment in the past. The best upper limits are still those of Lubin et al (1983): $T_p/T_0 \lesssim 2-4 \times 10^{-5}$ for the dipole and quadrupole components.

Anisotropy on degree scales. If the CBR last scattered at $z \approx 1000$, the present angular scale corresponding to the causal horizon at last scattering is $1°-2°$. Any anisotropy in the CBR on scales larger than this cannot have been smoothed away by causal processes, and thus carries information about the primordial spectrum of density perturbations in the Universe. Recently, Davies and his colleagues (1987) have claimed to detect fluctuations in the CBR corresponding to $\Delta T/T_0 = 3.7 \times 10^{-5}$ at $\lambda = 3$ cm on a scale of $8°$. Some workers in the field are skeptical of this claim and prefer to regard this result as an upper limit; in any case, measurements at degree scales are important and deserve further work (COBE's smallest angular scale is $7°$). N. Mandolesi, P. Crane and I have a project underway, and P. Lubin is making both ground-based and balloon measurements on this angular scale. One way to push the limits way down would be to use an array of sensitive bolometers to make a rough map of an area of the microwave sky; Dave Wilkinson at Princeton, with colleagues at Bell Labs and Haverford, is planning such a project.

Anisotropy on scales of $\sim 10'$. In many (but not all) scenarios for the origin of large-scale structure in the Universe, the amplitude of $\Delta T/T$ fluctuations has a maximum at $\sim 10'$ (see, e.g., Bond and Efstathiou, 1984;

Group	Berkeley	MIT/UBC	Moscow	Princeton	Princeton
Reference	Lubin et al (1985)	Halpern et al (1988)	Strukov et al (1987) Klypin et al (1987)	Fixsen et al (1983)	Boughn et al (1989)
Wavelength, mm	3	~ 1.7	8	12	15
Vehicle	balloon	balloon	satellite	balloon	balloon
Detector	heterodyne	bolometric	heterodyne	heterodyne	maser ampl.
Dipole amplitude, T_1, mK	3.4 ± 0.2	3.4 ± 0.4	3.16 ± 0.12	3.1 ± 0.2	3.47 ± 0.04
Direction of solar motion, R.A. and Dec.	$11^h.2 \pm 0^h.1$ $-6° \pm 1.5°$	$12^h.1 \pm 0^h.24$ $-23° \pm 5°$	$11^h.3 \pm 0^h.16$ $-7.5° \pm 2.5°$	$11^h.2 \pm 0^h.05$ $-8° \pm 0.7°$	$11.1^h \pm 0.1^h$ $-5.9° \pm 1.5°$
Limit on quadrupole moment, T_2, mK	0.4*	n.a.	≤ 0.08**	≤ 0.19	n.a.

Table 3. Measurements of the dipole moment T_1 and limits on T_2. The results are expressed in thermodynamic temperature.

*Calculated from Table I of Lubin et al by the present author, by taking the quadrature sum of the measured coefficients Q_1 . . . Q_5.

**Taking the more conservative, model-independent upper limit.

Vittorio and Silk, 1984). This scale is accessible to conventional filled aperture telescopes, and the upper limits on ΔT/T are consequently very tight: at λ = 1.5, and for θ = 7.5, ΔT/T ≤ 1.7×10⁻⁵ (Readhead et al, 1989; see also Uson and Wilkinson, 1984, for earlier results). These results are reviewed extensively in the literature, so I will not consider them further here.

Anisotropy on scales < 1′. In the galaxy formation scenarios referred to above, fluctuations on scales ≲ 1′ are smeared out (because the surface of last scattering has a finite thickness). In other models, however, particularly those invoking explosions to produce density perturbations, a higher amplitude of CBR fluctuations on scales ≤ 1′ may result (Ostriker and Vishniac, 1986; Vishniac, 1987). Thus several observers have considered it worthwhile to probe arcsecond scales (Fomalont et al, 1988; Martin and Partridge, 1988; Partridge, Nowakowski and Martin, 1988).

To achieve such resolution*, we need to employ a different technique, aperture synthesis, in which an array of telescopes, rather than a single antenna, is used to map the sky. This technique produces images of the microwave sky at a resolution set by the size of the array (see Verschuur and Kellermann, 1974 for details, or Partridge, 1988). This technique has been used by two groups working at the Very Large Array (VLA) operated by the U. S. National Radio Astronomy Observatory in New Mexico (Fomalont et al, 1984 and Fomalont et al, 1988; and Knoke et al, 1984, Martin and Partridge, 1988, Partridge, Nowakowski and Martin, 1988). Most observations reported to date were made at a wavelength of 6 cm, the wavelength at which the most sensitive receivers have been available. As shown in Table 4, angular scales of 6″ to 160″ were investigated. As is also clear from the table, the sensitivity of this technique is not yet quite comparable to the sensitivity of searches using conventional, filled-aperture radio telescopes (see Partridge, 1988, for details). On the other hand, typically 100–1000 independent sky elements are available in each map. Both groups begin by making a synthesized map of a region of the sky, such as the one shown in Figure 2. The area mapped is chosen to be much larger than the primary diffraction maximum of the individual antennas of the array (called the "primary beam" of the instrument). Thus the instrument is insensitive to radiation from sources at the edge of

*One exception to this statement is the recent 1 mm observation reported by Kreysa and Chini (1989).

Reference	λ, cm	θ, arcsec	$\Delta T/T \times 10^4$
Fomalont et al (1988)	6	18"	< 1.3
" "	6	60"	< 0.8
Martin & Partridge (1988)	6	18"–80"	1.7 ± 0.5
" "	6	36"–160"	1.3 ± 0.2
Hogan & Partridge (1989)	2	6"	< 6.3
" "	2	18"	< 1.6
Proposed Observations	3.5	12"	< 0.5
" "	3.5	40"	< 0.2

Table 4. Limits on fine-scale anisotropy in the CBR (95% confidence). Note that our proposed sensitivity exceeds the limits of Readhead et al (computed here for Gaussian fluctuations).

the map. Indeed that is clear from Figure 2; the radio sources in the field are visible only towards the center of the map. Likewise, any fluctuations in the CBR intensity will be detectable only near the center of the map where the primary beam response is large. On the other hand, instrumental and atmospheric noise will be distributed evenly over the entire map (see Knoke et al, 1984 or Fomalont et al, 1984). A comparison of the variances of the measured flux densities first at the edge of a map and then at its center thus provides a measurement of real fluctuations in the sky; these will produce extra variance at the center. It is important to note that both groups working at the VLA do find such excess variance at the centers of their maps, and that the observational results are in quantitative agreement even though the two groups looked at different regions of the sky, for different intervals of time, and using different map-making techniques.

Nevertheless, as Table 4 shows, the two groups reach different conclusions about CBR fluctuations. While we claim a ~ 3σ detection (σ here is statistical error only), they report only upper limits. The issue is the role played by faint radio sources. In any VLA map at λ = 6 cm, there will be foreground radio sources; several appear in fig. 2. The obvious sources may be removed from a map in several ways. But what about the fainter sources just at or below the threshold of detectability? These will add to the sky variance at the center of a map. One obvious effect is to add a long "tail" of positive flux readings to the map--see
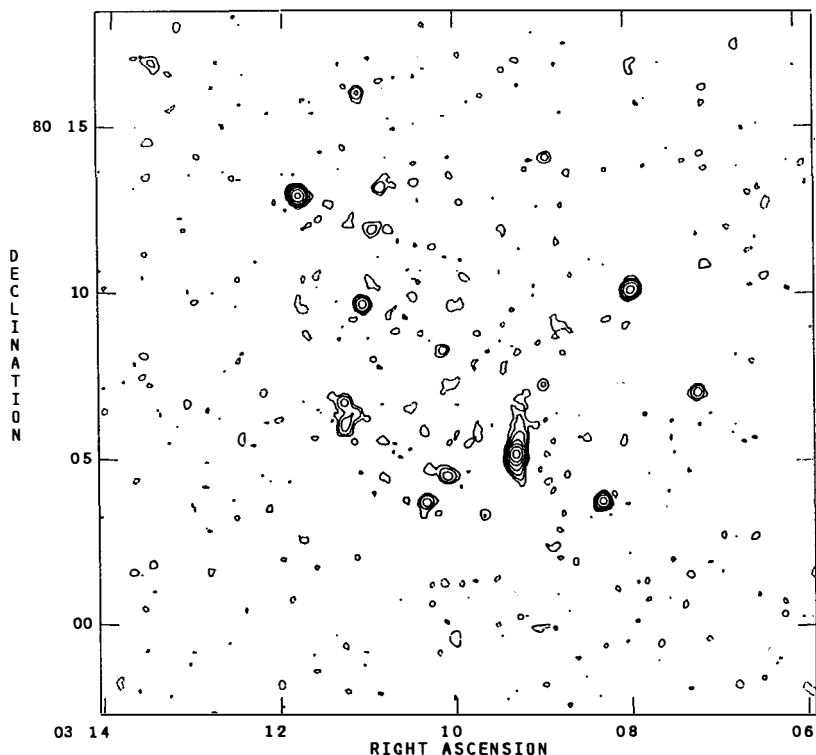
2. 6 cm contour map. Note the concentration of foreground
   sources near the center. Aside from the sources, is there
   excess noise near the map center?

the histogram of values of flux per resolution element at our map center
(fig. 3). Both groups modeled these contributions by extrapolating counts
of radio sources at higher flux densities and/or lower frequency. Does
the variance introduced by these faint sources explain all the excess
variance at the map centers? Here is where we disagree. Martin and I say
no (though it is close). Fomalont et al (1988) say yes. They have
included an effect which we neglected--the fact that any source in a VLA
map will have side-lobes (in physical terms, weak secondary interference
maxima). These side-lobes appear with both positive and negative flux
density in an aperture synthesis map. Although the amplitude of these
side-lobe signals is low (1-2% of the peak response), they do add to the
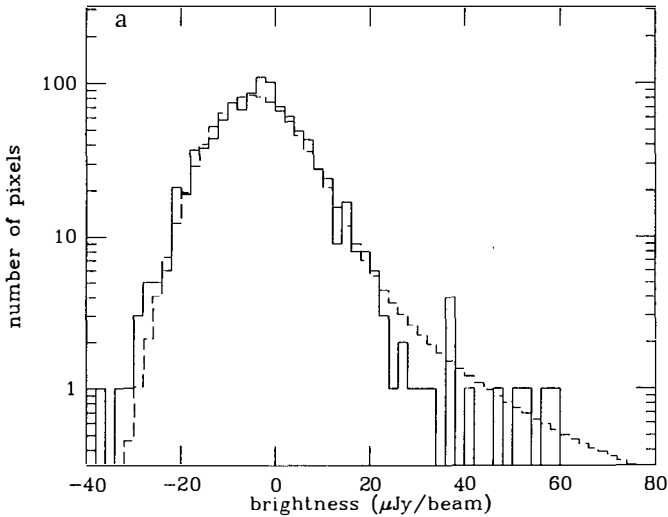
3. Observed brightnesses in central $(2.5)^2$ of the map shown in
    fig. 2, <u>after</u> sources were removed. The dashed line is our
    model fit, including faint radio sources (Martin and
    Partridge, 1988).

variance, broadening the histogram (see Fomalont et al, 1988; Partridge,
1989). In our analysis, we included only positive fluctuations, and hence
may have underestimated the full effect of weak sources. On the other
hand, an independent analysis of Fomalont et al's data by Franceschini et
al (1989) suggests that Fomalont et al would get a better fit to their
observations with a <u>non-zero</u> value of CBR fluctuations.

Clearly, more work is required before we settle on a final value for
or upper limit on ΔT/T at ⊕ ~ 18". One approach is to observe at higher
frequency: expressed in temperature, the spectrum of typical foreground
(synchrotron) radio sources is $T(\nu) \propto \nu^{-2.7}$. Thus higher frequency
observations can sharply reduce the problem caused by foreground sources.
Hogan and I (1989) therefore remapped a small area of the sky already
studied at 6 cm at the shorter wavelength of 2 cm, again at the VLA. The
2 cm receivers are less sensitive, so we have only marginal results (see
Table 4). The 2 cm results do not decide the issue, but <u>were</u> almost
entirely free of sources. In 1989, Hogan and I will join forces with
Fomalont and his colleagues at NRAO to use the VLA with its sensitive new
4 cm receivers to make one more concerted effort to detect CBR

fluctuations on scales $10" \lesssim \theta \lesssim 50"$. Our hoped-for sensitivities are shown in Table 4. At $\lambda = 4$ cm, we can, we think, do as well as the best currently available limit on arcminute scales. We ought also to be able to put models like Vishniac's (1987) to the test. In the meantime, I would suggest taking limits like 1.5×10^{-4} and 1.0×10^{-4} on $\Delta T/T$ on scales of 18" and 60", respectively.

I might also mention that these VLA observations may be used to put constraints on fluctuations produced in the microwave sky by the Sunyaev-Zel'dovich effect in distant clusters of galaxies (Rephaeli, 1981). The inverse-Compton scattering of the CBR photons in the intergalactic plasma in clusters will produce ~ 0.1-1 mK "holes" in the CBR on scales of roughly $1'$ (Korolev et al. 1986; Schaeffer and Silk, 1988). A student, Pat Hartnett, and I have shown that the 6 cm observations already available are barely consistent with the specific model presented by Korolev et al. The planned 4 cm observations may provide a more critical test.

Conclusion and Acknowledgements. The 7 measurements or upper limits I have mentioned have all proven useful in cosmology; particularly, I would say the measurement of T_1 and the limit on $\Delta T/T_0$ on arcminute scales. In a science starved for data, it is nice to be able to contribute 7 numbers.

My thanks to the organizers of this good meeting, and to both the National Science Foundation and Haverford College which supported my trip. Finally, I should confess that a few paragraphs of this article are borrowed, essentially verbatim, from a review I prepared for the Third ESO/CERN Symposium in 1988.

<div align="center">References</div>

Adams, F. C., Freese, K., Levin, J., and McDowell, J. C. 1989, submitted to *Ap. J.*

Basko, M. M., and Polnarev, A. G. 1980, *Mon. Not. Roy. Astr. Soc.*, 191, 207.

Bersanelli, M., Witebsky, C., Bensadoun, M., De Amici, G., Kogut, A., Levin, S. M., and Smoot, G. F. 1989, *Ap. J.*, 339, 632.

Bond, J. R., Carr, B. J., and Hogan, C. 1986, *Ap. J.*, 306, 428.

Bond, J. R. and Efstathiou, G. 1984, *Ap. J. (Letters)*, 285, L45.

Boughn, S. P., Cottingham, D. C., Cheng, E. S., and Fixsen, D. J. 1989, in preparation.

Davies, R. D., Lasenby, A. N., Watson, R. A., Daintree, E. J., Hopkins, J., Beckman, J., Sanchez-Almeida, J., and Rebolo, R., 1987, *Nature*, 326, 462.

Fixsen, D. J., Cheng, E. S., and Wilkinson, D. T. 1983, *Phys. Rev. Letters*, 50, 620.

34

Fomalont, E. B., Kellermann, K. I., Anderson, M. C., Weistrop, D., Wall, J. V., Windhorst, R. A., and Kristian, J. A. 1988, *A. J.*, 96, 1187.

Fomalont, E. B., Kellermann, K. I., and Wall, J. V. 1984. *Ap. J. (Letters)*, 277, L23.

Franceschini, A., Toffolati, L., Danese, L., and De Zotti, G. 1989, in preparation.

Fukugita, M. 1988, *Phys. Rev. Letters*, 61, 1046.

Halpern, M., Benford, R., Meyer, S., Muehlner, D. and Weiss, R. 1988, *Ap. J.*, 332, 596.

Hayakawa, S., Matsumoto, T., Matsuo, H., Murakami, H., Sato, S., Lange, A. E., and Richards, P. L. 1987, *Publ. Astron. Soc. Japan*, 39, 941.

Hogan, C., and Partridge, R. B. 1989, in press at *Ap. J.*

Johnson, D. G., and Wilkinson, D. T. 1987, *Ap. J. (Letters)*, 313, L1.

Klypin, A. A., Sazhin, M. V., Strukov, I. A., and Skulachev, D. P. 1987, *Soviet Astron. Letters*, 13, 104.

Knoke, J. E., Partridge, R. B., Ratner, M. I., and Shapiro, I. I. 1984, *Ap. J.*, 284, 479.

Kogut, A., Bersanelli, M., De Amici, G., Friedman, S. D., Griffith, M., Grossan, B., Levin, S., Smoot, G. F., and Witebsky, C. 1988, *Ap. J.*, 325, 1.

Korolev, V. A., Sunyaev, R. A. and Yakubtsev, L. A. 1986, *Sov. A. J. Letters*, 12, 141.

Kreysa, E., and Chini, R. 1989, in *Third ESO/CERN Symposium.*

Lacey, C. G., and Field, G. B. 1988, *Ap. J. (Letters)*, 330, L1.

Lubin, P., Melese, P. and Smoot, G. 1983, *Ap. J. (Letters)*, 273, L51.

Lubin, P. M., and Villela, T. 1985, in *The Cosmic Background Radiation and Fundamental Physics*, ed. F. Melchiorri, Editrice Compositori, Bologna.

Martin, H. M. and Partridge, R. B. 1988, Ap. J., 324, 794.

Matsumoto, T., Hayakawa, S., Matsuo, H., Murakami, H., Sato, S., Lange, A. E., and Richards, P. L. 1988, *Ap. J.*, 329, 567.

Negroponte, J., Rowan-Robinson, M., and Silk, J. 1981, *Ap. J.*, 248, 58.

Negroponte, J., and Silk, J. 1980, *Phys. Rev. Letters*, 44, 1433.

Ostriker, J. P. and Vishniac, E. T. 1986, *Ap. J. (Letters)*, 306, L51.

Partridge, R. B. 1985 in *The Cosmic Background Radiation and Fundamental Physics*, ed. F. Melchiorri, Editrice Compositori, Bologna.

Partridge, R. B. 1988, *Reports on Progress in Physics*, 51, 647.

Partridge, R. B. 1989, *3 K: The Cosmic Microwave Background Radiation*, in preparation for Cambridge University Press.

Partridge, R. B., Nowakowski, J., and Martin, H. M. 1988, *Nature*, 331, 146.

Readhead, A. C. S., Lawrence, C. R., Myers, S. T., Sargent, W. L. W. Hardebeck, H. E., and Moffet, A. T. 1989, submitted to *Ap. J.*

Rephaeli, Y. 1981, *Ap. J.*, 245, 351.

Schaeffer, R., and Silk, J. 1988, *Ap. J.*, 333, 509.

Shivanandan, K., Houck, J. R., and Harwit, M. O. 1968, *Phys. Rev. Lett.*, 21, 1460.

Smoot, G. F., De Amici, G., Friedman, S., Witebsky, C., Sironi, G., Bonelli, G., Mandolesi, N., Cortiglioni, S., Morigi, G., Partridge, R. B., Danese, L., and De Zotti, G. 1985, *Ap. J. (Letters)*, 291, L23.

Smoot, G. F., Levin, S. M., Witebsky, C., De Amici, G., and Rephaeli, Y. 1988, *Ap. J.*, 331, 653.

Strukov, I. A., Skulachev, D. P., Boyarskii, M. N., and Tkachev, A. N. 1987, *Soviet Astron. Letters*, 13, 65.

Uson, J. M. and Wilkinson, D. T. 1984, *Nature*, 312, 427.

Verschuur, G. L. and Kellermann, K. I., eds. 1974, *Galactic and Extra-galactic Radio Astronomy*, Springer-Verlag, New York.

Vishniac, E. T. 1987, *Ap. J.*, 322, 597.

Vittorio, N., and Silk, J. 1984, *Ap. J. (Letters)*, 285, L39.

Woody, D. P., and Richards, P. L. 1979, *Phys. Rev. Lett.*, 42, 925.

Yahil, A., Tammann, G. A., and Sandage, A. 1977, *Ap. J.*, 217, 903.

Cosmic Background Radiation Temperature

at 2.64 mm, 1.32 mm, and 0.6 mm

Philippe Crane
European Southern Observatory, Munich
Marc L. Kutner
Rennsalear Polytechnic Institute, Troy
Dennis J. Hegyi
University of Michigan, Ann Arbor
J. C. Blades
Space Telescope Science Institute, Baltimore
and
E. Palazzi, and N. Mandolesi
Istituto TE.S.R.E., Bologna

Abstract

The Cosmic Background Radiation temperature has been measured by means of interstellar absorption lines at wavelengths of 2.64 mm, 1.32mm, and at 0.56 mm. At 2.64 mm, a precise value of $T_{CBR} = 2.796(+0.019; -0.039)$K is determined. This result includes conservative estimates for all reasonable sources of error. At 1.32 mm, a value of 2.83 ± 0.07 K has been found in the direction of the star HD154368. The error in this result is dominated by uncertainties in the equivalent widths, but includes a substantial uncertainty due to the saturation correction. Observations of interstellar CH toward ζ Oph have yielded a one standard deviation upper limit to T_{CBR} at 0.56 mm of 3.60 K.

1 Introduction

Interstellar absorption lines provide an interesting alternative technique for studying the Cosmic Background Radiation spectrum at wavelengths that are difficult or impossible using direct ground based techniques.

It is perhaps curious that the first realization that this technique could be used to determine the existence of a universal background radiation was used as an argument against the Big Bang cosmologies. Apparently in the early 1950's, Hoyle and collaborators, working on a steady state cosmology, knew of the work of Adams(1941) who had found a CN excitation temperature of about 2 K, and the work of Gamow and collaborators who had predicted a universal background radiation with a characteristic temperature of about 20K. Although this is not published, it is understood that Hoyle used this discrepancy between measurement and prediction as an argument against the Big Bang cosmology proposed by Gamow.

Subsequent to the eventual detection and measurement of the Cosmic Background Radiation in 1964 by Penzias and Wilson(1965), there were several papers reporting determinations of the CBR temperature using the interstellar lines of CN as well as those of CH and CH^+. A useful review of work prior to 1972 can be found in the article of Thaddeus(1972). In the decade following Thaddeus' review, very little work on measuring the CBR temperature using molecular absorption lines was done. However, the field was revitalized in 1985 and 1986 with the appearance of the works of Meyer and Jura(1985) and Crane, Hegyi, Mandolesi, and Danks(1986). The arrival of a new generation of detectors providing high signal-to-noise at high spectral resolution allowed these investigators to achieve close to an order of magnitude increase in the precision with which the weak absorption lines needed to determine the CBR temperature could be measured.

In fact, the error in the value of the CBR temperature using the CN absorption lines toward ζ Ophiuchi is now dominated by the uncertainty in the knowledge of the physical conditions in the interstellar cloud and how these conditions might effect the excitation of the CN rotational levels. A crucial assumption in all measurements of the CBR temperature from interstellar absorption lines is that the measured excitation temperatures are in fact the CBR temperature or very close to it. Of course, the most

precise measurements must check this assumption as was first recognized by Field and Hitchcock(1966), and first attempted by Penzias, Jefferts, and Wilson(1972)

The results from the interstellar absorption lines are subject to relatively few systematic errors, and the major source of statistical error is in the determination of the optical absorption line strengths. This is especially true for the features which are sensitive to the CBR at wavelengths less than 2 mm. where the statistical uncertainties dominate the errors. There are two other effects which have to be accounted for; saturation corrections and possible excitation of the rotational states by sources other than the CBR. The saturation correction requires knowledge of the true shape of the observed absorption feature. This is difficult even at the maximum resolution of 150,000 used for the optical observations. Correcting for the non CBR excitation is in principle possible by observing the expected emission at say 2.64 mm which would be present if CN were excited by collisions with electrons or by *any* other mechanism.

In view of the possibility of excess radiation in the submillimeter region suggested by the recent Berkeley-Nagoya rocket flight (Matsumoto *et al.*,1988), and of a possible difference between ground based radiometer measurements of T_{CBR} and other measurements (Crane *et al.*,1989), the results presented here are particularly timely.

This paper presents data from three different sets of observations which measured or set limits on the CBR temperature at 2.64 mm, 1.32mm and 0.56 mm. All the optical data described here were obtained at the ESO 1.4 Coudè Auxilliary Telescope and associated Coudè Spectrograph. The millimeter observations were obtained at both the NRAO 12 meter and the SEST telescopes.

Figure 1 shows a schematic level diagram of CN and CH for the transitions of interest for this work. For CN, the R(0) line in combination with either the R(1) or P(1) lines provided the data needed to determine the CBR temperature at 2.64 mm. The R(1) or P(1) lines in combination with either the R(2) or P(2) lines are useful in determining T_{CBR} at 1.32 mm. For CH, the ratio of the strengths of the $R_1(1)$ line to the $R_2(1)$ line is sensitive the CBR intensity at 0.56 mm.

In the following sections, the results at 2.64 mm toward ζ Oph, the results at 1.32 mm toward HD154368, and at 0.56 mm toward ζ Oph are discussed. Since the detailed procedures were similar for all three sets of data, they are discussed only in the next
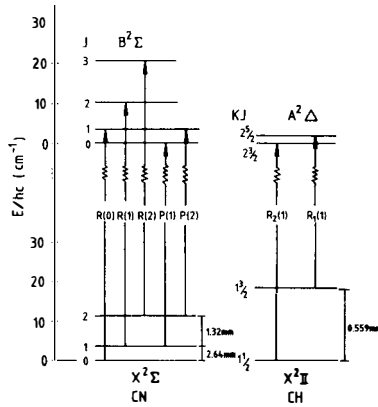
Figure 1: Schematic level diagram of CN and CH

section on results at 2.64 mm. The final section summarizes the results and discusses some of the implications.

2 T_{CBR} at 2.64 mm

The optical data used to determine T_{CBR} at 2.64 mm were obtained in two observing runs in 1984 and 1985 and have been reported previously by Crane *et al.*(1986). These data were obtained for the interstellar cloud along the line of sight to the star ζ Oph. The new results which we report (Crane *et al.*,1989) come from an improved analysis technique(Crane and Hegyi, 1988) which gives a better understanding of the nature of the errors in the data. In addition, a careful search for CN emission at 2.64 mm has set a new limit on possible departures of the CN rotational levels from thermal equilibrium with the CBR. Also, a careful investigation of the assumptions in the saturation correction technique has given greater confidence in the error assigned to this possible systematic effect. We discuss each of these briefly.

In reanalyzing the data, each 20 minute spectrum was taken separately and values for the R(0), R(1), and the P(1) lines' equivalent widths were determined. There were 61 spectra in all, but, in each case, only about 55 were used to determine the final equivalent width. The five or six spectra that were excluded from each data set had
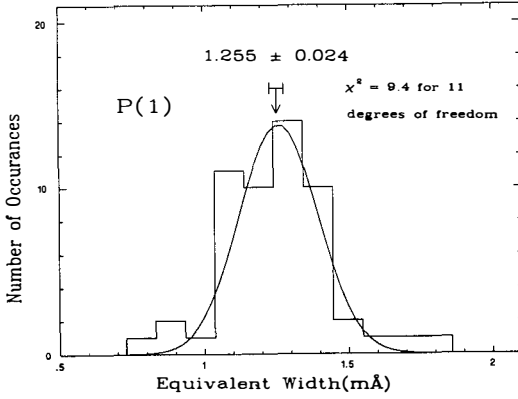
Figure 2: Histogram of the equivalent widths of the CN P(1) line. Each entry is for a single 20 minute spectrum. The line is a fitted gaussian. The arrow indicates the best fit value and the error.

various anamolies such as a noisy continuum or a cosmic ray hit in an absorption feature. The resulting equivalent widths were binned into histograms, and these histograms were fit to a gaussian to determine the best value and the error. Figure 2 shows the results for the P(1) line. Table 1 lists the measured equivalent widths.

Table 1: ζ Oph CN Equivalents Widths

Line	λ_{air} A A	Equivalent Widths mÅ
R(0)	3874.608	7.746 ± 0.041
R(1)	3873.998	2.454 ± 0.021
P(1)	3875.763	1.255 ± 0.020

In order to check the assumption that the CN molecule is in thermal equilibrium with the CBR radiation, a careful search for emission from CN at 2.64 mm. was performed at the NRAO 12 meter telescope on Kitt Peak with a total on source integration time of 30 hours. The observations yielded the formal result:

$$T_R^* = -9.5 \pm 5.2 mK$$

where T_R^* is the source antenna temperature corrected for atmospheric, ohmic and all spillover losses (Kutner and Ulich, 1981). However, this must be related to the excitation of CN due to local processes in the interstellar cloud through the relation

$$T_R^* \approx (0.74)T_{loc}(1 - e^{-\tau}) = 0.079 T_{loc}$$

where τ is the optical depth in the millimeter lines at 2.64 mm. ($\tau = 0.113$) We find $T_{loc} = -120 \pm 66$mK. This result implies that it is rather unlikely that there is *any* local procss contributing to the excitation of the CN rotational state populations. However, in order to derive an upper limit for T_{CBR}, we have used the following arguments.

There are no mechanisms that we know of that can produce values of $T_{loc} < 0$, or cool CN below the CBR temperature. Thus our result is formally unphysical, and we need to produce an upper limit to T_{loc}. If we take our result to be 0 with an uncertainty of 66 mK and ask below what value of T would 68%(1 σ) of the observed values fall if the observations were repeated many times. Following this procedure, and using a gaussian distribution for the errors, we find:

$$T_{loc} \leq 31 mK$$

Although the lines have small optical depths, a saturation correction must be made, and this presents the possibility of further systematic errors. The saturation correction requires an accurate knowledge of the absorption line profile. This knowledge is very difficult to acquire using optical resolutions of 2 km s^{-1} since the lines have width of at most 1.5 km s^{-1}. Previous work (Crane *et al.*, 1986) measured a width(FWHM) of 1.46 km s^{-1} for the CN R(0) line. However this assumed a single component line with a gaussian profile. Subsequent observations of CO toward this cloud (Langer *et al.*,1987) showed several narrower components which might reproduce the observed optical profile (Black and van Dishoeck, 1988). However, since there seems to be some differences between the CH 9 cm line profiles, and the CO 3mm line profiles(Crane, 1989), it is not clear how to model the CN. Therefore, we have used a single gaussian line profile with a FWHM of 1.46 km s^{-1} as the basis for the saturation correction model in the results below, but have allowed for the possibility that this model is wrong in the error budget.

The resulting value of $T_{CBR} = 2.796(+0.019; -0.039)$ is directly the measured CN excitation temperature and includes uncertainties of 13.3 mK due the equivalent widths, 5 mK due a scale uncertainty, -18 mK for the saturation correction, and -31 mK for possible local excitation effects. These results are summarized in Table 2.

Table 2: T_{CBR} at 2.64 mm

Ratio	T_{raw}	T_{exc}
R(1)/R(0)	2.9578 ± 0.0162	2.7960 ± 0.0156
P(1)/R(0)	2.9944 ± 0.0276	2.7968 ± 0.0251
Average		2.7962 ± 0.0133
Saturation Uncertainty		-0.018
Scale Error		± 0.005
Local Excitation		-0.031
Final T_{CBR}		$2.796(+0.014; -0.039)$

3 T_{CBR} at 1.32 mm

The value of T_{CBR} at 1.32 mm has been determined from the CN absorption lines toward the star HD154368 (Palazzi *et al.*,1989). The CN column density toward this star is about 10 times greater than toward ζ Oph and, therefore, the strength of the R(2) and P(2) lines which are sensitive to T_{CBR} at 1.32 mm are also 10 times stronger. The star is, however, about 10 times fainter than ζ Oph. The determination of very weak absorption lines is limited by detector performance at very high signal-to-noise and possibly by weak atmospheric lines. HD154368 is a better choice for measuring T_{CBR} at 1.32 mm. than ζ Oph since the required features are stronger relative to the continuum and hence limited by statistical uncertainties and not by detector systematics.

Figure 3 shows a composite of the spectra obtained toward HD154368. Table 3 lists the equivalent widths determined in this work. We note that the ^{13}CN equivalent width implies $^{12}C/^{13}C = 105 \pm 15$.

A search for CN emission at 2.64mm toward HD154368 has yielded a weak line with $T_R^* = 19.0 \pm 5.1$ mK. Following the same procedure as for the ζ Oph, we determine an

Table 3: HD154368 CN Equivalent Widths

Line	λ_0 (Å)	Equivalent Width	log N(cm^{-2})
R(0)	3874.608	24.62 ± 0.13	13.32
R(1)	3873.998	15.12 ± 0.11	12.97
P(1)	3875.763	9.74 ± 0.09	12.98
R(2)	3873.369	0.810 ± 0.107	11.53
P(2)	3876.310	0.545 ± 0.088	11.53
^{13}CN R(0)	3876.784	0.822 ± 0.096	11.32

excitation temperature at 2.64 mm towards HD154368 of

$$T_{loc} = 35 \pm 10 mK$$

This result also can be used to determine the contribution to the CBR temperature at 1.32 mm from local sources. If we assume that electrons are the dominant cause of this local excitation, then, following the procedures outlined by Thaddeus(1972), we find:

$$T_{loc}(1.32mm) = \frac{1}{3}T_{loc}(2.64mm) = 12 \pm 3mK$$

If other mechanisms contribute to the local excitation such as collisions with neutral atomic or molecular hydrogen, we expect an even smaller contribution to T_{loc}.

In addition to the result at 1.32 mm, the data provide a measurement of the CBR at 2.64 mm, but the required saturation correction is large, and its uncertainty dominates the errors. Therefore, these data do not provide an competitive value for T_{CBR} at 2.64 mm.

Since the features that determine to T_{CBR} at 1.32 mm are not as sensitive to the saturation effects or to possible sources of local excitation as the 2.64 mm data, HD154368 can provide a precise measurement at 1.32 mm. Table 4 lists the excitation temperatures and the saturation corrected excitation temperatures determined from the equivalent widths in Table 3.

The intrinsic width of the CN lines needed for the saturation correction was determined from high resolution Reticon spectra. The line width of 14.0 mÅ determined from fitting the observed R(0) line is considerably narrower than the linewidth of 19.0
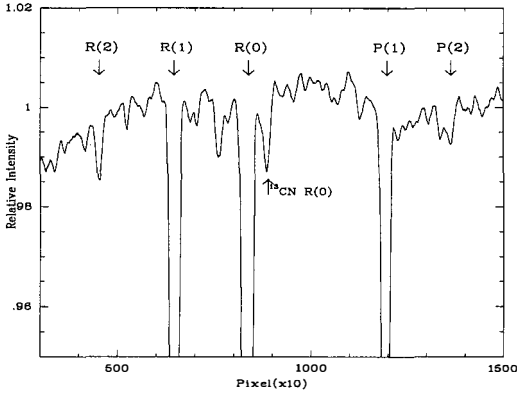
Figure 3: Composite of spectra CN absorption spectrum towards HD154368. The ^{12}CN lines are indicated as well as the ^{13}CN R(0) line. An unexplained line is visible to the left of the R(0) line.

Table 4: T_{CBR} at 2.64 mm from HD154368

Line Ratio	$T_{raw}(K)$	$T_{exc}(K)$
R(1)/R(0)	4.616 ± 0.072	2.849 ± 0.037
P(1)/R(0)	5.877 ± 0.091	2.889 ± 0.037
Weighted mean		2.869 ± 0.026
Saturation correction uncertainty		0.000 ± 0.080
Local excitation correction		-0.035 ± 0.010
T_{CBR}		2.834 ± 0.085

Table 5: T_{CBR} at 1.32 mm

Line Ratio	$T_{raw}(K)$	$T_{exc}(K)$
R(2)/R(1)	3.271 ± 0.16	2.852 ± 0.092
P(2)/P(1)	3.047 ± 0.14	2.834 ± 0.112
Weighted Average		2.845 ± 0.071
Saturation Correction Error		0.000 ± 0.007
Local Excitation Correction		-0.012 ± 0.003
T_{CBR}		2.833 ± 0.071

mÅ found for the ζ Oph cloud. In addition to the Reticon results, there are two other independent methods to determine this result. The requirement that the ratio of the R(1) to P(1) lines give a relative strength of 2 after correction for saturation yields a value for the intrinsic width of the lines. Also, a comparison of the red and violet line strengths can be used to constrain the intrinsic width of the lines (van Dishoeck and Black, 1989). All of these techniques give essentially the same result.

4 $\mathbf{T}_{CBR}$ at 0.56 mm

The CH molecule ground state rotational levels provide the possibility of studying the CBR spectrum at 0.56 mm. The $R_1(1)$ line at 4303.947Å can be compared to the stronger $R_2(1)$ line at 4300.321Å to yield a measure of the CBR temperature. For ζ Oph, the star we have observed, the expected strength of the $R_1(1)$ line is 0.005 mÅ if T_{CBR} is 2.8 K, or 0.010 mÅ if the radiation temperature is 3.12 K at 0.56 mm. This latter is close to what might be anticipated if the Berkeley-Nagoya results(Matsumoto et al.,1988) are correct.

We have measured the $R_2(1)$ line at 4300.321Å, and found an equivalent width of 18.2 ± 0.2 mÅ. We have searched for the $R_1(1)$ line and have established an upper limit of 0.030 mÅ Using the relation

$$T = 25.784/\ln\left(1.524\frac{N(R_2(1))}{N(R_1(1))}\right)$$

yields a limit of $T_{CBR} \leq 3.60$ K at 0.56 mm after correction for saturation.

Further observations may be able to push this limit down to the point where this technique will yield interesting results.

5 Discussion

In view of the increasing interest in the short wavelength spectrum of the CBR, the results reported here provide an independent method of determining the CBR spectrum. The interstellar absorption lines provide a relatively simple and inexpensive alternative to the other techniques.

The present results are limited mainly by the detectors. Very weak absorption must be determined from the stellar continuum as detected. Non-uniformities in the detector response or low level semi-periodic noise has not been totally eliminated. Also, weak telluric features may represent a more fundamental limitation to this technique.

At wavelengths longer than 1 mm, all measurements are consistent with the CBR being a pure black body spectrum with a characteristic temperature of 2.777 ± 0.012 K (Crane *et al.*,1989). At shorter wavelengths, the Berkeley-Nagoya results indicate considerable excess radiation compared to a 2.78 K black body. Numerous papers have proposed explanations of this excess radiation (Daly, 1988; Smoot *et al.*,1988). These explanations are severely constrained by the high precision result reported here at 2.64 mm. The result reported here at 1.32 mm is entirely consistent with other results at $\lambda \geq 1.0$ mm, but the precision is not quite good enough to constrain models or to indicate a possible deviation from a pure black body.

References

Adams, W.S., 1941, *Ap. J.*,**93**,11.

Black, J.H., and van Dishoeck, E., 1987,*Ap. J.*,**331**,986.

Crane, P., 1989 (to be published).

Crane, P., Hegyi, D.J., Mandolesi, N., and Danks, A.C., 1986 *Ap. J.*,**309**,822.

Crane, P., and Hegyi, D.J., 1988,*Ap. J.(Letters)*,**326**,L35.

48

Crane, P., Hegyi, D.J., Kutner, M.L., and Mandolesi, N., 1989, *Ap. J.*(November 1).

Daly, R.A.,1988,*Ap. J.(Letters)*,**333**,L1.

Field, G.B, and Hitchcock, J.L., 1966, *Ap. J.*,**146**,1.

Kutner, M.L., and Ulich, B.L.,1981,*Ap. J.*,**250**,341.

Langer, W.C., Glassgold, A.E., and Wilson, R.W., 1987, *Ap. J.*, **322**,430.

Matsumoto, T., Hayakawa, S., Matsuo, H., Murakami,H., Sata, S., Lange, A.E., and Richards, P.L.,1988, *Ap. J.*,**329**,567.

Meyer, D.M., and Jura, M., 1985,*Ap. J.*,**297**,119.

Palazzi, E., Mandolesi, N., Crane, P., Kutner, M.L., Blades, J.C., and Hegyi, D.J., 1989, *Ap. J.*(in preparation).

Penzias, A.A., and Wilson, R.W., 1965, *Ap. J.*,**142**,419.

Penzias, A.A., Jefferts, K.B., and Wilson R.W., 1972, *Ap. J.*, **28**,772.

Smoot, G.F., Levin, S.M., Witebsky, C., DeAmici, G., and Raphaeli, Y., 1988,*Ap. J.*,**331**,653.

Thaddeus, P.,1972,*Ann. Rev. Astr. & Astrophy.*,10,305.

van Dishoeck, E., and Black, J.H., 1989,*Ap. J.*,**340**,273.

CAN ONE "WEIGHT" THE COSMIC STRINGS WITH THE MICROWAVE BACKGROUND

FRANÇOIS R. BOUCHET

Institut d'Astrophysique de Paris, Paris, France;

and Centre de Physique Théorique de l'Ecole Polytechnique, Palaiseau, France.

In collaboration with D. P. BENNETT, Princeton University,USA,

and A. STEBBINS, CITA, Toronto, Canada.

(and a CRAY-2 at L.L.N.L., Livermore, USA)

ABSTRACT

We present estimates of the cosmic microwave background anisotropy that is produced by a network of cosmic strings. String networks were evolved dynamically in a flat matter-era cosmology, by using the code developed by D. Bennett and myself to study the relaxation to, and the properties of, the scaling solution. Using a formalism developed by A. Stebbins for calculating microwave anisotropy generated gravitationally by moving objects, we have computed the temperature patterns produced by these networks. The angular size of the resulting temperature maps depends on the redshift of last scattering but will be in the range $7° - 40°$. The temperature maps have $\langle \Delta T/T \rangle_{\mathrm{RMS}} \sim 17 G\mu/c^2$ where μ is the model-dependent linear mass density of the strings. Comparison with anisotropy experiments places an upper limit of 5×10^{-6} on $G\mu/c^2$, $i.e.$ we cannot quite yet "weight" the strings, but present day experiment already put an interesting upper limit on their mass per unit length.

Cosmic Strings are topologically stable linear defects that form in many grand unified theories (GUT) during a symmetry breaking phase transition in the early Universe.[1,2] They might also be fundamental string remnants of an earlier phase. Contrary to monopoles and domain walls (the zero- and two-dimensional defects), they are not obviously a disaster for Cosmology. In fact, the idea that they might account for the formation of galaxies and large scale structure has recently generated a lot of interest. If the string tension μ is at the GUT scale (*i.e.* $\mu \sim (10^{16}GeV)^2$), they could provide appropriate seeds for the matter accretion in the matter era (or for the Ostriker – Thomson – Witten explosions,[3,4] if they are superconducting). Furthermore they have interesting observable signatures, like a non-zero residual of the millisecond pulsar timing measurements,[5-7] or their gravitational lensing effects,[8,9] or the expected step-like discontinuities in the microwave background.[10,11] For the value of μ aforementioned (corresponding to $G\mu/c^2 \sim 10^{-6}$, G being Newton's constant), these might soon be detectable. In the following, we concentrate on the imprinted anisotropies on the Cosmic Microwave Background (hereafter CMB).

In order to understand the origin of these imprinted anisotropies, let us first consider the case of a straight infinite string,[12] which we place for convenience along the z axis. Since the string has no structure in the z direction, it must be invariant under Lorentz-boosts in that direction. Together with the conservation law, this is enough to imply

$$\tilde{T}_{\lambda\nu} = \delta(x)\delta(y) \int T_{\lambda\nu} \, dx \, dy = \mu \, diag(1,0,0,-1)\delta(x)\delta(y),$$

where $\tilde{T}_{\lambda\nu}$ is the stress energy tensor averaged over the string cross section which is absolutely tiny ($\sim 10^{-30} cm$ for GUT scale strings) as compared to any relevant cosmological scale. This exhibits a remarkable property, *i.e.* the tension along the string is equal to its energy density, which has important consequences on the coupling of strings with gravity. Indeed, let us recall that for matter which is static and of stress energy tensor of the form

$T_{\lambda\nu} = diag(\rho, -P_1, -P_2, -P_3)$, the Einstein equations yields in the Newtonian limit the Poisson equation

$$\nabla^2 \Phi = 4\pi G(\rho + P_1 + P_2 + P_3),$$

we discover that straight infinite strings have no Newtonian gravity! If one now works out the metrics resulting from the Einstein equations, one finds[13]

$$ds^2 = dt^2 - dz^2 - dr^2 - (1 - 4G\mu)r^2 d\theta^2,$$

where we recover that the surrounding space is everywhere (locally) flat. But it also shows that if one follows a close path along the string, the angle ϕ will change by $2\pi(1-4G\mu)$ instead of 2π. In other words, this metrics describes the structure of a cone, so that one can represent the effect of a string by assuming a Minkowskian plane geometry, by removing a wedge of angle $8\pi G\mu$, and by identifying the edges. Thus a background object will be lensed by the string (if it is less than $8\pi G\mu$ away from the plane defined by the string and the observing point), and the two images will be separated by $8\pi G\mu$.

If the string is moving, two other interesting effects appear. First, if we consider two particles at rest and a string moving with velocity v, in the reference frame of the string the particles move with parallel velocities equal to the string velocity, and in the opposite direction. One can use the previous construction to see that the effect of the conical geometry is to add a relative velocity toward each other $\delta v = 8\pi G\mu v$: the string "focused" the particles. A moving string in a medium will thus leave behind a wake. Such wakes are quite interesting since they might provide the initial conditions to obtain the large scale sheets[14] observed in the distribution of galaxies. But the details of their distribution, which depends on the evolution of string networks, has not yet been fully worked out, although analytical estimates are promising.[15] The other effect concerns the effect on a photon source. As in the lensing case, an observer will see two images of a source. But if the string is moving, as in the wake case, the two images of the source will be seen by the observer with different relative velocities. The observer will thus see two images, one

blueshifted and the other redshifted. If one now considers an homogeneous photon background, one expects to see a step-like discontinuity (along the string) of the "temperature" of this background, with a magnitude

$$\Delta T/T \sim 8\pi G\mu\, v\cos\theta$$

where $v\cos\theta$ is the projected string velocity perpendicular to the line of sight. All that was said above strictly applies only to the case of a straight infinite string. Nevertheless, it should provide a reasonable description whenever the curvature of the string may be neglected, *i.e.* when one considers the effect of a string on scales which are small as compared to the curvature radius of the strings.

The CMB anisotropies generated by "real" (*i.e.* not straight) strings are quite difficult to compute, in particular when one considers scales comparable to the horizon ($\propto ct$). Nevertheless, for strings embedded in a minkowsky space, Stebbins has showed [16] that, in the limit of an infinitely remote observer

$$\Delta T/T \sim -4\frac{G\mu}{c^2}\oint\frac{\mathbf{u}\cdot(\mathbf{x}_\perp - \mathbf{r}^{proj})}{\mid\mathbf{x}_\perp - \mathbf{r}^{proj}\mid^2}\,d\sigma,$$

where σ is the string parameter. $\mathbf{x}_\perp$, $\mathbf{r}^{proj}$, and $\mathbf{u}$ all live in the plane orthogonal to the photon direction (unit wavevector $\mathbf{k}$), and $\mathbf{x}_\perp$ marks the photon direction, $\mathbf{r}^{proj}$ marks the string element (so that $\mid\mathbf{x}_\perp - \mathbf{r}^{proj}\mid$ is the distance in the plane of the string element to the photon), and

$$\mathbf{u} = \left(1 - \frac{(r\prime\cdot\mathbf{k})^2}{(1-\dot{\mathbf{r}}\cdot\mathbf{k})^2)}\right)(\dot{\mathbf{r}} - (\dot{\mathbf{r}}\cdot\mathbf{k})\mathbf{k})\,.$$

The meaning of the above formula is made clearer if one notes that it can be cast in the form of a (two-dimensional) Laplace's equation

$$\nabla^2\left(\frac{\Delta T}{T}\right) = -8\pi\frac{G\mu}{c^2}\oint\mathbf{u}\cdot\nabla_{x_\perp}\delta^{(2)}(\mathbf{x}_\perp - \mathbf{r}^{proj})\,d\sigma.$$

In this limit, the temperature anisotropy field is given by a sum over a collection of infinitesimal dipoles (gradient of δ) along the string, the dipole moments being $\mathbf{u}$. It is thus easy to compute in Fourier space, provided one knows the source term, *i.e.* the time evolution of the interacting system.

David Bennett and myself have shown that a string system, interacting by intercommutation in an expanding Universe relaxes toward a universal scaling solution which amounts to say that the relaxed state is invariant when one uses the horizon size H ($\propto ct$) as a meter stick, and that whatever the initial conditions might be, the string system always relaxes to the same state (when expressed in horizon units). Such a result confirmed earlier findings by Albrecht and Turok,[19] although with different numerical values. It is interesting to note that the preliminary results of the simulations by Allen and Shellard[20] appear to confirm our numerical values. The new results of Albrecht and Turok[21] are different but might be compatible since they aknowledge large possible systematic errors (by a factor of 4, which is precisely the difference between our value and theirs). We find that the long string system may be viewed as a collection of brownian walks with persistence length $\xi \sim H/3$, and the long string density is of the order of 50 Horizon length H of long string per horizon volume H^3 in the radiation era, and about $30H/H^3$ in the matter era (note that $H^{-2} \propto a^{-4}$ in the radiation era, a being the metrics expansion factor, and $H^{-2} \propto a^{-3}$ in the matter era). This shows that, through their intercommuting, long strings dump enough energy into loops (that can ultimately disappear by gravitationally radiating all their mass) to have their energy density scale as the rest of the dominant material in a given era: the long string density at the horizon scale is a fixed and small fraction of the total energy density ($\delta\rho_{LongStrings}/\rho_{tot} \sim 50G\mu$ in the radiation era, $G\mu \sim 10^{-6}$).

One should be aware that although the long strings dynamics is fairly well understood, the loop sizes distribution is not well known.[7] From our result, we can only set an upper limit on the typical loop sizes chopped off the long string network, which turns out to be tiny ($R_{Loop} < 10^{-4}H$). In the matter era, the (total) projected angular length of string in the redshift interval $[z_i, z_f]$ scales on average as $\theta_{string} \propto \sqrt{z_i} - \sqrt{z_f}$, i.e. most of the string length we see is concentrated at high redshift. This means that most of the temperature anisotropies will be imprinted near the last scattering surface. If there is no reionization episode in the history of the universe, then the last photon scatterings occur at a redshift $z_{ls} \sim 1000$, and the angle subtended

by the horizon at that time is only $\theta_H \sim 1.8°$ ($10°$ for $z_{ls} \sim 30$), which is not much larger than the resolution of small angular scale CMB anisotropy experiments (typically $\sim 1°$). Thus one expects that all the CMB anisotropies of present day experiment will be imprinted by the long strings only. This can indeed be confirmed by looking at the topology of the maps we generated and by computing their power spectrum which is peaked at a scale $\sim 3/\theta_H$. Thus, although the loops's size distribution is poorly known, we can safely predict the expected CMB anisotropies, even at the degree scale.

Now in order to actually generate some CMB maps, we propagate photon planes in our simulation box along different axes during matter era simulations. At each time step, we record the positions and the transverse velocity (*i.e.* in the plane) of the strings poking through or in the photon plane. At the end of the simulation the recorded position in the plane perpendicular to the photon direction of propagation simply correspond to the projected string configuration on the backward observer's light cone. We take the last scattering surface to be the face of the cube from which the photon plane is launched. We are thus missing no visible strings from behind the simulation cube, but we are missing strings from between the front face of the cube and us. By how much? Since in such simulations the horizon increases from $H = L/4$ to $H = L$ (where L is the box size), $z_f = z_i/16$, *i.e.* we miss 25% of the total string length, if $z_i = z_f \sim 1000$. We compensate for this by superposing to this result the result of another simulation scaled by a factor four (1/16 of its resulting map), *i.e.* we place two simulation end-to-end, in effect covering 256 expansion factors. If the last scattering surface occurred at $z_{ls} \sim 1000$, we now miss only 6% of the projected string length, and we have 18% too many strings if the last photon scattering occurs at $z_{ls} \sim 30$, which seems a reasonable compromise. An example of such a superposition of projected string configuration on the backward observer's light cone is shown in figure 1.
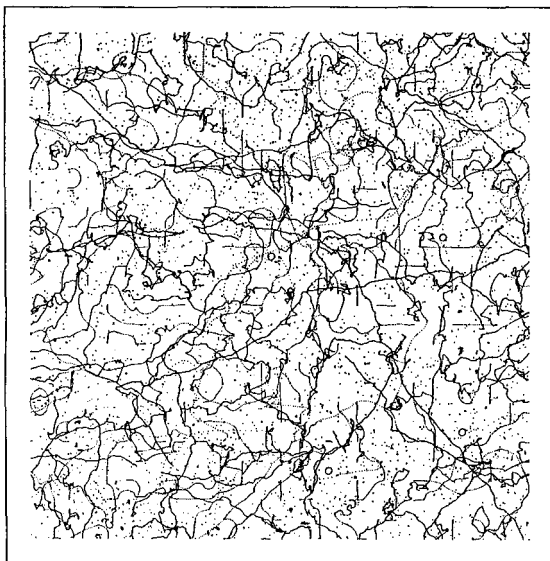
Figure 1

Projected String configuration

Since the horizon is initially a quarter of the box size, the angle subtended by the box is four times the horizon angle at the last scattering epoch, which thus sets the angular scale of our maps $\theta_L \sim 7°$ if $z_{ls} \sim 1000$, and $\theta_L \sim 30°$ if $z_{ls} \sim 30$.

The $\delta T/T$ maps can only be appropriately visualized by using color graphics; The interested reader should thus refer to one of our already published maps.[11] In order to compare with the results of real observations, it is best to emulate as closely as possible the experimental procedure. This is fairly easy in this case since we have available the "source" of the signal, and we just need to convolve our maps with a beam pattern appropriate for a given experiment. It is fortunate that the current experimental set-ups are rather appropriate to detect string induced anisotropies. Indeed the anisotropy patterns are lines of temperature discontinuity and the recorded signal is the difference between what is received from one patch of the sky and what is received from another patch (which might be the average of the signal received in 2 different directions as is the case in the three beam switching

experiments). The experiments thus record a differential map which is in principle fairly optimal[22] for the detection of line discontinuities.

On the other hand a truly optimal set-up does depend on the characteristic (angular) spacing between the discontinuities. It is easy to see in the simple case of an infinitely fine beam that for a very large beam throw the 2 patches of the sky will be many discontinuities away from each other and one thus expects a quasi- gaussian signal. On the other hand, for a tiny beam throw, in most cases, the 2 patches will not be separated by a temperature discontinuity at all, thereby yielding a null signal. In a few instances though, the patches will correspond to regions on each side of a discontinuity yielding a strong signal which would be extremely improbable in the gaussian case.

Figure 2.a

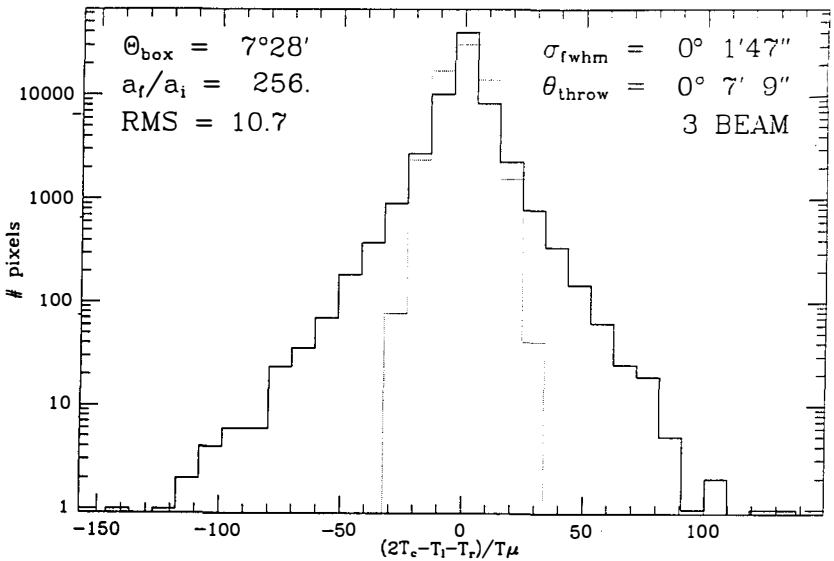*Number of pixels (out of 65 536) of a map convolved with a three beam pattern of beam throw of about 8 arcs minute, each gaussian beam having a FWHM of 1 arc minute 47 arc second. The "gaussian" case (dotted line) was generated from a string induced one by Fourier transforming the map, randomizing the phases, and transforming back.*

Figure 2 presents the result of two convolutions corresponding to two

three-beam-switching experiment of different geometrical configuration as a number of pixels as a function of the corresponding $\Delta T/T$.
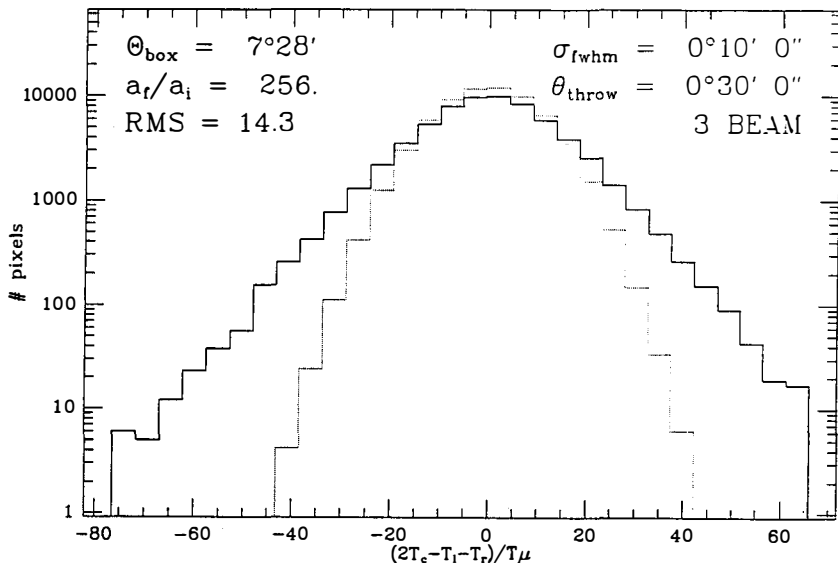
Figure 2.b

Same as Figure 2.a, but with a beam throw of 1/2 degree and a beam FWHM of 10 arcs minutes.

One can obviously now use the convolved maps in a more quantitative fashion in order to extract a limit on $G\mu$ (which is just an overall multiplicative factor of the maps) that a particular experiment places. But for rough estimates, one cannot use directly the quoted numbers by the observers since their analysis procedure generally assumes gaussian statistics. It is thus necessary to apply the same analysis procedure (based on maximum likelihood techniques) to extract a reliable number. It turns out that the tightest constraint comes form the Owens valley experiment (provided $z_{ls} \sim 1000$) since it yields $G\mu \lesssim 5\,10^{-6}$. This appears to be nearly the best limit available so far, since more indirect constraints coming from the residuals of millisecond pulsar timing measurements presently yield a limit[7] of $4\,10^{-6}$.

One should stress at this point that the previous upper limit is fairly conservative since the perturbations induced by density and velocity perturbation on the last scattering surface have not been accounted for. A full calculation of these perturbations will require to propagate in time the metrics perturbations induced by the strings up to the last-scattering surface, which involves a numerical integration of the (linearized) Einstein equations whose source term may be obtained at each time step of the simulations from the stress-energy tensor of the perturbing strings. Such a calculation does not pose any problem of principles and will be undertaken in a near future. Still, these perturbations are expected to be in the same angular range and of the same amplitude than those already computed. They will also add incoherently, thereby tightening the limit by a factor that should be of the order of $\sqrt{2}$.

Thus one cannot yet quite "weight" the cosmic strings by using the Cosmic Microwave Background as a pair of scales, although the current experiments already pose some interesting constraints on the cosmic string scenario of structure formation. One thus wait with great interest the results of new experiments, and in particular the full sky map with a resolution of 7 degrees that the satellite COBE should make available with good sensitivity. Unfortunately, the previous results cannot be used directly due to the difference in angular scales involved, and work is currently underway in order to obtain firm predictions, preferably before COBE flies...

REFERENCES

1. Y. B. Zel'dovich, Mon. Not. R. Astron. Soc. **192**, 663 (1980).

2. A. Vilenkin, Phys. Rev. Lett. **46**, 1169, 1496(E) (1980).

3. E. Witten, Nucl. Phys. **B249**, 557 (1985).

4. J. P. Ostriker, C. Thompson and E. Witten, Phys. Lett. **B180**, 231 (1986).

5. C. Hogan and M. Rees, Nature **311**, 109 (1984).

6. J. H. Taylor, Princeton University preprint to be published in the proceedings of the US-USSR Workshop on High Energy Astrophysics, Tbilisi and Moscow, June, 1989.

7. F. R. Bouchet and D. P. Bennett, Princeton University preprint, PUPT-89-1128, (1989).

8. A. Vilenkin, *Astrophys. J.* **282** (1984) L51.

9. J. R. Gott, *Astrophys. J.* **288** (1985) 422.

10. N. Kaiser & A. Stebbins, *Nature* **310** (1984) 391.

11. F. R. Bouchet, D. P. Bennett, and A. Stebbins, Nature, **335**, 410, (1988).

12. A. Vilenkin, *Physics Reports* **121** (1985) 263.

13. *e.g.* Gott, J. R., *Ap. J.* **288** (1985) 422.

14. Vashaspati, T., *Phys. Rev. Letters* **57** (1986) 1655.

15. Stebbins, A., Veeraraghavan, S., Brandenberger, R., Silk, J., and Turok, N., *Ap. J.* **322** (1987) 1. But the authors used numerical values which are now considered innacurate which changes their conclusions and make them much more optimistic.

16. Stebbins, A., *Ap. J.* **288** (1985) 422.

17. D. P. Bennett and F. R. Bouchet, Phys. Rev. Lett. **60**, 257 (1988).

18. D. P. Bennett and F. R. Bouchet, Princeton University preprints, PUPT-89-1137 and PUPT-89-1138, (1989).

19. A. Albrecht, and N. Turok, Phys. Rev. Lett. **54**, 1868 (1985).

20. B. Allen and E. P. S. Shellard, MIT preprint (1989).

21. A. Albrecht and N. Turok, Princeton University preprints, PUPT-89-1119 and PUPT-89-1133, (1989).

22. Gott, J.R., Park, R., Juszkiewicz, R., Bies, W. E., Bennett, D. P. , Bouchet, F. R., and Stebbins, A., Submitted to the Ap. J., Princeton Observatory Preprints POP-317.

III. THE PRESENT DENSITY OF THE UNIVERSE AND THE COSMOLOGICAL PARAMETER

THE DENSITY OF THE UNIVERSE FROM PRIMORDIAL NUCLEOSYNTHESIS

Jean AUDOUZE

Institut d'Astrophysique de Paris-CNRS
98bis, boulevard Árago, 75014 Paris, France

ABSTRACT

The outcome of primordial nucleosynthesis is compatible with the observed abundances of the lightest elements only if the baryonic density is much lower than the critical density. If we live in a Universe governed by an inflationary cosmology and such that the overall density of the Universe is equal to its critical value, the existence of large amounts of non baryonic particles is unavoidable.

I- INTRODUCTION

It is currently assumed that the lightest elements (D, ^{3}He, ^{4}He and ^{7}Li) are synthetized by the nucleosynthetic processes occuring during the primordial phases of the Universe. The outcome of the simplest (often referred to as canonical) Big Bang models is such that $\rho_B \approx (0.01\text{-}0.1) \, \rho_c$ where ρ_B is the baryonic density and ρ_c is the critical density. The purpose of this note is to claim that this range of baryonic density is presently unavoidable even in the frame of more complicated models attempting to reconcile $\rho_B \approx \rho_c$.

II - A VERY BRIEF REVIEW OF NON STANDARD MODELS OF PRIMORDIAL NUCLEOSYNTHESIS

Among the many attempts to reconcile the outcome of primordial nucleosynthesis with higher density values I would like to comment on two different types of models:

a) those requiring the existence of non baryonic particles (e.g. heavy neutrinos, gravitinos and photinos) able to decay by releasing high energy photons,

b) those taking into account possible inhomogeneities induced by the quark-hadron phase transition.

For the first set of models such as those studied by Audouze et al., 1985 and Salati et al., 1987 the agreement between the calculated abundances and the observations is at most barely satisfactory. The existence of such massive particle decaying into high energy photons is compatible with the existence of the lightest chemical species only for an extremely narrow set of mass and lifetime conditions.

In the more interesting case of inhomogeneous models the ^{7}Li nucleosynthesis provides a very stringent limitation both on the degree on inhomogeneity of such models and on the upper limit of baryonic density (see e.g. Audouze et al., 1988). Contrary to the expectation of Malaney and Fowler (1988) who have considered a very contrived set of possibilities it seems impossible to reconcile a high value of baryonic density with the observed ^{7}Li abundances.

The isotope ^{6}Li itself has been found to be useful to set stringent limitations on the existence of massive particles decaying into energetic hadron showers (Audouze and Silk, 1989).

III- MY CONCLUSIONS

Distinguished colleagues such as Professor W.A. Fowler are still convinced that there is a possibility to reconcile the observed abundances of the lightest elements with $\Omega_b=1$ where Ω_b is the baryonic cosmological parameter.

I am convinced that in all cases primordial nucleosynthesis provides very stringent upper limits on the baryonic density such that $\Omega_B \sim 0.1$.

This means that in order to live in a universe such that $\Omega=1$ (as proposed by all current inflationary models) the existence of copious amounts of non baryonic particles is still mandatory.

REFERENCES

Audouze, J., Delbourgo-Salvador, P. and Salati, P. 1988 in
"Dark Matter", ed. J. Audouze and J. Tran Thanh Van,
Editions Frontières, p. 277

Audouze, J., Lindley, D. and Silk, J. 1985, Ap. J. Letters,
293, L53

Audouze, J. and Silk, J. 1989, Ap. J. Letters

Malaney, R.A. and Fowler, W.A., 1988, Ap.J. Letters

Salati, P., Delbourgo-Salvador, P. and Audouze, J. 1987,
Astron. Astrophys., 173, 1

PRIMORDIAL NUCLEOSYNTHESIS AND THE DENSITY OF NUCLEONS IN THE UNIVERSE

GARY STEIGMAN

Physics Department, The Ohio State University,
Columbus, OH 43210, U.S.A.

ABSTRACT

The synthesis of the light elements D, ^{3}He, ^{4}He and ^{7}Li during the first $\sim$ thousand seconds of the evolution of the Universe depends on one adjustable parameter, the density of nucleons. By comparing the presently observed abundances of the light elements with the predictions of the "standard" (isotropic, homogeneous, ...) hot big bang cosmology, constraints on the present ratio of nucleons-to-photons, η, may be obtained. The confrontation of theory and observation reveals consistency with the standard model and bounds $\eta(\eta_{10} \equiv 10^{10}\eta)$: $3 \lesssim \eta_{10} \lesssim 5$. The constraints on η correspond to limits to the product of the present nucleon density parameter ($\Omega_{NO} \equiv$ the ratio of the nucleon mass density to the critical density) and the square of the present value of the Hubble parameter $H_O \equiv 100h_Okms^{-1}Mpc^{-1}$: $0.01 \lesssim \Omega_{NO}h_O^2 \lesssim 0.02$; for $0.04 \lesssim h_O \lesssim 1$ this leads to: $0.01 \lesssim \Omega_{NO} \lesssim 0.12$. Nucleons can account for the dynamically determined mass associated with the luminous parts of galaxies ($\Omega_{NO} \gtrsim \Omega_{GAL}$) and may account for much of the "dark" mass inferred from halos, groups and clusters of galaxies. The Universe fails by $\sim$ an order of magnitude (or more) to be "closed" by nucleons.

INTRODUCTION

In the standard, hot big bang cosmology the light elements deuterium, helium-3, helium-4 and lithium-7 are synthesized during the first $\sim$ thousand seconds of the evolution of the Universe. Within the context of the standard model, the primordial abundances of the light elements depend on one free parameter: the nucleon density or, equivalently, the nucleon-to-photon ratio $\eta \equiv N/\gamma$. For a review and a bibliography of the original work see, for example, reference 1. By comparing the predicted primordial abundances with those inferred from current observations, it is possible to constrain the allowed range of η and, consequently, the present density in nucleons can be bounded. It is those bounds which will be discussed here. Of particular interest is the *upper* bound to the nucleon density which, as is by now well known, suggests that our Universe is *not* "closed" by nucleons. As will be seen, however, much of the "dark matter" in the Universe may well be nucleonic.

As this subject – primordial nucleosynthesis – has been much reviewed lately[2,3], the abundance constraints will merely be quoted here; the reader is referred to references 1-3 for further details and bibliography. In the next section the abundance constraints will be presented and bounds on η will permit us to constrain Ω_{NO}, the fraction of the present critical density contributed by nucleons. In the following section Ω_{NO} will be compared to estimates of Ω_O, the ratio of the present total density to the critical density, and the issue of "dark" nucleons will be discussed. In the last section our results will be summarized.

ABUNDANCES AND N/γ

If η, the nucleon-to-photon ratio, were known, then the present density in nucleons could be calculated.

$$\rho_{NO} = m_N n_{NO} = m_N \eta n_{\gamma O}. \tag{1}$$

The present (number) density of photons is,

$$n_{\gamma O} \approx 4 \times 10^2 (T_{\gamma O}/2.7K)^3 cm^{-3}, \tag{2}$$

where $T_{\gamma O} = 2.76 \pm 0.05 K$[4]. If $\eta_{10} \equiv 10^{10}\eta$, then $\rho_{NO} \approx 38\eta_{10}(T_{\gamma O}/2.7K)eVcm^{-3}$. The "critical" (Einstein-deSitter) density is,

$$\rho_{CO} \equiv \frac{3H_O^2}{8\pi G} \approx 10.5 \times 10^3 h_O^2 eVcm^{-3}, \tag{3}$$

where the Hubble parameter is $H_O \equiv 100h_O kms^{-1}Mpc^{-1}$. The density parameter, Ω_{NO}, is the ratio $(\rho_N/\rho_C)_O$.

$$\Omega_{NO} = 3.53 \times 10^{-3}\eta_{10}(T_{\gamma O}/2.7K)^3 h_O^{-2}. \tag{4}$$

For $T_{\gamma O} = 2.76 \pm 0.05 K$,

$$10^3 \Omega_{NO} = (3.8 \pm 0.2)\eta_{10} h_O^{-2}. \tag{5}$$

It is clear from (4) and (5) that, even if η_{10} were known, Ω_{NO} would have a large uncertainty due to our ignorance of H_O. For subsequent comparisons, a very generous range for the Hubble parameter, $40 \lesssim H_O \lesssim 100 km s^{-1} Mpc^{-1} (0.4 \lesssim h_0 \lesssim 1)$, will be employed.

In the early Universe, deuterium is quickly burned to ^3H, ^3He and ^4He. The higher the nucleon density at nucleosynthesis ($\propto \eta$), the faster D is burned away and, the smaller its primordial abundance. Numerical integration of the evolution equations reveal that an excellent fit to the predicted primordial abundance of deuterium is[3],

$$y_{2P} \equiv (D/H)_P = 48 \times 10^{-5} \eta_{10}^{-5/3}. \tag{6}$$

Deuterium is only destroyed during the course of galactic chemical evolution so that, the primordial abundance can be no smaller than the present interstellar abundance ($y_{2ISM} \gtrsim 1 - 2 \times 10^{-5}$) or, the presolar nebula abundance[3] ($y_{2\odot} \gtrsim 2 \times 10^{-5}$). Using the solar system constraint, an *upper* bound to the nucleon-to-photon ratio is inferred.

$$y_{2P} \gtrsim 2 \times 10^{-5} \Rightarrow \eta_{10} \lesssim 7. \tag{7}$$

Although deuterium is easily destroyed, the primordial abundance of D cannot have been much in excess of that observed in the ISM or the solar system. The reason is that D is first burned in stars to ^3He and, some ^3He survives stellar processing[5,6]. Using the solar system (meteoritic) abundance of ^3He, it has been inferred[5] that,

$$y_{23P} \lesssim 6 - 10 \times 10^{-5} \Rightarrow \eta_{10} \gtrsim 3 - 4, \tag{8}$$

where $y_{23} \equiv (D + {}^3He)/H$.

Thus, observations of deuterium and helium-3, although very local, permit us to bound the nucleon-to-photon ratio.

$$D, {}^3He: \quad 3 \lesssim \eta_{10} \lesssim 7 \tag{9}$$

Is this range of η consistent with the observed abundances of lithium and of helium-4?

Lithium is produced primordially in two ways. For relatively low η values ($\eta_{10} \lesssim 3$) direct production via $^3H(\alpha,\gamma)^7Li$ dominates. As η_{10} is increased from very low values ($\ll 3$), lithium is burned away. Thus, for $\eta_{10} \lesssim 3$, lithium decreases with increasing η. However, for higher nucleon densities, ^7Be is formed via $^3He(\alpha,\gamma)^7Be$. Later, ^7Be will capture an electron to become ^7Li. Thus, for $\eta_{10} \gtrsim 3$, the primordial yield of ^7Li increases with η; minimum production of $y_{7P} \equiv ({}^7Li/H)_P \approx 1 \times 10^{-10}$ is achieved at $\eta_{10} \approx 3$[7].

Observations of lithium on the surface of young, Pop I stars most likely yield the lithium abundance in the gas out of which those stars formed[8]. The "high" Pop I abundance, $y_{7PopI} \approx 1 - 2 \times 10^{-9}$, is achieved primordially either for very low nucleon densities, $\eta_{10} < 1$, or, for relatively high densities $\eta_{10} \gtrsim 10$. *If* the Pop I abundance (or, an even higher value, to allow for some destruction) were identified with the primordial abundance, the "standard", hot big bang model would be ruled out since, either deuterium would have

no primordial origin ($\eta_{10} \gtrsim 10 \Rightarrow y_{2P} \lesssim 1 \times 10^{-5}$) or, *too much* deuterium would be produced ($\eta_{10} < 1 \Rightarrow y_{2P} \gtrsim .50 \times 10^{-5}$).

The discovery of lithium in very old, very metal poor (Pop II) halo and disk stars[9] has, perhaps, removed this discrepancy. The *low*, Pop II abundance ($y_{7\,PopII} \approx 1.2 \times 10^{-10}$) is consistent[7] with a nucleon-to-photon ratio in the range: $2 \lesssim \eta_{10} \lesssim 5$.

Is lithium on its way up (Pop II$\approx$ Primordial) or, on its way down (Primordial $\gtrsim$ Pop I)? Recent theoretical[10] and observational[11] work is beginning to supply an answer. The absence of observed lithium in the LMC in front of SN87A[11] suggests that lithium started "low" and is on its way up. The discovery that lithium can be produced in significant amounts in SN explosions[10] provides a mechanism for lithium to increase in the course of galactic chemical evolution. At present, then, it is not unreasonable to identify the Pop II lithium abundance with the primordial value.

$$Pop\,II \quad {}^7Li: \quad 2 \lesssim \eta_{10} \lesssim 5. \tag{10}$$

Therefore, consistency between the predictions of primordial nucleosynthesis in the standard, hot big bang cosmology and the observed abundances of deuterium, helium-3 and lithium-7 is obtained for,

$$D,\, {}^3He,\, {}^7Li: \quad \eta_{10} = 4 \pm 1. \tag{11}$$

What of ^{4}He? Because of the gap at mass-5 (no stable nucleus) and, because ^{4}He is the most tightly bound of the light nuclei, virtually all the neutrons available when nucleosynthesis begins ($T \approx 100 keV$, $t \approx 100$ sec.) are incorporated in ^{4}He. As a result, the ^{4}He mass fraction $Y_P \equiv 4y_P(1 + 4y_P)^{-1}$ (where $y_P \equiv {}^4$He/H), is very insensitive to η. For the "standard" three families of two-component, light ($m_\nu \ll MeV$) neutrinos ($N_\nu = 3$) and, for a neutron half-life in the range $10.2 \lesssim \tau_{1/2} \lesssim 10.5$ min., the primordial helium mass fraction is predicted to lie in the range: $0.236 \lesssim Y_P \lesssim 0.247$. Note that, if there is a fourth family of light neutrinos ($N_\nu = 4$), the *minimum* helium abundance increases to $Y_P \gtrsim 0.248$.

Being, next to hydrogen, the most abundant element in the Universe, helium-4 is easily observed throughout the Universe. Of most value are observations of helium recombination radiation from extragalactic HII regions. These data must be corrected for unseen neutral helium and, more significantly, for contamination by helium from the debris of stellar evolution. The best data[12] at present suggest[13,14] that $Y_P = 0.23 \pm 0.01$. This inferred primordial abundance is not inconsistent with that predicted for $3 \lesssim \eta_{10} \lesssim 5$ and $N_\nu = 3$; $N_\nu = 4$ would appear to be excluded.

BOUNDS TO THE NUCLEON DENSITY

Nucleosynthesis constrains the present nucleon-to-photon ratio to lie within narrow bounds: $\eta_{10} = 4 \pm 1$; it is purposeful that only one significant figure has been quoted (e.g., $\eta_{10} = 3$ may mean $\eta_{10} = 2.5$ is not excluded but $\eta_{10} = 2$ is ruled out). From equation (5) we obtain the bounds on the present density of nucleons,

$$0.011 \leq \Omega_{NO}h_O^2 \leq 0.020. \tag{12}$$

From our generous range of uncertainty in the Hubble parameter ($0.4 \lesssim h_O \lesssim 1$) this yields,

$$0.01 \lesssim \Omega_{NO} \lesssim 0.12. \tag{13}$$

For our "best guess" values of $\eta_{10} = 4$ and $T_{\gamma O} = 2.76K$, $\Omega_{NO}h_O^2 \approx 0.015$ so that, for $h_O = \frac{1}{2}$, $\Omega_{NO} \approx 0.06$.

It is clear that the biggest source of uncertainty in the constraints on Ω_{NO} is due to our ignorance of H_O. If, however, as is currently fashionable, we *assume* that $\Omega_O = 1$ (i.e., the *total* density is equal to the critical density) and that the cosmological constant vanishes, then the age of the Universe today is: $t_O = (2/3)H_O^{-1} \approx 6.5h_O^{-1}$ Gyr. We may then replace the uncertainty in H_O with the uncertainty in t_O.

$$\Omega_{NO} = (0.015 \pm 0.001)\eta_{10}\left(\frac{t_O}{13Gyr}\right)^2 \tag{14}$$

In Table 1 is shown the Hubble parameter and the range in Ω_{NO} (for $3 \leq \eta_{10} \leq 5$) corresponding to several choices for the age of the Universe.

Table 1: t_O, H_O and Ω_{NO}

t_O (Gyr)	$H_O(kms^{-1}Mpc^{-1})$	Ω_{NO}
10	65	0.02-0.05
13	50	0.04-0.08
15	43	0.06-0.11

What is the significance of these bounds on the universal density of nucleons? First, it is abundantly clear that the Universe is not closed by nucleons ($\Omega_{NO} \neq 1$). Indeed, $\Omega_{NO} = 1$ would require $\eta_{10} \gtrsim 40$ which would have yielded a primordial abundance of deuterium a hundred times smaller than that observed and an abundance of lithium an order of magnitude higher than the observed Pop I abundance (and two orders of magnitude higher than the Pop II abundance). For $\Omega_{NO} = 1$, the primordial helium mass fraction exceeds 0.27. Although it has been recently suggested that inhomogeneous nucleosynthesis[15] might be consistent with $\Omega_{NO} = 1$, more careful calculations[16] reveal that both ^{7}Li and ^{4}He are overproduced. Even for inhomogeneous nucleosynthesis – with

at least three more adjustable parameters than for standard nucleosynthesis – it seems likely[16] that $\eta_{10} \lesssim 10$ so that $\Omega_{NO} \lesssim 0.2$.

To compare our bounds on the nucleon density with various dynamical estimates of the total mass density on various scales in the Universe, we may define the mass-to-light ratio due to nucleons by,

$$\left(\frac{M}{L}\right)_N \equiv \Omega_{NO}\left(\frac{M}{L}\right)_C = \left(6.0^{+1.9}_{-1.7}\right)\eta_{10}h_O^{-1} \tag{15}$$

In (15) the mass-to-light ratio is in solar units and $(M/L)_C = (1600 \pm 400)h_O$ and $T_{\gamma O} = 2.76 \pm 0.05K$. For $\eta_{10} \gtrsim 3$, the *minimum* nucleon mass-to-light ratio is $(M/L)_N \gtrsim 13h_O^{-1}$; for $h_O \lesssim 1$, $(M/L)_N \gtrsim 13$. At the other extreme, the maximum value of $(M/L)_N$ for $\eta_{10} \lesssim 5$ is $(M/L)_N \lesssim 40h_O^{-1}$; for $h_O \gtrsim 0.4(0.5)$, $(M/L)_N \lesssim 99(79)$.

For the disk of the Galaxy in the Solar Neighborhood, $(M/L)_{DISK} \approx 2$. Since dissipation is necessary to concentrate the mass in a thin disk, the mass of the disk is almostly certainly dominated by nucleons. Since $(M/L)_{N,MIN} > (M/L)_{DISK}$, big bang nucleosynthesis is consistent with the, locally observed, galactic mass.

As is well known, on larger scales, $(M/L)_{OBS}$ increases[17]. For the *luminous* parts of galaxies[14], $(M/L)_{GAL} \approx (10 - 20)h_O$. Here, too, nucleons are entirely capable of accounting for the inferred mass density associated with (the luminous parts of) galaxies: $(M/L)_{N,MIN} \approx (M/L)_{GAL} < (M/L)_{N,MAX}$.

On the still larger scales probed by pairs, groups and clusters of galaxies, most of the dynamically inferred mass[18] is *dark*: $\Omega_{DYN} \approx 0.2 \pm 0.1$. Here, we encounter the first suggestion that the Universe may be dominated by exotic matter[19]. For only if Ω_{DYN} is at the lower end of its inferred range (≈ 0.1) and, Ω_{NO} at the upper end of its predicted range (≈ 0.1), could there be overlap between Ω_{DYN} and Ω_{NO}. However, it is clear that, at least *some* of the dark mass in the Universe *could* be nucleonic. Indeed, in the (perhaps atypical) environment of rich clusters of galaxies, it is known that most nucleons are "dark". In such rich clusters the mass of the x-ray emitting, intracluster gas (of *nucleons*) exceeds the mass of the luminous, cluster galaxies.

The bottom line, however, is that if, indeed, as inflation/naturalness suggests, $\Omega_O = 1$, then the Universe is definitely *not* dominated by nucleons.

SUMMARY

Primordial nucleosynthesis in the standard[1] (isotropic, homogeneous, ...) hot big bang cosmology predicts the abundances of the light elements D, ^{3}He, ^{4}He and ^{7}Li which are in accord with current observational data. In contrast, inhomogeneous nucleosynthesis[15] predicts ^{4}He and ^{7}Li in excess[16] of the primordial abundances as inferred from current data[11,12,13,14]. For the standard model, consistency between theory and observation is obtained for the nucleon-to-photon ratio (at present) in the narrow range: $3 \lesssim \eta_{10} \lesssim 5$ (a value as low as $\eta_{10} = 2.5$ may be allowed). The lower bound is set by the requirement that deuterium (and helium-3) be not overproduced; the upper bound by the Pop II abundance of lithium-7. For a present cosmic background radiation temperature

in the range $2.7 \lesssim T_{\gamma O} \lesssim 2.8K$, this range for η corresponds to a present mass density in nucleons in the range: $0.11 \lesssim \rho_{NO} \lesssim 0.21 keV cm^{-3}$. This leads to bounds on $\Omega_{NO} h_O^2$: $0.011 \lesssim \Omega_{NO} \lesssim 0.020$ and, for a Hubble parameter in the (generous) range, $40 \leq H_O \leq 100 km s^{-1} Mpc^{-1}$: $0.01 \lesssim \Omega_{NO} \lesssim 0.12$. Thus, at *least* 1% of the critical density is contributed by nucleons; nucleons *fail* by a wide margin to "close" the Universe.

The nucleon density at present is predicted from physics which occurred when the Universe was much younger ($\sim 10^2 - 10^3$ sec) and much hotter ($kT_\gamma \sim 100keV$). The predictions are consistent with the density of nucleons inferred from observations of the dynamics of luminous galaxies. This is strong support for the standard hot big bang cosmology. The nucleosynthesis bounds can account for the presently observed nucleons and, permit some (perhaps all, if $\Omega_{DYN} \approx 0.1$) of the dark matter in the Universe to be nucleonic. If, however, $\Omega_O = 1$ then, something other than nucleons dominate the Universe.

ACKNOWLEDGMENTS

REFERENCES

1. Boesgaard, A.M. and Steigman, G. 1985. Ann. Rev. Astron. Astrophys. 23, 319.

2. Steigman, G. 1988. AIP Conf. Proc. 183, 310.

3. Steigman, G. 1989. Ann. N.Y. Acad. Sci. (In Press).

4. Partridge, R.B. 1988. Rep. Prog. Phys. 51, 647;
   Crane, P. 1989. This Volume.

5. Yang, J., Turner, M.S., Steigman, G., Schramm, D.N. and Olive, K. A. 1984. Ap. J. 281, 493.

6. Dearborn, D.S.P., Schramm, D.N. and Steigman, G. 1986. Ap. J. 306, 35.

7. Kawano, L., Schramm, D.N. and Steigman, G. 1988. Ap. J. (Lett.) 327, 750.

8. Zappala, R.R. 1972. Ap. J. 72, 57.

9. Spite, F. and Spite, M. 1982. Astron. Astrophys. 115, 357.

10. Dearborn, D.S.P., Schramm, D.N., Steigman, G. and Truran, J.W. 1989. Ap. J. (In Press).

11. Sahu, K.C., Sahu, M. and Pottasch, S.R. 1988. Astron. Astrophys. 207, Li.

12. Pagel, B.E.J. and Simonson, E.A. 1989. Rev. Mex. Astron. Astrofis. (In Press).

13. Steigman, G., Gallagher, J.S. and Schramm, D.N. 1989. Comments on Astrophysics (In Press).

14. Torres-Peimbert, S., Peimbert, M. and Fierro, J. 1988. Ap. J. (In Press).

15. Applegate, J.H., Hogan, C.J. and Scherrer, R.J. 1987. Phys. Rev. D35, 1151;
    Alcock, C., Fuller, G.M. and Mathews, G.J. 1987. Ap. J. 320, 439;
    Terasawa, N. and Sato, K. 1988. Preprints (UTAP79,83).

74

16. Reeves, H., Richer, J., Sato, K. and Terasawa, N. 1989. Preprint;
    Kurki-Suonio, H., Matzner, R.A., Olive, K.A. and Schramm, D.N. 1989. Preprint.
17. Faber, S.M. and Gallagher, J.S. 1979. Ann. Rev. Astron. Astrophys. 17, 135.
18. Davis, M. and Peebles, P.J.E. 1983. Ap. J. 267, 465.
19. Schramm, D.N. and Steigman, G. 1981. GRG 13, 101.

Cosmological and astronomical lithium.

HUBERT REEVES
Section d'Astrophysique, CENS Saclay
and
JACQUES RICHER
Département de Physique, Université de Montréal

KATSUHIKO SATO

Department of Physics, Faculty of Science,
University of Tokyo, Bunkyo-ku, Tokyo, 113, Japan.

NOBUO TERASAWA,
Department of Physics, Faculty of Science,
The University of Tokyo, Bunkyo-ku, Tokyo, 113, Japan
and
National Astronomical Observatory
Mitaka-shi, Tokyo 181, Japan

ABSTRACT
We give arguments to prove that the Pop II lithium abundance can be used for cosmological determination of the baryonic density. We show that is dominated by the contribution of Big Bang nucleosynthesis, with negligible contributions from early GCR and stellar processes.

A range of baryonic density Ω_b between 0.01 and 0.2 Taking is obtained when recent studies of the influence of the quark-hadron phase transition and the uncertainties attached to its parameter, Big-Bang nucleosynthesis yields are taken into account. These rather large uncertainties on Ω_b could be reduced by a better knowledge of the parameters of the phase transition . They do not appear to be large enough to allow the baryons to close the universe: $\Omega_b < 1$.

We give arguments in favor of the idea that small stars (with lifetime longer than a few billion years) are probably the main contributors of the extra source of lithium needed to account for Pop I lithium abundance.

LITHIUM IN POP II STARS

One of the most important events in observational cosmology in recent years has been the discovery of lithium in PopII stars by the Spite (1983 a and b). Later, a number of other observations have confirmed their data and added a wealth of new measurements (Spite *et al.* 1985; Hobbs and Duncan 1987; Rebolo, Molaro and Beckman 1987)

The mean abundance of lithium in Pop II stars is $^7Li / H = 1.6 \times 10^{-10}$ with a dispersion of a factor of two (Rebolo *et al.* 1987). This small dispersion is the main argument in favor of the hypothesis that this lithium abundance has not suffered much depletion by processes associated with the stellar surfaces (Michaud 1986). Following the same logic, it appears reasonable to estimate that *the fractional depletion should not be larger as the observed dispersion*. A recent study of some (but not all possible) surface depletion processes by Delyannis *et al.* (1988) has confirmed this estimate. In consequence we estimate an initial value of $^7Li / H = 2.0 \pm 0.5 \times 10^{-10}$.

Vauclair (1987, 1988), studying the effect of rotational mixing on stellar lithium, has argued that the depletion may be larger and that the primordial value may be the same as the Pop I value ($^7Li / H = 1.0 \times 10^{-9}$). It remains to be seen if the theory will be able to reproduce the small abundance dispersion displayed in Figure 1. More work is being done on this subject.
Studies of lithium abundances in the Magellanic Clouds are of great importance in this respect. An upper limit of $^7Li/H < 10^{-10.1}$ has been reported in the interstellar medium toward SN 1987 A in the Large Magellanic CLoud. (Sahu et al 1989) . The ratio of K/ Li is used to correct for lithium depletion on grains.
Theses observations have rather large correction factors . Despite these uncertainties they make it highly unlikely that the primordial lithium value could be as large as 10^{-9}
What is the origin of these lithium atoms? As we shall discuss later, a lithium contribution of stellar origin seem to be needed in order to account for the Pop I surface abundances. In principle the corresponding formation mechanism could also have enriched the Pop II surfaces. A mere look at Figure 1 (from Cayrel 1986, 1988) suggests that *this is most probably not the case*. On the abcissa is plotted the ratio of iron to hydrogen, in units of the solar ratio. This parameter is a measure of the importance of stellar nucleosynthesis on a galactic scale at the birth of the corresponding star. The star on the farthest left, for instance, was born when the galactic gas contained less than one part in 3500 of the solar iron abundance. A very primitive star indeed...
The left part of Figure 1 displays, in ordinate, the corresponding magnesium abundance. As expected from typical products of stellar nucleosynthesis, both elements (iron and magnesium) grew together. The case of lithium is completely different (figure on the right) : the abundance of lithium remained almost constant while iron grows from .0003 to 0.1 of the solar value. The message is clear : *the lithium in this range is not mostly produced by stellar processes*. There exists a primordial component which dominates the stellar contribution all through this range.

Observations have shown that this component is mostly made of ^7Li : ($^7Li / ^6Li > 10$, Maurice *et al.* 1984). This, however, is not a very tale-telling result since in typical stellar outer layers ^6Li is thermonuclearly destroyed one hundred times faster than ^7Li.
What about galactic cosmic rays?
Very interesting result come from beryllium and boron, two elements which are produced in Galactic Cosmic Rays (Meneguzzi *et al.* 1971) but not in BBN (Wagoner *et al.* 1967). The rate of formation of lithium (both isotopes) is, to better than a factor of two, the same as the rate of formation of boron (both isotopes). It is approximately ten times larger than the rate of formation of beryllium (Reeves and Meyer, 1978, Walker *et al.* 1985). Furthermore, lithium, at all relevant temperature, is destroyed faster than beryllium and boron by stellar processes. Thus the abundance of beryllium gives an estimate of the GCR contributed lithium in a star while the abundance of the boron gives an upper limit to the GCR contribution.
Beryllium has been recently detected in Pop II stars (Rebolo, Molaro, and Beckman 1988) with hydrogen ratio $^9Be / H = 2 \times 10^{-12}$. The corresponding GCR lithium is only one tenth of the observed Pop II abundance.

A search for boron (Molaro 1987) in a Pop II star (HD 140283) has yielded an upper limit of B / Li < 0.04 . The corresponding upper limit to the ^{7}Li isotope is (^{7}Li/ H) $_{GCR}$ < 10^{-11}, at least an order of magnitude smaller than the Pop II observations (Figure 2). Thus we may conclude that *the primordial component observed in Figure 1 is not the result of hypothetical primordial cosmic rays* (Montmerle 1977). The only other process known to us to generate ^{7}Li in interesting amount is BBN and we may thus conclude that the lithium in Pop II stars is mostly of cosmological origin.

To summarize, both a stellar and a GCR origin can be eliminated as major contributor to the Pop II lithium abundance leaving the BBN origin as the most likely source.

Lithium in cosmology

The importance of lithium in cosmology stems from two happy circumstances. The first one is the fact that, for homogeneous baryonic density model, the BBN yield of lithium (^{7}Li / H) as a function of baryonic density (ρ_b) shows a deep minimum (a dip). The second one is the fact that the Pop II observations of lithium correspond to the lithium yield at the bottom of the dip. As a result this element is particularly well suited to test the hypothetical presence of baryonic inhomogeneities at the moment of BBN.

The physics of the quark-hadron phase transition (or transitions, since there is a chiral transition and a confinement transition) is presently the object of intense studies (Iso *et al.* 1986; Satz 1985, 1987; Leutwyler 1988) Many of the parameters of the transitions are still poorly known despite the vigourous effort being made in QCD calculations on networks(Irbäck et al (1988),Brown et al (1988), Bacilieri et al (1988). The hydrodynamics ha been considered by Blaizot (1987), Miller and Pantano (1988). A summary of the present status has been presented by Ukawa (1989) A review of its cosmological relevance for BBN has been prepared by Reeves (1989).

The relevant parameters, as far as BBN is concerned, are the following. First: the order of the transitions. After several years of debate the matter is not settled . Most authors believe that in the baryonic density range of the BBN, the transitions are *first order*, leading to nucleation and to bubbles of high density matter in a low density background However the recent work of the Roman group (Bacileri et al 1988) reopens the discussion. If the transition is truly of second order, it has no effect on the yields of BBN.

Second : the critical temperature T_c of the transitions. In the baryonic chemical potential range of cosmological interest($\mu_b/T_c \ll 1$), the transitions appear to occur at the same T_c and to be simultaneous. QCD calculations give a range of 150 MeV < T_c < 250 MeV. Recent chiral perturbation calculations have been published which quote a narrower range of 180 MeV < T_c < 220 MeV (Gasser and Leutwyler, 1987, 1988, Gerber and Leutwyler (1988)).

In the case of a first order transition , the likely scenario is the following. After some overcooling , nucleation of hadronic bubbles takes place which rapidly reheats the matter to the critical temperature , after which no more nucleation take place. The bubbles expands by surface hadronization , until the transition to hadrons is completed everywhere.

The nucleation rate is a very important parameter since it fixes the mean distance between bubbles , which itself influences the amount of later particle diffusion. It depends crucially on *surface energy of the bubbles:* the *smaller* this energy, the *smaller* the minimum size of the bubbles ; the *larger* the nucleation rate and the *smaller* the mean distance between the bubbles.

The baryonic number density in the hadronized phase is lower than in the quark phase . The ratio R between the high and low baryonic density phases can be computed, assuming chemical potential equilibrium between the two phases (Sale and Matthews 1986), (Applegate and Hogan 1985), (Applegate, Hogan and Sherrer 1987), (Alcock *et al.* 1987) (Fuller *et al.* 1987), (Kapusta and Olive 1988), (Reeves *et al.* 1987).. The result depends strongly on the value of the assumed critical temperature. At low T_c, the computed value of R is larger than ten, decreasing gradually at higher T_c.

For BBN calculations we need the density profile of baryonic matter around and below one MeV. We expect this profile to be composed of a number of overdensity regions (bubbles), with mean intercenter distances d, characterized by a baryonic density decreasing gradually from the center outside (Matthews, G.J. Fuller, G.M. Alcock, C.R. , and Kajino, T. UCRL 98943 June 1 88) .

As the universe cools from T_c at approximately 20 μsec, to one MeV at one second, the neutron to proton ratio (n /p), governed by weak processses is given by the Boltzmann formula of mass-action. Below one MeV the weak processes are no more in thermal equilibrium. The neutrons diffuse from high density phases into low density phases, changing both their density and their (n / p) ratio. The extent of neutron diffusion is a function of both the fractional volume in each phases and of the mean distance d between the high density blobs .

A convenient unit is the present value of d in light-hours (h) . One h today correspond to 2.5×10^5 cm at $T_9 = 1$ and approximately one meter at the Q-H phase transition , when the horizon scale was approximately ten km . For large values of d in this range ($d \approx 10^4$ lh), neutron diffusion can be neglected and we recover the inhomogeneous density BBN. At the other end of the scale , d << 1 lh or so, proton diffusion becomes important and we find back the results of the standard homogeneous density BBN.

Several generations of models have already been published , based on increasingly realistic models . The first generation were two-phase models characterized by a contrast density R and a fractional volume of the high density phase f_v , with the further assumptions of 1) complete neutron homogeneization between the two phases before the onset of BBN and 2) no further neutron diffusion during BBN . These models appeared to be able to reconcile the D, ^{3}He and ^{4}He calculated at critical baryon density $\Omega_b = 1$ with the observations , with however important overproduction of ^{7}Li.

A second generation of models take into account the effect of the interbubble comoving distance d on the neutron and proton diffusion before and during BBN . Several sets of calculations have been published for selected sets of points in the parameter space composed of ρ_b, R ,f_q and d (Terasawa and Sato 1988 , Mathews et al 1988 , Kurki-Suonio et al 1988, Kurki-Suonio and Matzner 1988),

For the discussion to be presented here we have also used new unpublished results extending the work of Terasawa and Sato. These are two-zone calculations covering the range: $1 < R < 10^4$; $0.5 \times 10^{-31} < \rho_b < 2 \times 10^{-31}$; $0 < f_v < 1$; d = 1 , 3 and 10 lh. The agreement between the various calculations is good enough for our following discussion to be of relevance.

In this work , another approach has been used which is complementary to the previous calculations . An analysis of the BBN results including neutron diffusion suggest a simplified approach which allows an easier systematic exploration of the whole parameter space. It is a standard two-phase model in which the effect of neutron diffusion are parametrized by a quantity f_n which vary from 0 to 1. A fraction f_n of the neutron *excess* in the high density (q) phase is supposed to have diffused, after the weak interactions fell out of equilibrium, but before the onset of nucleosynthesis, into the low density (h) phase. The neutron excess is defined here as the difference, at the time of weak interaction freeze-out, between the neutron mass density in the original quark phase, and the universe average neutron mass density; f_n is then a measure of the degree of homogenization of the *neutron* distribution throughout the universe just before nucleosynthesis ($f_n = 1$ corresponds to a homogeneous neutron distribution, which is as far as diffusion could ever go, and $f_n = 0$ corresponds to no diffusion at all). An analysis of the results of Terasawa and Sato (1988) and Matzner and Kurki-Suonio (1988) show that the neutron back-diffusion during BBN can be approximately simulated ,for a given model, by a reduction in the selected value of f_N . Thus we may expect to include theses later effects by letting f_n run from 0 to 1.

More details on the calculations are given in the appendix. The results are displayed in the figures 3 to 7 . In Figure 3 we have plotted the yields of the four isotopes has a function of ρ_b and y. The shaded areas correspond to the regions allowed by the observational abundances.

The effect of the quark -hadron phase transition can be estimated with the help of these figures. The assumed mean baryonic density defines an horizontal line in each diagram , which , together with a vertcal line drawn at y = o, divides each diagram into four parts. Each scenario with a given set of parameter is represented by a pair of points , one in the upper left corner and one in the lower left corner. The effect of including neutron back-diffusion is quite generally equivalent to a reduction of the value of f_n over the value selected for the no-back-diffusion model.

The figure 4 to 7 describe the influence of the parameter f_q for various choice of R and f_n, the fractional neutron diffusion. Again the shaded areas correspond to the regions allowed by the observational abundances.

It may be a long time before we get definite results on the effect of the quark-hadron phase transitions on the formation rate of the cosmological nuclides. Nevertheless the computations described before hopefully give us the general trends. Our present ignorance of the exact values of many relevant parameters of the Q-H transition can be assimilated to corresponding uncertainties on the final results. These uncertainties are likely to decrease as more detailed studies of the transition become available.

Many authors (Boesgaard and Steigman 1985, Cayrel 1987, Pagel 1987) have recently discussed the question of the relevant abundances of the light nuclides D , ^{3}He , ^{4} He ^{7} Li to be used for comparison with BBN calculations . The differences between these authors are mostly with the allowed fork of uncertainties. Here I will tend to use rather large forks .

The case of deuterium is still plagued with the problem of astration since we have no data prior to the birth of the solar system. Several galactic models of galactic evolution have been used to set constraints on the primordial abundances (Rocca-Volmerange and Schaeffer 1988) (Vangioni-Flamm and Audouze 1988) A deuterium fork of 10^{-5} (minimum astration) < D/H < 10^{-4}(maximum astration) is selected.

The uncertainties on the cosmological abundance of ^{3}He are even larger . So large that this isotope ,taken alone or summed with D does not yield interesting information for our quest.

For Y , the mass fraction of ^{4}He, we have used the rather large fork: $0.23 < Y < 0.26$. For ^{7} Li a fork of $10^{-10} < ^7\text{Li} / H < 10^{-9.5}$ is our best choice . In view of the possibility of a rotational destruction of ^{7}Li in enveloppe of Pop II stars (Vauclair (1988) We have also considered an upper limit of 10^{-9}, although , taking into account the Li limit estimate on LMC , this value appears to be quite unlikely.

It will appear later that the upper limits on the allowed range of both ^{4} He and ^{7} Li are critical for the evaluation of the upper limit on the baryonic density. For instance if , as many authors have already claimed , one can already exclude the range range Y > 0.25 and /or the ^{7}Li / H > $10^{-9.5}$ the baryonic range will be considerably reduced.

First we discuss the acceptable range of baryonic density (always given here in units of 10^{-31} g cm^{-3}). Agreement between calculations and observations is found for *some values* of the parameters *in the whole range* $2 < \rho_b < 50$, in the range $1\,lh < d < 10\,lh$

Deuterium and helium-4 are the limiting factors in the lower part of the range. At $\rho_b < 2$ helium-4 is too small and also D is too large(unless the fractional D destruction during galactic life is more than a factor of ten which probably the upper limit tolerable by galactic models).

In the range $2 < \rho_b < 5$ the observational abundances can be met for quite a large range of values of the parameters. As we move to higher baryonic densities the allowed range of parameters is progressively restricted . Increasingly larger values of R are needed together with rather large values of the fractional volume(applicable to the two -zone calculations) $f_v \approx 0.3$ to 0.6 . For instance at $\rho_b = 7$, we need $R > 5$; and at $\rho_b = 10$, we need $R > 9$.

The range $\rho_b > 20$ requires rather marginal coditions : very large values of $R > 100$, a value of f_v close to 0.3 together with the extreme observational limits of $Y \approx 0.26$ and $^7Li / H$ = $10^{-9.0}$. It is excluded if the Pop II lithium value is the correct one .

Even fragmentary knowledge of the likely values of these parameters will help in restricting this range.

The best estimate of the critical temperature of the phase transition (180 MeV $< T_c < 220$ MeV) leads to values of R between 5 and 10 at chemical potential equilibrium. The effective R , taking into account hydrodynamical effects should be somewhat but not much larger (Fuller et al 1988), thus favoring the lower part of the density range.

The same conclusion applies if f_v turns out to be small ($f_v < 0.1$) , as suggested by the computations of Fuller et al (1988) .

According to Kurki- Suonio (1988) there are some reasons to believe that d should be small ($d < 1$ lh) . If d is less than 0.1 lh we are again restricted to the lower part of the density range.

The previous remarks suggest that , although there is *some* possible agreement between the calculations and the observations all through the range $2 < \rho_b < 50$, we may reasonably already exclude the upper range and select a reasonable fork of $2 < \rho_b < 10$ (x 10^{-31} g cm^{-3}) This tentative conclusion will be the base of the following discussion.

Discussion

Given all the uncertainties including those on the Hubble parameter, the corresponding range of Ω_b goes at most from 0.2 to 0.01. Although this is appreciably larger than in the case of a homogeneous density universe. This does not appear to be large enough to allow the baryons to close the universe ($\Omega_b < 1$).

The cosmic density of luminous matter (stars and X-ray cluster gas) is $\Omega_L = 0.01$ within a factor of two while the density of clustered matter needed to account for the stability of clusters of galaxy or large scale motions is $\Omega_G = 0.1$ to 0.2.

Thus, within the uncertainties, at one end of the scale the baryonic matter could be entirely luminous (no baryonic dark matter) while at the other end of the scale the clustered matter could be entirely baryonic (no non-baryonic dark matter).

LITHIUM IN POP I STARS

The observed abundance of lithium in Pop I undepleted stars is $Li / H = 10^{-9}$ (within a factor of two). Normalized to Si and to the solar Si / H abundance, we find, for the meteoritic matter, a value $Li / H = 2 \times 10^{-9}$ in agreement, given the uncertainties,with the Pop I stellar

values.
     The isotopic ratio in the solar system is: $(^7Li / ^6Li) = 12.6$ For stars we have only lower limits : $^7Li / ^6Li > 10$. There are indications of possible larger values in interstellar matter (Ferlet and Dennefeld 1986).

     The ^6Li, ^9Be, ^{10}B and ^{11}B isotopes are satisfactorily accounted for by the GCR bombardment of interstellar matter during the galactic life (Meneguzzi _et al._ 1971; Reeves and Meyer 1978; Audouze and Reeves 1988),
     Can it also be responsible for the increase of lithium abundance from the Pop II value to the Pop I ?   The answer is most likely no. This discussion requires an estimate of the formation ratio of the isotopes of Li, Be and B in the GCR bombardment.
     One important parameter, in study of the galactic ray origin of the light elements, is the energy spectrum of the bombarding particles. Observational data on the spectrum of the galactic cosmic ray (GCR) is avalaible from the TeV region down to the hundreds of MeV. Because of solar modulation effects, nothing is known about the lower range.
     Using only the high energy spectrum (above 300 MeV) Meneguzzi _et al._ (1971) were able to account for the observations of ^6Li, ^9Be and ^{11}B. However the calculated lithium isotopic ratio $(^7Li / ^6Li)calc = 1.4$ was far too small with respect to the solar system ratio. And the calculated boron isotopic ratio $(^{11}B / ^{10}B)_{calc} = 2.6$ was also too small but with a lesser discrepancy : $(^{11}B / ^{10}B)_{obs} = 4.05 \pm 0.2$ in the solar system.
     Satisfactory agreement with the boron isotopic ratio could be obtained (Meneguzzi, and Reeves 1975; Reeves and Meyer 1978) by assuming low energy components similar to the solar energetic particles, presumably emerging from the stellar population of the galaxy. This result was later confirmed by Walker _et al._ (1985) with improved data and more elaborate computations.
     However we have no guarantee that these low energy components do indeed exist and are responsible for "adjusting " the boron isotopic ratio. In truth, no other mechanisms have ever been proposed and it is difficult to come out with an acceptable idea. Proton capture by boron atoms would alter the ratio in the wrong way while neutron capture would have left much more important (and unobserved) effects on other elements such as gadolinium (an extended discussion is given in (Reeves 1974).
     The existence and spallating action of these low energy fluxes of cosmic rays can in principle be tested by gamma ray astronomy (Meneguzzi and Reeves 1975). The 4.4 MeV line from carbon-12 and the 8.8 MeV line from oxygen-16, emitted after inelastic excitation of the corresponding nuclear states should be the best witnesses of the existence of these flux components.
     The detection threshold of the past gamma-ray telescopes have not been low enough to give a definite answer to question of the existence of a background of low energy gamma ray lines, yielding information on the existence of these fluxes and on the credibility of the hypothesis that they are responsible for adjusting the boron isotopic ratio to its observed value.
     In view of our ignorance, we shall consider separately the two corresponding hypothesis: a) the low energy component exist and is responsible for the boron isotopic ratio b) some other mechanism has altered the ratio.

     The numerical values of the formation ratios are given in Table 1 from Walker _et al._ (1985). "GCR alone" means that only the high energy fluxes corresponding to presently observed galactic cosmic rays are included. "GCR + 5" and "GCR + 7 " means that we have assumed the presence of lower energy particles (carrots) with a power kinetic energy spectrum with exponents 3, 5 and 7 as suggested by solar energetic particles.

Table 1: Relative formation yields of the isotopes of lithium, beryllium and boron by energetic particles in space.

Ratio	GCR alone	GCR + 3	GCR + 5	GCR + 7	obs
7/9	6.6	33	21	12	65 (x2)
7/6	1.4	2.6	2.9	2.2	12.6 (±0.2)
11/10	2.5	4.0	4.0	4.0	4.05 (±0.1)
11/7	1.8	0.7	1.0	1.80.	0.13 (x2)

At this point we ask again: can we account for the Pop I lithium abundance solely by the combination of the BBN and GCR contribution?

To answer this question we use the fact that the stellar Be abundance has remained quite uniform at $Be/H = 2 \times 10^{-11}$ (within a factor of two) over at least the last five billion years and probably more (Budge $et\ al.$ 1987). Using the numbers given in Table 1 the corresponding abundance of ^7Li and ^6Li can be computed for various assumptions about the presence, or not, of the low energy GCR particles and their energy spectra. Then, using the value of the Pop I lithium stellar abundance ($^7Li/H = 1$ to 2×10^{-9}) the solar system isotopic ratio ($^7Li/^6Li = 12.6$) and adding the BBN value of $^7Li/H = 3 \times 10^{-10}$ we find that _we need an extra contribution amounting to about sixty per cent_ of the observed Pop I lithium value.

Thus another lithium generating another process appears to be needed which is likely to be associated with stellar nucleosynthesis. A similar conclusion has been reached by Audouze $et\ al.$ (1983) and Abia and Canal (1988). This will be the subject of the next section.

Lithium from stars

Before proceeding with this discussion, one general remark is of importance. The observed large dispersion of stellar iron abundances with respect to stellar ages makes it clear that nucleosynthesis does not proceed uniformly with time in the galaxy. For this reason the nucleosynthetic evolutionnary curve of individual elements are often easier to understand when they are plotted as a function of iron abundance than as a function of galactic age.

It appears from the previous section that we need a third source of cosmic lithium. Plausible stellar mechanisms have been invoked in relation for instance to novae (Starrefield $et\ al.$ 1978) super-massive objects (Norgaard and Fricke 1976) novae (Audouze and Truran 1973), red giant interiors (Cameron and Fowler 1971, Dean $et\ al.$ 1977). But the uncertainties related to their efficiency are far too large for any believable calculated contribution to be quoted (Arnould 1986) .

We have three reasons to think that ^7Li is not made in massive stars but in rather small stars with Main Sequence lifetime of a few billion years.

The first one is based on a study of the correlation between various chemical elements in Pop II stars. As these stars were born shortly after the birth of the galaxy, their chemical abundances should only result from the nucleosynthetic yields of rather massive stars. In the range $[Fe/H] < -1.0$, we have the following observed ratios : $[Mg/Fe] = +0.5$ dex, $[Si/Fe] = +0.35$ dex, $[S/Fe] = +0.6$ (François 1987) (the square bracket notation means the logarithm to the base ten of the ratio of the abundances in units of solar abundances). As discussed by Matteucci (1987) all these observations are explained in the frame of conventional galactic evolution theory by the fact that the corresponding elements are generated in massive stars. Their abundances are expected and observed to be overabundant relative to iron. The fact that lithium shows no correlation with these elements can be taken as evidence that it is not produced in massive stars.

The second argument is based on the relative growth of lithium with respect to the iron abundance in the _later_ chapter galactic evolution. Some information about this period where [Fe/H] > -1.0 **can** be obtained from Figure 12 of Rebolo, Molaro and Beckman (1988). The upper envelope of the Li stellar abundances appears to grow approximately linearly with iron ([Li /Fe] = 0) in the range from one sixteenth to twice the solar abundance (-1.2 < [Fe /H] < + 0.3).

This argument should however be seen with caution; we have no convincing arguments to prove that the stars on the upper envelope have not suffered _some_ depletion.

The linear growth of lithium, if confirmed by values intermediate between the Pop II and Pop I abundance value, would indicate that lithium is probably not made by massive stars. Novae and small red giants would, off-hand, be better candidates.

The third argument is in relation with the lithium abundances in the Magellanic Clouds. The SMC galaxy is two or three times less metal-rich than the Milky Way and the rate of star formation appears to have been almost constant with time (Lequeux 1984). The fact that the lithium abundances in the Magellanic Clouds   is comparable with the Pop II value in our galaxy(Sahu et al 1989, Spite et al 1989, Ritchler et al 1989) is another indication that the contribution of lithium by massive stars is not a dominant factor.

The favored mechanism is the conversion of ^{3}He into ^{7}Be and ^{7}Li with   production of s-process elements, in the late stage of evolution of red giants (Cameron and Fowler 1971). This idea is observationally supported by the detection of very large lithium abundances in a few carbon stars such as WZ Cassiopea.

One counter argument could come from the recent observation of lithium in the old open cluster NGC 188, with solar iron abundance, by Hobbs and Pilachowski (1988). The estimated age of the cluster is 5 to 10 x 10^9 years. The mean value of Li / H is 2 x 10^{-10}, averaged over five stars with surface temperature around 5850 K. We note in passing that this is almost the same value found for Pop II stars (Molaro, Rebolo and Beckman 1987 revised value).

As discussed by Hobbs and Pilachowski this lithium value is surprisingly large for such old Pop I stars at that temperature. The sun, at the same surface temperature and one half the age, has twenty times less lithium. The 5 x 10^9 year old M67 cluster also show far less lithium at this surface temperature.

How much lithium depletion took place at the surface of the stars in NGC 188 ? What were the initial stellar lithium values ? Were they as high as 10^{-9} as claimed by the authors in their discussion? Can that be used as a proof that the lithium abundance has not increased in the last 5 to 10 x 10^9 years? In view of the many processes influencing surface abundances (Michaud *et al.* 1986) we find it difficult to come to a conclusion.

As mentionned before, despite the fact that the observed values are hardly larger than the Pop II values, the fact that NGC 188 has a solar iron abundance makes it likely that its lithium abundance has been increased over and above the Pop II values, probably by the stellar mechanism discussed previously.   Since the cluster is some 10^{10} years old, this fact limits the strength of our argument that the lithium- producing stellar process is restricted to small long-lived stars.

The main question at this point is : what was the age of the galaxy at the time of birth of NGC 188 ? What was, then, the mass of it's smallest dying stars? Even with a galactic age as short as 13 x 10^9 years, they could be appreciably smaller than two solar masses. This would also be required by the fact that the cluster has as much iron as the sun, since iron is believed to be mostly a product of small stars.

CONCLUSIONS

1) The Pop II lithium abundance is dominated by the contribution of Big Bang nucleosynthesis, with negligible contributions from early GCR and stellar processes. This conclusion supports the use of the Pop II data for cosmological arguments.

Taking into account the possible effects of the quark-hadron phase transition on the nucleosynthetic yields of the light nuclides , the range of baryonic densities compatible with the observations is somewhat larger than in the case of the standard (homogeneous) Big Bang , but ,most likely , not large enough to reach the critical density.

At one end of the range of uncertainties , the baryonic density may be small enough to avoid the need of an important contribution of dark baryonic matter. At the other end of the scale , it may be large enough to avoid the need of non-baryonic matter. Progresses in the evaluation of the parameters of the Q-H may help in reducing these uncertainties.

2) The contribution of GCR to the Pop I lithium abundance can be evaluated through a combination of the stellar beryllium abundance, the relative   Li / Be yield in GCR (Table 1) and the lithium isotopic ratio in the solar system. These data constrain the GCR produced ^{7}Li to more than twelve but less than thirty percent of the Pop I lithium abundance depending on the presence and slope of the low energy GCR particles.

3) A stellar contribution is therefore required to contribute most of approximately $^7Li/H = 10^{-9}$ therefore becoming the major source of ^7Li (approximately sixty per cent depending again upon the low energy GCR spectrum). The BBN contribution being approximately twenty per cent we conclude that the three contributions differ by at most a factor of five.

4) The lithium producing stellar process appears to be restricted to rather small stars (less than a few solar masses).

Bibliography:

Abia, C., and Canal., R. 1988, _Astron. Astrophys._, **189**, 55.

Alcock, C.R., Fuller, G.M., and Mathews, G.J. 1987, _Ap. J._, **320**, 439.

Applegate, J.H., and Hogan, C. 1985, _Phys. Rev._, **D30**, 3037.

Applegate, J.H., Hogan, C.,and Sherrer R.J. 1987, _Phys Rev._, **D35**, 1151.

Arnould, M. 1986, _Prog. Part. Nucl. Phys._, **18**.

Arnould,M., and Forestini M., " Proceedings of the III La Rabiba School on Nuclear Astrophysics". (Springer Verlag, Berlin 1988°

Audouze, J., and Reeves, H. 1982, in _Essays in Nuclear Astrophysics_, eds. C.A. Barnes _et al._, Cambridge University Press, p. 355.

Audouze, J, Boulade, O., Malinie, G., and Poilane, Y. 1983, _Astr. Astrophy._ **127**, 164.

Audouze, J. and Truran. J.W. 1973, _Ap. J._, **192**, 487.

Bernaschi, M., Cabasino, S. Cabbibo, N., Fernandez, L.A. Marinari, E., Paolucci, P., Parisi, G., Salina, G., Tarancon , A., Coppola, F., Lombardo, M.P., Simeone, E. Trippiccione, R., Fiorentini, G., Lai, A., Marchessini, P.A., Marzano, F., Rapuano, F., Tross, W. preprint, ROM2F 88 020

Beaudet, G., and Reeves H. 1984, _Astr. Astrophys._, **134**, 240.

Beaudet, G., and Yahil, A. 1977, _Ap. J._, **218**, 253.

Blaizot, J.P., Acta Physica Polonica, **B18**, 661, (1988)

Boesgaard, A.M. and Steigman G. 1985, _Ann. Rev. Astr. Ap._, **23**, 319.

Brown, F.R., Christ, N.H., Yuefan Deng, Y., Gao, M., Woch, T.J., preprint Columbia University.

Budge, K.G., Boesgaard, A., and Varsik, J. 1987, IAU Symposium 132, Paris.

Cameron, A.G.W., and Fowler, W.A. 1971, _Ap. J._, **164**, 111.

Caughlan, G.R., and Fowler, W.A. 1988, "Thermonuclear Reaction Rates", preprint.

Cayrel, R. 1986, I.A.U. Symposium no. 126, Cambridge.

Cayrel, R. 1988, Proceedings of the Alpbach Summer school.

Clegg, R.E.S., Lambert, D.L., Tomkin, S. 1981, _Ap. J._, **250**, 262.

Dean. C.A., Lee P. and O'Brien A. 1977, _Publ. Astron. Soc. Pac._, **89**, 222.

Delbourgo-Salvador, P., 1988, private communication.

Ferlet, R., and Dennefeld, M. 1986, _Astron. Astrophys._, **138**, 303.

François, P. 1986, _Astron. Astrophys._, **160**, 264.

François, P. 1987, in preparation.

Fuller, G.M., Mathews, G.J., and Alcock, C.R. 1988, _Phys. Rev._, **D37**, 1380.

Gerber, P., and Leutwyler, H., preprint, BUTP 88/30

Hobbs, L.M., and Duncan, D.K. 1987, _Ap. J._, **317**, 796. (Li in halo stars)

Hobbs, L.M., and Pilachowski, C. 1988, _Lithium in old open clusters : NGC 188_, Preprint.

Irbäck, A., Karsh, F., Peterson , B., and Wyld , H.W.. preprint, CERN TH 5130/88

Kawano, L., Schramm, D., and Steigman, G. 1987, Fermilab preprint.

Kawano, L., and Schramm, D. 1988, _Ap. J._, **327**, 750.

Kapusta ,J.I. and Olive K.A. University of Minnesota preprint UMN- TH- 647 (1988)

Kurki-Suonio, H., Matzner, R.A.., Centrella, J.M., Rothman, T., and Wilson, J.R. 1988, _Physical Review D_. 38 1091 (1988)

Kurki-Suonio, H. _Physical Review D_. **37** , 2104, (1988)

Kurki-Suonio, H., Matzner, R.A. preprint (1988)

Lequeux, J., 1984. I.A.U . Symposium no 108.
Matteucci, F. 1987, ESO preprint 550.
Matthews, G.C., Fuller, G.M., Alcock, C.R., Kajino, T. preprint UCRL 98943 (1988)
Maurice, E., Spite, F., and Spite, M. 1984, *Astr. Astrophys.*, **132**, 278.
Meneguzzi, M., Audouze, J., and Reeves, H. 1971, *Astr. Astrophys.*, **15**, 337.
Meneguzzi, M., and Reeves, H. 1975, *Astr. Astrophys.*, **40**, 91.
Miller , J.C., and Pantano, O, preprint SISSA Trieste.
Molaro, P. 1987, *Astr. Astrophys.*, **183**, 394.
Montmerle , T. 1977 Ap . J . **217**, 872 .
Nissen, P.E., Edvardsson, B., Gustafsson. B. 1985, in *Production and distribution of CNO elements*, eds I.J., Danziger, F. Matteucci and K. Kjär, ESO preprint, p. 131.
Norgaard. H., and Fricke K.J. 1976, *Astron. Astrophys.*, **49**, 337.
Rebolo, R., Beckman,J. and Molaro, P. 1987, *Astron. Astrophys.*, 172, L17. (Li in G 64 -12)
Rebolo, R., Molaro, P., and Beckman, J. 1988, *Astron. Astrophys.*, **192**, 192.
Reeves, H. 1974, *Ann. Rev. Astron. Astrophys.*, **12**,437.
Reeves, H., and Meyer J.P. 1978, *Ap. J.*, **226,** 613.
Reeves, H. 1987, Varenna School "Confrontations between Observations and Theories in Cosmology", eds J.A.Audouze and F Melchiorri, to be published.
Reeves, H., Delbourgo-Salvador, P, Audouze, J., and Salatti, P. 1988, *European Journal of Physics* ,**9**, 179.
Reeves, H., 1989 to appear in Physics Report.

Sahu, K.C., Sahu, M., and Pottasch,S.R., 1989 IAP preprint, 261.
Sale, K.E. and Mathews, G.J. 1986, *Ap.J.*, **309**, L1.
Spite, M and Spite, F. 1982a, *Nature*, **297,** 483.

Spite, F., Spite, M., Peterson, R.C., and Chafee, F.H. 1987, *Astron. Astrophys.*, 172, L9.

Starrefield, S., Truran, J.W., Sparks. and Arnould, M. 1978, *Ap. J.*, **222**, 600.
Terasawa, N., and Sato, K. 1989 Prog. Theor . Phys. Lett 81, 254
Terasawa, N., and Sato, K. 1988, preprint UTAP 79
Ukawa, A., 1988 CERN Preprint TH 5266
Vauclair, S., Vauclair, G., Schatzman, E. and Michaud, G. 1978, *Ap. J.*, **223**, 567.
Vauclair, S. 1987, Procedings of Meudon IAU Symposium (July 1987).
Vauclair, S., 1988, p. 269 , in Dark Matter Ed J. Audouze and Tran Van . Editions Frontières
Walker, T.P., Mathews, G.J. and Viola, V.E. 1985, *Ap.J.*, **299**, 745.
Yang, J., Turner, M.S., Steigman, G., Schramm, D.N., and Olive, K. 1984, *Ap.J.*, **281**, 493.
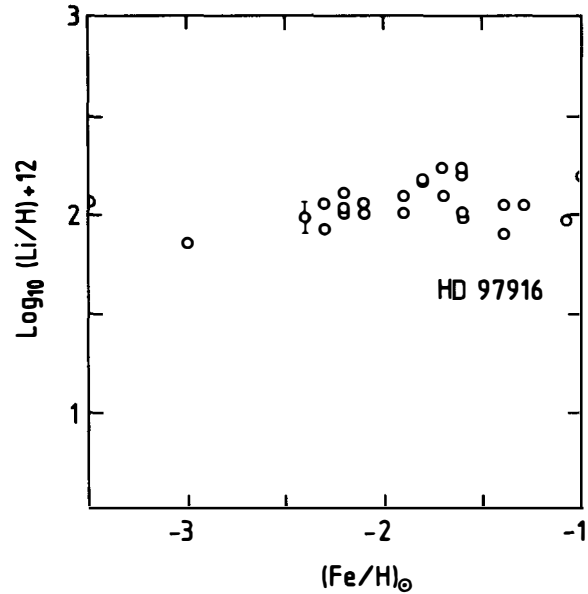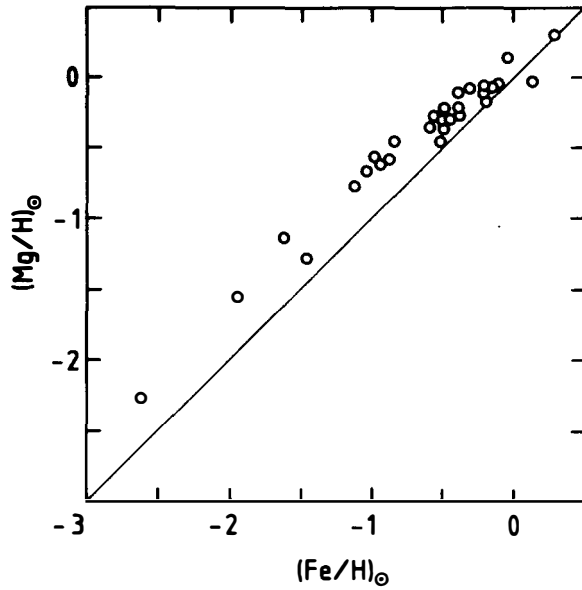
Figure 1: On the origin of Pop II lithium abundances: stellar- nucleosynthetic contribution.

The two figures show the correlation between iron abundances (in abcissa, normalized to the solar abundance) and the abundances of Pop II Li (on the left) and Mg (on the right) on a number of field stars (from R. Cayrel, IAU Symposium no 1986). Typically a product of stellar nucleosynthesis, Mg is seen to increase in steps with iron. The Pop II Li abundances appears to be independant of the amount of nucleosynthetic activity, suggesting a primordial origin.
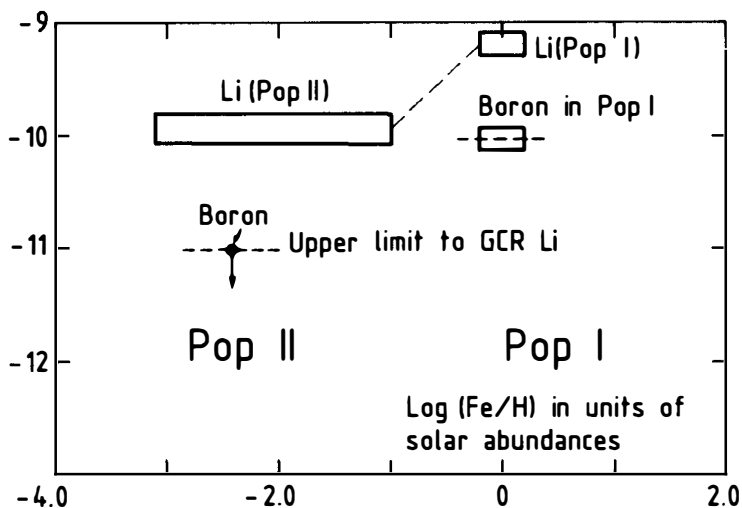
Figure 2: ●n the origin of Pop II lithium abundances: Galactic Cosmic Ray (GCR) contribution. The figure displays the observations of stellar lithium and boron abundances (a pure GCR product) as a function of the iron abundances. For PopII we have only one upper limit of B abundance. The GCR contribution to boron is quite similar to its contribution to lithium. The dashed line shows the upper limit of the GCR contribution to Li in PopII stars.
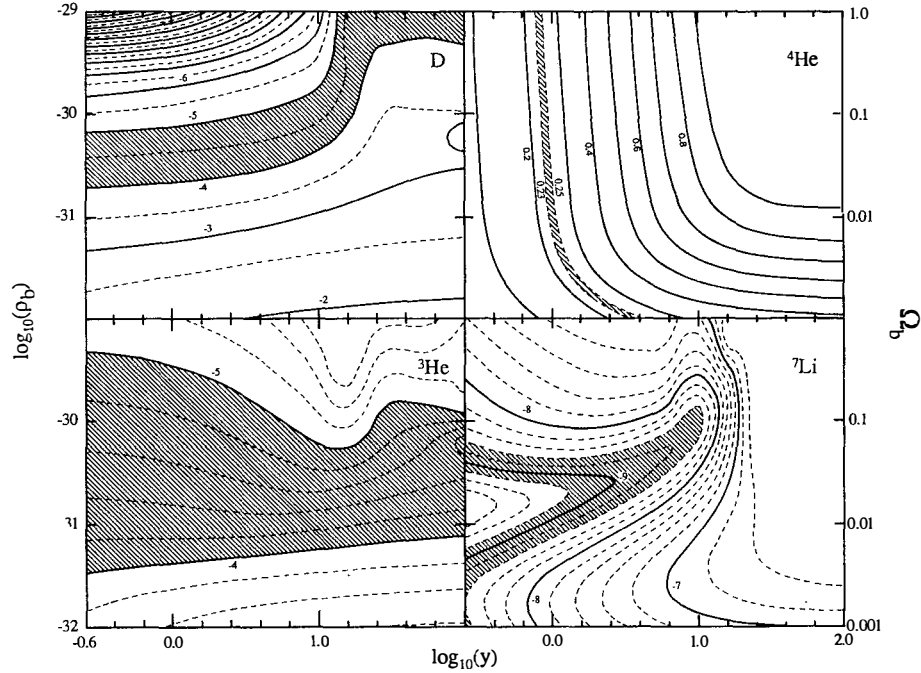
Figure 3: Deuterium, ^{3}He, ^{4}He and ^{7}Li primordial nucleosynthesis in a homogeneous universe, as a function of the present baryonic density ρ_b (or the corresponding Ω_b value, with Hubble constant ≈ 75 km/sec/Mpc), and of the (n/p) ratio just prior to nucleosynthesis. The (n/p) ratio is given in units of the standard Big-Bang thermal equilibrium value: $y = (n/p)/(n/p)_{equ}$. Level curves of $\log_{10}$ (mass fraction) are shown for D, ^{3}He and ^{7}Li; level spacing is constant. Mass fraction is shown for ^{4}He. Hatched areas show the current observational constraints discussed in the text. A change in the temperature at which $(n/p)_{equ}$ is defined results in a mere translation of the whole diagrams along the (n/p) axis.
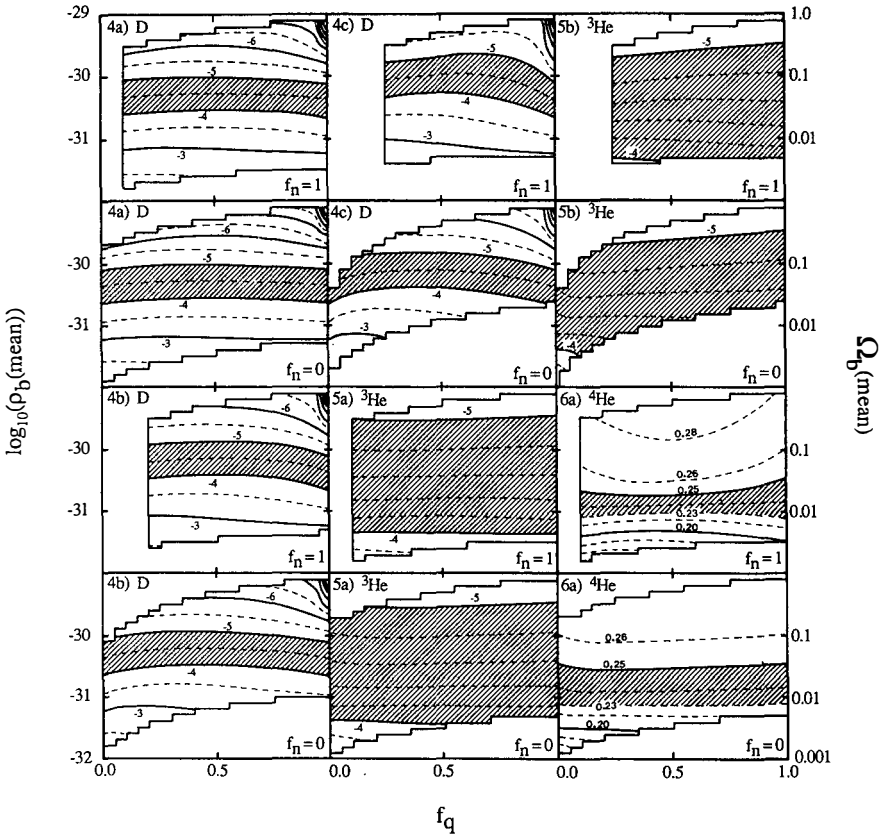
Figures 4 to 7: Deuterium, ^{3}He, ^{4}He and ^{7}Li primordial nucleosynthesis yields in the two phase model universe, as a function of the present *average* baryonic density ρ_b(mean), the volume fraction f_q of the universe that was in the high density "quark" phase at the time of nucleosynthesis, the density contrast R between the two phases, and the neutron diffusion efficiency parameter f_n. The figures come in pairs, with the top part corresponding to $f_n = 1$ (maximum diffusion), and the bottom part to $f_n = 0$ (no diffusion). **4)** Deuterium: a) R=5, b) R=10, c) R=20; **5)** ^{3}He: a) R=5, b) R=20; **6)** ^{4}He: a) R=5, b) R=10, c) R=20; **7)** ^{7}Li: a) R=3, b) R=5, c) R=10, d) R=50. Again, hatched regions show observational constraints. Log_{10}(mass fraction) values are shown, as in Figure 3 (except again for ^{4}He).
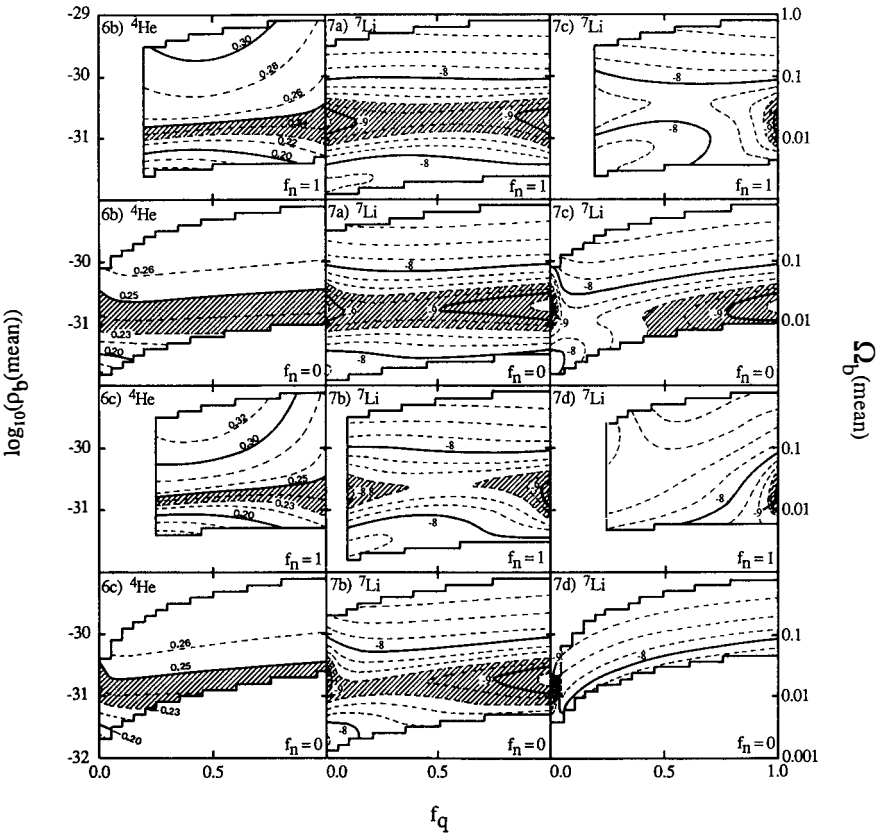
EXPANSION OF HADRONIC BUBBLES

DURING THE COSMOLOGICAL QUARK-HADRON TRANSITION

Ornella Pantano[*]   and   *John Miller*[*†]

[*]*International School for Advanced Studies (S.I.S.S.A.), Trieste, Italy.*
[†]*Department of Astrophysics, University of Oxford, England.*

Abstract

We discuss the structure of the hydrodynamical flow produced by an expanding hadronic bubble during a first order quark-hadron phase transition. Results are presented from computations which calculate the bubble growth from the initial nucleation time onwards.

I. Introduction

The study of the properties of strong interactions by means of numerical lattice simulations seems to indicate that the transition of strongly interacting matter between the normal low density hadronic phase and a high density quark-gluon plasma phase, might be of first order. Although no final conclusion has yet been reached on this[1], the relevance which first order phase transitions in the early universe can have for the dark matter problem and for the formation of structure makes it worthwhile to explore the possible cosmological consequences which might result if the quark-hadron transition is of first order. Of particular interest is the possibility, suggested by Witten[2], that the quark confinement process (which occurred in the early universe at a temperature of about $150\,MeV$), might have produced inhomogeneities in baryon number density as a result of the different bulk properties of hadronic matter and of the quark-gluon plasma which favour baryon number staying in the plasma phase. If the inhomogeneities were able to survive until the time of cosmic nucleosynthesis, they might have altered the generally accepted picture for this[3]. It has been suggested that the observed abundances of light elements may then be consistent with values of Ω_b (the ratio between the density of baryonic matter and the critical density) higher than those given by the standard picture[4].

A first order phase transition is characterized by an associated release of latent heat which produces temperature gradients and, in the present case, might lead to quite large local bulk velocities representing significant deviations away from the Hubble flow. Apart from the intrinsic interest of such perturbations, they can also cause a rearrangement of the baryon number distribution and so study of the baryon fluctuations cannot be separated from a hydrodynamical study of the transition.

For the hadronization process, we consider here the scenario in which the expanding plasma first supercools to slightly below the critical temperature for the transition (T_c) and thermal fluctuations then give rise to nucleation of bubbles of the low temperature phase[5]. The formation of a phase interface with finite surface tension has the consequence that only bubbles larger than a critical radius r_c can survive and grow while smaller ones shrink and disappear[6]. However, the probability of nucleating bubbles decreases rapidly with increasing size and so, for practical purposes, only those with $r \sim r_c$ are of interest. The growing bubbles eventually coalesce giving rise to discon-

nected quark regions which then shrink. Surface tension plays an important role during the early stages of bubble growth, at coalescence and then again when the disconnected quark regions have contracted to small dimensions.

As long as changes within each phase occur on scales which are large compared with the strong interaction length scale, transition regions between the two phases can be described as discontinuity surfaces with junction conditions being imposed across them. A phase interface could, in principle, move either supersonically (as a detonation) or subsonically (as a deflagration) relative to the quark medium. However, detonations would require more supercooling than is expected here and would produce hadrons in a superheated state[5,7,8]. Therefore, in practice, it is the deflagration solutions which are of interest.

We concentrate here on the early stages of bubble growth and present some numerical results which we have obtained for the case of a single spherical hadronic bubble expanding into an initially uniform medium. This sort of study is an essential step towards a more complete understanding of the transition and is relevant in providing initial conditions for a subsequent analysis of bubble collision and coalescence. The aim is to see how the flow structure evolves from the initial stages, in which the dynamics is dominated by surface effects, towards a possible asymptotic similarity solution[8].

In Section II we present the hydrodynamical equations together with the junction conditions imposed at the interface. Results are presented in Section III and Section IV contains final remarks. We use units for which $c = \hbar = k = 1$.

II. Relativistic hydrodynamical equations

In this section we present the system of equations used for studying numerically the expansion of a spherical bubble (see also Ref. 9). Since the energy density in both phases is provided almost entirely by relativistic particles, it is necessary to use relativistic hydrodynamics even in the limit of small bulk velocities. Each phase is here taken to behave as a perfect fluid which is a reasonable assumption for the stages of bubble growth where long-range energy transport by particles with long mean free path is not important. We use a Lagrangian formulation and write the space-time metric as

$$ds^2 = -a^2 dt^2 + b^2 d\mu^2 + R^2 \left(d\theta^2 + sin^2\theta \, d\phi^2 \right), \tag{1}$$

with μ being a comoving radial coordinate having its origin at the centre of the bubble. For small net baryon number, it is a reasonable approximation to take the energy density e and the pressure p as depending only on temperature so that $p = p(e)$. The system of hydrodynamical equations can be written as

$$u_t = -a \left[4\pi R^2 \frac{\Gamma}{w} p_\mu + G \left(\frac{m}{R^2} + 4\pi p R \right) \right], \qquad (2)$$

$$R_t = au, \qquad (3)$$

$$\frac{(\rho R^2)_t}{\rho R^2} = -a \left(\frac{u_\mu}{R_\mu} \right), \qquad (4)$$

$$e_t = w\rho_t, \qquad (5)$$

$$\frac{(aw)_\mu}{aw} = \frac{(e_\mu - w\rho_\mu)}{w}, \qquad (6)$$

$$m_\mu = 4\pi R^2 e R_\mu, \qquad (7)$$

$$\Gamma = 4\pi \rho R^2 R_\mu = \left(1 + u^2 - 2Gm/R \right)^{1/2}, \qquad (8)$$

$$b = \left(4\pi R^2 \rho \right)^{-1}. \qquad (9)$$

Here u is the radial component of fluid four-velocity in the associated Schwarzschild frame, R is the Schwarzschild circumference coordinate, Γ is the general relativistic analogue of the Lorentz factor, ρ is the relative compression factor, w is the specific enthalpy $(= (e + p)/\rho)$, and the subscripts denote standard partial derivatives. The mass function m can also be calculated using the alternative equation

$$m_t = -4\pi R^2 apu. \qquad (10)$$

As mentioned earlier, it is reasonable to treat the phase interface as an exact discontinuity with the fluid variables on either side being linked by suitable junction conditions. Unlike a shock, a transition front separates two different media and surface

effects need to be taken into account. The required junction conditions for energy-momentum conservation may be derived with the aid of the Gauss-Codazzi formalism. For the particular case where the surface tension σ is independent of temperature one obtains:

$$\left[eb^2\dot{\mu}_s^2 + pa^2\right]^{\pm} = -\frac{\sigma}{2}f^2\left\{\frac{1}{ab}\frac{d}{dt}\left(\frac{b^2\dot{\mu}_s}{f}\right) + \frac{f_{\mu}}{ab} + \frac{2}{fR}\left(b\dot{\mu}_s u + a\Gamma\right)\right\}^{\pm}, \qquad (11)$$

and

$$\left[ab(e+p)\right]^{\pm} = 0. \qquad (12)$$

where $\mu_s(t)$ is the interface location, $\dot{\mu}_s = d\mu_s/dt$, $f = \left(a^2 - b^2\dot{\mu}_s^2\right)^{1/2}$, and $[A]^{\pm} = A^+ - A^-$, $\{A\}^{\pm} = A^+ + A^-$ with the superscripts $\pm$ indicating quantities immediately ahead of and behind the interface. The comoving derivative is taken along the world-line of the interface. There are also three metric junction conditions coming from continuity across the interface of $R, dR/dt$ and ds:

$$[R]^{\pm} = 0 \qquad (13)$$

$$[au + b\dot{\mu}_s\Gamma]^{\pm} = 0 \qquad (14)$$

$$\left[a^2 - b^2\dot{\mu}_s^2\right]^{\pm} = 0 \qquad (15)$$

The mass function m receives a contribution from the surface energy. At the time of nucleation of the bubble, conditions are essentially Newtonian so that

$$[m]^{\pm} = 4\pi R^2\sigma, \qquad (16)$$

and the subsequent time evolution is given by

$$\frac{d}{dt}[m]^{\pm} = 4\pi R^2\left[b\dot{\mu}_s\Gamma e - apu\right]^{\pm}. \qquad (17)$$

For an ordinary shock or a strong detonation front, the junction conditions together with the hydrodynamical equations in each phase are sufficient to completely determine the solution when initial and boundary values have been specified. However,

as discussed in detail in Ref. 9, the situation is different for a deflagration which is the case of interest here. For a deflagration, the rate of flow of energy across the interface depends on the details of the transformation process and so the hydrodynamical and junction equations should be supplemented by an additional expression setting the hydrodynamical energy flux across the interface

$$F_H = \frac{a w \dot{\mu}_s}{4 \pi R_s^2 (a^2 - b^2 \dot{\mu}_s^2)},$$ (18)

equal to the transformation rate (F_T) as derived from separate physical considerations. A simple expression for F_T (see Ref. 9) is given by

$$F_T = \alpha \left[\Phi \left(T_q \right) - \Phi \left(T_h \right) \right],$$ (19)

where $\Phi \left(T_q \right)$ represents an ideal thermal flux away from the interface (at temperature T_q) into the hadron medium, $\Phi \left(T_h \right)$ is the corresponding flux from the hadronic matter towards the interface and α is an accommodation coefficient which takes account of deviations away from the ideal situation ($0 \leq \alpha \leq 1$). This approach is analogous to that used for calculating the net mass transfer across a vapour-liquid interface in classical bubble dynamics[10].

The solution of the above set of equations is complicated by the fact that, for a deflagration, the state of the fluid ahead of the interface is not independent of conditions behind it and so one has to solve the equations for fluid ahead and behind simultaneously with the junction conditions and this requires an iterative procedure. We have numerically integrated the hydrodynamical equations for each phase using a largely explicit Lagrangian finite difference method, while motion of the interface was followed using a characteristic method which gives a very accurate solution. For simplicity, we took the equation of state for the hadronic matter to be that for an ideal gas of massless point-like pions:

$$e_h = 3 p_h = g_h \left(\frac{\pi^2}{30} \right) T^4,$$ (20)

where T is the temperature and g is the degeneracy number. The corresponding expression for $\Phi \left(T \right)$ is:

$$\Phi \left(T \right) = \frac{1}{4} g_h \left(\frac{\pi^2}{30} \right) T^4.$$ (21)

The deconfined quarks and gluons cannot be considered as entirely free and for these we used an approximate equation of state which takes account of the interactions[11]:

$$p_q = g_q \left(\frac{\pi^2}{90}\right) \left[1 - \left(\frac{T_r}{T}\right)^n\right] T^4, \tag{22}$$

$$e_q = g_q \left(\frac{\pi^2}{30}\right) \left[1 + (n/3 - 1) \left(\frac{T_r}{T}\right)^n\right] T^4. \tag{23}$$

For $n = 4$ this reduces to the M.I.T. bag model, with bag constant $\left(\pi^2/90\right) g_q T_r^4$, while $n = 3$ provides the best fit to results obtained from QCD lattice calculations[11]. In addition to the strongly interacting matter, there are also photons and relativistic leptons present within each phase and these satisfy an equation of state similar to that given above for the hadronic matter. When they are in equilibrium with the strongly interacting particles, their contribution can be included by suitably incrementing the values of g_h and g_q and rescaling T_r.

III. Computations of flow structure

Numerical integration of the hydrodynamical equations presented in the previous section allows us to study the dynamics of an expanding hadronic bubble from the time of its nucleation onwards. We here report results from a simplified calculation in which only strongly interacting particles are considered, taking $g_h = 3$ and $g_{q.} = 37$ (appropriate for two relativistic quark flavours), $T_c = 150\,MeV$ and $n = 4$. Runs have been made for various values of the surface tension, transition rate parameter α and nucleation temperature. Such calculations are directly relevant for the first stages of the bubble expansion when the bubble radius is much smaller than the mean free paths of the photons and leptons which are also present. However, they need to be modified after this stage to include these other particles as well. We will return to this point in the Conclusion but proceed in this section with a discussion of calculations made considering only strongly interacting matter throughout.

The surface tension has been parametrized in terms of an adimensional quantity σ_0, such that $\sigma = \sigma_0 T_c^3$ (where, reasonably, $10^{-2} \lesssim \sigma_0 \lesssim 10$)[13]. For any given temperature, the critical radius of a bubble at nucleation grows with σ and one expects that the effects of surface tension will remain significant for a longer time during the

expansion when σ is larger. In fact, if the gravitational terms can be neglected, the hydrodynamical equations (2) – (17) are invariant under the transformations

$$R/\sigma_0 \to \widetilde{R}/\widetilde{\sigma}_0, \qquad t/\sigma_0 \to \widetilde{t}/\widetilde{\sigma}_0 \quad \text{and} \quad b\,d\mu/\sigma_0 \to (\widetilde{b}\,d\widetilde{\mu})/\widetilde{\sigma}_0 \tag{24}$$

showing that all times and distances will then scale linearly with σ. For the circumstances being considered here, the gravitational terms are indeed negligible and so there is a family of similar solutions, for different values of σ_0, related through the transformations (24).

Figures 1 and 2 show, respectively, the velocity and energy density profiles in the fluid as functions of R at various times during the bubble expansion (for nucleation temperature $T_n = 0.98\,T_c$, $\alpha = 1$ and $\sigma_0 = 1$). Initially, surface tension dominates but its role progressively decreases during the expansion until eventually its effect becomes negligible and an asymptotic regime is reached where the interface velocity is almost constant. This happens when the bubble radius has increased by about two orders of magnitude above its nucleation value. The hadronic material inside the bubble is then essentially at rest and the compression wave expanding out through the quark medium is becoming self-similar (cf Ref. 8). There is no evidence for any shock forming at the
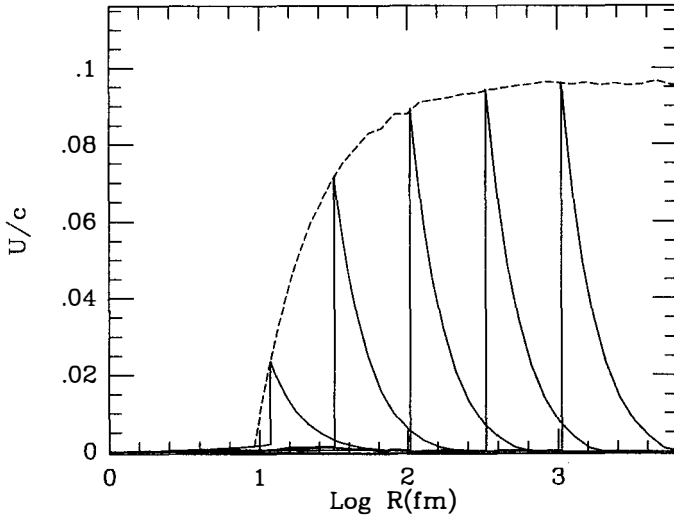
Fig. 1. Fluid velocity at successive times (continuous lines), is plotted against radius R. (See text for the parameters of the run.) The dashed line shows the behaviour of the fluid velocity just ahead of the interface as the bubble expands.

Fig. 2. Behaviour of the energy density as a function of R for the same run as in Fig. 1.

Fig. 3. Evolution of the temperatures immediately ahead of and behind the interface (continuous and dashed lines respectively) for the same run as in Fig. 1. The temperatures are plotted as functions of bubble radius R_s.

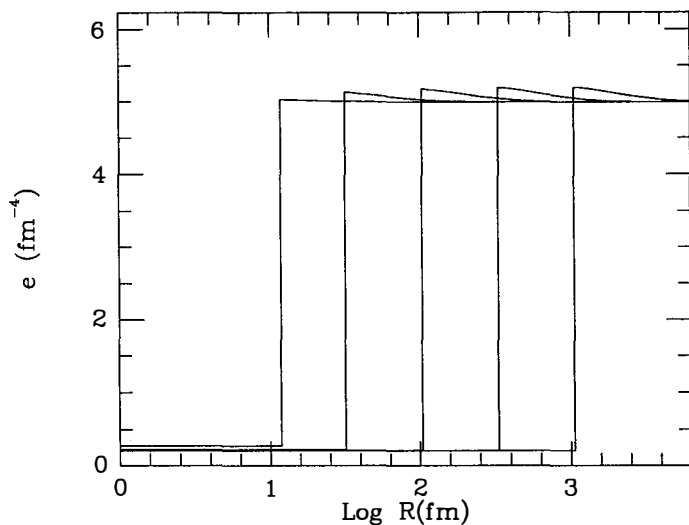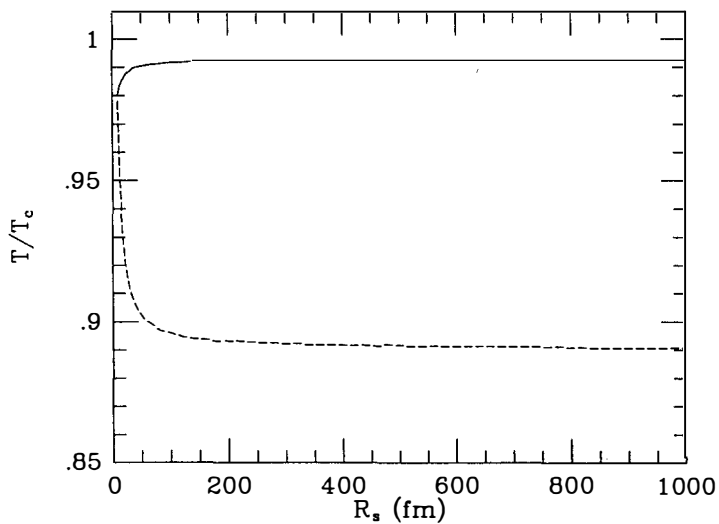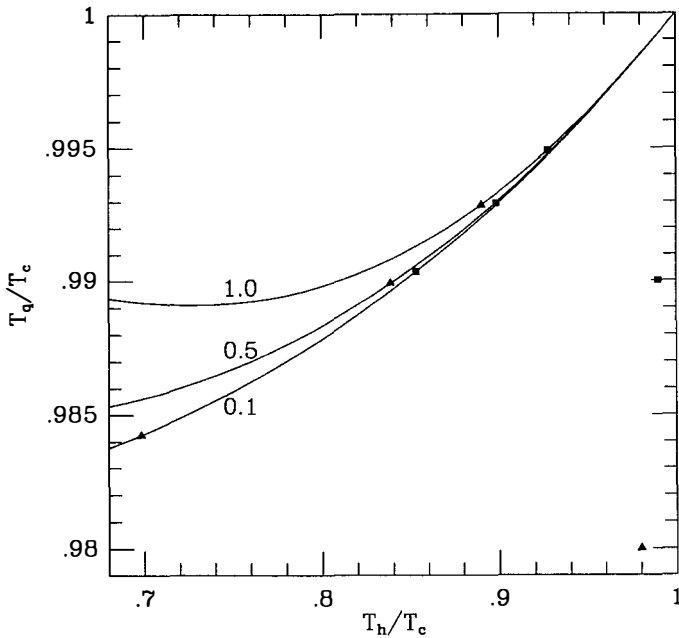*Fig. 4. The continuous lines show the relationship between the temperatures ahead of and behind the interface for a hadronization deflagration front when surface tension is neglected. The labels show the the value of α used for each curve. The triangles indicate the initial and asymptotic values for runs with $T_n = 0.98\,T_c$ and various values of α (see corresponding curves). The squares indicate corresponding points for $T_n = 0.99\,T_c$.*

leading edge of the compression wave but this is not surprising in view of the fact that the maximum velocity attained by the bubble surface (0.103 in this case) is small compared with the sound speed $(1/\sqrt{3})$. Most of the latent heat released in the transition does, in fact, go into thermal energy of matter in the compression wave but this is nevertheless a very small perturbation of the pre-existing quark energy density and the velocity profile is very similar to that for an incompressible fluid.

Figure 3 shows the behaviour of the temperature immediately ahead of and behind the interface for the same case as described above. The temperature ahead rises as the bubble expands while that behind decreases. The asymptotic values reached have also been plotted in Figure 4 together with ones obtained from other runs with various values of α ($= 0.1$, 0.5 and 1.0) and T_n ($0.98\,T_c$ – denoted by triangles – and $0.99\,T_c$ – denoted

by squares). Once the value of α has been specified, the transition rate equation (19) together with the junction conditions (11) and (12) (neglecting surface tension) give a direct relationship between the temperature behind the interface and the temperature ahead which should be appropriate for the asymptotic regime[14]. This relationship (for the same values of α as above) is shown by the solid lines in Figure 4. It is interesting to note which points on the curves are reached by computed evolutions starting from the different values of T_n.

IV. Conclusion

As emphasized at the beginning of Section III, calculations involving only strongly interacting particles are a reasonable approximation for the first part of the bubble expansion but this ceases to be the case when the bubble radius begins to get near to the mean free path of the electromagnetically interacting particles which will also be present ($\lambda_e \simeq 10^3 \, fm$). First, these particles start to provide a significant long range energy transport mechanism causing deviations away from the previous solution. Later, when the characteristic length scales of the problem become large compared with λ_e, they may be taken as being in thermal equilibrium with the strongly interacting matter and moving together with it as a single fluid. The perfect fluid hydrodynamic equations may then be used as before except that the additional degrees of freedom must be included in the equations of state. For the parameters used in Figures 1 – 3, the contribution of the electromagnetically interacting particles becomes important before the asymptotic regime is reached and, at this point, the solution would change tending eventually towards another asymptotic regime corresponding to the new g factors. These new asymptotic solutions are qualitatively similar to those discussed in Section III but are characterised by lower velocities, smaller compressions and smaller temperature differences between the two phases.

At even larger scales, the effect of long range energy transport by neutrinos becomes important when the bubble radius approaches the neutrino mean free path ($\lambda_\nu \simeq 1 \, cm$). However, it is possible that the mean distance between bubble nucleation sites might be smaller than this so that bubble coalescence would occur before neutrino transport became important.

102

References

1] H. Reeves, to appear in *Phys. Rep.* (1989).

2] E. Witten, *Phys. Rev. D* **30**, 272 (1984).

3] For a review see the articles by J. Audouze and G. Steigman in these proceedings.

4] J.H. Applegate, C.J. Hogan and R.J. Scherrer, *Phys. Rev. D* **37**, 1151 (1987);
   G.M. Fuller, G.J. Mathews and C.R. Alcock, *Phys. Rev. D* **37**, 1380 (1988);
   H. Kurki-Suonio, R. Matzner, J.M. Centrella, T. Rothman and J.R. Wilson, *Phys. Rev. D* **38**, 1091 (1988);
   R.A. Malaney and W.A. Fowler, *Astrophys. J.* **333**, 14 (1988).

5] K.Kajantie and H. Kurki-Suonio, *Phys. Rev. D* **34**, 1719 (1986).

6] L.D. Landau and E.M. Lifshitz, *Statistical Physics*, Pergamon Press, Oxford, 1980.

7] M. Gyulassy, K. Kajantie, H. Kurki-Suonio and L. McLerran, *Nucl. Phys.* **B237**, 477 (1984).

8] H.C. Kurki-Suonio, *Nucl. Phys. B* **255**, 231 (1985).

9] J.C. Miller and O. Pantano, to appear in *Phys. Rev. D.* (1989).

10] T.G. Theofanous, L. Biasi, H.S. Isbin and H.K. Fauske, *Chem. Eng. Sci.* **24**, 885 (1969).

11] S.A. Bonometto and L. Sokołowski, *Phys. Lett.* **107A**, 210 (1985).

12] M.I. Gorenstein and O.A. Mogilevsky, *Z. Phys. C* **38**, 161 (1988).
   F. Karsch, *Z. Phys. C* **38**, 161 (1988).

13] K. Kajantie and L. Kärkkäinen, Helsinki preprint HU–TFT– 88–22;
   Z. Frei and A. Patkós, Fermilab preprint Pub–89/47–A.

14] O. Pantano, to appear in *Phys. Lett. B.* (1989).

THE MEAN DENSITY FROM THE GALAXY DISTRIBUTION

Valérie de Lapparent
Institut d'Astrophysique de Paris
98 bis, Boulevard Arago
75014 Paris, France

ABSTRACT

Some of the characteristics of the galaxy distribution in the CfA redshift survey extension are reviewed, and their implications on the mean mass density of the universe are discussed. This survey shows that the largest structures in the galaxy distribution pose problems for determination of the mean density of matter underlying structures of galaxies. New surveys designed for sampling efficiently many more structures than in the nearby surveys will provide tighter constraints on the distribution and mean density of matter in the universe.

1. GENERALITIES

The cosmological parameter Ω_0, measuring the mean mass density of the universe, is strongly constrained by redshift surveys: these "three-dimensional" maps provide information on both the spatial galaxy distribution and its dynamics, and thus provide estimates of the mean mass density attached to galaxies and to the structures they form on large scales (~ 1 to $100h^{-1}$ Mpc; $H_0 = 100\ h$ km s^{-1} Mpc^{-1}).

The spatial luminosity density for galaxies (derived from galaxy counts per luminosity interval) multiplied by the M/L ratio of individual galaxies yields an estimate of the mean density which accounts for the dark matter in halos of galaxies. For a value of the luminosity density in large redshift surveys in the range of $1 - 2\ 10^8 h L_\odot$ Mpc^{-3} (Davis and Peebles 1982; Kirshner et al. 1983; de Lapparent, Geller, and Huchra 1989) and $M/L \sim 30h M_\odot/L_\odot$ (from the rotation curve of galaxies; see Binney and Tremaine, 1987, and references therein), the resulting density parameter is $\Omega_0 \sim 0.01 - 0.02$.

However, estimates based on the clustering dynamics suggest the presence of larger amounts of dark material on scale of $\gtrsim 1h^{-1}$ Mpc. Following are four different methods (in order of increasing characteristic scale) which are used for deriving the dynamical estimates of Ω_0: the pairwise peculiar velocities in the field (Davis and Peebles 1983; Bean et al. 1983); the velocity dispersion in cluster cores (Kent and Gunn 1982; Kent and Sargent 1983; Kurtz et al. 1985; Ostriker et al. 1989); the velocity profile in the cluster outskirts (Shectman 1982; Regös and Geller 1989); the velocity field at large distance from clusters (Aaronson, Huchra, Mould, Shectman 1981, for the Virgo-centric flow; see also Davis and Peebles 1983). These estimates yield consistent values of Ω_0 ranging between 0.1 and 0.3.

Thus, values of the mean mass density as derived from the largest known coherent structures of galaxies reach an upper limit of $\sim$ one-third the closure density. Therefore, to make $\Omega_0 = 1$ as suggested by the concept of "inflationary universe" (Guth 1981, 1986), we need to invoke the presence of a component of dark matter which has a different spatial distribution from that for the galaxies, and is supposedly distributed more uniformly than galaxies (see Peebles 1986). Because baryons can account at most for the dark matter found by the dynamical estimates on scales of groups and clusters of galaxies (see the results from nucleosynthesis; Steigman, this volume), the inflationary picture requires that most of the mass in the universe be non-baryonic.

2. THE CFA REDSHIFT SURVEY EXTENSION

The recent extension of the CfA redshift survey to $m_{B(0)} = 15.5$ suggests a new picture of the galaxy distribution, in which galaxies are distributed in thin sheet-like or shell-like structures surrounding vast voids. Figure 1 shows a pie-diagram of the first "slice" of the CfA survey extension, bounded by $26.5° \leq \delta \leq 32.5°$ in right ascension, and $8^h \leq \alpha \leq 17^h$ in declination (de Lapparent, Geller, and Huchra 1986). Here, we show how this survey raises new difficulties in estimating the mean mass density of the universe from redshift surveys.
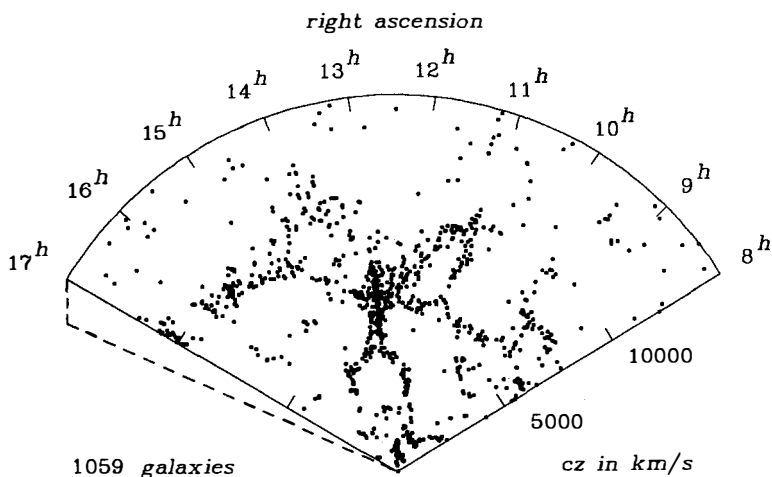
Figure 1. Map of the velocity versus right ascension for the galaxies with $cz \leq 15,000$ km s^{-1} in the first slice of CfA redshift survey. The thickness of the slice (indicated by the dashed lines) is 6° in declination.

The dense region in the center of the map in Figure 1 is the Coma cluster of galaxies. The elongation of the cluster along the line of sight, caused by the velocity dispersion of galaxies in the gravitational potential of the cluster, is used to derive the dynamical estimate of the mass of the cluster. However, the cluster is at the intersection of several sheets of galaxies, with one of them parallel to the line of sight and in the foreground of the cluster. Therefore, velocity dispersion of the cluster might be overestimated by the confusion of spatial sheet-like structure with the velocity profile of the cluster.

Reliable estimates of Ω_0 from clusters of galaxies require maps of the surroundings of the clusters which are appropriate for clean separation of the spatial structures from the velocity structure.

Direct estimation of the mean density from the average number of galaxies in the survey is also susceptible to biases. In Figure 1, the size of the largest underdense region (nearly circular on one side, and centered at 15^h and 7,000 km s^{-1}) has a diameter ($\sim$ 5,000 km s^{-1}) comparable to the characteristic depth of the survey ($\sim$ 10,000 km s^{-1}). Therefore, this survey does *not* represent a fair sample of the galaxy distribution. The fluctuations in the counts are directly related to the size of the voids and to how close-packed they are. A simple geometric model shows that the fractional uncertainty in the mean number density of galaxies is proportional to the inverse of the square-root of the number of large voids (under reasonable assumptions on the spectrum of void diameter), giving an uncertainty of $\sim$ 25% for the slice in Figure 1. Therefore, the fluctuations in the mean are not simply reduced by increasing the number of galaxies in the sample, but by increasing the number of large voids in the survey (de Lapparent, Geller, and Huchra 1988).

The predicted fluctuations in the mean density are confirmed by direct calculation of the luminosity density for the slice. The shape of the luminosity function for this catalog can be derived by an inhomogeneity-independent method (*i.e.* unbiased by the selection effects introduced by the strong inhomogeneities in the sample), and thus allows to correct the selection effect related to the apparent-magnitude limiting of the catalog. The luminosity density can then be derived by averaging over structures at different redshifts. For the slice, the luminosity density fluctuates by $\sim$ 25% of its median value ($1.5\ 10^8 h L_\odot$ Mpc^{-3}) when the redshift cut-off out to which galaxies are counted varies from 5,000 km s^{-1}to 10,000 km s^{-1}. Moreover, the luminosity density does not seem to converge within the depth of the survey (de Lapparent, Geller, and Huchra 1989).

It is interesting to note that similar estimates of the luminosity density for the earlier CfA redshift survey (limited to $m_{B(0)} = 14.5$, equivalent to a depth of 6,000 km s^{-1}; Huchra *et al.* 1983) show smaller fluctuations with varying depth that in the slice, consistently with the ratio of the volumes of space sampled by the two surveys (a ratio of $\sim$ 15). However, blind comparison of these results is misleading: the shallower survey is not closer to a fair sample than the deeper slice because it does not contain any

structure as large as the $\sim 5,000$ km s^{-1} void centered at 15^h and $7,000$ km s^{-1} in the slice. The shallow sample would be barely large enough to contain one such structure.

Redshift surveys can also provide indirect constraints on the mean mass density in the universe: the characteristics of the large-scale clustering constrain the theoretical models for the formation of large-scale structure, and thus the initial conditions and physical mechanisms which lead to the observed structures. Quantitative measures of the clustering are therefore necessary for reliable comparison of the data with the results of N-body models. Because the structures in the CfA slice are highly asymmetric and contrasted, these measures must depend on the high-order moments of the distribution. Several sophisticated statistics have been designed to describe the galaxy distribution (Gott, Melott, and Dickinson 1986; Maurogordato and Lachièze-Rey 1987; Ryden 1988; Gott *et al.* 1989; Ryden *et al.* 1989; see also Maurogordato, this volume). However, simpler measures can already constrain some of the models: for example, the filling factor for the galaxies ($\sim 20\%$ in the CfA slice; de Lapparent, Geller, and Huchra 1989) puts limits on the relative distribution of galaxies and dark matter in the pancake models (White *et al.* 1987; Melott 1987; see also Bouchet, this volume). In these models, $\Omega_0 = 1$, and the galaxies form only at the peaks of the matter distribution.

3. PROSPECTS

Deep surveys which can sample many voids like those in the CfA slice will improve the description of the galaxy distribution, and lower the fluctuations in the number of the largest voids. One such program is being undertaken at the European Southern Observatories facilities (de Lapparent *et al.* 1989). The survey has the configuration of a thin strip of $\sim 2° \times 0.2°$ reaching out to a redshift of ~ 0.5 (an order of magnitude deeper than the CfA slice). Because this survey should cut through ~ 50 voids of average diameter 3,000 km s^{-1}, we will obtain better constraints on the spectrum of void diameter and thus on the mean density of galaxies. This survey might also uncover even larger voids than in the CfA slice ($\gtrsim 10,000$ km s^{-1} in diameter), which could not have been detected in the CfA slice. This survey has been designed to sample efficiently structures similar to those found in the CfA slice: $0.2°$ are equivalent to ~ 300 km s^{-1} at the depth of the strip, which is comparable to the typical separation of the galaxies in the sheets of the CfA slice. This new survey will therefore probe through distant sheets with a sufficient density contrast for reliable detection.

Note that the choice of a smaller thickness for this deep strip would lead to over-

estimation of the size of the voids: some of the sheets might be "missed". On the other hand, a larger thickness would yield redundant information on the position of the voids and sheets. This effect is well illustrated by comparison of the first CfA slice (Fig. 1) with the adjacent 6° slice to the north (Geller, Huchra, and de Lapparent 1987; Geller 1988): there is a strong coherence of the sheets and voids from one slice to another because the thickness of each slice along the declination coordinate (indicated by dashed lines in Fig. 1; $\sim 1,000$ km s^{-1} at a depth of 10,000 km s^{-1}) is smaller than the $\sim 3,000$ km s^{-1} mean diameter for the voids.

REFERENCES

Davis, M. and Peebles, P. J. E. 1983, *Ann. Rev. Astr. Ap.*, **21**, 109.

Binney, J., and Tremaine, S. 1987, *Galactic Dynamics,* Princeton Series in Astrophysics, ed J. P. Ostriker (Princeton: Princeton University Press).

Geller, M. J. 1988, in *Large-Scale Structure in the Universe,* ed. L. Martinet (Saas Fee Lectures 1987), **17th Advanced Course of the Swiss Society of Astronomy and Astrophysics.**

Geller, M. J., Huchra, J. P., and de Lapparent, V. 1987, in *Observational Cosmology,* eds. A. Hewitt *et al.* (Dordrecht: D. Reidel), **IAU Symposium 124**, p. 301.

Gott, J. R. III, Melott, A., and Dickinson, M. 1986, *Ap. J.*, **306**, 341.

Gott, J. R. III, *et al.* 1989, *Ap. J.*, **340**, 625.

Guth, A. 1981, *Phys. Rev*, **D23**, 347.

Guth, A. 1986, in *Inner Space/Outer Space,* ed. E. W. Kolb *et al.* (Chicago: University of Chicago Press, p. 287.

Huchra, J., Davis, M., Latham, D., and Tonry, J. 1983, *Ap. J. Suppl.*, **52**, 89.

Kent, S. M., and Gunn J. E. 1982, *Astr. J.*, **87**, 945.

Kent, S., and Sargent, W. 1983, *Astr. J.*, **88**, 697.

Kirshner, R. P., Oemler, A. Jr., Schechter, P. L., and Shectman, S. A. 1983, *Astr. J.*, **88**, 1285.

Kurtz, M. J., Huchra, J. P., Beers, T. C., Geller, M. J., Gioia, I. M., Maccacaro, T., Schild, R. E., and Stauffer, J. R. 1985, *Astr. J.*, **90**, 1665.

de Lapparent V. 1986, *Ph. D. thesis,* Université de Paris 7.

de Lapparent, V., Mazure, A., Mathez, G., et Mellier, Y. 1989, *The Messenger*, **55**, 5.

de Lapparent, V., Geller, M. J., and Huchra, J. P. 1986, *Ap. J. (Letters)*, **302**, L1.

de Lapparent, V., Geller, M. J., and Huchra, J. P. 1988, *Ap. J.*, **332**, 44.

de Lapparent, V., Geller, M. J., and Huchra, J. P. 1989, *Ap. J.*, **343**.

de Lapparent, V., Geller, M. J., and Huchra, J. P. 1989, in preparation.

Maurogordato, S., and Lachièze-Rey, M. 1987, *Ap. J.*, **320**, 13.

Melott, A. L. 1987, *Mon. Not. Roy. Astr. Soc.*, **228**, 1001.

Ostriker, E. C., Huchra, J. P., Geller, M. J., and Kurtz, M. J., *Astr. J.*, **96**, 1775.

Regös, E., and Geller, M. J. 1989, in preparation.

Ryden, B. S. 1988, *Ap. J. (Letters)*, **333**, L41.

Ryden, B. S., *et al.* 1989, *Ap. J.*, **340**, 647.

Peebles, P. J. E. 1986, *Nature*, **321**, 27.

Shectman, S. A. 1982, *Ap. J.*, **262**, 9.

White, S. D. M., Frenk, C. S., Davis, M., and Efstathiou, G. 1987, *Ap. J.*, **313**, 505.

THE MEAN DENSITY AND GALAXY STATISTICS IN THE SSRS

by

Sophie Maurogordato [1,2]

1. DAEC Observatoire de Paris Meudon France

2. on leave from Service d'Astrophysique CEN Saclay France

Abstract

High-order statistics, as the Counts Probabilities in cells, are computed on the tri-dimensionnal Southern Sky Redshift Survey, which represents up to day one of the "fairest galaxy sample" of the Universe . Comparison to the theoretical predictions issued from the "Scaling Invariant" models defined by Balian and Schaeffer 1988, helding on a very general relation between n-point correlation functions, gives very good agreement with these models, directly explaining the various "scaling laws" evidenced by the data.

Introduction

Supposing homogeneity for the Universe at very large scales, the mean mass distribution can be described by the mean mass density and the expansion rate. The value of the mean mass density normalized to the critical one, is particularly important in order to determine the evolution of the Universe through Einstein equations. However, the value of Ω deduced from nucleosynthesis or from galaxy observations is smaller than the $\Omega = 1$ wanted by the theoretical inflationary scenario. Some scenarios invoking non-baryonic matter, and for example the "biased galaxy formation" models, can be compatible with an Universe of critical density. The statistical analysis can be of great help both for direct estimation of Ω and for comparing model predictions to data from which it allows to extract a quantified information. As the Fair Sample Hypothesis is being supposed to perform this analysis, the catalogs used are needed to be large enough to be representative of the whole Universe. At the moment, large tridimensional surveys of galaxies as the Center for astrophysics Redshift Survey (Huchra et.al 1983) the Southern Sky Redshift Survey (da Costa et.al unpublished), the Arecibo Perseus Survey (Giovanelli and Haynes 1989) and the Supergalactic Plane Survey (Dressler et.al 1989) allow to compute spatial statistics. The Southern Sky Redshift Survey (next SSRS), not domined by very rich clusters, is particularly adapted to the Statistical analysis by its homogeneity and representativity. High order statistics, as the count probabilities functions are then computed on this sample (Maurogordato, Schaeffer, da Costa, 1989), extending the algorithm developped by Maurogordato and Lachièze-Rey 1987 for the Void Probability Function analysis.

Statistical tools and characteristical scales

The most "known" and "fruictful" statistical tool used up to now has been the 2-point correlation function, ξ, introduced in cosmology by Peebles in the seventies. It was shown to follow a power law versus the radius tested (Davis and Peebles 1983)

$$\xi(r) = (r/r_0)^\gamma, \text{ with } \gamma = -1.8 \text{ and } r_0 = 5.4h^{-1}Mpc$$

On the same way is defined the whole hierarchy of the n-point correlation functions. As all the orders were shown to be important to characterize the whole distribution, more attention was paid in order to determine the correlation up to higher orders. From observations, they were calculated until order 4, showing a relation linking the n-point correlation function to the 2-point correlation function. In order to go further , related statistics are for example the moments of the counts of neighbors, and integrated values as

$$J_3 = \int r^2 \xi(r)dr \quad N_c = \frac{\int \delta V_1 \delta V_2 \xi(r)}{V^2}$$

Complementary indicators have been developped , involving the high order correlation functions, as the nearest neighbor distance (Turner and Gott,1979), the void probabilities (White 1979, Schaeffer 1984, Fry 1986, Bouchet and Lachièze-Rey 1986, Maurogordato and Lachièze-Rey 1987) and the counts in cells (Peebles 1980,Balian and Schaeffer 1988)

Apart from the correlation length, at the scale transition for linearity for the 2-point correlation function, one can define two interesting characteristical scales. The first one is defined as the "clustering length": When calculating the counts of randomly placed cells , their fluctuations can be separated in two contributions:

$$\Delta^2 = < (N- <N>^2>$$

$$\Delta^2 = nV[1 + \frac{\int\int \delta V_1 \delta V_2 \xi(r)}{V^2}]$$

$$\Delta^2 = nV[1+ N_c]$$

the Poisson and the correlated part through the N_c integral. In the regime where the power law approximation for $\xi(r)$ can be applied, it is directly infered to N_c . The scale r_c corresponding to $N_c = 1$ can be traduced as the switch between the Poisson and the correlated case. A void radius r_v is defined too, corresponding to the radius to which the VPF has a given value, e^{-1} for example. These scales are normalized according to the density dependance, in order to get characteristical values of the galaxy clustering. It results a clustering radius of about $1h^{-1}Mpc$ and a mean void radius around $6h^{-1}$Mpc.

Counts probabilities in the SSRS and comparison to the SI models

We have performed the counts in cells in the SSRS, and compared to the predictions issued in the frame of the "scale invariant models" defined by Balian and Schaeffer (1988). The SSRS covers galactic latitudes $b_{II} < -30°$ and declinations souther than $-17.5°$, with 1676 galaxies in 1.75 steradian up to apparent diameter $log(d) > .1$ arcmin. For the statistical purpose, subsamples limited both in distance and absolute diameter are extracted from the initial sample.

The previous "scale-invariant" models (next SI) helds only on a very general scaling relation between N-point correlation functions:

$$\xi_N(\lambda r_1, ..., \lambda r_N) = \lambda^{-(N-1)\gamma} \xi_N(r_1, .., r_N)$$

This relation is compatible with the correlations extracted up to day and with the BBGKY hierarchy analysis. These SI models cover the so-called hierarchical models which suppose a more precise relation between N-point and 2-point correlation functions.

As the counts probabilities can be expressed as density derivatives of the VPF,

$$P_N(r) = \frac{(-n)^N}{N!} \frac{d}{dn}^N P_0(r)$$

and the VPF explicitly depends on the n-point correlation functions:

$$Ln P_0(r) = \sum (-n)^N \int d^3 r_1 ... d^3 r_N \, \xi_N(r_1, ..., r_N)$$

The behaviour of the VPF and of the counts probabilities should then reflect any relation between the n-point correlation functions . It is therefore interesting to compare the direct estimations from the data to the analytical predictions. First, the VPF deduced from the SI models verifies a "scaling law" : when normalized to Poisson, it is an universal function only dependant on the integral N_c. More, this function $\sigma(N_c)$ is expected at larges scales to show a power law behaviour,

$$\sigma(N_c) \propto a N_c^{-\omega}$$

when

$$N_c \to \infty$$

In this regime, the void probability function $P_0(r)$ can be expressed as:

$$P_0(r) = e^{-N_v^{1-\omega}}$$

The universality of the representation $\sigma(N_c)$ has been shown in the CfA by Maurogordato and Lachièze-Rey 1987, and in the SSRS by Maurogordato, Lachièze-Rey and da Costa 1989, deducing the variable $N_c(r)$ from the two-point correlation extracted directly from the data, which are simply related in the power-law approximation by: $N_c(r) = K(\gamma)\xi(r)$. In a new approach, (Maurogordato, Schaeffer, da Costa 1989), the scaling variable $N_c(r)$ is directly estimated from the data, computing the mean number of neighbors for each galaxy. The scaling invariance is then confirmed in the SSRS respectively limited to 40, 60, 80 h^{-1} Mpc, and to the corresponding absolute diameters (Fig 1.). This scaling law is being verified on the SSRS between radius ranges from .5 to about $14 h^{-1} Mpc$, defining an universal law governing the void distribution at all scales up to the size of the big voids of the Universe defined by de Lapparent et.al 1986. The power law behaviour is too clearly evidenced at large scales, well fitted by parameters of $a = .92$ and $\omega = 0.7$
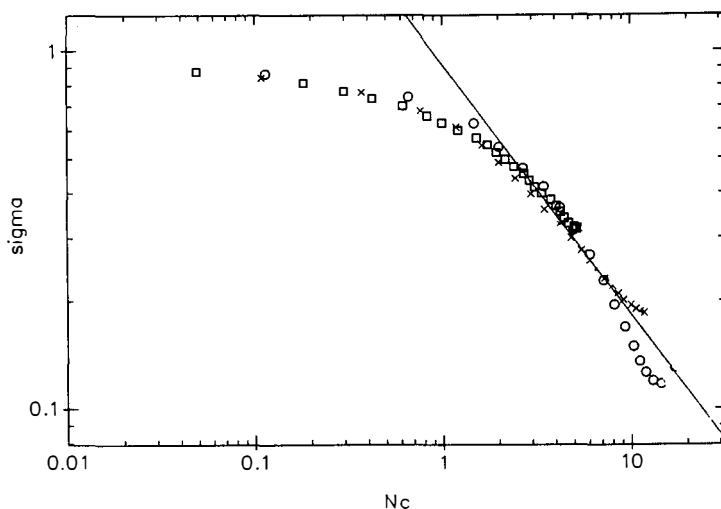
$$\sigma = \frac{log[P_0(r)]}{nV} \, versus \, N_c = \frac{\int \delta V_1 \delta V_2 \xi(r)}{V^2}$$

The behaviour of the P_N with the count N, in the SSRS is completely coherent with the predictions from the SI models as shown in Fig.2 for the subsample of the SSRS distance-limited to $60h^{-1}Mpc$ and diameter limited to $21.9h^{-1}$ Kpc (next SS60) At small scales of $r < rc$, an exponential decrease is expected for the P_N. At large scales, however, between r_c and r_v, a power-law behaviour is predicted:

$$P_N = \frac{1-\omega}{\Gamma(\omega)} \frac{1}{N_c < \xi(r) >} \frac{N^{\omega-2}}{N_c}$$

with a lower-cutoff for $N = N_v$, and an upper cut-off for $N = N_c$. From the data, the evolution of the upper cut-off with the radius agrees well with the corresponding increase of N_c.

Count probabilities
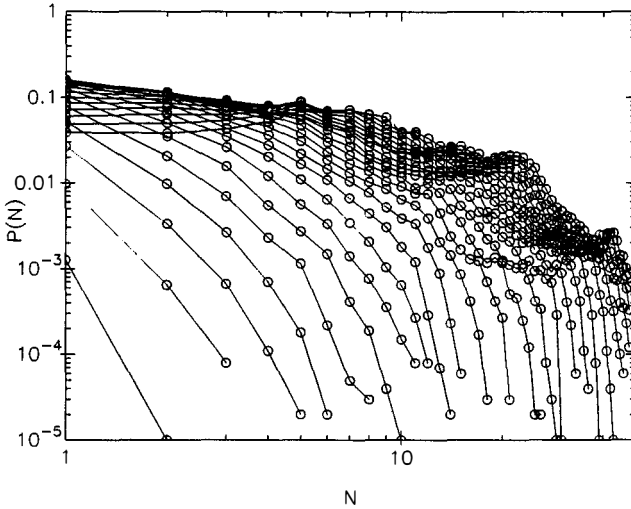
Fig.2 : The evolution of the counts probabilities P_N with N. Each connected curve corresponds to a different radius tested (incremented with .5 h^{-1}Mpc steps)in the SS60.

More, scaling laws are predicted too for the P_N for two extreme regimes: for $1 < N < N_c$, $N P_N$ behaves as $\frac{N}{N_v} g(\frac{N}{N_v})$ and for $N > N_v, N > 1, N_c > 1, N^2 P_N$ behaves as $\frac{N}{N_c} h(\frac{N}{N_c})$ Fig.3 shows for the subsample SS60, $N^2 P_N$ as $\frac{N}{N_c}$ in the adequate regime. Allthough the P_N versus N were systematically shifted for each radius scale, the new representation shows the curves all gathering together for the different scales tested.

Fig 3 : Scaling relation for $N^2 P_N$ with $\frac{N}{N_c}$ in the SS60.

Conclusion

The SSRS, deeper and more homogeneous than the previous 3D surveys, allows to compute high order statistics as the void probability function or the counts probabilities, up to tested radius of 12, $14h^{-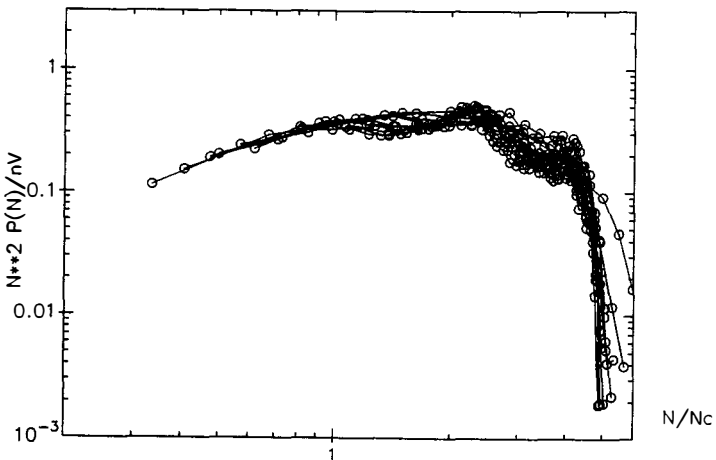1}$ Mpc. The scaling laws and power law behaviours exhibited both by the VPF and the counts are directly predicted in the frame of the scale-invariant models defined by Schaeffer and Balian 1988. Combining these statistics to the SSRS, likely to be a "fair sample" representative of the Universe, allows us to reach the conclusion the Universe presents a scale-invariant behaviour until the greater scales surveyed up to now.

References

Balian, R. and Schaeffer, R. 1989, *submitted to Astron.and Astrophys.* .

Bouchet, F. R., and Lachièze-Rey, M. 1986, *Astrophys J. Lett.*, **302**, L37.

da Costa, L.N., Pellegrini, P.S., Sargent, W.L.W., Tonry, J., Davis, M., Meiksin, A. and Latham, D.W. 1988, *Astrophys. J.*, **327**, 544.

de Lapparent, V., Geller, M.J. and Huchra, J.P. 1986, *Astrophys J. Lett.*, **302**, L1.

Huchra, J., Davis, M., Latham, D. ,Tonry, J. 1983, *Astrophys. J. (supplts)*, **52**, 89.

Maurogordato, S., and Lachièze-Rey, M. 1987, *Astrophys. J.*, **320**, 13.

Maurogordato, S., Lachièze-Rey, M. and Bouchet,F. 1988, *Astron. and Astrophys. (Letters)*, **206**, L23.

Maurogordato, S., Lachièze-Rey, M., daCosta, L., N. 1989, *in preparation*.

Maurogordato, S., Schaeffer, R., daCosta, L., N. 1989, *in preparation*.

Peebles, P. J. E. 1980, *The Large Scale Structure of the Universe*, Princeton University Press, Princeton.

Schaeffer, R. 1984, *Astron and Astrophys. Lett*, **134**, L1.

White, S. D. M. 1979, *M. N. R. A. S.*, **186**, 145.

QUARK NUGGETS, DARK MATTER AND PULSAR GLITCHES.

Jes Madsen
Institute of Astronomy
University of Aarhus
DK-8000 Aarhus C, Denmark.

ABSTRACT

Very tight constraints are put on the occurrence of stable lumps of quark matter (quark nuggets) in our Galaxy. Only nuggets heavier than 10^{15} grammes remain possible candidates for the dark matter. A suggestion for solving the solar neutrino problem is ruled out, and some restrictions are set on models trying to explain Centauro cosmic ray primaries or cygnets as quark nuggets. The existence of strange stars in binaries is questioned. The conclusions come from assuming that pulsar glitches can occur only in neutron stars, not in strange stars. As a consequence not a single quark nugget can have penetrated to the neutron drip region in a pulsar, and no quark nuggets can have been caught by the pulsar progenitor, since then the pulsar would have been converted to a strange star. This leads to limits on the galactic flux of quark nuggets many orders of magnitude better than limits from Earth-based detectors. The presentation is based on a recent publication[20], but unpublished results on the fate of nuggets during supernova explosions and during collisions with neutron stars are included as well.

I. PHYSICS AND ASTROPHYSICS OF QUARK NUGGETS

Quark matter composed of up, down and strange quarks in roughly equal propor-
tions (*strange matter*) could be stable in bulk (i.e. stronger bound than ^{56}Fe) at
zero temperature and pressure for significant ranges of strong interaction
parameters and strange quark masses.[28],[12]

Quark nuggets (lumps of strange matter) could be the most bound state of
baryonic matter for baryon number A in the range 10-$100 \lesssim A \lesssim 2 \times 10^{57}$. Nuggets
with masses above a few percent of a solar mass are significantly influenced by
gravity and correspond to neutron stars - so called *strange stars*. Such objects
could be the direct result of Type II supernova explosions, or be created by
conversion of ordinary neutron stars. A Chandrasekhar-type instability limits A
to be less than 2×10^{57}. Quark nuggets with $A \lesssim 10^{56}$ are bound by the strong
interactions alone. Shell effects give a lower bound of order 10-100 on A for
stable nuggets.

Nuggets where gravity is negligible have constant mass density throughout,
typically of order 3.6×10^{14}gcm^{-3}, and masses $m = A/6 \times 10^{23}$g. The quark surface is
well-defined and surrounded by an atmosphere of electrons. Nuggets with
$A \lesssim 10^{15}$ have their outermost electrons in Bohr-like orbits out to a radius
$\approx 10^{-8}$cm, whereas larger nuggets with quark-radius exceeding this value have
electrons up to 400 fermi above the quark surface.

Due to the extended electron atmosphere a typical nugget has a Coulomb
barrier of order $+10$MeV at the quark surface, making it inert in low-energy
collisions with ordinary matter, whereas free neutrons are efficiently absorbed
and converted into quark matter.

The stability of strange matter is generally increased if a finite pressure is
imposed, such as would be the case inside neutron stars/strange stars.[10] On the
other hand finite temperature effects tend to decrease the stability,[10],[25] so
that even if strange matter is the most stable phase of baryonic matter at $T=0$,
it may not be so at high temperatures. The details of stability as a function
of temperature and pressure are even less secure than the situation at $T=0$.
This is important since we shall in fact be looking at nuggets in hot environ-
ments such as the Big Bang and supernova-explosions. However as will be dis-
cussed in context later it is not only the overall thermodynamical stability of a
nugget that matters, but also whether the lower energy state is accessible on
the time-scales involved.

Quark nuggets have been looked for but not seen in laboratory-
experiments.[9] Very low-mass nuggets might appear as abnormally heavy isotopes
of well-known elements. Another natural place to look is in ultrahigh energy

heavy ion collisions, but it is not obvious that existing accelerators reach the interesting region, especially since the baryon number involved in collisions is low.

Instead it is interesting to look for extraterrestrial sources. Witten[28] suggested two astrophysical settings for quark nugget formation : The quark-hadron phase transition 10^{-5} seconds after the Big Bang, and the transformation of neutron stars into strange stars (with the possibility that strange star collisions may lead to further spreading).

Formation of quark nuggets during the quark-hadron phase transition in the early Universe could take place if neutrino cooling of regions in the quark phase was sufficiently fast compared to the transport of baryon number across the surface separating the quark phase from the hadron phase. Whether this is the case has been questioned by Applegate and Hogan[6], who prefer a less extreme scenario leading to full conversion of the quark phase, but with resulting inhomogeneities in the hadron phase and subsequent interesting consequences for Big Bang nucleosynthesis. In view of our present knowledge of QCD-physics it seems fair to leave all possibilities open and pursue the consequences of primordial quark nuggets further. (In particular since the nugget hypothesis is one of the few dark matter explanations that allows the relative amounts of dark matter and ordinary baryonic matter to be calculated - at least in principle. Witten found that the relative amounts might work out right).

The mass-spectrum of primordial nuggets (if they are created) is poorly constrained. Witten estimated a very tentative most likely range $10^{33} < A < 10^{42}$. A reasonable upper bound is the mean baryon number within the horizon at the QCD-transition, $\approx 10^{49}$. A lower bound, $A \gtrsim 10^{20} \Omega_Q^3$, where Ω_Q is the present nugget density in units of the critical density, can be derived from Big Bang nucleosynthesis.[22] The efficiency of neutron absorption by nuggets means that many small nuggets present during nucleosynthesis could eat most neutrons, thus leaving no helium. A more thorough investigation of nucleosynthesis with nuggets is in progress.

Even if nuggets are created they do not necessarily survive until the present. Alcock and Farhi[1] argued that neutron and proton emission from the nugget surface at high temperatures would lead to evaporation of primordial nuggets with $A < 10^{52}$-10^{55}. Madsen, Heiselberg and Riisager[21],[15] showed, that nuggets with $A \gtrsim 10^{46}$ survived the evaporation as a consequence of significant reductions in the emission rates due to u and d quark depletion in the surface layers (the emission rate is controlled by competition between kaon and nucleon emission). They also showed that much smaller nuggets might survive due to reabsorption of hadrons, but a detailed study of this process was not possible. Alcock and Olinto[4] have recently proposed that all primordial nuggets boil away

in a manner that makes discussion of the surface evaporation irrelevant, unless the surface tension is rather high.

If nuggets survived from the Big Bang or were spread in our galaxy by secondary processes such as strange star collisions, there should be a potentially observable flux of nuggets hitting the Earth. De Rujula and Glashow[11] suggested "experiments" suitable for searching for these nuggets in the form of fast-moving meteors, special looking earthquakes, etchable tracks in ancient mica, etcetera. The only data actually investigated in their paper came from a nega-tive search for tracks in ancient mica, and corresponded to a lower nugget flux limit of $8 \times 10^{-19} \mathrm{cm}^{-2} \mathrm{s}^{-1} \mathrm{sr}^{-1}$, for nuggets with $A \gtrsim 1.4 \times 10^{14}$ (smaller nuggets are trapped in layers above the mica samples studied). For later comparisons it is useful to write this limit as an excluded region

$$1.4 \times 10^{14} \lesssim A \lesssim 8 \times 10^{23} \rho_{24} v_{250}, \tag{1}$$

where $v \equiv 250 \mathrm{kms}^{-1} v_{250}$ and $\rho \equiv 10^{-24} \mathrm{gcm}^{-3} \rho_{24}$ are the typical speeds and mass den-sity of nuggets in the galactic halo. (The speed is given by the depth of the gravitational potential of our galaxy, whereas $\rho_{24} \approx 1$ corresponds to the density of dark matter.) In these units the number of nuggets hitting the Earth per cm^2 per second per steradian is $6.0 \times 10^5 A^{-1} \rho_{24} v_{250}$.

Later investigations utilizing cosmic ray-, proton decay-, and gravitational wave-detectors have improved these flux limits somewhat. The most stringent Earth-based flux-limits[24] are shown in Figure 1 as curves a, b, c, and d. It will be shown in the following, that a significant improvement of these limits can be achieved using much larger and longer-lived "detectors", namely radio pulsars and their progenitors.[20]

II. GLITCHING RADIO PULSARS - NEUTRON STARS, NOT STRANGE STARS

Because of the importance of gravity, strange stars with masses in the region of observed neutron star masses are hard to distinguish from ordinary neutron stars in terms of their radius or total moment of inertia.[28],[14],[2],[3]

One important feature however seems to distinguish strange stars from neu-tron stars in a manner with observable consequences, and that is the distribu-tion of the moment of inertia inside the star. Ordinary neutron stars older than a few months have a crust made of a crystal lattice or an ordered inhomogene-ous medium reaching from the surface down to regions with density $2 \times 10^{14} \mathrm{gcm}^{-3}$. This crust contains about 1% of the total moment of inertia. Strange stars in contrast can only support a crust with density below the neutron drip density

$(4.3 \times 10^{11}\,\mathrm{g\,cm^{-3}})$. This is because free neutrons would be absorbed and converted by the strange matter. Such a strange star crust contains at most 10^{-5} of the total moment of inertia. This is an upper bound, since the strange star may have no crust at all, depending on its prior evolution.

As pointed out by Alpar[5], and also partly by others[14],[2], this difference in the moment of inertia stored in the crust of neutron stars and strange stars seems to pose significant difficulties for explaining the glitch-phenomenon observed in radio pulsars with models based on strange stars. Glitches are observed as a sudden speed-up in the rotation rate of pulsars. The fractional change in rotation rate Ω is $\Delta\Omega/\Omega \approx 10^{-6}\text{-}10^{-9}$, and the corresponding fractional change in the spin-down rate $\dot{\Omega}$ is of order $\Delta\dot{\Omega}/\dot{\Omega} \approx 10^{-2}\text{-}10^{-3}$. Regardless of the detailed model for the glitch phenomenon the jump in $\dot{\Omega}$ must involve the decoupling and recoupling of a component in the star containing a fraction $I_1/I \approx \Delta\dot{\Omega}/\dot{\Omega} \approx 10^{-2}\text{-}10^{-3}$ of the total moment of inertia. This role is played by the inner crust of an ordinary neutron star, but the crust around a strange star is much too small.

It therefore seems reasonable to conclude, that glitching pulsars must be ordinary neutron stars, not strange stars. Of course one might hope to invent a completely different model for strange star glitches[3], but with our present knowledge it does seem hard to circumvent the moment of inertia argument outlined above. We shall therefore assume that glitching pulsars are ordinary neutron stars.

If strange quark matter is stable, neutron stars can be converted to strange stars by a number of different mechanisms, such as pressure-induced transformation to uds-quark matter via ud-quark matter, sparking by high-energy neutrinos, or triggering due to the intrusion of a quark nugget.[2] As soon as a lump of strange matter comes in contact with free neutrons it starts converting them into strange matter. The burning of a neutron star into a strange star is therefore expected to take place on a rather small time-scale.[7],[23] The transformation may even involve a detonation.[16]

Independent of whether the conversion takes place as a slow combustion or as a detonation the time-scale is sufficiently short, that any neutron star hit by a quark nugget capable of penetrating to the neutron drip region will quickly transform into a strange star. Furthermore, if the progenitor star during its lifetime has captured even a single nugget in its core, a strange star will result from the supernova explosion. The existence of glitching pulsars, that are neutron stars, not strange stars, can therefore be used to place limits on the flux of galactic quark nuggets.[20] To do this we shall first investigate the accretion rate and capture of quark nuggets hitting neutron stars and their progenitors.

III. STELLAR ACCRETION AND CAPTURE OF NUGGETS

For an infinite bath of positive energy nuggets with an isotropic, monoenergetic distribution function, the number accretion rate of nuggets onto the surface of a star of mass M and radius R is given by

$$F = 1.39 \times 10^{30} \text{s}^{-1} \text{A}^{-1} \left[\frac{M}{M_\odot} \right] \left[\frac{R}{R_\odot} \right] \rho_{24} v_{250}^{-1} \left[1 + 0.164 v_{250}^2 \left[\frac{R}{R_\odot} \right] \left[\frac{M}{M_\odot} \right]^{-1} \right], \qquad (2)$$

where $M_\odot$ and $R_\odot$ denote the solar mass and radius.

For the Sun the second term in parenthesis (the geometrical term) contributes only slightly to the accretion rate, and the contribution is even less important for more massive stars and for compact objects like neutron stars. In the following we shall therefore only take the first term (gravitational) into account.

To convert a neutron star into strange matter a quark nugget should not only hit a supernova progenitor but also be caught in the core. Similarly, nuggets hitting a neutron star after its creation have to penetrate the outer layers and reach the neutron drip region. It is therefore important to consider the question of quark nuggets penetrating stars.

A nugget passing through matter will displace the matter in its path and suffer energy loss at a rate[11] $dE/dx = -\alpha \rho v^2$, where α is the effective surface area ($3 \times 10^{-16} \text{cm}^2$ for nuggets with $A < 10^{15}$ and $3 \times 10^{-26} A^{2/3} \text{cm}^2$ for $A > 10^{15}$ for interactions with charged matter; $3 \times 10^{-26} A^{2/3} \text{cm}^2$ for all A for interactions with neutrons), ρ is the density of the medium, and v is the speed of the nugget. At low energies the displacement of matter takes place via elastic or quasi-elastic collisions due to the positive electrostatic potential at the quark-surface of the nugget.

If x denotes the (positive) distance below the stellar surface and ε is the structural energy density of possible crystalline material, the motion of the nugget is described by the equation :

$$m(x)v(x)\frac{dv(x)}{dx} = -\alpha(x)\rho(x)v^2(x) + \frac{GM(x)m(x)}{R^2(x)} - \varepsilon(x)\alpha(x) \qquad (3)$$

where R and M are the stellar radius and mass interior to that radius.

The first term on the right-hand-side of equation (3) describes the drag force due to removal of the mass $\alpha \rho dx$ encountered when moving the distance dx. The second term is gravity, and the third term is the structural resistance of an ionic lattice ($\varepsilon = 0$ except in white dwarfs and neutron star crusts; in these systems it will be approximated by $\varepsilon(x) \approx n_i Z_i^2 e^2 / a_i \approx 1 \times 10^{13} \text{ergcm}^{-3} \rho^{4/3} Z_i^2 A_i^{-4/3}$, where n_i and a_i denote number density and lattice

spacing of ions with mass number A_i and charge Z_i).

The initial velocity $v(0)$ is mainly caused by gravitational acceleration of the nugget, $v(0) \approx (2GM/R)^{1/2}$. For the Sun $v(0) \approx 617 \mathrm{kms}^{-1}$, and it is higher for more massive main sequence stars and for compact objects. This means that nuggets to a good approximation can be assumed to move on radial trajectories. Nuggets hitting neutron stars are accelerated to kinetic energies of order 200 MeV per baryon, leading to inelastic collisions with ions (and of course with neutrons). We shall neglect relativistic corrections to the equations of motion, but will return to other consequences of the large impact energy later.

The solution of equation (3) is discussed elsewhere.[20] The important point here is that nuggets are stopped after sweeping up a mass comparable to their own. This happens for $A \leq A_{\mathrm{stop}}$, where

$$A_{\mathrm{stop}} = \begin{cases} 5.8 \times 10^{-6} D^3 & A \gtrsim 10^{15} \\ 1.8 \times 10^8 D & A \lesssim 10^{15} \end{cases} \tag{4}$$

with column density $D \equiv \int_0^x \rho(x)dx$.

IV. CAPTURE IN PRE-SUPERNOVA STARS

The total column density encountered by a nugget moving the distance $2R$ on a radial orbit through a star described by a $\gamma = 4/3$ polytrope is $5.0M/R^2$, so that $A_{\mathrm{stop}} \approx 5.0 \times 10^{31}(M/M_\odot)^3(R/R_\odot)^{-6} \approx 5.0 \times 10^{31}(M/M_\odot)^{-1.8}$, where the last equality comes from $R \sim M^{0.8}$ for upper main sequence stars. Nuggets with $A > A_{\mathrm{stop}}$ pass unhindered through main sequence stars, whereas nuggets with $A \ll A_{\mathrm{stop}}$ are effectively stopped and will settle near the center.

The Sun would in this way accrete $3.7 \times 10^{-20} \rho_{24} v_{250}^{-1} M_\odot$/year, or a total of $10^{-10} \rho_{24} v_{250}^{-1} M_\odot$ in its total lifetime on the main sequence. Very low-mass nuggets collected near the solar center in this manner might have an impact on the energy production,[17] but the effect is negligible unless the electrostatic barrier at the nugget surface is much smaller than expected, or unless very special circumstances allow nuggets to catalyze nuclear reactions.[26] It was originally suggested to study the impact of quark nuggets on solar structure and in particular on solar oscillations[19], but according to Thompson[27] the mass of a quark nugget core in the Sun must exceed 10^{-4}-$10^{-3} M_\odot$ before the dramatic change in the central gravitational potential of the Sun leads to observable consequences with the present quality of helioseismological data. This mass limit is orders of magnitude above the maximally accreted mass of nuggets in the solar lifetime, so

solar oscillations are only capable of tracing a strange matter core (or neutron star) in the Sun in the rather unlikely case where the Sun formed by condensation around a pre-existing very massive nugget. The situation may improve if g-mode oscillations probing the central parts of the Sun are observed.

In any case the results of the present investigation rule out that the Sun has accreted any nuggets at all in its lifetime.

Conversion of a neutron star into a strange star will happen if even a single nugget is present near the stellar center at the time of neutron star formation. According to equation (2) a nugget has hit the star if $Ft > 1$, or $A < A_1$, where

$$A_1 = 4.4 \times 10^{37} (t/\text{years})(M/M_\odot)(R/R_\odot)\rho_{24} v_{250}^{-1}. \tag{5}$$

Approximating the main sequence lifetime of massive Population I stars by $t_{MS}(\text{years}) \approx 3.7 \times 10^9 (M/M_\odot)^{-1.9}$, it follows that $A_{\text{stop}} \ll A_1$ for $\rho_\infty \gg \rho_{\min} \approx 3.0 \times 10^{-40} \text{g cm}^{-3}(M/M_\odot)^{-1.7} v_{250}$, so that A_{stop} is the relevant capture limit. For $\rho_\infty < \rho_{\min}$ the capture limit is $A < A_1 \approx 1.6 \times 10^{47}(M/M_\odot)^{-0.1}\rho_{24} v_{250}^{-1}$.

The total column density of a star increases when it leaves the main sequence, due to central density concentration. Immediately prior to a supernova explosion of Type II, the central region of a massive Population I star resembles a $\gamma = 4/3$ white dwarf with $M_{\text{cent}} \approx 1.4 M_\odot$ and $R_{\text{cent}} \approx 10^{-2} R_\odot$, corresponding to $A_{\text{stop}} \approx 10^{44}$. Since in this case $A_{\text{stop}} \gg A_1$, the neutron star will contain quark nuggets if nuggets with $A < A_1 \approx 10^{35} \rho_{24} v_{250}^{-1}$ are present in our Galaxy. Nuggets with slightly higher baryon number may be caught between the main sequence phase and the explosion.

For the pre-supernova rates of nugget capture to be used for limiting the nugget flux, the nuggets must survive in the stellar core during the explosion, so that they are available for converting the nuclear matter to strange matter. As discussed in section I, quark nuggets in the early Universe may evaporate partially by emission of hadrons (mainly neutrons, protons and kaons) from a thin surface layer. A similar effect might be expected in the hot interior of a (proto-)neutron star during the initial stage of a supernova explosion. Temperatures may reach 10-30 MeV for a few seconds following core collapse, resulting in high surface emission rates of hadrons. Formation of a strange star would be prevented if nuggets could dissolve.

However due to the extreme density of the nucleon gas surrounding the nugget, no such evaporation takes place. On the contrary, net neutron absorption by the nugget is quickly initiated. To see this one may compare the rates of neutron emission, λ_{em}, and neutron absorption, λ_{abs}, per nugget in the neutron star. These rates are (for a non-degenerate gas)[21]

$$\lambda_{em} = \frac{2m_n(kT)^2}{\pi\hbar^3}e^{(\mu_n-m_n)/kT}r^2 \tag{6}$$

$$\lambda_{abs} = n_n v_n 4\pi r^2 = \frac{\rho_n}{m_n}\left[\frac{kT}{2\pi m_n}\right]^{1/2}4\pi r^2, \tag{7}$$

where m_n, v_n, ρ_n and n_n are the neutron mass, speed perpendicular to the nugget surface, mass density and number density respectively. The radius of the quark part of a nugget is r, and μ_n is the neutron chemical potential given as $\mu_n = \mu_u + 2\mu_d$, where μ_u and μ_d are the up and down quark chemical potentials in the nugget surface layer.

Thus the ratio of the rates is independent of r,

$$\frac{\lambda_{em}}{\lambda_{abs}} = \frac{m_n^{5/2}(kT)^{3/2}}{2^{1/2}\pi^{3/2}\rho_n\hbar^3}e^{(\mu_n-m_n)/kT}$$

$$= 7.94\times10^{-3}\left[\frac{T}{MeV}\right]^{3/2}\left[\frac{10^{14}\text{gcm}^{-3}}{\rho_n}\right]e^{(\mu_n-m_n)/kT} \tag{8}$$

In the limit where the effective neutron binding energy, $I_n = m_n - \mu_n$, goes to zero one finds that $\lambda_{em} < \lambda_{abs}$ for $T \lesssim 40\text{MeV}$, assuming $\rho_n \gtrsim 2\times10^{14}\text{gcm}^{-3}$. Thus nuggets present grow rather than evaporate.

In case of complete degeneracy the neutron absorption rate is increased relative to the non–degenerate rate by the factor $(3\pi^{1/2}/8)\left[\varepsilon_F/kT\right]^{1/2}$, where $\varepsilon_F \approx 30\text{MeV}\left[\rho_n/10^{14}\text{gcm}^{-3}\right]^{2/3}$ is the neutron Fermi–energy. At the same time the emission–rate of neutrons is decreased since the low–energy part of neutron phase space is occupied. The emission rate of protons is not influenced in the same amount by phase space blocking, so it is more relevant to compare the (non–degenerate) proton emission rate with the (degenerate) neutron absorption rate. In any case the conclusion is unchanged : Nuggets absorb nucleons faster than they are emitted, even at the high temperatures in proto–neutron stars.

Whether nuggets are stable at $T \approx 10\text{-}30\text{MeV}$, or whether it is energetically favorable to dissolve nuggets into a gas of hadrons, is another matter that depends on poorly constrained QCD–parameters. Studies of this question for bulk quark matter in weak equilibrium indicate, that stability is probably retained, assuming stability at $T=0$, $P=0$, especially at the high pressures present in neutron star interiors.[10]

Thus it seems, that nuggets absorbed by a pre–supernova star are able to survive the heating of the stellar interior during the explosion.

V. CAPTURE IN NEUTRON STARS

A nugget capable of reaching layers in a neutron star with densities exceeding the neutron drip density ($4.3 \times 10^{11} \text{gcm}^{-3}$) will convert the neutron star to a strange star. An upper bound to the baryon number of nuggets hitting a neutron star of age t is given by equation (5), but several events may hinder the nugget from ever reaching the free neutrons.

Neutron stars are too hot to build up a solid crust during the first few months of their lifetime. In this molten phase $\varepsilon = 0$, and any nugget hitting the star and surviving the impact will convert it to strange matter. An upper bound to the baryon number of nuggets hitting the star in this phase of its life is $A < A_1 \approx 6.3 \times 10^{32} (t_m/\text{years})(M/M_\odot) R_{10} \rho_{24} v_{250}^{-1}$, where t_m is the duration of the molten phase, and R_{10} is the neutron star radius in units of 10km. A lower bound on A stems from the stopping of small nuggets by the expanding supernova shell: $A_{\min} = 4.6 \times 10^{10} (M_{sh}/M_\odot) v_{250}^{-2} (t_m/\text{years})^{-2} \approx 10^{12}$.

Whether these nuggets can convert the neutron star into strange matter depends crucially on their ability to survive the collision with the neutron star. Due to the strong gravitational potential, nuggets reach the star with kinetic energies of order $200A$ MeV. Therefore the collisions with ions (and in deeper layers with neutrons) are inelastic. Ions easily penetrate the electrostatic barrier of a nugget, until the nugget has lost most of its kinetic energy. As $A_{stop} \gg A_1$ nuggets are stopped above the neutron drip layer, and they absorb a mass comparable to their initial mass during the stopping.

The absorption of ions destabilizes the nuggets in two ways. First the nuggets are significantly heated, which reduces their stability. Secondly ion absorption increases the amount of u and d quarks relative to s quarks, which also reduces the stability. A detailed study of the kinetics of such collisions has not been attempted, but consideration of the time-scales involved gives an impression of the physics involved.

Let us concentrate on large nuggets ($A > 10^{15}$) hitting neutron stars with $R_{10} = M/M_\odot = 1$. For these the stopping time-scale, t_{stop}, can be approximated as $t_{stop} \approx x_{stop}/v(0) \approx 2.92 \times 10^{-12} \text{s} A^{2/15}$. Quarks moving at the speed of light inside nuggets at temperature T can equilibrate the temperature across a nugget radius on the diffusion time-scale $t_{diff} \approx 10^{-28} \text{s} A^{2/3} T_{MeV}^2$. One notes that t_{diff} exceeds t_{stop} as long as $A > 10^{31} T_{MeV}^{-15/4}$, which means that heat is distributed inefficiently through a large, hot nugget (t_{diff} is an increasing function of T because Pauli blocking prevents scattering at low temperatures).

The neutrino emissivity of strange matter is of order $2 \times 10^{31} T_{MeV}^8 \text{ergcm}^{-3}\text{s}^{-1}$.[13] This cooling rate is much too low to remove the heat

distributed in a nugget when the nugget loses $200A$MeV of kinetic energy in a time t_{stop}.

A hot nugget emits hadrons, in particular neutrons, from the surface. With the emission rate λ_{em} given from equation (6) an estimate of the evaporation time of a nugget is $t_{em} = A/\lambda_{em} = 4.3 \times 10^{-20} s A^{1/3} T_{MeV}^{-2} \exp(I_n/kT)$. For typical neutron star parameters t_{em} is small compared to t_{stop} as long as $A < 1.3 \times 10^{39} T_{MeV}^{10} \exp(-5I_n/kT)$. This comparison assumes isotropic emission from an isothermal nugget, but it seems clear, that significant evaporation will take place for nuggets in the mass-range likely to hit young neutron stars.

The most likely outcome of the inelastic collisions involved when nuggets are stopped in the outer layers of a neutron star is, that the nugget is severely damaged. It probably starts to disintegrate, beginning in the direction of motion. However since characteristic weak interaction time-scales are long compared to t_{stop} for $A \lesssim 10^{35}$-10^{40} a large number of s-quarks have to be incorporated in the fragments, so it is quite possible, that smaller lumps of strange matter are among the disintegration products.

Only a small fragment of a nugget has to survive in order to finally convert a molten neutron star, so it seems likely that the nugget flux limit derived for molten neutron stars is relevant in spite of (partial) disintegration.

The situation is more uncertain when it comes to neutron stars older than a few months. After the crust solidifies, it becomes difficult for a nugget to reach the region where free neutrons are available for conversion. The column density of the 5×10^{28}g solid crust above the neutron drip region is $D_{crust} \approx 4 \times 10^{15}$ gcm^{-2}. Only nuggets with $A > A_{stop} \approx 4 \times 10^{41}$ penetrate this outer crust freely. Smaller nuggets are slowed down and perhaps destroyed. Fragments will only be able to reach the neutron drip region if gravity exceeds lattice resistance for fragments surviving collision. This happens for $A_f > 2.5 \times 10^{36} \varepsilon_{28}^3 (M/M_\odot)^{-3} R_{10}^6$, where A_f is the baryon number of surviving nugget fragments. For neutron star age t this excludes nuggets with $10^{36} \lesssim A_f \lesssim A \lesssim 10^{33} (t/\text{years}) \rho_{24} v_{250}^{-1}$. For the glitching pulsars Crab and Vela we may use $t \approx 10^3$ and 10^4 years respectively. (The age of Vela has recently been questioned[8]). Strong glitches have been observed in the pulsar PSR0355+54, which has a characteristic age derived from its period and period derivative of 6×10^5 years.[18] Assuming the characteristic age to be a good measure of the true age, PSR0355+54 excludes the highest A-values. Higher values of A may be excluded if glitches are found in those millisecond pulsars, which are presumably old neutron stars spun up by accretion from a binary companion.
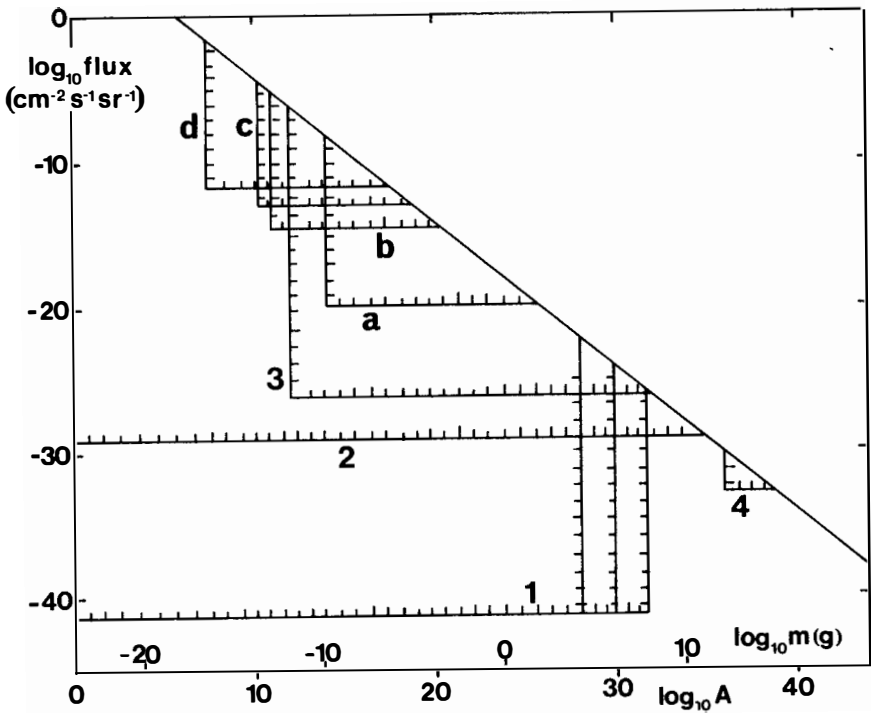
Figure 1 :

Limits on the flux of nuggets reaching the Earth as a function of nugget mass and baryon number. Regions on the hatched side of lines are excluded. Curves a, b, c, and d are the best Earth-based limits[24]. Curves 1 correspond to nugget capture in the main sequence phase of supernova progenitors with masses of 100, 10, and $1 M_\odot$. Curve 2 shows capture in supernova progenitors after the main sequence phase. The area surrounded by curve 3 is excluded by nugget capture during the molten neutron star phase, provided that just a tiny lump of strange matter survives the impact. Finally the region denoted by 4 is excluded by capture in the solid crust neutron star phase for the pulsar PSR0355+54, provided that nugget fragments with baryon number exceeding 10^{36} survive the impact. The diagonal curve is the upper flux limit corresponding to the galactic dark matter. Astrophysical limits are shown for $v_{250}=1$.

VI. CONCLUSIONS

Figure 1 illustrates limits on the flux of quark nuggets hitting the Earth (or rather its upper atmosphere). Curves a-d are the best ground-based detector-limits,[24] and the curves 1-4 show the astrophysical limits derived here and in ref.20). The diagonal curve is an upper flux limit given by the total density of galactic dark matter.

Most of the astrophysical flux-limits depend on the parameter $\rho_{24} v_{250}^{-1}$, which enters in the gravitational accretion rate in equation (2). Limits derived with Earth-based detectors depend on the geometrical accretion term, which is proportional to $\rho_{24} v_{250}$. The astrophysical limits in Figure 1 have therefore been plotted assuming $v_{250} = 1$.

Throughout the investigation it has been assumed that only nuggets with a single value of A contributed to the flux. If a distribution of A-values is involved the *upper limits* on excluded A at a given $\rho_{24} v_{250}^{-1}$ remain valid if the density is hidden in nuggets with a distribution of A below that limit, but above the *lower limit*, when that exists. If the distribution extends to values of A exceeding the upper boundaries of the excluded regions, the density ρ_{24} should be interpreted as the density contribution from nuggets in the excluded region.

With these reservations it is easily seen from the figure that the astrophysical nugget flux-limits are many orders of magnitude better than those derived from experiments on Earth. Neutron stars and their progenitors are very sensitive quark nugget detectors.

The dark halo around our Galaxy is expected to have $\rho_{24} v_{250}^{-1} \approx 1$, so Earth-based experiments exclude nuggets with $3 \times 10^7 \lesssim A \lesssim 5 \times 10^{25}$ as being responsible for the dark matter. For comparison capture in pulsar progenitors during the main sequence phase excludes $A \lesssim 10^{30}$. Stopping of nuggets in the giant phase rules out $A \lesssim 10^{35}$. Capture during the molten phase of the neutron star life could exclude $10^{12} \lesssim A \lesssim 10^{32}$ if a tiny fraction of the incident nugget survives the collision, and capture in solid crust neutron stars may exclude nuggets as large as $A \lesssim 6 \times 10^{38}$, if the age of PSR0355+54 is estimated correctly, and if fragments with baryon number $A_f \gtrsim 10^{36}$ survive. Only very large nuggets may explain the dark matter.

The pulsar glitch argument excludes nuggets with $A \lesssim 10^{28}$ even at fluxes 18 orders of magnitude below that of the halo dark matter, since these nuggets would have been absorbed by the neutron star progenitor in its main sequence phase. At even lower fluxes the excluded region due to main sequence capture is approximately $A \lesssim 10^{47} \rho_{24} v_{250}^{-1}$. This seems to rule out the suggestion[26] that nuggets of very low A accreted in the Sun could catalyze nuclear reactions,

thereby reducing the solar neutrino problem. If such nuggets were around in our Galaxy they would have been accreted by neutron star progenitors as well.

Furthermore the very existence of strange stars may be questioned on the basis of these flux-limits. If strange stars exist our Galaxy almost inevitably contains a background flux of quark nuggets due to mass ejection in strange star collisions (in systems like the binary pulsar). A single event releasing $0.1M_\odot$ of nuggets would correspond to a mean density in the galactic disk of $10^{-35} \mathrm{gcm}^{-3}$ under the (rather unlikely) assumption that the nuggets are spread evenly in the disk. At this density and even at densities of $10^{-42} \mathrm{gcm}^{-3}$ nuggets with $A \lesssim 10^{28}$ are excluded. Thus strange stars probably never existed in compact binaries unless most of the nuggets spread by stellar collisions have $A > 10^{28}$, or the orbits of the nuggets avoid the galactic disk.

Quark nuggets have been suggested as candidates for the Centauro cosmic-ray events. Centauro primaries may have a flux as high as $10^{-14} \mathrm{cm}^{-2}\mathrm{s}^{-1}$ and $A \approx 10^3$. Since Centauro primaries move at relativistic speeds they are destroyed by inelastic collisions when hitting a star, so the flux-limits given in this paper cannot directly be used to rule out quark nuggets as Centauro primaries. However the mechanism producing the primaries must be tuned so that it only produces relativistic quark nuggets in order not to conflict with the flux-limits for non-relativistic nuggets. Similar arguments constrain attempts[7] to invoke nuggets in explanations of cygnets.

In summary the allowed occurrence of quark nuggets in our Galaxy is very tightly constrained. Only very massive nuggets remain possible dark matter candidates. A suggestion for solving the solar neutrino problem is ruled out, and some restrictions are set on models trying to explain Centauro primaries or cygnets as quark nuggets. The very existence of strange stars is questioned, at least as members of systems resembling the binary pulsar. The lack of strange stars may be taken as an indication that strange matter is *unstable* in bulk. This would have significant implications for the range of QCD-parameters allowed.

The basic assumption underlying these conclusions is, that pulsar glitches can not occur in strange stars. This assumption seems to be well motivated. Should a mechanism for glitches in strange stars nevertheless be shown to work, the conclusions mentioned above would not hold. No limits on the galactic flux of quark nuggets could then be set from the glitch argument, but the "excluded region" in Figure 1 could then instead be interpreted as the combinations of nugget flux and baryon number capable of converting *all* neutron stars into strange stars. Some of the flux limits presented above may in fact still be applicable (regardless of the validity of the glitch argument) if the consequences of neutron star conversion turn out to be more dramatic than any

events observed. This may in particular be the case if a detonation rather than a slow combustion is involved.

Thanks are due to the organizers for a very interesting workshop.

REFERENCES

1) Alcock, C., and Farhi, E. 1985, *Phys. Rev.*, D32, 1273.
2) Alcock, C., Farhi, E., and Olinto, A. 1986a, *Ap. J.*, 310, 261.
3) Alcock, C., and Olinto, A. 1988, *Ann. Rev. Nucl. Part. Sci.*, 38, 161.
4) Alcock, C., and Olinto, A. 1989, *Phys. Rev.*, D39, 1233.
5) Alpar, M. A. 1987, *Phys. Rev. Letters*, 58, 2152.
6) Applegate, J. H., and Hogan, C. J. 1985, *Phys. Rev.*, D31, 3037.
7) Baym, G., Kolb, E. W., McLerran, L., Walker, T. P., and Jaffe, R. L. 1985, *Phys. Letters*, 160B, 181.
8) Bignami, G. F., and Caraveo, P. A. 1988, *Ap. J. (Letters)*, 325, L5.
9) Brügger, M., *et al.* 1989, *Nature*, 337, 434.
10) Chmaj, T., and Slominski, W. 1987, preprint.
11) De Rujula, A., and Glashow, S. L. 1984, *Nature*, 312, 734.
12) Farhi, E., and Jaffe, R. L. 1984, *Phys. Rev.*, D30, 2379.
13) Haensel, P. 1987, *Acta Phys. Pol.*, B18, 739.
14) Haensel, P., Zdunik, J. L., and Schaeffer, R. 1986, *Astr. Ap.*, 160, 121.
15) Heiselberg, H., Madsen, J., and Riisager, K. 1986, *Physica Scripta*, 34, 556.
16) Horvath, J. E., and Benvenuto, O. G. 1988, *Phys. Letters*, 213B, 516.
17) Jändel, M. 1988, *Z. Phys.*, C40, 599.
18) Lyne, A. G. 1987, *Nature*, 326, 569.
19) Madsen, J. 1986, in *Second ESO-CERN Symposium - Cosmology, Astronomy and Fundamental Physics*, ed. G. Setti and L. Van Hove (München: ESO), p. 279.
20) Madsen, J. 1988, *Phys. Rev. Letters*, 61, 2909.
21) Madsen, J., Heiselberg, H., and Riisager, K. 1986, *Phys. Rev.*, D34, 2947.
22) Madsen, J., and Riisager, K. 1985, *Phys. Letters*, 158B, 208.
23) Olinto, A. V. 1987, *Phys. Letters*, 192B, 71.
24) Price, P. B. 1988, *Phys. Rev.*, D38, 3813.
25) Reinhardt, H., and Dang, B. V. 1988, *Phys. Letters*, 202B, 133.
26) Takahashi, K., and Boyd, R. N. 1988, *Ap. J.*, 327, 1009.
27) Thompson, M. J. 1987, Ph.D. thesis, Cambridge (unpublished).
28) Witten, E. 1984, *Phys. Rev.*, D30, 272.

Constraints on Cosmological Parameters from High-Redshift Galaxies

B. ROCCA–VOLMERANGE[1,2] and B. GUIDERDONI[1]
1-Institut d'Astrophysique du CNRS, Paris, 75014, France
2-Université de Paris XI, F-91405 Orsay-Campus

Abstract
    Stellar populations of galaxies have been detected on a large scale of distances till cosmological ones. Hubble diagrams, color diagrams from $z=0$ to 2, energy distributions of extreme high-z galaxies (up to redshifts $z \geq 3$) are used as constraints of models describing the evolution of star formation for distant galaxies. Ages and epoch of formation of these high-z galaxies are estimated and an approach of cosmological parameters is then possible from a lower limit for the age of the Universe. Our analysis of the set of present observables converges to old (≥ 17Gyrs) galaxies and an old Universe. As a consequence, cosmological parameters such as the Hubble constant $H_0 \simeq 50$ km s^{-1} Mpc^{-1} and the density parameter $\Omega_0 \simeq 0.1$ appear to be extremely low. For the future, several ways must be pursued: i) to understand if our galaxy samples are homogeneous. More specifically do different parameters (metallicity, dust, merging process,..) rule evolution of the reddest galaxies? ii) to analyse the sensitivity of our present results to the models. What would become these galaxy ages if ages of the stellar clusters change? For the first time, observational cosmology can be approched from the lower part of redshift up to primeval epochs. The stake of such an analysis is sufficient to explore in details its ins and outs.

I. Introduction

Distant galaxies open a new era for understanding the main steps of galactic evolution and for discovering the earliest populations of galaxies until possibly the primeval galaxies. When galaxies are observed at such remote epochs, their appearances are affected by at least two simultaneous effects which are respectively a cosmological effect and the intrinsic evolution of their stellar populations younger than our nearby galaxies in an Universe in expansion. A fundamental problem is to disentangle respective contributions of these two effects. Other effects could also modify appearance of galaxies as interaction with environment, amplification by gravitational lensing, etc.. They will be also taken into account if necessary. We briefly recall the basic principles of our approach of galactic evolution, already given in several papers (see review by Rocca-Volmerange and Guiderdoni, 1989 and references therein). Our atlas of synthetic galaxies (Rocca-Volmerange and Guiderdoni, 1988), based on the recent version of our models (Guiderdoni and Rocca-Volmerange, 1987) fits at the present epoch the Hubble Sequence by standard scenarios of evolution . Comparisons of the synthetic spectra with observations are given. Only a significant fit of these spectra with observations justifies to use them as reference spectra to calculate cosmological (k-) and evolutionary (e-) corrections which affect the apparent magnitudes of distant galaxies relatively to the nearby ones. Several observational independent tests at high-z are possible: magnitude or color versus z diagrams, and stellar energy distribution of the most distant galaxies ($z \geq 3$). We shall use these tests as clues for the main questions:
-Do high-z galaxies confirm the scenarios of galactic evolution proposed for fitting nearby galaxies?
- Can Hubble diagrams give an estimate of the deceleration parameter q_0?
-What ages are given from a comparison of observations with models?
-What are the most influent parameters on the age estimates?
-Is it significantly possible to induce an age of the Universe and to approach the cosmological parameters?

II. Evolution of high-z galaxies

i) The samples
Intense star formation in distant galaxies is detected through their stellar energy distribution from far–UV to infrared or from the emission lines emitted by the gas excited by energetic photons of massive stars. Star formation activity can follow a coherent continuous scenario of galactic evolution, implicitly depending upon the total mass and stimulated by a gaseous environment. It can also be affected by some randomly distributed interactions with other galaxies or be triggered by a strong radio activity. To analyse the homogeneity of our samples,we shall separately consider galaxies in clusters, field galaxies as the sample of Koo's 1986 or those analysed by Guiderdoni and Rocca-Volmerange, 1989 and in this

conference, and radiogalaxies from the 3CR and Parkes catalogues, as infiuence of the radio power may possibly modify their star formation activity (Mc Carthy et al, 1989). Optical counterparts of the 3CR radiogalaxies until z≃2 (see reviews from Spinrad, 1987, 1988 and Djorgovski, 1987 and references therein) with extreme Lyman α equivalent widths (≥ 1000Å) are firstly considered as well as the most recently discovered but rare extreme high-z galaxies from Lilly,1988 at z=3.395 and Miley and Chambers,1988 at z=3.8. Then the Parkes Selected Region sample for which Dunlop et al, 1989a gave the optical and infrared counterparts, consists of fainter radio luminosity galaxies, which are compared to our models (Dunlop et al, 1989b).

ii)Modelisation

As presented in several papers and reviews, the main free parameter of our evolutionary models is the star formation rate (SFR(m,t)=τ_*(t) Φ(m)), which is assumed to be depending upon a star formation history τ_*(t) and the initial mass function (IMF) Φ(m)= m^{-x}. In the present version of our models, IMF is constant with an index x=0.25, 1.35 and 1.7 respectively between the limits 0.1$M_\odot$,1$M_\odot$,2$M_\odot$ and 80$M_\odot$ based on Scalo, 1986 analysis and star formation laws describe 8 different morphological types of the Hubble sequence (Elliptical to Irregular) from far–UV to visible, with bursts or continuousscenarios varying with the gas content. Table 1 gives the adoptedscenarios and time scales t$_*$ (Guiderdoni and Rocca–Volmerange, 1987, hereafter GRV). The correspondence with gas density $g(t)$, B-V and morphological type is also given.

$\tau_*(t)$ $M_\odot \, \mathrm{Gyr}^{-1} \, M_\odot^{-1}$	t_* Gyr	age Gyr	$B - V$	"average" type
1 Gyr burst	0.63	17.4	0.88	red envelope
exp $-t$	1.0	13.2	0.97	UV–cold E/SO
1$g(t)$	0.9	13.2	0.92	UV–hot E/SO
0.4$g(t)$	2.2	12.5	0.74	Sa
0.3$g(t)$	3.0	12.5	0.66	Sb
0.1$g(t)$	9.0	12.5	0.51	Sc
0.060	10.5	12.5	0.45	Sd
7.7 $10^{-4}t^2$	13.5	12.5	0.35	Im

TABLE 1

The model is essentially based on input data which are the stellar evolutionary tracks in the Hertzprung-Russell diagram and the library of stellar spectra. The star population forms from the Zero-Age-Main-Sequence and evolves as a function of time along the tracks. At each time, a stellar spectrum of the library can be assigned to any star and a composite spectrum of a synthetic galaxy is computed. We hereafter present results issued from the adopted set of input data as described in GRV. The sensitivity of such results to parameters is most important. It will be discussed below and in further papers. From now, stellar library is essentially observational from IUE satellite atlases in UV (Wu et al, 1983, Heck et al, 1983) and the visible atlas from Gunn and Stryker, 1983. The stellar tracks are derived from internal structure models and atmosphere models fitted

on the main properties of the globular and open clusters. Tracks compiled in our present models are based on the Yale isochrones, Becker, 1981 and Maeder,1981 for massive stars. The first point to emphasize is the time duration of various phases of stellar evolution. These times may vary from one track set to another and they affect the estimated ages of the clusters as well as those of galaxies. Due to the age-metallicity relation, ages are also depending on the metal content which modifies lifetimes of stars as well as the effective temperatures of the giant branches. We successively adopt a fit on globular clusters (Cohen et al, 1978) for the metal-deficient populations (Rocca-Volmerange et al, 1981) till the Yale isochrones for normal populations (Sweigart and Gross, 1978).

iii) Outputs of models

An Atlas of synthetic spectra of galaxies (Rocca-Volmerange and Guiderdoni, 1988, RVG), based on scenarios of evolution for 8 morphological types to simulate the Hubble Sequence is computed. An exemple is given on Figure 1.

FIGURE 1: Stellar energy distribution from far-UV to IR emitted during and after a burst 1Gyr at various ages (0.4 Gyr to 17.4 Gyr) in relative units. Absorption lines and nebular emission lines are indicated.

Caracteristics of the Atlas are:
- a wavelength range 200Åto 2.5µm
- a resolution $\Delta\lambda=10$Å from 1200Åto 1µm.
- a time step $\Delta t \simeq 1$ Gyr.

These spectra are used to calculate cosmological and evolutionary corrections(respectively k- and e- corrections). which allow to predict apparent magnitudes and colors of distant galaxies according to:

$$m_\lambda(z) = M_\lambda(0) + (m-M)_{bol}(z) + k_\lambda(z) + e_\lambda(z)$$
$$c_\lambda(z) = C_\lambda(0) + k_{\lambda,c}(z) + e_{\lambda,c}(z)$$

with $M_\lambda(0)$ and $C_\lambda(0)$ respectively the intrinsic magnitude and color at the present epoch.

These corrections are published in tables (RVG) for these 8 morphological types and a large range of z (Table 2). Also apparent magnitudes and colors have been computed through Johnson's photometric system and the Space Telescope filters (Guiderdoni and Rocca-Volmerange, 1988).

burst

z	V k	U k	B k	V e	U e	B e
0.000	0.00	0.00	0.00	0.00	0.00	0.00
0.050	0.07	0.24	0.23	0.04	-0.08	-0.03
0.100	0.15	0.49	0.48	0.09	-0.15	-0.06
0.150	0.24	0.75	0.74	0.12	-0.23	-0.09
0.200	0.36	1.03	0.99	0.11	-0.31	-0.15
0.300	0.72	1.69	1.45	-0.04	-0.57	-0.34
0.400	1.15	2.43	1.90	-0.30	-0.89	-0.58
0.600	1.92	3.65	2.91	-0.73	-1.78	-1.07
0.800	2.65	4.72	3.98	-1.27	-2.91	-1.90
1.000	3.52	5.94	4.93	-1.97	-3.60	-3.03
1.200	4.39	6.30	5.85	-2.73	-3.83	-4.17
1.400	5.18	6.16	6.68	-3.66	-2.91	-4.47
1.700	6.25	6.37	7.30	-4.84	-2.05	-4.72
2.100	7.58	8.28	7.40	-5.27	-3.80	-3.99

TABLE 2:
k-corrections and e-corrections calculated through the VUB bands of Johnson system and a 1 Gyr burst. Cosmolgical parameters are $H_0 = 50$ km s^{-1} Mpc^{-1} and the density parameter $\Omega_0 = 0.1$. RVG give other photometric systems and cosmology.

III. Ages of galaxies

A comparison of observations (spectra or colors) with the synthetic stellar energy distributions gives ages of the stellar population. We present some estimates from the present version of our models (GRV) and shall discuss these results in section V. Due to the large extent of redshift $z=0$ to 3.5 for the observed samples, emissivity appears in visible to be dominated by various subpopulations of stars: old giant stars in nearby galaxies to young massive stars in extremely distant galaxies, including these two types in intermediate -z populations showing significant effects of evolution. The so-called ages correspond with the time duration elapsed from the first stars formed until to the current time when the galaxy is observed. Ages cannot be separated from metallicity considerations. In the following, we shall assume an about half-solar to solar metallicity for the evolved galaxies and we shall discuss the implications of such an assumption.

i) The Hubble Sequence

Color-color diagrams from far-UV to visible colors (GRV) and stellar energy distribution of ellipticals (Rocca-Volmerange, 1989) fit models with an 12-13 Gyr age for most galaxies. Similar ages are obtained by fitting spirals of the A370 cluster from Mellier et al, 1987. Spectral comparisons are in Rocca-Volmerange and Guiderdoni, 1989.
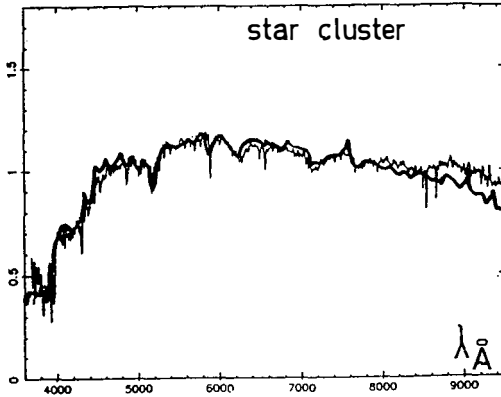
FIGURE 2: Comparison of the observed stellar globular cluster (Bica and Alloin, 1986) of 16.5 Gyr (thin line) age to our burst model at 17 Gyr (thick line).

The older population of the globular cluster spectrum with a metallicity $[Z/Z_\odot]$=-0.4 observed by Bica and Alloin, 1986 is compared to our burst model for a roughly half solar metallicity (figure 2). The estimated age 17Gyr is quite comparable to the age 16.5 Gyr adopted for this cluster by the observers. Note that these ages are essentially based on Yale tracks. It will be important to have new estimates by the more recent VandenBerg, 1985 tracks.

ii) Hubble and color-z diagrams

In visible as in infrared, such diagrams are statistically meaningful. A color is not significantly dependent on the distance modulus and only in a differential way on the effect of extinction. Moreover there is no evidence that an amplification effect by gravitational lens modifies colors of galaxies. Blue to red colors extended up to $z \simeq 2$, are compared with our models. They show that an evolution effect does exist for $z \geq 0.7$. This evolution effect is higher in blue than in red colors (Guiderdoni and Rocca-Volmerange, 1988, Dunlop and Longair, 1987). Diagrams have been analysed for cluster galaxies (Dressler and Gunn, 1983) as well as for the deep samples from Koo, 1986 in GRV, 1988 (figure 3a). The analysis of the Parkes Selected Region Sample with our models is also proposed by Dunlop et al, 1989b.

Galaxies of these samples are well fitted in various colours by models of 13Gyr age and the 8 scenarios of evolution. However in all samples, an important part of the reddest galaxies including the Bright Cluster Members are not fitted (figure 3a) by our 13 Gyr models. GRV,1988 and Dunlop et al, 1989b propose an interpretation of this excess by an age effect. An old giant population (≥ 17Gyr) is a possible explanation of such red colors (figure 3b). This is extremely constraintful for ages of galaxies.
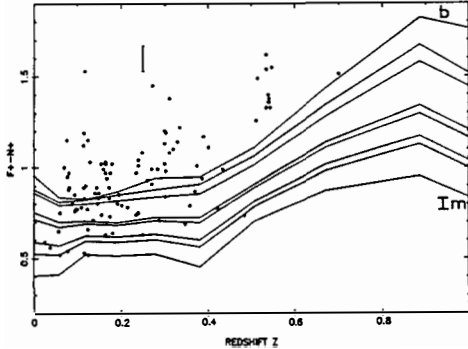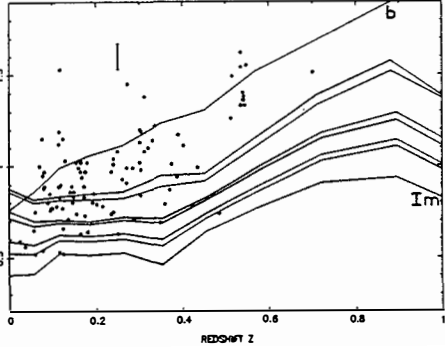

| FIGURE 3a: | FIGURE 3b: |

Deep sample of faint objects from Koo, 1986 are compared to the predictions of our scenarii of evolution. Case (a) is computed for h_0=0.5 and Ω_0=1. Case (b) is for h_0=0.5 and Ω_0=0.1 Differences of cosmology imply an age 13Gyr for case (a) and 17 Gyr for case (b).

iii) The $z \geq 3$ radiogalaxies

The best example is given by the radiogalaxy 0902+34 which has been discovered by Lilly, 1988. Its redshift is z=3.395 estimated from Lyα and CIV emission lines. These lines show evidences of a non-thermal component and of metal enrichment. It has been selected on the basis of a faint infrared emissivity associated to a very red color J-K ≥ 2.75. Its emissivity in Lyα line ($\simeq 2.1 \times 10^{-18}$ W m^{-2}) and its equivalent width ($\simeq 1000$ km s^{-1}) are about similar to those of the 3CR radiogalaxies observed by Djorgovski et al, 1984. The best fit of the integrated U'BVRIJK colors, corrected from the Lyα line (figure 4a) is obtained from the sum of two intense bursts of respective ages 0.1 Gyr and $\simeq$ 3Gyr (Rocca-Volmerange, 1988). Aperture corrections in the K band (Lilly,1989) and recent stellar tracks from Maeder and Meynet(1988) models can explain the gap from V to K bands by a supergiant population with an age $\leq$ 1Gyr (figure 4b). In this last case, the Lyman α emission line could not be only produced by photoionisation. (Rocca-Volmerange and Guiderdoni, 1989, in preparation).
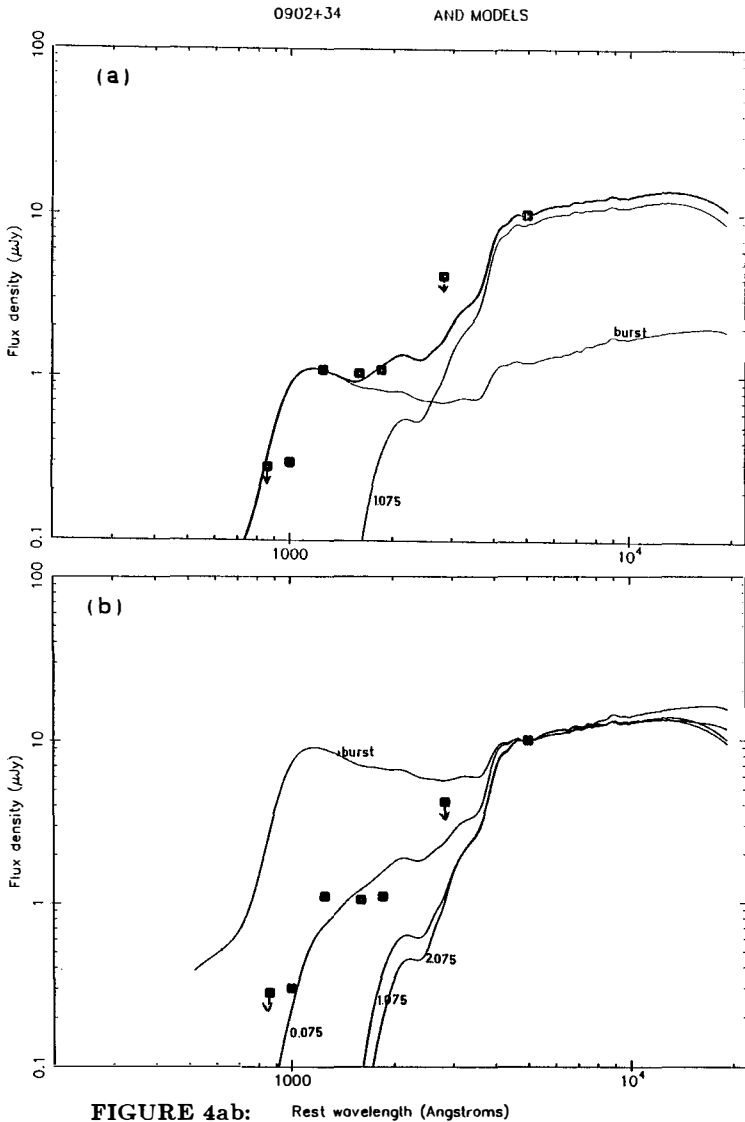
FIGURE 4ab: Rest wavelength (Angstroms)

U'BVRIJK fluxes of the radiogalaxy 0902+34 are compared to -
case(a): a sum of a current burst and a stellar population of $\simeq 1.075$Gyr after the
1Gyr burst.

- case(b): a unique population at successive ages 0.075 (supergiant),
1.075 and 2.075 Gyr after a 1Gyr burst. Data in the K band have been corrected
according to Lilly,1989. New tracks (Maeder and Meynet, 1988) are used.

—————————————— TABLE 3: ——————————————

	$\Omega_0=0$	$\Omega_0=0.1$	$\Omega_0=1.$
Universe Age in Gyr	19.56	17.57	13.04
t(3.395) in Gyr	4.45	3.13	1.41
$t(z_{for})$ in Gyr	3.45	2.13	0.41
for an age 1Gyr			
z_{for}	4.5	5	≥ 10

IV. Constraints on Cosmological Parameters

A classical cosmological model such as the Friedmann-Lemaître model gives a relation between the redshift z and the cosmic time $t(z)$. This relation essentially depends on the cosmological parameters: the Hubble constant H_0, the density parameter Ω_0 and the cosmological constant Λ_0. The age of a stellar population substracted to the cosmic time of the observed redshift is the cosmic epoch of the galaxy formation redshift z_{for} according to:
$$t(z_{for}) = t(z)\text{-age}$$

i) An age for the Universe
Estimates of ages for galaxies would have to imply a lower limit of age for the Universe t_0:
$$t(z_{for}) \leq t_0$$
From the different samples considered in the previous section, all converge to an old Universe.

The globular clusters of our Galaxy give a limit 17Gyr which could be increased to 20 Gyr (Sandage, 1988) for metal deficient clusters, assumed to form at the same epoch than the halo of our Galaxy.

The color-color diagrams are strongly constrained by the reddest galaxies of each sample (cluster, field or radiogalaxies) These red colors are explained by an age effect (increasing the population of red giants relative to blue main sequence stars). Also an envelop of these observations is given by an extreme model of initial burst at 17 Gyrs or more (figure 3b).

The case of $z \geq 3$ galaxies is still uncertain. The two solutions proposed in figures 4a and 4b are not significantly different in terms of cosmological parameters. Table 3 present possible redshifts and epoch of formations for the galaxy 0902+34 at the age 1Gyr . Cosmology $\Omega_0=1$ is not excluded by any solution as it was firstly thought from the first results. More constraints on the Lyman α emission and colours are needed.

The cosmological parameters $\Omega_0 =0.1$ and $H_0= 50$ km s^{-1} Mpc^{-1} and a null cosmological constant correspond to an age $\simeq$ 17Gyr for the Universe.

ii) A low value for Ω_0?

Ages deduced from evolution models give a low estimate of Ω_0. Another possibility to approach this parameter could be the Hubble diagrams (Tinsley,1972, Lilly and Longair, 1984) Most of them are strongly affected by evolutionary effects which are difficult to disentangle from cosmological effects. The best approach would be to observe in the K band in which the faintest evolution corrections are observed. However accuracy of observations or/and sensitivity of models to other parameters prevent to find at present a solution from such diagrams.

From fitting the faint galaxy counts (Guiderdoni and Rocca-Volmerange, 1989 and this session), a low value of the density parameter $\Omega_0 \leq 0.1$ is also obtained. It may be noticed that in this case, the distributions of galaxies in magnitudes, colors and redshifts are not only sensitive to the evolutionary scenarios but also to the structure of the Universe. Discussions on these results are given by the authors.

Concerning H_0, our models are not so sensitive to its value. The low value deduced from ages is not in disagreement with Sandage, 1988, who recently proposed an extremely low value down to $\simeq$ 40 km s^{-1} Mpc^{-1}.

The consequences of such values of Ω_0 and H_0 are fundamental since they are in contradiction with $H_0= 100$ km s^{-1} Mpc^{-1} (Roland and Pelletier, 1989) and $\Omega_0=1$ currently admitted by some models of galaxy formation such as the Cold Dark Matter model.

V. Discussion and Conclusion

The convergence of previous results to old galaxies and an old Universe could be the simple effect of the basic modelisation. Let us consider the parameters which are the most influent in this age determination.

i) the stellar tracks

They define, with the scenarios of star formation, the scale times of our models. Most of previous models (from Tinsley,1972 to Bruzual, 1983) used various set of tracks which are in agreement with old globular clusters as our present models. But a large amount of Galactic globular clusters has been recently analysed by VandenBerg,1983, with several improvements: atmosphere models, color-temperature relations, opacities and a detailed significant comparison with observations. His conclusion is 18 Gyrs for the oldest clusters of our Galaxy. This is not fundamentally different from previous estimates but his new set of tracks are needed in our models to estimate how different are estimates of galaxy ages. Another important set of tracks to test with our models are those computed by Maeder and Meynet, 1988 including overshooting and mass loss which accurately fit a large range of open and globular clusters. These new data are at present running in our models.

ii) Metallicity effect

Due to the well-known age-metallicity relation observed by Twarog, 1980 and Carlberg, 1985 in our Galaxy and verified (figure 5) in our models (Rocca-Volmerange and Schaeffer, 1989), the assumption of an half solar metallicity, reached after 1 Gyr of efficient star forming process, appears available. Most galaxies observed at high-z form such an amount of stars, likely evolved as in the galaxy 0902+34, that their metallicity has not to be so far from solar. If metallicity is 2-3 $Z\odot$, a problem of analysis does exist since metal-rich clusters are extremely rare and their data are not so meaningful. However metallicity effect could be an explanation of the reddest galaxies observed in the color $-z$ diagrams. The case of metal deficiency is completely different and plays a fundamental role in young star formation sites, for example in starbursts and possibly in the primeval galaxies.
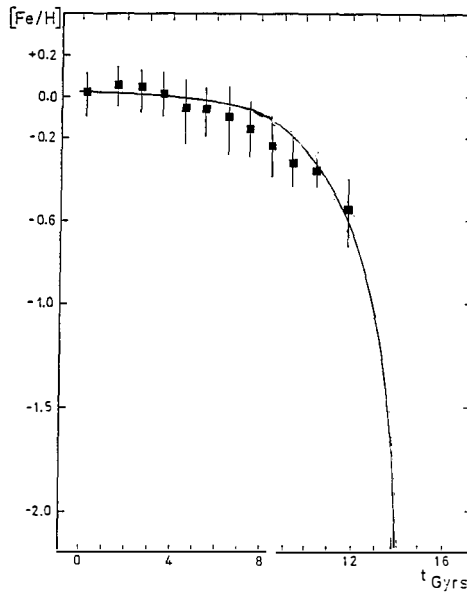
FIGURE 5:

Relation metallicity-age in the solar neighborhood (Twarog, 1980) compared to our evolutionary models. Age of the Galaxy is 13-14 Gyrs. (from Rocca-Volmerange and Schaeffer, 1989)

ii) Scenarios of evolution

They are not important for extreme cases of the color-z diagrams or the most extreme radiogalaxies where a burst is assumed. In this case, main parameters are efficiency, timescale and duration of bursts. Spectral distributions of nearby and intermediate -z galaxies are the most sensitive to the Hubble sequence scenarii. Only deeper observations will confirm our proposed evolutionary histories. Faint galaxy counts also bring some interesting constraints on these scenarii.

A last but not least parameter to consider is the dust. Reddening of galaxies could be attributed in a large part to a differential extinction. The main problem will be to conciliate this extinction with the strong emission lines, likely partly due to photoionisation.

An old Universe ($\geq$ 17Gyrs) and a low value of $q_0 \simeq 0.05$ are the present conclusions of our model fits. Extremely dependent on the ages of the globular clusters, these results could be modified from new sets of stellar tracks , as proposed by VandenBerg, 1983, 1985 and by Maeder and Meynet, 1988, also by metallicity and dust effects. Anyway if more detailed computations are running from now, it appear very difficult to conciliate all the data with a young age for the Universe and $\Omega_0 = 1$.

references

Becker, S.A., 1981, Astrophys. J. Supp. Series, 45, 475

Bica, E., Alloin, D., 1986, Astron. Astrophys., 162, 21

Bruzual, G., 1983, Astrophys. J., 273, 105

Cohen, J.G., Frogel, J.A., Persson, S.E., 1978, Astrophys. J., 222, 165

Djorgovski, S., Spinrad, H., Marr, J., 1984, " New Aspects of Galaxy Photometry", J.L. Nieto (ed.), Springer–Verlag, p. 193

Djorgovski, S.G., 1987, "Towards Understanding Galaxies at Large Redshift", Kron, R.G., Renzini, A. eds., Kluwer, p.259

Downes, A.J.B., Peacock, J.A., Savage, A., Carris, D.R., 1986, Mon. Not. R. astr. Soc., 218, 31

Dressler, A., Gunn, J.E., 1983, Astrophys. J., 270, 7

Dunlop, J., Longair, M.,1987," High Redshift and Primeval Galaxies", Ed Bergeron, Kunth, Rocca-Volmerange, Tran Thanh Van, Ed Frontieres, p. 93

Dunlop, J., Peacock, J.A., Savage, A., Lilly, S.J., Heasley, J.N., Simon, A.J.B., 1989a, Mon. Not. R. Astr. Soc., in press

Dunlop, J., Guiderdoni, B., Rocca-Volmerange, B., Longair, M., Peacock, J., 1989b, Mon. Not. R. Astr. Soc., in press

Guiderdoni, B., Rocca–Volmerange, B., 1987, Astron. Astrophys., 186, 1 (GRV)

Guiderdoni, B., Rocca–Volmerange, B., 1988, Astron. Astrophys. Supp. Ser.,74, 185

Guiderdoni, B., Rocca–Volmerange, B., 1989, Astron. Astrophys., in press

Gunn, J.E., Stryker, L.L., 1983, Astrophys. J. Suppl. Series, 52, 121

Johnson, H.L., 1966, Astrophys. J., 143, 187

Koo, D.M., 1986, Astrophys. J., 311, 651

Laing, R.A., Riley, J.M., Longair, M.S., 1983, Mon. Not. R. astr. Soc., 204, 151

Lilly, S., 1988, Astrophys. J., 333, 161

Lilly, S., 1989, Berkeley Conference on Radiogalaxies

Lilly, S., Longair, M., 1984, Mon. Not. R. Soc., 211, 833

Mc Carthy, P. J., Van Breugel, W., 1989, "The epoch of Galaxy formation", Frenk et al, eds, NATO ASI Series C, vol 264, p. 57

Maeder, A., 1981, Astron. Astrophys., 102, 401

Maeder, A., Meynet, M., 1988, Astron. Astrophys. Supp Series, 76, 411

Mellier, Y., Soucail, G., Fort, B., Mathez, G., 1987, Astron. Astrophys., 199, 13

Miley, G., Chambers, K., 1989, in preparation

Rocca-Volmerange, B., Lequeux, J., Maucherat-Joubert, M., 1981, Astron. Astrophys., 104, 177

Rocca–Volmerange, B., Guiderdoni, B., 1989, Evolutionary Processes in galaxies, Ed. J. Beckman, in press

Rocca–Volmerange, B., Guiderdoni, B., 1988, Astron. Astrophys. Supp. Series, 75, 93 (RVG)

Rocca–Volmerange, B., 1989, Mon. Not. R. astr. Soc., 236, 47

Rocca–Volmerange, B., 1988, the Messenger, 53, 26

Rocca–Volmerange, B., Schaeffer, R., 1989, submitted

Roland, J., Pelletier, J., preprint

Sandage, A., 1988, preprint

Scalo, J.M., Fundamental of Cosmic Physics, 11, 1

Spinrad, H., 1987, High Redshift and Primeval Galaxies, Ed. J. Bergeron, D. Kunth, B. Rocca-Volmerange, Tran Thanh Van, Ed Frontieres, p. 59

Spinrad, H., 1988, "The epoch of Galaxy formation", Frenk et al, eds, NATO ASI Series C, vol 264, p. 57

Sweigart A.V., Gross, P.G., 1978, Astrophys.J. Supp. Series, 36, 405

Tinsley, B.M., 1972, Astron. Astrophys., 20, 383

VandenBerg, Don A., 1983, Astrophys. J. Supp. Series, 51, 29

VandenBerg, Don A., Bell, R.A., 1985, Astrophys. J. Supp. Series, 58, 561

CONSTRAINTS ON q_0 FROM FAINT GALAXY COUNTS

B. Guiderdoni[1] and B. Rocca-Volmerange[1,2]

1) Institut d'Astrophysique de Paris, 98bis Boulevard Arago, F-75014 Paris

2) Laboratoire René Bernas, Bât. 108, Université Paris XI, F-91405, Orsay-Campus

ABSTRACT. We interpret faint galaxy counts by analysing the intrinsic evolution of high-redshift galaxies with our model of spectrophotometric evolution. We take into account scenarios of evolution depending on the spectral type and reproducing the colours and type mix of nearby galaxies. We show that, under the assumption of *pure* luminosity evolution, the magnitude distributions are consistent only with scenarios of evolution in which a significant fraction of the galaxies formed at high redshift ($z_{for} \simeq 10$ or more) in a universe with low q_0 (below $\simeq 0.25$ at 2σ) if $H_0 = 50$ km s^{-1} Mpc^{-1}. A good fit is given with $q_0 = 0.05$ and $z_{for} = 30$, and high past Star Formation Rates. The colour distributions are correctly reproduced in range and amplitude without any additional free parameter. The redshift distribution of the Durham Faint Survey is also naturally predicted by the fit. The rejection of $q_0 = 0.5$ or $z_{for} = 2$ (for all galaxies) is strong ($\simeq 4\sigma$) and does not seem to depend on misestimates of input data. In order to save the value $q_0 = 0.5$, one would have to relax the assumption of *pure* luminosity evolution and introduce strong *number* evolution.

1. Introduction

In this paper, we present an analysis of faint galaxy counts. In principle, these counts can be used to constrain the value of the deceleration parameter q_0. But at apparent magnitudes brighter than $m \simeq 24$, the effect of the predicted intrinsic evolution dominates the pure *geometric* effect of varying q_0 between plausible values (Brown and Tinsley, 1974). This behaviour is also found in other classical cosmological tests involving galaxies such as the well-known Hubble diagram. This is the reason why, up to now, the analysis of faint galaxy counts was only considered to understand the evolution of galaxies. But at magnitudes fainter than $m \simeq 24$, the influence of geometry on the counts becomes stronger when evolution is simultaneously taken into account. As a matter of fact, we shall see that the current observations down to $m \simeq 27$ (Tyson, 1988) can actually give constraining upper limits, in contrast with the former studies limited to brighter magnitudes.

The no-evolution slope of the counts is predicted to be $d \log N(m)/dm \sim 0.3$ at $20 < m < 24$ while the observations give $\sim 0.4 - 0.6$ depending on the photometric band from red to blue (see e.g. Koo, 1986). These faint objects do not belong to a local population of dwarf galaxies, as shown by the analysis of their colours (Tyson, 1988) or of their redshift distribution (Broadhurst et al., 1988). The increasing surface density of galaxies as one observes at fainter magnitudes suggests (1) intrinsic luminosity evolution due to younger stellar population and higher star formation rates at more remote look-back times (respectively the so-called "passive" and "active" evolutions), and/or (2) number density evolution, the present-day galaxies being the result of the merging of the large number of galaxies seen in the past. In any way, some evolution is needed as a *prediction* of the standard cosmological models. The bluer colours of faint galaxies are a strong evidence of at least some passive intrinsic evolution in the past (Shanks et al., 1984, Koo, 1986, Tyson, 1988). So we choose to restrict our analysis to the examination of the case for *pure* luminosity evolution.

The intrinsic evolution can be analyzed by means of a model of spectrophotometric evolution which allow to compute evolving synthetic spectra of galaxies from a minimum set of assumptions about the star formation history. By coupling these results with Friedmann–Lemaître cosmological models, apparent magnitudes and colours can be derived, which take into account the entangling of the cosmological and passive/active evolutionary effects in a consistent way. The interpretation of faint galaxy counts must use these realistic magnitude and colour computations. Tinsley, 1980, Bruzual and Kron, 1980, Shanks et al., 1984, King and Ellis, 1985, and Yoshii and Takahara, 1988, already proposed predictions of faint galaxy counts based on their model of evolution of galaxies, under the assumption of pure luminosity evolution. The general trend of their conclusions based on data brighter than $m \simeq 24$ is that small values of q_0 are required to fit the observed slope of the magnitude distribution (see e.g. the review by Koo, 1988). Nevertheless, in one of the most recent papers on this subject (Yoshii and Takahara, 1988), their "best fit" of the observations is still poor and the authors conclude that "if the observational uncertainty is taken into account, it may be safe to conclude that $0 < q_0 < 0.5$ is an allowable range".

In this paper, we use our model of spectrophotometric evolution (Guiderdoni and Rocca–

Volmerange, 1987, Rocca–Volmerange and Guiderdoni, 1988, hereafter GRV and RVG) to propose our own analysis and predictions for faint galaxy counts. These results are more completely described and discussed in Guiderdoni and Rocca–Volmerange, 1989.

2. Predictions of faint galaxy counts

2.1 Principles

In their simplest form, the predictions of faint galaxy counts are based on the assumption that the comoving number of galaxies of each type is conserved once the galaxy formed at redshift z_{for}. Let $d^2 A_j(m_\lambda, z)$ be the number of galaxies of spectral type j and redshift $[z, z + dz[$ contributing to the counts per steradian and magnitude bin around apparent magnitude m_λ. This elementary contribution simply reads:

$$d^2 A_j(m_\lambda, z) = \Phi_j(M_\lambda)(1 + z)^3 \frac{dV}{dz} dm_\lambda dz \qquad (1)$$

dV/dz is the volume element per steradian of the shell $[z, z + dz[$ given in classical textbooks (e.g. Weinberg, 1972). $\Phi_j(M_\lambda)$ is the luminosity function per volume unit for type j determined from the analysis of *nearby* galaxies. The absolute magnitude through the λ filter is computed from the apparent magnitude m_λ by means of the formula:

$$M_\lambda = m_\lambda - (m - M)_{bol}(z) - k_{j\lambda}(z) - e_{j\lambda}(z) \qquad (2)$$

$(m - M)_{bol}(z)$ is the bolometric distance modulus (Weinberg, 1972). The quantities $k_{j\lambda}(z)$ and $e_{j\lambda}(z)$ are the $k-$correction and the $e-$correction which depend on type j. The $k-$correction accounts for the cosmological redshift of the spectra of distant galaxies. The $e-$correction accounts for the intrinsic evolution of the rest–frame spectra of distant galaxies with respect to nearby standards. They are computed from evolving synthetic spectra according to formulae recalled in RVG.

The total counts per steradian and magnitude bin dm_λ are obtained by integrating the elementary contribution on z and summing on j

$$N(m_\lambda) \equiv \sum_j \int_0^{z_{max,j}} d^2 A_j(m_\lambda, z) \qquad (3)$$

$z_{max,j} = min(z_{for,j}, z_{lim})$ with z_{lim} being the redshift above which the Lyman continuum break enters the λ filter: $1 + z_{lim} \simeq \lambda/912$ Å. Even if galaxies form at high z_{for}, they appear in the $J-$band ($\lambda_{eff} \simeq 4620$ Å) counts only below redshift $z_{lim} \simeq 4$. $N(m_\lambda)$ is a number of galaxies per steradian and magnitude bin dm_λ.

2.2 Luminosity functions

The luminosity function for each spectral type j has a Schechter form. The values of the $J-$band magnitude M_j^* of the knee and of the slope α_j for each type are taken from King and Ellis, 1985, and tabulated in Table 1 for $h = 0.5$, with $h \equiv (H_0/ 100 \text{ km s}^{-1} \text{ Mpc}^{-1})$. These values are consistent with the overall determination of Efstathiou et al., 1988, leading

Table 1: Parameters of the Schechter luminosity function for each type. Col. (2) and (3): J–band absolute magnitude of the knee (for $H_0 = 50$ km s^{-1} Mpc^{-1}) and slope. Col. (4) and (5): observed fractions f_j in a magnitude–limited field survey with $J < 16.75$, from Shanks et al., 1984, and computed "density fractions" g_j in the luminosity functions.

type	M_j^*	α_j	f_j	g_j
(1)	(2)	(3)	(4)	(5)
E/S0	-21.10	-1.00	0.43	0.35
Sa	-20.90	-1.00	0.07	0.07
Sb	-20.90	-1.00	0.19	0.18
Sc	-20.90	-1.00	0.18	0.17
Sd	-20.45	-1.00	0.09	0.15
Im	-20.45	-1.00	0.04	0.08

Table 2: History of star formation for each type, according to scenarios A, B and C described in sections 2.3 and 3.1. Scenario B predicts fainter and redder galaxies in the past than scenario A. Scenario C is intermediate.

type	scenario A/C(*)		scenario B	
	SF law	$B - V$ at 12–16 Gyr	SF law	$B - V$ at 12–16 Gyr
E/S0	$1g(t)$ (*) (UV–hot)	0.92–0.91	$\tau(t) = 1$ ($t < 1$ Gyr) (1 Gyr burst)	1.00–0.95
Sa	$0.4g(t)$	0.74–0.84	$b/d = 1.6$	0.85–0.78
Sb	$0.3g(t)$	0.67–0.78	$b/d = 0.86$	0.76–0.70
Sc	$0.1g(t)$	0.51–0.58	$b/d = 0.11$	0.49–0.51
Sd	0.060	0.42–0.47	0.060	0.42–0.47
Im	$7.7 \ 10^{-4}t^2$	0.31–0.34	$7.7 \ 10^{-4}t^2$	0.31–0.34

$g(t) \equiv M_{gas}(t)/M_{tot}$.

(*) For A: all E/S0 are UV–hot. For C: 50 % of E/S0 are UV–hot and 50 % are 1 Gyr bursts as in scenario B.

to $M^* = -20.90 \pm 0.10 + 5\log(h/0.5)$ in the J band, and $\alpha = -1.07 \pm 0.05$, but they are preferred to the latter because of their type dependence. The "density fractions" g_j are computed from the observed fractions f_j in a magnitude–limited sample of nearby galaxies (brighter than $J = 16.75$) taken from Shanks et al., 1984. Since evolution is small at the look–back times corresponding to these magnitudes, these values are almost unsensitive to the choice of the evolutionary corrections. Since the value of ϕ^* in the luminosity function is not well determined, we choose to normalise the predicted counts to the observations at magnitude $J = 19$. Table 1 summarizes these input ingredients.

2.3 $k-$ and $e-$corrections

The computation of the $k-$ and $e-$corrections is based on the set of evolving synthetic spectra given in RVG for various spectral types of the Hubble sequence. These spectra are the main outputs of our model of spectrophotometric evolution (GRV). This model has a number of improvements with respect to the previous ones: (i) The theoretical stellar tracks include the last stages of stellar evolution (Horizontal Branch, Asymptotic Giant Branch). (ii) The rest–frame UV flux, which is fundamental for the predictions of apparent magnitudes of high–redshift galaxies in the visible, are estimated from the complete library of the IUE stellar atlas (Wu et al., 1983). (iii) The model gives good fits of observational spectra and colours of nearby galaxies and the spectral types are considered "templates" (see e.g. the reviews by Rocca–Volmerange and Guiderdoni, 1988b, 1989). The Hubble sequence is simply described by varying a characteristic time scale for the conversion of gas into stars, in the expression of the Star Formation Rate (SFR). In particular, we keep a constant Initial Mass Function (IMF) $d\mathcal{N}(m_*)/d\ln m_* \propto m_*^{-x}$. We use Scalo, 1986, observational slope $x = 1.7$ for the IMF of massive stars ($80M_\odot > m_* > 2M_\odot$) which emit the crucial rest–frame UV light. For the low–mass stars, the slopes are the classical $x = 1.35$ for $2M_\odot > m_* > 1M_\odot$ and $x = 0.25$ for $1M_\odot > m_* > 0.1M_\odot$. Finally, the internal extinction and the nebular emission are taken into account.

The E/S0 are represented by the so–called "1 Gyr burst" and "UV–hot" models depending on the amount of UV excess which we assigned to star formation (Rocca–Volmerange and Guiderdoni, 1987). The 1 Gyr burst model followed by passive stellar evolution is the "red envelope" of the possible colours, with no UV excess. The range of observed UV excesses in the nuclei of nearby galaxies spans between this model and the UV–hot model (Rocca–Volmerange, 1989b) which reproduces the UV and visible spectrum of the nuclei of M87 and NGC 4649. We shall investigate the influence of these two histories of the SFR on the high–redshift predictions. For late–type galaxies, we shall also test two possible histories of the SFR. In the first one, we assume that there is no interruption of star formation between the formation of the bulge and the disk. The spectral types from Sa to Sc are described with SFRs proportional to the gas content after formation at redshift z_{for}. In the second one, bulge and disk evolutions are followed separately, as in King and Ellis, 1985 (bulges evolve as the 1 Gyr burst model and disks evolve with a constant SFR). In the first scenario, Sa, Sb and Sc become redder as they age. In the second one, they become bluer since the luminosity of the bulge strongly decreases while that of the disk is nearly constant. In an
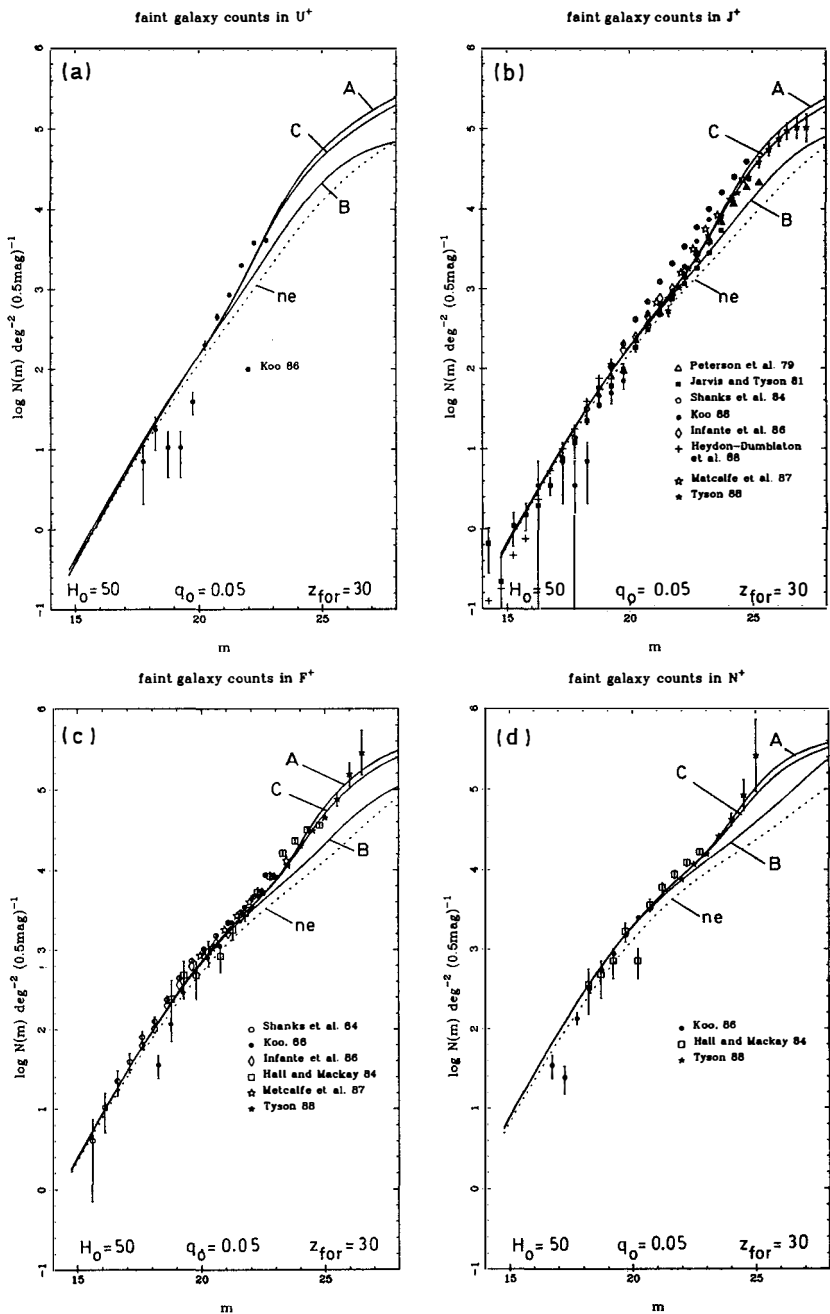
faint galaxy counts in U⁺

(a)

faint galaxy counts in J⁺

(b)

faint galaxy counts in F⁺

(c)

faint galaxy counts in N⁺

(d)

Figure 1a–d: Influence of the scenario of evolution on the magnitude distributions in the $U^+ J^+ F^+ N^+$ photometric bands. Scenarios A, B and C are recalled in Table 2. Scenario A is "bright", scenario B is "faint". In scenario C, half of the E/SO evolve according to the burst model and the other half according to the UV–hot model, with late-type galaxies as in scenario A. The redshift of galaxy formation is $z_{for} = 30$ and $q_0 = 0.05$. Solid lines: with evolution (Scenarios A, B and C). Dotted line: no evolution.

average, galaxies in the past are fainter in the second scenario than in the first one. Finally, Sd and Im are respectively described with constant and increasing SFR. Table 2 summarizes the various SFR histories which will be used to reproduce the Hubble sequence. The range of predictions with these models illustrates the uncertainty due to the possible histories of star formation in ellipticals and spirals.

2.4 Adopted value of H_0

The H_0 dependence of the counts is weak. On the one hand, the luminosity function dependence in H_0^3 cancels that of the volume element dV/dz in H_0^{-3}. On the other hand, the effect on the bolometric distance modulus $(m - M)_{bol}$ is cancelled by the H_0 dependence of M_j^*. The only H_0 dependence is that of the e–corrections through the relation of galaxy ages $t_{gal}(z)$ to redshift z.

The values of H_0 and q_0 determine an upper limit for the current age of the stellar population in a galaxy. The values $H_0 = 100$ km s^{-1} Mpc^{-1} and $0 \leq q_0 \leq 0.5$ lead to ages of the universe $6.5 \leq t_0 \leq 9.8$ Gyr. The corresponding evolutionary time scales produce colours which are much too blue and cannot fit a number of objects, as shown in Guiderdoni and Rocca–Volmerange, 1988, from the comparison of predicted colours with a compilation of cluster and field galaxies at $z < 0.8$. Consequently, we hereafter retain $H_0 = 50$ km s^{-1} Mpc^{-1}, giving ages $13.1 < t_0 < 19.6$ Gyr for $0 < q_0 < 0.5$, with small values of q_0 to be preferred on the basis of the reddest observed colours.

3. Magnitude distributions

We compiled data available in the literature and reduced the systems used by the various authors to the Kron, 1980, and Koo, 1985, photographic plate system U^+ ($\lambda_{eff} \simeq 3660$ Å), J^+ ($\lambda_{eff} \simeq 4620$ Å), F^+ ($\lambda_{eff} \simeq 6170$ Å), N^+ ($\lambda_{eff} \simeq 7940$ Å). Tyson, 1988, proposes a correction for confusion at faintest magnitudes in his deep counts. This correction is taken into account with its large error bars. The Poisson errors reported in the figures are probably underestimates of the real uncertainties, since the various authors are not in complete agreement. In particular, the counts by Shanks et al., 1984, in the direction of the South Galactic Pole are a factor $\simeq 2$ above the other counts. Infante et al., 1986, and Metcalfe et al., 1988, commented on this discrepancy, which could be due to zero–point differences in the photometry (CCD with respect to photographic plates, for instance) as well as to real fluctuations in galaxy counts from field to field.

3.1 The history of star formation and the redshift z_{for}

Figure 1 shows the influence of the scenario of evolution on the magnitude distributions in the $U^+ J^+ F^+ N^+$ photometric bands, with $z_{for} = 30$ in a $q_0 = 0.05$ universe. We introduce three sets of scenarios (recalled in Table 2) which give almost the same *visible* colours for nearby galaxies, but evolved differently in the past. Scenario A gives "bright" galaxies in the past by using the UV–hot model for the E/S0 and SFRs proportional to the gas content for late–type galaxies. Scenario B gives fainter and redder galaxies in the past with respect to scenario A by using the 1 Gyr burst model and separate bulge/disk evolutions. We take redshifts of formation $z_{for}^b = 30$ for the bulges and $z_{for}^d = 5$ for the disks, and bulge/disk
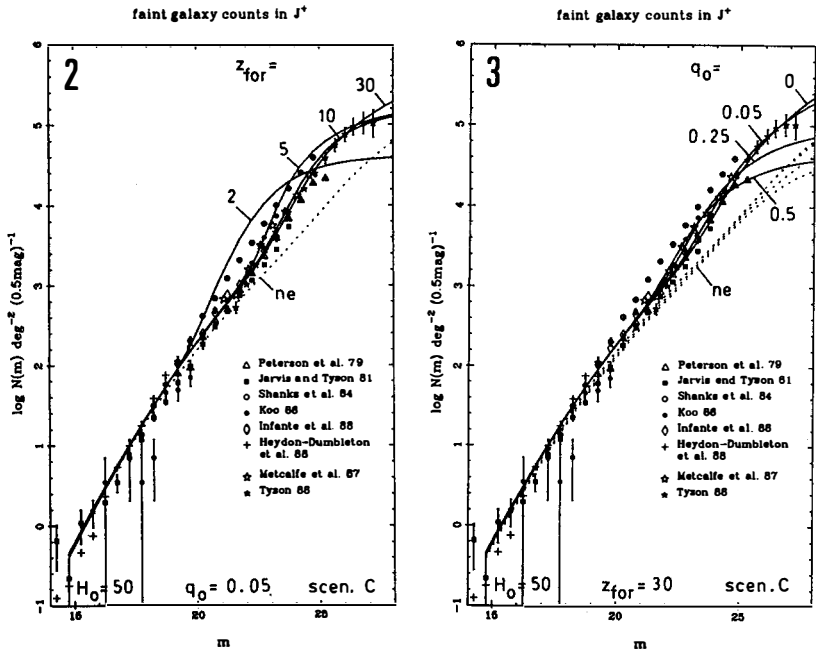
faint galaxy counts in J^+

faint galaxy counts in J^+

Figure 2: Influence of z_{for} on the faint galaxy counts. $q_0 = 0.05$. Solid lines: with evolution (scenario C). Dotted line: no evolution. Large values of z_{for} are required to fit the slope and the plateau fainter than $J^+ \simeq 25$.

Figure 3: Influence of q_0 on the faint galaxy counts. $z_{for} = 30$. Solid lines: with evolution (Scenario C). Dotted line: no evolution. Small values of q_0 are required to fit the slope and the plateau fainter than $J^+ \simeq 25$.

luminosity ratios b/d in the J^+ band are fixed in order to reproduce a plausible range of visible colours for present Sa, Sb and Sc. Finally, in scenario C, half of the E/S0 evolves according to the 1 Gyr burst model and the other half according to the UV–hot model, with later–type galaxies as in scenario A. The models are normalised to the data at $J^+ = 19$. The fit of the counts in the four photometric bands is good for scenario A and C, and the uncertainties due to the scenario of evolution are comparable to those appearing from the data, especially from the scatter of the observational results from one author to another, and from the correction for confusion given in Tyson, 1988, deep counts. Scenario B appears too faint. The influence of varying z_{for}^d (provided that $z_{for}^b = 30$) or the luminosity ratio is much smaller than the difference between A and B. So the fit of the magnitude distributions seems to need scenarios of "active" star formation in the past. This is the first trend. In the following sections, we shall take scenario C, keeping in mind the scatter of figure 1.

Figure 2 shows the influence of varying z_{for} for $q_0 = 0.05$. z_{for} acts in the computation of the e–corrections and in the upper limit of the integral of the counts (see equation (3)) which is larger for higher z_{for}. Large values of z_{for} are required to fit the counts. This is the second trend. The value $z_{for} = 5$ predicts a bump around $J^+ = 24$ which is not in the data. The value $z_{for} = 2$ does not reproduce the slope fainter than $J^+ = 20$, and the predicted faint–magnitude plateau is strongly discrepant with the data, at $\simeq 4\sigma$, in one takes into account only the level of the plateau ($J^+ > 25.5$) compared to the error bars arising from the correction for confusion.

3.2 The value of q_0

Figure 3 shows the predictions with various q_0 and $z_{for} = 30$. The various predictions without evolution are shown. They slightly differ one from each other because of the influence of q_0 on geometry (the bolometric distance modulus $(m - M)_{bol}(z)$ and the volume element dV/dz are smaller at fixed z for smaller q_0). The observed counts have a slope steeper than the predictions without evolution, whatever the values of q_0 may be. The predictions with evolution are much more sensitive to q_0 than the predictions without evolution. In fact, the deceleration parameter influences the counts with evolution through *geometry* and through *time scales* $t(z)$ in the computation of the e–corrections. The plateau occurs at lower levels for higher q_0, with a factor $\simeq 4$ shift in the counts between $q_0 = 0$ and $q_0 = 0.5$. Small values of q_0 are strictly required to fit the counts. The predicted plateau for $q_0 = 0.5$ is not consistent with the data at $\simeq 4\sigma$, with the previously–mentioned significance. The value $q_0 = 0.25$ is discrepant only at 2σ and can be marginally retained. This is the third trend. Tyson, 1988, counts fainter than $J^+ \simeq 25$ are particularly constraining. The value $q_0 = 0.05$ gives a good fit from the bright end down to $J^+ \simeq 27$.

3.3 Comments

The above–mentioned conclusions can be rapidly summarized. (i) The ~ 0.4 slope at $20 < J^+ < 24$ can be reproduced provided that the luminosity evolution is large enough with respect to the present–day galaxies. This can be done through the choice of the SFR at the early epochs, of z_{for} and of q_0. High SFR and q_0 or low z_{for} increase the slope. With "active" SFR designed to reproduce the colours of present galaxies (say scenario A or C), $q_0 = 0.5$ or
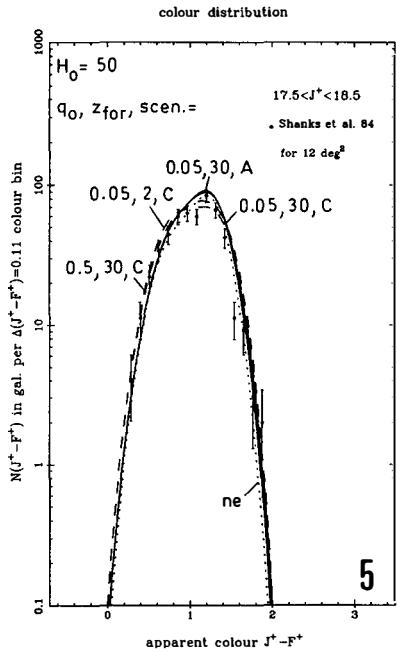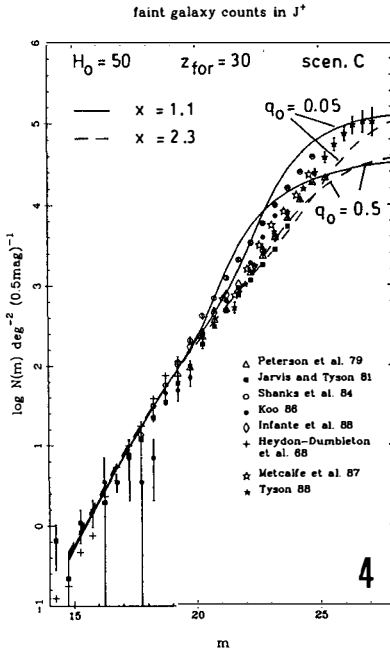
faint galaxy counts in J⁺

colour distribution

Figure 4: Influence of the slope of the IMF $d\mathcal{N}(m_*)/d\ln m_* \propto m_*^{-x}$ for massive stars $(80 M_\odot > m_* > 2 M_\odot)$. The predictions for $x = 2.3$ (Miller and Scalo, 1979, dashed lines) and $x = 1.1$ (solid lines) are computed with $z_{for} = 30$ and scenario C, in the cases $q_0 = 0.05$ or 0.5. The value $q_0 = 0.5$ is not consistent with the data, whatever the slope of the IMF may be.

Figure 5a–b: (a) Colour distribution for $17.5 < J^+ < 18.5$. The observed number of galaxies per colour bin in a 12 deg² area is drawn from Shanks et al., 1984. (b) Colour distribution for $23 < F^+ < 24$. The observed number of galaxies per colour bin in a 0.036 deg² area is drawn from Tyson, 1988. The normalisation of the computed counts was fixed by the total counts, with no additional free parameter. Solid lines: with evolution (scenarios A and C), $z_{for} = 30$ and $q_0 = 0.05$. Dashed lines: with evolution (scenario C), $z_{for} = 2$, $q_0 = 0.05$ or $z_{for} = 30$, $q_0 = 0.5$. Dotted line: no evolution.

colour distribution   redshift distribution
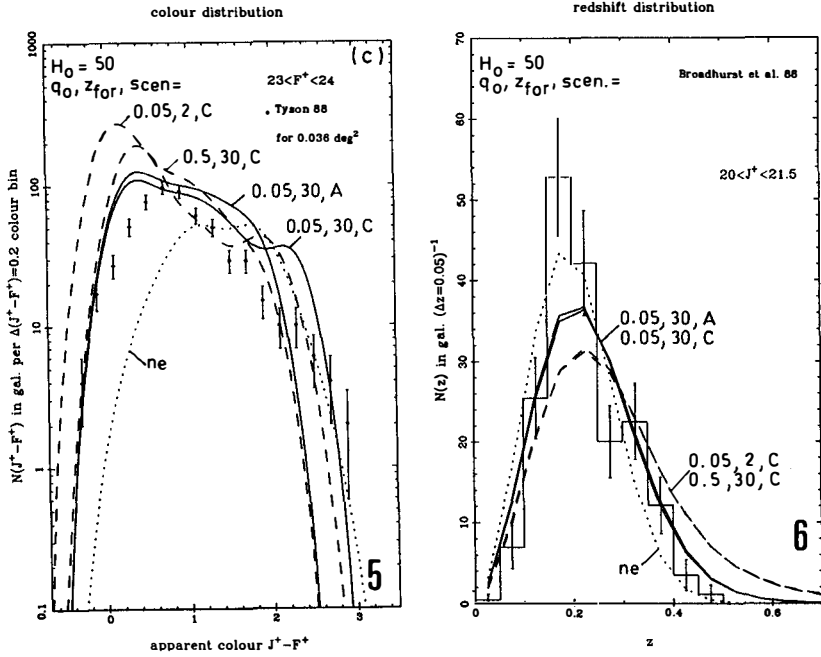
Figure 6: Redshift distribution for $20 < J^+ < 21.5$. The data are drawn from Broadhurst et al., 1988. The various predictions are computed per 0.05 mag bin in the area surveyed by the authors. The counts are normalised to the observed total number of galaxies. Solid lines: with evolution (scenarios A and C), $z_{for} = 30$ and $q_0 = 0.05$. Dashed lines: with evolution (scenario C), $z_{for} = 2$, $q_0 = 0.05$ or $z_{for} = 30$, $q_0 = 0.5$. Dotted line: no evolution.

$z_{for} = 2$ would give too steep slopes. With low q_0 and high z_{for}, "active" scenarios (A or C) are required to fit the slope. Nevertheless, the various lines are very close at $J^+ < 24$. This is the reason why it has been so difficult to disentangle the effects of the various scenarios of SFR and cosmological models on the basis of data brighter than this limit, although this conclusion was already reached in a qualitative form (see the review by Koo, 1988). (ii) The plateau at $J^+ > 25$ is not reproduced with $q_0 = 0.5$ because of the smaller volume elements and bolometric distance modulus, nor with $z_{for} = 2$ because of the lack of galaxies at very high redshift. In fact the plateau would appear at much fainter magnitudes if evolution was not taken into account. So its position has a "geometric" origin, but it is "enhanced" by the evolution which makes it appear at the relevant apparent magnitudes. Even with small q_0 and large z_{for}, only the most active SFRs can reproduce the observed plateau.

Here we get good fits of the magnitude distributions in all surveyed photometric bands, from $J^+ \simeq 16$ down to $J^+ \simeq 27$, with $q_0 = 0.05$. We emphasize the fact that the fit is naturally obtained on a ten−magnitude range with standard scenarios of evolution derived from the study of nearby and high−redshift galaxies. The rejection of $q_0 = 0.5$ appears to be a strong conclusion of the model on the basis of Tyson's results. Is this rejection reliable ? In fact, if the luminosity evolution in our models was underestimated, we should artificially get low values of q_0 from fits of the data.

For instance, a systematic change of the IMF in the past might be responsible of such an underestimate. We checked this possibility by varying the Salpeter index for the slope of massive stars ($m_* > 2M_\odot$). In our standard model, it is $x = 1.7$. We tested the values $x = 2.3$ (Miller and Scalo, 1979) and a flat IMF, with $x = 1.1$. The results are shown in figure 4. With $q_0 = 0.05$, it is clear that, for scenario C, an intermediate slope is needed (precisely our choice $x = 1.7$), or SFRs more active (resp. less active) than scenario C if one wants to keep the value $x = 2.3$ (resp. $x = 1.1$). With $q_0 = 0.5$, the level of the faint−magnitude plateau is weakly dependent on the choice of x. Thus the rejection of $q_0 = 0.5$ cannot be avoided by these changes of the IMF. Guiderdoni and Rocca−Volmerange, 1989, also show that neither nebular emission nor internal extinction could lead to a sufficient misestimate of the luminosity evolution.

Finally, one could remark that the evolutionary time scales derived for high−redshift galaxies rest on the input stellar tracks and particularly on the Giant Branches which are the dominant contributor in evolved galaxies (see GRV). Could models with input stellar tracks leading to shorter evolutionary time scales modify the conclusion ? In fact, the rejection of $q_0 = 0.5$ on the basis of the faint galaxy counts is mainly due to the level of the faint−magnitude plateau, which is a "geometric" effect enhanced by the evolution. As it is the case for a shallower−slope IMF, one can expect that shorter time scales or stronger luminosity evolution will increase the slope of the counts and shift the plateau towards brighter apparent magnitudes, without improving the fit.

4. Colour and redshift distributions

4.1 Constraints from colour distributions

Figure 5 gives the colour distribution for $17.5 < J^+ < 18.5$, from Shanks et al., 1984, and for $23 < F^+ < 24$ from Tyson, 1988. The model predictions with the chosen normalisation are simply rescaled to the sky areas quoted by the observers. So there is no additional free parameter in the fit of the colour distributions with respect to the fit of the magnitude distributions proposed in section 3. The colour distribution with $17.5 < J^+ < 18.5$ is very well reproduced. Since the colour evolution is still weak at these magnitudes, the excellent fit only reinforces the strong consistency of the choice of normalisation, parameters of the luminosity function and mix of spectral types. The fit of Tyson, 1988, colour distribution is fair. The predicted histogram show a bump at $J^+ - F^+ = 0.4$ which is not observed. This might be due to the beginning of confusion. Tyson estimates that the correction for the blue objects missed in the observations could bluen the mean of the colour distribution by $\simeq 0.1$ mag (Tyson's figure 17). On the other hand, it is expected that the colours at this depth are more sensitive than the slopes of the counts to the details of the SFR history. The red part of the distribution strongly depends on the choice of the evolution model for E/S0. As a matter of fact, our scenario C seems to still have too few "UV–hot" early types. Nevertheless, the general agreement with the total number and colour range of observed objects, and especially the large number of observed *blue* objects (with respect to no evolution) is surprisingly satisfactory, since no additional ad hoc modelling has been introduced.

Finally, one must recall that the faint galaxy counts show a scatter of a factor 2 from one field to another (one author to another ?) So one can expect that it will be difficult to obtain a good agreement of the colour distributions in magnitude slices. Nevertheless, it is pretty clear that scenarios with low z_{for} or high q_0 are not consistent with the data. They predict the existence of too many very blue galaxies which are not observed. The scenario with low q_0 and large z_{for} gives the best trend for the bump bluer than $J^+ - F^+ \simeq 1.2$, with respect to the no–evolution predictions.

4.2 The Durham Faint Survey

We took the redshift distribution of faint galaxies with $20 < J^+ < 21.5$ from the Durham Faint Survey (hereafter, DFS, Broadhurst et al., 1988). The data are summed on $\Delta z = 0.05$ bins corresponding to the predictions. Figure 6 shows the redshift distribution for $20 < J^+ < 21.5$ from the DFS, with predictions of various models. The models are normalised in order to give the same total number of galaxies as the observed sample. The peak at $z = 0.175$ is due to some clustering in one field (the so–called SGP) among the five surveyed, as noticed by the authors themselves. At these redshifts, the intrinsic evolution is weak. Anyhow, the above–mentioned conclusion leading to high values of z_{for} in a low–q_0 universe is consistent with this redshift distribution.

Broadhurst et al., 1988, proposed two quantitative tests for the distribution: the average redshift $< z >$ in the magnitude slice $20.5 < J^+ < 21.0$, where their data are more complete, and the slope $\gamma \equiv d \log N(m)/dm$ of the magnitude distribution between $J^+ = 20$ and 24. The data give $< z >= 0.225 \pm 0.015$ and $\gamma = 0.43 \pm 0.02$. The fit by scenario C has $< z >= 0.220$ and $\gamma = 0.442$ (respectively differring from the observed means by only 0.3σ and 0.6σ).

5. Conclusions

The luminosity and spectral evolution predicted by our model in the case of *pure* luminosity evolution have been compared to apparent magnitude and colour distributions obtained from faint galaxy counts in four photometric bands from 3600 Å to 7900 Å.

(i) Low q_0 (say, below 0.25 at 2σ, with σ being the error of the correction for confusion given by Tyson, 1988) and large z_{for} (say, above 10) are required to fit the slope of the counts on a ten-magnitude range, and the plateau observed down to $J^+ \simeq 27$. The values $q_0 = 0.05$ and $z_{for} = 30$ give a good fit. The values $q_0 = 0.5$ or $z_{for} = 2$ are in strong discrepancy with the data, since they miss to reproduce the faint-end plateau at 4σ. This rejection appears to be very strong and does not come from misestimates of stellar data (with respect to previously-published models), internal extinction, nebular emission, or IMF, as discussed in Guiderdoni and Rocca-Volmerange, 1989. Tyson, 1988, magnitude and colour distributions are particularly constraining.

(ii) Among the plausible scenarios of evolution depending on the spectral type, and fitting the properties and distribution of nearby galaxies, scenarios with "active" past SFR, for instance with a large number of UV-hot early-type galaxies and SFR of late types proportional to the gas content, are to be preferred.

(iii) The colour distributions of faint galaxies reinforce this conclusion. The redshift distribution of the DFS is also naturally reproduced. On the basis of this distribution, we do not see any evidence for a dominant contribution of the burst-driven luminosity evolution claimed by Broadhurst et al., 1988.

In order to escape from this conclusion and to save $q_0 = 0.5$ ($\Omega_0 = 1$) predicted by inflationary scenarios (if $\Lambda = 0$), one could invoke the entangling of number evolution and luminosity evolution (which is anyhow absolutely needed by the standard cosmological models). Since an accurate modelling of the evolution of luminosity after merging is needed before any definitive conclusion, we keep low q_0 and high z_{for} as a conservative conclusion of the present paper.

References

Broadhurst, T.J., Ellis, R.S., Shanks, T., 1988, *Month. Not. Roy. Astron. Soc.*, 235, 827

Brown, G.S., Tinsley, B.M., 1974, *Astrophys. J.*, 194, 555

Bruzual, G., Kron, R.G., 1980, *Astrophys. J.*, 241, 25

de Vaucouleurs, G., de Vaucouleurs, A., Corwin, H.G., 1976, *The Second Reference Catalogue of Bright Galaxies*, University of Texas Press, Austin

Efstathiou, G., Ellis, R.S., Peterson, B.A., 1988, *Month. Not. Roy. Astron. Soc.*, 232, 431

Guiderdoni, B., Rocca-Volmerange, B., 1987, *Astron. Astrophys.*, 186, 1 (GRV)

Guiderdoni, B., Rocca-Volmerange, B., 1988, *Astron. Astrophys. Suppl. Series*, 74, 185

Guiderdoni, B., Rocca-Volmerange, B., 1989, *Astron. Astrophys.*, *in press*

Hall, P., Mackay, C.B., 1984, *Month. Not. Roy. Astron. Soc.*, 210, 979

Heydon-Dumbleton, N.H., Collins, C.A., MacGillivray, H.T., 1988, *preprint*

Infante, L., Pritchet, C., Quintana, H., 1986, *A.J.*, 91, 217

Jarvis, J.F., Tyson, A.T., 1981, *A.J.*, 90, 418

King, C.R., Ellis, R.S., 1985, *Astrophys. J.*, 288, 456

Koo, D.C., 1985, *A.J.*, 90, 418

Koo, D.C., 1986, *Astrophys. J.*, 311, 651

Koo, D.C., 1988, in *The Epoch of Galaxy Formation*, C.S. Frenk, R.S. Ellis, A. Heavens, J. Peacock and T. Shanks eds., Kluwer Academic Publishers

Kron, R.G., 1980, *Astrophys. J. Suppl. Series*, 43, 305

Metcalfe, N., Fong, R., Jones, L.R., Shanks, T., 1988, in in *High-redshift and Primeval Galaxies*, J. Bergeron, D. Kunth, B. Rocca–Volmerange and J. Tran Thanh Van eds., Editions Frontières

Miller, G.E., Scalo, J.M., 1979, *Astrophys. J. Suppl. Series*, 41, 513

Peterson, B.A., Ellis, R.S., Kibblewhite, E.J., Bridgeland, M.T., Hooley, T., Horne, D., 1979, *Astrophys. J. Lett.*, 233, L109

Rocca–Volmerange, B., Guiderdoni, B., 1987, *Astron. Astrophys.*, 175, 15

Rocca–Volmerange, B., Guiderdoni, B., 1988a, *Astron. Astrophys. Suppl. Series*, 75, 93 (RVG)

Rocca–Volmerange, B., Guiderdoni, B., 1988b, in *High-redshift and Primeval Galaxies*, J. Bergeron, D. Kunth, B. Rocca–Volmerange and J. Tran Thanh Van eds., Editions Frontières

Rocca–Volmerange, B., Guiderdoni, B., 1989, in *The Epoch of Galaxy Formation*, Durham, *in press*

Rocca–Volmerange, B., 1989b, *Month. Not. Roy. Astron. Soc.*, 236, 47

Scalo, J.M., 1986, *Fundam. Cosmic Phys.*, 11, 1

Shanks, T., Stevenson, P.R., Fong, R., MacGillivray, H.T., 1984, *Month. Not. Roy. Astron. Soc.*, 206, 767

Tinsley, B.M., 1980, *Astrophys. J.*, 241, 41

Tyson, J.A., 1988, *A.J.*, 96, 1

Weinberg, S., 1972, *Gravitation and Cosmology*

Wu et al., 1983, *IUE Ultraviolet Spectral Atlas*, NASA No22

Yoshii, Y., Takahara, F., 1988, *Astrophys. J.*, 326, 1

THE TECHNIQUE OF FIT IN THE HUBBLE DIAGRAM

G. Bigot [1] and R. Triay [2]

Centre de Physique Théorique*
CNRS - case 907 - Luminy
F - 13288 - Marseille Cedex 9 (France)

(Presented by R. Triay)

ABSTRACT

We present some results prior to publication of an investigation on the methodology to determine the deceleration parameter q_o. The goal is to obtain a formal value of q_o from the distance-magnitude relation of brightest cluster galaxies. The differences between the maximum likelihood approach with the usual technique(s) of fit are mainly emphasized. The correct Malmquist corrections, which depend on the world model, are derived. An application to the Hoessel, Gunn and Thuan (1980) data provides an unlikely formal value, which shows that the (usual) statistical model is poorly defined. This result has consequences which cannot be neglected because a reliable determination of q_o requires a secure evolutionary model as well as a correct statistical description of the sample to fit the data to the world model.

*) Laboratoire Propre, LP7061; [1]) Université d'Aix-Marseille II ; [2]) Université d'Aix-Marseille I

1. Introduction

The most preferred method to determine the deceleration parameter q_o has long been a least square fit of the log redshift-magnitude relation in the Hubble diagram. This technique was widely performed on brightest cluster galaxies because of the small dispersion in their intrinsic absolute magnitudes (see Humason, Mayall and Sandage 1956; Sandage 1972a,b,c; Gunn and Oke 1975, herein GO; Sandage, Kristian and Westphal 1976). It is clear that, since the true value of q_o cannot be ruled out without a perfect knowledge of evolutionary effects, the most pressing step to achieve is to derive a model of spectroscopic evolution of the sources. However, by comparing the results obtained by Kristian, Sandage and Westphal 1978; Hoessel, Gunn and Thuan 1980 (herein HGT), Hoessel and Schneider 1985, it turns out that decades of effort for collecting and analyzing data in order to estimate (at least) a formal value of q_o has led unfortunately to inconsistent conclusions. While this difficulty has not yet been clearly understood, it is generally believed that the uncertainty lies in the correction of observational data. Herein, because it is of interest to make clear the statistical approach before utilizing any evolutionary model, we have adopted a complementary point of view by questioning the statistical technique.

The low redshift sample of HGT, for which the effects of evolution can be neglected, is used as support of this investigation. Note that the determination of q_o is certainly not accurate when using a low redshift sample but this is not the goal of this investigation. The details of these results are given in Bigot and Triay (1989a,b).

2. The distribution of the data

In this section we describe the most common statistical model used to describe a sample of brightest cluster galaxies. The (linear) Hubble diagram is introduced as a graphical tool which permits to check apparent disagreements between the data and the model.

2.1. The usual statistical model

The usual statistical model assumes a Gaussian luminosity distribution function and a uniform spatial distribution of the sources. Instead of using the absolute magnitude M, let the luminosity distribution function be written in terms of the reduced absolute magnitude, hereafter RAM, $\mu = M + 5log(c/H_o) - 5$, as follows: $g_G(\mu;\mu_o,\sigma)$; where μ_o is the mean and σ the

standard deviation. If the selection effects depend on a monochromatic (apparent) magnitude S, called sampling magnitude by GO, and on the redshift z, then the density of probability describing an observed object is given by

$$d\mathcal{P}r_{dat} = \frac{1}{A(\mu_o,\sigma)}\, \mathcal{P}_{mag}(S)\mathcal{P}_{red}(z)\, g_G(\mu;\mu_o,\sigma)d\mu\, dV\, d\mathcal{P}r_{abs} \tag{1}$$

where $A(\mu_o,\sigma) = \int \mathcal{P}_{mag}(S)\mathcal{P}_{red}(z)\, g_G(\mu;\mu_o,\sigma)d\mu\, dV\, d\mathcal{P}r_{abs}$ is a normalization factor, dV is the comoving volume element, $d\mathcal{P}r_{abs}(r)$ is the density of probability describing the distribution of the reddening correction terms $r_k = A_S(\vec{x}_k)$, $\mathcal{P}_{mag}(S)$ and $\mathcal{P}_{red}(z)$ are technical functions describing the selection effects. If the sample is complete to the limiting search magnitude S_{lim} within the redshift range $z_{min} < z < z_{max}$, the technical functions read by means of the Heaveside distribution function

$$\begin{aligned}\mathcal{P}_{mag}(S) &= \theta(S_{lim} - S)\\ \mathcal{P}_{red}(z) &= \theta(z - z_{min})\theta(z_{max} - z)\end{aligned} \tag{2}$$

In general, S is identified to the magnitude which is obtained bracketing the galaxy within a constant linear sampling radius in a particular world model $q_o = q_o^*$ (i.e. by adopting a diaphragm radius $z \to \gamma(z)$ as given by a particular function of the redshift z). Hence, by writing the luminosity as a power law in the projected diaphragm radius, the redshift-magnitude relation reads

$$S - r = \mu + \xi(z) + K_S(z) \tag{3}$$

where $K_S(z)$ is the K-correction, $\xi(z)$ is the distance modulus

$$\xi(z) = 5log(1+z) + 5\Big((1-\alpha/2)\, log\, Z_{q_o}(z) + (\alpha/2)\, log\, Z_{q_o^*}(z)\Big) \tag{4}$$

α is the structure parameter and $Z_{q_o}(z)$ is the dimensionless measure of the luminosity distance, see GO and Bigot and Triay (1989a). Finally, the density of probability describing the distribution of N objects reads $d\mathcal{P}r_{dat}^{\otimes N} = \prod_{k=1}^{N} d\mathcal{P}r_{dat}^{(k)}$, where $d\mathcal{P}r_{dat}^{(k)} = d\mathcal{P}r_{dat}$ is defined by Eq. (1).

2.2. The (linear) Hubble diagram

It is clear that the real situation might not be so clear cut as that, and plots can be utilized for checking the validity of the working hypotheses. Two kind of problems are expected : the effects due to the evolution (which are not described in the statistical model) and the ones due to selection

effects (which might not be sufficiently well described by the technical functions (2)). It is well known that the Hubble diagram is not well adapted to discriminate between the effects of evolution and the one due to the geometry, and furthermore it turns out that it does not overcome the problems of selection effects. Indeed, the feature which does not facilitate the analysis of selection effects is that the coordinates are both redshift dependant (*log z* versus the apparent magnitude corrected for the reddening and the K-dimming $m^{R,K} = S - r - K_S(z)$). Moreover, the K-correction term makes curved the boundary of the distribution of the data at the faint branch of the Hubble diagram (i.e. when $m^{R,K} = S_{lim} - r_{min} - K_S(z)$ at high redshift) where the deviation from a straight line is expected to be the most important.

To overcome these problems of recognition (evolution and selection effects), it is more convenient to use the (linear) Hubble diagram, see Bigot and Triay (1989b). This diagram displays the distribution of the data in the $[\zeta,m^R]$ coordinates,

$$m^R = S - r$$
$$\zeta(z) = \xi(z) + K_S(z) \tag{5}$$

The only difference between the Hubble diagram is that all redshift dependence lies in the function $\zeta(z)$. Hence, the bound of the distribution of the data at the limiting search magnitude $S_{lim} - r_{min}$ is a straight cutoff which does not depend on redshift. Additionally, any discordance with the working hypotheses (2) produces an anomaly in the distribution of the data which is either vertical or horizontal (and thus orthogonal) depending on which variable (the redshift or the apparent magnitude) the technical functions does not fit. Note that this diagram is model dependent because $\zeta = \zeta(z)$ depends of the value of q_o . This unusual feature permits to inquire on the luminosity evolution. Indeed, the effects of evolution can be described by rewriting the density of probability (1) as follows : to account of the luminosity evolution, the mean RAM transforms $\mu_o(z) = \mu_o + \Delta\mu_o(z)$, which depends on redshift by means of a the variation $\Delta\mu_o(z)$; and a factor $h(z)$ is included to account of the number evolution (hence, the spatial distribution function reads $\propto h(z) \, dV$). Therefore, in accordance with (3) and (5), when plotting the data with bogus values of q_o , the distribution lies about a curve of equation $m^R \approx \mu_o + \zeta(z) + \Delta\mu_o(z) - \Delta\xi(z)$ where the term $\Delta\xi(z)$ accounts of the error on the value of q_o . Note that the distribution has an asymetrical dispersion : it is Gaussian at constant ζ and with probability density function equal to $h(z) \, dV_t/d\zeta$ at constant m^R ; where $\zeta_t = \zeta - \Delta\xi$ and V_t are defined for the true value of q_o . Then, when plotting the data for the true

value of q_o (ie : $\Delta\xi = 0$), the distribution lies within a straight line of unit slope in the case of no luminosity evolution (ie : $\Delta\mu_o(z) = 0$). Conversely, the effect of luminosity evolution is emphasized by a persistent residual curvature in the diagram when choosing a value of q_o to make the distribution as linear as possible. In this case, a minimal amount of evolution can be even estimated by the term $(\Delta\mu_o)_{min}(z) = \Delta\mu_o(z) - \Delta\xi(z)$. Actually, this estimate is valid as long as the geometry does not act exactly as an effect of evolution (ie : $\Delta\mu_o(z) - \Delta\xi(z) = 0$), that would be a peculiar situation. The problem of choosing a such value for q_o is related to the statistic which is used.
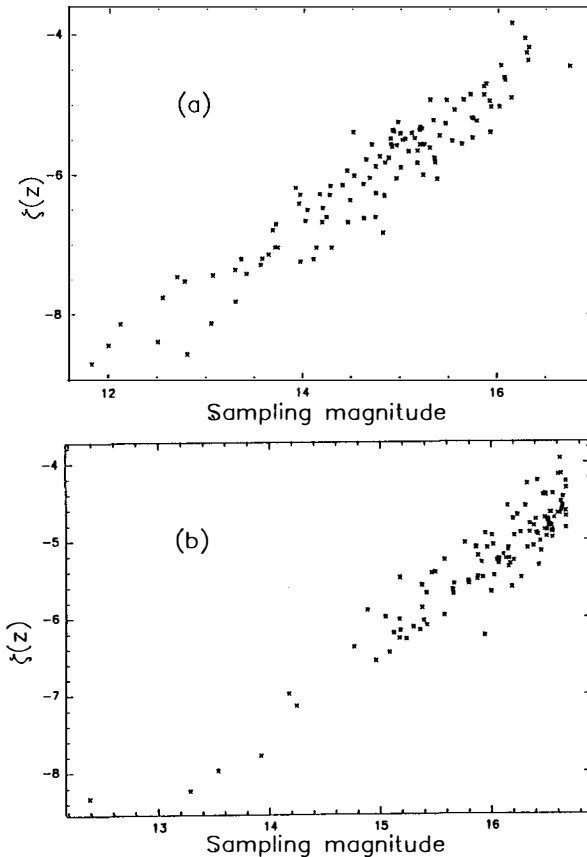
Figure 1 : The (linear) Hubble diagram with $q_o = 1/2$: (a) the HGT's data, (b) a characteristic simulation.

2.3. The data

The low redshift sample of HGT is used as support of this investigation. We have simulated 50 random samples $\{(\mu, V)_k\}$ in the Standard model ($q_o = 1/2$) following the statistical model as defined by (1) and with characteristics similar to HGT's data : 116 objects, completeness to the limiting search magnitude $S_{lim} = 16.8$ with $\mu_o = 20.78$ and $\sigma = 0.34$; the sampling magnitudes S_k are obtained from (3) by utilizing uniform randomly distributed values of r_k ($0 < r_k < 0.35$) to simulate the galactic absorption, the K-correction used is a smoothed version of the one obtained by Schild and Oke (1971) as given by GO, and with a constant structure parameter of $\alpha = 0.49$.

Figure 1 shows the (linear) Hubble diagram with $q_o = 1/2$: (a) the HGT's data, (b) a characteristic simulation. It turns out that, by comparing these diagrams, it is clear that the working hypotheses do not describe the HGT's data. Accordingly to the above discussion on this diagram, the effect due to a luminosity evolution cannot account of the difference between the two distributions and particularly because of the small redshift extent of the sample $z_{max} \approx 0.15$. This statistical analysis is given in Bigot, Fliche and Triay (1988); it suggests that, if the working hypothesis (1) is kept, the selection effect on the apparent magnitude is not simply described by a cutoff at the limiting magnitude but by a decreasing tendency (roughly exponential versus the magnitude S) to select the fainter objects; a similar analysis is presented at this conference by Bigot. The consequences of this uncertainty on defining the statistical model when using a technique of fit to determine q_o is discussed at the end of the following section.

3. The techniques of fit

In this section, the usual techniques of fit as well as the one given by the maximum likelihood (ML) technique are described. The application of these techniques with simulated and real brightest cluster galaxies samples are performed and compared; further details are given in Bigot and Triay (1989a)

3.1. The usual techniques of fit

The question on how to perform the fit, either at constant redshift or at constant magnitude, has long been discussed and no definite solution has been proposed. It must be noted that the

common feature of these approaches consists as a matter of fact to minimize a dispersion function. With Eq. (3), these dispersion functions read as follows : (a) for a fit at constant redshift one has

$$D_{red}(q_o) = \frac{1}{N} \sum_{k=1}^{N} \left[m_k^{R,K} - \left(\xi(z_k) + \mu_o \right) \right]^2 \tag{6}$$

where $m^{R,K}$ is the apparent magnitude corrected for the reddening and the K-dimming, and (b) for a fit at constant magnitude one has

$$D_{mag}(q_o) = \frac{1}{N} \sum_{k=1}^{N} \left[log(z_k) - log\left([\xi^{-1}](m_k^{R,K} - \mu_o) \right) \right]^2 \tag{7}$$

where $[\xi^{-1}]$ is the inverse function of $\xi(z)$ which is defined in (4). It is clear that in both Eq. (6) and (7), the mean μ_o must be obtained by a statistic which removes the Malmquist bias. To simplify the discussion we assume that μ_o is correctly estimated and that the sample is not distance limited.

In general, the use as well as the construction of a particular dispersion function is suggested by an heuristic approach of the Hubble diagram that we summarize as follows. Regardless of selection effects, the fit at constant redshift, see Peach (1970), might be preferred because the residuals are randomly Gaussian distributed and do not depend on cosmology, see Sandage (1972a). In the other hand, in accordance with GO, as long as the limiting search magnitude exists, the fit at constant magnitude is recommendable to avoid the cut off problem. Nonetheless, let us points out that, in this case, the conditions of utilization of a least square fit are not any more confirmed because the dispersion of the distribution at constant magnitude is not symmetrical !

Moreover, note that the dispersion function (6) reads also $D_{red}(q_o) = (1/N) \sum_{k=1}^{N} (\mu_k - \mu_o)^2$, which is a biased statistic (the Malmquist effect) of the variance σ^2, and by expanding $logo[\xi^{-1}]$ about $\xi = m_k^{R,K} - \mu_k$, the dispersion function (7) reads with a similar form $D_{mag}(q_o) \approx (1/N) \sum_{k=1}^{N} \pi_k^2 (\mu_k - \mu_o)^2$, where $\pi_k = \pi(z_k)$ is the slope of the distribution in the Hubble diagram. Therefore, one see that the minimization of (7) does not provides the same result as (6) unless the weighing factor π_k is constant. And, if the fit by means of (6) does not avoid the problem due to the cut off at the limiting search magnitude then the one by means of (7) also does not avoid this problem because the factor π_k does not account for that.

In a theoretical point of view, the weakness of these techniques is that they are not covariant. This failure explains the difficulty to argue a fit rather than the other one. A covariant version of these approaches, which reaches properly the desired goal, would be actually to minimize the statistic $D_\sigma(q_o) \rightarrow \sigma$ which provides the standard deviation. Moreover, this approach seems advantageous since the uniform hypothesis on the spatial distribution, which is probably too strong because of clustering tendency of the clusters themselves, see Abell (1982), does not intervene apparently. Nevertheless, this heuristic approach is not valid. Indeed, note that the arguments developed in favor of D_{red} or D_{mag}, and as well as the ones for $D_\sigma(q_o)$, are meaningless since they use one dimensional probability distribution functions (as obtained by fixing constant one of the coordinates) which are of null measure.

3.2. The maximum likelihood approach

While it might be not unique, a correct approach is given by the ML technique, which is described as follows : with the density function (1), the natural logarithm of the likelihood function reads

$$L(\mu_o, \sigma, q_o) = N \left(L_{Gauss} + L_{Unif} - L_{Bias} \right) \qquad (8)$$

where

$$\begin{cases} L_{Bias} = Ln(A) - Ln\left(V(z_{max}) - V(z_{min})\right) \\ L_{Gauss} = -Ln(\sigma) - \frac{1}{2}Ln(2\pi) - \frac{1}{N}\sum_{k=1}^{N}\frac{(\mu_k - \mu_o)^2}{2\sigma^2} \\ L_{Unif} = \frac{1}{N}\sum_{k=1}^{N}Ln\left(\frac{dV}{dz}(z_k)\right) - Ln\left(V(z_{max}) - V(z_{min})\right) \end{cases} \qquad (9)$$

The "maximum likelihood principle" asserts that the values of the parameters μ_o, σ and q_o should be chosen so that the function $L(\mu_o, \sigma, q_o)$ is maximized; which gives in some case equations and hence statistics of the parameters. It turns out that the likelihood equations provide statistics of μ_o and σ^2 which read as two interdependent equations

$$\begin{cases} \langle\mu\rangle = \frac{1}{N}\sum_{k=1}^{N}\mu_k \underset{CL}{\approx} \mu_o - \sigma^2 B_0(\mu_o, \sigma) \\ \frac{1}{N-1}\sum_{k=1}^{N}(\mu_k - \langle\mu\rangle)^2 \underset{CL}{\approx} \sigma^2 + \sigma^4 \left(B_1(\mu_o, \sigma)/\sigma^2 - B_0^2(\mu_o, \sigma)\right) \end{cases} \qquad (10)$$

Note that Eq. (10) provides the statistic (or dispersion function) $D_o(q_o) \to \sigma$ (the covariant version of the usual techniques). These equations are similar to the Malmquist (1920)'s ones but with corrections depending on q_o through the functions

$$B_k(\mu_o,\sigma) = \frac{1}{A(\mu_o,\sigma)} \int (\zeta-\zeta_o(\mu_o,r))^k \, g_G(\zeta;\zeta_o(\mu_o,r),\sigma) \, \mathcal{P}_{red}(z) \frac{dV}{dz} dz \, d\mathcal{P}_{rabs} \qquad (11)$$

where $\zeta_o(\mu_o,r) = S_{lim} - \mu_o - r$. For a given value of q_o , the equation (10) is solved by means of the Newton's method, which gives estimates of μ_o and σ. These values are inserted into (9) to provide the dispersion function $D_{ML}(q_o) = -\mathcal{L}(\mu_o,\sigma,q_o)$ to minimize. The order of magnitude of the terms (11) for $q_o = 1/2$, as obtained from the simulations, are $B_0 \approx 1.06 \ (\neq 1.382)$ and $B_1 \approx 0.12$.

Let note that Eq. (9) gives the natural logarithm of likelihood functions of well known densities of probability, $\mathcal{L}_{Gauss}$ accounts for the Gaussian distribution and the $\mathcal{L}_{Unif}$ for the uniform distribution[1]. The term $Ln(V(z_{max}) - V(z_{min}))$ has been inserted artificially to show the decomposition (8) but it must be removed in case of a not distance limited sample while the uniformity is still checked. These functions are maximized to the detriment of the coupling term $\mathcal{L}_{Bias}$ which accounts for the Malmquist bias[2]. It is clear that, contrary to the usual techniques of fit, all the working hypotheses are taken into account and contribute with equal weights in Eq. (8).

3.3. Application to simulated and real samples

While the simulations has been obtained in the Standard model, the determination of the world model by the previously described techniques has been performed on Friedmann-Lemaître models without assuming (a priori) a null cosmological constant $\Lambda = 3 H_o^2 \ (\Omega_o/2 - q_o)$; this permits the determination of expected negative estimates of q_o (because of the accuracy due to statistical fluctuations) without using an unauthorized extrapolation of Mattig's formulas (1958), see GO and HGT; however, the estimates corresponding to unphysical models (bounced), which represents 15% of loss, have been rejected. In principle, two cosmological parameters should be optimized

---

[1] The probability density function describing a uniform spatial distribution within $[V_{max} , V_{min}]$ reads

$\theta(V - V_{min}) \ \theta(V_{max} - V) \ dV \ (V_{max} - V_{min})^{-1}$.

[2] $\mathcal{L}_{Bias}$ is the natural logarithm of the likelihood function as given by the probability to observe an object within the redshift range $[z_{min}, z_{max}]$.

but the (reduced) density parameter has been fixed to $\Omega_o = 1$, since the small redshift range of the sample does not provide information on Ω_o. The results of the optimization of q_o by these techniques are shown in Table 1; the fist line represents the mean optimized value of q_o as obtained by means of these approaches when using the simulations. For the dispersion functions given by (6) and (7), the mean μ_o has been calculated following Eq. (10), as well as for σ.

Sample	D_{red}	D_{mag}	σ	D_{ML}
‹Simulations›	≈ 27	0.5±1.5 (1σ)	≈ 20	0.5±1.5 (1σ)
HGT's data	0	7	9	12

Table 1. The optimized value of q_o as determined by the quoted techniques

It is clear that the use of D_{red} and σ yields to overestimate q_o. In the other hand, the maximum likelihood approach gives back the value used for the simulations. Surprisingly, it turns out that the use of D_{mag} gives also the good estimate and seems equivalent to the ML approach; this behavior has not yet been clearly understood. When these techniques are performed with the HGT's data (not corrected for the Bautz-Morgan type and richness effects), see line 2 of Table 1, the ML approach gives a (very) overestimated value of q_o while the optimized value obtained from a least square fit at constant redshift (which is biased) looks reasonable. The qualitative analysis of the (linear) Hubble diagram of the data, in the Section 2.2 and 2.3, has suggested that the working hypothesis (2) are certainly not valid (the difficulty to select the fainter objects is described by a smoother technical function than a simple cutoff at the limiting magnitude). The comparison between the two lines of Table 1 gives the bias on determining q_o by a technique of fit in such a case. However, this is not the only possible explanation, among all working hypotheses to be questioned on defining the statistical model, another one would be that the selection effects are not actually described by the sampling magnitude S (as it is formally suggested in the literature). This suggestion is motivated by the fact that the galaxies are found on plates as far they can be distinguished from the brightness of the sky before the aperture correction is applied (i.e. by its isophotal diameter); this approach will be developed in a future paper

5. Conclusion

It has been shown that a least square fit in the Hubble diagram is not a covariant technique and that the arguments suggesting what kind of fit must be used are inconsistent. The maximum likelihood approach provides the valid Malmquist corrections (for high redshifts) and shows the rule of the working hypotheses when using a technique of fit. By utilizing the (linear) Hubble diagram and with the results as obtained by the ML technique of fit, it turns out that the usual statistical model, defined by the working hypotheses (1) and (2), does not described the HGT's data.

It is clear that the most pressing step to achieve in the determination of q_o is to derive a model of spectro-photometric evolution of the sources, but a correct statistical description of the data must be worked out in order to provide unbiased methods which can be used with evolutionary models.

References

Abell, G.O., 1982, *Galaxies and the Universe* , p.638, Mid. rep.Vol 9, G.P. Kuiper (Ed.)

Bigot, G., Fliche, H.H., Triay, R., 1988, Astron. Astrophys., 206,1

Bigot, G., Triay, R., 1989a, in prep. will be submitted to A & A (Main journal)

Bigot, G., Triay, R., 1989b, in prep. will be submitted to A & A (Letter to the Editor)

Gunn, J.E., Oke, J.B., 1975, Astrophys. J. **195**,255

Hoessel, J.G., Gunn, J.E., Thuan, T.X., 1980, Astrophys. J. **241**,486

Hoessel, J.G., Schneider, D.P., 1985, Astron. J. **90**,1648

Humason, M.L., Mayall, N.U., and Sandage, A., 1956, Astron. J., **61**,97

Kristian, J.A., Sandage, A., Westphal, J.A., 1978, Astrophys. J. **221**,383

Malmquist, K.G., 1920, Medd. Lund Astron. Obs. (ser. 2) **22**, 9

Mattig, W., 1958, Astr. Narch., **284**, 109

Peach, J.V., 1970, Astrophys. J. **159**, 753

Sandage, A., 1972a, Astrophys. J., **173**,485

Sandage, A., 1972b, Astrophys. J., **178**,1

Sandage, A., 1972c, Astrophys. J., **178**,25

Sandage, A., Kristian, J.A., Westphal, J.A., 1976, Astrophys. J. **205**,688

Schild,R.E.,Oke,J.B., 1971, Astrophys. J. **169**,209

A NULL CORRELATION TECHNIQUE TO DETERMINE q_o

G. Bigot [1] and R. Triay [2]
Centre de Physique Théorique*
CNRS - case 907 - Luminy
F - 13288 - Marseille Cedex 9 (France)

(Presented by G. Bigot)

ABSTRACT

We present a method to obtain a formal value (no evolution) of the deceleration parameter q_o from brightest cluster galaxies which is free of selection effects on apparent magnitude such as the Malmquist bias and the Scott effect. At the contrary of the usual techniques of fit, the forms of the luminosity function and of the technical function describing the selection effects on apparent magnitude are derived. The application of this technique to a (complete) sample of brightest cluster galaxies gives a formal value of $q_o \approx -0.76 \pm 0.6$ and confirms the Gaussian form of the luminosity function for these sources, while the effects of selection (by the apparent magnitude) are not described by a simple cut-off at the limiting search magnitude. If the evolutionary effects are neglected, because of the small redshift range ($z < 0.15$) of this sample, this value of the deceleration parameter suggests a non-zero cosmological constant (with repulsive vacuum) to have a density of order of $\Omega_o \approx 0.1$. The corrections for the Bautz-Morgan and richness classes as well as the effect of nuclei multiplicity are derived for this world model. In the orther hand, when iterating the procedure (corrections applied to the data - determination of q_o - determination of corrections), a stable solution is reached at $q_o \approx 0.54$. A such discrepancy with the previous result suggests that the statistical model is not yet clearly defined.

1. Introduction

The dependence on distance of the visual magnitude for brightest cluster galaxies has been widely utilized to determine (a formal value of) q_o but without convincing results. A typical example is the disagreement between the estimate of $q_o = -0.55\pm0.45$ as obtained from a complete sample limited to $z_{max} < 0.15$, Hoessel, Gunn, and Thuan (1980), hereafter cited as HGT, with the $q_o = 1.6\pm0.4$ as given by Kristian, Sandage and Westphal (1978), from a sample extending up to $z_{max} < 0.4$ (both values indicating a deviation of the Hubble diagram from a straight line, $q_o = 1$). Because of the opposite sign of these estimates and the small redshift range of these samples, other reasons than effects of evolution must be found to account of a such discrepancy. In general, the usual statistical model describing a not evolving population, defined by [i] the completeness to a limiting magnitude, [ii] a Gaussian luminosity function and [iii] a uniform spatial distribution of the sources, is assumed to warrant the technique of fit. Slight differences in the approaches of these groups of authors are on the aperture correction and on the technique of fit. The aperture correction used in HGT works for any world model, see Gunn and Oke (1975), while Kristian, Sandage and Westphal (1978)'s data were corrected separately for assumed values of $q_o = 0, +1$ (for which the subsequently computed values of q_o differ by only 0.2) and a iterative procedure was used to produce a self consistent estimate. The main difference as a matter of fact is the technique of fit, this points has been discussed by Triay (this conference) and it turns out that one still obtains unsatisfactory results when using the one given by the maximum likelihood approach. This failure suggests that the statistical model is not enough accurate, since the parameters are optimized so that the expected distribution of the data fits as well as possible the real one. Therefore, even with a better understanding of the evolutionary effects, the statistical approach still remain to be improved.

Herein, we give a new approach for which the working hypotheses [i] and [ii], as well as the corrections for the Bautz-Morgan and the richness classes (which are used to describe the sample in accordance with [ii]), are rendered unnecessary. The null correlation test has been performed with the low redshift sample of HGT (which is known to be complete to a limiting magnitude) by Bigot, Fliche and Triay (1988), hereafter cited as BFT, and gave the formal value of $q_o \approx -1.2\pm0.6$. In this paper, we give the estimate as obtained with more accurate data of the HGT's sample given by Hoessel and Schneider (1985), hereafter cited as HS. We need hardly mention

that this work is an investigation on the methodology rather than a determination of q_o .

2. The theory

The null correlation test was developed by Fliche and Souriau (1979) in the case of quasars and adapted for extended brightest cluster galaxies by BFT, which pointed out also the technique to determine the luminosity function as well as the technical function describing the effects of selection. Herein, we describe briefly the theoretical framework of these techniques by utilizing the notations and quantities defined by Triay (this conference).

2.1. The null correlation test

By assuming a uniform spatial distribution of brightest cluster galaxies and that the selection effects depend on a monochromatic magnitude S , the density of probability describing an observed object reads

$$d\mathcal{P}r_{dat} = \frac{1}{A} \varphi_{mag}(S) f(\mu) d\mu \, dV \, d\mathcal{P}r_{abs} \tag{1}$$

where $A = \int \varphi_{mag}(S) f(\mu) d\mu \, dV \, d\mathcal{P}r_{abs}$ is a normalization factor, S denotes the magnitude (sampling magnitude) obtained bracketing the galaxy within a constant linear sampling radius, see Gunn and Oke (1975), hereafter cited as GO, $\varphi_{mag}(S)$ is a technical function describing the selection effects, μ is the reduced absolute magnitude, $f(\mu)$ is the luminosity distribution function, dV is the comoving volume element, $d\mathcal{P}r_{abs}(r)$ is the density of probability describing the distribution of the reddening correction terms $r_k = A_S(\vec{x}_k)$. The distance magnitude relation reads

$$m^R = \mu + \zeta(z) \tag{2}$$

where $m^R = S - r$ is a monochromatic apparent magnitude corrected for the reddening and $\zeta(z) = \xi(z) + K_S(z)$ is a function which includes all redshift dependance, $\xi(z)$ is the (aperture corrected) distance modulus and $K_S(z)$ is the K-correction.

The technique is summarized as follows : with the variables transformed $(\mu, V) \rightarrow (\mu, m^R)$, the density of probability (1) reads

$$d\mathcal{P}r_{dat} = \rho(z) \times \frac{1}{A} f(\mu) d\mu \, \varphi_{mag}(m^R + r) dm^R \, d\mathcal{P}r_{abs} \tag{3}$$

where $\rho(z) = |\partial V / \partial m^R| = |\partial V / \partial \zeta|$ is a computable function of the redshift z . From the

equations, one note that $\rho(z)$ cannot be written as a product of independent functions of the variables m^R and μ, therefore this function is as a matter of fact a correlation function of these random variables. Let $g(\mu, m^R)$ be a function which reads $g(\mu, m^R) = \rho(z)^{-1} g_1(\mu) g_2(m^R)$. In accordance with (3), the expectation of $g(\mu, m^R)$ is equal to $\mathcal{P}r_{dat}[g] = A^{-1} G_1 \times G_2$ where $G_1 = \int g_1(\mu) f(\mu) d\mu$ and $G_2 = \int g_2(m^R) \varphi_{mag}(m^R + r) dm^R d\mathcal{P}r_{abs}$ depend on the functions g_1 and g_2 separately. Let $z \rightarrow \omega_\beta(z)$ be the function defined as follows

$$\omega_\beta(z) = w_\beta(z) \, / \, \sum_{i=1}^{N} w_\beta(z_i)$$

$$w_\beta(z) = \rho(z)^{-1} \, 10^{\beta \zeta(z)/5}$$

(4)

where β is an arbitrary constant. One note that the function $\omega_\beta(z)$ has the required form which was described previously for the function $g(\mu, m^R)$. The proof is straightforward by using Eq. (2) and by noting that the average $\langle w_\beta(z_k) \rangle$ becomes as less sensitive to additional sample values as N increases (in accordance with the central limit theorem). Therefore, if the working hypotheses used to defined the density of probability (1) are correct, the expected value of the function

$$\Gamma(q_o) = \sum_{k=1}^{N} \omega_\beta(z_k) \left(\mu_k - \langle \mu \rangle \right) \left(m^R_k - \langle m^R \rangle \right)$$

$$where \quad \langle \mu \rangle = \sum_{i=1}^{N} \omega_\beta(z_i) \, \mu_i \quad and \quad \langle m^R \rangle = \sum_{j=1}^{N} \omega_\beta(z_j) \, m^R_j$$

(5)

has a limiting distribution about zero (i.e. : $\mathcal{P}r_{dat}[\Gamma(q_o)] \rightarrow 0$ as N increases) for the true values of q_o. Conversely, the equation " $\Gamma(q_o) = 0$ " should provided the values of q_o which agrees with observed data[1]. An equivalent description of this test by means of weighted probabilities is given by BFT ; the function $\Gamma(q_o)$ defined in Eq (5) denotes the weighted covariance and the $\omega_\beta(z_k)$ are the weighting factors. In practice, the value of the arbitrary constant β is chosen so that the values $\{\omega_\beta(z_k)\}_{k=1,N}$ are as similar as possible in order to minimize the statistical fluctuations, Fig. 1 shows these weighing factors in the model $q_o = -0.76$ for the data which are described in Section 3.1.

---

[1] Described by the density of probability (1).
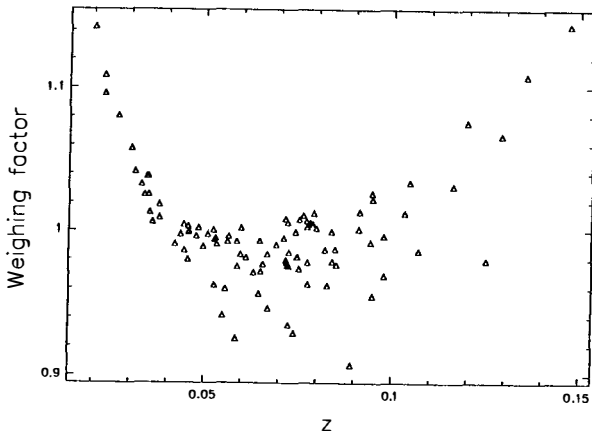
Figure 1 : The weighing factors for HGT sample (99 objects) of the HS data (175 objects). The world model is defined by $q_o = -0.76$ and $\Omega_o = 0.1$. The dots scatter from a continuous curve $z \rightarrow \omega_\beta(z)$ because of the individual α-corrections (aperture).

2.2. The luminosity function and the selection effects

In accordance with the equations (3,4), for a sufficiently large N , we have

$$F_{st}^*(\mu) = \sum_{k=1}^{N} w_\beta(z_k)\, \theta(\mu - \mu_k) \propto \int_{-\infty}^{\mu} 10^{-\beta\mu/5} f(\mu)d\mu$$

$$\Phi_{st}^*(m^R) = \sum_{k=1}^{N} w_\beta(z_k)\, \theta(m^R - m^R{}_k) \propto \int_{-\infty}^{m^R} 10^{\beta m^R/5} \langle\varphi\rangle(m^R)dm^R$$

(6)

where θ is the Heaveside distribution function and $\langle\varphi\rangle(m^R) = \int \varphi_{mag}(m^R + r)d\mathcal{P}_{abs}$ is the technical function averaged in the field of the observation (one has roughly $\langle\varphi\rangle \approx \varphi$). Therefore, if the equation $\Gamma(q_o) = 0$ holds, the luminosity function $\mu \rightarrow f(\mu)$ and the technical function $m^R \rightarrow \varphi(m^R)$ are derived a posteriori by inverting Eq. (6). We obtain

$$f(\mu) \propto \frac{F_{st}^*(\mu+\Delta_r\mu) - F_{st}^*(\mu-\Delta_l\mu)}{\Delta_r\mu+\Delta_l\mu} 10^{\beta\mu/5}$$

$$\varphi(m^R) \propto \frac{\Phi_{st}^*(m^R+\Delta_r m^R) - \Phi_{st}^*(m^R-\Delta_l m^R)}{\Delta_r m^R+\Delta_l m^R} \cdot 10^{-\beta m^R/5}$$

(7)

where the intervals $\Delta_l x$ (resp. $\Delta_r x$) contains at least $\sqrt{N}/2$ values $< x$ (resp. $> x$) in

order to minimize the statistical fluctuations. In practice, only the forms of these functions are induced from the plots of step-functions given in Eq. (7) within the statistical fluctuations. Hence, by inserting these candidate functions in the right hand terms of Eq. (6), we can derive statistics providing the values of parameters which fix them and utilize the Kolmogorow-Smirnov test to estimate the likelihood of these hypotheses.

2.3. Discussion

Compared to the usual techniques of fit in the Hubble diagram, without accounting of the evolutionary effects, it must be noted the following advantages : (a) the luminosity function is not assumed a priori Gaussian, (b) the completeness of the sample is not required as long as the selection effects are only described by means of the S-magnitude and (c) the null correlation test is an hit-or-miss approach. These aspects are developed in the following :

(a) The form of the luminosity function is generally assumed Gaussian because of a natural upper limit to the absolute luminosity of individual galaxies in clusters. However, Scott (1957) pointed out that it might not be a sharp cutoff. In such a situation, since the tail of the luminosity function toward the bright magnitudes could be much more stretched than a Gaussian trend, a least-square fit technique would make to overestimate q_o. Moreover, since the determination of q_o is as much difficult as the distribution of brightest cluster galaxies is scattered, correction for Bautz-Morgan and Richness classes are performed. The aim is that the whole sample can be described by a single Gaussian luminosity function. However, it turns out that these corrections have not yet been determined independently of the world-model. Finally, it is clear that, since the form of the luminosity function is not assumed in the working hypotheses, the null correlation test is free of previous effects.

(b) It is obvious that a limiting search magnitude exists, but that a sample is indeed complete to this magnitude is a guess of observers (which might be more likely by utilizing automatic technics of recognition on plates). If this effect is not negligible, the consequences in fitting the data are drastic since the Malmquist (1920) correction is not any more valid.

(c) At the contrary to fitting techniques, which consist to adjust the parameters without been secure that the working hypotheses are adapted to the data, the null correlation test may or not provide a solution, i.e. : a value of q_o such that the equation $\Gamma(q_o) = 0$ holds (for example, it turned out that a solution could not be found for the 3CR sample of radio galaxies which shows a

strong evolution, see Bigot, Rauzy and Triay 1989).

3. Application of the technique

The determination of the world model has been performed on Friedmann-Lemaître models without assuming (a priori) a null cosmological constant $\Lambda = 3\,H_o^2\,(\Omega_o/2 - q_o)$; the motivation can be found in BFT and in Triay (this conference). The forms of the previous equations do not change while another cosmological parameter must be optimized. Since the redshift-magnitude relation is not sensitive to reasonable variations of the (reduced) density parameter, because of the small redshift range of the sample, the null correlation test was performed at constant density for two values : at $\Omega_o = 0.1$ and at $\Omega_o = 1$.

3.1. The data

The HGT's sub-sample of the HS's data consists of 99 objects chosen from all Abell clusters with richness class greater than or equal to 1 ; distance class 4 or less and galactic latitude above 30°, and extending up to the redshift $z \approx 0.15$. The photometric data correspond to the apparent magnitude in the g and r passbands within a standard sampling radius of $16kpc$ (assuming $\Omega_o^* = 2q_o^* = 1$ and $H_o = 60$ km/s/Mpc), the reddening correction, which is based on Burstein and Heiles (1978) measurements, and the k-correction are given in Schneider, Gunn and Hoessel (1983). The RAM μ stands for the k-corrected apparent g -magnitude of an object placed at a luminosity distance of one Hubble radius. Herein, each object has its own measurement of the structure parameter "α" while BFT used a constant value $\alpha = 0.49$ as given by HGT, this is the main difference between these analysis.
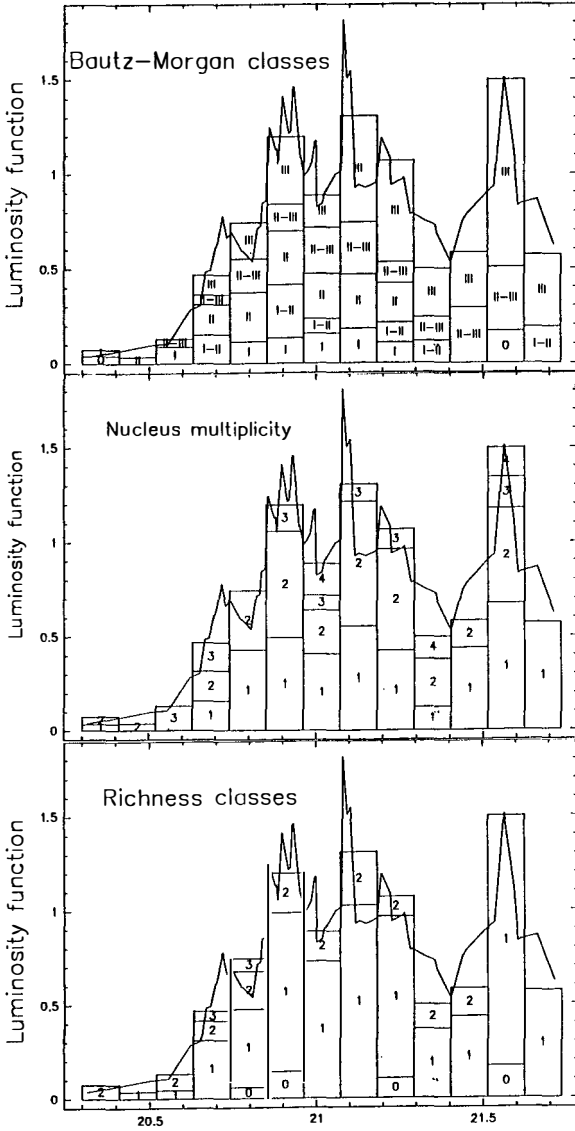
Figure 2 : The luminosity function $f(\mu)$. The contribution of classes (Bautz-Morgan type, Richness class and nucleus multiplicity) is shown by the histogram of weighing factors in each classes, the code 0 corresponds to clusters lacking classification.

3.2. Determination of the deceleration parameter

The optimized estimates of the deceleration parameter, which verify the statistic $\Gamma(q_o) = 0$ were found $q_o = -0.76$ (for $\Omega_o = 0.1$) and $q_o = -0.91$ (for $\Omega_o = 1$). For convenience, the world model defined by the first of these values will be used in the following in the text. The (intrinsic) accuracy of the method as obtained by BFT was of $\Delta q_o \approx 0.6$. However, this order of magnitude is underestimated since the mean value of the structure parameter $\langle \alpha \rangle_{HS} \approx 0.75$ is almost twice larger[2] than the constant value $\langle \alpha \rangle_{HGT} = 0.49$ used by BFT.

3.3. Description of the luminosity function and of selection effects

The figures 2 display the luminosity function as given by Eq. (7). It turns out that the general trend (continuous line) of the diagram shows a Gaussian form like. Hence, in accordance with Eq. (6), by assuming that the luminosity function is indeed Gaussian, then its mean and standard deviation are given by the following equations

$$\sigma_\mu^2 \approx \frac{N}{N-1} \sum_{k=1}^{N} \omega_k (\mu_k - \langle \mu \rangle)^2$$

$$\mu_o \approx \langle \mu \rangle + \frac{\beta \ln(10)}{5} \sigma_\mu^2$$

(8)

Hence, we obtain a mean of $\mu_o = 21.17$ and a standard deviation $\sigma_\mu = 0.31$ at a significance level of 75% (estimated by the Kolmogorov-Smirnov test). This result supports a posteriori the Gaussian hypothesis. In the other hand, it turns out that the sample is as a matter of fact not complete. Indeed, the probability that the measured deviation of the technical function $\varphi(S)$ from a cutoff $\theta(S_{lim} - S)$ at a limiting magnitude S_{lim} is due to statistical fluctuations is found of $\approx 10^{-21}$; these results are in agreement with the BFT's investigation.

The mean RAM in each classes (Nucleus multiplicities, Richness and Bautz-Morgan classes) is shown in Table 1 (first column in each class), these values are free of selection effects such as the Malmquist bias (1920) and the possible Scott effect (1957).

---

[2] For $\alpha = 2$ no cosmological information can be derived, see Eq. (4) in Triay (this conference).

CLASS	Nucleus multiplicity			Richness class			Bautz-Morgan type		
	$\langle\mu\rangle_{class}$	$\langle\mu\rangle_{class} - \mu_o$	N	$\langle\mu\rangle_{class}$	$\langle\mu\rangle_{class} - \mu_o$	N	$\langle\mu\rangle_{class}$	$\langle\mu\rangle_{class} - \mu_o$	N
0	***	***	(00)	(21.18)	(+0.01)	(05)	(21.03)	(−0.14)	(02)
1	21.22	+0.05	44	21.23	+0.06	72	20.99	−0.18	12
2	21.14	−0.03	39	21.00	−0.17	20	21.13	−0.04	11
3	21.01	−0.16	12	20.83	−0.34	2	21.03	−0.14	20
4	21.35	+0.18	04	***	***	**	21.21	+0.04	19
5	***	***	**	***	***	**	21.31	+0.14	35

Table 1. Mean RAM (first column) in each classes as obtained from the HS's data of 99 HGT's objects with $q_o = -0.76$ (for $\Omega_o = 0.1$). The number of objects involved in each estimate is indicated by N (third column). The Bautz-Morgan classes run form 1 to 5 instead to I to III ; the code 0 corresponds to clusters lacking classification.

One can note a tiny correlation of these values with the class identification while the individual α-corrections would remove a such effect. This correlation has a similar trend but with a smaller amplitude of the one found by HS which used the Standard world model ($q_o = 0.5$). However, the contribution of each classes (Bautz-Morgan type, Richness class and nucleus multiplicity) in the luminosity function, which is shown in Figure 1, is evenly distributed and has no significant tendency toward a correlation, this suggests that is might be a statistical fluctuation. But, if the (subjective) classifications in classes of richness and BM type, as well as the nucleus multiplicity, is free of selection effects, the null correlation test is independent of quantized corrections, see the discussion in section 2.3 (a). Herein, we have checked this independence by using corrections which were estimated as follows : for each class (Bautz-Morgan, Richness and Nucleus multiplicities, and in this order) the values $\langle\mu\rangle_{class} - \mu_o$ are estimated and subtracted to the data until this procedure converges.

Table 2 shows these corrections with $q_o = -0.76$. Hence, a new optimized value of q_o is found ($\Gamma(q_o) = 0$) and the related corrections are estimated. The global procedure was repeated 9 times until a stable solution was found, which gives a formal value of $q_o = 0.54$ ($\Omega_o = 0.1$) ; the journal on these iterations in given in Table 3. In this world model the data corrected for Bautz-Morgan type, Richness class and Nucleus multiplicities are described by a Gaussian luminosity function with mean of $\mu_o = 21.19$ and a standard deviation $\sigma_\mu = 0.26$ at a significance level of 82%. In accordance with this procedure, this mean RAM (in the stable solution) is exactly the same for all classes.

CLASS	Nucleus multiplicity			Richness class			Bautz-Morgan type		
	$q_o = -0.76$	$q_o = 0.54$	N	$q_o = -0.76$	$q_o = 0.54$	N	$q_o = -0.76$	$q_o = 0.54$	N
0	***	***	(00)	(+0.01)	(−0.01)	(05)	(−0.09)	(−0.06)	(02)
1	+0.03	+0.03	44	+0.05	+0.05	72	−0.13	−0.14	12
2	−0.01	≈0.00	39	−0.13	−0.13	20	−0.03	−0.05	11
3	−0.11	−0.13	12	−0.38	−0.34	2	−0.14	−0.13	20
4	+0.10	+0.10	04	***	***	**	+0.03	+0.03	19
5	***	***	**	***	***	**	+0.12	+0.13	35

Table 2. The $\langle\mu\rangle_{class} - \mu_o$ corrections as obtained in the world models $q_o = -0.76$ and $q_o = 0.54$ with $\Omega_o = 0.1$ for the HS data of 99 HGT objects. The number of objects involved in each estimate is given (third column). The Bautz-Morgan classes run form 1 to 5 instead to I to III ; the code 0 corresponds to clusters lacking classification.

n°	it. corr.	q_o	μ_o	σ	Gaussian	Cutoff
1	5	−0.76	21.17	0.31	0.75	$2\,10^{-21}$
2	6	+0.17	21.17	0.27	0.92	$8\,10^{-22}$
3	5	+0.44	21.18	0.27	0.83	$3\,10^{-21}$
4	4	+0.51	21.19	0.27	0.86	$1\,10^{-20}$
5	3	+0.53	21.19	0.27	0.83	$4\,10^{-21}$
6	2	+0.53	21.19	0.26	0.82	$4\,10^{-21}$
7	2	+0.54	21.19	0.26	0.82	$4\,10^{-21}$
8	1	+0.54	21.19	0.26	0.82	$4\,10^{-21}$
9	0	+0.54	21.19	0.26	0.82	$4\,10^{-21}$

Table 3. The results of the optimization by using the corrections to the data. The iterate number (column 1), the number of iterations required for consistent corrections (column 2) in the world model defined by the value of q_o (column 3) are given ; with these values the mean RAM and the standard deviation are given (columns 4 and 5) at a significance level (as defined by the Kolmogorov-Smirnov test) given in column 6 ; the likelihood testing the cutoff at a limiting magnitude is given in column 7.

The related corrections to the data are given in Table 2, one can note their stability in changing of q_o. Therefore, if these corrections are valid, the world model describing the data is defined by $q_o \approx 1/2$. Nevertheless, this result is inconsistent with the properties of the test. This failure is not yet clearly understood but indicates that the statistical model (1) is not adapted. At first glance it is obvious that, among the usual working hypotheses, the one which identifies S to the

magnitude obtained bracketing the galaxy within a constant linear sampling radius must is incorrect since the objects are detected on plates before the aperture luminosity is measured. This approach is part of an a work in progress.

3.4. Application to the HS sample.

The null correlation test was also performed with the whole HS sample which consists of the HGT's sample in addition of the richness-based sample of Schneider, Gunn and Hoessel (1983), extending to a redshift of $z \approx 0.25$ and giving a total of 175 objects. By performing the test, the following values $q_o = 6.26$ (for $\Omega_o = 0.1$) and $q_o = 5.97$ (for $\Omega_o = 1$) were obtained, HS found a value of $q_o = 4.4 \pm 1.1$ (for $\Omega_o = 1$) with another technique. It is clear that these estimates are biased since the related selection effects of the additional sample are not only described by a technical function of the variable S .

Sampling magnitude
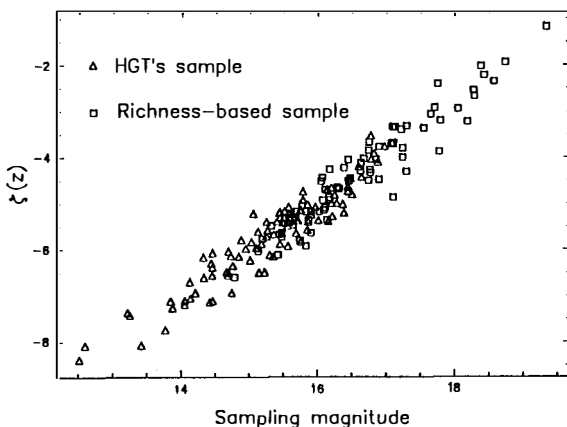
Figure 3 : The (linear) Hubble diagram of the HS data for $q_o = -0.76$ and $\Omega_o = 0.1$. HGT sample : triangles ; Schneider, Gunn and Hoessel (1983) richness-based sample : squares. No apparent deviation from a straight line can be found in the distribution.

Moreover, Figure 3 displays the (linear) Hubble diagram of these data for the world model defined by $q_o = -0.76$ and $\Omega_o = 0.1$, and no apparent deviation from a straight line can be found in the distribution ; which suggests also that no evolutionary effects are present in this

sample (unless the geometry masks this effect), see Triay (this conference) about the (linear) Hubble diagram.

4. CONCLUSION

For samples with no indication about the luminosity function and their completeness, as long as the objects are selected by means of their apparent magnitude, the null-correlation approach offers a powerful test to determine the deceleration parameter (if the evolutionary effects can be neglected).

If the selection effects in the HGT sample can be roughly described by the apparent magnitude as obtained bracketing the galaxies at a constant linear standard radius, the null-correlation test enables us to estimate a formal value of the deceleration parameter $q_o = -0.76 \pm 0.6$ ($\Omega_o = 0.1$). If the evolutionary effects are neglected (since $z_{max} \approx 0.15$), this result suggests that the data are consistent with a Friedmann-Lemaître model with a positive cosmological constant (in the sense that the vacuum is repulsive). It turns out that these selection effects are not described by a cutoff at a limiting magnitude (but a much smoother technical function), which confirms the Bigot, Fliche and Triay (1988) analysis. The distribution in aperture luminosities can be approximated by a Gaussian curve of dispersion ≈ 0.31 mag. In the other hand, by performing corrections for Bautz-Morgan, Richness classes and Nucleus multiplicity, the value of $q_o = 0.54$ ($\Omega_o = 0.1$) was found and the dispersion in aperture luminosities is ≈ 0.26 mag. However, the disagreement between these results suggests that the statistical model describing the HGT sample is not well determined.

REFERENCES

Bigot, G., Fliche, H.H., Triay, R.1988, Astron. Astrophys. **206**,1

Bigot, G., Rauzy, S., Triay, R., 1989, in prep. will be submitted to A & A (Main journal)

Burstein, D., Heiles, C., 1978, Astrophys. J. **225**,40

Fliche, H.H., Souriau, J.M., 1979, Astron. Astrophys. **78**,87

Gunn, J.E., Oke, J.B., 1975, Astrophys. J. **195**,255

Hoessel, J.G., Gunn, J.E., Thuan, T.X., 1980, Astrophys. J. **241**,486

Hoessel, J.G., Schneider, D.P., 1985, Astron. J. **90**,1648

Kristian, J., Sandage, A., Westphal, J.A., 1978, Astrophys. J. **221**,383

Malmquist, K.G., 1920, Medd. Lund Astron. Obs. (ser. 2) **22**, 9

Schneider, D.P., Gunn, J.E., and Hoessel, J.G, 1983, Astrophys. J. **264**,337

Scott E.L., 1957, Astrophys. J. **62**,248

IV. THE COSMOLOGICAL CONSTANT

VARYING COSMOLOGICAL CONSTANT
AND THE EARLY UNIVERSE

Katsuhiko SATO, Nobuo TERASAWA and Jun'ichi YOKOYAMA
Department of Physics, Faculty of Science, University of Tokyo
Bunkyo-ku, Tokyo 113, Japan

K.Sato

Abstract

Cosmological constant (or the vacuum energy density) is necessary for the universe to be created without singularity, but observations show that the value at the present universe must be extremely small. We investigated effects of varying cosmological constant on the baryogenesis and the primordial nucleosynthesis. It is shown that stringent constraints on the value of the vacuum energy density are imposed from primordial nucleosynthesis, but very loose constraints can be imposed from the baryogenesis, i.e., the baryogenesis is insensitive to the remaining cosmological constant. From these two results, we speculate that the universe inflate extremely rapidly by the slowly-decaying cosmological constant in the period between the baryogenesis and the primordial nucleosynthesis.

1. Introduction

The cosmological constant Λ is a constant term in the Einstein equation, $G_{ij} - \Lambda g_{ij} = 8\pi G T_{ij}$. If we interpret this term Λg_{ij} as a energy momentum tensor of the empty space or vacuum, T_{ij}^{vac}, i.e., $\Lambda g_{ij} = 8\pi G T_{ij}^{vac}$, the existence of the cosmological constant means that the vacuum possesses a constant energy density $\rho_v = \Lambda/8\pi G$ and the negative pressure $p_v = -\Lambda/8\pi G$, which neither decrease nor increase by cosmic expansion. This cosmological constant is introduced by Einstein in order to prevent his static universe from collapsing against gravity, since the cosmological constant with positive sign plays as a universal repulsive force for space. As is well known, however, he said, "The introduction of the cosmological constant is the biggest blunder of my life," after the discovery of cosmic expansion. Nevertheless I want to stress that its introduction is not his blunder but one of the biggest brilliance in his life, because in this decade it has become very clear that the cosmological constant is an important key for the universe to be created[1],[2] and for the created mini-universes to inflate to macroscopic universes[3]−[6].

For example, if we take a scenario proposed by Vilenkin[1], universes are created from "nothing" via tunneling effect. Let us assume, for simplicity, that universes are closed, homogeneous and isotropic, and are filled only with vacuum energy ρ_v, then the Lagrangian of this mini-superspace model is given by

$$L = \frac{3\pi}{4G}(-a\dot{a}^2 + a - \frac{a^3}{\ell^2}),$$

(1)

where a is the scale factor of the universe and ℓ is the characteristic length of this universe model, $\ell = (8\pi G\rho_v/3)^{-1/2} = (\Lambda/3)^{-1/2}$. Then we get the Hamiltonian by using the standard procedure of classical mechanics,

$$H = -\frac{2G}{3\pi a}[\frac{1}{2}p^2 + V(a)],$$

(2)

where p is the canonical momentum, $p \equiv \partial L/\partial \dot{a} = -3\pi a\dot{a}/2G$, and

$$V(a) \equiv \frac{3\pi a^2}{4G}(1 - \frac{1}{3}\Lambda^2 a^2).$$

(3)

Then we get the Wheeler-de Witt equation by replacing p with $-id/da$,

$$[\frac{1}{2}(-i\frac{d}{da})^2 + V(a)]\Psi(a) = 0.$$

(4)

Vilenkin showed that the tunneling probability from the state of "nothing", $a = 0$, to the starting point of the classical universe, $a = (\Lambda/3)^{-1/2}$, is given by

$$P \propto \exp(-\frac{3\pi}{G\Lambda}).$$

(5)

This means that the larger the cosmological constant is, the greater is the tunneling probability. Thus the classical singularity at $a = 0$ is avoided and the non-singular universe is created thanks to the existence of the cosmological constant. It is obvious at present stage that the introduction of the Λ is one of the biggest brilliance in Einstein life, and never the biggest blunder. The cosmological constant is an important key for the universe to be created.

On the other hand, we know that stringent upper limit of the cosmological constant is imposed from cosmological observations, $\Lambda \leq H_0^2 \sim 10^{-55} \text{cm}^{-2}$ or $\rho_v \leq 10^{-120} m_p^4$, where H_0 and m_p are present Hubble parameter and the Planck mass, respectively. This implies that the "cosmological constant" is not a constant but evolves in the history of the universe[7)-10)].

2. Evolution of the Cosmological Constant and Constraints on its variation

As I stressed in Section 1, the cosmological constant must exist at the Planck time in order for universes to be created without a singularity, and to inflate exponentially. After the inflation, it is usually assumed that the vacuum energy density vanishes, but it is rather natural to consider that Λ remains still after the inflation, although it decreases greatly. As a model of its evolution, Peebles and Ratra[7)] proposed a model that the ratio of the vacuum energy density to that of radiation, ρ_v/ρ_r, varies as $a^{8/(-\alpha+2)}$ in radiation dominated universe. This evolution comes from the rolling over of a scalar field with the potential $V(\phi) = \lambda\phi^\alpha$, $\alpha < 0$. They showed that models with $\alpha = -4$, or -6 are consistent with observations of the present universe, such as $m - z$ relation and the number density$-z$ relation. This model, however, suffers from a fine tuning problem when we go back to early universe as noticed by Peebles and Ratra themselves[7)]. For example, if we take $\alpha = -6$, ρ_v/ρ_r is only 10^{-32} at the Planck time. Since the natural scale of the vacuum energy at this epoch is m_p^4, the fine tuning of the order of 10^{-32} is necessary. In order to avoid this fine tuning, α must be very small, then ρ_v/ρ_r becomes almost constant. It seems reasonable that the vacuum energy density evolves along the line of $\rho_v \sim \rho_r$ in the early stage of the universe, though it conflicts observations in the present or late stages. Then models we can consider would be the following two.

Model A: $\rho_v \propto a^{-4}$, i.e., the ρ_v evolves just like radiation.

Model B: ρ_v is a piece-wise constant function of a which decreases with a stair-like manner.

It is easily presumed that the stringent constraints on these models are imposed from the baryogenesis and the primordial nucleosynthesis. In the present work, we show that this presumption is true for the nucleosynthesis but not for the baryogenesis. That is, it

196
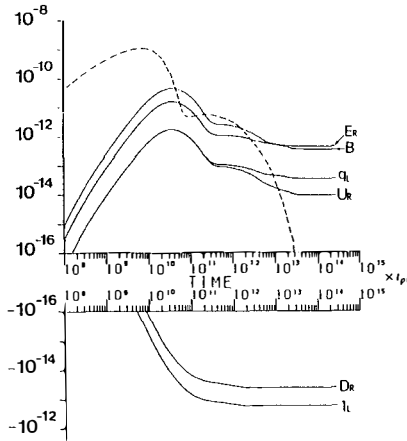
Fig. 1 Time evolution of baryon asymmetry in the model $\rho_v = 0, M_H = 2 \cdot 10^{13}\text{GeV}, \epsilon = 10^{-7}$, and $C_v = 2 \cdot 10^9\text{GeV}$.

turns out that baryogenesis can set only a very loose constraint on the magnitude of the vacuum energy.

3. Constraint from the baryogenesis

In the present status of high energy physics theories by which we should describe the early history of the universe, we cannot, unfortunately, single out any definite model of baryogenesis among numerous possible candidates. It seems, however, the model investigated by Yokoyama et al [11] is a typical and natural model. In this work, we investigated the constraint on the evolution of the vacuum energy by using this model. In this model, the evolution of the inflaton field ϕ in the reheating phase is governed by the following equation,

$$\ddot{\phi} + 3H\dot{\phi} + C_v\dot{\phi} = V'(\phi), \tag{6}$$

where $V'(\phi)$ is the derivative of the potential

$$V(\phi) = \frac{1}{2}M^2\phi^2 + \rho_v(a). \tag{7}$$

The value of M is taken to be $2 \cdot 10^{13}$ GeV in order for the appropriate amplitude of density fluctuations remain after inflation. In this model, there remains the vacuum energy density

$\rho_v(a)$, which is given by

$$\rho_v(a) = \text{const.} \cdot a^{-4}, \qquad \text{for Model A,}$$
$$= \text{constant during baryogenesis, for Model B.} \qquad (8)$$

We assume that the inflaton's energy is transferred to Higgs bosons $(H, \overline{H})$ via viscosity term $C_v \dot{\phi}$, and baryon number asymmetry, as well as the entropy of the universe, is generated by their decay. The decay modes and rates are as follows.

$$\Gamma(H \to U_L^c E_L^c) = \alpha_U R_H, \qquad \Gamma(\overline{H} \to U_R E_R) = \alpha_U R_H(1 + \epsilon),$$
$$\Gamma(H \to U_L D_L) = 2\alpha_U R_H, \qquad \Gamma(\overline{H} \to U_R^c D_R^c) = 2\alpha_U R_H(1 - \epsilon/2),$$
$$\Gamma(H \to U_R^c E_R^c) = \alpha_D R_H, \qquad \Gamma(\overline{H} \to U_L E_L) = \alpha_D R_H, \qquad (9)$$
$$\Gamma(H \to D_R^c \nu_R^c) = \alpha_D R_H, \qquad \Gamma(\overline{H} \to D_L \nu_L) = \alpha_D R_H,$$
$$\Gamma(H \to U_R D_R) = \alpha_D R_H, \qquad \Gamma(\overline{H} \to U_L^c D_L^c) = \alpha_D R_H,$$

where U, D, E and ν represent up-like and down-like quarks, electron like leptons and neutrinos, respectively. Here R_H is related with the Higgs boson mass, M_H, as $R_H = 3M_H/16$ and coupling constants are taken to be $\alpha_U = 3 \cdot 10^{-4}$ and $\alpha_D = 7 \cdot 10^{-6}$ depending on the quark masses. ϵ is the CP breaking parameter and net baryon asymmetry of $\epsilon/3$ is produced by the decay of a pair of H and $\overline{H}$.

In Fig. 1, a typical example of the evolution of asymmetries in various species is shown for a model with the vanishing vacuum energy density[11]. In the first step asymmetry is made by decay of Higgs bosons, in the second step it is decreased by the effect of inverse decays to Higgs bosons and is eventually frozen out when the temperature drops too low for these processes to occur.

In Fig. 2, baryon asymmetry generated in the Model A is shown as the function of the ratio ρ_v/ρ_r when the baryogenesis and the entropy production terminate. As seen in this figure, for the case $C_v = 10^{10}$GeV, the baryon asymmetry first increases with the vacuum energy density, until the ratio $R = \rho_v/\rho_r$ becomes as large as 10^6. This is because the decrease of the asymmetry by the inverse decay is suppressed by the rapid expansion of the universe due to the remaining vacuum energy density. In the region $R > 10^6$, however, the baryon entropy ratio b/s decreases monotonically with increasing R as $b/s \propto R^{-1/4}$.

This relation is easily derived: The entropy production and baryogenesis effectively occur when the cosmic expansion decelerates and becomes $H = C_v$, where the cosmic expansion rate, H, is given by $H = (8\pi G \rho_v/3)^{1/2}$ in the limit $R \to \infty$. Then the baryon/entropy ratio b/s is approximately given by

$$\frac{b}{s} \approx \frac{\epsilon \Gamma n_H}{\Gamma n_H M_H/T^*} = \frac{\epsilon T^*}{M_H}, \qquad (10)$$
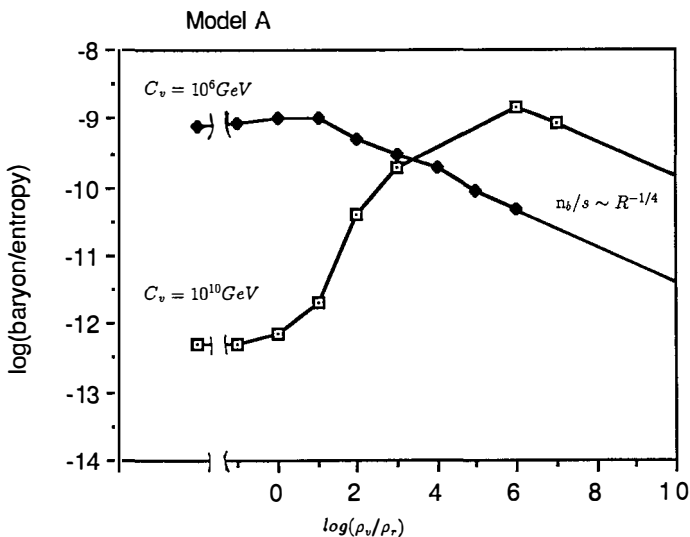
Fig. 2 Baryon/entropy ratio in the Model A(ρ_v =const·a^{-4} is shown as the function of $R = \rho_v/\rho_r$ when the baryogenesis and entropy production terminate. The values of parameters are $M_H = 2 \cdot 10^{13}$GeV and $\epsilon = 10^{-7}$.

where Γ is the mean decay rate of Higgs bosons and T^* is the cosmic temperature at the time when $H = C_v$, which is given by

$$T^* \approx (\rho_r^*)^{\frac{1}{4}} = (\frac{\rho_v^*}{R})^{\frac{1}{4}} = (\frac{3C_v^2}{8\pi GR})^{\frac{1}{4}}. \tag{11}$$

Substituting this temperature into (10), we get

$$\frac{b}{s} \approx (\frac{3}{8\pi G})^{\frac{1}{4}}(\frac{\epsilon}{M_H})C_v^{\frac{1}{2}}R^{-\frac{1}{4}}. \tag{12}$$

From the observation, $b/s > 10^{-11}$, we can get the constraint on the ρ_v/ρ_r ratio,

$$\frac{\rho_v}{\rho_r} < 10^{15}(\frac{C_v}{10^{10}\text{GeV}})^2(\frac{\epsilon}{10^{-7}}). \tag{13}$$

This is a surprisingly loose constraint in spite that there remain uncertainties on the value of C_v and ϵ.

In Fig. 3, baryon asymmetry in the Model B (ρ_v =const during baryogenesis) is shown as a function of the vacuum energy density. As shown in this figure the baryon asymmetry becomes almost vanishing when the vacuum energy density exceeds a critical value. At this point the expansion rate H_v becomes greater than the viscosity coefficient C_v, $H_v > C_v$,

Model B (const. Vacuum energy density)
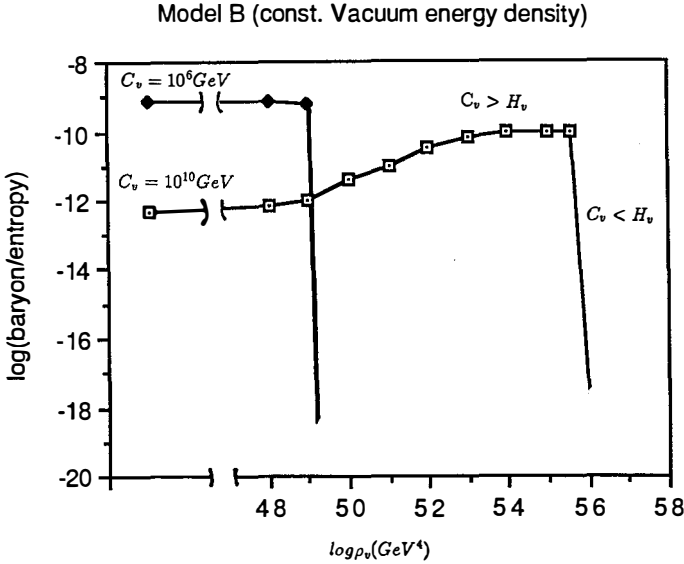
Fig. 3 Baryon/entropy ratio in the Model B(ρ_v =const) is shown. The values of parameters are $M_H = 2 \cdot 10^{13}$GeV and $\epsilon = 10^{-7}$.

where $H_v^2 = 8\pi G \rho_v/3$. This is because that the exponential expansion due to the remaining vacuum energy begins before the baryogenesis. From the observation, we get an upper limit on the remaining vacuum energy density as

$$\rho_v < \frac{3C_v^2}{8\pi G} = (10^{14}\text{GeV})^4 (\frac{C_v}{10^{10}\text{GeV}})^2. \tag{14}$$

We get again only a very loose constraint on the remaining vacuum energy density.

4. Constraint from nucleosynthesis

In the Model A $(\rho_v/\rho_r = x; constant)$, the upper limit of the ρ_v is easily obtained from the ⁴He abundance as the upper limit of the neutrino species is obtained. As is well known, with increasing the total energy density, $\rho = \rho_v + \rho_r = (1 + x)\rho_r(T)$, the cosmic expansion is accelerated and as a result, ⁴He abundance is increased. From the upper limit of the ⁴He abundance $Y \leq 0.26$, x must be smaller than 0.16, i.e.,

$$\frac{\rho_v}{\rho_r} \leq 0.16. \tag{15}$$

Recently Freese et al[12] derived $x \leq 0.1$ assuming that the sum of the radiation energy and the vacuum energy is conserved.

Constraint on the vacuum energy density in Model B (the vacuum energy is constant during the nucleosynthesis) is also easily obtained by modifying a nucleosynthesis program. In Fig. 4, the synthesized abundances are shown as a function of the vacuum energy density. As seen in Fig. 4, ^{4}He abundance increases with increasing the vacuum energy density, since free neutrons remain after the freezing of beta process by the rapid cosmic expansion. However, in the limit of large vacuum energy density, ^{4}He abundance turns to decrease because no more nuclear reactions can catch up the cosmic expansion (see Fig. 5). As a result, very abundant D and ^{3}He are synthesized. Then, a constraint on the vacuum energy density

$$\rho_v < (0.034\text{MeV})^4. \tag{16}$$

is obtained from the condition that $(\text{D} +^3 \text{He})/\text{H} < 10^{-4}$.
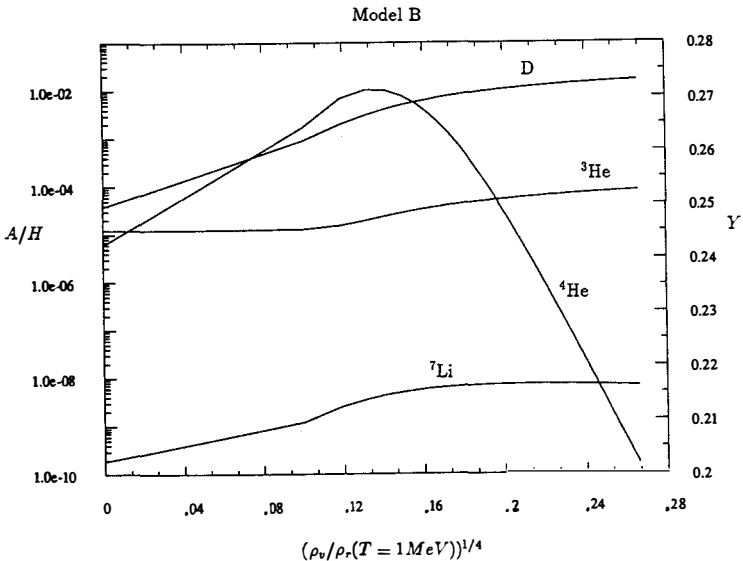
Fig. 4 Synthesized abundance of light elements in Model B (the vacuum energy density is constant during the primordial nucleosynthesis). The abscissa is the vacuum energy density in units of radiation energy density when the cosmic temperature is $T = 1$ MeV.
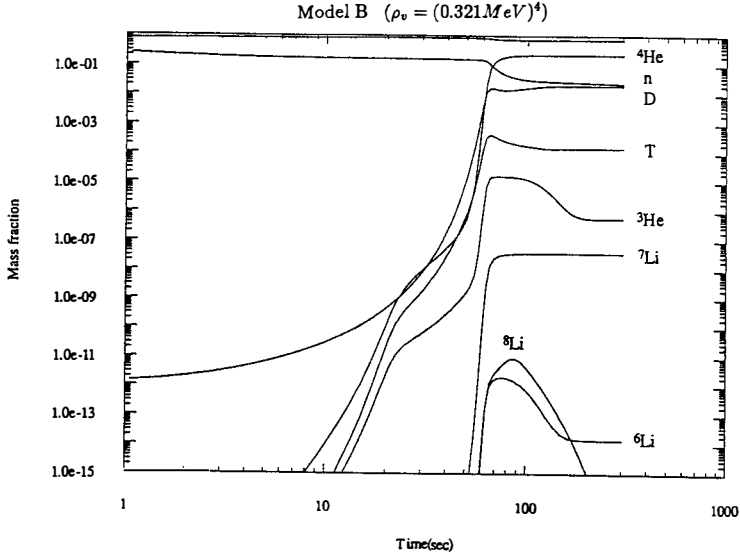
Model B $(\rho_v = (0.321MeV)^4)$

Fig. 5 The time evolution of light elements abundance in Model B ($\rho_v = (0.321\text{MeV})^4$ and $\eta = 5 \cdot 10^{-10}$)

5. Conclusion and Remarks

As shown in preceding sections, it was shown that stringent constraints on the value of the vacuum energy density are imposed from primordial nucleosynthesis,

$$\frac{\rho_v}{\rho_r} \leq 0.16 \qquad \text{for Model A,} \tag{17}$$

and

$$\rho_v < (0.034\text{MeV})^4 \quad \text{for Model B.} \tag{18}$$

However, it was shown that very loose constraints on the vacuum energy density is imposed from the baryogenesis. It is surprising that the baryogenesis is insensitive to the remaining cosmological constant.

From these two results, we can speculate that the universe inflate extremely rapidly by the slowly decaying cosmological constant in the period between the baryogenesis ($t \sim 10^{-36}$sec, the characteristic time scale of GUTs(grand unified theories)) and the primordial nucleosynthesis ($t \sim 1$sec). It seems rather natural to consider that a fraction of the vacuum energy density remains after the primordial inflation or after phase transitions of vacuum.

If we assume that the remaining vacuum energy density is of the order of GUT scale and almost constant, and it decays just before the nucleosynthesis without producing entropy, the universe would have cooled exponentially within 10^{-34}sec. Then what observational effects can be expected from this scenario? We may presume that phase transitions which are expected to occur between the cosmic temperature 10^{15}GeV and a few MeV become of very strong first order, since the transition cannot catch up the cosmic expansion until the universe stops the extremely rapid expansion. Then the large density fluctuations are produced by the quark hadron phase transition. In order for the present rapid cooling scenario to work, the remaining vacuum energy density and the kinetic energy of the scalar field must disappear by cosmic expansion without dissipation. It, however, depends on the model of the potential of scalar field ϕ: If we assume the potential,

$$V(\phi) = \lambda \phi^n \tag{19}$$

then, oscillation energy damps as

$$\rho_\phi = \frac{1}{2}\dot{\phi}^2 + V(\phi) \propto a^{-6n/(n+2)}. \tag{20}$$

Then ρ_ϕ decreases faster than ρ_r, if $n > 4$. If we take the potential,

$$V(\phi) = \lambda \exp[-(8\pi Gn)^{1/2}(\phi - \phi^*)], \tag{21}$$

which is adopted in Peebles and Ratra[7], the oscillation energy damps as

$$\rho_\phi = V(\phi^*)(\frac{a^*}{a})^n. \tag{22}$$

If we take $n > 4$, ρ_ϕ can damp quickly.

Details of the present talk will be reported elsewhere soon[13].

References

1) A. Vilenkin, Phys. Rev., **D33** (1986), **3560** and **D37**(1988), 888.

2) J. B. Hartle and S. W. Hawking, Phys. Rev., **D28**(1983), 2960.

3) K. Sato, Month. Not. Roy. Astron. Soc, **195**(1981), 467, and Phys. Lett. **B99**(1981), 66.

4) A. H. Guth, Phys. Rev., **D23**(1981), 347.

5) A. D. Linde, Phys. Lett. **108B**(1982), 389.

6) A. Albrecht and P. J. Steinhardt, Phys. Rev. Lett. **48** (1982), 1220.

7) P. J. E. Peebles and B. Ratra, Astrophys. J., **325**(1988), L17.

8) A. A. Dolgov, in *The Very Early Universe*, ed. by G. W. Gibbons, S. W. Hawking and S. T. C. Siklos, (Cambridge Univ. Press, 1982), 449.

9) Y. Fujii, Mod. Phys. Lett. A, to be published.

10) S. Weinberg, Rev. Mod. Phys., **61**(1989), 1.

11) J. Yokoyama, K. Sato and H. Kodama, Phys. Lett., **196B** (1987), 129.

12) K. Freese, F. C. Adams, J. A. Frieman and E. Motttola, Nucl. Phys., **B287**(1987), 797.

13) K. Sato, N. Terasawa and J. Yokoyama, in preparation.

NUCLEOSYNTHESIS IN THE INHOMOGENEOUS UNIVERSE AND NEUTRON DIFFUSION

Katsuhiko Sato and Nobuo Terasawa

Department of Physics, Faculty of Science,
The University of Tokyo, Bunkyo-ku, Tokyo 113, Japan

K.Sato

Abstract

We investigate nucleosynthesis in the universe with isothermal baryon density fluctuations taking into account nucleon diffusion during the nucleosynthesis. We find $\Omega_B = 1$ universe is marginally consistent with the light element abundances (D, ^{3}He, ^{4}He, ^{7}Li) if the density contrast, R, is very high, $\gtrsim 300$ and the other parameters are tuned.

It has been suggested that isothermal baryon density fluctuations are generated during the quark-hadron phase transitions[1]-[5]. These fluctuations significantly affect primordial nucleosynthesis through 2 effects: (1) The abundances of elements sensitively depend on the local baryon-photon ratio, and the final average abundances of the elements are much different from those in the uniform universe. (2) When the temperature falls down to $\sim 1\,\mathrm{MeV}$, the weak interactions among nucleons cannot catch up with cosmic expansion and decouple. Then the neutron diffusion length becomes significantly longer than the proton diffusion length and neutron-proton segregation occurs.[6]

Applegate et al.[6], Alcock et al.[7], and Fuller et al.[8] investigated the nucleosynthesis in this model and showed that the light element abundances are greatly modified in particular by the effect of (2): They showed that ^{4}He overproduction in the high-density region is suppressed by the escape of neutrons and also synthesized abundance of D is enhanced in the low-density region by neutrons which come from the high-density region. Their most important and interesting result is that in this scenario, $\Omega_B = 1$ universe can be consistent with the observations of the abundances of light elements except for ^{7}Li[9] provided that the baryon density contrast between high and low density regions is sufficiently large. If the ^{7}Li problem is removed, the dark matter can be baryonic and no more speculative candidates, such as photinos, gravitinos etc. are necessary.

In early works, however, nucleosynthesis was calculated independently in the high-density and in the low-density regions and neutron diffusion during the nucleosynthesis was neglected as criticized by several authors.[10]-[15] Since neutron diffusion length keeps growing during nucleosynthesis [6], neutron diffusion cannot be neglected. Moreover, Applegate, Hogan, and Scherrer[12] suggested that heavy elements are formed via a primordial r-process which may take place in neutron-rich regions.

To examine the effects of the nucleon diffusion after the onset of nucleosynthesis and how much seed nuclei of r-process is produced, we calculate nucleosynthesis incorporating the neutron diffusion and the proton diffusion in the wide ranges of parameters using the extended reaction network including up to ^{32}S.[16]

In the present work, we assume the universe consists of two regions; a high-density region whose volume fraction is f_v and a low-density region $(1 - f_v)$. The average baryon density is then, $\rho_b = f_v \rho_h + (1 - f_v)\rho_l$, where ρ_h and ρ_l are the baryon densities in the high and the low density regions respectively. The ratio of ρ_h to ρ_l is changed by nucleon diffusion. In this investigation, initial value, $R \equiv \rho_h^0/\rho_l^0$, is a parameter.

In order to take into account the nucleon diffusion between the high and the low density regions, diffusion terms are added to nuclear reaction networks;

$$\dot{Y}_i^h = -(Y_i^h - \rho_l Y_i^l/\rho_h)/f_v \tau_i, \tag{1}$$

$$\dot{Y}_i^l = -(Y_i^l - \rho_h Y_i^h/\rho_l)/(1 - f_v)\tau_i, \tag{2}$$

where Y_i^h and Y_i^l $(i = n,\ p)$ are the mass fractions of nucleon in the high and the low density region respectively. The time scale of diffusion τ_i is given by

$$\tau_i = \frac{d^2}{6D_i}\left(1 + \frac{\lambda_i}{d}\right) \tag{3}$$

where d is the physical size of high density zone, D_i is the diffusion coefficient and λ_i is the mean free path of neurons or protons. The second flux-limiter term in the parenthesis
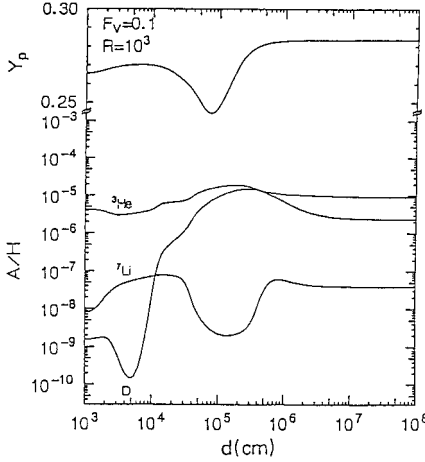
Fig. 1 The abundances of D, ^{3}He, ^{4}He, and ^{7}Li plotted against the scale of density fluctuations d at $T = 1\,\mathrm{MeV}$ for $\Omega_B = 1, f_v = 0.1$, and $R = 1000$.

is added to avoid the overestimation of diffusion since the diffusion approximation breaks down when the mean free path of nucleons becomes longer than the length scale of density fluctuations.[17] For the diffusion coefficients of neutrons and protons, we use those given by Applegate et al.[6].

The neutron lifetime and the number of neutrino species are taken as $\tau_n = 898\,\mathrm{sec}$[18] and $N_\nu = 3$, respectively. Thus intrinsic parameters of the calculation are the average baryon density parameter Ω_b, the volume fraction of the high-density region f_v, and the initial ratio of the baryon density of the 2 regions R, and the physical size of the high density zone d at $T = 1\,\mathrm{MeV}$. Calculated rages are $\Omega_b = 0.01 \sim 1(H_0 = 50\mathrm{kmMpc}^{-1}\mathrm{sec}^{-1}, T_0 = 2.7\mathrm{K})$, $f_v = 0 \sim 0.5$, $R = 1 \sim 10000$, and $d(T = 1\,\mathrm{MeV}) = 10^3 \sim 10^8\mathrm{cm}$.

In Fig. 1, the calculated abundances of D, ^{3}He, ^{4}He, and ^{7}Li are plotted against $d(T = 1\,\mathrm{MeV})$ for $f_v = 0.1$ and $R = 1000$.

In the range $d(T = 1\,\mathrm{MeV}) < 10^3\mathrm{cm}$, the diffusion time scale of neutrons is so short that the universe becomes uniform before the onset of the nucleosynthesis and the abundances turn out to be equal to those of uniform universe. In the range $10^3\mathrm{cm} \lesssim d(T = 1\,\mathrm{MeV}) \lesssim 10^4\mathrm{cm}$, neutrons which diffused out in the early stage from the high-density zone diffuse back as soon as the nucleosynthesis in the high density zone begins. Thus the low-density zone does not become neutron rich and abundances of light elements synthesized there are very small. Hence the D abundance is smaller than that in the uniform case, and the ^{4}He abundance and the ^{7}Li abundance turn out somewhat greater in this range.

The most interesting point is the behavior of the abundances in the range $10^4\mathrm{cm} \lesssim d(T = 1\,\mathrm{MeV}) \lesssim 10^6\mathrm{cm}$. For density fluctuations in this range, the diffusion time scale of neutrons is long enough and the nucleosynthesis in the low-density region starts before neutrons diffuse back to the high-density region. Hence the low-density region becomes neutron rich and

neutron-rich nucleosynthesis occurs there.
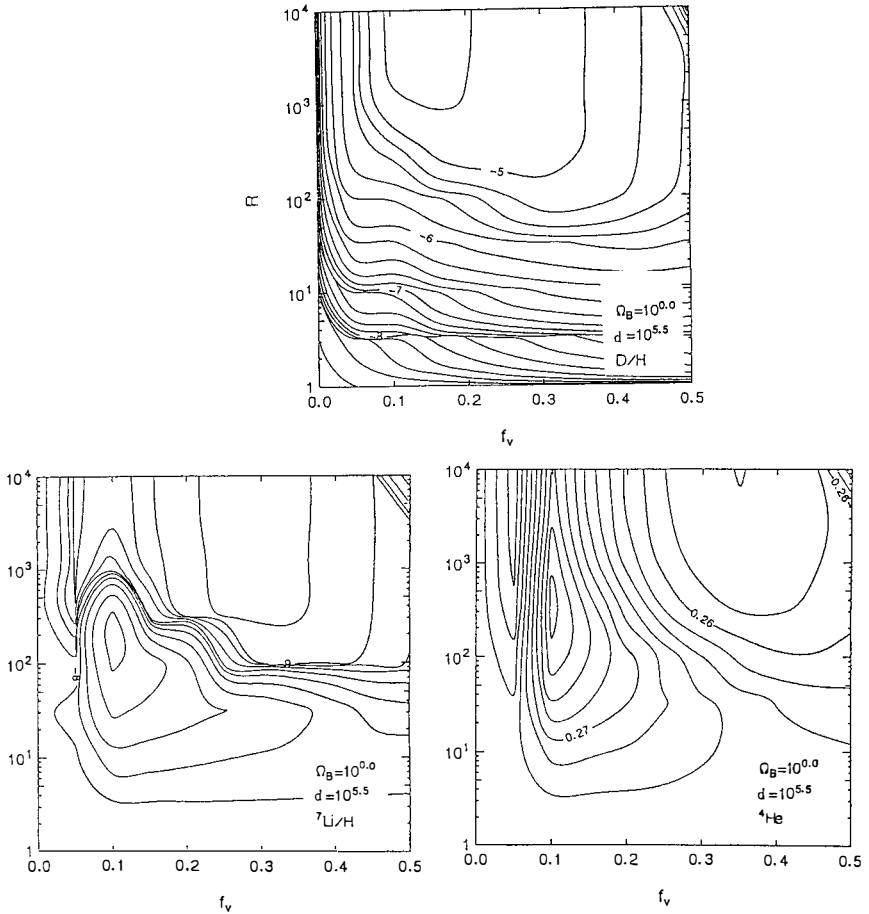
Fig. 2   The average abundances of D, ^{4}He, ^{7}Li, and heavy elements on the $R - f_v$ plane for $\Omega_B = 1$ and $d = 10^{5.5}$ cm, (a): log(D/H). (b): The mass fraction of ^{4}He(Y). (c): log(^{7}Li/H).

Since the nucleosynthesis in the low-density region begins late, the neutron fraction becomes small and the ^{4}He abundance turn out to be small in consequence. Thus we find that the ^{4}He abundance is consistent with the primordial abundance at $d(T = 1\,\mathrm{MeV}) \sim 10^5$cm. The decrease of the ^{7}Li abundance in this range, $10^4 \sim 10^6$cm, comes from the destruction of ^{7}Be in the high-density region by the neutron diffusion (via ^{7}Be$(n,\ p)^7$Li$(p,\ \alpha)^4$He) and from the destruction of ^{7}Li in the low-density region by the proton diffusion (via ^{7}Li$(p,\ \alpha)^4$He) although it is compensated by the synthesis of ^{7}Be in the high-density region due to the
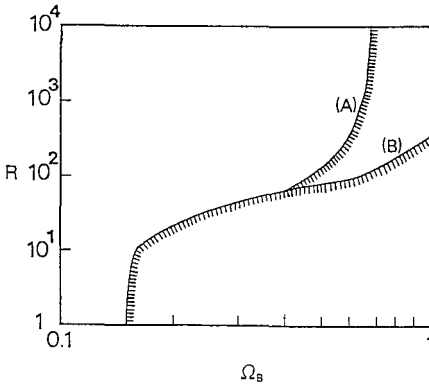
Fig. 3 The allowed range of R displayed against Ω_B in the range $0.1 \leq \Omega_B \leq 1$. (A): $Y < 0.25$, D/H $> 10^{-5}$, and ^{7}Li/H $< 10^{-9}$. (B): $Y < 0.26$, D/H $> 10^{-5}$, and ^{7}Li/H $< 10^{-9}$.

proton diffusion. The increase of the D abundance in the range $d(T = 1\,\text{MeV}) \gtrsim 10^4$cm is essentially due to the segregation of the high-density region and the low-density region.

In the range $d(T = 1\,\text{MeV}) \gtrsim 10^6$cm, the diffusion time scale is so long that two regions are almost independent each other and the final abundances of elements turn out to be a simple average of those of two independent regions.

In the case of Fig.1, we cannot find a range in which the primordial abundances of all the light elements are consistent simultaneously because the ^{7}Li abundance is too large ^{7}Li/H $> 10^{-9}$.[19] It is, however, obvious the intermediate region $10^{5.5\pm1}$cm is the most interesting region, because the abundances of ^{4}He and ^{7}Li have dips. Now let's investigate the abundance in the wide range of parameters R and f_v, assuming $d(T = 1\,\text{MeV}) = 10^{5.5}$cm.

As shown in Fig.2(a), the D abundance is consistent with the primordial abundance, D/H $> 10^{-5}$[19], if R is large enough as $R > 200$ and $0.1 < f_v < 0.35$. The ^{4}He abundance is also consistent with primordial abundance in the ranges $R > 100$ and $f_v > 0.2$ (Fig.2(b)), if we adopt a loose constraint on the primordial abundance $Y < 0.26$.[20] However, if we take the recent estimate by Steigman, Gallagher III, and Schramm [21], $Y < 0.25$, there exists no consistent region. The ^{7}Li abundance is consistent with the primordial abundance, ^{7}Li/H $< 10^{-9}$, in the ranges $R > 100$ and $0.15 < f_v < 0.45$ as we can see in Fig.2(c). We find, after all, that the $\Omega_B = 1$ is consistent with the primordial abundances of light elements in the ranges $R > 300$ and $0.2 < f_v < 0.35$ if we take the upper bound $Y < 0.26$.

In Fig.3, the allowed range of R is displayed against Ω_B. This constraint on R and Ω is derived by searching for the lowest value of R, which is consistent with a given set of constraints on the primordial abundances, on the $d - f_v$ plane for a fixed Ω. If we take a stringent constraint on the primordial ^{4}He abundance as $Y < 0.25$, $\Omega_B = 1$ is excluded and $\Omega_B = 0.7$ is marginal. If the present value of the Hubble constant, however, is as small as $H_0 = 40$kmMpc^{-1}sec^{-1}, $\Omega_B = 1$ is consistent with such a stringent constraint. This value is very small compared with the values usually accepted, $H_o = 50 \sim 100$kmMpc^{-1}sec^{-1}, but it cannot be necessarily excluded.[22] If the mean lifetime of neutrons, otherwise, is as short as 870sec., the ^{4}He abundance turns out to ^{4}He $= 0.25$ for $\Omega_B = 1(H_0 = 50$kmMpc^{-1}sec^{-1}) and

$\Omega_B = 1$ is also consistent with the light element abundances. This value of τ_n is about 2σ smaller that the value given by Particle Data Group, $\tau_n = 898 \pm 16\text{sec}$.[18], but it is consistent with the recent measurement by Last et al., $\tau_n = 876 \pm 21\text{sec}$. within the error.[23] Thus $\Omega_B = 1$ is not completely inconsistent with the abundances of light elements. However it is allowed for a rather marginal set of the parameters and these results are based on a 2-zone model. Hence it should be considered open. Details of the results and systematic discussion will be shown in the forthcoming paper.[24]

Finally, we would like to mention about heavy elements. The mass fraction of heavy elements is at most 10^{-9} and it is dominated by ^{11}B produced in the high-density region. The abundances of CNO elements are, for instance, $X(^{12}C) = 1.3 \times 10^{-11}, X(^{14}N) = 5.3 \times 10^{-12}, X(^{16}O) = 1.1 \times 10^{-13}$ in the case that $d = 10^{5.5}$ cm, $f_v = 0.1$ and $R = 1000$. It must be stressed that the abundance of heavy elements in the neutron-rich and low-density region is very small; $X(^{12}C)$ is 100 times smaller than the abundances in the high density region and the abundances of elements heavier than ^{12}C are negligibly small. This suggests that the contribution of primordial r-process proposed by Applegate, Hogan, and Scherrer[12] is small.

References

[1] E. Witten, Phys. Rev. D**30** (1984) 272.

[2] J. H. Applegate and C. J. Hogan, Phys. Rev. D**31** (1985) 3037.

[3] K. Iso, H. Kodama, and K. Sato, Phys. Lett. **169B** (1986) 337.

[4] K. Kajantie and H. Kurki-Suonio,Phys. Rev. D**34** (1986) 1719.

[5] H. Kurki-Suonio, Phys. Rev. D**37** (1988) 2104.

[6] J. H. Applegate, C. J. Hogan, and R. J. Scherrer, Phys. Rev. D**35** (1987) 1151.

[7] C. R. Alcock, G. M. Fuller, and G. J. Mathews, Astrophys. J. **320** (1987) 439.

[8] G. M. Fuller, G. J. Mathews, and C. R. Alcock, Phys. Rev. D**37** (1988) 1380.

[9] J. Audouze, P. Delbourgo-Salvador, H. Reeves, and P. Salati, in *The Origin and the Distribution of the Elements*, edited by G. Mathews(World Scientific, Singapore).

[10] R. A. Malaney and W. A. Fowler, preprint, 1988(to be published).

[11] H. Kurki-Suonio et al., preprint, 1988(to be published).

[12] J. H. Applegate, C. J. Hogan, and R. J. Scherrer, Astrophys. J. **329** (1988) 572.

[13] G. J. Mathews, G. M. Fuller, C. R. Alcock, and T. Kajino, 1988, preprint(to be published).

[14] R. A. Matzner, J. M. Centrella, T. Rothman, and J. R. Wilson, Center For Relativity preprint, 1987 (to be published).

[15] N. Terasawa and K. Sato, Prog. Theor. Phys. **81** (1989), 254. and **81** (1989) No.5.

[16] N. Terasawa and K. Sato, Astrophys. J. **294** (1985) 9; Prog. Theor. Phys. Lett.**72** (1985) 1262.

[17] There are many papers on the flux-limited diffusion. See for instance; C. D. Levermore and G. C. Pomraning, Astrophys. J. **248** (1981) 321.

[18] Particle Data Group, Phys. Lett. **170B** (1986)1.

[19] A. M. Boesgaard and G. Steigman, Ann. Rev. Astron. Astrophys. **23** (1985) 319.

[20] J. Yang, M. S. Turner, G. Steigman, D. N. Schramm, and K. A. Olive, Astrophys. J. **281** (1984) 493.

[21] G. Steigman, J. S. Gallagher III, and D. N. Schramm, 1987, preprint(to be published).

[22] D. Branch et al., Astrophys. J. **270** (1983) 123.

[23] J. Last et al., Phys. Rev. Lett. **60** (1988) 995.

[24] N. Terasawa and K. Sato, Phys. Rev. D**39** (1989) 2893.

THE COSMOLOGICAL CONSTANT AND WEYL SYMMETRY

J. Solà

Grup de Física Teòrica,
Universitat Autònoma de Barcelona,
08193 Bellaterra (Barcelona), Catalonia, Spain

ABSTRACT

We discuss the possible rôle played by gauge Weyl invariance as a distinguished symmetry to be shared by matter and gravitational fields in order to achieve stability of flat spacetime.

1. INTRODUCTION

In this talk we discuss a possible framework to tackle the (theoretically) unun-derstood observational value of the cosmological constant. As it is well known, the observation of small clusters of galaxies (the lowest density systems to which one applies Newtonian theory with some success) puts an upper limit to the allowed value of the effective cosmological constant Λ_{eff} (i.e. bare term plus induced con-tributions) in Einstein's equations. Similarly, if we believe that our universe can be described by a Friedmann–Robertson–Walker model, the combined observation of the deceleration parameter and of the average energy density sets another upper bound on Λ_{eff}. In both cases one obtains, roughly, the same extremely stringent bound: $\Lambda_{eff} < 10^{-84} GeV^2$ [1] , which is unprecedented in the history of physical measurements. Since Λ_{eff} is a dimensionful parameter, its smallness can be better assessed by noticing, for example, that its experimental upper value is 34 orders of magnitude smaller than the smallest upper bound available on the photon mass squared: $m_\gamma^2 < 10^{-50} GeV^2$.

The former limit on Λ_{eff} can be interpreted as an experimental limit on the vacuum value of the trace of the energy–momentum tensor: $< T_\mu^\mu > < 10^{-46} GeV^4$. Since the various, and very much dissimilar, mass scales of spontaneous symmetry breaking (SSB) in quantum field theory (e.g., chiral symmetry breaking in QCD, electroweak and grand unified phase transitions etc.) induce an effective cosmological term, which is very many orders of magnitude off the permitted one, we are faced with a big problem: the longstanding cosmological constant problem [2]

Needless to say, there have been innumerable previous attempts at solving this problem using a variety of different approaches. In particular, let us first focus our attention on dynamical mechanisms [3] and specifically on a proposal (the Cosmon model [4,5]) in which the cosmological constant is related to the fate of dilatation symmetry. One obvious motivation for considering dilatation symmetry is that the divergence of the dilatation current is linked to the trace of the energy–momentum tensor [6] . In order that mass scales may appear explicitly in the theory, this dilata-tion symmetry must be realized in a Nambu–Goldstone manner, being spontaneously broken at a high scale M, possibly near M_P (the Planck mass).

The Standard Model (SM) can be easily written in a (globally) scale- invariant fashion [4,6] by introducing a coefficient factor $e^{S/M}$ for each mass parameter (essen-tially the Higgs mass parameter, μ_ϕ) entering the action, where S is the non–linearly realized dilaton field, which in ref.[4] played the rôle of the Cosmon. Furthermore, if we include a scale-invariant kinetic energy term for S and a dilatation symmetric gravity piece, the action reads (in an obvious notation)

$$I = \int d^4x \sqrt{-g}\Big\{ h\chi^2 R + \frac{1}{2}g^{\mu\nu}\partial_\mu\chi\partial_\nu\chi + \mathcal{L}_{SM}(g^{\mu\nu}, \phi, \psi, W_\mu, \mu_\phi^2 e^{2S/M}) \Big\}, \quad (1)$$

where as in ref.[4] we defined

$$h = \frac{1}{16\pi}\Big(\frac{M_P}{M}\Big)^2 \quad (2)$$

and

$$\chi = Me^{S/M}. \tag{3}$$

The action (1) is invariant under global Weyl transformations:

$$\phi(x) \rightarrow e^{\alpha}\phi(x), \tag{4a}$$

$$\psi(x) \rightarrow e^{\frac{3}{2}\alpha}\psi(x), \tag{4b}$$

$$W_{\mu}(x) \rightarrow W_{\mu}(x), \tag{4c}$$

$$g_{\mu\nu}(x) \rightarrow e^{-2\alpha}g_{\mu\nu}(x) \tag{4d}$$

and

$$S(x) \rightarrow S(x) + \alpha M , \tag{5}$$

where α is, at this point, a constant.

Notice that in Weyl's formulation of scale invariance there is no coordinate dilatation: $x \rightarrow x$. Although it is possible to keep the metric unchanged while transforming the coordinates[6] this is not convenient in the presence of gravity, since global Weyl dilatations commute with general Einstein transformations whereas coordinate dilatations do not.

We would like to extend the global dilatation invariance of the Cosmon model[4] to **local** scale invariance (α in eqs. (3)–(4) becoming now an arbitrary local spacetime function $\alpha(x)$), as this is more in the spirit of general relativity. Now, local Weyl invariance is usually assumed to be an "accidental" or "hidden" symmetry of the fundamental action[7] rather than another gauge symmetry. The problem with this approach is that the conformal variances of the first two terms in eq.(1) cancel each other only for $h = -1/12$, which is unacceptable. In principle this could be arranged by reversing the relative sign of the two relevant terms, but this would render S a ghost and special prescriptions would be needed to avoid conflicts with unitarity[8] . An alternative formulation[9] that avoids this problem is obtained by implementing conformal invariance as a gauge symmetry, i.e. along the same lines than Weyl's original approach to a geometric unification of gravity and electromagnetism[10] .

2. GAUGE WEYL INVARIANCE

To fulfil our program we need: i) to introduce a new vector boson C_{μ} (Weyl's conformal gauge boson), ii) to enlarge the SM covariant derivatives in order to include the new gauge symmetry, and iii) to modify the metric connection such that it be conformally invariant.

Under a conformal gauge transformation, the Weyl gauge boson changes as

$$C_\mu \to C_\mu - \frac{1}{g_c}\partial_\mu \alpha(x) \, , \tag{6}$$

(g_c being a dimensionless coupling constant). To guarantee local conformal invariance, the $SU(2) \times U(1)$ covariant derivative for scalars must be enlarged as follows

$$\nabla_\mu \to \nabla_\mu + g_c C_\mu \, , \tag{7}$$

while the one for fermions in the following different way

$$\tilde{\nabla}_\mu \to \tilde{\nabla}_\mu + \frac{1}{2} i\omega_{\mu ab} S^{ab} \, , \tag{8}$$

where the last term of eq.(8) is constructed from the ordinary spin connection (see ref.[9] for detailed formulas) and from $S^{ab} = (i/4)[\gamma^a, \gamma^b]$, the spin matrices. It is remarkable that the fermion covariant derivative need not to involve C_μ nor any other conformal gauge boson. Thus, eq.(8) is just the usual covariant derivative for spinors in Einstein's general relativity, having the property that under general coordinate transformations, it transforms as a covariant vector, while under local Lorentz transformations it transforms like any spinor.

Now, in order to build a conformally–invariant coupling of the Cosmon to gravity, we need to modify the metric connection in a suitable manner. The usual Christoffel symbols, $\Gamma^\eta_{\mu\nu}$, are replaced by the dotted ones

$$\dot{\Gamma}^\eta_{\mu\nu} = \Gamma^\eta_{\mu\nu} - g_c(g^\eta_\nu C_\mu + g^\eta_\mu C_\nu - g_{\mu\nu} C^\eta) \, , \tag{9}$$

which are invariant under conformal transformations. The new geometry no longer has a zero covariant derivative of the metric. Thus, although angles are preserved, lengths are not preserved under affine transport of vectors.

The corresponding conformally–invariant Riemann and Ricci tensors are, respectively,

$$\dot{R}^\lambda_{\mu\nu\eta} = \partial_\eta \dot{\Gamma}^\lambda_{\mu\nu} - \partial_\nu \dot{\Gamma}^\lambda_{\mu\eta} + \dot{\Gamma}^\rho_{\mu\nu}\dot{\Gamma}^\lambda_{\eta\rho} - \dot{\Gamma}^\rho_{\mu\eta}\dot{\Gamma}^\lambda_{\nu\rho} \tag{10a}$$

and

$$\dot{R}_{\mu\nu} = \dot{R}^\lambda_{\mu\lambda\nu} \, . \tag{10b}$$

The Ricci scalar of this geometry is not invariant; it has conformal weight -1 :

$$\dot{R} \to e^{2\alpha}\dot{R} \, . \tag{11}$$

Contrary to what happened in the original Weyl theory[10] , its variance is compensated by that of χ. Notice, furthermore, that the Ricci tensor (10b) is not symmetric;

its antisymmetric part is proportional to the field strength of the conformal gauge boson

$$\dot{R}_{\nu\mu} - \dot{R}_{\mu\nu} = 4C_{\mu\nu} \ , \tag{12}$$

where

$$C_{\mu\nu} = \partial_\mu C_\nu - \partial_\nu C_\mu \ . \tag{13}$$

On expanding $\dot{R}$ in terms of the original Riemannian curvature we find, from eqs. (9)-(10),

$$\dot{R} = R - 6g_c(D_\mu C^\mu - g_c C_\mu C^\mu) \ . \tag{14}$$

We are now in position to write down a generally coordinate invariant, $SU(2) \times U(1)$ gauge symmetric, action which is also invariant, term by term, under gauge Weyl transformations (eqs.(4)-(6)). The action (1) must be substituted for a suitable action in which the replacements (7)-(10) have been incorporated, i.e.

$$\begin{aligned} I \to \int d^4x \sqrt{-g} \, [& h\chi^2 \dot{R} + \xi\Phi^\dagger\Phi\dot{R} + \frac{1}{2}g^{\mu\nu}\nabla_\mu\chi\nabla_\nu\chi + g^{\mu\nu}(\nabla_\mu\Phi)^\dagger(\nabla_\nu\Phi) \\ & - \frac{1}{4}g^{\mu\alpha}g^{\nu\beta}(W_{\mu\nu}W_{\alpha\beta} + C_{\mu\nu}C_{\alpha\beta}) + \bar{\psi}e_a^\mu\gamma^a\tilde{\nabla}_\mu\psi \\ & - (f_\psi\bar{\psi}\Phi\psi + h.c.) - V(\Phi^\dagger\Phi, \chi^2) + ...] \ . \end{aligned} \tag{15}$$

Allowance is made for the scalar doublet, Φ, to be conformally coupled with curvature. Here ξ and f_ψ are dimensionless constants and e_a^μ is the vierbein, transforming as

$$\delta e_a^\mu \to \alpha(x)e_a^\mu \ ; \ \delta e_\mu^a \to -\alpha(x)e_\mu^a, \tag{16}$$

In eq.(15) we have not explicitly included some possible conformally invariant higher derivative terms. As for the potential it is assumed to be dilatation invariant, as in eq.(1).

3. AN ALTERNATIVE TO THE HIGGS MECHANISM

Let $G_k(k = 1,2,3)$ be the standard "would-be" Goldstone bosons associated to the internal $SU(2) \times U(1)$ symmetry. Under a gauge transformation with parameters β_k they shift as

$$G_k \to G_k + \beta_k v \ , \tag{17}$$

where $v = 2^{-1/4}G_F^{-1/2} \simeq 250\,GeV$. This law of transformation is similar to that of eq.(5) for the dilaton, the "would-be" Goldstone boson associated to dilatation symmetry. In both of these laws the inhomogeneous term is the signal of spontaneous symmetry breaking; namely, in eq.(5) it is specified by the scale M and in eq.(17) by the scale v. We may entertain the possibility that both conformal and internal gauge invariance of the action (15) may be described in terms of the transformation laws of

the full set of Goldstone bosons S and G_k. To this end we parametrize Φ as follows $(T_k = \tau_k/2)$:

$$\Phi = exp\left[\frac{S}{M} + i\frac{G_k T_k}{v}\right]\begin{pmatrix} 0 \\ \frac{v}{\sqrt{2}} \end{pmatrix} \tag{18a}$$

$$= exp\left[i\frac{G_k T_k}{v}\right]\begin{pmatrix} 0 \\ \frac{v}{\sqrt{2}}e^{S/M} \end{pmatrix}, \tag{18b}$$

which is a generalization of the usual representation of the scalar doublet after suitable rotation of the isospin axes. The field S (G_k) enters the real (imaginary) part of eq.(18) because it is a scalar (pseudoscalar) Goldstone boson. Notice furthermore that the purported Higgs degree of freedom (associated to the length of Φ) is subsumed within the dilaton field. Scale invariance is not broken by the presence of v because this scale is accompanied by the coefficient $e^{S/M}$. Our theory is aimed to be invariant under any change in the length of Φ.

The generalization of the parametrization (18) in case of having several scalar fields involving on the whole n real degrees of freedom is (T_k being now a $n \times n$ matrix representation)

$$\Phi = \exp\left[\frac{S}{M} + i\frac{G_k T_k}{v}\right]\begin{pmatrix} \vec{0} \\ \sin\theta_1 \sin\theta_2 ... \sin\theta_{r-2} \cos\theta_{r-1} \\ \sin\theta_1 \sin\theta_2 ... \sin\theta_{r-2} \sin\theta_{r-1} \\ \sin\theta_1 \sin\theta_2 ... \cos\theta_{r-2} \\ \vdots \\ \sin\theta_1 \cos\theta_2 \\ \cos\theta_1 \end{pmatrix}\frac{v}{\sqrt{2}}, \tag{19}$$

where $r = n - 3$ and $\vec{0}$ is a 3-dimensional null vector. The column multiplet with θ-fields is unimodular. As before the field S describes the (gauge) degree of freedom associated to the length of Φ:

$$|\Phi|^2 = \frac{v^2}{2}e^{2S/M}. \tag{20}$$

Our action integral (15) can be rewritten in a special gauge ("conformal unitary gauge") in which the scales v and M appear explicitly in the Lagrangian and the Goldstone bosons G_k and S are eaten to give masses to the gauge bosons $W_\mu^\pm, Z_\mu$ and C_μ, respectively. This gauge is defined by the Weyl rescalings

$$\psi(x) \to e^{\frac{3}{2}S(x)/M}\psi(x), \tag{21a}$$

$$g_{\mu\nu}(x) \to e^{-2S(x)/M}g_{\mu\nu}(x), \tag{21b}$$

$$e_\mu^a(x) \to e^{-S(x)/M}e_\mu^a, \tag{21c}$$

and

$$C_\mu \to C_\mu - \frac{1}{g_c}\partial_\mu \frac{S(x)}{M} \qquad (21d)$$

(S does not transform). Scalar fields other than Goldstone bosons would transform, if present, as

$$\varphi(x) \to e^{S(x)/M}\varphi(x) . \qquad (21e)$$

We assume that the internal $SU(2) \times U(1)$ unitary gauge is also fixed. A straightforward calculation (using eqs.(11),(14),(19)-(21)) brings eq.(15) into

$$I = \int d^4x \sqrt{-g} \ [\frac{M_P^2}{16\pi}R + \frac{1}{2}g^{\mu\nu}\Gamma_{ab}(\theta_1...\theta_{r-1})\partial_\mu\theta^a\partial_\nu\theta^b$$
$$-\frac{1}{4}g^{\mu\alpha}g^{\nu\beta}C_{\mu\nu}C_{\alpha\beta} + \frac{1}{2}M_c^2 C_\mu C^\mu - W_{eff}(S)] , \qquad (22)$$

with

$$M_c = g_c\sqrt{v^2 + M^2 + \frac{3M_P^2}{4\pi}} \simeq g_c\sqrt{M^2 + \frac{3}{4\pi G_N}} , \qquad (23)$$

$$G_N = (16\pi hM^2 + 8\pi\xi v^2)^{-1} \simeq (16\pi hM^2)^{-1} . \qquad (24)$$

The internal metric structure Γ_{ab} (a,b =1...r-1) in θ –space takes on the S^{r-1} form

$$\Gamma_{ab}(\theta_1...\theta_{r-1}) = \begin{pmatrix} 1 & & & & & \\ & \sin^2\theta_1 & & & & \\ & & \sin^2\theta_1\sin^2\theta_2 & & & \\ & & & \cdot & & \\ & & & & \cdot & \\ & & & & & \cdot \\ & & & & & \sin^2\theta_1...\sin^2\theta_{r-2} \end{pmatrix} , \qquad (25)$$

which defines an harmonic map Lagrangian[11] (a generalization of the nonlinear σ model). The ordinary SM terms (letting aside the Higgs terms) have not been explicitly included in eq.(22), although they are exactly reproduced. By construction, there is no trace of the Higgs field in the action (22). As for the dilaton, S, it has deposited its degree of freedom into the longitudinal component of C_μ. Notice that since V is, by hypothesis, dilatation invariant at the classical level, even the potential in eq.(22),

$$W = e^{-4S/M}V, \qquad (26)$$

is independent of S in the absence of quantum corrections. Matters nevertheless change when we jump to the quantum theory, i.e. when W is replaced by the effective potential W_{eff}.

It should be clear that the parametrization (18)-(19) has nothing to do with the presence of the scalar potential V; in particular, the scale v need not be tied to the possibility that Φ acquires a nonvanishing vacuum expectation value (VEV). In the usual Higgs mechanism for the SM a nonvanishing VEV, $< \Phi > \neq 0$, is postulated as a means to generate SSB of the electroweak symmetry and, by inputing its value from experiment, as a way to introduce the Fermi scale into the model. The scalar field in this context performs dynamical oscillations around the constant background $< \phi >$, considered to be the expansion point of perturbation theory. Such oscillations are connected with the physical existence of the Higgs particle. In our case, however, we have no such particle and the appearence of the electroweak scale v may be linked[12] to the boundary conditions of the scalar multiplet at spatial infinity. In our context this means the following. If we expect that the class of metrics allowed in the action integral (15) are those metrics which are spatially symptotically flat, the condition by which the fields in Weyl basis (21) do not violate this prescription reads

$$\lim_{|\vec{x}| \to \infty} S(x) = 0. \tag{27}$$

From eq. (20) it now follows that

$$\lim_{|\vec{x}| \to \infty} \mid \Phi(x) \mid = \frac{v}{\sqrt{2}}. \tag{28}$$

Therefore, we see that the scale invariance of our initial action integral (15) is spontaneously broken by the asymptotic value that $\mid \Phi \mid$ takes at spatial infinity. It is this boundary condition on the low energy scalar multiplet that sets the Fermi scale in our "standard" model. Due to the rôle played by S, however, the presence of v does not break scale invariance in eq.(15). This symmetry is only broken when we set the conformal unitary gauge. It is precisely in this gauge where in the next section we propose to perform a probabilistic adjustment of the cosmological constant.

4. ADJUSTING Λ_{eff} A LA HAWKING

First of all, let us stress the fact that the effective cosmological constant may exhibit a rich variety of S-dependences as soon as the vacuum value of W_{eff}, $< W_{eff} >$, is itself S-dependent . Of special significance are the S-dependences induced by short distance effects. To illustrate this point[4,9] , notice that even non-perturbative contributions to the effective potential, like e.g. the QCD anomaly, $< \Theta_{QCD} > \sim \Lambda^4_{QCD}$, may be given a vacuum S-dependence through the change of long and short distance β-functions at a scale $M_X = v_X e^{S/M}$ ($v << v_X \lesssim M$) defining the SSB of some unified theory, G_X, in which the dilatation symmetric SM is assumed to be embedded. Explicitly, from simple renormalization group analysis (at the 1-loop level) we find

$$\Lambda_{QCD}(S) = v_X \ exp\left(\frac{g_0}{2\beta_3}\right)\left(\frac{\mu_0}{v_X}\right)^{\beta_X/\beta_3} exp\left\{\left(1 - \frac{\beta_X}{\beta_3}\right)\frac{S}{M}\right\} . \tag{29}$$

$g_0 = g(\mu_0)$ is the unified coupling, defined at a scale μ_0 beyond M_X, and β_X, β_3 are the β-functions above and below M_X (where $g(M_X) = g_3(M_X)$). The S-dependence

of eq.(29) is patent; it only vanishes for $\beta_X = \beta_3$, i.e. only in the unlikely case that it were possible to extend the SM to infinitely short distances. As for the contribution to $\Lambda_{eff}(S)$ from the scalar effective potential of G_X, the multiplet (19) constitutes a subset of a larger family of scalar fields used to cause a suitable chain of SSB of G_X down to $SU(3)_c \times U(1)_{em}$. If we denote collectively by φ these scalar fields, their VEV's become S-dependent through eq.(21e) and the condition

$$\frac{\partial W_{eff}(S,\varphi)}{\partial \varphi}\bigg|_{<\varphi>} = 0. \tag{30}$$

The well–known fact that quantum fluctuations break classical scale invariance in a hard manner shows up in this context through an explicit dependence of the effective potential (and so of Λ_{eff}) on the undynamical scalar S. (Notice that its value must be constant in vacuum,

$$< S(x) >= S_0 , \tag{31}$$

otherwise the gravitational field equations could not be satisfied without violating the Bianchi identities of the Riemann tensor.)

In the Weyl basis (21), the renormalization mass scale is given by $\bar{\mu} = \mu e^{-S/M}$, so that the anomalous divergence of the dilatation current is given by

$$\partial_\mu J_D^\mu = -\sqrt{-g} M \frac{\partial W_{eff}}{\partial S} = \sqrt{-g}\Theta , \tag{32}$$

where Θ stands for the anomalous trace of the energy–momentum tensor, $\Theta \equiv T_\mu^{\mu}$[6]. It is easy to check that this formula gives the correct dilatation anomaly in any Coleman-Weinberg type effective potential and also reproduces the standard QCD trace anomaly.

We think this is enough for the purpose of illustrating the fact that the total effective cosmological constant is, in our framework, a complicated function of S that is sensitive to both long–distance and short–distance properties of the theory. This feature may be used to make Λ_{eff} a dynamical quantity. To be more precise, we would like to invoke Hawking's suggestion[13] that a scalar field with a potential term, but no kinetic term (as it is the case of S in eq.(22)), can be utilized to generate a " hidden" dynamical cosmological constant. (Other alternatives to produce a similar scenario involve topological fluctuations of the metric[14] or the existence of a three–index antisymmetric tensor field in the context of certain supergravity theories[15] .) Hawking's mechanism[13] for relaxing the cosmological constant to zero is to be thought of as a "probabilistic adjustment" rather than as a "dynamical field adjustment". It is based on the Euclidean formulation of quantum gravity[16] (in which the action, I, is replaced by the Euclidean action, I_E) and on the notion of the wave function of the Universe[17] . This function determines the probability for the matter and metric field histories in the Euclidean path integral. Quite recently, Coleman[18] has exploited this approach from the point of view that "wormhole" configurations can exist in Euclidean spacetime and have the net effect of inducing a probability distribution for the local interactions in the input Lagrangian.

As remarked by Hawking[13] , in order to promote the cosmological constant to a dynamical variable one should include it in the set of fields that are integrated over in the path integral defining the ground state wave function of the Universe, Ψ_0. In our case we may effectively do this by integrating over S under the constraint (31), i.e.

$$
\begin{aligned}
\Psi_0 &\sim \int [dS][dg_{\mu\nu}][d\phi_m]\, \delta(S(x) - S_0)\, e^{-I_E(S, g_{\mu\nu}, \phi_m)} \\
&\sim \int dz \int [dS][dg_{\mu\nu}][d\phi_m]\, e^{-I_E + iz(S(x) - S_0)} \\
&\sim \int dz\, e^{-\Gamma_E(z, S, <\phi_m>(S))} \sim e^{-\Gamma_E^{vac.}(S_0)}
\end{aligned}
\tag{33}
$$

(ϕ_m stands for the matter fields). We have introduced the effective action, Γ_E, evaluated at some (presumably existing) stationary point with respect to all the fields. In particular, the stationary solution for the gravitational field is taken to be Euclidean de Sitter spacetime (see below).

For field configurations near the vacuum state, the fields are essentially static and the action (22) reduces (in Euclidean space) to

$$
\Gamma_E^{vac.} = -\frac{M_P^2}{16\pi} \int d^4x \sqrt{-g}(R - 2\Lambda_{eff}(S)) ,
\tag{34}
$$

where Λ_{eff} includes (apart from a bare term, Λ_0) perturbative constrictions from $< W_{eff}(S, \varphi) >$, whose S-dependence is fixed by eqs.(19) and (30), and also contributions from all sorts of non-perturbative phenomena associated to S-dependent intrinsic mass scales, of which eq.(29) is the simplest example.

By the saddle point approximation, we expect that the dominant contribution to the Euclidean path integral comes from metrics near solutions of Einstein's equations with a Λ_{eff} term. If we restrict to positive-definite (compact Euclidean) metrics, then the Euclidean action (22) is an extremum for a spacetime of constant (positive) curvature. As stated before, it is identified to be Euclidean de Sitter spacetime; namely, the 4-sphere of radius $\sqrt{3/\Lambda_{eff}(S)}$, with the metric induced by embedding it in 5-dimensional Euclidean space. The surface area of such a sphere is $24\pi^2/\Lambda_{eff}^2(S)$ and the Ricci scalar is $4\Lambda_{eff}(S)$, whence[13]

$$
\Gamma_E^{vac.} = -3\pi M_P^2/\Lambda_{eff}(S)
\tag{35a}
$$

and

$$
\Psi_0 \sim exp(+3\pi M_P^2/\Lambda_{eff}(S)) .
\tag{35b}
$$

Clearly, Hawking's mechanism selects those configurations such that the, so-far undetermined, constant (31) is a root of the equation

$$
\Lambda_{eff}(S_0) = 0
\tag{36}
$$

−assuming the root to exist. Thus the value of S is decided by the requirement that the vacuum field configurations for which the total effective cosmological constant vanishes are (by far) the most probable ones.

Some comments are now in order. The model, at this stage, says nothing about why the various mass scales of our world are where they are. This is the hierarchy problem, also present in the global model[4] . The only thing we can say (as a matter of experimental evidence[1]) is that today's value of the cosmological constant is zero (or very nealy zero), and hence that the actual hierarchy of mass scales (being S-dependent in our model) was "frozen" at its present state when eq.(36) happened to hold. A second related point is that there is no reason, in principle, why eq.(36) should have ever been true in early epochs of the history of our universe; this could perhaps "explain" the peculiarity of our present state. As a matter of fact, Hawking's mechanism cannot be extrapolated back in physical time, at least in an obvious way. This is because the mechanism itself works in Euclidean space, and in general there is no guarantee that eq.(36) is recovered when we analitically continue the Euclidean action back to the Minkowski action. For positively curved Friedmann universes, however, the Euclidean section intersects the physical spacetime at the moment of maximum expansion[16] . Thus one would expect that eq.(36) should be asymptotically fulfilled for large volume universes (our present universe?). By the same token, an inflationary era in the early stages of the cosmic evolution is not precluded in this framework, as Λ_{eff} could have been very large at that time. This is a nice feature, not shared by many models that could not avoid concluding that $\Lambda_{eff} = 0$, at all times, if they would succeed in setting $\Lambda_{eff} = 0$ at the present time.

5. SUMMARY AND CONCLUDING REMARKS

In the gauge formulation of conformal invariance (Cf. eq.(15)) each term of the action is independently local scale invariant. Two covariant derivatives, eqs.(7)-(8), were specially designed to insure this fact, but only a single conformal gauge boson, C_μ, was necessitated. In this framework, a multiplet of scalar fields, with a fixed nonvanishing boundary condition at spatial infinity, is conformally coupled to gravity. Its phase as well as its length, are described by the "would-be" Goldstone bosons G_k and S. We have shown that there is a "biunitary" gauge (i.e. internal and conformal unitary gauge) where our model boils down to the observable (i.e. non-Higgs) part of the Standard Model, including Einstein gravity, plus perhaps (if $r > 1$) a nonlinear sector of scalars fields. These are essentially decoupled from the SM fields and show up in the theory in the form of an harmonic map Lagrangian with target space S^{r-1}. No low energy ($\lesssim \mathcal{O}(TeV)$) object bearing any resemblance to a Higgs particle is expected in this formulation of the SM. In its stead we expect the presence of a very heavy ($\lesssim M_P$) new vector field, the aforementioned Weyl conformal gauge boson, whose only interactions are of gravitational type. One may conjecture that it could contribute significantly to the arsenal of dark matter in the Universe. From our analysis, therefore, we coincide with ref.[12] in regarding the Higgs potencial as an unessential tool to reproduce the observable features of the SM. Finally, we have shown that the S-dependences induced by the quantum fluctuations of all fields (long and short distance fields) in the "biunitary" gauge can be utilized to endow Λ_{eff} with a dynamical nature. This feature is exploited to perform a probabilistic adjustment of the total effective cosmological constant on the grounds of Hawking's mechanism[13] .

We would like to finish with a brief comment concerning the nonrenormalizability of the present alternative version of the SM. It is true that at low energies we are left with three patent sources of nonrenormalizability; namely, i) a massive Yang-Mills theory, ii) an harmonic map Lagrangian and iii) the Einstein gravitational interaction. This list of deseases notwithstanding, it could be that their troublesome effect on the theory is nothing but a low energy "mirage"; after all, the short distance behaviour of the theory, being conformally invariant at the very fundamental level, might well be controlled by a non–trivial fixed point[19]. If this is so the theory, although it is not renormalizable in the conventional sense, it would be "asymptotically safe"[20], which means that it would be anyhow a perfectly sensible quantum field theory.

Acknowledgements

I would like to thank the organizers, J. Audouze and J. Trân Thanh Vân, for the invitation to the conference and for the warm hospitality and excellent organization of the Rencontre de Moriond meetings.

REFERENCES

1. A. Sandage, *Observatory* **88** (1968) 91;
   S. Bludman and M. Ruderman, *Phys. Rev. Lett.* **38** (1977) 1

2. Ya. B. Zel'dovich, *Sov. Phys. Usp.* **11** (1968) 381;
   A. D. Linde, *JEPT Lett.* **19** (1974) 183;
   For a recent review, see S. Weinberg, *Rev. Mod. Phys.* **61** (1989) 1 and A. Dolgov, Proc. of the XXIVth Rencontre the Moriond, Electroweak Interactions, ed. J. Trân Thanh Vân (Frontières, 1989).

3. A. Dolgov, The very early universe, ed. G. Gibbons, S. W. Hawking and S. T. Siklos (Cambridge University Press, 1983);
   F. Wilczek, Erice Lectures (1983);
   L. Abbot, *Phys. Lett.* **150B** (1985) 427;
   A. Zee, High energy physics, Proc. of the 20th Annual Orbis Scientiae, ed. S. L. Mintz and A. Perlmutter (Plenum, New York, 1983);
   S. M. Barr, *Phys. Rev.* **D36** (1987) 1691.

4. R. D. Peccei, J. Solà and C. Wetterich, *Phys. Lett.* **195B** (1987) 183;
   C. Wetterich, *Nucl. Phys.* **B302** (1988) 688.

5. For a detailed discussion of the phenomenological consequences of the Cosmon model, see R. D. Peccei, Proc. of the Latin American Meeting on High Energy Physics, Valparaiso, Chile, 1987; see also the talks by E. Fischbach, C. Wetterich and C. Taldmage, in: 5th Force, Neutrino Physics, Proc. of the XXIIIth Rencontre the Moriond, ed. O. Fackler and J. Trân Thanh Vân (Frontières, 1988)

6. S. Coleman, in: Dilatations, Erice Lectures (1971)

7. E.S. Fradkin and A. A. Tseylin, *Phys. Rep.* **119** (1985) 234;
   E. Englert, C. Truffin and R. Gastmans, *Nucl. Phys.* **B117** (1976) 407.

8. I. Antoniadis and N. C. Tsamis, *Phys. Lett.* **144B** (1984) 55.

9. J. Solà, Univ. Autònoma de Barcelona preprint UAB-FT-202/89

10. H. Weyl, in: Gravitation und Elektrizität, Sitz. Preuss. Akad. Wiss. (Berlin, 1918) p. 465, reprinted in: The principle of relativity (Dover, New York, 1923) p. 201.

11. C. W. Misner, *Phys. Rev.* **D18** (1978) 4510

12. H. Cheng, *Phys. Rev. Lett.* **61** (1988) 2182;
    H. Cheng and W. F. Kao, MIT preprint (1988).

13. S.W. Hawking, *Phys. Lett.* **134B** (1984) 403.

14. S.W. Hawking, *Nucl. Phys.* (1978) 349.

15. A. Aurilia, H. Nicolai and P.K. Townsen, *Nucl. Phys.* **B176** (1980) 509.

16. S. W. Hawking, Proc. of the Einstein Centenary Survey, ed. S. W. Hawking and W. Israel (Cambridge University Press, 1979);
    S.W. Hawking, Recent Development in Gravitation , ed. M. Lévy and S. Deser (Plenum Press, 1979);

S.W. Hawking, Proc. of the Nuffield Workshop, ed. M.J. Duff and C.J. Isham (Cambridge University Press, 1982);
S. W. Hawking, Three hundred years of gravitation, ed. S. W. Hawking and W. Israel (Cambridge University Press, 1988).

17. J. B. Hartle and S. W. Hawking, *Phys. Rev.* **D28** (1983) 2960.

18. S. Coleman, *Nucl. Phys.* **B310** (1988) 643.

19. L. Smolin, *Nucl. Phys.* **B208** (1982) 439.

20. S. Weinberg, Proc. of the Einstein Centenary Survey, ed. S. W. Hawking and W. Israel (Cambridge University Press, 1979)

THE COSMOLOGICAL CONSTANT PROBLEM

A.D.Dolgov

Institute for Theoretical and Experimental Physics,

Moscow, USSR

Abstract
A review of the cosmological term problem is presented. Ba-
by universe model and the compensating field model are discus-
sed. The importance of more accurate data on the Hubble constant
and the Universe age is stressed.

Two major problem in particle physics originated from cosmology. The first one is the hidden mass problem which presents a serious challenge to experimentalists. Unfortunately, the chances to observe the hidden mass particles directly are negligible for a good lot of existing hypotheses on their nature. In a sence the problem of cosmological constant can be connected with the hidden mass problem because the corresponding vacuum energy may, at least to some extent, provide the hidden mass. Of course, the implication of cosmological constant is much wider than that. One can expect that the understanding why the cosmological constant is so small in the scale of the particle physics will have tremendous impact both on quantum field theory and cosmology. The discrepancy between theoretical expectations for its value and the observational upper bound are 100-50 orders of magnitude. This is a singular example when theoretical order of magnitude estimate differs by such an enormous amount from the real world. But we know that scientific development is based on contradictions between theory and experiment, so "the worse the better", this huge contradiction may lead to a great discovery as, for example, the observed stability of atoms has lead to quantum mechanics.

The cosmological term was introduced into Gereral Relativity equations by Einstein in 1918:

$$R_{\mu\nu} - 1/2 g_{\mu\nu} R = 8\pi G_N T_{\mu\nu} + \Lambda g_{\mu\nu} \qquad (1)$$

The right-hand side of this equation is a source of the gravitational field tensor $R_{\mu\nu\alpha\rho}$ (Rieman tensor) in (almost) the same sence as electromagnetic current j_μ is a source of the Maxwell field tensor F_μ. The first term in the r.h.s., $T_{\mu\nu}$, is the energy-momentum tensor of matter and the second one, $\Lambda g_{\mu\nu}$, is the cosmological term.

The l.h.s. is kinematically conserved

$$D_\mu (R^\mu_\nu - 1/2 g^\mu_\nu R) \equiv 0 \qquad (2)$$

This implies the conservation of the r.h.s. It is usually assumed that the energy-momentum tensor of matter is conserved

$$D_\mu T^\mu_\nu \equiv T^\mu{}_{;\nu} = 0 \qquad (3)$$

This is true if one starts with a Lagrangian field theory in which $T_{\mu\nu}$ is defined as functional derivative of action with respect to metric:

$$T_{\mu\nu} = \delta S / \delta g_{\mu\nu} = \frac{\delta}{\delta g^{\mu\nu}} \int d^4x \sqrt{-g} L \qquad (4)$$

where scalar function L is the Lagrangian density. In this case the second term in the r.h.s. must be also conserved and since $g_{\mu\nu;\alpha} = 0$ then

$$\Lambda = const \qquad (5)$$

The cosmological term can be interpreted as vacuum energy-momentum tensor

$$T_{\mu\nu}{}^{vac} = \rho^{vac} g_{\mu\nu} = \Lambda g_{\mu\nu} / 8\pi G_N \qquad (6)$$

This is the only tensor compatible with Lorentz invariance and in fact vacuum energy calculation in quantum field theory gives the expression for $T_{\mu\nu}{}^{vac}$ of this form. Thus there can exist nonvanishing vacuum source of gravitational field in contrast to, say, electrodynamics where nonvanishing vacuum currents $j_\mu{}^{vac}=0$ break Lorentz invariance.

Einshtein invented cosmological term in order to get a stationary cosmological model. He noticed that eq. (1) with $\Lambda = 0$ does not have stationary solutions for homogeneous and isotropic distribution of matter. Λ-term was introduced to compensate gravitational attraction of matter on large scales. But later on it became clear that the Universe is nonstationary, it expands and Einstein rejected the idea of Λ-term considering it to be the greatest mistake of his life. This term is permitted by general covariance but no other excuse for its existence was known. The principle "everything that is not forbidden is permitted" was not operative in physics at that time. Nevertheless Le Maitre advocated very much the existence of cosmological constant and, as we understand it now, he was right. Quantum field theory demands nonvanishing vacuum energy which must be fantas-

tically larger than the observed upper bound. The first physicist who understood the problem was to my knowledge G.Gamov. In his letter to A.Ioffe in 1930 he wrote about the gravitational interaction of the Dirac sea. The hystory of the problem starts from the paper by Zel'dovich [1] where it was explicitely stated that zero-mode oscillations must gravitate and the contributions of bosonic and fermionic degrees of freedom might be cancelled out.

It is well known that the ground state energy of quantal oscillator is nonzero

$$E_0 = \omega/2$$

where ω is the oscillatior frequency.

In quantum field theory the field is represented by an infinite set of oscillators in every space point with all possible frequences ω. Hence the energy of the ground state, i.e. the vacuum energy, is equal to

$$\rho_{vac}=E_{vac}/V=\Sigma\omega/2 \longrightarrow \int d^3p/(2\pi)^3 \omega_p/2 = \infty \qquad (7)$$

which is definitely larger than zero. Here $\omega_p = \sqrt{p^2+m^2}$, and m is the mass of the field quanta.

The lucky circumstance is that the fermionic contribution into ρ_{vac} is of the opposite sign. So if there were an equal number of bosons and fermions with the same masses (in pairs) the contribution of quantum fluctuations into total vacuum energy should cancel out. Such a symmetry between bosons and fermions is called supersymmetry. There exists a formal proof that in the limit of exact supersymmetry vacuum energy must vanish. But we know from experiment that supersymmetry is not exact. Masses of bosons and fermions are different and superpartners of the known particles, if exist, must be as heavy as at least several GeV.

If supersymmetry is broken spontaneosly then vacuum energy must be nonvanishing and be of the order of m_{susy} where m_{susy} is the mass scale of the supersymmetry breaking. Presumably $m_{susy} > 100$ GeV and correspondingly $\rho_{vac} > 10^8$ GeV^4. This conclusion can be avoided if sypersymmetry is local, i.e. the symmet

transformation can be done in different space-time points inde-
pendently. To compensate the action variation due to difference
of the transformation in different points one has to add into
the theory vector fields and, what's more, massless tensor field
with spin 2. The latter is the graviton field. So this theory
automatically includes gravity. In the supergravity frameworks,
even if the symmetry is broken, vacuum energy may be zero. There
exist models in which vacuum energy rather naturally vanishes on
the classical and one-loop level but no explanation is found for
the vanishing of the higher order quantum corrections. This is-
sue is discussed in some detail in the recent review paper [2]
where one can find the corresponding list of references. This
review is much more exhaustive than the present talk and may be
recommended for a deeper study of the Λ-term problem. My aim
here is to give an elementary introduction to the subject diges-
table to experimentalists and astronomers.

Thus supersymmetry let one expect that vacuum energy is fi-
nite but gives by an order of magnitude estimate a very huge
number for it. No specific mechanism leading to vanishing of
ρ_{vac} in the frameworks of supersymmetric theories has yet been
found.

Advent of gauge theories with spontaneousdy broken symmetry
has produced another source of contributions into vacuum energy.
The phase transition from symmetric state to the state with bro-
ken symmetry is accompanied by a change in the vacuum energy

$$\Delta T_{\mu\nu} = \Delta\rho \, g_{\mu\nu} \tag{8}$$

where $\Delta\rho_{GUT} = 10^{60}$ GeV^4 for Grand Unification models,
$\Delta\rho_{EW} - 10^9$ GeV^4 for electroweak theory, and $\Delta\rho_{QCD} \approx 0.1$ GeV^4 for
quark-hadron phase transition in quantum chromodynamics. These
phase transitions took place in the course of the Universe ex-
pansion and cooling down [3,4]. So to get $\rho_{vac}=0$ today the Cre-
ator must prepare the initial state with $\rho_{vac}\neq0$ and with such
an accuracy that the subsequent phase transitions would cancell
it to the degree better than 10^{-100}, which clearly seems to be a
difficult job.

I would like to stress that there definitely exists nonzero
contribution into vacuum energy of the order of 0.1 Gev^4 from

gluon condensate [5]

$$\langle G_{\mu\nu} \, G^{\mu\nu} \rangle \neq 0$$

The existence of this condensate is, in a sence measured experimentaly. So the situation looks absolutely crazy since this contribution must be exactly cancelled out either by vacuum energy of some other field or by real cosmological term adjusted to ρ_{vac} with accuracy better than 10^{-46}.

Up to the present day no convincing resolution of the Λ-term problem is known. There are several possibilities discussed in the literature, but no one is absolutely satisfactory. A list of possible ways of the solution which is by no means complete looks as follows:

1. A compensating field (like axion?).
2. Baby universes.
3. Anthropic principle.
4. Modification of gravity.
5. ? ...

The order reflects my own preferences which may not coincide with those possessed by some other physicists. In what follows the first two cases are mostly discussed and only a few comments are made on the last ones. Those who are interested in them are addressed to review [2]. One thing which is definite is that the cancellation of the cosmological term is a low energy phenomenon which is operative at long time and distance scales.

Modification of gravity does not seem very appealing to me because General Relativaty is a too nice theory to be spoiled. But who knows... It may be premature to judge about the beauty of not yet existing modification.

Anthropic principle states that the Universe must have appropriate conditions for life otherwise there would be no observer who could put a question about e.g. cosmological term. Using this idea S.Weinberg [4] has found the upper bound on the (positive) vacuum energy density $\rho_{vac} < 100 \, \rho_m$, where ρ_m is the contemporary energy density of matter in the Universe. With a larger ρ_{vac} the Universe expansion rate would be too high to permit the galaxy formation. A comparable (by the absolute value) bound is valid for negative ρ_{vac} since very large $(-\rho_{vac})$ would re-

sult in too small time duration from the Big Bang till recollap-
se.

As was claimed by Linde [7] anthropic constraint on the va-
cuum energy density can be made as strong as $\rho_{vac} < 10^{-10000}$
g/cm³ if one assumes the validity of chaotic inflation scenario
with eternally existing Universe and eternally and continuously
existing Life.

Arguments using anthropic principle would be more close to
religion than to science if there were no chances for existence
of universes (or parts of the Universe) with quite different
conditions, physical laws, and so on. In the approach based on
the baby universes different values of the so called fundamental
constants like particle masses, coupling constants, and at last
Λ-term can be realized. Thus it can give a justification of
anthropic principle. In fact one expects even more. Baby univer-
se model may permit to calculate the probability distribution
for all the constants and so makes them caculable. In particular
the probability of vanishing Λ-term is claimed to be infinitely
large in comparison with all the other values of Λ . Here lies
an essential difference between the baby universe model and the
compensating field model. The latter predicts that vacuum energy
is not exactly cancelled out but only up to terms of the order
of m_{Pl}^2/t^2 i.e. of the order of the critical energy density. So
there is a way to distinguish between these two models.

Before going into further theoretical details I shall bri-
efly comment on the present observational status of Λ-term. If
Λ=0 the Universe age can be expressed as follows

$$t_u \approx H_0^{-1}/(1+1/2J\Omega)=9.8 \text{ Gyr } h_{100}^{-1}/(1+1/2J\Omega) \quad (9)$$

where $H_0 = (100 \text{ km/s/mpc})h_{100}$ is the Hubble constant and
$\Omega=\rho/\rho_c$ is the ratio of the average energy density in the Uni-
verse to the critical energy density $\rho_c=3H^2/8\pi G$. Inflationary
universe model predicts $\Omega=1\pm10^{-4}$. Observations give a smaller
value $\Omega=0.1\div0.3$ but they are sensitive to the clustered matter
only and not to that uniformly distributed. For the latter the
result presented here by Rowan-Robinson is valid which is
$\Omega=0.7^{+.3}_{-.16}$. The chances that inflationaty model is true are very
high so it seems safe to assume that $\Omega=1$. It was stated by Peeb-

les in his summary talk at this conference that $h_{100}=0.65\pm0.15$ so if Λ =0 the Universe age must be smaller than 13.5 Gyr. As Rood and Schramm have told us the age of globular clusters and nuclear chronology are compatible with 12 Gyr < t_u < 18 Gyr. So we are still uncertain. If however the bound claimed by Rocca-Volmerange, t_u >17 Gyr, is valid we either have to admit that $\Lambda \neq 0$ or Λ =0, $h_{100}=0.5$ and $\Omega=0.1$ i.e. the inflationary model is wrong. Constraints on decceleration parameter, q_0, presented here by Guiderdoni and Triay seem to be in favour of nonvanishing Λ but systematic errors could be large.

Nonvanishing neutrino mass can help to resolve the problem because the Gerstein-Zeldovich bound

$$m_\nu < 400 \text{ eV } (9.8 \text{ Gyr}/t_u - h_{100})^2, \qquad (10)$$

if we are lucky, may be violated. That would mean that Λ -term is not zero. The positive result on neutrino mass obtained by the ITEP group is still neither confirmed nor rejected. Hopefully it will be done (in one or other way) in the nearest future.

To conclude the modern data seem to trend to a nonvanishing Λ -term but of course they are not decisive.

The idea that the cosmological constant is most probably zero originated from the Hawking's paper [9]. Shortly his arguments are the following. The probability of a field configuration is assumed to be defined by action S in Euclidean space-time which is achieved by analytic continuation to imaginary time, $t \to it$. S is taken to be the Einstein action with Λ -term and without matter:

$$S = (m_{Pl}^2/16\pi) \int d^4x \sqrt{g} (-R+2\Lambda) \qquad (11)$$

It is also assumed that quasiclassical approximation is valid so S is calculated on the solution of the classical equations of motion. In the case under consideration the latter are the Einstein equations and their solution is the four-dimensional Euclidean sphere with radius $\sqrt{3/\Lambda}$ (if $\Lambda > 0$). Hence, the action is $(S_{cl}=-3\pi m_{Pl}^2/\Lambda$ and one could expect that the probability of the cosmological term being equal to Λ in a universe is

$$W \sim exp\{3\pi m_{pe}^2 / \Lambda\} \qquad\qquad (12)$$

So universes with vanishingly small Λ are infinitely more probable than any other.

This result heavily rests on the Euclildean approach and the sign nondefiniteness of the gravitational action. In a sence these two statements are contratictory. The continuation to Euclidean space is made in order to achieve the convergence of the integral over fields by transforming the oscillating function $exp(iS)$ into the decreasing one, $exp(-S)$. But this is not the case if S is not positive definite. One hopes however that the method is nevertheless correct and will be justified in the future.

Another objection against this result is that Λ is not a dynamical variable in this approach but a constant. To overcome this the third quintized theory of baby universe was proposed (for the list of references and the detailed review see paper ⁹⁾). This is an absolutely new theory which does not follow from quantum field theory (second quantized theory) as quantum field theory does not follow from quantum mechanics (first quantized theory) and quantum mechanics does not follow from classical mechanics. Still some analogy between lower and higher quantized theories is kept. Quantum field theory is constructed as quantum mechanics of a system with infinitely many degrees of freedom when the value of a field in any space point is considered as quantum variable. Third quantized theory deals with whole universes in any three-geometry. Fundamental objects in quantum field theory are elementary particles and those in third quantized theory are universes. In analogy with particle creation-annihilation operators a_p^+ and a_p one introduces universe creation-annihilation operators A_j^+ and A_j, where index j refers to different kinds of universes.

It is assumed that only small size baby universes $(l \sim m_{pe}^{-1})$ are essential for our Universe. The formation of large scale universes is suppressed as $exp(-m_{pe}^2 l^2)$. Whether this is the case or not is still an open question. Another assumption is that the interaction between the baby universes is negligible and so the action is the bilinear function of A_j and A_j^+:

$$S = \Sigma f_J A_J A_J$$

Here f_J can be represented as the ingegrals over whole space-time (to be more exact, over Euclidean four dimensional space) of scalar functions L_J:

$$f_J = \int d^4x \sqrt{g} L_J$$

This follows from the condition that baby universes do not posses nonvanishing energy and momentum because they are closed. By the same reason they do not posses any conserved charge. Functions L_J depend upon the properties of the baby universes and are of the form

$$L_0 = 2\Lambda - R,$$
$$L_1 = m\bar{\psi}\psi,$$
$$L_2 = gv_\alpha \bar{\psi} J^\alpha \psi \ , \ etc$$

Averaging over small size baby universes gives an effective Lagrangian in our large Universe. One sees that all the "fundamental constants" like m, g, etc. can have arbitrary values depending upon the average $< A_J^+ A_J >$. The latter generally are different for different large universes.

Nonrenormalizable couplings like, e.g. $(\bar{\psi}\psi)^2$ must also be present. Their absence at the available energies is probably explained by their power law rescaling, $\sim (E/m_{Pl})^n$, whereas renormalizable couplings rescale as logarithms of energy.

Now cosmological constant has become variable so one can talk about its probability distribution. Of course, in one universe Λ =const but it can be different in different universes.

Summing over all noninteracting baby universes ane gets an extra exponential in comparison with eq.(12) and obtains the following probability distribution

$$W \sim exp\{exp(3\pi m_{Pl}^2 / \Lambda \ )\} \tag{13}$$

This result and to the large extent the method belong to Coleman [10].

The theory seems to be very promising. All the fundamental constants might be calculable quantities if their their probabi-

lity distributions prove to be peaked at some specific values as it was demonstrated for Λ –term. At the moment however the way seems to be long and hard. First of all the validity of Euclidean approach and quasiclassical approximation can be questioned. Universe behaviour in real (not imaginary) time is obscure. If the Universe was created with the characteristic Planck scales how was it sensitive to a quantity which is more than one hundred orders of magnitude smaller? And at last but not the least how the objects which do not interact with our Universe, since their energy and momentum are zero from the point of view of observers in our world, can influence the Universe evolution? All these questions reflect our poor understanding of the relation between real and imaginary time.

Now let us turn to the compensating field models. The idea is extremely simple and is the following. The curvature of space-time is assumed to induce the formation of a classical field condensate which by its back reaction cancells out its own source. As a result the exponential expansion of the universe turns into power law one. As a toy model let us consider the theory with the Lagrangian [11].

$$L = - M^2 /16\pi (R-2\Lambda) + 1/2(f_{,\alpha}f^{,\alpha} - \frac{1}{3}Rf^2) \qquad (14)$$

It leads to the following equation of motion of scalar field f:

$$f_{,\alpha}^{,\alpha} + \frac{1}{3}Rf = 0 \qquad (15)$$

If R <0, long-wave fluctuations of f are unstable and there exist rising solutions of this equation. This rise is exponential while the total energy-momentum tensor is dominared by the vacuum term $T_{\mu\nu} \approx (\Lambda M^2/8\pi)g_{\mu}$:

$$exp\{(-3/2 + \sqrt{9/4 - 12\frac{1}{3}})\sqrt{\Lambda/3}\ t\} \qquad (16)$$

The solution may be taken spatially homogeneous because the Universe expansion $a \sim exp(\sqrt{\Lambda/3}\ t)$ quickly smooths down the inhomogeneities of f. When f becomes large its contribution into T_μ must be taken into account. Using the Einstein equations one ob-

$$R= \frac{4 \Lambda M^2+8\pi(6\frac{3}{2}-1)\dot{f}^2}{M^2+8\pi \frac{3}{2}(6\frac{3}{2}-1)f^2} \tag{17}$$

With encreasing f, R becomes smaller and the exponential rise of f slows down. At large t $f\approx\sqrt{\Lambda}$ Mt, $R\sim t^{-2}$, and $H=\dot{a}/a\sim t^{-1}$. Thus we have got the desired result that the scale factor behaves as a power of t, $a\sim t^k$. Unfortunately this is achieved by the price of vanishing of the gravitational coupling constant:

$$G(t)=(M^2-8\pi \frac{3}{2} f^2)^{-1}\sim \Lambda^{-1}(Mt)^{-2} \tag{18}$$

To get the presently measured value $G_N=m_{p\ell}^{-2}=10^{-38}$ GeV^{-2} one has to assume that

$$M \approx m_{p\ell}/(\sqrt{\Lambda}\ t_u) \tag{19}$$

where $t_u \approx 5\cdot10^{17}$ sec is the Universe age. Of course, in such a naive version the model can not stand cosmological tests. In particular there exist a very strong upper bound on possible time variation of G_N. The bound might be avaded if there would be a conspiracy between time variation of different coupling constants and masses. Probably the model of this type can be worked out. An idea of consistent variation of masses together with G(t) was considered by Fujii [12].

The problem of vanishing of $G_N(t)$ persisted in the models with more general coupling of f with gravity as it has been shown by Ford [13]. Attempts to resolve it with the help of the conformal anomaly did not prove to be very succesful [11,14]. It was claimed in ref.[15] that in theories with torsion one is able to get rid of the cosmological constant along the lines considered without destroying gravity.

Another attempt to save gravity was made in a model with vector field V_α instead of scalar one [16]. The Lagrangian has the form

$$L = 1/4 F_{\alpha\rho} F^{\alpha\rho} + 1/2 (D_\alpha V^\alpha)^2 + \tfrac{3}{2} R(m_1^2/16\pi) \ln (1 + V^2/m_2^2) \qquad (20)$$

where $F_{\alpha\rho} = \partial_\alpha V_\rho - \partial_\rho V_\alpha$ is the field strength. Potential of this type may arise due to radiative correction. In this model field V_μ is unstable and asymptotically increases as

$$V_\mu \sim \delta_{\mu t}(At + Bt^{-1}) \qquad (21)$$

Its back reaction cancells out vacuum energy so that $R \sim t^{-2}$ and $H \sim t^{-1}$. In contrast to the case of scalar field, energy-momentum tensor of V_μ is asymptotically proportional to $g_{\mu\nu}$ so that all the components of the total energy-momentum tensor go down as the Univers expands. Effective gravitational coupling constant decays only logarithmically,

$$G^{\text{eff}}(t) = [m_0^2 + m_1^2 \ln(1 + A^2 t^2)]^{-1} \qquad (22)$$

which may be consistent with observations.

Energy density in this theory is not positive definite but field quantization over classical background (21) seems safe.

It is noteworthy that the cancellation of cosmological term in such models proceeds only on large scales comparable with the horizon. In fact gravitational field drives the formation of condensate of f or V_μ if it is homogeneous at the distance

$$1 > M(32\pi \rho |\tfrac{1}{3}|)^{-1/2} \qquad (23)$$

where ρ is the energy density. So gravitational field of usual astronomical bodies is not influenced by this mechanism. It could only be essential in black holes.

All the models considered have the common feature that the vacuum energy is not completely cancelled out but only up to terms which give rise to the power expansion law. It seem to be the generic feature of compensating field models. This could change the standard scenario of the Universe evolution, influence large scale structure formation and so on. The cosmological models with unstable scalar field have been considered in refs.[17,18] and by Sato at this meeting. In the frameworks of

such models large values of the Hubble constant and the Universe age can be compatible.

In this short talk I am unable to cover many other interesting possibilities. Their large number shows the importance of the problem as well as it is still far from the resolution. I am not so optimistic as to believe that it will be solved to the next conference but I hope that it will be done in this millenium and in one of the future Rencontres de Moriond a single and correct model of Λ-term cancellation will be presented.

References

1. Zel'dovich, Ya.B (1968), Uspekhi Fiz. Nauk, 95, 209.
2. Weinberg, S. (1989), Rev. Mod. Phys., 61, 1.
3. Kirzhnits, D.A. (1972) Pis'ma ZhETF, 15, 745.
4. Kirzhnits, D.A. and Linde, A.D. (1972), Phys.Lett., 42B, 385.
5. Shifman, M.A., Vainshtein, A.I., and Zakharov, V.I. (1979) Nucl.Phys. B147, 385.
6. Weinberg, S. (1987) Phys.Rev.Lett. 59, 2607.
7. Linde, A.D. (1988) DESY 88-147. Plenary talk at the XXIV International Conference on High Energy Physics.
8. Hawking, S.W. (1984) Phys.Lett., 134B, 403.
9. Strominger, A. (1988) Baby Universes. Lectures presented at the TASI summer school. Brown University.
10. Coleman, S. (1988) Nucl.Phys., B310, 643.
11. Dolgov, A.D. (1982) Nuffield Workshop on the Very Early Universe. Cambridge, 1982. Ed. G.Gibbons, S.W.Hawking, and S.T.C.Siklos (Cambrdge University Press, Cambridge, 1983).
12. Fujii, Y. (1988) University of Tokio preprint UT-Komaba 88-14.
13. Ford, L.H. (1987) Phys.Rev. D35, 2339.
14. Peccei, R.D., Sola, J., and Wetterich, C. (1987) Phys.Lett. 195B, 183.
15. R. de Ritis, P.Scudellaro, C.Stornaillo (1988) Universita di Napoli preprint.
16. Dolgov, A.D. (1985) Pis'ma ZhETF, 41, 280.
17. Freese, K., Adams, F.C., Frieman, J.A., and Mottola (1987) Nucl.Phys. B287, 797.
18. Peebles, P.J.E. and B.Ratra (1987) Astrophys. J., 325, L17-L20.

Weakly Unstable Dark Matter

David Eichler

Dept. of Physics, Ben Gurion University
and
Dept. of Physics and Astronomy, University of Maryland

ABSTRACT

The ranges of allowed masses and coupling strengths for massive dark matter particles falls within a limited range of a two dimensional parameter space. In particular, their mass may not exceed several Tev if their lifetime exceeds the Hubble time. Here we discuss whether such particles, if weakly unstable, could manifest themselves astrophysically via their decay. In particular, we show that decay of particles of several Tev due to symmetry breaking at the grand unification scale could account for the anomalous positrons in the galactic cosmic radiation at E>10 Gev. The viability of the right-handed neutrino as weakly unstable dark matter is also discussed.

Introduction

There are currently some motivations for considering unstable particles that decay over a cosmological timescale. Particle decay has been widely invoked in the literature to provide revisionist scenarios for big bang nucleosynthesis, to account for the reported Wein excess in the microwave background, and to remove most of the closure density from superclusters . For several years, the anomalous positron excess in the cosmic radiation at E>10 Gev has aroused the curiosity of this author since "conventional" astrophysical explanations for it , though not inconceivable, are neither easy to come by. We considered[1] whether they could result from the annihilation of massive Dirac neutrinos with a mass of ~20 Gev and found that this supplied a plausible explanation. At about the same time however, Avignone, Drukier and co-workers [2] announced that they could rule out such particles in the galactic halo, and we had to accept that this result invalidated our hypothesis.

The motivations for hypothesizing non-baryonic dark matter have been long aired and have been discussed at length at this conference. An attractive choice of parameters for the dark matter particles are such that $\Omega = 1$, i.e. that the total density of the universe, most of which is dark matter, is the closure density, as predicted from inflationary models of the early universe with vanishing cosmological constant. However this is not insisted upon by most cosmologists.

Dark matter and unstable particles are related topics in that they both invite the theorist to invent unknown candidate particles. Dark matter, of course, need not be unstable, and unstable matter, if its half life is small compared to the Hubble time, cannot currently be dark matter. But if dark matter lasts for a Hubble time and is nevertheless weakly unstable, perhaps we could detect it via its decay products. Most massive particles may be unstable at the grand unification (GUT) scale, so weakly unstable dark matter may not be much more radical a notion than the stable variety.

If the reported Wein excess is to be attributed to Comptonization via plasma that has undergone decay heating, several constraints must be obeyed.[3] To live for cosmological timescales, the particle must be able to escape from a collapsing star if produced thermally at the core. If it eventually decays into gamma rays, the decay products due to supernovae greatly exceed the observational limits on the gamma ray background. So either the particle is not thermally produced in collapsing cores or its rest mass is sufficiently small that the high Lorentz factor at Mev energies stabilizes it over a Hubble time. In the latter case however, the decay photons of big bang relics would heat the cosmic plasma very inefficiently. Typically, the constraint that the particle not be thermally produced in collapsing stellar cores constrains the mass to be above 100 Mev.

In addition, a) the total energy density of the decay products should not exceed about 10% of the blackbody background, b) the decay must take place late enough to allow the Comptonization distortions to survive rethermalization ($z<10^6$) . If the particles annihilate in the big bang according to conventional particle physics, constraints a) and b) typically require the particle mass to be above a Gev or so.   In this case, radiative decay scenarios via weak interactions yield too short a lifetime to obey b). Thus, if weakly unstable massive particles are to account for the reported Wein excess, they must be protected against rapid decay by some new consideration.

Having reviewed the general motivations above, this paper discusses a couple of specific examples of a weakly unstable massive particle. As emphasized in the discussion, assumptions are introduced (e.g. a low energy symmetry) to protect the particle against rapid decay.

Tev Particles

The annihilation cross section that leaves $\Omega = 1$ is given by [4,5] $<\sigma v> =$ 4×10^{-27} h^{-2} cm^2 s^{-1}, where h is the Hubble constant in units of 100 km s^{-1} Mpc^{-1}. Now if the mass M of the mediating particle that governs the annihilation is lower than the mass of the dark matter particle m, the annihilation cross section will not depend significantly on M, and, in fact, is comparable to the electromagnetic annihilation cross section. The "electron-positron" cross section, scaled appropriately to the mass of the dark matter particle, is given by $<\sigma v> = \pi\alpha^2 m^{-2}$. If there are j species of lighter particles that couple to the same mediating boson, the annihilation cross section is raised above the electron - positron annihilation cross-section by a factor of $(2j + 1)$ because the decay can process via a virtual boson[5]. It follows that the dark matter gives an Ω of unity if m=0.7h(2j+1) Tev.

This mass estimate is otherwise quite general in that it doesn't assume a particular value for M, only that M<m.

The usual strong assumption one must make is that the dark matter particle is protected by an extremely good quantum number. We shall now assume that this quantum number is good up to the GUT energy scale, and that at this scale there are interactions that can cause the dark matter particle to decay. The lifetime of the particle is then given by

$$\tau = 3 \times 10^{16} \text{ yr } (\tau_p/10^{33} \text{yr.})(\sin\theta)^{-4}(2 \text{ Tev}/m)^5,$$

where τ_p is the proton lifetime and θ is a mixing angle. Though the decay time is much longer than the Hubble time, allowing the particle to currently exist as dark matter, the decay products are cosmic rays and could be detectable even if only a very small fraction of the dark matter has decayed.

An example of dark matter that is unstable at the GUT scale might be the lightest of a fourth generation of leptons. If fourth generation lepton number is a good quantum number up to the GUT energy scale, then decay to less massive leptons must proceed through the hadronic sector. This will in fact happen if there is Cabibbo mixing between the fourth generation quarks and lighter ones.

The dark matter mass density in the halo is about 0.3 proton masses per cm^3.[6] In the present scenario, this implies a positron emissivity Z in the galactic halo of about

$$Z = 1.5 \times 10^{-27}(\#/10)(\sin\theta)^4(m/2\ Tev)^4\ (10^{33}yr./\tau_p)\ e^+/cm^3\ s,$$

where # is the positron multiplicity per decay. If the decay involves a quark jet, # could easily be of the order of 10.

The positron emissivity required to sustain a galactic excess above 10 Gev at the reported level, i.e. the number density divided by the escape time, is 10^{-29} cm^{-3} s^{-1}. Details are given in references 1 and 7. This is in good agreement with the emissivity estimated above from GUT decay dark matter particles if # = 10, $\tau_p=10^{33}$yr., and $m\sin\theta$ = 0.6 Tev.

The idea that weakly unstable dark matter gives rise to the positron anomaly at E>10 Gev in the galactic cosmic rays, if crazy, is at least testable in several ways. First, dark matter particles with masses of several Gev can be detected in laboratory experiments. If they have spin-independent interactions, they are close to being detected with current technology.[2] Secondly, the positrons should have a characteristic inverse-Compton loss spectrum, as calculated by Tylka and Eichler.[1] This spectrum will be measurable with great accuracy with the superconducting magnet facility on the space station. Thirdly, the flux of gamma rays accompanying the positrons from any quark jet, and also the inverse-Compton gamma rays from prompt Tev lighter leptons should be easily detectable with the EGRET experiment on the Gamma Ray Observatory [7]. Fourthly, since the dark matter particles are in the several Tev range, the physics is well within the range of the planned superconducting supercollider.

Right-Handed Neutrinos

Right-handed neutrinos are required in many particle physics scenarios. Left - right (L- R) symmetric scenarios require them, and L - R symmetry breaking enables the v_R to be much heavier than v_L. If the Dirac v mass is of order the electron mass, as in standard "see-saw" models, the v_R decays rapidly into v_L, e+, and e-. However, if the Dirac v mass happens to vanish then the v_R can be stable. It is possible, however, that a tiny but finite Dirac mass can be acquired through higher order loop corrections. In this case, cosmologically interesting lifetimes can in principle result even though the v_R is very massive.

An illustrative model has been sketched by Babu, Eichler, and Mohapatra,[8] in which the right-handed neutrino decays via a virtual W_R that is mixed with the W_L . (Note that the "right-handed" W_R is the weak gauge boson that couples to v_R; here the subscript R does not refer to the helicity of the W.) This mixing is accomplished by loops of very massive particles that appear as radiative corrections to the W propagator, that , by virtue of their Dirac mass, mix the left and right handed sectors. (Note that by definition, a Dirac mass term mixes left and right components.) Electrons and quarks (e,u,d) are assumed to acquire a Dirac mass only via their coupling to these massive fermions (E,U,D), as in "universal see-saw" models,[9] i.e. the mixing between the left and right sectors is accomplished only by these heavy partners. The neutrino fails to pick up a Dirac mass simply because (by assumption) it has no massive partner . It turns out that mixing at the one (quark) loop level can cause too fast a decay, so in this particular model a discrete symmetry is invoked to prevent one of the heavy quark partners (say the D) from directly mixing the left and right sectors. The mixing d_R and d_L is accomplished by yet another coupling,this time between the d and u quarks via a charged scalar particle, and the L-R mixing takes place through the U. The mass of this scalar particle and its coupling strength to the quarks determine the decay rate of the right-handed neutrino. There are many free parameters in the theory. Babu, Eichler and Mohapatra [8] choose a v_R mass of 30 Gev, and with other mass scales suitably chosen, the v_R lives for about 10^{25} s. With these parameters, the v_R can comprise the closure density as well as account for the high energy positron anomaly . If we readjust the mass of the v_R to be 100 Gev, and readjust the strength of the coupling between left- and right-handed sectors, we can arrange for the v_R to comprise an Ω of about $0.1h^{-2}$ (until it decays, of course) and for the lifetime to be merely $\cdot 10^{10}$ s, corresponding to a decay redshift of $\cdot 10^5$ in an Einstein - de Sitter universe. This would then account for the reported Wein distortion, for, at a redshift of 10^5, the rest energy density of the v_R's would be about 0.05 of that in the blackbody background.

For completeness, we note that although the lightest supersymmetric partner is usually taken to be completely stable, its protecting quantum number, R-parity, may not be exactly conserved. If so, then the lightest supersymmetric partners could be weakly unstable. However, we refrain here from quantitative speculation.

To summarize, weakly unstable massive particles (m>Gev) that have a cosmologically interesting decay rate are possible, if not probable, given the current understanding of particle physics. If they are still around and still decaying, they could be highly conspicuous through their decay products.

References

1. Tylka, A. and Eichler D. 1987 unpublished preprint
2. Ahlen, S.P., Avignone, F.T., Brodzinski, R.L., Drukier, A.K. Gelmini, G, and Spergel D.N. 1987, Physics Letters B, 195, 605
3. Turner, M.S. 1981, Proc. of Neutrino '81 (Maui), and Dar, A. Nussinov,S. and Loeb, A. 1989, preprint
4. Steigman, G. 1979, Ann. Rev. Nuclear and Particle Phys, 29, 313 and references therein
5. Wolfram, S. 1979, Phys. Lett.B, 81, 65
6. Caldwell, J.A.R. and Ostriker, J.P.1981, Astrophys. J., 251, 61
7. Eichler, D., 1989, Phys Rev. Lett. (submitted)
8. Babü, K.S., Eichler, D., and Mohapatra, R. 1989, Phys Lett. (submitted)
9. Davidson, A. and Wali, K.C., 1987, Phys. Rev. Lett. 59, 393

V. DETECTION, MASS AND LIFE TIME OF NON BARYONIC PARTICLES

THE COSMIC MICROWAVE BACKGROUND:
A PROBE OF PARTICLE PHYSICS

Joseph Silk
Departments of Astronomy and Physics
and
Center for Particle Astrophysics
University of California
Berkeley, CA 94720

ABSTRACT

I review the current status of spectral distortions and angular anisotropies in the cosmic microwave background, with emphasis on the role played by weakly interacting particle dark matter. Theoretical predictions and recent observational results are described, and prospects for futrue progress are summarized.

1. Introduction and Historical Review

Study of the earliest epochs in the Universe is the ultimate goal of the cosmologist, thereby providing a probe of the very beginnings of time. The microwave background provides our only direct glimpse of the first million years of the cosmic expansion. Its spectrum resembles that of an ideal blackbody, and is produced during the first year of the big bang, when the universe was sufficiently hot and dense to generate thermal radiation. The seed fluctuations from which all large-scale structures are generated leave their imprint in the microwave background. Indeed, over angular scales in excess of a few degrees, the isotropy of the background is attributable to the homogenizing legacy of an inflationary epoch of rapid expansion that occurred during the first 10^{-35} second or so after the big bang. Nevertheless, both the existence of fluctuations at a level of a fraction of a percent, and infinitesimal deviations from perfect blackbody radiation, are inevitable, given our existence. Without such blemishes in the idealized big bang, galaxies could not have formed. The microwave background is a unique testament to our origins in a remote and fiery past.

The cosmic microwave background (CMB) was almost discovered on several occasions, being anticipated by Gamow,[1] by Alpher and Herman[2], and independently, but twenty years later, by Dicke.[3] The first near-discovery was by McKellar[4] in 1941, who studied interstellar CN molecules at high spectral resolution to investigate the rotational fine structure of the ground electronic state. The rotational levels were excited, apparently by radiative pumping through a microwave transition at 2.64 mm which required a radiation field with equivalent blackbody temperature of about 2.3°K. However electron collisions could also have produced rotational excitation, and without more detailed analysis, only an upper limit on the interstellar radiation field was deduced. Not until after the discovery of the 3K cosmic blackbody radiation was the interstellar CN excitation reexamined. The most recent study[5] achieves 30μA resolution, and limits the role of electron excitation, providing one of the most precise absolute measurements of the cosmic microwave background

flux. This molecular "thermometer" verifies the universality of the cosmic microwave background, since it can be applied along different lines of sight. The CMB was first detected in 1964 at 7cm wavelength by Penzias and Wilson[6] who were calibrating the Bell Laboratories' horn antenna that was used originally for the first trans-oceanic television broadcast via the Telstar satellite, in order to study the diffuse galactic background.

The early experiments found that the spectrum was consistent with that of a blackbody at about 3K, but it required a modern generation of millimeter and submillimeter experiments to make precise spectral measurements. Penzias and Wilson were content to state that the microwave background was isotropic to better than 10 percent, and this limit also has been greatly improved over the past two decades. However, only over the past year or two has the first substantial evidence, still unconfirmed, emerged for spectral distortions and angular anisotropies, apart from the well established dipole anisotropy due to our motion relative to the rest-frame of the microwave background. This review will summarize the evidence for spectral distortions and angular fluctuations and I will explore the implications of these observations for particle physics. I will conclude with a brief discussion of future prospects.

2. Spectral Distortions

To a flux level of ± 10 percent or better, the cosmic microwave background radiation is described by a blackbody spectrum with a temperature of 2.74K. Its blackbody spectrum is determined by the efficient thermalization processes that occurred in the first year of the Big Bang at $z \sim 10^7$. The spectrum is subsequently frozen, apart from any late input of energy into the universe. The blackbody photons, numbering about $400 (1+z)^3 \mathrm{cm}^{-3}$, undergo frequent scatterings off of electrons prior to recombination of the primeval plasma at $z \sim 1000$. This epoch of last scattering, which can occur at a redshift as late as $z \sim 10$ if the universe subsequently becomes reionized, marks the effective photosphere of the universe. On this last scattering surface, one can see fluctuations in the radiation brightness that

track the seed fluctuations in the matter distribution and gravitational field from which large-scale structure subsequently emerged.

These fluctuations do not perturb the thermal spectrum, however, unless the scattering medium is subsequently reheated to a temperature in excess of 10^8K. Galaxy formation necessarily distorts the CMB spectrum, at an expected level of about one percent in νi_ν, the spectral energy density per decade of frequency, with the specific frequency dependence of the distortion depending on the detailed processes of early star formation.

The reality of spectral deviations from a blackbody spectrum has only recently received strong, if not yet definitive, support. I summarize in Figure 1 the various spectral measurements[7]. These include ground-based observations above 1 cm wavelength, and measurements from rocket or balloon-born platforms as well as indirect measurements causing excitation of interstellar molecules, at wavelengths shortward of 1 cm. Two inferences may be drawn from Figure 1. There appears to be a systematic offset of about 0.1K in brightness temperature between the measurements at $\lambda \gtrsim 1$ cm and those below 1 cm, in the sense that the long wavelength data points appear, on the average, to be slightly low. Two of the submillimetric channels from the Nagoya-Berkeley rocket-borne bolometer[8] show a significant excess relative to the Wien tail of the CMB. The reported energy excess amounts to about 15 percent of the energy density in the unperturbed CMB. Such a result is extremely difficult to understand, and, pending experimental confirmation of the spectral distortion, three classes of theoretical models have been advanced to account for the excess flux.

One class of explanations appeals[9] to the out-of-equilibrium decay of some exotic species of massive particles, $\chi \rightarrow \chi' + \gamma$. This decay must occur after thermalization first becomes ineffective at kT $\lesssim 1$ keV, so that for direct decays to result in a feature near the blackbody peak, one requires the particle mass to be $\lesssim 1$ keV. However such particles must also be thermally produced during the course of stellar evolution, when temperatures of 10 keV or more are attained. It has been shown[10] that horizontal branch mor-
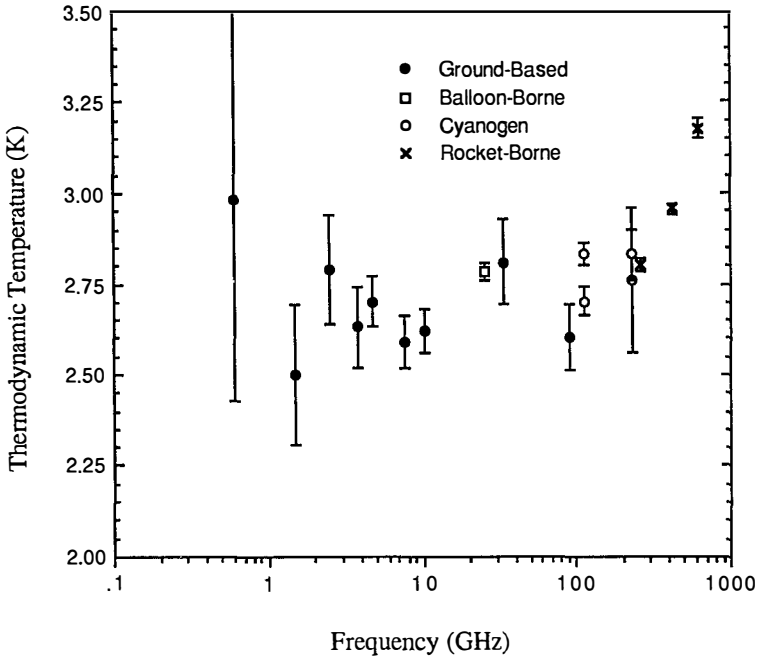
Figure 1: Brightness temperature of the cosmic microwave background. Measurements summarized by Matsumoto *et al.* and Smoot.

phologies would be grossly affected by decays of the form $e^+ + e^- \rightarrow \bar{\chi} + \chi'$ if the particle

mass and decay lifetime were in the range required to account for the distortion, namely

$m_\chi \sim 10\text{eV}/(\tau_\chi/10^5\text{yr})^{1/2}$. The only remaining loophole is for a very massive particle

$m_x > 1\text{MeV}$ to decay at $t \sim 10^6$ sec into photons plus other particles, and the resulting in-

complete thermalization could give a distortion near the blackbody peak. Not only does

this possibility need considerable fine-tuning of the particle parameters, but it most likely

yields a chemical potential (low frequency) distortion in the spectrum of the same order

as the Comptonization (high frequency) distortion near the peak. Limits on the chemical

potential distortion, due to the inefficiency whereby bremsstrahlung reprocesses the low-

frequency photons less rapidly than Comptonization upscatters these photons, constrain

the early energy injection in low frequency photons to about one percent of the total energy density.[11] However, detailed limits have not yet been studied for injection of energetic $(h\nu > m_e c^2)$ photons.

A second class of explanations invokes reheating of the intergalactic medium to a temperature in excess of 10^8K, and the consequent Comptonization of the cosmic microwave background photons. This can occur at recent epochs, when the density is low, and the chemical potential distortion is correspondingly suppressed: it is only significant for energy injection at redshift $z \gtrsim 10^4$. The immediate problem with Comptonization models arises with the energetic requirements. The scattering process $\gamma + e \rightarrow \gamma + e$ heats photons from frequencies below the blackbody peak to frequencies above the peak, and the energy transfer efficiency is characterized by the product of scattering probability and energy transfer per scattering, namely

$$y \equiv \int_t^{t_0} cn_e\sigma_T[k(T_e - T_\gamma)/m_e c^2]dt$$

integrated up till the present epoch t_0. The spectral distortion amounts to an excess energy density $\Delta\rho_\gamma/\rho_\gamma \approx 4y$, so that the Nagoya-Berkeley result requires $y \approx 0.03$. Detailed fits[12] actually specify y=0.0256. Since $y \sim \tau \cdot (kT/m_e c^2)$, and the electron scattering optical depth τ only approaches unity at redshift $z \gtrsim 10$, it is clear that one needs a temperature of $\gtrsim 10^8$K for the intergalactic medium at $z \sim 10$ in order for this model to work. Mechanisms involving baryonic matter become increasingly more extravagant in energy at higher redshift because one has to overcome the redshifting of photon energy relative to baryonic rest mass to account for a given amount of excess energy today. The energy requirement is severe: a rest mass fraction of 0.001 percent of the IGM must be in the form of thermal energy to attain 10^8K. This means that utilizing as much as ten percent of the luminous baryons now observed in stars ($\Omega \sim 0.005$–0.01) or allowed by primordial nucleosynthesis constraints ($\Omega \lesssim 0.1$) to burn at nuclear efficiency (~ 0.007) with a modest estimate of the fraction of non-thermal energy that is available as a heat source (~ 0.01) for a conventional (solar neighborhood) initial mass function, falls short by an order of magnitude or more.[13]

A proposed solution for energizing and ionizing the IGM appeals to ionizing photon production from decaying particles.[4),5),6)] Consider an unstable neutrino-like massive particle decaying via $\nu' \rightarrow \nu + \chi$ with ν a lighter (or massless) neutrino species and χ a majoran or familon that allows neutrino flavor-charging decays. A small branching ratio $\nu' \rightarrow \nu + \gamma$ into photons is assumed. The astrophysical constraints are that the enery density of the decay products account for the dark matter of the universe (or do not exceed it), that the decay photons yield the energy density in the submillimeter excess, and that the decay photons can efficiently comptonize the microwave background photons by heating the intergalactic medium. This restricts the decay parameters to $m_{\nu'} > 20\text{keV}$, $\tau(\nu' \rightarrow \nu_\chi) \sim 10^{10(\pm1)}$ sec, and a photon branching ratio $B \sim 10^{-5}$. Remarkably, these parameters are consistent with galaxy formation theory, the massive neutrino allowing an earlier period, prior to the standard matter-radiation epoch of equal densities, of matter-dominated expansion. During this early phase, fluctuation growth occurs, and only after the neutrino decays have occurred does a second period of radiation domination commence. Direct observation of the decay photons provides a constraint on this model, and the decay photons may even produce a detectable signature near 2μ with an energy density comparable to that associated with the submillimeter excess.[17)] Inclusion with constraints on neutrino decays from SN1987A futher restricts the allowable model parameter space to $m_{\nu'} = (12 \pm 6)\text{keV}$, $\tau_d = 5(\pm2) \times 10^{12}\text{sec}$, $\Omega_\chi = 0.1(\pm0.2)$, and $B = 6(\pm2) \times 10^{-4}$.

A third class of models consists of dust re-emission, with the dust either in protogalaxies or distributed in the intergalactic medium. It was pointed out a decade ago, in response to the reported Woody–Richards CMB distortion,[18)] that dust emission led naturally to spectral distortions in the vicinity of the CMB peak.[19)] Despite the retraction of the Woody–Richards distortion,[20)] the reported Nagoya–Berkeley submillimeter excess has revitalized theoretical studies of dust emission in the early universe. However, both the high UV dust optical depth that is inferred from the spectral form of the distortion and the energy density associated with the excess severely constrain theoretical models. Ordinary

stars fail to produce enough energy at a redshift that is high enough to give the required optical depth ($\gtrsim 20$). One has to resort to more exotic objects such as accreting massive black holes or very massive stars ($\gtrsim 10^3 M_\odot$) that produce little enrichment but a considerable amount of light.[21]

In fact, anisotropy upper limits already pose a strong constraint on dust models. The most stringent limit is at 0.13cm, where at a resolution of $11''$, Kreysa and Chini[22] report that $\Delta T/T < 2.6 \times 10^{-4}$. For any dust emissivity model, objects emitting in the submillimeter spectral region still contribute strongly at this wavelength. This limit translates into a limit on intensity fluctuations in the region of the distortion that amounts to about 1 percent. The required number density of emitting galaxies is large, and may be estimated from

$$\Delta f/f = (n_g \sigma \Delta \ell)^{-1/2}$$

where $\sigma \equiv \pi R^2$ is the effective cross-section of a galaxy, $\Delta \ell \equiv c \Delta t_0 (1+z)$ is the thickness of the redshift shell at the emission redshift, and $t_0 \equiv c/H_0$. This expression yields[23]

$$\Delta f/f = (5 \times 10^{-3}/\theta \text{ arc-min}) (\ell/\Delta \ell)^{1/2} (h^3 \text{ Mpc}^{-3}/n_{go})^{1/2}$$

in terms of the comoving number density of bright galaxies n_{go}. With the experimental resolution $\sigma = 11''$ and emission shell thickness $\ell/\Delta \ell \sim 10$, one needs $n_{go} \gtrsim 100 h^3 \text{Mpc}^{-3}$ for typical models. This means that the required abundance of infrared-bright galaxies correspond to a huge comoving density of dwarf galaxies. This seems implausible, although one cannot rule out such a hypothesis. The requirement of so many luminous objects at $z > 20$ challenges the ingenuity of any model with $\Omega = 1$, and in particular, that of cold dark matter. Evidently, both the anisotropy measurement and the submillimeter spectral distortion need to be confirmed before jumping to any theoretical conclusions.

3. Anisotropies

Inflationary cosmology provides the backdrop for the origin of the fluctuations that gave rise to galaxies.[24] Density fluctuations driven by gaussian quantum fields are inevitably present at the threshold of classical cosmology, the Planck epoch at $\sim 10^{-43}$

sec. These are expected to have magnitude of order unity on the horizon scale, although a detailed description awaits a definitive theory of quantum gravity. Inflation is triggered by a phase transition that sets in at the epoch of grand unification symmetry breaking, $\sim 10^{-35}$sec, and is completed by $\sim 10^{-33}$sec. During this phase, the universe undergoes a strongly accelerated phase of expansion, which effectively enlarges the particle horizon to a comoving scale far larger than its present value. The inflationary phase is time-translation-invariant, and the residual quantum fluctuations that emerge from the horizon, as the standard Friedmann-Robertson-Walker expansion resumes, retain a scale-invariant spectrum. This is equivalent to a fluctuation distribution with constant metric (or gravitational potential) fluctuations, the amplitude of which can, in principle, be specified in terms of the inflationary field, but, in practice, is treated phenomenologically as a free parameter pending development of a compelling theory of inflation.

Inflation predicts[25] that the universe should be isotropic, nearly homogeneous, devoid of magnetic monopoles, and should be dark-matter dominated with $\Omega = 1$; gaussian scale-invariant curvature fluctuations are its primary legacy for large-scale structure. Inflation may end with a second phase transition that can result in the production of cosmic strings. These non-linear objects provide a non-gaussian mode of density fluctuations that also, on large-scales, has a scale-invariant distribution of amplitudes when decomposed into a power-spectrum. Matter is freely accreted by strings once the universe becomes dominated by non-relativistic matter, and this results in a viable alternative for galaxy and cluster formation.

If the universe is dominated by baryonic matter, the preferred mode of fluctuations is via entropy perturbations. This results in the so-called isocurvature mode, which leaves a negligible imprint on the universe at very early epochs.[26] Because these fluctuations are dynamically unimportant at early epochs, inflationary models provide little guidance to the late-time spectrum. In the absence of a plausible model for primordial entropy fluctuations, the slope of the isocurvature power spectrum is specified phenomenologically by the

requirements of large-scale structure. For a power spectrum of density fluctuations

$$|\delta_k|^2 \propto k^n, \text{ with } \delta\rho/\rho \equiv \int e^{ik\cdot r} d^3k \propto M^{-\frac{1}{2}-\frac{n}{6}},$$

comparison with the observed galaxy correlations limits the power law index to lie in the range $0 \gtrsim n \gtrsim -2$, $n = 0$ being white noise. The scale-invariant spectrum of primordial curvature fluctuations has $n=1$, since specifying an index n is equivalent to primordial curvature fluctuations with spectrum $\delta\kappa \propto M^{(n-1)/6}$,. The ensuing sub-horizon density fluctuations during the matter-dominated era, generated by curvature perturbations

$$\delta K \sim GM/LC^2 \sim (\delta\rho/\rho)(L/ct)^2 \sim (\delta\rho/\rho)(M/M_h)^{2/3},$$

have an effective index equal to $n-3$.

The radiation field has a dominating influence on the growth of primordial fluctuations. The epoch of equal densities of (non-relativistic) matter and radiation occurs at $1 + z_{eq} = \rho_{mo}/\rho_{ro} = 2 \times 10^4 \Omega h^2$, where $\rho_{mo} \equiv \Omega(3H_0^2/8\pi G)$ is the present matter density in units of the critical density for closure, $3H_0^2/8\pi G$, ρ_{ro} is the present radiation density, equivalent to a blackbody at $T_{ro} = 2.74K$, and $h = H_0/100 \text{km s}^{-1} \text{ Mpc}^{-1}$. Prior to this epoch, the universe is radiation-dominated, and growth of linear density fluctuations is inhibited. For an uncoupled dominant component of weakly interacting massive particles (cold dark matter) that is nonrelativistic at $1 + z < 1 + z_{eq}$, there is a weak logarithmic growth at $1 + z < m_p c^2/kT_{ro}$. However, if the dominant mass component is baryonic, matter and radiation are strongly coupled and there is no fluctuation growth, but rather damping of the adiabatic fluctuation component. Early universe physics thereby acts both as a source of the fluctuations, for example via the inflationary cosmology that generates scale-invariant gaussian fluctuations, and as a filter, modifying the primordial spectrum.

The horizon scale at z_{eq} is consequently a critical scale for the fluctuation spectrum: for example, in a cold-dark-matter dominated universe, it characterizes the (gradual) transition between larger and larger scales ($L \gtrsim 2ct_{eq}$) which first enter the horizon at later

and later times, subsequently undergoing uninterrupted sub-horizon growth, and those scales ($L \gtrsim 2ct_{eq}$) which have their sub-horizon growth frozen until t_{eq}, subsequently all sharing a common growth factor. One therefore expects that the comoving length scale $L_{eq} = 2ct_{eq}(1 + z_{eq}) = 12(\Omega_0 h^2)^{-1}$ Mpc will be the principal surviving imprint of the early universe on the residual linear density fluctuation spectrum that seeds the large-scale structure of the universe via the action of gravitational instability.

Last scattering of the radiation occurs at a redshift of about 1000, some 3×10^5 yr after the initial singularity, and the corresponding comoving scale of the horizon at this epoch is about 100 Mpc. The radiation subsequently propagates freely, and thereby demarcates the largest scale on which any causal processes may be expected to have acted, subsequent to any inflationary epoch, to erase or induce any structure in the cosmic microwave background. This projects to an angular scale of about 2 degrees (Figure 2). Any detection of temperature fluctuations on larger scales would therefore probe primordial fluctuations in the matter distribution. On smaller angular scales, the interpretation of any fluctuations is model-dependent, but still may provide a useful probe.

The matter fluctuations continue to grow by gravitational instability, eventually achieving non-linearity at $z \lesssim 100$, and producing galaxies, galaxy clusters, and even larger structures. Normalization of the fluctuation spectrum to the observed large-scale structure can be performed via the galaxy correlation function or via large-scale peculiar velocities, either of which directly probe the linear fluctuation regime. Once normalized, the cosmic microwave anisotropies provide a unique window on the very early universe, hopefully allowing us to distinguish between rival theories.
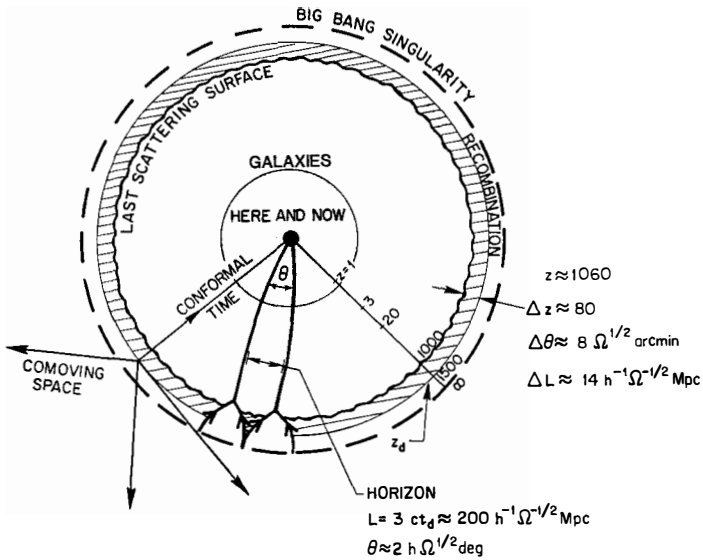
Figure 2: Conformal space-time diagram of the Big Bang.

Large Angular Scales (2°–90°)

Gravitational potential fluctuations on the last scattering surface and around the observer result in gravitational redshifts or blueshifts, respectively, of the CMB photons.[27] The magnitude of the resulting temperature fluctuations is

$$(\delta T/T)_{sw} \approx \frac{1}{3}\delta\phi/c \approx \frac{1}{3}(\delta\rho/\rho)_{\ell s}(L/ct)_{\ell s}^2,$$

where $\delta\phi$ is the potential fluctuation on scale L and $\delta\rho/\rho$ is the amplitude of the associated matter density fluctuation. For a fluctuation spectrum that is scale invariant, with constant space curvature, $\delta\rho/\rho \propto L^{-2}$ on large scales, so that the Sachs-Wolfe effect is independent of the epoch at which it is evaluated. It is the dominant source of primeval anisotropy on scales $L \gg L_{eq}$, which represents the asymptotic regime where $\delta\rho/\rho \propto M^{-2/3}$ for a scale-invariant spectrum. This effect is produced both by adiabatic fluctuations at all epochs, and by the orthogonal mode of isocurvature fluctuations, although in this latter case, the Sachs-Wolfe effect in the matter-dominated era is supressed by a factor $\sim \rho_r/\rho_m$.

Intermediate Angular Scales (10′–2°)

On scales such that $L \lesssim 3(ct)_{\ell s}$, *i.e.*, the horizon at last scattering, $L \lesssim 100\text{Mpc}$, there are two other contributions to temperature fluctuations that usually dominate over the Sachs-Wolfe effect. Flows of partially ionized gas, associated with infall of matter relative to the expansion into the shallow potential wells described by the fluctuation spectrum, generate temperature fluctuations at last scattering of order[28]

$$(\delta T/T)_{rel} \approx v/c \approx (\delta\rho/\rho)_{\ell s}(L/ct)_{\ell s}$$

On scales $L \gg L_{eq}$, where the scale-invariant fluctuation spectrum $\delta\rho/\rho \propto L^{-2}$, the velocity induced fluctuations dominate on scales $L_{eq} \lesssim L \lesssim (ct)_{\ell s}$.

An adiabatic fluctuation spectrum has a third component of fluctuations, which if decoupling of matter and radiation were instantaneous, would be described by[29]

$$(\delta T/T)_{ad} \approx \frac{1}{3}(\delta\rho/\rho).$$

The net adiabatic contribution is reduced relative to this estimate because the fuzziness of the last scattering surface partially erases the temperature fluctuations. The visibility function $e^{-\tau}d\tau/dz$, where τ is the electron scattering optical depth along a line of sight to redshift z, measures the magnitude of this smearing,[30] peaking at z=1060, and described approximately by a gaussian distribution in z, with a half-width $\triangle z \approx 80$. The last scattering surface is deduced to have a similar half-thickness of ~ 4 Mpc, which corresponds to an angular smearing of relic fluctuations amounting to $\triangle\theta \approx 8'$.

Fine-Scale Anisotropy ($\lesssim 10'$)

On angular scales below 10′, the relic adiabatic temperature fluctuations fall off rapidly with decreasing scale, because of the last scattering surface fuzziness, approximately as θ^2. There is an additional thermal contribution to temperature anisotropies on very small angular sizes which arises from Comptonization of the CMB by passage through hot gas in

newly formed galaxy clusters and galaxies. This is the Sunyaev-Zel'dovich effect, which amounts to

$$(\delta T/T)_{sz} \sim (kT/m_e c^2)\tau.$$

It is usually very small: for the evolution of inhomogeneities as predicted by the cold dark matter spectrum, sufficiently hot gas is generated only at $z \lesssim 10$, and induces $(\delta T/T)_{sz} \lesssim 10^{-6}$. Reionization of the intergalactic medium, a process which if it occurred sufficiently early (see below) would have erased primordial fluctuations, itself would have generated new fluctuations via the Sunyaev-Zel'dovich effect. There are also contributions to fine-scale anisotropy from discrete radio sources: these should be distinguishable, however, by their distinctive non-thermal spectral signature.

Significance of Large Angular-Scale Anisotropy

The angular scale subtended by the last scattering surface, at redshift $z_{\ell s}$, is $\theta_{\ell s} \approx (\Omega/z)^{1/2}$ rad, the angular size appropriate to the particle horizon at this epoch. For $z_{\ell s} \sim 1000$, as expected if there has been no ensuing reionization, $\theta_{\ell s} \approx 2°$. Since the thermal history of the universe is not well known, however, a more conservative estimate of last scattering is to assume that the universe has indeed been reionized. In this case, optical depth unity occurs at a redshift

$$z_{\ell s} \approx 70(\Omega/0.2)^{1/3}(0.02/\Omega_b)^{2/3}.$$

The corresponding angular scale $\theta_{\ell s} \approx 10°$.

The significance of this angular scale is the following. For any causal process responsible for reionization, primordial fluctuations would be erased, and new fluctuations introduced, on scales $\lesssim \theta_{\ell s}$. However, on larger angular scales, the primordial CMB fluctuations will be preserved. This thereby provides a motivation for designing experiments to study large-angular scale anisotropies, since these can provide a relatively model-independent probe of the primordial fluctuation spectrum.

Amplitude of δT/T

Experiments have been designed in two modes, either beam-switching with a single dish, or mapping with an interferometer. Hitherto, the best limits have been obtained in the former mode, and results will be described below. The theoretical predictions are usually described as a temperature correlation function between directions γ_1 and γ_2 and evaluated at the present epoch:

$$C(\theta) \equiv (\delta T/T)^2 =< \delta T/T(\gamma_1)\delta T/T(\gamma_2) >; \cos\theta = \gamma_1 \cdot \gamma_2.$$

Detailed computations of the transfer function through last scattering are required for fine-scale anisotropy fluctuations. On large angular scales, however, simple estimates suffice to give a crude estimate of the desired accuracy. For example, rich clusters and superclusters, which are forming at the present epoch, have velocity dispersions $v/c \approx 3 \times 10^{-3}$ and represent gravitational curvature fluctuations $\delta\phi/c^2 \approx (v/c)^2 \approx 10^{-5}$. The Sachs-Wolfe contribution is therefore expected to be of order $\frac{1}{3}\delta\phi/c^2$, or $(\delta T/T)_{sw} \approx 3 \times 10^{-6}$ over angular scales of tens of arcminutes or larger, for a scale-invariant spectrum.

Observational Constraints

The quantity that one uses to construct observational maps of the CMB is the angular power spectrum, defined by expanding $C(\theta)$ in spherical harmonics

$$C(\theta) = \frac{1}{4\pi} \sum_{\ell>2}(2\ell + 1)C_\ell P_\ell(\cos\theta),$$

where

$$C_\ell = \int \frac{k^2}{8\pi}dk|\delta\rho_{r\ell}(k, t_0)|^2.$$

Here $\delta\rho_{r\ell}(k, t_0)$ is the Fourier component of the radiation density at the present epoch (t_0) as a function of comoving wavenumber and expanded over angular harmonics in $\cos\theta$. The unobservable monopole ($\ell = 0$) and the gauge-dependent dipole terms have been subtracted; the remaining expression is gauge-invariant.

The rms quadrupole amplitude $C_2^{1/2}$ is directly measurable via an all-sky map, and the upper limit on its amplitude is 5×10^{-5} (95 percent confidence) from the RELICT satellite experiment.[31] This limit is a factor of two smaller if scale-invariant fluctuations are assumed. On smaller angular scales, construction of a map utilizes the full power spectrum C_ℓ. Hitherto, experiments have utilized a single telescope that beam-switched to reduce systematic errors.

A typical experiment has an angular response that is determined by its beam pattern, which might involve a simple subtraction between two beams, as performed by Melchiorri et al.[19] with FWHM=5° and switching angle $\theta = 6°$, or might measure the temperature difference between one direction and that on either side in a three-beam experiment, as carried out by Uson and Wilkinson[32] for a beam of $1'.5$ switched over $4'.5$. We then have either

$$(\triangle T/T)^2 = 2[C_B(0) - C_B(\theta)]$$

$$\text{or} \quad (\triangle T/T)^2 = \langle [T_0 - \frac{1}{2}(T_1 + T_2)]^2 \rangle = 2[C_B(0) - C_B(\theta)] - 1/2[C_B(0) - C_B(2\theta)],$$

respectively, where $C_B(\theta) = \frac{\langle \triangle T(\gamma_1) \triangle T(\gamma_2) \rangle}{T^2}$ with $\cos\theta = \gamma_1 \cdot \gamma_2$ is the beam-smeared temperature correlation function. Limits from these two experiments are

$$\triangle T/T \leq 7.4 \times 10^{-5} \quad (\theta = 6°)$$

and

$$\triangle T/T \leq 2.8 \times 10^{-5} \quad (\theta = 4'.5)$$

at 95 percent confidence. A recent experiment[33] reports a slightly stronger small-scale anisotropy limit utilizing a double beam-switching technique for a $1'.9$ beam and $\theta = 7'.15$, with an upper limit $\triangle T/T \leq 1.7 \times 10^{-5}$. The Uson-Wilkinson result has been criticized as being overly optimistic:[34] a more realistic upper limit may be 4×10^{-5} over $4'.5$.
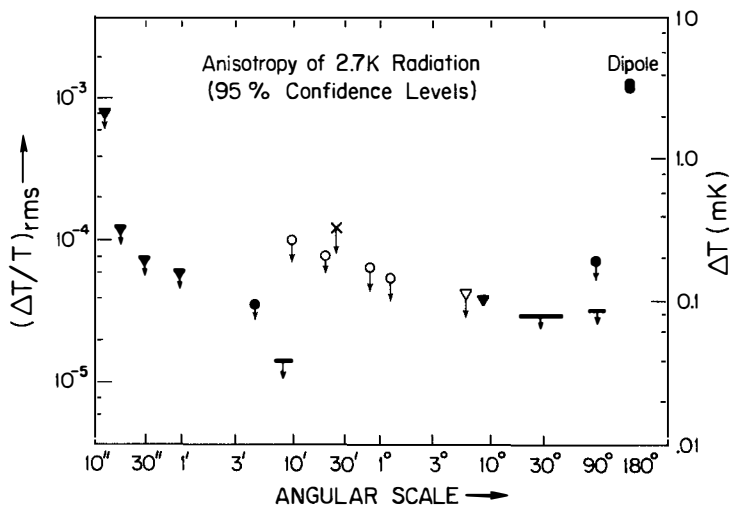
Figure 3: Upper limits on the rms temperature fluctuations in the CMB. Measurements are summarized in the text.

A detection has been reported[35] of fluctuations at $\theta = 8°.2$ (FWHM beam $8°.3$) with a dedicated experiment at Tenerife at a level $\Delta T/T = 3.7 \times 10^{-5}$. This experiment has hitherto been performed at one wavelength (3 cm), and evaluation of a possibly major contribution to the signal, the patchy low-level galactic diffuse emission, must await completion of a survey at longer wavelength. If the experimental result were confirmed as a measurement of the CMB anisotropy, the implications would be remarkable: the reported level of $\Delta T/T$ exceeds that expected in cold dark matter-dominated cosmologies, and indeed in any model with primordial gaussian, scale-invariant fluctuations, by an order-of-magnitude. One should compare the Tenerife result with the upper limits reported by RELICT and also by the balloon data[36] on intermediate angular scales: at 95 percent confidence,

$$[C(\theta)]^{1/2} \lesssim 5 \times 10^{-5} \quad (\theta \geq 20°) \text{ and}$$

$$[C(\theta)]^{1/2} \lesssim 3.7 \times 10^{-5} \quad (\theta \geq 10°),$$

respectively, for a FWHM beam of 7°. The various observations are summarized in Figure 3.

Interferometric techniques, using aperture synthesis at the VLA, have been used to map the CBR with sub-arc-minute resolution.[37),38)] The strongest upper limits are[39)] $\Delta T/T \leq 0.6 \times 10^{-4}(60'')$, $0.8 \times 10^{-4}(30'')$, and $8.5 \times 10^{-4}(12'')$ at 95 percent confidence. Only a small area of sky has been searched at 5 GHz ($\sim 10^3$ square arc min) with this resolution.

4. Implications and Future Prospects

In the context of inflationary models and curvature fluctuations, baryon-dominated cosmology is almost untenable as a consequence of the intermediate angular-scale anisotropy limits.[40),41)] One needs $\Omega_b = 1$ and a primordial adiabatic fluctuation power-spectrum $(\delta\rho/\rho)_k^2 \propto k^n$ with n > 2 to suppress the large-scale temperature fluctuations. However such a spectrum gives an unacceptable fit to the galaxy-galaxy and large-scale velocity correlations, and, moreover, has a small-scale divergence that one has to cure by fine-tuning the initial conditions. This is not regarded as an attractive means for saving the theory. An isocurvature fluctuation spectrum in a baryon-dominated universe avoids this divergence problem, since the local curvature associated with fluctuations, by definition, vanishes, and even allows one to live with $\Omega_b \approx 0.1$, the value consistent with the primordial nucleosynthesis constraint. One has to pay the price, however, of adjusting the power spectrum shape, by forcing n to lie in the range $0 \gtrsim n \gtrsim -1$. The index n has to be carefully tuned to fit the statistical probes of large-scale structure provided by the galaxy and velocity pairwise correlations, and the intermediate angular scale CMB anisotropy must also be suppressed. For example, isocurvature fluctuations with a Zel'dovich initial spectrum (equivalent to n=−3) have been eliminated as a possible contender because of excessive intermediate angular scale anisotropy.[42)] It is worth noting that if n > −3, non-linearity is inevitable at an early epoch. This means that reheating most likely occurred as a consequence of the energy input associated with early galaxy formation. Vishniac[43)] pointed out that a quadratic (second order) contribution in $\delta \mathbf{n} \cdot \mathbf{v}$ to temperature fluctuations would be important on small, sub-arcminute, angular scales. One can improve matters somewhat by

adding a cosmological constant (or vacuum density) to maintain a spatially flat universe: $\Omega_{vac} = 0.9$, $\Omega_b = 0.1$. This boosts fluctuation growth, and helps alleviate the difficulty with the CMB anisotropy.

Such an approach is not very compelling, however, to a theorist. The key observational constraint is that baryonic matter is restricted by primordial nucleosynthesis constraints, at least in the standard and simplest big bang model, to $\Omega_b \lesssim 0.1$, whereas consideration of the physics of the very early universe, and in particular the inflationary cosmological models, favors a density parameter $\Omega = 1$. The dominant form of matter must, in this case, be some form of non-baryonic, weakly interacting particle. The dominance of non-baryonic dark matter means that fluctuation growth can occur prior to the decoupling epoch, although it is only efficient during the matter-dominated era that commences at z_{eq}. Thus the prevalence of non-baryonic matter acts to reduce the required amplitude (Figure 4). The reduction factor amounts to $(1 + z_{dec})/(1 + z_{eq}) \sim 0.1$.
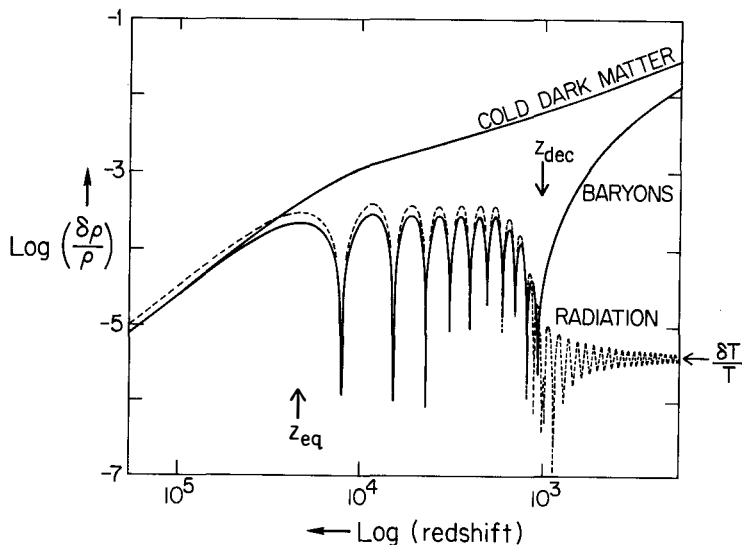
Figure 4: Time-evolution of density fluctuations in CDM, baryon and radiation in the early universe (N. Vittorio, in preparation.)

In addition, linear growth ceases if $\Omega \ll 1$ at a redshift $\sim \Omega^{-1} - 1$. This implies that the expected fluctuation amplitude at last scattering is increased by a factor $\sim \Omega^{-1}$ relative to what is expected in a universe with $\Omega = 1$. Reducing Ω also affects L_{eq}, which therefore shifts the characteristic scale of roll-over between the $\delta\rho/\rho \sim$ constant (small L) and $\delta\rho/\rho \sim L^2$ (large L) regimes to larger scales. This behaviour leads to a characteristic large-scale signature, and suggests that one should consider a cold dark matter-dominated cosmology, with Ω allowed to be a free parameter. Such a model could be consistent with inflation if $\Omega_{vac} + \Omega_{CDM} = 1$.

The fine-scale upper limit on the CMB anisotropy may be used to constrain such models, which predict that[44)−47)]

$$\triangle T/T \approx 1 \times 10^{-5} \Omega^{-1} (2h)^{-4/3} (\Omega_b/0.1)^{1/3} b^{-1}.$$

Here Ω_b is the baryon density, augmentation of which tends to enhance $\triangle T/T$ due to the Doppler contribution on the last scattering surface, and b is the bias factor, defined to be the ratio of $\delta N_g/N_g$, the observed galaxy count fluctuations averaged over a sphere of radius $8h^{-1}$Mpc, to $\delta\rho/\rho$, the underlying mass fluctuations. The ever-improving upper limits (Figure 5), culminating most recently with the Readhead et $al.$ result,[32)] constrain Ω to be $\gtrsim 0.4$ in a CDM-dominated universe.

Hot dark matter models are also severely constrained by the fine-scale anisotropy limits (Figure 5). In these models, non-linearity occurs far too late to allow any smoothing of primordial temperature fluctuations by reionization. For a hot dark matter model to survive with $\Omega = 1$, one requires non-linearity and galaxy formation to occur at a redshift $\lesssim 1$. This is probably inconsistent with the recent discovery of galaxies at a redshift of $\gtrsim 3$.

However hot dark matter has attracted renewed interest in the guise of a universe wherein density fluctuations are seeded by cosmic strings. Cosmic strings are non-linear topological defects from an early phase transition that effectively accrete matter in the
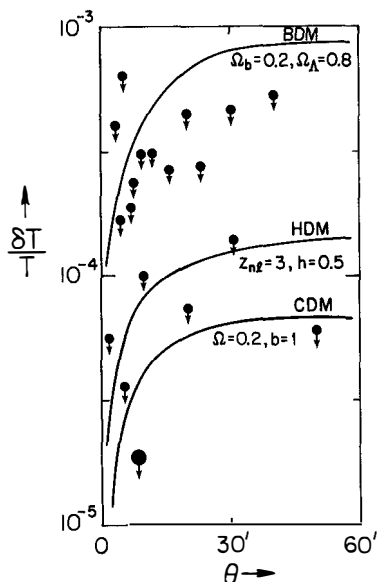
Figure 5: Comparison of fine-scale upper limits for beam switching experiments with three different models: CDM ($\Omega=0.2,b=1$), HDM ($z_c=3,h=0.5,\Omega=1$), and BDM ($\Omega_b=0.2,\Omega_{vac}\equiv\Omega_\Lambda=0.8$).

matter-dominated era. In fact, the accretion is so efficient that strings may even be incompatible with a cold dark matter-dominated cosmology, [48] with excessive small-scale power being generated in the form of galaxy correlations. Hot dark matter tends to suppress accretion on sub-galactic scales until recently, and provides the most attractive complement to cosmic strings. An interesting test of cosmic strings arises because of their non-gaussian character. One has to recall that only very limited areas of sky have been studied, and any theory invoking non-gaussian fluctuations statistics would meet with very different constraints from the CMB anisotropy limits. Bouchet et al.[49] compute the temperature pattern induced in the CBR by a network of cosmic strings, and find that the rms temperature anisotropies are $\Delta T/T = 17~G\mu/c^2$, where μ is the parameter that specifies the mass-density of the strings: typical models that seed large-scale structure require $G\mu/c^2 \sim 10^{-6}$. The temperature fluctuations possess a "stringy," non-gaussian character, with the small-scale power concentrated in rare discontinuities. With sufficient sky coverage, it should be

possible to distinguish string-induced temperature anisotropies from those expected in the principal rival theory for large-scale structure, namely the inflationary model, which predicts gaussian adiabatic scale-invariant fluctuations in a (cold-) dark-matter-dominated universe.

The existing theories are not faring particularly well with regard to accounting for recent data on the large-scale structure of the universe. Reanalysis of the galaxy angular correlations utilizing an automated deep survey of galaxy counts, suggests excessive large-scale power relative to what is expected in cold dark matter models,[50] which were only marginally compatible with the Groth-Peebles[51] angular correlation function from the Shane-Wirtanen counts. Reports persist of large, ~100 Mpc, structures in the galaxy distribution, including the Perseus-Pisces filament,[52] Geller's great wall,[53] and Tully's agglomerations of galaxy clusters over scales[54] of ~300 Mpc.

Another observational result that suggests the presence of excess large-scale power in the primordial fluctuation spectrum, relative to what would be expected for scale-invariant initial conditions, is the evidence for large-scale bulk flows. While these rely on knowledge of distance indicators to an accuracy of about 10 percent, where there is some scope for hitherto unrecognized sources of systemic error or bias, the tentative conclusion that coherent velocity flows of several hundred km s^{-1} persist over scales of $\gtrsim 30h^{-1}$Mpc remains unshaken.[55],[56] If these motions are gravitationally driven, one has to appeal to linear fluctuations of order $\delta\rho/\rho \sim v/ct$ on these large-scales. These same linear fluctuations must inevitably induce Sachs-Wolfe anisotropies of order.[57]

$$\Delta T/T \approx (\delta\rho/\rho)(L/ct)^2_{\ell s} \approx v(L/ct)_{\ell s} \approx 3 \times 10^{-5} \left(\frac{v}{500 \text{kms}^{-1}}\right) \left(\frac{L}{50h^{-2} \text{ Mpc}}\right)$$

over $\theta \sim 2(L/50h^{-1} \text{ Mpc})\Omega$ degrees. Here L is the scale over which the bulk flow component v is measured. Pending experiments, which are expected to have a sensitivity of at least one part in 10^5 to temperature fluctuations, should be capable of testing the reality of the large-scale bulk flows.

Models that are still tenable include cold-dark-matter cosmology, with adiabatic, scale-invariant fluctuations and $\Omega = 1$, and string-seeded models with a universe dominated by cold, hot, or even baryonic dark matter. There are still discouragingly many choices between rival hypotheses about the nature of the seed fluctuations that gave birth to galaxies, galaxy clusters and superclusters. However the next generation of CBR experiments, including balloon-borne experiments (UCSB, MIT, Princeton, Rome) and proposed ground-based dedicated aperture synthesis arrays (Cambridge, Caltech), should be expected to provide definitive clues to the origin and nature of the large-scale structure in the universe.

For example, one area that is largely unexplored from the theoretical perspective is large angular scale anisotropy, precisely where one anticipates progress from the forthcoming all-sky maps to be obtained by the COBE and RELIC 2 satellite experiments. Curved models do not yield simple unambiguous predictions of $\Delta T/T$ on scales larger than the angle subtended on the sky at the last scattering surface by the curvature radius $R_{curv} = (c/H_0)(1 - \Omega_0)^{-1/2}$. The reason for this is that Fourier decomposition, the definition of wave-number and wavelength, and the concept of mass or energy fluctuations, all acquire a new level of complexity in a curved background. One no longer has the prediction of a Zel'dovich spectrum, and one has to generalize the definition of wave number onto a spatially curved spacelike surface in order to apply linear perturbation theory. One may obtain some insight by comparing the curvature scale with the horizon radius, $R_{hor} = 2(c/H_0)\Omega_0^{-1}$, to infer that as Ω_0 decreases below a critical value of 0.85, R_{curv} becomes smaller than R_{hor}. Since R_{curv} determines the role of geodesic focussing, we may expect geometrical focussing to tend to suppress the quadrupole and low order multipoles of the CBR anisotropy in low Ω cosmologies. A similar effect manifests itself as the "'ring of fire" in curved Bianchi models, and has been studied[40] for infinite single mode plane wave perturbations of open Friedmann models. The characteristic angular scale of the features, observable as a peak in the multipole structure, is $[\Omega_0/(1 - \Omega_0)]^{1/2}$ radian. One

might hope ultimately to disentangle both Ω and the intrinsic fluctuation spectrum from the CMB anisotropies.

One important challenge for the forthcoming experiments that are designed to probe the $\Delta T/T < 10^{-5}$ range will lie in circumventing the various backgrounds. Once atmospheric fluctuations are under control, by judicious choice of observing platform and wavelength, the galactic background is the next obstacle one runs into. It already seems likely that this is the cause of fluctuations seen in experiments at $\sim 500\mu$ and at 15 GHz. At ~ 40 GHz or 0.3 cm, the atmospheric background is minimal from a high altitude site. The galactic background, due to synchrotron and HII region emission at the lower frequency, and to IRAS cirrus at the higher frequency, is poorly known at the $10\mu K$ level that will be necessary to probe $\Delta T/T$. Moreover, the contribution from unresolved extragalactic radio sources also becomes significant at this level[58]. Finally hot gas in galaxy clusters, super-clusters, groups and halos produces Sunyaev-Zel'dovich distortions with an expected amplitude of $(10-100)\mu K$.[59),60)] The filling factor of this hot gas component could be appreciable, and one ideally requires x-ray observations to map out the thermal gas distribution. It seems apparent that multi-frequency measurements, mapping with a wide range of angular resolutions, and extensive sky coverage are all necessary ingredients that will have to be incorporated into any definitive detection of the primordial cosmic microwave background anisotropies. Such a detection, as well as confirmation of any spectral distortions, will constitute a crucial element in our understanding of the ultimate origin of the large-scale structure of the universe.

Acknowledgments

References

1. Gamow, G. 1948, *Phys. Rev.*, **74**, 505.

2. Alpher, R. and Herman, R. 1948, *Nature*, **162**, 774.

3. Dicke, R. H. *et al.* 1965, *Ap.J.*, **142**, 414.

4. McKellar, A. 1941, *Pub. Dominion Astr. Obs*, **7**, No. 15.

5. Crane, P. *et al.* 1989, (in press).

6. Penzias, A. and Wilson, R. 1965, *Ap.J.*, **142**, 419.

7. From Smoot, G. 1989, in proceedings of *Particle Astrophysics Workshop*, ed. E. Norman (in press).

8. Matsumoto, T. *et al.* 1988, *Ap.J.*, **329**, 567.

9. Kawasaki, M. and Sato, K. 1987, *P.A.S.J.*, **39**, 337.

10. Raffelt, G., Dearborn, D., and Silk, J. 1989, *Ap.J.*, **336**, 61.

11. Smoot, G. *et al.* 1987, *Ap.J. (Letters)*, **317**, L45.

12. Hayakawa, S. *et al.* 1987, *P.A.S.J.*, **39**, 941.

13. Lacey, C. and Field, G. B. 1988, *Ap.J. (Letters)*, **330**, L1.

14. Fukugita, M. 1988, *Phys.Rev. Lett*, **61**, 1046.

15. Field, G. B. and Walker, T. P. 1989, preprint 1787 (Center for Astrophysics).

16. Fukugita, M. and Kawasaki, M. 1989, preprint TU-339 (Tohoku University).

17. Wang, B. and Field, G.B. 1989, preprint (Center for Astrophysics).

18. Woody, D. P. and Richards, P.L. 1981, *Ap.J.*, **248**, 18.

19. Rowan-Robinson, M., Negroponte, J., and Silk, J. 1979, *Nature*, **281**, 635.

20. Bernstein, G. *et al.* 1989, *Ap.J.* (in press).

21. Adams, F. *et al.* 1989, *Ap.J.* (in press).

22. Kreysa, E. and Chini, A. 1989, in *Proc. 3rd ESO-CERN Symposium Astronomy, Cosmology, and Fundamental Particles* (in press).

23. Bond, J.R., Carr, B.J., and Hogan, C. 1989, *Ap.J.* (in press).

24. e.g. see *The Early Universe*, Kolb, E. and Turner, M.S. 1989, (Springer-Verlag) (in press).

25. Guth, A. 1981, *Phys.Rev.D*, **27**, 347.

26. Peebles, P.J.E. 1987, *Ap.J. (Letters)*, **277**, L1.

27. Sachs, R.K. and Wolfe, A.M. 1967, *Ap.J.*, **147**, 73.

28. Zel'dovich, Ya. B. and Sunyaev, R.A. 1969, *Astrophys. Space Sci.*, **4**, 301.

29. Silk, J. 1968, *Ap.J.*, **151**, 459.

30. Jones, B.J.T. and Wyse, R.F.G. 1985, *Astr. Ap.*, **149**, 144.

274

31. Strukov, I.A., Skulachev, D.P., Klypin, A.A. and Sazhin, M.V. 1986, *Special Astrophysical Observatory Report*, **53**, 67.

32. Uson, J. and Wilkinson, J. 1984, *Nature*, **312**, 427.

33. Readhead, A., *et al.* 1988 in , *The Large-Scale Structures of the Universe*, ed. J. Audouze, M.C. Pelletan and A. Szalay (Dordrecht: D. Reidel), p.37.

34. Partridge, R.B. 1988, *Reports on Progress in Physics*, **51**, 647.

35. Davies, R.D., *et al.* 1987, *Nature*, **326**, 462.

36. Fixsen, J., Cheng, E. and Wilkinson, J. 1983, *Phys. Rev. Lett.*, **50**, 620.

37. Fomalont, E. Kellerman, K. and Wall, J. 1984, *Ap.J.*, **277**, L23.

38. Martin, H.M. and Partridge, R.B. 1988, *Ap.J.*, **324**, 794.

39. Fomalont, E.G., *et al.* 1989, *Ap.J.*, (in press).

40. Wilson, M. and Silk, J. 1981, *Ap.J.*, **243**, 14.

41. Wilson, M. 1983, *Ap.J.*, **277**, 2.

42. Efstathiou, G. and Bond, J.R. 1986, *M.N.R.A.S.*, **218**, 103.

Vishniac, E. 1987, *Ap.J.*, **322**, 597.

44. Bond, J.R. and Efstathiou, G. 1984, *Ap.J. (Letters)*, **295**, L45.

45. Vittorio, N. and Silk, J. 1984, *Ap.J (Letters)*, **285**, L39.

46. Bond, J.R. 1987, in *The Early Universe*, ed. J. Unruh (Dordrecht: Reidel) (in press).

47. Vittorio, N. and Silk, J. 1989, in preparation.

48. Bertschinger, E., Melott, A. and Scherrer, R. 1989 (in press).

49. Bouchet, F., Bennett, D. and Stebbins, A. 1988, *Nature*, **335**, 410.

50. Efstathiou, G. and Maddox, S. 1989, (in preparation).

51. Groth, E. and Peebles, P.J. E. 1977, *Ap.J.*, **217**, 385.

52. Haynes, M.P. and Giovanelli, A. 1986, *Ap.J. (Letters)*, **306**, L55.

53. Geller, M. 1989, in proceedings of *Particle Astrophysics Workshop*, ed. E. Norman (in press).

54. Tully, R. B. 1987, *Ap.J.*, **323**, 1.

55. Dressler, A., *et al.* 1987, *Ap.J. (Letters)*, **313**, L37.

56. Faber, S. and Burstein, D. 1988 in *Large-Scale Motions in the Universe*, ed. V. Rubin and G. Coyne (Princeton: Princton University Press), 116.

57. Suto, Y. *et al.* 1988, *Nature*, **332**, 328.

58. Franceschini, A. *et al.* 1989 (in press).

59. Schaeffer, R. and Silk, J. 1988, *Ap. J.*, **733**, 509.

60. Cole, S. and Kaiser, N. 1988, *M.N.R.A.S.*, **233**, 137.

MASSIVE COMPOSITE BOLOMETERS FOR DARK MATTER DETECTION

N. CORON[1], P. de MARCILLAC[2], G. ARTZNER[1], J. LEBLANC[1],

G. JEGOUDEZ[1], G. DAMBIER[1], J.P. LEPELTIER[1], M. BARTHELEMY[1], R. ROTHENFLUG[3],

P. PARI[4], A. TARRIUS[3], F. AMOUDRY[5], H. STROKE[6], O. TESTARD[3]

Presented by N. CORON

ABSTRACT

Massive composite bolometers cooled below 100 m°K can detect recoil energy of particles with a very high efficiency. By using different absorber materials (Al_2O_3, Ge, Si, LiF, Cr_2O_3, TiO_2...) some identification of dark matter particles will be possible. Resolutions in the 10 eV range for 1 kg of absorber are theoretically possible at 10 m°K if the thermistor is well matched to the substrate (for the heat capacity) and to the electronics (for the impedance). We have successfully developed and tested a 25-gram sapphire bolometer, the heaviest to date, at 100 m°K and obtained on a 60 KeV γ line a 16 KeV FWHM resolution limited by extraneous noise.

First bolometric spectra of radioactivity and cosmic ray background obtained at sea level are presented.

1   LPSP-IAS, B.P. 10, 91371 Verrières le B., France, Tél. : (1) 64 47 43 08 - Fax : (1) 69 20 39 07
2   IAP, 98bis, boulevard Arago, 75014 Paris, France
3   S.A.p.-CEN, B.P. 2, 91190 Gif sur Yvette, France
4   S.P.S.R.M.-CEN, B.P. 2, 91190 Gif sur Yvette, France
5   LMRI-CEN, B.P. 2, 91910 Gif sur Yvette, France
6   New York University, 4 Washington Place, N.Y. 10003, U.S.A.

1   INTRODUCTION

Massive bolometers (in the 1-1000 gram range) for single event particle detection were, only a few years ago, still a purely prophetic anticipation[1-4]. But, since 1984, thermal spectrometry is seeing an increasing development in the world[5-16]. First, little bolometers were proven to have good resolution on X-rays[6] and α-particles[7]. More recently massive bolometers (over 1 gram) have been successfully tested[5,11,15,16]. Detection of cold dark matter particles through measurement of the recoil energy in a massive target (in the 10-1000 gram range) cooled below 100 m°K to reach 100 eV resolution was proposed several years ago[17-19]. We analyse below the operation and possible performance of the composite bolometer for dark matter detection. We also detail a new design of such a detector and the successful tests of a 25 gram sapphire composite bolometer achieving a resolution better than 16 KeV.

2   COMPOSITE BOLOMETERS AND DARK MATTER DETECTION

A large proportion of the mass in the universe may be under the form of non baryonic particles weakly interacting with matter (W.I.M.P.)[17-21]. Present detection of these particles can be attempted only with germanium[22] or silicon detectors[24] in which only about 25 % of the recoil energy can be transformed into an electrical current. Observing recoil energies smaller than 5 KeV is nearly hopeless. Moreover these detectors have few non-zero spin nuclei, so that the interaction rate is expected to be very low for certain particle candidates such as the photino (see 17, 18, 19). Massive composite bolometers have potentially several advantages :

- the material of the target can be chosen among several possibilities, as LiF, TiO_2, Cr_2O_3 ...A set of composite bolometers with different targets can help to determine the nature of the interacting particles ;
- the ultimate resolution depends essentially on temperature and can be in the 10 eV range for a 1 kg low heat capacity single crystal cooled below 10 m°K ;
- the quanta of thermal energy modes (phonons) are in the 10^{-3}-10^{-4} eV range, so that intrinsic statistical noise is very low (≈ 0.3 eV on a 100 eV recoil energy !).

The collision between a dark matter particle (with mass m_x) and a nucleus (with mass m_N) of the target deposits in the bolometer a recoil energy E, the average value of which is[21] :

$$< E > \approx 2 \text{ KeV} \frac{m_N}{1 \text{GeV}} [\frac{m_x}{m_N + m_x}]^2 \qquad (1)$$

For $m_x = 5$ GeV and for ^{27}Al with $m_N = 25$ GeV we get $< E > = 1.4$ KeV.

Because of the three times better recoil energy detection efficiency and of the better matching of masses, a 1 KeV (nominal threshold) LiF bolometer will detect cosmions of 2.6 GeV while a 1 KeV (nominal threshold) classical Ge detector[22] will detect only cosmions with mass above 12 GeV. Bolometers with diamond, germanium, silicon or sapphire targets are now classical ones. All hard single crystals will work as well. For an absorber with bad thermal properties a composite-sandwiched target can be a solution as we proposed earlier[10].

Interaction rates will depend strongly on the nature of the particle and of the spin of the target[17-21]. The calibration of such detectors will be possible on recoils from neutrino scattering[23] or on collimated neutrons[24]. Several groups in the world are now developing low temperature cryogenic thermal detectors for dark matter[5,20,22]. In France extensive collaborations are developing on this subject and the "Institut des Sciences de l'Univers" supports this program[25] helped also by international collaborations (N.Y. University, Göteborg University, CERN-ISOLDE). We present below our most recent theoretical and experimental results.
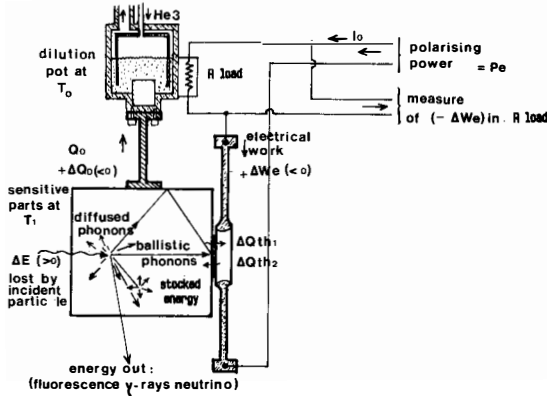
Figure 1 - Schematic diagram of a composite bolometer and of energy balance
when an incident particle looses ΔE by collision on the target.

3   OPERATION AND THERMODYNAMICS OF THE COMPOSITE BOLOMETER

Present bolometer theories implicitly suppose that the whole energy is finally confined in the sensor. We think that this is not exact for the composite bolometer (except perhaps in an hypothetic ballistic phonon detector mode). The composite bolometer consists mainly of an absorber or target with heat capacity C_a, very well thermally connected to a sensor or thermistor with heat capacity C_{th}. By construction these two elements are always at nearly the same temperature T_1 (in the frequency bandpass of the whole bolometer). They are connected to the refrigerator by a thermal link of thermal conductance G optimised so that the thermal time constant $\tau_{th} = (C_a + C_{th})/G$ has the wanted value.

When a particle strikes the target with an absorbed energy ΔE the sensor receives a fraction of it as heat, ΔQ, with :

$$\Delta Q = (\frac{C_{th}}{C_a + C_{th}}) \Delta E \tag{2}$$

Up to now, small bolometers had $C_{th} \gg C_a$ and normal theory with $\Delta Q = \Delta E$ was appropriate. But for massive bolometers a new question arises : what is the optimal C_{th}/C_a ratio ? We attempt an answer : we suggest to consider the composite bolometer system as a

thermodynamic engine in which the heat reservoir is the composite sensitive part at T_1 and the cold reservoir is the cryostat at T_0. The second principle of thermodynamics states that only a fraction η_t of heat ΔQ extracted from the heat reservoir at T_1 can be transformed into (electrical) work, with $\eta_t = 1 - T_0/T_1$.

The maximum useful signal that can be transferred to a measurement is thus:

$$\Delta We = \eta_t \frac{C_{th}}{C_a + C_{th}} \Delta E \tag{3}$$

We must now reestimate the two fundamental noise sources existing in a bolometer : the thermodynamic noise and the "polarising" noise. The first noise is due to statistical fluctuations of the thermal energy in the sensor[26,28] which will be converted into noise signal with maximal efficiency η_t ; this noise after conversion in work is $\Delta N1_{rms}$:

$$\Delta N1_{rms} = \eta_t \sqrt{kT_1^2 C_{th}} \tag{4}$$

where k is the Boltzmann constant.

The second noise is due to the statistical fluctuations ($= \Delta Pe_{rms}$) of the polarising power Pe which maintains the bolometer at the optimal temperature T_1. This noise is called either the "Johnson noise" if the sensor is electrically polarised, or the "photon noise" if the sensor is optically polarised. As long as Pe is transmitted by quanta of energy $\delta E \ll kT_1$ we get (demonstrated in ref.29 for photons) :

$$\Delta Pe_{rms} = \sqrt{Pe} \sqrt{kT_1} \sqrt{B} \tag{5}$$

where B is the bandpass.

But the fraction of Pe available to change energy in the sensor is only Pe_{th} with :

$$Pe_{th} = Pe \times \frac{C_{th}}{C_a + C_{th}} \text{ and } \Delta Pe_{th} = \sqrt{Pe_{th}} \sqrt{kT_1} \sqrt{B} \tag{6}$$

We'll suppose here that power fluctuations ΔPe_{th} are converted into signal noise $\Delta N2_{rms}$ with an efficiency equal to one (voltage fluctuations not converted into heat),while measuring energy ΔE. We introduce τ_e, the electrical time constant of the pulse connected to the true time constant τ_{th}, by $\tau_e = \phi\tau_{th} = \phi\frac{C_a + C_{th}}{G}$ where ϕ is a coefficient depending slightly on the thermistor sensitivity.Then, with optimal filtering of the signal pulse, it is demonstrated[28] that $\Delta E_{rms} = \sqrt{\tau_e} \Delta Pe_{rms}/\sqrt{B}$. As applied here:

$$\Delta N2_{rms} = \sqrt{\tau_e} \Delta Pe_{th}/\sqrt{B} = \sqrt{Pe \frac{C_{th}}{C_a + C_{th}}} \times \sqrt{kT_1} \times \sqrt{\tau_e} \tag{7}$$

Using $Pe = G(T_1 - T_0)$ and $\phi = 0.5$ (typical value of good thermistors) we can simplify (7) to :

$$\Delta N2_{rms} = \sqrt{C_{th} kT_1 (T_1 - T_0)/2} \tag{8}$$

Then the ultimate resolution for a composite bolometer becomes :

$$\Delta E_{rms} = \frac{C_a + C_{th}}{C_{th}} \times \frac{1}{\eta_t} \sqrt{\Delta N_{1rms}^2 + \Delta N_{2rms}^2} = \frac{C_a + C_{th}}{\sqrt{C_{th}}} \times f(T_1, T_0) \tag{9}$$

If C_a and C_{th} vary as T_1^3 this expression goes through a minimum when

$$T_1/T_0 = \theta_m = 1.2 \tag{10}$$

and

$$C_{th}/C_a = \psi_m = 1 \tag{11}$$

It can be shown that this minimum is always obtained for values of θ_m around 1.2 and of ψ_m around 1 independent of the rates of variation of C_{th} and C_a with T_1, or of the electrical characteristics of the sensor.

a   b
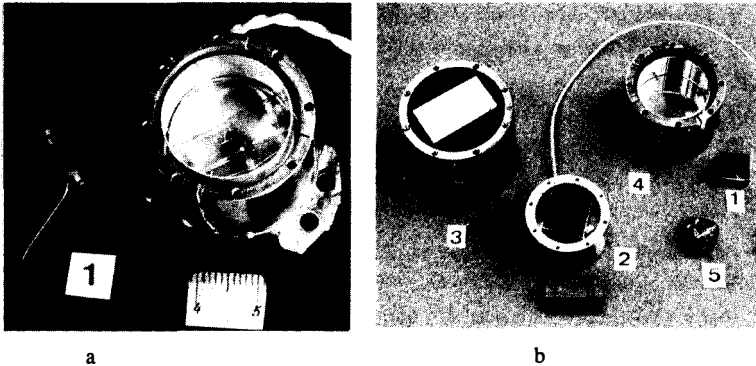
Figure 2

a- A classical infrared bolometer with collecting optics compared to the 25 g bolometer for dark matter

b- Massive bolometers under construction with different materials :

Ge (1, 2, 3);Sapphire(4);Diamond(5)

So from thermodynamic considerations only, we have established that for all composite bolometers the best resolution is obtained when the thermal capacity of the sensor equals the thermal capacity of the target. This general new theorem was first demonstrated by Buhler and Umlauf in the particular case of the magnetic bolometer[11] and was generalised by us[5].

Our analysis is for the pessimistic case where no amplification exists through the sensor. If some amplification exists we obtain the same conclusions after replacing η_t by $\eta_e = (1 - \tau_e/\tau_{th})$, but the ultimate calculated resolution would be better. This amplification mecanism may also introduce supplementary noise proportional to η_t/η_e. So for the dark matter detector we'll use the thermodynamic limit independent of the sensor.

Finally, the possible resolution of a composite massive bolometer optimized with $C_a = C_{th} = \frac{C_b}{2}$ at a working temperature T_1 and maintained by the polarising power at $T_1 = 1.2\, T_0$ is (with $\Delta E_{FWHM} = \sqrt{8\ln2}\, \Delta E_{rms} = 2.35\, \Delta E_{rms}$) :

$$\Delta E_{FWHM} = 5.7\, \sqrt{kC_b(T_0)} \times T_0^2 \qquad (10)$$

So, for dark matter detection,the ultimate possible resolution of a composite bolometer with a 1 kg single crystal target is :

$$\Delta E_{FWHM} = 4.2 \times 10^{-8}\, T_0^{5/2}\, \theta_D^{-3/2}\, M_A^{-1/2} \quad \text{in Joule}/\sqrt{kg} \qquad (11)$$

where θ_D is the Debye temperature and M_A the atomic mass (in grams) of target material.

These ultimate performances will only be obtained if :

a the thermal gradients are minimised between sensitive parts at T1 ;

b the conversion of recoil energy into heat is complete and stable : no energy stocked in defaults, or trapped charges ;

c the current noise in the sensor is negligeable ;

d non interesting sources of energy are filtered : windows must stop infrared photons ; filters must stop electrical interferences ;vibrations must be stopped in the bandpass of the bolometer ($\approx$ 10 Hz to 10 KHz) ;

e the cooling system is stable ($\frac{\Delta T}{T} < 1\ \%$) and with no microphonics ;

f the noise temperature of the preamplifier is less than 2 To.

Massive bolometers in the 1- kg range will necessitate a substantial volume of material for the sensor which must also be perfectly homogeneous in response. At the present time, we think that only the germanium thermistor, heavily doped by normal techniques, available in large volume, will be useful for massive bolometers with electrical polarisation.

4   THE HEAVILY DOPED GERMANIUM THERMISTOR

Up to now the best results have been obtained with heavily doped semiconductor (Ge or Si) for the thermistor[5,9]. Then, at low temperature, electrical conduction comes from the "hopping" mechanism where electrical carriers jump from an occupied site to an unoccupied one with a probability increasing steeply with temperature[31,32]. The resistance varies exponentially with temperature and the difficulty is to obtain a sensor with an impedance matched to electronic and time constant constraints, typically in the 10 KΩ-100 MΩ range, at a working temperature T_0. For example, the resistivity at 0.1°K varies as the 140-th power of the doping concentration or of room temperature resistivity (see Figure 3).

To solve this difficulty, and make bolometers of reasonable impedance, we monitor with very high precision the resistivity of germanium wafers at 300°K with the four-probe method. We use a specially designed, low pressure, 400 μm spacing, four-point probe. At 300°K we have to measure values around 0.06 ohm.cm resistivity with a few per thousand precision. The typical map of a 15 x 15 mm^2 region is shown in Figure 4 for a wafer doped for 0.1°K temperatures with $<\rho> \approx 0.052$ ohm.cm.

Resistivities of several tested thermistors (made of Ga doped Germanium) are plotted as a function of temperature in Figure 5. Curve labelled "Bol 143" is for the 25 g bolometer thermistor : there is a very sharp transition from conduction to non-conduction at 80 ± 20 m°K, typical of good doping homogeneity and of a measurement without parasitic background in the
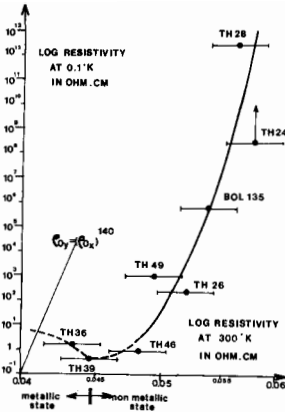
Figure 3
Resistivity of heavily doped germanium thermistors measured at 0.1°K as a function of room temperature resistivity (T = 298°C). Large error bars are due to errors on size measurements.
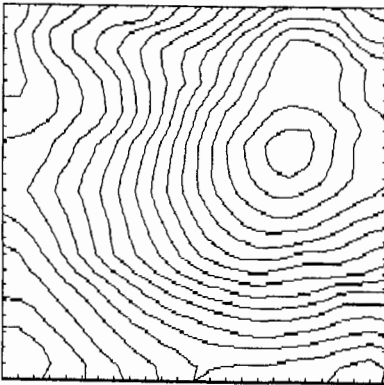
mapped area=15mm x 15mm
Δρ/ρ per contour interval=.002
ρmax=.0525 ohm.cm

Figure 4 - Resistivity maps of a 15 x 15 mm^2 slice of heavily doped Ge ; resistivity varies 5 per cent around 0.05 ohm cm between top and bottom ,corresponding to three orders of magnitude at 0.1° K. This map needed 100 hours of robotic measurement
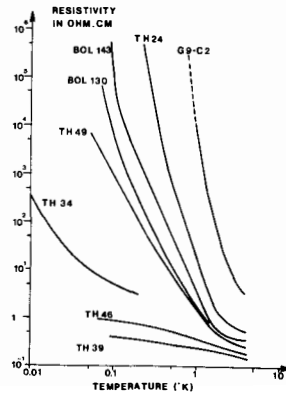
Figure 5 - Resistivity of typical doped Ge sensors as a function of temperature below 4°K

From these measurements we can conclude that, in normally grown germanium, the gradient in doping concentration is $\Delta Na/Na \approx 0.006$ per mm.This confers on sensors, with volumes in the mm^3 range, a resistivity at $0.1\,°K$ varying by ± 30 per cent in the whole volume. We believe that such an homogeneity is at least as good as other techniques for doping (N.T.D. or ion implantation). Anyway, improvements in doping homogeneity will have to be made for sensors of large bolometers working at 10 m°K. Heat conductivity and heat capacity measurements on these sensors are reported in ref. 5.

5   TOWARDS THE OPTIMAL DESIGN FOR COMPOSITE BOLOMETERS

A good approximation of the optimal design of a dark matter bolometer is our design of the 25 grams sapphire bolometer schematically shown in Figure 6 ; it incorporates several of our earlier developments : the thermistor is monolithic with shaped extremities so that solder heat capacity is "unseen" ; contacts are made of deposited In whose heat capacity in the superconductive state is very low. The heat capacity of the 3 mm^3 sensor is matched at $0.1\,°K$ with the 25 g sapphire heat capacity.
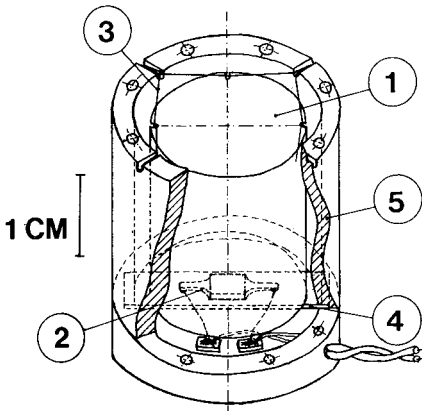
Figure 6 - Schematic of a massive composite bolometer with a 25 grams sapphire substrate (1) and a 5 mm^3 germanium thermistor (2) The suspension is made of 32 nylon threads (60 microns diameter) (3), while the heat link to the thermostat is a thin sapphire strip (4).
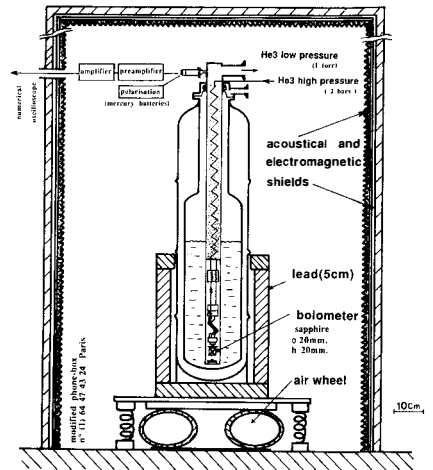
Figure 7 - Schematic diagram of the experimental set-up for tests at 100 m°K with protection against electromagnetic and accoustic interference and cosmic rays

The thermal link is made by a separate sapphire strip and can be easily changed. In this design we have five materials or components used in the sensitive part : nylon thread, epoxy, doped Ge, indium deposit, sapphire substrate, sapphire thermal link ! We foresee that massive composite bolometers will have more and more components !

6 TESTS AND RESULTS ON MASSIVE BOLOMETERS ; THE 25 GRAMS BOLOMETER

We have constructed several massive bolometers of 0.07, 0.15, 2.5 and 25 grams respectively (see Fig.2). In several aspects the larger ones work better and are easier to make than X-ray composite little bolometers ! We don't find extraneous heat capacity (sometimes a factor 10) as we found in the 1 mg bolometers.

We present below results obtained on the 25 gram bolometer. It has benefited from our earlier tests with lower masses and it is currently the best massive bolometer in the world, as far as we know, since it reaches a $\Delta E/\sqrt{m}$ of 1×10^5 eV/$\sqrt{Kg}$. As shown in Figure 6, it consists of a sapphire cylinder (20 mm diameter, 20 mm high) suspended by 32 nylon wires. The thermal sensor has a large volume (5 mm^3) and a thin sapphire strip links the system to the 0.1°K thermostat so that the measured time constant is 30 ms. The good quality of the sensor is seen in the V-I curve of Fig.8 since, at 0.1°K, a polarising power of 0.6 x 10^{-9} watt can be applied without too much "hot carrier effect".

We have used a special French-made dilution refrigerator[13] installed inside a metallic cabin (see Fig. 7). For calibrations we used an ^{241}Am source cooled at 4°K placed at 15 mm from the 1.5 mm diameter diaphragm in front of the bolometer. A removable 5 cm thickness lead wall was also installed around the cryostat to reduce external radioactivity and cosmic ray background (see §7 below).

An external ^{60}Co source placed at 50 cm of the cryostat was clearly detected giving many pulses per second around 1 MeV. So we have no doubt that this detector works through the entire volume. A typical analog output from the amplifier is given in Figure 9. The small peaks on the base line between the α peaks are true signals due to γ-rays in the 20 KeV-100 KeV range. Typical α pulses are plotted in Figure 10.

First tests were made without any analog filtering : at 0.1 K we obtained a 35 KeV FWHM resolution on the 5.48 MeV α line of ^{241}Am after numerical filtering of each pulse[5].

Second tests were made with a 10 -100 Hz analog filter and triggering on γ's : the 59.54 KeV γ-line of Am^{241} appears at the right place -deduced from linear extrapolation of the α's amplitude- and a 16 KeV FWHM resolution was obtained[5]. This resolution is not the ultimate one possible with this detector. We still have considerable parasitic noise from 1/f electrical noise and from low frequency microphonics (cf. Fig. 11). The heat capacity deduced from the signal obtained on 5.48 MeV α's is $2 \pm 1 \times 10^{-9}$ J/K. This value is twice the theoretical heat capacity of the sapphire cylinder. The ultimate resolution possible given by formula (10) is 600 eV with this bolometer at 0.1°K .
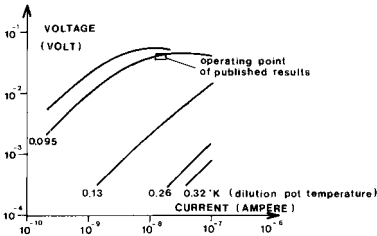
Figure 8 - V-I curve of the 25 g bolometer under vacuum at different temperatures (95 m°K, 135 m°K, 260 m°K, 320 m°K)
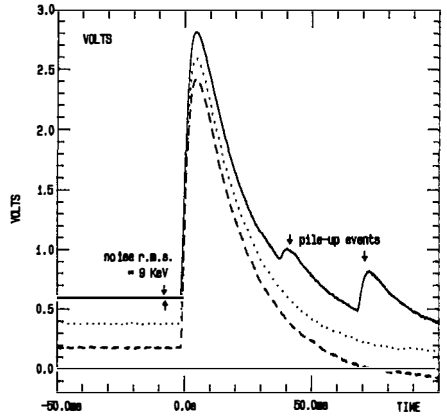
Figure 9 - Three typical single 5.48 MeV events in the 25 g bolometer without any filtering Units in the abcissa are ms
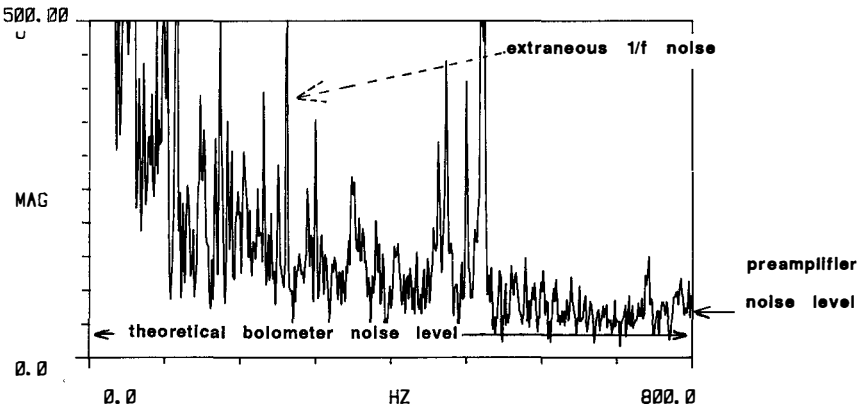
Figure 10 - Spectrum of the voltage noise measured on the 25 g bolometer at 0.1°K with a room temperature amplifier : this noise corresponds to spectra with 16 KeV resolution. If this extraneous noise is eliminated, the resolution should reach 600 eV

7   PRELIMINARY MEASUREMENTS OF THE RADIOACTIVE AND COSMIC BACKGROUND

For dark matter detection the major problem will be the limitations due to the background. In this developement phase of massive bolometers our goal is to lower the background sufficiently so that the resolution of the bolometer can be determined at sea level.

We report a first attempt to measure the background due to cosmic rays or radioactivity in a 6.28 cm^3 sapphire crystal (Al$_2$O$_3$). Results are presented in Figures 11 et 12.
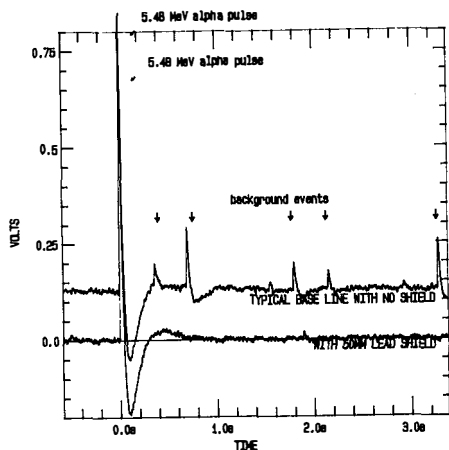
Figure 11 - Comparison of base lines between α's calibration pulses without protection (upper curve) and with 5 cm thickness lead shield (lower curve). In the latter case γ rays with energies in the 100 KeV-1 MeV range have disappeared.

The experimental set up was the following :

- location : Verrières le Buisson, near Paris (Lat ≈ 49°) about 150 meters above sea level. The experiment is made on the first floor of a building, surmounted by about 1 meter of millstone ;
- integration time : 5 hours for the high-energy events ;
- calibration : α's from an ^{241}Am source (5.48 MeV). This prevents us from obtaining any useful data in the 5→6 MeV range;
- shielding : we used a 5 cm thickness of contemporary lead, total mass ≈ 700 kg, located at a 20 cm mean distance from the sapphire crystal (see Figure 7). For experimental convenience, a zenith window of 0.4 sr (half angle 20°) with respect to the detector was left unshielded. Materials between the lead and crystal were Cu 2 mm thick (bolometer support) and stainless steel 3 mm thick (cap and cryostat).
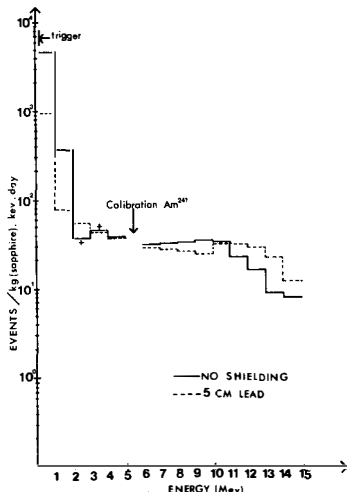
Figure 12 - Comparison of background spectra with and without shielding in the 25 g sapphire bolometer. Data are extrapolated to a 1 kg crystal. Trigger threshold is set at 200 keV level. Crosses indicate poor statistics

Evidence is shown of a substantial noise reduction of events due to background up to 10 MeV. Further improvements are expected on our very crude shielding with selected and different materials, and increasing the thickness, since conventional passive shielding requires at least 15 cm of lead. These results can be compared to experimental data[33] which report very low background, using Ge spectrometers for the study of neutrinoless double β decay of ^{76}Ge. Rates are normalised to equivalent masses (1 kg), but attention is required to differences between materials -Ge or Al_2O_3- and thus efficiencies, or on bulk effects -multiple Compton scattering- both of which may raise the extrapolated rates for sapphire.

Of course substantial improvements are required to lower the present rates down to 1 event/keV.kg.day in the low energy channels, where higher background rates are expected, but these first tests were made with existing normal cryostats.

Material	Size	Mean rate per kg (500 keV -1MeV)	Shielding
Al_2O_3	6 cm^3	940 events/keV.kg.day	5 cm lead, this experiment
Ge ref. (33)	135 cm^3	80 events/keV.kg.day	10 cm lead, typical cryostat
	135 cm^3	0.5 events/keV.kg.day	Rebuilt cryostat 1438 m underground without electronic anticosmic shielding

An extra noise, associated with the presence of the lead shielding, appears in Fig.12 in the high energy region. Though we did not possess any independent way of identifying the particles responsible for such an effect, it may be attributed to the muonic component of the cosmic ray and its interaction with Pb nuclei according to $\mu^- + p \rightarrow n + \nu_\mu$.

Neutron production in lead following muon capture has been studied by several authors[34]. A mean neutron multiplicity of about 1.7 in Pb is reported, 85 % of which are attributed to an evaporation process : a compound nucleus is formed and energy distributed among all nucleons; neutrons of energy up to 5 MeV may then escape from the nucleus. The remaining 15% lead to "direct" capture ;neutrons with energy as high as 50 MeV emitted in this way account for the high energy tail of the emission spectrum (it falls in an exponential manner $N(E) \propto \exp(-E/E_0)$ with a decay constant $E_0 \approx 9$ MeV for Pb). Excess counts with energy release in the crystal greater than 10 MeV could be thus attributed to this last process.
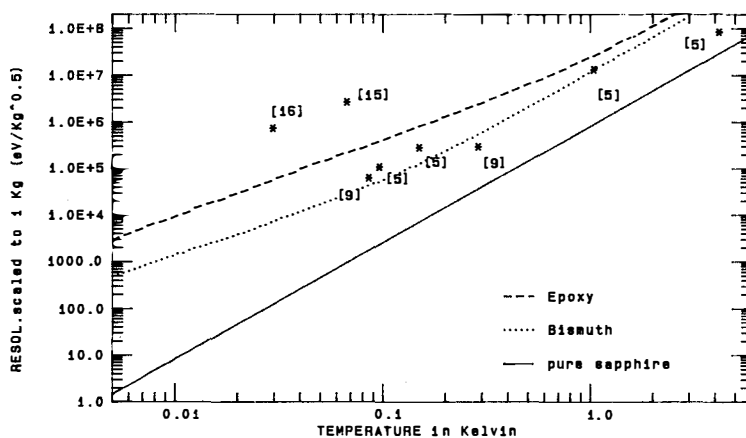
Figure 13 - Comparison of resolutions in published spectra obtained in thermal spectrometry by different groups and bolometry techniques : the resolution plotted in ordinate, is $\Delta E = \Delta E/\sqrt{m}$ in unit of $eV/\sqrt{Kg}$. Curves are theoretical estimations of ultimate resolution per $\sqrt{Kg}$ in sapphire, bismuth and epoxy as a function of temperature.

8   FUTURE PROSPECTS AND CONCLUSION

Massive composite bolometers cooled below $100 \, m°K$ are very promising detectors of weakly interacting particles provided that sensor and target are matched so that they have about the same heat capacity. Characteristics and optimisation of the heavily doped germanium thermistor have been analysed. In Figure 13 we summarise the results we obtained on a 25 grams bolometer and those of other groups with less massive ones. We present theoretical limits possible in 1 kg of sapphire or bismuth absorber.

Extrapolation of data show that a resolution of 800 eV in 1 kg at 10 m°K is a very immediate realistic goal. By dividing this same mass in 20 detectors (50g each) we would obtain a resolution better than 200 eV at 10 m°K. If placed in an underground location they would (in a few weeks) either detect new particles or place very new upper limits on the unknown quantity of non-baryonic dark matter in the solar system.

References

1) F. Simon, Nature, 135, 763, 1935

2) E. Fiorini, T.O. Niinikoski, Nucl. Instr. Meth., 224, 83-88 (1984)

3) A. de Rujula, M. Lusignoli, Phys. Lett., 118B, 429-434 (1982)

4) B. Cabrera, L. Krauss, F. Wilczek, Phys. Rev. Lett., 55, 25-38 (1985)

5) N. Coron, G. Artzner, P. de Marcillac, H. Stroke, A. Benoit, F. Amoudry, H. Ravn, B. Jonson, J.P. Torre, O. Testard, G. Dambier, J. Leblanc, G. Jegoudez, J.P. Lepeltier, in "Superconducting and Low-Temperature Detectors", G. Waysand and G. Chardin editors, Elsevier, 115-125, 1989.

6) D. Mc Cammon, S.H. Moseley, J.C. Mather, R.F. Mushotzky, J. Appl. Phys., Vol. 56(5), 1263-1266, 1984

7) N. Coron, G. Dambier, G.J. Focker, P.G. Hansen, G. Jegoudez, B. Jonson , J. Leblanc, J.P. Moalic, H.L. Ravn, H.H. Stroke, O. Testard, Nature, 314, 75-76, 1985

8) N. Coron et al., SPIE, Vol. 597, X-ray Instr. in Astronomy, 389-396, 1986

9) D. Mc Cammon, M. Juda, J. Zhang, S.S. Holt, R.L. Kelley, S.H. Moseley, A.E. Szymkowiak, Japan Journal of Appl. Phys. Vol. 26, suppl. 26-3, 1987 and S.H. Moseley et al., IEEE Trans. Nucl. Sci. NS32, N° 1, 134-138, 1985

10) N. Coron, G. Artzner, H. Stroke, J. Rich et al., Proceedings of VIIth Moriond Workshop, Editions Frontières, 421-, jan, 1987

11) M. Buhler, E. Umlauf, Europhys. Lett. 5(4) p. 297-301, 1988

12) N. Wang, B. Sadoulet et al., Trans. on Nucl. Sci., 35, N° 1, 55-58 , 1988

13) D. Bassi, M.G. Dondi, F. Tommasini, F. Torello, U. Valbusa, Phys. Rev. A, Vol. 13, N° 2, 584-594, 1976

14) H.H. Andersen, N.I.M., Vol. B12, pp. 437-439, 1985

15) A. Allessandro, D.V. Camin, E. Fiorini, A. Giuliani, Phys. Lett. B, 202(4), p. 611, 1988

16) A. Allessandro, C. Brofferio, D.V. Camin, E. Fiorini, A. Giuliani, IEEE Trans. on Nucl. Sci., Vol. 36, 141-145, 1989

17) M.W. Goodman, E. Witten, Phys. Rev. D., Vol. 31, 3059-3063, 1985

18) I. Wasserman, Phys. Rev. D., Vol. 33, 2071-3078, 1986

19) A. Druckier, K. Freese, D. Spergel, Phys. Rev. D., Vol. 33, 3495, 1986

20) L. Gonzales-Mestres, D. Perret-Gallix, in "Dark matter", J. Audouze, J. Tran Thanh Van Editors, Editions Frontières, 85-94, 1988 and also in same book thom 22, pp. 1-36 (review paper).

21) J. Rich, same book as ref.20, 43-53, 1988

22) D.O. Caldwell et al. in "Low temperature detectors for neutrinos and Dark matter", Editions Frontières, edited by L. Gonzales-Mestres and D. Perret-Gallix, 55-66, 1988

23) C.J. Martoff, Science, Vol. 237, 507-509, 1987

24) G. Gerbier et al., this book, 1989

25) N. Coron, P. de Marcillac, G. Artzner, C. Goldbach, G. Nollez, A. Vidal-Madjar, F. Amoudry, Scientific proposal to INSU, internal report IAP PM/MchP/599, 25 Sept 1988

26) C. Kittel, H. Kroemer in "Thermal Physics" W.H. Freeman and Cpy, San Francisco, p. 84, 1980

27) J.C. Mather, Appl. Opt. Vol.21 N° 6, pp. 1125-1129, 1982

28) S.H. Moseley, J.C. Mather, D. Mc Cammon, J. Appl. Phys., Vol. 56(5), pp. 1257-1262,1984

29) R.A. Smith, F. Jones, R. Chasmar in "The detection and measurement of I.R. radiation", Oxford University Press, p. 214-22, 1968 and N. Coron, Infrared Phys., Vol. 16, p. 411-419, 1976

30) J.C. Mather, Appl. Opt. Vol 23, N° 4, pp. 584-588, 1984

31) Fritzsche, Phys. Rev., Vol. 119, 1238- (1960) and all precedent papers

32) P.P. Edwards and C.N.R. Rao, The Metallic and nonmetallic states of matter, Taylor et Francis ed., 1985

33) F.T. Avignone, III, R.L. Brodzinski, D.P. Brown, J.C. Evans, Jr., W.K. Hensley, H.S. Miley, J.H. Reeves, and N.A. Wogman Phys. Rev. Lett., Vol. 54, n° 21, 2309- (1985)

34) P. Singer, Review talk, Muon Physics Conference Colorado State University, 6-10 september 1971.

SEARCHES FOR NON-BARYONIC DARK MATTER PARTICLES

Bernard Sadoulet

Center for Particle Astrophysics,
Department of Physics and Lawrence Berkeley Laboratory
University of California, Berkeley, CA 94720,USA.

Abstract
This paper just reviews the experimental challenges encountered in the detection of the Weakly Interacting Massive Particles which may constitute Dark Matter. It then describes the recent results obtained by the groups associated to the Center for Particle Astrophysics both with ionization and phonon mediated detectors.

1 WEAKLY INTERACTING MASSIVE PARTICLES

It is quite natural in many particle physics models to expect non-baryonic particles to be produced in the hot early universe, and to have today a density high enough to explain the observed Dark Matter. In fact, the hypothesis that dark matter consists of a non-baryonic particle species is much less vague that could be supposed *a priori* and in most cases, is directly testable. In particular, if these dark matter particles have been *once in thermodynamic equilibrium* with the quarks and leptons and if they were *non relativistic*, at the time they dropped out of equilibrium their current density is completely determined by their annihilation rate at the time of freeze-out[1].

This can be seen in the following way. We are considering a species of particles that we will call δ since our considerations cover equally well heavy neutrinos ν_H, supersymmetric neutralinos $\tilde{\gamma}$, $\tilde{h}$, $\tilde{\nu}$, $\tilde{z}$, technicolor particles, etc. We assume that it has once been in thermal equilibrium with quarks (q) and leptons (l), presumably through the reactions

$$\delta \bar{\delta} \leftrightarrow q \bar{q}, l \bar{l}$$

(1)
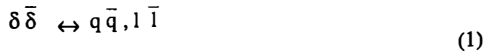
As explained in more details in Griest and Sadoulet[2], this simple hypothesis leads to a present δ density in the universe that is a function of their annihilation rate at the time they went out of equilibrium (the "freeze-out" time). The argument is simple: Let us first assume that there is *no initial asymmetry* and the number of δ's is the same as the number of their antiparticles. In the very early universe, at temperatures bigger than the mass of the δ's, the reactions above go both ways. As the universe expands and cools down, when the temperature reaches $\approx m_\delta/20$, the equilibrium is displaced to the right. If the annihilation rate is much faster than the rate of expansion of the universe, the δ's all disappear and they cannot constitute the present dark matter. If on the other hand, the rate is too small, the expansion quickly dilutes the δ's, which soon cannot find an antiparticle to annihilate with, and their abundance now will be too large. For δ masses above 300 MeV/c^2, the freeze-out temperature is about a twentieth of the rest mass of the particle, and the annihilation cross section is for δ mass in the Gev/c^2 region:

$$<\sigma v> \approx 10^{-26} / (\Omega_\delta h^2) \text{ cm}^3/\text{s},$$

(2)

where Ω_δ is the current ratio of the δ average density to the critical density and h is the Hubble constant in units of 100 km/s/Mpc.

Such a result is interesting because of two facts:

- For $\Omega_\delta \approx 1$ this annihilation rate has the value expected from weak interaction, while nowhere in the argument, had we to assume a particular interaction scale. Hence these particles are usually known as WIMPs (Weakly Interacting Massive Particles). This may be a numerical

coincidence, or a precious hint that physics at the W scale is important for the problem of dark matter and therefore something like supersymmetry exists!

- The interaction scale is fixed and gives the experimentalist some idea of what to expect.

Moreover it is a lower limit. For we could imagine *an initial asymmetry*, similar to the one usually assumed for baryons and antibaryons. In this case, the cross section could become large enough for all the pairs $\delta\bar{\delta}$ to disappear and the small excess of one component to make up the dark matter. Therefore, in the general case, we have

$$<\sigma v> \gtrsim 10^{-26}/(\Omega_\delta h^2) \text{ cm}^3/\text{s} \qquad (3)$$

This annihilation cross section at a specific energy can be related to other potentially detectable processes. And the experimentalist discovers with interest that this general hypothesis may be testable in a rather model independent way through a combination of experiments. This is shown schematically in Figure 1.

Given the form of the effective Lagrangian (e.g., vectorial, axial vectorial) one can extrapolate from the freeze-out energy to high energy, where accelerator experiments provide useful constraints. It can be shown[2] that e^+e^- data (ASP,MAC,CELLO) bound the δ mass from below around a few GeV. The cross section can also be extrapolated to very low energy to predict the annihilation rate today in the halo of our galaxy. The annihilation would give rise to a low-energy flux of antiprotons and positrons and to a gamma-ray flux. The present experimental constraints however are weak[3,4] since the expected rate varies rapidly with mass and is completely dependent on the assumed confinement time in the halo.

Given the same matrix element, the annihilation cross section can be related by crossing to the elastic cross section of δ on ordinary quarks. Usually the matrix elements are of the same order of magnitude

$$M(\delta\bar{\delta} \to q\bar{q}) \sim M(\delta q \to \delta q) \text{ and for } m_\delta \geq 1 \text{GeV/c}^2, \qquad (4)$$

$$\sigma_{el} \geq 10^{-38} \text{ cm}^2 \text{ x coherence factor.} \qquad (5)$$

This leads to two consequences: first, the elastic scattering rate of halo δ on ordinary matter in the laboratory may be large enough to be detectable[5]. This is the main subject of this paper. The second consequence is that the δ's can be trapped in the sun and in the planets, modifying their core temperature and leading to enhanced annihilations which may be detectable as a high energy neutrino flux[6,7]. So far no excess of neutrinos has been seen coming from the sun. While this observation presumably excludes scalar neutrinos above a mass of 4 GeV/c^2, no limit can be put on the case of the photino because of the uncertainties on axial couplings[8].

In the case of the sun, it may even be possible to solve[9,10,11] the solar neutrino puzzle[12]. We will refer to the particles which have the restricted properties necessary to provide such

an explanation, as "Cosmions"[13] (reserving "WIMPs" for the general class of massive dark matter particles).

2. DIRECT DETECTION BY ELASTIC SCATTERING: THE EXPERIMENTAL CHALLENGE

2.1 Rates And Energy Deposition.

The arguments outlined above lead to a rather model-independent estimate of the elastic cross section of δ's on nuclei. The coherence factor in our previous estimate has to be included because the particles to be detected have the typical virial velocity of the halo of our galaxy, some 300 km/s and the resulting small momentum transfer corresponds to a de Broglie wavelength bigger than the size of the nucleus[5]

Taking into account the known density of the galactic halo, it is then possible to calculate the expected interaction rate. Complications arise from the coherence factor and a possible initial asymmetry[2],[41].

For some types of matrix elements (e.g. the vectorial current $\bar{u} \gamma^{\mu} u$), the coherence adds up the relevant quark charges, and cross sections will go essentially as the square of the atomic number of the target nucleus. Unfortunately, for other couplings (such as the axial one, $\bar{u} \gamma^{\mu} \gamma_5 u$, which is the case of standard photinos), it is the spin which is the additive quantum number and the final cross section is proportional to $s(s+1)$ where s is the nuclear spin of the target. The coherent effects are then minimal and there is no elastic scattering on spin zero nuclei which make up the major part of natural silicon and germanium.

In the latter case, for favorable target the event rate would be of the order of a fraction of a fraction of an event per kg of target and per day, as given by Fig 2a or b. We assumed $\Omega_\delta h^2 = 1/4$, a root mean square velocity of 300km/s and a halo density of $0.7 \ 10^{-24}$ g/cm^3.

A second case, which is more favorable, is that of an additive quantum number proportional to A, or the number of protons or neutrons (as for heavy neutrinos). The rate is much bigger (by a factor $\sim A^2$) but still decreasing as $1/m_\delta$ for $m_\delta < M$.

As a last archetype of what could happen, we should consider an initial asymmetry between the number of δ's and their antiparticles. The annihilation cross-section can be much bigger than the Lee-Weinberg limit. Fig 2c gives the example of a heavy neutrino coupling with the full Z^0 strength. The rates are much bigger and as we will see, double β experiments already put limits on such models of dark matter.

It is also easy to compute the energy deposition and Figure 3 shows the predicted energy deposition in eV for a particular example.

These two calculations clearly identify the two major technical challenges of the proposed experiment:

- The need for very low thresholds (100eV) for detectors of a few kilograms and therefore of rms noise less or equal to 20eV.

- The need for very low radioactive background.

We now review these experimental challenges.

2.2 Backgrounds

The basic experimental problem is to extract from the background the rather small signals that we have predicted above. We have to distinguish between four background sources.

1. Cosmic rays can be vetoed and they deposit so much energy that they can be rejected easily.

2. The main background will come presumably from the residual radioactivity in the detector elements and in their surroundings.

Internal radioactivity of the detectors is expected to be negligible if crystals such as Ge, Si are used. Spallation products such as ^{68}Ge[4] or tritium[5] produced during the time the detectors elements were exposed to the cosmic radiation at the surface of the earth, may be quite disturbing because the decay energy is in the range of interest. Tritium is particularly annoying because of its broad β spectrum and its long life time. For crystals grown in an hydrogen atmosphere, the original tritium is presumably displaced at the time of this operation. After that it is therefore important to minimize exposition of the detector to cosmic–rays. A direct consequence is that direct detection experiments have to be located underground.

An important source of background will presumably come from the surroundings (refrigerator, dewar, shield). Small range particles such as α's and β's can be eliminated completely in a position-sensitive detector by imposing a fiducial region. Fast neutrons from U and Th decays or μ captures, are potentially dangerous but can be thermalized easily with 40cm of water. Slow neutrons which may create γ rays can be absorbed by a borated shield. By far the most difficult background to deal with is the γ rays from lines, nγ reactions and β bremsstrahlung. They produce a flat Compton background which may be quite difficult to decrease appreciably even with an active veto.

3. The mechanism which is potentially the most dangerous is the feed-down from high energy to low energies because of defects of the detector: bad collection efficiency, dead regions, edge effects etc. This could produce in some instances an energy spectrum peaked at low energy, like the expected signal. Localization of the interaction is essential to set up fiducial regions in the detector and reject events in region of doubtful sensitivity.

4. Close to the threshold, the upper end of the electronics noise may also simulate a dark matter signal.

These four types of effects are seen in the double β decay experiments of LBL/UC/UCSB[14] and PNL/USC[16]. As an example, figure 4 gives the present results of the LBL/UC/UCSB group.

2.3 Signatures

In the case a low energy signal is observed, how can one be sure that it is due to dark matter interactions and not to a misunderstood behavior of the detector?

1. The measurement of the direction of the scattered nucleus would be a powerful discrimination tool[17] since it will show whether or not the signal is linked to the galaxy. The halo has not collapsed significantly and is predicted to have a very small overall angular velocity. Because of the rotation of the sun inside the halo, dark matter particles will come preferentially from one direction. The expected asymmetry is sizeable. However measuring it is extremely difficult. Reconstructing a track is excluded in a solid because the range of the recoiling nuclei may not be larger that a few tens of angstroms. An interesting possibility is that the ballistic phonons produced may keep a memory of the initial direction of the momentum (in spite of umklapp processes!). J. Rich and M. Spiro[18] have suggested that the use of a gas at low enough pressure may also provide a rough directionality.

2. Another unambiguous evidence would be a change in the event rate and the spectrum of energy deposition with the time of the year. This annual modulation is demonstrated in figure 3. The reason is simple[19],[20]. While the sun goes around the galaxy and therefore through the halo at 250km/s the earth is adding or subtracting half of its velocity to the sun velocity in the summer or the winter. The mean energy deposition varies by about $\pm 4.5\%$ and the rate varies by about $\pm 2.5\%$. In order to observe such an effect at 3 σ, about 3700 events are needed and therefore very large mass detectors (of the order of 10 kg) will be required for the unambiguous detection of LSP's in a reasonable amount of time (2 years).

3. The shape of the spectrum is an important datum. To take a simple example, spectra in germanium contaminated by ^{68}Ge show gallium, zinc and copper X ray lines between 8.9 and 10.6 keV which cannot be confused with a potential signal for a detector with appropriate energy resolution[14]. Such a line would be however fatal for a "threshold" detector such as superconducting granules operated in a simple mode providing only a yes-no answer. For such detectors, the threshold will have to be varied in order to effectively measure the spectrum. This may be too time consuming for such experiments which are intrisically rate limited.

4. Another important handle is the behavior as a function of the material`which effectively allows the measurement of the mass of the δ particle.

5. As emphasized above, an important discrimination against background is the spatial distribution of the energy in the detectors.

6. Finally, an important signature would be to know that the interaction has occurred on a nucleus and not on an electron as would be the case for β or γ interactions. This or the spectrum of the phonons generated in the interaction can deduced from a simultaneous measurement of the ionization and the total energy.

In summary, three major signatures may have eventually to be used: if possible the directionality, the annual modulation which requires several thousand events to measure and the fact that the interaction occurs on a nucleus, which could be evidenced by a low ratio between the ionization and the total energy deposited. Although already encouraging, the current state-of-the-art

background (a fraction of an event per keV kg day (see Fig. 4) has to be considerably improved for the detection of massive photinos, for instance.

2.4 Proposed Strategy.

How to attack this difficult challenge of detecting dark matter particles? We propose the following strategy.

a) In the short term, we can only use existing detector technology: proportional chambers or solid state ionization detectors. In particular, low radioactive background systems have been developed for double β decay experiments and they can be modified to have lower thresholds. These detectors can already put limits on large cross section WIMP's (see section 3) and will be very important in understanding the background problems.

b) However, it seems difficult for these detectors to provide the amount of redundancy which is, in the long run, necessary to decrease the background sufficiently for the detection of the lightest supersymmetry particle, for instance. A gain of a factor of 100 is necessary.

For that purpose, it seems natural to attempt to use quanta of smaller energies than those involved in ionization processes: Cooper pairs in a superconductor have binding energies of the order of 10^{-3} eV and phonons in a crystal at 100 mK have energies of 10^{-5} eV. If efficient detection schemes using broken Cooper pairs ("quasiparticles") or phonons can be implemented, the small energy of quanta involved will lead to very low thresholds and have signals sufficiently high to be analyzed for redundancy. In order to prevent thermal excitation of the quanta to be detected, such detectors have to be maintained at very low temperature, typically much below one Kelvin, and are thus called cryogenic detectors. The potentialities of such methods for dark matter searches and other applications has been recognized for some time[19],[21],[22],[23].

These detectors can be classified into two main categories: detectors of quasiparticle in a superconducting crystal and phonons detectors in an insulator. This field has recently been reviewed by Sadoulet[24] with an extensive list of references. Superheated Superconducting Colloids are an example of the first category. They are discussed in this volume by L. Gonzales-Mestres and D. Perret Gallix. In section 4, we discuss phonon mediated detectors. The main idea is that when more than 90% of the energy is dissipated in phonons, they are the component which should be measured. They may provide some of the signatures (directionality, nucleus recoil signature) that are important to establish a potential signal.

3. IONIZATION DETECTORS

3.1 Present Results.

Two double β decay groups, the PNL/USC collaboration[16] and the LBL/UC/UCSB group[14], are using their experiments to put limits on WIMPS. Figure 4 shows the most recent distribution of the equivalent electron energy observed by the LBL/UC/UCSB collaboration. The total integration is 6364 kg-hours. Above the sharp peak due to electronic noise and before the

background reaches the level of 0.3 events per keV per kg and per day which is thought to come from a combination of β decays and unvetoed Compton scattering, we can identify a prominent contribution of tritium at the level of 25 events per kg and per day, which severely limits the sensitivity of the experiment. The peaks are Ga and Cu X ray peaks due to ^{68}Ge and ^{65}Zn decays. As explained above, both features are thought to be the result of exposure to cosmic rays while the detectors were at the earth surface. This distribution allows to exclude a Dirac neutrino of 11.5 GeV/c^2 mass for which the expected contribution is shown in Fig 4 as the dashed line. More generally a large region in the mass/cross-section plane can be excluded (Fig 5).

3.2 New Developments.

The two groups are attempting to improve these results in two directions.

a) On one hand, the Berkeley–Santa Barbara group is decreasing the detector threshold. In particular, four silicon detectors of 60 g total mass have been recently installed and provide a threshold of about 1 keV equivalent electron energy. The main motivation of this effort in which Saclay is also involved, is to be able to put limits on Cosmions[25]. The Saclay group is currently measuring the ratio between the ionization produced by a Si recoil and that produced by an electron of the same kinetic energy[26]. In addition, the Berkeley group is preparing a new germanium detector using a gradient of dopant concentration to increase the electric field in the drifting ion and allow thus to decrease the electrode capacitance[27]. This should lead to a factor of three improvement on the current threshold (3 keV) for a one kilogram detector.

b) On the other hand, both the PNL/USC and LBL/UCB/UCSB groups are attempting to decrease the contamination by spallation products (^{68}Ge and ^{3}H). PNL/USC has recently installed in the Homestake mine an ~1 kg germanium detector which has been processed as fast as possible. The low capacity germanium detector of the Berkeley has also been subjected to a minimum exposure to cosmic rays. Both groups should have results soon.

4. PHONON MEDIATED DETECTORS

4.1 Calorimetry.

One of the oldest methods for detecting energy is calorimetry, where the absorbed energy ΔE results in a measurable temperature rise ΔT

$$\Delta T = \frac{\Delta E}{C} \qquad (6)$$

where C is the heat capacity. If this is done at low enough temperature for C to be very small, the method can be in principle very sensitive and able to detect individual particles[22],[28],[29]. In practice a small thermistor is fixed to or implanted in a high quality crystal which acts as an absorber and its resistance gives the temperature. This is a detector of *thermalized* phonons and, because of their discrete nature, the detector will experience thermal energy fluctuation. Standard optimal filtering

methods[30] taking into account, in addition,the Johnson noise in the thermistor give a statistical uncertainty on the energy

$$\delta E = \xi \sqrt{k \ T^2 \ C} \qquad (7)$$

where ξ depends on the responsiveness dR/dT of the thermistor. At temperatures above 100 mK the best thermistors investigated so far are doped semiconductors leading to $\xi \approx 2$. This thermal limit has nearly been achieved at 100 mK by Moseley *et al.*[31] for a small crystal of 10^{-5} gram of Si and by Coron[32] for a mass of 25 grams.

The above formula indicates the route for extrapolation to larger devices[22]. Since C is proportional to the mass, and for an insulator proportional to

$$(\frac{T}{T_D})^3 \qquad (8)$$

where T_D is the Debye temperature,

$$\delta E \sim \xi \ T^{5/2} \ M^{1/2} \qquad (9)$$

and a large augmentation in mass can in principle be compensated by a modest decrease in temperature. Extrapolating from the results obtained by Moseley[31], it should be possible if the thermistor responsiveness is maintained at low temperature, to get at 15 mK less than 10eV rms noise for crystals of 320g of boron, 200g of silicon, 100g of germanium! 15mK are relatively easily obtained by modern dilution refrigerators and cooling down a few kilograms is technically feasible.

However, while attempting to extrapolate down in temperature, serious difficulties are encountered with thermistors. As the Berkeley group have shown, with neutron transmutation doped germanium thermister, in the 20 – 30 mK region, the I–V characteristics become very non–linear (Fig. 6a), limiting the bias current and therefore the sensitivity[33]. Moreover, the pulse response is extremely slow (Fig. 6b)[34]. The main effect at these low temperatures seem to be the decoupling of the charge carriers in the thermistor from the thermal phonons in the lattice. With a very naive model describing a thermal impedance between the charge carriers and the phonons, the Berkeley group is able to explain semiquantatively both the I–V and AC behaviors (solid lines in Fig. 6). The reason for such a decoupling appears to be very fundamental, as the volume of phase space in the final state which appear in any transition probability, goes to zero at low temperature!

4.2 Ballistic Phonons.

It should be noted, however, that basically for the same reason, the picture outlined above is fundamentally incorrect. At low temperatures, the poor couplings and the low density of thermal phonons in the crystal will prevent phonons originating from the interaction from thermalizing efficiently and the energy of a significant number of them is expected to stay relatively high, around a few milli-electron-volts[35],[36]. Such phonons will be ballistic, that is travel in straight lines and

bounce off surfaces, and the concepts of temperature and heat capacity that we used before are inadequate to describe such a system. These effects are well known to solid state physicists for large energy depositions, and have been recently unambiguously demonstrated in the context of particle detection[37].

Instead of being a nuisance ballistic phonons may ease the detection job. Instead of the heat capacity of the global crystal, what counts now is the efficiency of the phonon energy collection. The crystal acts as a phonon guide. Because of this fast propagation, these phonons may allow a timing on several faces of the crystal. This requires a fast rise time of the sensor signal. In addition, the fact that energy propagates in preferred directions ("focussing") may allow the localization of the event by pulse division between several sensors[36]. Accuracies of a millimeter may be within reach.

These ideas are quite attractive, especially in the context of dark matter detector where large volume are necessary. Moreover, as mentioned before, it remains to be proven that such detectors can be implemented. Two kinds of sensor are being studied, highly dopped semiconductor thermistors which, in addition to being able to measure the crystal temperature, should be sensitive to high energy phonons[38] and superconducting film[36].

Figure 7 shows results obtained by the Berkeley group with thermistors irradiated by 60 keV and 18 keV X–rays. Contrary to what happens with thermal phonons, the rise time is fast (limited by the electronics at $\approx$ 200 μs). A possible explanation is that X–rays create high energy phonons which couple very rapidly to the charge carriers since the phase space argument given above is no more valid. This interpretation is supported by the fact that another thermistor sharing the same lattice but not irradiated by the source, keeps a constant temperature. The estimated absorption length of these high energy phonons is a few hundred microns. Therefore thermistors appear as good high energy phonon detectors. However if thermistors have really to be 200 μ thick to absorb efficiently the phonons, they cannot be fabricated by implantation in the crystals. The problem is then to design an interface which transmit efficiently high energy phonons with the minimum of down conversion. The Berkeley group is currently testing a method based on a very thin Germanium–Gold eutectic layer (< 2000 Å).

Figure 8 shows the results obtained by the Stanford group who detect phonons generated in a silicon wafer 200 μ thick with a superconducting thin film of titanium (1.5 μ wide, 300 Å thick), operated at 300 mK[39]. Figure 8a shows the meander pattern they used. The experimental pulse height obtained for a mixture of 60 keV and 29 keV X–rays is shown in Fig. 8b. No definite line is obtained in the pulse height spectrum. The observed behavior is due to the fact that he area of the region which becomes normal is a strong function of the distance of the point of interaction, and is in excellent agreement with what is expected from a simple Monte Carlo calculation (Fig. 8c and d). When the interaction occurs closely, a small area becomes normal leading to a small pulse height. At the opposite for distant interactions the flux is insufficient to break superconductivity in more than a small area. In between an optimal pulse height is obtained. This interpretation is further supported by the correlation observed between the pulse height and the pulse width which is a function of the temperature reached by the film. The group is currently working with films deposited on the two

faces of the wafer. This should allow to obtain directly the position of the interaction point and therefore deconvolve the pulse height spectrum.

4.3 Simultaneous Measurement of Ionization and Heat.

The simultaneous detection of the ionization and phonon components allow in principle to give an unambiguous signature for an elastic scattering off a nucleus[40],[41]. In that case the ratio of the ionization energy to the total energy released will be 4 to 6 times smaller than for an electron interaction involving the same deposited energy, and only a rough measurement of the ionization yield may be necessary. This attractive method requires the combination of two difficult techniques at very low temperature. As P. Luke has noted in a very interesting paper[42], the drift of changes will usually create more heat that deposited in the initial interaction, an effect which has, in itself, the potentiality of greatly increasing the sensitivity of ionization detectors. Figure 9 shows his detection of alpha particles by the heat produced by the drifting charges carriers. Therefore the naive idea of applying a DC electric field to a calorimeter does not work as is and more complex schemes have to be imagined. P. Luke is currently working on this problem.

5. CONCLUSION.

In the hypothesis where dark matter is made of massive non-baryonic particles which have been in thermal equilibrium with the universe, the current density of dark matter leads unexpectedly to a wek interaction annihilation rate. Even if this is a numerical coincidence, the fact that the W and Z physics scale could be responsible for dark matter has to be checked.

The most direct method to search for those particles is to attempt to detect them by elastic scattering on a target in the laboratory. This is a challenging experimental task since the expected rates are low and the energy deposition is small.

In the short run, it is likely that the main physics results will be obtained through improvement in the threshold of "conventional" solid state detectors.

In the long term, cryogenic detectors will become the instruments of choice, if they can be made to work for large masses, because of the low thresholds, the variety of materials they should allow and maybe, the signatures of a nuclear interaction and of direction. These detectors face however a long development because of the complexity of the solid state physics and materials technology which has to be mastered, and the inconvenience of ultra low temperature refrigerators.

References

1] Lee, B.W., Weinberg, S., Phys. Rev. lett., **39**, (1977), 165.

2] Griest, K., Sadoulet, B., "Model Independence of Constraints on Dark Matter Particles", to appear in the proceedings of the Second Particles Astrophysics School on Dark Matter, Erice, Italy, (1988), (in press; 1989).

3] Ritz, S., in Proceedings of the High Energy Physics Conference, Munich, (1988).

4] Ellis, J., et al., "Cosmic Ray Constants on the Annihilation of Relic Particles in the Galactic Halo," Phys. Lett., **B214**, (1988b), 403.

5] Goodman, M.W. and Witten, E., Detectability of Certain Dark-Matter Candidates, Phys. Rev., **D31**, (1985), 3059.

6] Srednicki, M., Olive, K.A. and Silk, J., "High Energy Neutrinos from the Sun and Cold Dark Matter." **UMN-TH-553/86** (1987)

7] Krauss, L.M. et al., Ap.J., **299**, (1985), 1001.

8] Ellis, J., and Flores, R.A., and Ritz, A., Implications for Dark Matter Particle of Searches for Energetic Solar Neutrinos, Phys.Lett., **198**, (1987), 393.

9] Press, W.H., Spergel, D.N., Ap. J., 296, (1985), 679.

10] Faulkner, J. and Gilliland, R.L., Ap. J., **299**, (1985), 994.

11] Gilliland, R.L., Faulkner, J., Press, W.H. and Spergel, D.N., "Solar Models with Energy Transport by Weakly Interacting Particles," Ap. J., **306**, (1986), 703.

12] Davis, R., AIP Conference Proceedings No. 126, "Solar Neutrinos and Neutrino Astronomy", (1986).

13] Gelmini, G.B., Hall, L.J. and Lin, M.J., Nucl. Phys., **B281**, (1987), 726.

14] Caldwell, D.O. et al., Laboratory Limits on Galactic Cold Dark Matter, Phys. Rev. Lett., **61**, (1988), 510.

15] Martoff, C.J., Science, Vol. **237**, (1987), 507.

16] Ahlen S.P. et al., Phys. Lett., **B195**, (1987), 603.

17] Spergel, D.N.,The Motion of the Earth and the Detection of WIMPS, Astrophysics Preprint Series, IASSNS-AST 87/2, (1987).

18] Rich, J. and Spiro, M., DPhPE, CEN-Saclay preprint, (1987).

19] Drukier, A.K., Freese, K. and Spergel, D.N., Detecting Cold Dark Matter Candidates, Phys. Rev., **D33**, (1986), 3495.

20] Freese, F. and Frieman, J. and Gould, A., Signal Modulation in Cold Dark Matter Detection, SLAC preprint SLAC-PUB-4427, (1987).

21] Drukier, A.K. and Stodoloski, L., Phys. Rev., **D30**, (1984), 2295.

22] Cabrera, B. and Krauss, L.M. and Wilczek, F., Bolometric Detection of Neutrinos, Phys. Rev. Lett., **55**, (1985), 25.

23] Cabrera, B. and Caldwell, D.O. and Sadoulet, B., Low temperature Detectors For Neutrino Experiments and Dark Matter Searches in Proceedings of The 1986 Summer Study on the Physics of the Superconducting Supercollider, ed. Donaldson, R. and Marx, J., (New York:DPF, American Physical Society) p. 704, (1987).

24] Sadoulet, B., Cryogenic Detectors of Particles:Hopes and Challenges, IEEE Trans. on Nucl. Sci., NS35, (1988b), 47.

25] Sadoulet, B. *et al.*, Testing the WIMP explanation of the solar neutrino puzzle with conventional silicon detectors, Ap. J. Lett., 324, (1988a), L75.

26] Gerbier, G., Conventional Techniques for Dark Matter Detection, this volume, (1989).

27] Luke, P.N., Goulding, F.S., Madden, N.W. and Pehl, R.H., "Low Capacitance Large Volume Shaped–Field Germanium Detector," IEEE Trans. on Nucl. Sci., NS–36, (1989), 976.

28] Niinikoski, T. O. and Udo, F., CERN preprint, (1974).

29] Fiorini, E. and Niinikoski, T.O., Low-Temperature Calorimetry for Rare Decays, Nucl. Insts. and Meth., 224, (1984), 83-88.

30] Moseley, S.H., Mather, J.C. and McCammon, D.,Thermal Detectors as X-Ray Spectrometers, J.Appl.Phys., 56, (1984), 1257.

31] Moseley, S.H., *et al.*, IEEE Trans. on Nucl. Sci., NS 35, (1988), 59.

32] Coron, N., *et al.*, "Thermal Spectrometry of Particles and γ–rays with Cooled Composite Bolometers of Mass up to 25 Grams." in G. Waysand and G. Chardin, Proceedings of the Conference on Superconducting and Low Temperature Particle Detectors, Strasbourg, (1988, 1989)

33] Wang, N., Sadoulet, B., Shutt, T., *et al.*, IEEE Trans. on Nucl. Sci., NS 35, (1988), 55.

34] Wang, N., *et al.*, "Electrical and Thermal Properties of Neutron Transmutation Doped Germanium at 20mK," *Submitted for publication*, (1989b)

35] Maris, H.J., Design of Phonon Detectors for Neutrinos, Fifth International Conference on Phonon Scattering in Condensed Matter, Urbana, Illinois, June 2-6, COO-3130TC-29, (1986).

36] Neuhauser, B., Cabrera, B. and Martoff, C.J. *et al.*, Phonon-Mediated Detection of Alpha Particles with Aluminum Transition Edge Sensors, Proc. 18th Int.Conf. on Low Temperature Physics, Kyoto Jap. Journ. of Applied Physics, 26, (1987).

37] Peterreins, Th. and Proebst, F. and Feilitzsch, F. and Krauss, H., Phonon Mediated Position Resolved Detection of Alpha Particles with Superconducting Tunnel Junctions, IEEE Nuclear Symposium, San Francisco, (1987).

36] Wang, N., *et al.*, "Particle Detection with Semiconductor Thermistors at Low Temperatures," IEEE Trans. on Nucl. Sci., NS–36, (1989a), 852.

39] Young, B.A., Cabrera, B., *et al.*, "Phonon Mediated Detection of X-rays in Silicon Crystals using Superconducting Transition Edge Phonon Sensors," IEEE Trans. on Magnetics, 25, (1989), 1347.

40] Krauss, L. and Srednicki, M. and Wilczek, F.,Solar System Constraints on Dark Matter Candidates, Phys. Rev., **D33**, (1986b), 2079.

41] Sadoulet, B., Prospects for Detecting Dark Matter Particles by Elastic Scattering, in Proceedings of the 13th Texas Symposium on Relativistic Astrophysics, ed. Ulmer, M.L., (Singapore:World Scientific) p. 260, (1987).

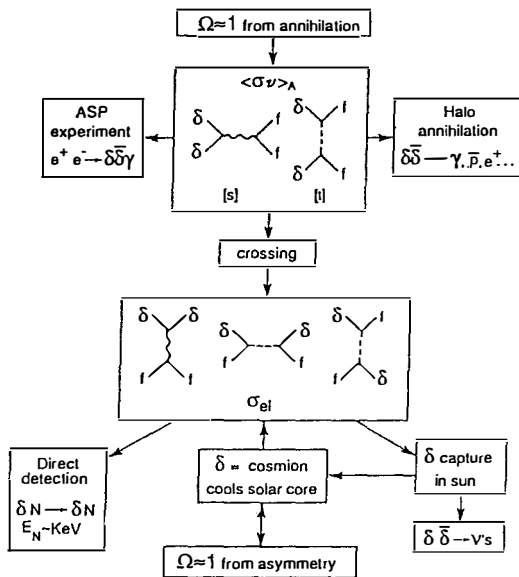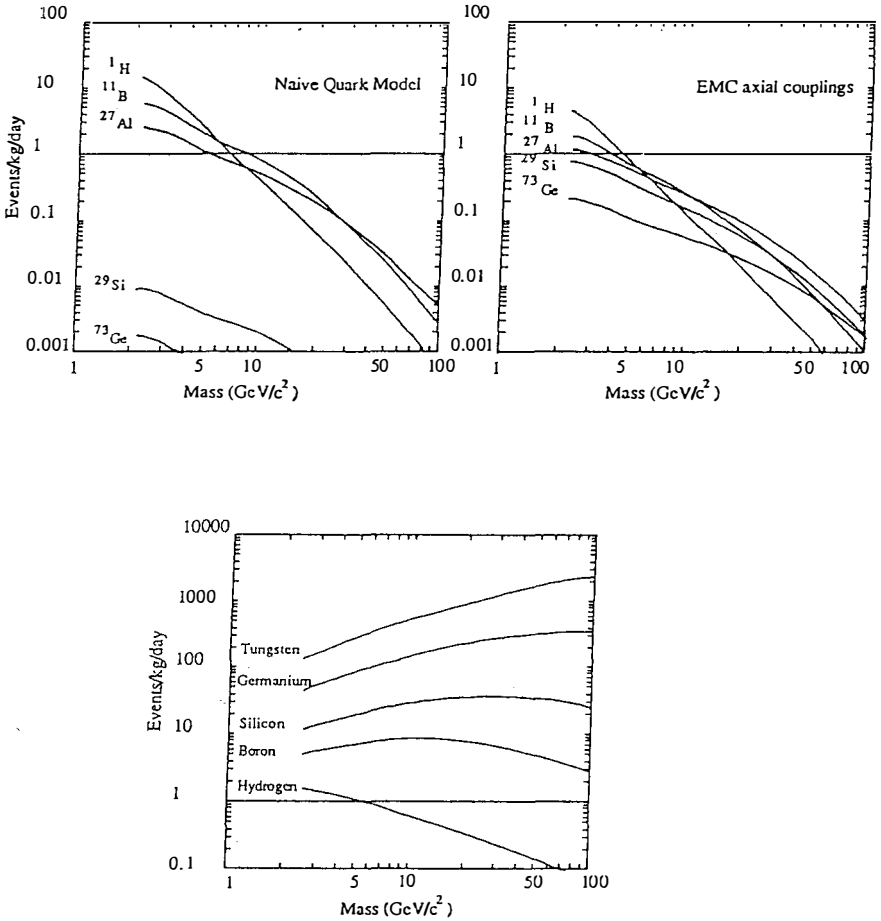42] Luke, P.K., "Voltage-Assisted Bolometric Ionization Detector." Submitted to Appl. Phys., Univ. of CA, Berkeley (1988)

Fig. 1 The searches for Dark Matter Particles.

Fig. 2 Interaction rates of WIMPS (Assumed to form the DM halo of our Galaxy) versus mass for various target materials.

a) Case of a pure photino with $\Omega_{\tilde{\delta}} \approx 1$. The sfermions are assumed to be degenerate with their mass determined so that $\Omega_{\tilde{\delta}} h^2 = 0.25$, $\rho_{halo} = 0.3$ GeV c^{-3}, $v_{\Theta} = 230$ km/s, and $<v^2_{halo}>^{1/2} = 270$ km/s. The axial couplings are determined from the naive quark model (*left*) and the recent European Muon Collaboration measurements (*right*), as discussed in Ellis and Flores (1987c).

b) the WIMP is a heavy Dirac neutrino ν with hypercharge 1/2 interacting via Z^0 exchange. (This model requires a $\nu - \bar{\nu}$ assymetry for mass above $\sim$ 4 GeV/c^2).
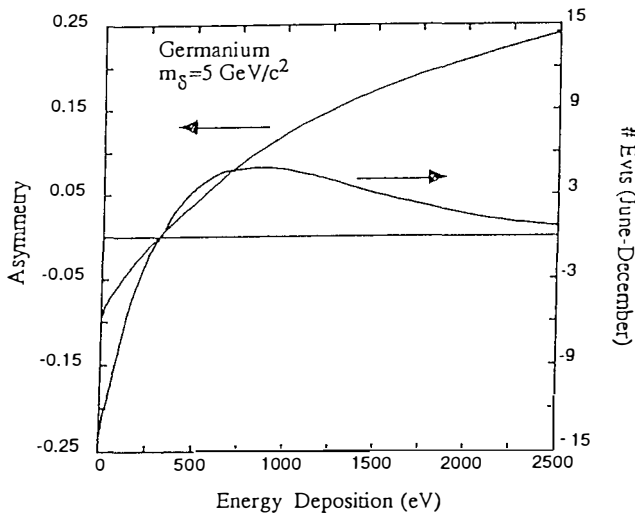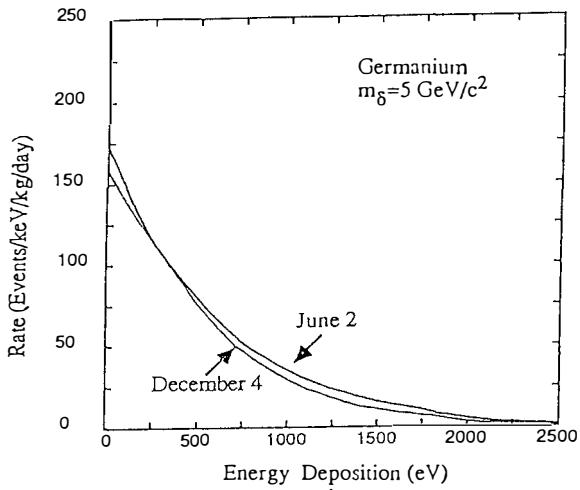
Figure 3 Energy deposition for a weakly interacting massive particle of 5 GeV/c^2 in germanium.

a) Rate for June 2 and December 4 vs deposited energy.

b) The June–December difference (right axis) and asymmetry (left axis) vs deposited energy. Note that although the asymmetry increases with the energy deposition, the rate and therefore also the June–December rate difference both decrease at high energy deposition.
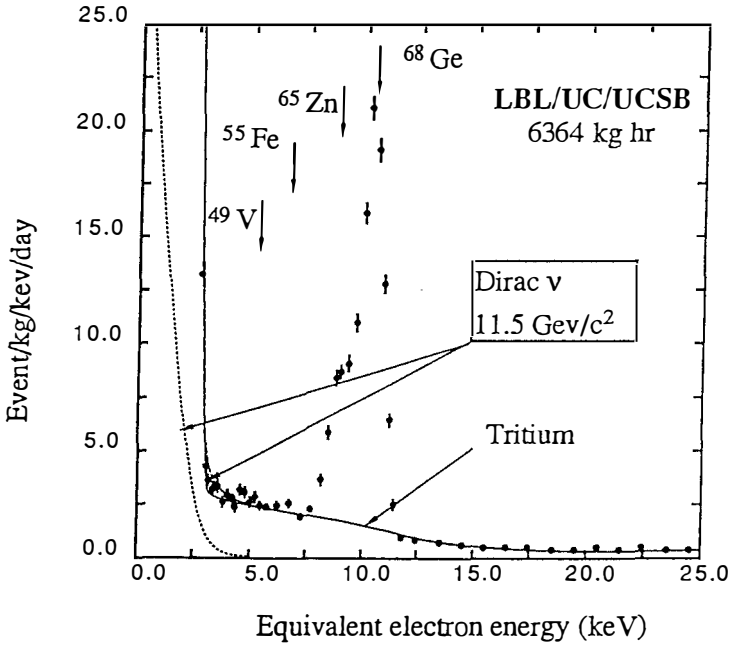
Fig.4 Equivalent-electron-energy spectrum obtained by the LBL-UC-UCSB Collaboration in two 900g germanium detector. X-ray peaks regions are not included in fit calculated for $\rho_{Halo} = 0.3$ GeV/cm^3, $\sqrt{<v^2>}_{Halo}=270$ km/s $v_{sun} = 230$km/s.
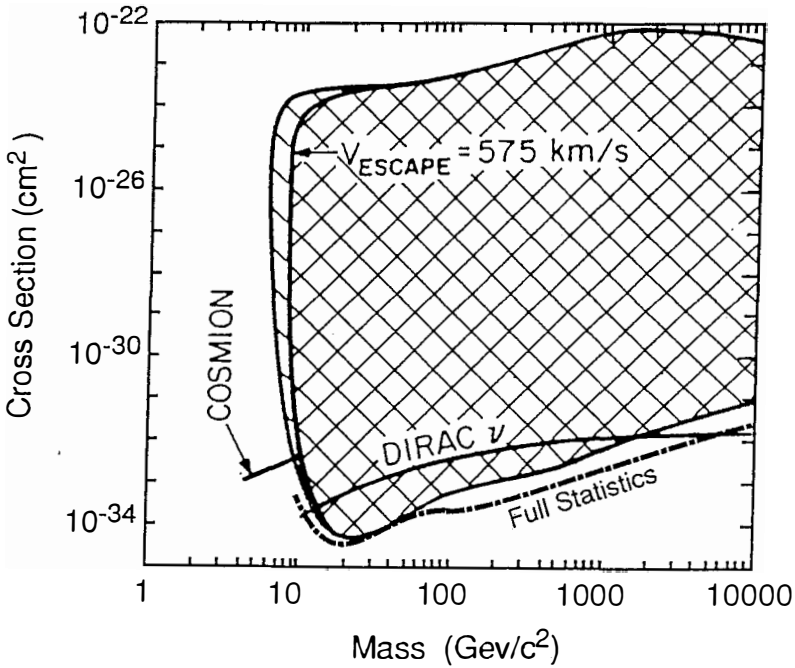
Fig. 5 Contraints on the mass and the cross section of Dark Matter particles, from the Fig. 4 spectrum (LBL–UCSB–UCB Collaboration). The dot-dash line gives the full statistics (6364kg hr). These limits are obtained for $\rho_{Halo}=0.3$ GeV/cm^3, $\sqrt{<v^2_{Halo}>} = 270$km/s, $v_{sun} = 230$km/s.
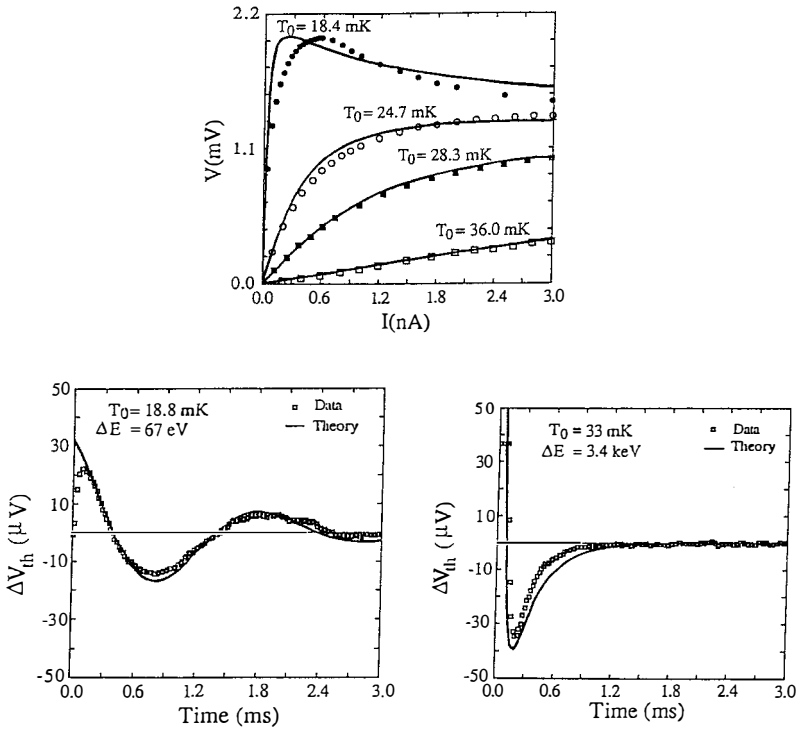
Fig. 6 Behavior of a thermistor at very low temperature (Wang *et al.*, 1989).
a) I–V curve at various temperatures.
b) Typical responses to a short electrical pulse. Dots are experimental data and solid lines prediction of a simple thermal impedence model.
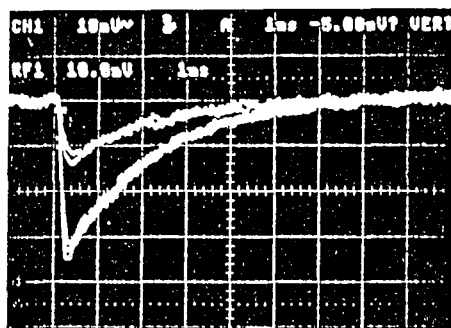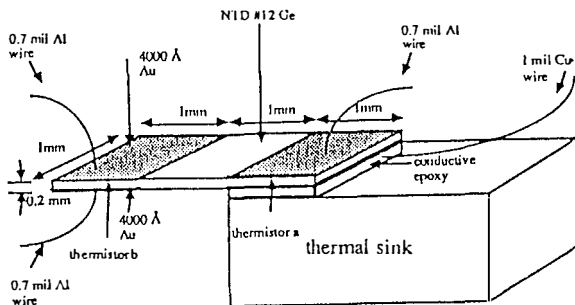
Fig. 7 Typical pulses obtained with a thermally clamped bolometer (Wang *et al.*, 1989)
a) Experimental set up.
b) Electrical pulses from X–rays of [241]Am incident on thermistor b at 18 mK. We chose
   typical pulses. The vertical scale is 100 μV/div, and the horizontal scale is 1 ms/div.
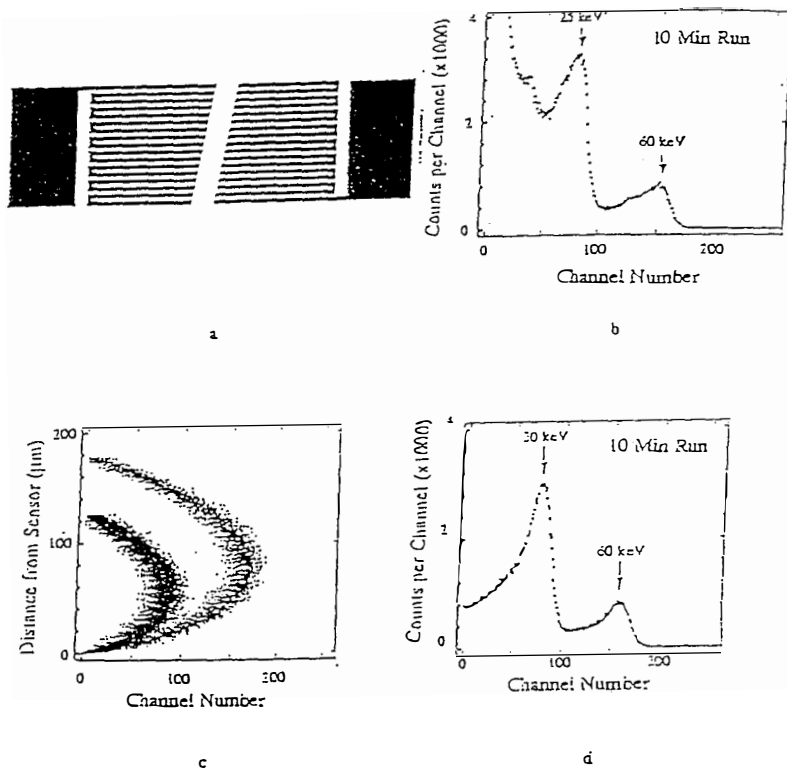
Fig. 8 Detection of high energy phonons with a superconducting film (Cabrera and coworkers, 1988).
a) The meander pattern.
b) Pulse height spectrum caused by 60 keV ^{241}Am photons incident on the backside of a 299–line Ti transition edge sensor for Sn absorber.
c) Calculated pulse height spectrum from hot spot model.
d) Calculated phase space plot of even depth verses pulse height, for 30 and 60 keV photons incident on the backside of a Ti transition edge sensor.
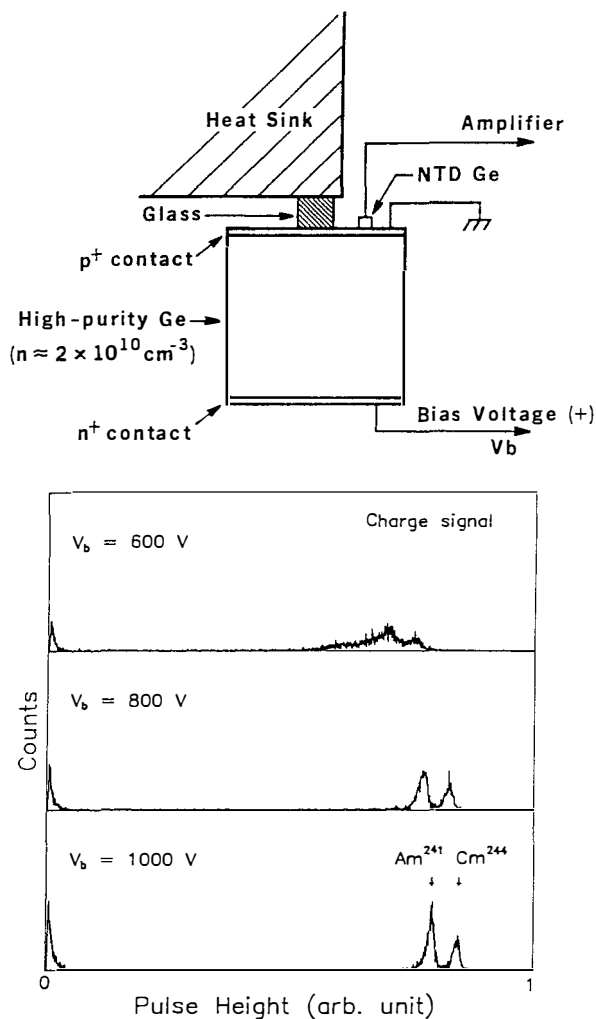
Fig. 9 Detection of ionization through the heat generated by the drift of the charge carriers in an electric field.
a) Set up.
b) Pulse height spectra obtained on the thermistor, as a function of the field.

The search for elusive dark matter: large scale experiments and new detection techniques

L. Gonzalez-Mestres and D. Perret-Gallix
L.A.P.P. Annecy

Abstract

We focus on dark matter candidates which do not exhibit the large event rates characteristic of coherent scattering off nuclei or cosmion interactions. Theoretical motivation for particle dark matter candidates is briefly reviewed, and specific problems related to the detection of each kind of "new" particle are dealt with. Current experiments and possible new detection techniques are described, with particular emphasis on WIMP (weakly interacting massive particles). Particle identification with hybrid cryogenic detectors is discussed as a new way to reject radioactive background.

1 INTRODUCTION

If dark matter is not baryonic, several types of candidates can be investigated. Apart from light neutrinos, all candidates presently envisioned are "new" particles whose existence has not yet been confirmed experimentally. Finding one of such candidates with a dark matter detector would therefore amount to the discovery of a new particle. Dedicated techniques that may eventually be used to detect these objetcs are presently being developed.

A galactic halo of non-baryonic dark matter would have an approximate particle density $n \simeq 0.3/m_x \ GeV/cm^3$, where m_x is the dark matter candidate mass. With a speed $v \approx 10^{-3} \ c$, such particles would present appreciable fluxes and lead to observable effects. However, their detection poses several problems concerning detector sensitivity and intrinsic radioactive background. This is the subject of the present talk.

2 MONOPOLES

In a Workshop entitled "The Quest for Fundamental Constants", it seems well suited to start our review by magnetic monopoles. The elementary magnetic charge would certainly be a very basic constant in Physics.

The monopole problem is a fundamental issue in modern physics, as the existence of magnetic charges would naturally complete the dual symmetry of Maxwell's equations. A dual transformation means exchanging (up to some phases): a) electric and magnetic charges; b) electric and magnetic currents; c) the electromagnetic strength tensor $F_{\mu\nu}$ by its Hodge transform $^*F_{\mu\nu} = \epsilon_{\mu\nu\rho\sigma}F^{\rho\sigma}$, which implies exchanging $\vec{E}$ (electric field) and $\vec{B}$ (magnetic field). Already noticed by Maxwell, the idea was further pursued by Dirac [1] within the framework of quantum mechanics, leading to quantization of electric and magnetic charges through the relation: $eg = h$, where e and g are respectively the units of electric and magnetic charge, and h the Planck constant.

Monopoles which are non-perturbative solutions (topological solitons) of grand-unified Yang-Mills theories appear at the classical level [2] and may have been formed in the early universe. The mass of such objects would be in the range $10^{16} - 10^{19} \ GeV$, and their flux is hard to determine from standard inflationary cosmology. Any program to search for such monopoles deserves a few words of caution. First, they are not genuine ($\Omega = 1$) dark matter candidates if Parker's bound [3] is to be believed. This bound is obtained from the persistence of the galactic magnetic field, and leads to F_{mon} (monopole flux) $\lesssim 10^{-15} \ cm^{-2} \ sr^{-1} \ s^{-1}$ for $m = 10^{16} \ GeV$. Secondly, bounds on monopole flux from the persistence of neutron stars are even more stringent [4] if monopoles are assumed [5] to catalyze baryon decay. Nevertheless, the cosmological implications of a precise knowledge of the monopole flux (if any) would be very far-reaching and searches with large area detectors are being undertaken.

1989 is an important date for monopole searches, as the first large surface detector, MACRO [6,7] has started running at GRAN SASSO Laboratory and will reach 10000 $m^2 sr$ in 1990. MACRO uses several conventional techniques in coincidence: a) liquid scintillator (horizontal and vertical layers); b) streamer tubes (He , C_5H_{10} again in horizontal and

vertical layers); c) plastic track-etch detectors (CR 39 in horizontal layers). The detector will be 72 m long (6 x 12 m), 12 m wide across hall, and 10 m high. 3 modules 12 m long x 12 m wide are presently installed. At the Parker limit, ≈ 4 $events/year$ are expected.

MACRO will thus be able by 1995, after five years of running, to reach a monopole flux sensitivity $\approx$ 10% of the Parker limit, and set 90% confidence limit excluding $\Omega_M > 0.03$ ($\Omega_M = \rho_M/\rho_c$, ρ_M = monopole density, ρ_c = critical density), for $m = 10^{16}$ GeV .

A delicate question is sensitivity to low beta ($\beta = v/c$) , as energy losses decrease at low speed and become smaller than ordinary ionization at $\beta < 10^{-2}$. Liquid scintillators should perform better than $\beta > 10^{-3}$, whereas plastic detectors would be sensitive to at least $\beta > 10^{-2}$ and gaseous detectors using Drell effect [8] may be sensitive to $\beta > 10^{-4}$. However, the interaction of slow monopoles with matter is not fully understood, and current estimates rely at some point on theoretical calculations or extrapolations not derived directly from first principles. The liquid scintillator used by MACRO was calibrated with slow recoil protons from exposure to neutrons [9]. Estimates of the response of several conventional detectors to a magnetic monopole are shown in Fig.1 .
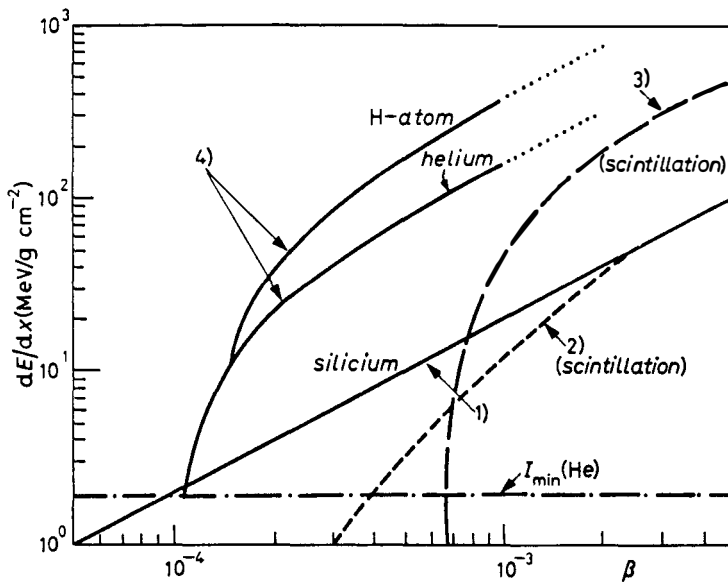

Fig.1 - Theoretical predictions for monopole energy losses in several materials, from: 1) S.P. Ahlen and K. Kinoshita, Phys. Rev. D26, 2347 (1982); 2) D. Ritson, 1983; 3) S.P. Ahlen and G. Tarle, Phys. Rev. D27, 688 (1983); 4) ref. [8] . The figure is from P. Musset, in Underground Physics 85.

A complementary approach is provided by "all beta" detectors, whose basic operating principle is independent of the monopole speed. Superconducting devices fulfill this property: a permanent current directly related to the monopole charge is generated by Faraday's law (a basic principle of electrodynamics) when a magnetic charge crosses the detector. Two superconducting monopole detectors have been proposed:

a) Induction loops. In this case, a monopole of charge g crossing the surface surrounded by a superconducting loop creates a supercurrent $i = 2\phi_0/L$, where ϕ_0 is the flux quantum ($\phi_0 \simeq 2\ 10^{-7}\ G\ cm^2$) and L the loop inductance. The current i is very weak, 1 nA for a circular loop of 25 cm diameter, and must be read out by a SQUID (Superconducting Quantum Interference Device [10]). The main problem for such detectors is electromagnetic background. As an example, fluctuations in the earth's magnetic field are $\approx 10^{-3}\ G$ and would provide a noise exceeding by several orders of magnitude the monopole signal.

Several ingeneous techniques have been used to bypass electromagnetic background problems: expansion at low temperature of initially collapsed superconducting Pb shielding cylinders [11], gradiometric techniques [12] and coincidence between several loops. They have allowed to build operating detectors in the $\approx 1\ m^2 sr$ range (Fig. 2), placing an overall bound $\approx 2\ 10^{-13} cm^{-2} sr^{-1} s^{-1}$ on the monopole flux. Development of new prototypes in the $\approx 1\ m$ diameter range is being carried on successfully, using more performant gradiometric techniques (Fig. 3).
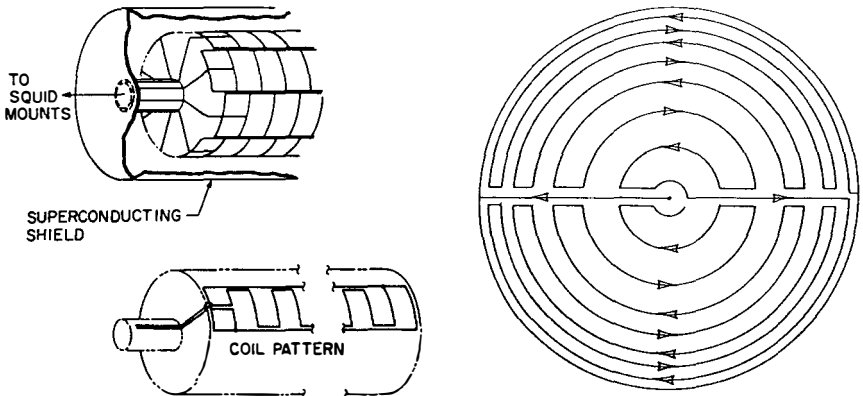

Fig. 2 (left) - A scheme of the Stanford monopole detector, with a eight SQUID 1.5 m^2 sensing area [13].

Fig. 3 (right) - Gradiometric loop studied by the CFM group to minimize electromagnetic noise [14]. Arrows indicate a possible direction for the induced current. The prototype was operated in a 125 $mGauss$ magnetic field.

In spite of technical difficulties, induction experiments are the only way to reach a direct measurement of the monopole charge. If only for that, any effort to pursue such a development appears to be justified.

b) Superheated superconducting granules (SSG). A brief introduction to SSG detectors can be found elsewhere in these Proceeedings [16] . Their use for monopole detection [17] would imply comparatively large grains, in the $30 - 100$ μm diameter range. A magnetic monopole of charge g crossing a type I superconductor would leave behind a flux tube $\phi = 2\phi_0$ injected into the sample. Inside this vortex, the order parameter is lowered and Cooper pairs broken. If the specimen is in a metastable state (superheating), the ends of the flux tube will originate nucleation centers of the normal state, leading to a phase transition of the whole sample. By this mechanism, the monopole is expected to flip a substantial amount of the grains it will cross, independently of their size and of the monopole speed. A large signal ($\approx 10^5$ ϕ_0) would then be obtained, as well as very good background rejection since large grains are not sensitive to minimum ionization.

A SSG monopole detector would be made of several planes parallel to each other, providing timing and tracking. The large signal expected should allow for a conventional electronic read out. Monopole speed and direction would then be determined with good accuracy.

Finally, a more recent development are Transient Response Induced Current Detectors [14]. The aim in such case would be to: a) work (if possible) with a high T_c superconducting coil; b) use conventional electronics or high T_c SQUIDs; c) escape low frequency magnetic field fluctuations, therefore avoiding expensive shields. The relevant frequency domain for the signal produced by a monopole with speed v in a coil of radius a is: $\omega \lesssim v/a$. For an upper cutoff in frequency ω_c , all monopoles of speed $v > a \omega$ turn out to give the same signal in a coil of radius a . It is thus possible to set a lower cutoff in speed, $v_{min} = 3.8 \ 10^{-5} \ c$ (the earth's escape velocity) and restrict the allowed size and shape of the monopole signal, improving background rejection. The required frequency cutoff would be $\omega_c \approx 10^5 \ Hz$ for $a \approx 10 \ cm$.

3 AXIONS

Quantum Chromodynamics has a topological winding number:

$$n = -g^2/32\pi^2 \ \int d^4x \ \epsilon_{\mu\nu\rho\sigma} \ Tr(F^{\mu\nu}F^{\rho\sigma}) \tag{1}$$

where $F^{\mu\nu}$ is the colour octet strength tensor from the gluon field. For each (integer) value of n , there is a vacuum state $\mid n >$ associated to the relevant topological sector. The ground state is then: $\mid \theta > = \Sigma_n \ e^{-in\theta} \mid n >$, where θ can take any value and is to be determined experimentally. The effect of topological vacua can be expressed in a simple modification of the effective lagrangian density:

$$L = L_{QCD} + g^2/32\pi^2 \ (\theta + arg \ detM) \ Tr(F^{\mu\nu} \ ^*F_{\mu\nu}) \tag{2}$$

where M is the quark mass matrix, and leads to a neutron electric dipole moment $d_n \simeq 10^{-15}(\theta + arg \ detM) \ e \ cm$ (e = electron charge). Experimental bounds [18] then suggest

the miraculous cancellation: $\theta + arg\ detM \lesssim 10^{-10}$.

To explain this situation, an additional symmetry $U(1)_{PQ}$, the Peccei-Quinn symmetry [19], was added to the lagrangian. After spontaneous breaking, a pseudoscalar Goldstone boson, the axion a , appears and acquires a small mass through the chiral anomaly:

$$m_a = A\ \sqrt{z}/(1+z)\ f_\pi m_\pi/f_a \qquad (3)$$

where: $z = m_u/m_d \simeq 0.56$, $m_\pi = 135\ MeV$, $f_\pi = 93\ MeV$; A is the colour anomaly of $U(1)_{PQ}$; f_a is proportional to $(\theta + arg\ detM)^{-1}$ times $< a >$, the vacuum expectation value of the axion field. We therefore expect: $f_a m_a \approx f_\pi m_\pi \approx 10^{16} eV^2$.

Axion couplings to matter are of the type: $\partial_\mu a\ (\overline{N}\gamma^\mu\gamma_5 N)$ for nucleons; $\partial_\mu a\ (\overline{e}\gamma^\mu\gamma_5 e)$ for electrons and positrons; $a\ \vec{E}.\vec{B}$ for photons. The effective coupling for the last term is:

$$g_{a\gamma\gamma} = 1/\sqrt{2\pi}\ e^2\ (\hbar c)^{1/2}\ m_a/m_\pi f_\pi \qquad (4)$$

and, numerically: $g_{a\gamma\gamma} \approx 10^{-34}\ MeV^{1/2}\ cm^{3/2}\ (m_a/10^{-5} eV)$. Laboratory limits on axions come from bounds on the processes: $K^+ \rightarrow \pi^+ + a$ (unseen axion), $J/\psi \rightarrow a + \gamma$ and $\Upsilon \rightarrow a + \gamma$, leading to: $f_a \gtrsim 10^3\ GeV$, $m_a \lesssim 6\ keV$ [20].

Helium ignition in red giants precludes an axion with mass $m_a \gtrsim 10^{-2} eV$ [21]. Even more stringent are bounds from the hot neutron star born as a result of SN1987 collapse, using the fact that too massive an axion would have accelerated the duration of the neutrino burst (less than 1 sec for $m_a \approx 10^{-2} eV$). The bound thus emerging from several works [22] is $m_a \lesssim 10^{-3}\ eV$. Finally, inflationary cosmology leads to and energy density of relic axions:

$$\Omega\ h^2 \approx (\Lambda_{QCD}\ /\ 200\ MeV)^{-0.7}\ (m_a/10^{-5} eV)^{-1.18} \qquad (5)$$

so that the universe may be closed by an axion of mass $m_a \approx 10^{-5}\ eV$ [23,24]. These numbers illustrate the difficulty to detect a non-relativistic cosmic axion.

The key mechanism for axion detection lies in the coupling a $a\gamma\gamma$ coming from axion-π_0 mixing. Sikivie [25] proposed to detect cosmic axions by a $a \rightarrow \gamma$ conversion in the presence of a strongly inhomogeneous magnetic field. The energy of the produced γ is then the total energy of the incoming axion. The main signature for cosmic axions would be a very narrow signal in frequency, where the finite width would be due to the axion kinetic energy $\approx 2\ 10^{-6}\ m_a$. Using a variable frequency electromagnetic cavity, with its resonant frequency tuned to a given value of the axion mass, and in the presence of a strong electromagnetic field, galactic axions of the relevant mass can convert into excitation quanta of an appropriate mode of the cavity. In this way, one may attempt to progressively explore the relevant domain of proposed axion masses. This amounts to covering the frequency range $1 - 10^3\ GHz$ by successive narrow band experiments. The expected power for a cylindrical cavity in the best suited vibration mode (T_{110}) is:

$$P \approx 10^{-20}\ Watt\ (V/500 liter)(B_0/8T)^2(\rho_a/0.5\ 10^{-24} g cm^{-3})(m_a/6\pi GHz)Min(Q/10^6,1) \qquad (6)$$

where V is the cavity volume, ρ_a the galactic halo density and Q the cavity quality factor.

A search for cosmic axions along these lines has been carried out at BNL [26] , at $\approx 1\ GHz$ frequencies. The experiment (Rochester-BNL-FNAL Collaboration) used a

$8.7\,T$ superconducting magnet with $15.2\,cm$ diameter and $40.6\,cm$ long bore, and a copper cavity at liquid helium temperature. The resonant frequency of the cavity is in the range $1\,GHz\ <\ f\ <\ 4GHz$, and can be tuned using a sapphire rod (Fig. 4) of electric constant $\epsilon = 10$, leading to an operating Q of 9 10^4 and a bandwidth of 13 kHz . The axion mass for such frequencies varies in the range 4.5 $\mu eV\ <\ m_a\ <\ 18\ \mu eV$, and the intrinsic bandwidth of the axion signal would be $\approx\ 130\ Hz$. No signature for axions was found, and the obtained bounds on the axion flux are shown in Fig. 5 , in terms of the energy spectral density $<\,d\rho/d\nu\,>_a$ and the coupling $g_{a\gamma\gamma}$ [27].
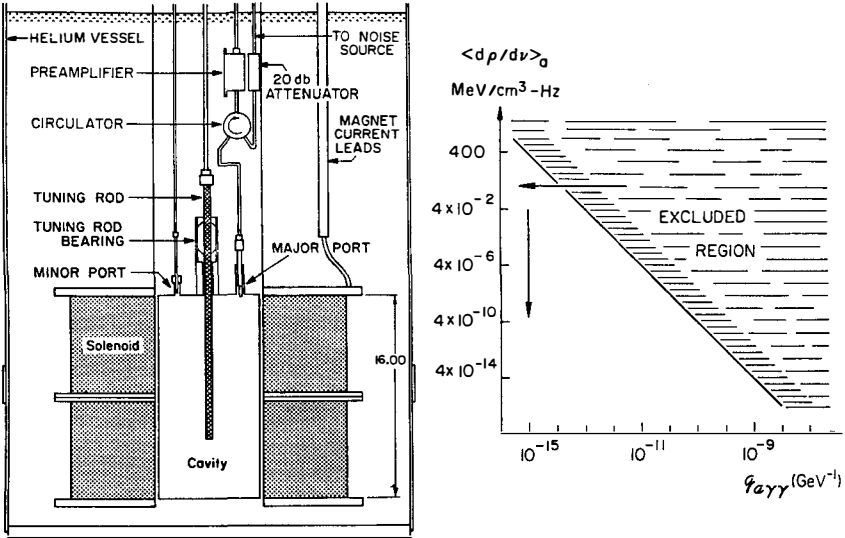
Fig. 4 (left) - A scheme of the Rochester - BNL - FNAL cosmic axion detector.

Fig. 5 (right) - Bounds from the same experiment. The abscissa is the $a\gamma\gamma$ coupling and $d\rho/d\nu$ stands for energy density per unit frequency. The vertical and horizontal arrow indicate respectively the predicted values of both variables for which axions may close the universe [23].

Assuming 100% of the galactic dark matter to be made of such axions, this bound lies 50 times above the value predicted by inflationary cosmological models based on the Peccei-Quinn symmetry [23]. The BNL experiment provides an encouraging start point for more ambitious searches. Technical problems that would be posed by a more efficient search are presently been studied. A second group, in Florida [28], has started a similar experimental program, with a 7 *liter* cavity inside a 9 *Tesla* superconducting solenoid. By cooling the detector down to 2.2 K , it is expected to lower the system noise temperature and to somehow improve the BNL bounds. A third detector is being built at KEK.

If axions are trapped in the solar system, and thermalized by its central core, they can reach earth with an energy of the order of the sun central temperature ($E \approx 1 \; keV$). It has indeed been shown [29] that axion-photon conversion in atoms yields acceptable cross-sections (axioelectric effect):

$$\sigma_{axioelectric} = (\alpha_{axion}/\alpha_{electromagnetic})(E_a/2m_e) \; \sigma_{photoelectric} \tag{7}$$

where:

$$4\pi\alpha_{axion} = (2x'_e m_e/f_a)^2 \tag{8}$$

and in most models $2x'_e \approx 1$. The solar axion flux is in turn taken from bremsstrahlung and gives:

$$F_a(solar) \approx 10^{13}(10^8 GeV/f_a)^2 \; sec^{-1} \; cm^{-2} \tag{9}$$

leading to a few $events/Kg.day$ with most target materials.

Based on this idea, double β germanium detectors [30,31] have been used to provide some interesting upper bounds on solar axions. The PNL-USC group [30] developed a 135 cc intrinsic Ge detector with a very low background in the keV energy region and a threshold at $E \approx 4 \; keV$. Installed at a water equivalent depth of 4000 $meters$ in the Homestake mine, the PNL-USC detector brought upper bounds allowing to exclude the range $f_a < 0.5 \; 10^7 \; GeV$. According to the above discussion, theory favors the region: $10^{10} \; GeV < f_\bullet < 10^{12} \; GeV$. Subsequently, the UCSB-LBL-UCB collaboration reported slightly better bounds, $f_a \gtrsim 10^7 \; GeV$. These results are shown in Fig. 6 , which also exhibits theoretical expectations for the solar axion spectrum. In order to reach cosmological bounds and cover the full spectrum of solar axions, two obvious requirements appear: a) background should still be lowered in order to reach full sensitivity to the expected solar axion flux; b) the energy threshold should be set an order of magnitude lower, which justifies the development of cryogenic devices.
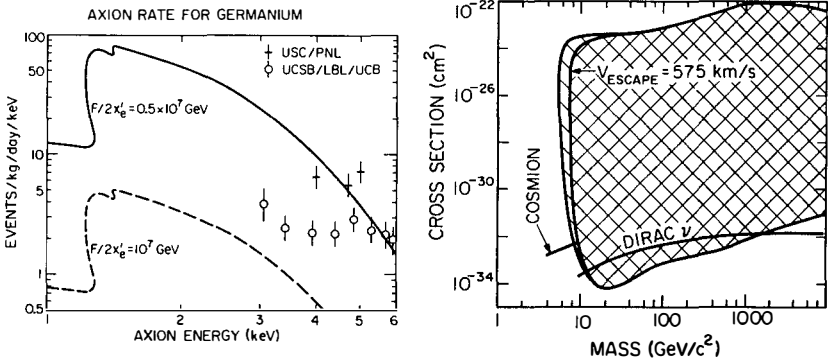

Fig. 6 (left) - Recent results on solar axions, from D.O. Caldwell et al. in [15] . On the figure, $F = f_a$ and theoretical predictions for the solar axion flux are also exhibited.

Fig. 7 (right) - Excluded region for Dirac neutrinos, s-neutrinos and cosmions in terms of the mass and cross section with germanium. From D.O. Caldwell et al. in [15] .

4   NEUTRINOS AND MAGNINOS

Light neutrinos are the only well established dark matter candidate, as the existence of three light flavours has been demonstrated experimentally and the role of neutrinos in the generation scheme of quarks and leptons is to some extent understood [32]. The electron neutrino is often thought to be the lightest one, with laboratory bounds on its mass: $m_{\nu_e} < 18 - 32~eV$ [33]. From cosmological arguments, the average density of neutrinos and antineutrinos in the universe for a given light flavour is:

$$n_\nu \approx 100~cm^{-3} \tag{10}$$

so that, if light neutrinos close the Universe, the following bound is obtained [34]:

$$\Sigma_i~m_{\nu_i}~<~100~eV~h^{-2} \tag{11}$$

where h is the Hubble constant in units of $100~Km/Mpc$. For $\Sigma_i~m_{\nu_i}~>~5~eV$, the neutrino contribution to the Universe mass density is found to exceed that of baryons. However, at galactic scale fermionic phase space limitations for free neutrinos would be consistent with $\Omega_\nu = 1$ only if $m_\nu~>~30~eV$ for large galaxies, and $m_\nu~>~500~eV$ for the smallest ones. These figures may be a difficulty for models where the electron neutrino is the cold dark matter candidate, but it is possible to build models (e.g. singlet Majoron [35]) where $\Omega_\nu~=~1$ with ν_μ or ν_τ having masses in the range $1~keV~-~35~MeV$, still leading to an acceptable scenario for galaxy formation.

Detection of non-relativistic light galaxy neutrinos is an extremely hard task. If they were clustered in the galactic halo, they would have a kinetic energy $E~<~10^{-4}~eV$ for ν_e , and $E < 100~eV$ for other families. It then follows that any recoil energy from elastic scattering with such neutrinos would be very small: at best, E_R (recoil energy) $<~10~eV$ for the heaviest possible neutrino. No detector is known that would be sensitive to such an energy deposition. Furthermore, at such energies elastic cross-sections would also be small and lead to hopeless event rates. If light neutrinos are Dirac fermions, their long wavelength would lead to comparatively large cross sections for coherent scattering and interaction with collective modes in matter (e.g. phonons) may be worth considering. In such case, rather than trying to detect neutrinos individually, the right strategy may be to look for some macroscopic effect (e.g., heat leaks in future very low temperature devices [36]) . Several laboratory experiments to detect cosmological light neutrinos have been proposed in the past, based on the motion of a macroscopic plate under radiation pressure [37], the torque of a ferromagnet under spin-spin interactions [38], coherent momentum transfer to superconducting electrons [39], ... But some of them have been refuted [40] and those which turned out to be correct lead to very small effects. Finally, a sea of cosmological light neutrinos may provide a target for very high energy cosmic rays [41], but again the feasibility of any experiment based on this phenomenon appears extremely difficult.

If the dark matter neutrino is not the lightest one, it will most likely be ustable and decay by ultraviolet gamma emmission. But, again, the expected ultraviolet cosmic photon flux seems very difficult to observe [42] .

Heavy neutrinos ($m_\nu~>~3~GeV$) arise from new families of fermions, $SU(2)_L \otimes SU(2)_R$ models or superstring theories. On general grounds, there is no obvious reason why they

should be stable, but they may eventually carry a new conserved quantum number. Heavy Dirac neutrinos, as well as s-neutrinos (the supersymmetric partners of the neutrinos), exhibit coherent scattering off nuclei and can therefore be detected through this process (see next section for more details).

The magnino [43] is a Dirac neutrino carrying a conserved number (to prevent unwanted annihilation rates) and an anomalous magnetic moment (to bring a sufficiently large scattering cross-section $\sigma \approx 10^2 \, \sigma_{weak}$). Then, with a mass in the range of 4 to 10 GeV and a magnetic moment $\approx 10^2$, the magnino can reproduce the requirements of the cosmion model [44]. The magnino is basically a new sequential neutrino associated to a heavy charged lepton. Therefore, its existence can in principle be checked by accelerator experiments.

Heavy Dirac neutrinos, as well as magninos, are the most accessible dark matter candidates for present and forthcoming experiments, due to the comparatively large cross sections involved. The basic detection principle would be elastic nucleus recoil, with energies in the range $50 \, eV \, < \, E_R \, < \, 10 \, keV$ for magninos and possibly much larger for heavier neutrinos. Intrinsic germanium has been able to provide some bounds on the cosmion flux (Fig. 7), but more sensitive detectors are required. The use of intrinsic (semiconductor) silicon is presently being studied [45,46], and some new bounds on dark matter have recently been reported from such a detector [46]. However, the development of cryogenic devices will most likely be the only way to comfortably cover the full range of cosmion masses. Fig. 7 also presents bounds on Dirac neutrinos and s-neutrinos, again based on nucleus recoil, where a large mass domain has been ruled out.

5 WEAKLY INTERACTING MASSIVE PARTICLES

The problem addressed is: how to detect dark matter in the laboratory if it is made of WIMP (Weakly Interacting Masive Particles)? By weak interaction we mean not only W or Z^0 exchange, but any other process leading to cross sections much smaller than electromagnetic. (e.g. the exchange of a scalar quark).

Many WIMP dark matter candidates have been considered, but special attention has in the recent years been paid to new particles generated by supersymmetry. The lightest supersymmetric particle (LSP) is often considered to be stable by R-parity conservation, although the validity of such a hypothesis is not completely general. Gravitinos and scalar neutrinos are not the LSP in most models [47] , the main candidates being the photino $(\tilde{\gamma})$ and the higgsino $(\tilde{H})$. One often has $m_{\tilde{H}} \, > \, m_{\tilde{\gamma}}$, which makes the photino the most popular LSP. The photino mass is rather model dependent, and present studies concern mainly the range $5 \, GeV \, < \, m_{\tilde{\gamma}} \, < \, 100 \, GeV$, for which $\Omega_{\tilde{\gamma}} \, \approx \, 1$ appears to come out quite naturally.

Accelerator experiments provide bounds on the supersymmetric partners of quarks and gluons, to which the photino mass is related in a model dependent way. In general, s-quarks $(\tilde{q})$ and gluino $(\tilde{g})$ are an order of magnitude heavier than the photino. UA1 data give $m_{\tilde{g}} \, > \, 53 \, GeV$, $m_{\tilde{q}} \, > \, 45 \, GeV$. Results from CDF at FERMILAB, as well as next runs from UA1 and UA2 at CERN, will push these lower bounds higher in mass. It must also be

realized that the photino mixes with higgsino and Zino ($\tilde{Z}$, the supersymmetric partner of the Z^0) . The lightest particle resulting from this mixing is in general photino-dominated and is called the neutralino (χ).

Note also that, within the framework of superstrings, some fashionable supersymmetric grand unified theories are based on flipped $SU(5) \otimes U(1)$ (another way of breaking the SO(10) grand unified symmetry [48]). A new dark matter candidate appears: the flatino [49], a neutral supersymmetric partner of the $SU(5)$ breaking Higgs boson. This neutral fermion may close the universe and be totally undetectable, except for gravitational effects. However, neutralino dark matter is not excluded in flipped $SU(5) \otimes U(1)$ [50].

Laboratory detection of galactic WIMP was discussed by Goodman and Witten [51], mainly based on the recoil energy of scattered nuclei. For a WIMP of kinetic energy E ($\approx 10^{-6}$ m) scattering a nucleus of mass M, the maximum recoil energy is:

$$T_{max} = 4 \, m \, M \, E \, / \, (M+m)^2 \tag{12}$$

For a reaction producing an excited nucleus of mass $M' = M + \Delta M$, relevant formulae can be found in [52] . WIMP weak cross-sections with nuclei can be cast in three categories:

5.1 Coherent scattering

Coherent scattering appears if a non-relativistic particle of well defined weak hypercharge interacts with a nucleus through the isoscalar components of the Z^0 current. The condition for coherent scattering is that the wavelegth defined by momentum transfer be larger than the size of the nucleus. The relevant matrix element is:

$$M = 4 \sqrt{2} \; G_F \; J^0_{WIMP} \; J^0_{TARGET} \tag{13}$$

If the WIMP is a fermion, we get:

$$J^0_{WIMP} = 1/4 \, (Y_L + Y_R) \tag{14}$$

where Y_L (Y_R) is the weak hypercharge of the left (right) chiral component of the WIMP. For a Majorana neutrino, $J^0_{WIMP} = 0$ and there is no coherent scattering off nuclei. On the contrary, s-neutrinos and Dirac neutrinos are expected to interact coherently with nuclei and should exhibit reasonably large event rates in the case they would form the dark matter of our galaxy.

5.2 Spin-dependent interactions

This is the case for galactic photinos interacting with nuclei through the exchange of a scalar quark (Fig. 8a). The nonrelativistic limit of the relevant Feynman diagram is equivalent to the exchange of a space-like pseudovector current. Then, assuming that valence quarks carry most of the spin of the nucleon, the nucleon couplings are proportional to [51] :

$$< p \, |\bar{u} \vec{\gamma} \, \gamma_5 u \, | \, p > = (1 + g_A) < p \, |\vec{S}| \, p > \tag{15}$$

$$< p \,|\overrightarrow{d\gamma}\, \gamma_5 d\, |\, p >= (1 - g_A) < p\, |\vec{S}|\, p > \qquad (16)$$

$$< n \,|\overrightarrow{u\gamma}\, \gamma_5 u\, |\, n >= (1 - g_A) < n\, |\vec{S}|\, n > \qquad (17)$$

$$< n \,|\overrightarrow{d\gamma}\, \gamma_5 d\, |\, n >= (1 + g_A) < n\, |\vec{S}|\, n > \qquad (18)$$

where experimentally $g_A \simeq 1.2$. Therefore, a u-quark in a proton or a d-quark in a neutron would have a larger matrix element than the converse case. Furthermore, the complete diagrams carry twice the coupling $\tilde{q}q\tilde{g}$, which is proportional to the charge of the interacting quark. It would then follow [51,53] that photino searches should be made with even-odd nuclei carrying an odd number of protons.

This conclusion has been reconsidered at the light of EMC data [54,55] which suggest that a sizeable part of the nucleon spin is carried by gluons or sea quarks. If this is the case for low values of Q (the momentum transfer), the above estimates should be seriously modified and a wide range of target elements could be used for dark matter detection (but with lower event rates). EMC data were taken at $Q^2 > 3\ GeV^2$, and there has been some controversy [56] on their interpretation and validity at $Q^2 \simeq 0$. Recent theoretical work [57] based on the Skyrme model at large N_c (number of colors) seems to support the idea that valence quarks are not the basic ingredient to build the proton spin. A complementary experimental information comes from νp and $\bar{\nu}\, p$ scattering [58], where data are not inconsistent with the EMC result and the new proton models.

Significant corrections to pure photino cross-sections may in some cases come from photino-higgsino-Zino mixing [59], where both higgsino and Zino exhibit coherent scattering (e.g. Fig. 8b).
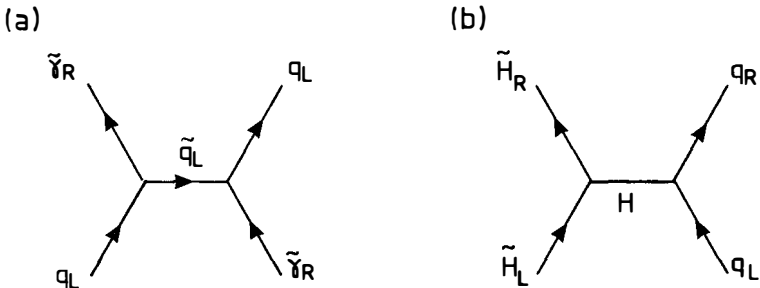

Fig. 8 - Feynman diagrams contributing to photino and higgsino scattering with matter.

Results of a calculation of neutralino cross sections in a minimal supergravity model are shown in Table 1 . In any case, spin-dependent interactions of WIMP with nuclei are likely to lead to event rates of $\approx 1\ event/Kg.day$, whereas the best background rate of germanium detectors at the relevant energies is of $1\ event/keV.Kg.day$, and it is far from

obvious that purity rates similar to that of germanium can be reached for other target materials. This is likely to be the main obstacle to the detection of galactic Majorana fermions, especially if purely calorimetric or ionization techniques are used.

Finally, Fig. 9 a and b show low background achievements in UCSB-LBL and USC-PNL double beta germanium detectors.

Isotope \ m_x	4 [GeV]	8 [GeV]	15 [GeV]	20 [GeV]	
$^{1}_{1}H$	1.1 / 3.6	0.12 / 0.39	0.018 / 0.059	0.0065 / 0.021	Event rates
$^{2}_{1}H$	0.022 / 2.8	0.0029 / 0.33	0.00050 / 0.051	0.00019 / 0.025	in
$^{3}_{2}He$	1.4 / 0.017	0.18 / 0.0030	0.032 / 0.00071	0.012 / 0.00033	$Kg^{-1} \ day^{-1}$
$^{7}_{3}Li$	1.0 / 3.1	0.18 / 0.55	0.039 / 0.12	0.016 / 0.048	
$^{9}_{4}Be$	0.66 / 0.0086	0.14 / 0.0021	0.030 / 0.00068	0.013 / 0.00035	Upper: according
$^{10}_{5}B$	0.016 / 2.0	0.0035 / 0.40	0.00090 / 0.092	0.00039 / 0.052	to EMC data
$^{11}_{5}B$	0.84 / 2.6	0.18 / 0.54	0.044 / 0.13	0.019 / 0.055	
$^{19}_{9}F$	1.2 / 3.5	0.29 / 0.87	0.083 / 0.25	0.038 / 0.12	
$^{27}_{13}Al$	0.42 / 1.3	0.11 / 0.33	0.036 / 0.11	0.018 / 0.051	Lower: according
$^{51}_{23}V$	0.23 / 0.71	0.068 / 0.21	0.026 / 0.076	0.014 / 0.040	to naive quark
$^{69}_{31}Ga + ^{71}_{31}Ga$	0.23 / 0.70	0.070 / 0.21	0.028 / 0.082	0.015 / 0.045	model
$^{75}_{33}As$	0.21 / 0.66	0.066 / 0.20	0.027 / 0.079	0.015 / 0.043	
$^{79}_{35}Br + ^{81}_{35}Br$	0.20 / 0.62	0.063 / 0.19	0.026 / 0.075	0.014 / 0.041	
$^{203}_{81}Tl + ^{205}_{81}Tl$	0.15 / 0.46	0.050 / 0.15	0.022 / 0.066	0.013 / 0.038	

Table 1 - Event rates predicted for elastic scattering of neutralino off nuclei, from [55] .

5.3 Inelastic scattering

For particles that do not scatter coherently off nuclei, Goodman and Witten proposed the use of special target nuclei, where the matrix elements for the transition to excited states:

$$\tilde{\gamma} + N \rightarrow \tilde{\gamma} + N^* \tag{19}$$

the excited state N^* decaying subsequently to the ground state:

$$N^* \rightarrow N + \gamma \tag{20}$$

may be almost as important as those of elastic scattering. Then, besides the recoil energy, it would be possible to detect a γ ray coming from the decay of the excited state. The

main drawback is our lack of knowledge of the actual nuclear wave functions and matrix elements. An estimate of inelastic neutralino scattering cross-sections with the most interesting isotopes has recently been performed [60] . In spite of its not well known cross-sections (a priori quite small), inelastic scattering may in some cases provide a specific signature (delayed time coincidence [52]) which appears potentially able to reject severe backgrounds. This may turn out to be a crucial point even if very large detectors are likely to be required. For isotopes allowing for a delayed time coincidence, 10 *ton* detectors are needed to reach a rate of the order of 1 *event/day* . Some well suited isotopes, after the theoretical calculation from [60] , would be (*i.a.* = isotopic abundance, τ = excited state lifetime):

$$^{169}Tm \ , \ \ 100\% \ i.a., \ \ \Delta E = 8.4 \ keV \ , \ \ \tau \ = 4 \ ns \ , \ \approx 1 \ event/ton.day \tag{21}$$

$$^{57}Fe \ , \ \ 2.2\% \ i.a. \ , \ \ \Delta E = 14.4 \ keV \ , \ \ \tau = 98 \ ns \ , \ \approx 0.2 \ event/ton.day \tag{22}$$

$$^{119}Sn \ , \ \ 8.6\% \ i.a. \ , \ \ \Delta E = 23.9 \ keV \ , \ \ \tau \ = \ 18 \ ns \ , \ \approx 0.1 \ event/ton.day \tag{23}$$
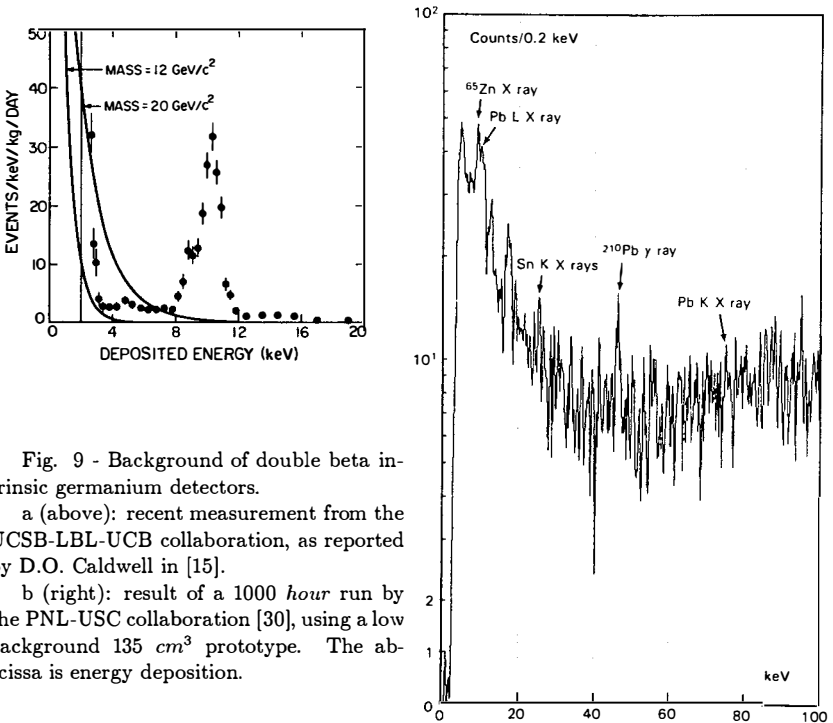
Fig. 9 - Background of double beta intrinsic germanium detectors.

a (above): recent measurement from the UCSB-LBL-UCB collaboration, as reported by D.O. Caldwell in [15].

b (right): result of a 1000 *hour* run by the PNL-USC collaboration [30], using a low background 135 cm^3 prototype. The abscissa is energy deposition.

Because of its long excited state lifetime, ^{57}Fe would be particularly well suited for a delayed coincidence, whereas ^{119}Sn can be used in the form of superconducting granules and ^{119}Tm may possibly be appropriate for very fast luminescent devices.

Assuming that detectors incorporating these matrix elements can be built, with high sensitivity and low background, the delayed time coincidence should in principle allow for a clean identification of dark matter events.

6 DETECTION TECHNIQUES FOR WIMP

For a WIMP mass of 1 GeV (100 GeV), dark matter detectors sensitive to < 1 keV (100 keV) energy deposition are required, if a recoiling target nucleus of mass $M = m$ is used. Since the last condition cannot be fulfilled a priori (the WIMP mass is unknown), a threshold at least an order of magnitude lower (below 100 eV) should be the requirement for a universal WIMP detector. This naturally hints to the development of low temperature devices. However, more conventional detectors have already provided some interesting bounds [61,62] and are still being considered for further experiments. Among the proposed detection techniques for WIMP are:

6.1 Conventional techniques

The pioneering role of germanium double beta detectors has already been mentioned previously. Semiconductor detectors have apparently not finished their role in the field, as intrinsic silicon is now being used [46,63]. The motivation for shifting to silicon is: a) higher energy deposition for light WIMPs; b) higher ionization yield for a given energy deposition; c) lower threshold, claimed to be in the 600 keV range in equivalent electron energy.

Another idea would be WIMP detection through proton recoil in a low pressure time proportional chamber [64] in the presence of a magnetic field. This would be particularly well suited for light photinos, where the track of a recoiling proton from CH_4 or CD_4 gas may well be observable.

The use of scintillators has equally been considered [52] for neutralino detection through inelastic scattering. Two preliminary steps appear to be necessary before going further in this development: a) find a very fast luminescent crystal with a high light yield, incorporating the target element under consideration; b) study in detail the scintillation yield (if any) from nucleus recoil at the expected WIMP kinetic energy scale. As will be seen later, luminescence may also in some cases be combined with cryogenic detection.

6.2 Crystal phonon devices

In a suitable insulating crystal cooled at very low temperature [65], a low energy particle will deposit most of its energy in the form of phonons. If the crystal is of very high quality, part of these phonons will be ballistic and can reach unscattered the walls of the crystal. Ballistic phonons propagate along the main cristallographic axis and can

travel a few *mm* without de-focusing. On the walls of the crystal, a phonon read-out of superconducting tunnel junctions (STJ) [66] or transition-edge superconducting strip, can detect the ballistic phonons in real time. In this way, it is possible to obtain position information on the event.

The alternative is thermal detection. In this case, a resistive thermometer (thermistor) implanted on one of the walls is used. In the theoretical limit where the energy resolution of such a bolometer would be given by energy fluctuations, a commonly used expression [67] is:

$$\Delta E \approx 2.5 \ (kT^2C)^{1/2} \tag{24}$$

where C is the heat capacity of the bolometric system (crystal + sensor). Taking

$$C \approx aMT^3 \tag{25}$$

where M is the mass of the crystal, the $T^{5/2} \ M^{1/2}$ dependence of ΔE from (24-25) suggests that it may be possible to obtain high sensitivity for comparatively large detectors if size is compensated by a decrease in working temperature.

A hybrid read-out involving both thermistor and phonon detectors can equally be considered. Phonon detectors are expected to provide low threshold (especially in thermal detection) and high energy resolution. Furthermore, being made of high quality crystals, a low impurity content (necessary to avoid radioactive background) appears to be naturally implemented, even if much higher purity will be required for a dark matter detector.

Recent results on thermal bolometers and ballistic phonon devices are very encouraging, and are dealt with in two contributions to this Workshop [68,16].

6.3   Superheated superconducting granules (SSG)

The idea originates from members of the Orsay Group on Superconductivity [69] , who proposed to use as particle detectors the colloids of metastable type I superconducting granules previously developed by J. Feder [70] . Very small spheres (ϕ , diameter, $\propto$ 1 μm) are mixed with some dielectric at $\propto$ 10 − 30% filling factor in volume. In the presence of an applied magnetic field, they remain superconducting above the critical value and reach a metastable state called superheating, that can be disrupted by the energy deposition of incoming particles. The phase transition of one or several granules is detected in real time through Faraday's law by a transient read-out of current loops sensitive to the disappearence of the Meissner effect in the sourrounding grains. SSG may be used to detect dark matter in several different ways: a) nucleus recoil [71] with Al, Cd, Ga or Zn grains; b) proton recoil using hydrogen from the dielectric material as the target [52] ; c) inelastic scattering with a ^{119}Sn target [72]. However, studies made in the last years [72] suggest that, at least in their conventional version, SSG fail to provide the required performances for dark matter detection (although recent progress in grain fabrication [73] may considerably improve the response of SSG devices).

We have recently proposed [72] a new way for SSG development based on a the concept of "amplification by thermal micro-avalanche". With a better handling of heat exchanges in the detector, and working at temperatures where the released latent heat is slightly

positive, the new scenario is particularly relevant for dark matter detection, since: a) the detector response to WIMP interactions is no longer reduced to a single granule flip, therefore energy resolution can be obtained ; b) the dielectric material surrounding the granules becomes part of the active target. However, if experimental evidence for thermal avalanches seems to exist, implementing in practice the micro-avalanche scenario for the required target elements is less simple and more experimental studies on the new version of SSG are required. If the basic physics of the micro-avalanche scenario works as expected, superconducting granules are likely to provide the best suited cryogenic detector for large volume experiments. Recent results on SSG development are presented in [16].

6.4 Hybrid devices

The backgound problems faced by WIMP detection, especially if interaction with nucleus is not full strength coherent, hint to the necessity of finding new, unconventional approaches to dark matter detection. Cryogenic devices are a step in this direction, but it is not obvious that they will be able to solve the problem as long as they remain purely calorimetric.

One possible way to improve background rejection may be the simultaneous detection of ionization and heat, as according to Lindhard et al. [74] and existing data with Ge and Si [75], a low energy nucleus recoil is expected to ionize much less than a beta or gamma particle of the same energy. Two developments have been proposed along these lines:

a) Cold semiconductors. Luke [76] has demonstrated that ionization can be measured in a germanium crystal at $1.3 \ K$ by detecting the heat produced when electrons drift in an electric field. More recent results on the subject are described in the talk by B. Sadoulet.

b) Luminescent bolometers [77] . The basic idea is to use a scintillating crystal exhibiting good luminescence properties at very low temperature, which seems indeed to be the case for BGO , $CdWO_4$, CeF_3 , intrinsic CsI and LiI , $GSO : Ce$, ... It would then be possible to simultaneously detect the optical and thermal signals separately, and even to use light as a timing strobe. We discuss this idea in some detail elsewhere in these Proceedings.

The idea of developing such hybrid devices is rather new, so that many practical problems remain to be solved and nontrivial basic studies are still necessary. But, in case of succes, hybrid techniques would provide a significant step forward in the field of dark matter detectors.

7   QUARK NUGGETS

Witten [78] proposed that quarks may form dense stable states where u, d and s quarks fill a Fermi sea up to very high values of the baryon number. Then, the gain in Fermi energy may eventually make the s quark stable inside a heavy nugget.

The interaction of cosmic quark nuggets (nuclearites) with matter has been discussed at length [79] and they turn out to be detectable in real time experiments [80] for masses and speeds in the range $10^{-13} \ g \ < \ m < \ 1 \ g$, $\beta \ > \ 10^{-4}$. Assuming that nuclearites are gravitationally dominant, present real time experiments exclude at least the region

$m < 10^{-7}$ g . The 10^4 m^2 sr underground MACRO detector [7] will be sensitive to much smaller fluxes, allowing to exclude nuclearite masses up to $m < 10^{-2}$ g .

Nuclearites lighter than 10^{-10} g would be trapped in earth, and could be detected using heavy ion beams [81] , the crucial point being that strange quark matter is expected to form bound states with ordinary matter. Searches along this line [82] have not reported any positive result.

Very heavy nuclearites ($m > 1$ g) would leave macroscopic tracks on rock and geological searches are possible [83] . Again, no candidate has been found, but further searches are required to cover such small fluxes.

Finally, it has been pointed out [84] that present day gravitational antennae are sensitive to nuclearites and can provide bounds in the region $m > 10^{-9}$ g , $\beta \gtrsim 10^{-3}$.

8 CONCLUSION

If dark matter is made of non-relativistic particles, its nature remains completely unknown and diversified laboratory searches would constitute a fundamental step forward. This, however, requires an important research and development effort in order to reach the necessary performance for dedicated detectors. Conventional techniques may still prove useful, but new tools (e.g. cryogenic detectors) are foreseen to completely handle the problem of particle dark matter.

If light neutrinos (as hot, warm or cold dark matter) are the right answer, their detection in the laboratory will be the greatest technological challenge ever faced by particle physics and astrophysics. The success of such an experiment would in turn be one of the most fundamental results in the recent history of science.

Detectors for axions, monopoles and some WIMP candidates are being developed, and the research program along these lines is providing interesting results. Experimental check of the cosmion hypothesis has already started and brought relevant bounds. On the other hand, the most prominent WIMP candidate, the photino-dominated "neutralino", poses rather severe backgound problems and requires quite sophisticated detection techniques, where cryogenic devices should play a crucial role if they indeed reach the theoretically expected sensitivity and energy resolution.

For elusive WIMP, where event rates are expected to fall below the best possible detector background, particle identification (allowing to distinguish between a nucleus recoil and a low energy ionizing particle) may be a surprisingly simple way out. It can possibly be achieved by looking simultaneously, in a well suited cryogenic device, at thermal and ionization signals. Then a recoiling nucleus would be seen to ionize much less than a low energy beta or gamma. We propose, in this perspective, the development of a luminescent bolometer based on some crystal scintillator cooled to very low temperature.

To conclude, Table 2 (next page) shows a list of dark matter candidates in particle physics, including dynamical origin, fluxes on earth and proposed detection techniques.

Table 2 - Dark matter candidates in Particle Physics.

PARTICLE	MASS	PRESENCE NEAR EARTH	ABUNDANCE	INTERACTION WITH MATTER	PROPOSED DETECTION TECHNIQUES
LIGHT NEUTRINO	$m < 30$ eV (Cosmology) $m < 18-32$ eV (Experiment) (Supernova ?)	COSMIC GALACTIC	$\Omega \sim 1$ if 5 eV $< m_\nu < 30$ eV	COHERENT SCATTERING IF DIRAC MASS	??
AXION	$m > 10^{-5}$ eV (Cosmology)	GALACTIC	$\Omega \sim 1$ if $m_a \sim 10^{-5}$ eV ?	$a \to \gamma$ conversion in a strong emf.	LOW TEMPERATURE ELECTROMAGNETIC CAVITIES
	$m < 10^{-3}$ eV (Stars)	SOLAR	flux on earth: 10^5 to 10^{11}cm^{-2}s^{-1}	$a \to \gamma$ conversion in atoms.	.SILICIUM DIODES .LOW TEMPERATURE DETECTORS
HEAVY NEUTRINOS	$m > 3$ GeV	GALACTIC	Eventually, $\Omega \sim 1$	WEAK (COHERENT IF DIRAC MASS)	.IONIZATION DETECTORS FOR HEAVY PARTICLES
LSP (Lightest supersymmetric particle)	Model-dependent (1-100 GeV ?)	GALACTIC	Eventually, $\Omega \sim 1$	SUPERSYMMETRIC (spin-dependent in most models)	. LOW TEMPERATURE DETECTORS FOR ENERGY DEPOSITS BELOW 1 keV: SSG
COSMIONS	4 GeV$< m <$ 10 GeV	SOLAR and GALACTIC	$\Omega \sim 1$ possible	$\sigma \sim 10^2 \sigma_{weak}$	PHONONS (Ballistic and thermal) HYBRID DEVICES
MONOPOLES	$m \sim 10^{16}$ GeV (GUTS)	GALACTIC TRAPPED AROUND SUN	• PARKER BOUND • BOUNDS FROM RUBAKOV EFFECT	ELECTROMAGNETIC	.CONVENTIONAL .SUPERCONDUCTING
QUARK NUGGETS	HEAVY (UNKNOWN)	GALACTIC	Eventually, $\Omega \sim 1$	ATOMIC COLLISIONS	ACCORDING TO MASS

References

[1] P.A.M. Dirac, Proc. Royal Soc. A133, 60 (1934); Phys. Rev. 74, 817 (1948).

[2] See, for instance:

Proceedings of the Monopole Meeting, Trieste 1981, Ed. N.S. Craigie, P. Goddard and W. Nahm, World Scientific Pub.

Q. Shafi, in Proceedings of the $XXIV$ Int. Conf. on High Energy Physics, Munich August 1988, Ed. World Scientific Pub., and references therein.

[3] M.S. Turner, E.N. Parker and T.J. Bogdan, Phys. Rev. D26 1296 (1982).

[4] E.W. Kolb, S. Colgate and J.A. Harvey, Phys. Rev. Lett 49 1373 (1982).

S. Dimopoulos, J. Preskill and F. Wilczek, Phys. Rev. Lett. 119B 320 (1982).

[5] V.A. Rubakov, ZhETF Pis'ma 33, 658 (1981).

[6] See, for instance, the MACRO Collaboration in the Proceedings of Underground Physics 85, Ed. Il Nuovo Cimento 1986.

[7] See, for instance, B.C. Barish for the MACRO Collaboration, Proceedings of the EPS Conference on High-Energy Physics, Uppsala 1987.

[8] S.D. Drell et al. , Phys. Rev. Lett. 50, 644 (1983).

[9] D.J. Ficenec et al., Phys. Rev. D36, 311 (1987).

[10] See, for instance, T. van Duzer and C.W. Turner, "Principles of Superconducting Devices and Circuits", Ed. Elsevier North Holland, New York 1969.

[11] See, for instance, B. Cabrera in the Proceedings of the Workshop on Superconductive Particle Detectors, Villa Gualino (Torino) October 1987, Ed. World Scientific Pub.

[12] J. Incandela, M. Campbell, H. Frisch, S. Somalwar, M. Kuchnir and H.R. Gustafson, Phys. Rev. D34, 2367 (1986).

[13] See, for instance, B. Cabrera in the Proceedings of the Moriond Workshop on Massive Neutrinos, January 1986, Ed. Frontieres.

[14] J. Incandela in [15].

[15] "Low Temperature Detectors for Neutrinos and Dark Matter- II", Ed. L. Gonzalez-Mestres and D. Perret-Gallix, Frontieres 1988.

[16] L. Gonzalez-Mestres and D. Perret-Gallix, these Proceedings.

[17] L. Gonzalez-Mestres and D. Perret-Gallix, Proceedings of Underground Physics 85, Nuovo Cimento 9C, (1986).

[18] D. Dubbers, Nucl. Instr. Meth. A264, 120 (1988).

[19] R.D. Peccei and H.R. Quinn, Phys. Rev. Lett. 38 , 1440 (1977).
R.D. Peccei and H.R. Quinn, Phys. Rev. D16, 1791 (1977).

[20] J.E. Kim, Phys. Rep. 150, 1 (1987).

[21] D. Dicus, E. Kolb, V. Teplitz and Wagoner Phys. Rev. D22, 839 (1978).
M. Fukugita, S. Watamura and M. Yoshimura, Phys. Rev. Lett. 48, 1522 (1982).

[22] See, for instance, M. Turner, FERMILAB preprint Conf.-89/104-A, and references therein.

[23] M. Dine, W. Fischler and M. Srednicki, Phys. Lett. 104B, 199 (1981).

[24] L. Abbot and P. Sikivie, Phys. Lett. 120B 133 (1983).
M. Dine and W. Fischler, Phys. Lett. 120B 137 (1983).
J. Preskill, M. Wise and F. Wilczek, Phys. Lett. 120B 127 (1983).

[25] P. Sikivie, Phys. Rev. Lett. 51 1415 (1983).

[26] S. de Panfilis et al., Contribution to Telemark IV, "Neutrino Mass and Neutrino Astrophysics", Ashland WI March 16-18 1987, Ed. World Scientific Pub.
B.E. Moskowitz et al., NIM A264, 98 (1988).
W. Wuensch, Thesis Univ. Rochester 1988.

[27] W.U. Wuensch et al., Rochester preprint ER 13065-574 UR-1107 (1989).

[28] University of Florida Development Project (1986).
S.I. Cho et al., Contribution to LT-18, Kyoto 1987.
P. Sikivie et al., Florida (Gainsville) preprints (1989).

[29] S. Dimopoulos, G.D. Starkman and B.W. Lynn, Mod. Phys. Lett. 1, 491 (1986).

[30] F.T. Avignone III et al., Phys. Rev. D35, 2753 (1987).

[31] D. O. Caldwell, NIM A264, 106 (1988).

[32] See, for instance, L. Di Lella in "A Unified View of the Macro- and the Micro-Cosmos".
Ed. A. de Rujula, P. Shaver and D.V. Nanopoulos, World Scientific Pub. 1987

[33] M. Fritschi et al., Phys. Lett. B173, 485 (1986).

[34] See, for instance:
K.A. Olive and G. Gelmini in "A Unified View of the Macro- and the Micro-Cosmos".
E.W. Kolb, D.N. Schramm and M.S. Turner, FERMILAB preprint Pub-89/97-A, and references therein.

334

[35] G. Raffelt and J. Silk, Berkeley preprint (1987).

G. Raffelt, in Proceedings of Telemark *IV* , World Scientific Pub. 1987.

E. Carlson and L.J. Hall, preprint UCB-PTH-89/10 LBL-27202 (1989).

[36] For a discussion of the potentialities of existing cryogenic devices, see T.O. Niinikoski, Proceedings of the "Rencontre sur la Masse Cachée dans l'Univers et la Matière Noire", Annecy July 1987, Ed. Annales de Physique (France).

[37] R. Opher, Astro. Ap. 37, 135 (1974); 108, 1 (1982).

[38] L. Stodolsky, Phys. Rev. Lett. 34, 110 (1974).

[39] P.F. Smith and J.D. Lewin, Ap. J. 318, 738 (1987).

[40] P. Langacker, J.P. Leveille and J. Sheiman, Phys. Rev. D27, 1228 (1983).

[41] See, for instance, B. Muller in Proceedings of the X Workshop on Particles and Nuclei: "Neutrino Physics", Heidelberg October 1987.

[42] A. de Rujula and S.L. Glashow, Phys. Rev. Lett. 45, 942 (1980).

[43] S. Raby and G. West, Phys. Lett. B194, 457 (1987)

[44] J. Faulkner and R.L. Gilliland, Ap. J. 299, 954 (1985).

D.N. Spergel and W.H. Press, Ap. J. 294, 954 (1985).

W.E. Press and D.N. Spergel, Ap. J. 296, 679 (1985).

[45] B. Sadoulet, J. Rich, M. Spiro and D.O. Caldwell, proposal Berkeley- Santa Barbara-Saclay (1987).

[46] G. Gerbier, these Proceedings.

[47] See, for instance:

J. Ellis, in the Proceedings of the EPS Conference on High Energy Physics, Uppsala 1987, and references therein.

J. Ellis, in "Proceedings of the IX Workshop on Grand Unification", Aix-les-Bains May 1988, World Scientific Pub. 1989.

[48] See, for instance, D.V. Nanopoulos, in the Proceedings of the III ESO-CERN Symposium, Bologna 1988, Ed. Kluwer, and references therein.

[49] J. Ellis et al., Phys. Lett. B209, 283 (1988).

[50] J. Mc Donald, Phys. Lett. B225, 133 (1989).

[51] M.W. Goodman and E. Witten, Phys. Rev. D312 3059 (1985).

[52] L. Gonzalez-Mestres and D. Perret-Gallix, in Proceedings of the "Rencontre sur la Masse Cachée l'Univers et la Matière Noire".

[53] A.K. Drukier, K. Freese and D. N. Spergel, Phys. Rev. D33, 3495 (1986).

[54] EMC Collaboration, as reported by T. Sloan at the EPS Conference on High Energy Physics, Uppsala 1987.

[55] J. Ellis and R. Flores, Nucl. Phys. B307, 883 (1988).

[56] F.E. Close and R.G. Roberts, Phys. Rev. Lett. 60, 1471 (1988).

[57] S.J. Brodsky, J. Ellis and M. Karliner, Phys. Lett. B206, 309 (1988).

[58] L.A. Ahrens et al., Phys. Rev. D35, 785 (1987).

[59] K. Greist, FERMILAB preprints (1988).
R. Barbieri et al., Pisa preprints (1988).

[60] See, for instance, R. Flores in [15].

[61] S.P. Ahlen, F.T. Avignone III, R.L. Brodzinski, A.K. Drukier, G. Gelmini and D.N. Spergel, Phys. Lett. 195, 603 (1987).

[62] D. O. Caldwell, R.M. Eisberg, D.M. Grumm, M.S. Witherell, F.S. Goulding and A.R. Smith, Phys. Rev. Lett. 59, 419 (1987).

[63] B. Sadoulet, J. Rich, M. Spiro and D.O. Caldwell, Ap. J. 324, LT5 (1988).

[64] J. Rich and M. Spiro, Saclay report DPhPE 88-04 (1988).

[65] S. Simon, Nature 135, 763 (1935).
T.O. Niinikoski, in "Liquid and Solid Helium" (Halsted, New York 1975), p.145.

[66] D. Twerenbold, Europhysics Letters 1, 209 (1985).

[67] S.H. Moseley, J.C. Mather and D. Mc Cammon, J. Appl. Phys. 56, 1257 (1984) and references therein.

[68] N. Coron, these Proceedings.

[69] H. Bernas, J.P. Burger, G. Deutscher, C. Valette and S.J. Williamson, Phys. Lett. 24A, 721 (1967).
C. Valette, Thesis (1971).

[70] J. Feder, S.R. Kiser and F. Rothwarf, Phys. Rev. Lett. 17, 87 (1966).

[71] A.K. Drukier and L. Stodolsky, Phys. Rev. D30, 2295 (1984).

[72] For a recent update see: L. Gonzalez-Mestres, D. Perret-Gallix in [15].

[73] M. Le Gros, A. Da Silva, B.G. Turrell, A. Kotlicki and A.K. Drukier, "A new Super-heated Superconducting Granule Detector", Vancouver and Landover, 1989.

[74] J. Lindhard et al., K. Dan. Vidensk. Selsk. Mat.-Fys. Medd. 33, 10 (1963); 36, 10 (1968).

[75] C. Chasman, K.W. Jones and R.A. Kristenen, Phys. Rev. Lett. 15, 245 (1965).

A.R. Sattler, F.L. Vook, and J.M. Palms, Phys. Rev. 143, 588 (1967).

[76] P.N. Luke, J. Appl. Phys. to appear.

See also: B. Sadoulet, these Proceedings.

[77] L. Gonzalez-Mestres and D. Perret-Gallix, Nucl. Instr. Meth. A279, 382 (1989).

J.P. Chaminade et al. in the Proceedings of the Moriond Workshop on "Tests of Fundamental Laws in Nature", January 1989, Ed. Frontieres.

[78] E. Witten, Phys. Rev. D30, 279 (1984).

[79] A. de Rujula, Nucl. Phys. A434 605 (1985).

A. de Rujula and S.L. Glashow, Nature 312, 734 (1984).

[80] K. Nakamura, H. Horie, T. Takahashi and T. Tanimori, Phys. Lett. 161B, 417 (1985).

B. Barish, G. Liu and C. Lane, in Proceedings of the EPS Conf. on High Energy Physics, Uppsala 1987.

[81] E. Farhi and R.L. Jaffe, Phys. Rev. D32, 2452 (1985).

[82] D. Elmore et al., "A search for anomalously heavy isotopes of low Z nuclei", Univ. of Michigan preprint 1986.

[83] P.B. Price and M.H. Salamon, in Proceedings of the XIX ICRC, La Jolla, 1985.

Cui Huanhua, O. Eugster, Ke Wei, P. Le Coultre and Tang Xiaowei, preprint IHEP Beijing-Univ. Bern-IHEP Zurich 1988.

[84] B. Barish and G. Liu, CALTECH preprint (1989).

NEW RESULTS ON DETECTOR DEVELOPMENTS FOR LOW ENERGY NEUTRINOS AND DARK MATTER

L. Gonzalez-Mestres and D. Perret-Gallix

L.A.P.P. Annecy

Abstract

The motivation and present status of detector developments for low energy neutrinos and dark matter are discussed. In particular, recently proposed cryogenic techniques are expected to reach unprecedented sensitivity and energy resolution. They may provide the next generation of low background, high sensitivity detectors. The critical overview of to-date results is completed by a sketch of new ideas and possible ways for further improvements. The possibility to develop hybrid detectors, measuring simultaneously ionization and heat, is given special attention.

1 INTRODUCTION

Astro-particle physics has provided in the last decade significant motivation for the development of a new generation of low backgound, highly sensitive detectors dedicated to: a) solar neutrino detection; b) neutrino mass measurements; c) double β experiments; d) dark matter searches, especially cosmions, axions or WIMP (weakly interacting massive particles). The basic technologies foreseen for most of the proposed experiments are closely linked among them, and are leading to the birth of a new cross-disciplinary field at the frontier between particle and nuclear physics, astronomy and material science.

The interpenetration between low energy neutrino physics and dark matter searches is twofold: first, a massive light neutrino may well be a candidate to hot, warm or cold dark matter; secondly, the detectors foreseen for cosmions, WIMP or even solar axions are very close to those proposed for the next generation of low energy neutrino experiments.

A nonvanishing electron neutrino mass may be observed by direct measurement of a β decay spectrum near the end point of maximum electron energy [1] , or indirectly through a double β decay event produced by one of the diagrams shown in Fig. 1 , where the electron neutrino is assumed to be a Majorana particle, with a small mass related to lepton number violation (neutrino-antineutrino oscillation) [2]. Similarly, the observed anomaly in the solar neutrino flux [3], if confirmed by the GALLEX experiment [4], may be an evidence for a flavour-changing neutrino mass matrix [5]. But, in the case of solar neutrinos, other explanations are possible: a) a new weakly interacting neutral particle conveying energy from the central core of the sun to colder regions (cosmion model [6]); b) an anomalous magnetic moment, leading to helicity flip of the produced neutrinos by the solar magnetic field (the neutrino should then have a small Dirac mass); c) finally, new data from Davis et al. [7] may indicate a systematic error in previous measurements, leading to a flux compatible with the standard solar model, but may also be due to time evolution in the solar activity having an influence on effect b) [8]. A plot of the solar neutrino spectrum predicted by the standard solar model [9] is given in Fig. 2 .
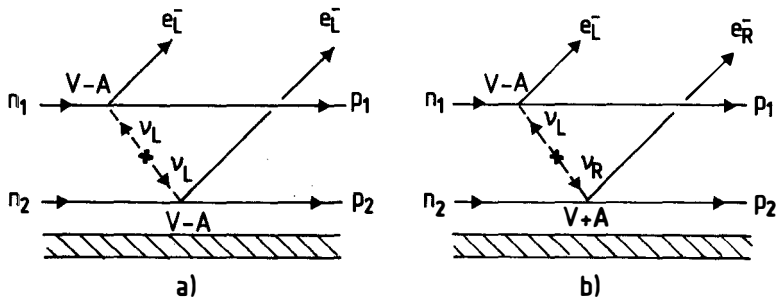

Fig. 1 - Diagrams contributing to neutrinoless double beta decay.

Dark matter candidates (see [10]) , such as cosmions or the magnino [11] , play a significant role in possible explanations of the solar neutrino puzzle. In turn, light neutrinos may themselves be dark matter candidates if they have masses in the range $5\ eV\ <\ m_{\nu_e}\ <\ 100\ eV$ or $1\ keV\ <\ m_{\nu_{\mu,\tau}}\ <\ 35\ MeV$ [12].
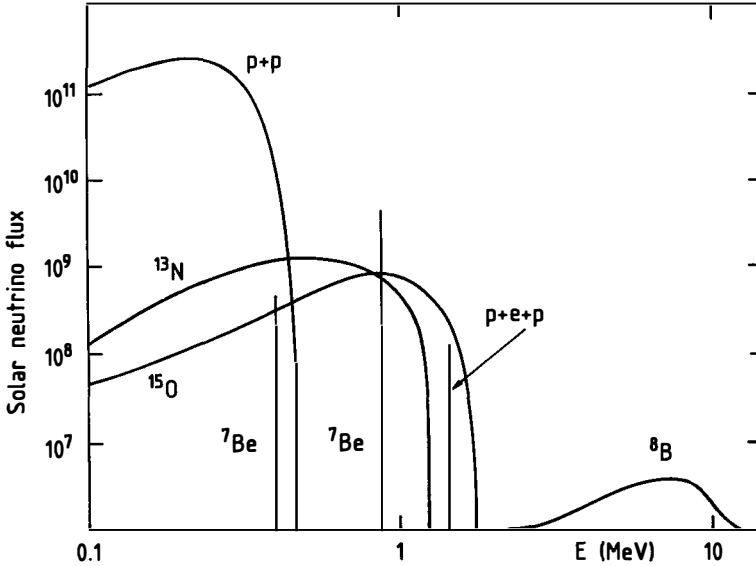

Fig. 2 - Solar neutrino spectrum (in $cm^{-2}\ sec^{-1}\ MeV^{-1}$), as predicted by the standard solar model. Narrow lines stand for integrated fluxes (in $cm^{-2}\ sec^{-1}$). See [13] .

2 NEUTRINO EXPERIMENTS

2.1 Neutrino mass

The mass of the electron neutrino has until now been measured through the tritium Kurie plot, where a nonzero mass would manifest itself at the $E\ \simeq\ E_0$ end point of the distribution:

$$dn/dE\ =\ F(E)\ p\ E\ (E_0\ -E)\ [(E_0\ -\ E)^2\ -\ m_{\nu_e}^2]^{1/2} \qquad (1)$$

p being the electron momentum, E its energy and $F(E)$ a smooth calculable Coulomb correction. E_0 is the maximum value of E if $m_{\nu_e}\ =\ 0$, $E_0\ =\ 18.6\ keV$ for tritium.

There is at present consensus that the best result in this line of research has been provided by the Zurich axial spectrometer [14] , with $27\ eV$ energy resolution on the electron energy, leading to the bound $m_{\nu_e}\ <\ 18\ eV$.

Although progress in axial spectrometry is still possible, new techniques are being

proposed based on low temperature phenomena: thermal detection with bolometers, or excitation of quasiparticles in superconductors detectable with superconductirg tunnel junctions (STJ). Both techniques will be dealt with later on.

2.2 Double beta experiments

Double beta decay with two neutrinos has been observed in a ^{82}Se experiment [15], leading to a lifetime $\approx 10^{20}$ $years$. $\beta\beta$ decay with Majoron emission was claimed with a half life $\simeq (6 \pm 1)$ 10^{20} $years$ in a ^{76}Ge experiment [16], but has not been confirmed by other germanium experiments [17], which give bounds better than $\tau > 10^{21}$ $years$. Other double beta isotopes used in present experiments are: ^{48}Ca , ^{100}Mo , ^{130}Te , and ^{128}Te.

Germanium detectors have until now dominated the search for $\beta\beta_{0\nu}$ events, due to the excellent energy resolution of intrinsic semiconductor germanium ($\approx 0.1\%$ in the $\approx 2-3$ MeV region), but various techniques are used in experiments with other targets. In the Irvine experiment [15] , a 7 mg / cm^2 thick enriched foil of ^{82}Se is used as the central electrode of a 80 cm × 80 cm × 20 cm Time Proportional Chamber (TPC) in a 700 G magnetic field. The LBL/Mt. Holyoke/New Haven experiment [18] uses 17 g of enriched ^{100}Mo foils between layers of $Si : Li$ detectors searching for coincidence events. ^{136}Xe is incorporated in a multiwire proportional counter by the Milan group [19] , and in a TPC by the Caltech/PSI/Neuchatel collaboration [20] .

Again, cryogenic devices may well provide a next generation of double beta experiments, continuing the line started by semiconductor germanium detectors where energy resolution was the main tool to reject background. Thermal bolometers are in this respect the best suited technique, and can incorporate almost any specifc material in an active target detector. Finally, the use of enriched isotopes (already started with ^{82}Se,^{100}Mo,^{76}Ge,...) is likely to become a general practice.

2.3 Solar neutrinos: ^8B sector

Since the (unique, and radiochemical) Homestake experiment [21] brought data in contradiction with the Standard Solar Model, a considerable effort has been devoted to the preparation of new solar neutrino experiments. KAMIOKANDE II , originally designed for proton decay, has been able to observe low energy events induced by ^8B solar neutrinos through ν_e e^- elastic scattering in a 3000 ton water Cherenkov detector [22]. A ^8B ν flux of 2.6 10^6 cm^{-2} s^{-1} within 30% 1 σ error may be inferred, possibly confirming a deficit with respect to the prediction of the Standard Solar Model, but obviously further experiments are needed. Another Cherenkov detector, using 1000 $tons$ of heavy water, is being proposed to be installed near Sudbury (Canada) [23] .

ICARUS [24] is a project to build a large liquid argon imaging chamber, expected to be sensitive to ^8B solar neutrinos through ν e^- elastic scattering, or through the reaction $^{40}Ar(\nu_e , e^-)^{40}K^*$, where the excited nucleus $^{40}K^*$ decays to the ^{40}K ground state by emitting a γ of 4.38 MeV . Finally, ^8B solar neutrinos may also be detectable by a boron-loaded liquid scintillator (BOREX experiment [25]) where boron can be incorporated in some compounds up to 20% in weight. The relevant reactions are: $^{11}B(\nu_e , e^-)^{11}C$

and $^{11}B(\nu_X, \nu_X)^{11}B^*$, where X stands for any arbitrary flavour. Feasibility studies of ICARUS and BOREX are presently in progress.

2.4 Solar neutrinos: low energy sector

Two experiments sensitive to low energy solar neutrinos will be radiochemical and based on the isotope ^{71}Ga instead of ^{37}Cl : one at GRAN SASSO (GALLEX) [4], and the second one at BAKSAN[26]. The reaction $^{71}Ga(\nu_e, e^-)^{71}Ge$ has a threshold of 235 keV in incoming neutrino energy, and therefore will be sensitive to a part of the pp solar neutrino spectrum.

Gallex uses 30 $tons$ of gallium in the form of $GaCl_3$, in acqueous solution of HCl . An event rate of ≈ 1 ^{71}Ge $atom/day$ is expected. $GeCl_4$ will be extracted by a nitrogen purge with a small amount of Ge carrier, transformed into GeH_4 after extraction, and finally the decay of ^{71}Ge into ^{71}Ga by electronic capture ($\tau_{1/2} \simeq 11.4$ $days$) will be detected with a proportional counter.

The BAKSAN experiment uses 60 $tons$ of gallium in metallic form, where an extraction method from melted metal has been developed.

The ultimate goal would, however, be a real time experiment sensitive to both the pp spectrum and the ^7Be ray, allowing for a clean event identification and with background rejection good enough to accurately measure the differential solar neutrino flux. This is possibly one of the most difficult challenges ever met by particle physics instrumentation. Until now, the main effort has been devoted to devices based on the reaction proposed by Raghavan [27]: $^{115}In(\nu_e, e^-)^{115}Sn^{**}$, with a threshold of 128 keV in the incoming neutrino energy. The excited state Sn^{**} de-excites 3.2 μs later, giving two γ rays of 116 and 490 keV , which are emitted simultaneously but can be detected in different cells of a segmented detector. In spite of its clean signature, the use of Raghavan's reaction presents the major drawback of ^{115}In radioactive background, with an event rate of $\simeq$ 1 β $decay$ $cm^{-3}sec^{-1}(E < 490\ keV)$, leading to 2 β , 3 β and (β - erratic γ) coincidences that may fake solar neutrino events. Since the expected solar ν event rate is very low ($\simeq 0.3$ $event$ $ton^{-1}day^{-1}$), such backgrounds can be rejected only by a detector having simultaneously very fine segmentation, fast response and good energy resolution.

Aiming mainly at a measurement of the ^7Be ray, new indium loaded liquid scintillators have been developed [28], incorporating 10% In in weight, still presenting reasonable optical properties. In such detectors, the 116 keV γ would not be detected separately, but rather with the first Compton scattering from the 490 keV γ. Detection efficiency for ^7Be solar neutrinos may be of $\approx$ 30%. Along similar lines, In coated scintillating fibres are given some attention [29], although the detection of the 116 keV γ becomes more problematic and efficiency may be less than 15% [30] . In both cases, very large detectors (200 ton or more for 1 $event/day$) are needed and the practical possibility to reject all kinds of backgrounds remains to be demonstrated.

Potentially able to detect pp solar neutrinos may be very high quality crystal scintillators [31], semiconductor InP [32], STJ [34] or superheated superconducting granules (SSG) [36]. The last two techniques will be discussed in the next section.

Fig. 3a shows a recently grown transparent single crystal of $InBO_3 : Tb^{3+}$ [37], and Fig. 3b its emmission spectrum when excited with 292.5 nm ultraviolet laser light. Lu-

minescence is very intense, but unfortunately Tb^{3+} fluorescence is too slow for a particle detector. The chemical feasibility of Ce^{3+} doping of several indium compounds is presently under investigation. Ce^{3+} doping is actually a nontrivial chemical challenge not only for indium borates [38], but also for well known phosphor silicates such as $Si_2In_2O_7$ [39].

InP is a very promising technique, as 1 cm^3 prototypes have already been constructed and show sensitivity to low energy electrons and photons [32]. Further material studies are required in order to optimize the response of the detector.

The main alternative to the indium program for low energy solar neutrinos would be nucleus recoil [40], where coherent scattering allows for large cross sections and a significant number of events can be reached with smaller detectors. However, energy deposition would be very small ($\approx$ 10 eV for ^7Be neutrinos interacting with a ^{27}Al target) and the event a pure recoil without specific signature. Even if such a signal were made detectable, background problems appear at first sight practically hopeless and, in any case, have never been dealt with at such low energy deposition.
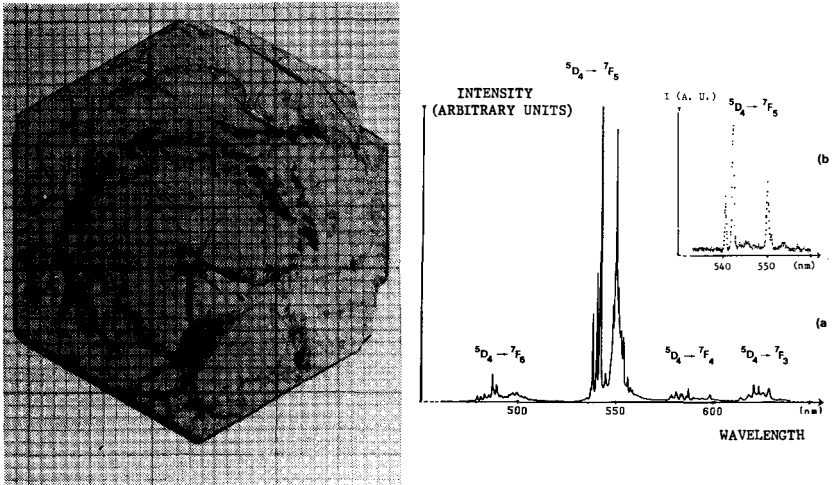
Fig. 3 - a (left): a transparent single crystal of $InBO_3$: Tb^{3+} grown by the flux method. b (right): its emission spectrum when excited by ultraviolet light. From [37].

3 CRYOGENIC DETECTORS

Low temperature devices are possibly the most significant noveltry in recent detector technology. Small cryogenic detectors have already been used in astrophysics, a well-known application being the study of possible anisotropies of microwave background radiation [41]. Particle physics applications [35,33] require: a) sensitivity to individual particles; b) comparatively large devices.

The use of low temperature detectors is expected to bring higher sensitivity and energy resolution, due to: a) the lower energy of elementary excitations (phonons, charge carriers, spin excitations...); b) the fast decrease of specific heats for dielectric crystals and superconductors; c) lower thermal noise for both detector and electronics. In addition, some low temperature effects provide specific signals (e.g. change in magnetization) or amplification effects (e.g. metastable phase transition in superconductors, latent heat release or quasiparticle multiplication). The wide variety of superconducting materials and crystal heat absorbers makes low temperature techniques attractive when active targets are needed.

Low temperature detectors are still at the stage of feasibility studies, but have already provided encouraging results. Current work concerns mainly the study of the basic properties of these new devices.

3.1 CRYSTAL CALORIMETERS (BOLOMETERS)

The specific heat of an insulating crystal at low temperature is dominated by lattice vibrations. An energy deposition E converted into heat will lead to an increase in temperature that can be detected with a resistive thermometer (thermistor). In the ideal case of very low read-out noise, energy resolution is given by phonon thermal fluctuations [42] :

$$\Delta E_{rms} \simeq \zeta \ (C/k)^{1/2} \ kT \propto T^{5/2} \ M^{1/2} \tag{2}$$

where C is the crystal heat capacity, k the Boltzmann constant and M the mass of the crystal. The heat capacity of the thermistor has been neglected, which may not always be justified, especially for small bolometers. The coefficient ζ depends on the details of detector architecture, but is often estimated to be in the range 1.5-2 . From (2), a sizeable increase in detector mass can be compensated by working at lower T.

The measurement of the ν_e mass from the ^3H Kurie plot can be made with detectors smaller than 1 mm^3 . Energy resolution of 10 eV $FWHM$ or less on 18.6 keV electrons is needed for such purposes. A diamond bolometer (0.25 mm^3) at 1.3 K reached $FWHM$ energy resolution of 36 keV on 5.5 MeV α particles [43] , and at 100 mK a composite Si micro-calorimeter brought 17 eV $FWHM$ resolution on 6 keV γ's [44] . Fig. 4a shows the scheme of the Wisconsin-Goddard Si bolometer, whereas Fig. 4b exhibits spectra obtained with this device.

More recently, the study of large bolometers has also been undertaken. Using a 0.7 g germanium absorber at 44 mK , the Milano group [45] obtained 1% energy resolution on α particles from a ^{228}Ra source in radioactive equilibrium with its daughters. Furthermore, a previous high flux irradiation allowed to implant daughter nuclei in the crystal producing a spectrum with satellite peaks shifted upwards by 100 keV (Fig. 5a). As the implanted nuclei decayed, satellite peaks disappeared and only single peaks from external α's remained (Fig. 5b). The authors conclude that the bolometer was sensitive to nucleus recoil, as expected from the 50 keV energy resolution. Similar evidence had been previously reported from work with small bolometers [46] . More recent results on large bolometers are being presented by N. Coron at this Workshop.

A new idea is the so-called "magnetic bolometer" [47]. Half of the deposited heat is converted into very low energy spin excitations ($\approx 10^{-6}$ eV) and a small change in the

magnetization of the crystal can be detected by a SQUID read-out. The authors report 30 keV noise level at 400 mK with 5.5 $MeV\alpha$'s on a 7.35 g sapphire absorber with a 135 mg $YAG : Eb^{3+}$ magnetic bolometer implanted on the sapphire.
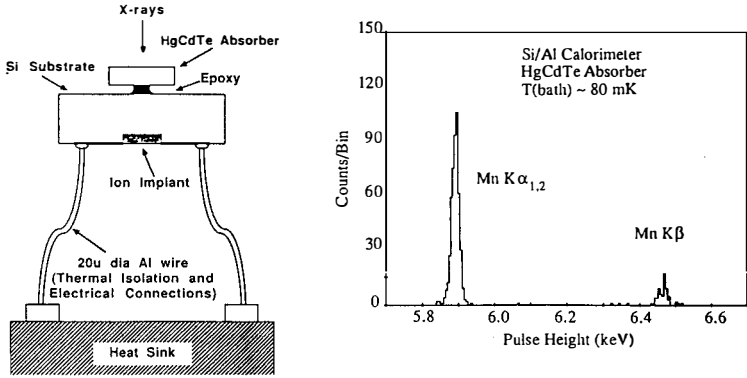

Fig. 4 - a (left): The silicon micro-calorimeter developed by the Wisconsin-Goddard group. b (right) low energy γ spectrum from [44] , obtained with a ^{55}Fe source, exhibiting $\Delta E \simeq 17$ eV for the width of the Mn K_α peak.
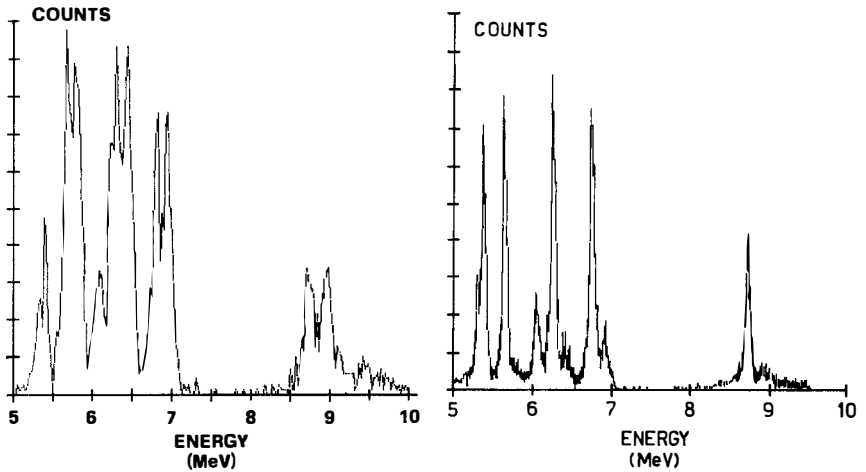

Fig. 5 : Energy spectra of the Milano bolometer [13] irradiated with a ^{228}Ra source. a) left: with daughter nuclei implanted in the crystal; b) right: two weeks later, after the implanted nuclei decayed.

Bolometer development must still undergo substantial progress before reaching theoretically expected performances. In particular, although in an ideal case one should have $\Delta E \simeq noise\ level$, in practice energy trapping by long lived electronic states, Frenkel pair formation, light emission, and other unwanted phenomena, imply substantial departures from the ideal behaviour of a purely thermal bolometer and degrade energy resolution. Furthermore, the specific heat of the sensor must also be taken into account and may limit the performance of small bolometers. To date, the main motivation for the development of large bolometers ($100\ g - 1\ Kg$) lies in neutrinoless double β decays [48] , where energy resolution is crucial for background rejection, and dark matter searches through nucleus recoil [49], where sensitivity to energy deposition below 1 keV is required. More difficult, because of background, would be a solar neutrino experiment based on $\nu - e^-$ scattering using several tons of bolometric detector [50]. Applications at reactors face similar feasibility problems.

3.2 SUPERCONDUCTING TUNNELING JUNCTIONS (STJ)

Superconductors provide the unique possibility of producing diodes with about $10^{-3}\ eV$ current carrier excitation energy. Then, a statistical $N^{1/2}$ law (Poisson distribution) for energy resolution leads again to exceptional performances for the detection of low energy particles. In a STJ with a small bias voltage, quasiparticles and holes tunnel across a thin insulating layer separating two superconducting samples, and the current can be read with conventional low noise pre-amplifiers. Usually, STJ are made of two metallic films separated by the insulating layer (Fig. 6) , and are not expected to be massive detectors. However, new ideas have recently emerged (e.g. quasiparticle trapping, which also provides multiplication [34]) to incorporate bulk superconducting specimens.
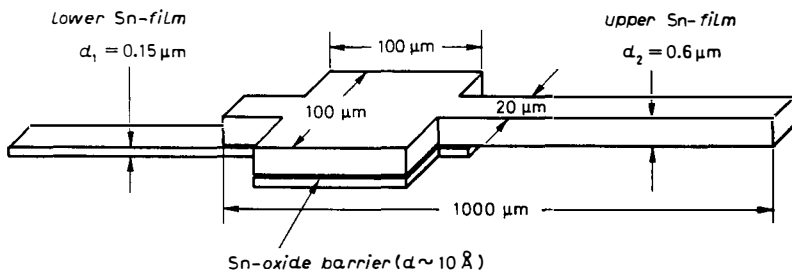

Fig. 6 - Scheme of a STJ prepared at PSI (Villigen) [51] .

The bias voltage creates a thermal current $I_{th} \propto exp(-\Delta/kT)$ that can be lowered by working at low reduced temperature ($t = T/T_c$). In order to prevent Cooper pair tunneling (DC-Josephson current), a magnetic field parallel to the oxide barrier is applied. An incoming particle will excite mainly electrons of energy much larger than the gap Δ , but these electrons will later relax emitting phonons. At $t \ll 1$, phonons mainly excite

quasiparticles, which can then tunnel across the junction or recombine.

The expected energy resolution in a STJ is:

$$\Delta E_{rms} \simeq (fE\epsilon)^{1/2} \qquad (3)$$

where f is the Fano anti-correlation factor ($0.1 < f < 1$) and ϵ the effective quasiparticle excitation energy ($\epsilon > \Delta$). Potentially, a $Sn - SnO - Sn$ detector with $f \simeq 1$ and $\epsilon \simeq \Delta \simeq 0.6$ meV , should reach 0.1% energy resolution on 6 keV γ's. Experimental results are not that good, but the SIN group claims [51] 48 eV $FWHM$ resolution on the ^{55}Mn K_α peak at 5.89 keV, whereas the Garching (TMU) group [52] reports 88 eV resolution, determined from the energy difference between the K_β ($6.49keV$) and K_α peaks. A typical signal rise time from existing STJ is of the order of 15 μs .

Using materials with higher T_c , good performances can also be obtaiend at higher temperatures. As an example, a 10 $\mu m \times 10\mu m$ $Nb/Al/Al_2O_3/Al/Nb$ junction [53] recently brought 250 eV energy resolution at $T = 1$ K .
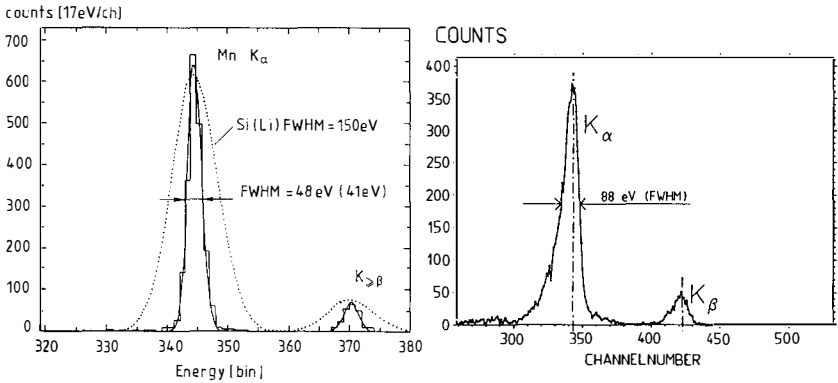
Fig. 7 : Recent results yielded by superconducting tunneling junctions. a) left: energy spectra (full line) of $E \simeq 6$ keV X rays obtained at PSI (Villigen) with a Sn STJ at 400 mK , as compared to the best performance of $Si : Li$ detectors at LN_2 temperatures (dotted line); b) right: similar spectra obtained by the Garching group.

Apart from the detection of low energy γ rays, a possible use of small STJ would be neutrino mass measurements [54] , but if larger devices can be made, they could be used [34] to detect low energy solar neutrinos through the ^{115}In Raghavan's reaction [27] . A ^{115}In detector may also be used for $\bar{\nu} \rightarrow \nu$ oscillation experiments at reactors.

STJ provide an interesting read-out for crystal phonon detectors, where ballistic phonons would be converted into quasiparticles. Since ballistic phonons propagate along the main crystallographic axis, it should be possible to extract information on the position of the event inside the crystal [50,55]. This possibility has been recently demonstrated by the Garching (TMU) group [55] using three aluminum STJ implanted on one of the faces of a Si wafer, and deplacing the external α source on the other side of the crystal. Position

information is seen to emerge from correlations between the signals observed at two different junctions. A parallel effort along similar lines is being pursued by the Stanford group [50] , using a superconducting strip read-out near the transition edge. Recent results from Garching are shown in Fig. 8 .
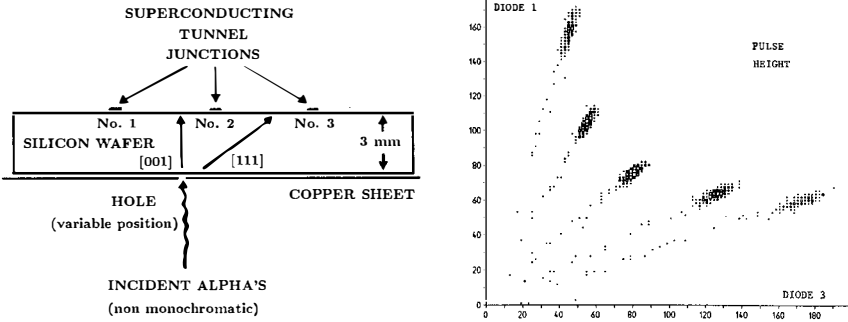

Fig. 8 - The Garching ballistic phonon experiment: a (left) schematic description of the set-up; b (right) two-junction signal scatter plot showing a clear separation between signals produced at the five different impact positions.

3.3   SUPERHEATED SUPERCONDUCTING GRANULES (SSG)

A type I superconductor with low enough κ (the Ginzburg-Landau parameter) can exhibit metastable states, due to the positive normal-superconducting interface energy. In particular, a superconducting sample may remain in this state for values of the external magnetic field larger than the critical field H_c (superheating). The superheated state and has been obtained for pure metal microspheres of $1 - 400\ \mu m$ diameter. It was proposed long ago [56] to use SSG as a particle detector in the form of a suspension of small microspheres into some dielectric material, with a read-out of current loops oriented in the plane normal to the applied magnetic field $\vec{H}_0$. The energy released by an incident particle would originate a fast transition of one or several granules, detectable through the disappearance of the Meissner effect.

A major drawback of SSG detector is the dispersion in effective superheated critical field observed in a realistic colloid with many granules. As the magnetic field is increased, the number of counts per unit increase in H_0 follows a rather wide distribution (the differential superheating curve). It is thus impossible to fix a value of the applied magnetic field in such a way that all the granules are set to a common small threshold in H_0, i.e. in energy deposition for a given size. Work in progress, however, seems to suggest [57] that new fabrication techniques may possibly circumvent such a difficulty and lead to very narrow superheating curves. This, in case of success, would be a major step forward.

Recently, progress has been made in the SSG real time read-out [58] and tin granules of

sizes $10-400$ μm have been shown to be sensitive to low energy sources down to 6 keV γ's [59] . The observed sensitivity can be theoretically understood and, when extrapolated to very small grains, gives encouraging figures: 1 μm diameter In grains at T = 200 mK would be sensitive to about 300 eV energy deposition with 80% efficiency, whereas good quality Al or Ga grains cooled to 100 mK would achieve a similar performance for 4 eV energy deposition. Such figures would be improved by narrower superheating.

Industrial manufacturers are now able to produce at large scale rather small grains of reasonable quality (Fig. 9 - 11) by conventional techniques. In the last months, recently produced Al and Zn grains were available and have been studied for the first time for detection purposes [60] , [61] . As an example, the Al grains of Fig. 11b were irradiated in Annecy with a ^{109}Cd source (β's and γ's of E < 88 keV) deposited on the grains before preparing the SSG colloid. The result obtained after 5 min irradiation time is shown in Fig. 12 . In Fig. 12a is exhibited the differential superheating curve, where dN/dH_0 is the number of counts per unit increase in H_0 . Fig. 12b shows the irradiated differential superheating curve, where the applied field stays at some fixed value (the point where the gap appears on the curve) for 5 min (irradiation period) before being further increased. The missing counts in Fig. 12b correspond to grains having changed state during the irradiation period, although contrary to previous tests with tin, not all of the flips under irradiation were detectable in real time with our electronics. The test was performed at T = 400 mK , and already indicates excellent sensitivity, which should still be considerably improved by working at T = 100 mK .

Encouraging as they may look, the above results are not sufficient for realistic detection purposes. Two examples:

1) It has been proposed [62] to use indium SSG as a detector for low energy solar neutrinos. A X-Y current loop read-out would allow to segment a 4 ton indium detector into 10^7 elementary cells, with only 10^5 electronic channels. However, such an instrumentation would require 5 $mm \times 1$ m current loops, which makes extremely difficult to detect the signal produced by 116 keV secondaries.

2) Dark matter searches through nucleus recoil encounter an even more severe difficulty, since only single grain flips are usually expected. We therefore have only a threshold detector, without any energy resolution.

To cure both diseases, we have proposed a new operating principle, based on the concept of "amplification by thermal micro-avalanche" [59]. Metastability allows for a positive latent heat in the superconducting to normal phase transition. Then, the flip of a single granule can release heat which, together with the deposited energy, will be dispersed in the detector. If heat exchanges through the dielectric material are efficient enough (low Kapitza resistances), new flips will be produced which in turn will release more latent heat. In such a scenario, with sufficiently small grains (1 μm in diameter), a signal in magnetic flux $\Delta \Phi \propto \Delta E$ is predicted even for a nucleus recoil. The appearance of extra flips is expected to lead an amplification effect (one or two orders of magnitude), which may solve the basic problems for a ^{115}In experiment. Calculations using the thermal conductivity of GE 7031 Varnish for heat propagation in the colloid yield time resolution in the range $10-100$ ns , and metallic spherical inclusions should not drastically change the result [63].
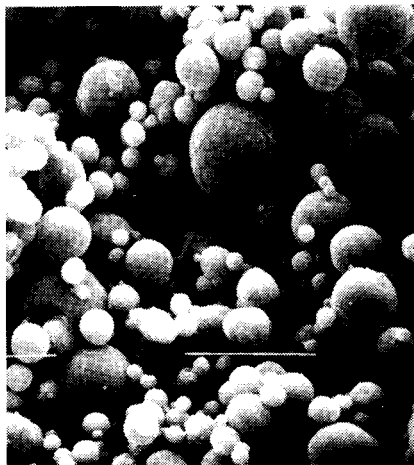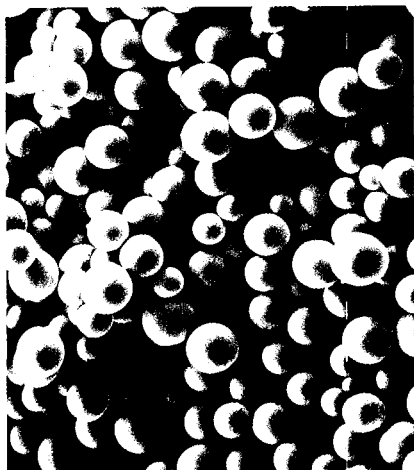
Fig. 9 (left) - ϕ (diameter) $<$ 25 μm Sn granules obtained by conventional sieving from a ϕ $<$ 40 μm collection produced by EXTRAMET. The mark is 10 μm.

Fig. 10 (right) - $\phi_{mean} \simeq 4$ μm superfine HEUBACH Zn powder. The mark is 10 μm.
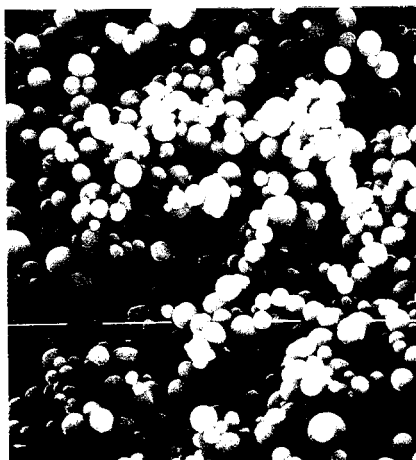

Fig. 11 - Aluminium samples obtained by centrifugation in air from a ϕ $<$ 63 ECKART-WERKE sample. a (left): ϕ $<$ 5 μm , the mark is 10 μm ; b (right): 12 μm $< \phi <$ 20 μm, the mark is 10 μm (a tail of smaller grains remains).
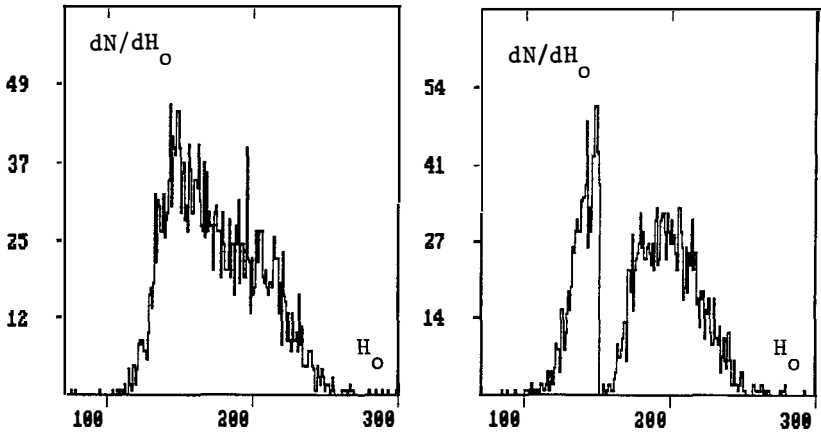
Fig. 12 - Irradiation result for the sample of Fig. 11b, with a ^{109}Cd source. a (left): differential superheating curve; b (right) irradiated superheating curve obtained staying for 5 min at a fixed value of H_0 before raising further the magnetic field (H_0 in a. u.).
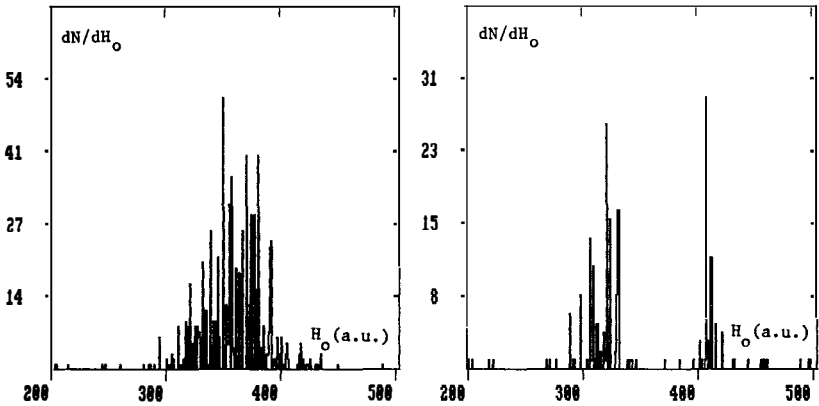

Fig. 13 - Similar test for 4 μm Zn grains. a (left) : the "avalanche" superheating curve; b (right) : irradiated "avalanche" superheating curve obtained after staying for 5 min at the value of H_0 where the gap starts. The source used was ^{36}Cl ($E < 714$ keV β's).

In case of success of the "micro-avalanche" scenario, other applications of SSG would become possible: double beta decays [64], X-ray imaging [65], dark matter searches through inelastic scattering with a ^{119}Sn target [59]. Furthermore, the dielectric material can provide an active target (hydrogen for dark matter searches [59]) ... However, if experimental evidence for global avalanches already exists [66] , further work is required to evaluate the real performance of the micro-avalanche effect.

We performed tests at $T = 400\ mK$ with the Zn grains shown in Fig. 10 , and possible new evidence for thermal avalanches was obtained. Very large and long pulses ($10-50\ \mu s$ risetime) were seen, whereas single grain flips could not be detected individually and previous tests with larger granules of the same origin had exhibited normal single grain pulses. Due to the superposition of a continuous slow signal and rapidly oscillating noise, each long pulse produced several counts in our read-out system leading to the distribution shown in Fig. 13a . We may call this (non reproducible) distribution the "avalanche" superheating curve. It was even possible to obtain interesting irradiation results, where practically no signal was observed during the irradiation period but in turn a large gap appeared in the irradiated superheating curve (Fig. 13b). Clearly, a careful study should be performed to really elucidate the nature of the phenomenon and further tests are in preparation down to $100\ mK$.

Development of industrial grain production should also be pursued to reach smaller sizes. ϕ_{mean} (average size) $\simeq 25\ \mu m$ tin granules are produced [67] at a rate of 5 $Kg/hour$ using a 40 KHz ultrasonic atomizer. A new development is underway in order to adapt the existing procedure to higher ultrasonic frequencies, up to 5 MHz according to the law [68] : $\phi_{mean} \propto f^{-2/3}$ (f = frequency). Other techniques seem also well suited to produce (possibly, after sieving by centrifugation) very small spheres in the $\sim 1\ \mu m$ range. For instance, direct atomization of molten metal with a nitrogen jet is currently being used for the production of Al and Zn powders [69] , [70] .

An independent application, using large grains, would be the detection of magnetic monopoles [71] , where the flux tube injected by the monopole would destroy the superconductivity of many granules. The advantage of SSG would be a comfortable signal (several orders of magnitude larger than in induction experiments), a good background rejection due to the large grain size, as well as tracking and timing allowing for a measurement of speed and direction.

3.4   OTHER CRYOGENIC DETECTORS

Energy deposited in superfluid ^4He at low temperature ($100\ mK$) would create rotons $\Delta/k = 8.65\ K$. A 200 keV electron from neutrino scattering is expected to originate $\approx 10^8$ elementary excitations, which will propagate ballistically in all directions. Some will hit the surface of the liquid and evaporate a sizeable number of helium atoms, that may be detected by bolometric techniques [72] . No experimental result exists yet on this technique, but a development is being carried on at Brown University. Even more ambitious is a proposal from the Lancaster group [73] , where superfluid ^3He (cooled below 1 mK) would produce $\approx 10^7$ quasiparticles per deposited eV . Unfortunately, such quasiparticles are neutral and their detection far from obvious.

Several ideas on the possible use of devices operating below 1 mK have been put forward by T.O. Niinikoski [74] , who was able to obtain bounds on dark matter from measured heat leaks in Cu adiabatic nuclear demagnetization refrigerators. On the other side, high T_c superconductors have already produced interesting devices, such as DC SQUIDs made of $YBaCuO$ ceramics [75] . More classical techniques, such as semiconductors ($InSb$, doped Ge ,...) operating at 4 K [76], or low temperature scintillators [77], may also play a significant role in the next generation of particle detectors.

4   HYBRID DEVICES

Background problems are rather difficult to handle in rare event detectors, when only one kind of signal (current, thermal pulse, scintillation...) is used. Furthermore, the way energy is degraded into elementary excitations depends crucially on the way it has been deposited (therefore, on the nature and energy of the incident particle, the type of interaction with matter, etc.). Thus, the measurement of only one component of the deposited energy may not be the best approach, as it implies a substantial loss of information (although some scintillators yield a two-component fluorescence signal). At room or LN_2 temperature, it is not possible to detect a single particle thermal pulse (large specific heat, high noise level...). At very low temperature, the extremely good performance expected from ideal thermal measurements often pushes developments in the opposite sense: only a thermal signal is aimed at, other kinds of energy losses are potentially a source of trouble spoiling energy resolution. We would like to argue, here, in favour of a simultaneous detection of ionization and heat in a composite cryogenic scintillator or semiconductor.

According to Lindhard et al. [78], a nucleus recoil at $E_R < 1\ MeV$ can be distinguished from an electron or photon by looking at the relative amount of energy converted into ionization (the nucleus ionizes 3 to 5 times less at $E_R = 10\ keV$). The smaller the recoil energy, the smaller the relative amount of ionization losses as compared to direct production of phonons. Similarly, fluorescence radiation sets a neat distinction between a slow α particle and a β or γ of the same energy, due to the dE/dx (ionization energy loss per unit length) dependence of the light yield [79]. It then follows that rare event experiments, having to face severe backgrounds, may seriously benefit from particle identification through simultaneous measurement of ionization and heat. This would in particular be the case for the search of WIMP dark matter candidates through nucleus recoil, but may also be relevant to a calorimetric double beta experiment, as far as the main background would be given by $\alpha's$. Two obvious possibilities arise when looking for ways to combine thermal and ionization measurements. One is the use of a semiconductor at very low temperature, and is discussed in the talk by B. Sadoulet. We would like here to discuss in detail the second possibility, based on suitably chosen scintillating crystals [80,37] .

Several intrinsic scintillators are known to present a high light yield when cooled down to ^4He temperatures. Undoped BGO produces 10 times more light than at room temperature [81] , whereas $CdWO_4$ improves slightly and CeF_3 fluorescence remains essentially unchanged [82] . Fluorescence decay time increases to about 200 μs for both BGO and $CdWO_4$ [81,37] but remains very fast ($\approx$ 40 ns) for CeF_3 [82], as well as for cerium-doped

luminophores [83]. Although further studies, down to 50 mK, are needed, commonly used models predict a flattening of the T-dependence of the basic fluorescence parameters, which all tend to some constant as $T \to 0$. This has indeed been observed for the fluorescence decay time of $CdWO_4$ [37] , which remains unchanged between 4 K and 1.5 K . Fig. 14a shows BGO emission spectra at several temperatures, as obtained from ultraviolet excitation. The increase in light output is explicit as the crystal is cooled down. Fig. 14b presents the T-dependence of BGO fluorescence decay time below 250 K . More recent results for BGO using radioactive sources (5.5 MeV ^{241}Am α's) [84] appear to show the same trend, although further tests with sources below 200 K would be useful in order to carefully study BGO fluorescence under several kinds of irradiation.

It may even happen that materials not exhibiting significant luminescence at room temperature become good luminophores at low T . Fig. 15 shows the T-dependence of $MoPbO_4$ light yield, where the 520 nm (green) component increases by four orders of magnitude when the crystal is cooled down to LN_2 temperature. Other molybdates exhibit analogous behaviour [85]. The time evolution of $MoPbO_4$ green fluorescence splits at very low temperature in two components: one with a decay time $\tau \simeq 10$ μs ; the slower one with $\tau \approx 100$ μs , similar to tungstates.
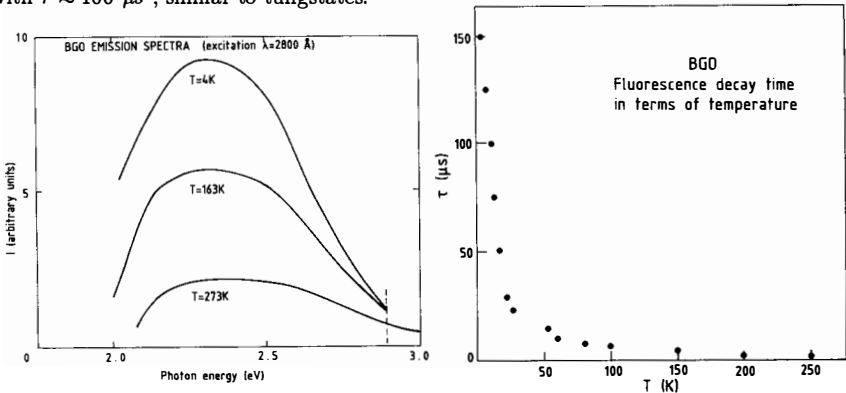

Fig. 14 - Temperature dependence of BGO fluorescence properties. a (left): emission spectrum under ultraviolet excitation ($\lambda = 280$ nm) at several temperatures; b (right): fluorescence decay time in terms of temperature. From [81].

The above conditions naturally suggest the development of a new hybrid device: the *luminescent bolometer*. A transparent scintillating crystal cooled to very low temperature would then carry a double read-out: a) a cryogenic photosensitive device; b) a thermistor. In this way, it would be possible to measure both light and heat and implement particle identification. A rough scheme (all faces painted but one, to prevent light from escaping) is shown in Fig. 16 . The main technical problem is possibly the choice or development of the best suited photosensitive device. Superconductive detectors and bolometers are possibly the best candidates, if light collection is to be made at bolometric temperature.
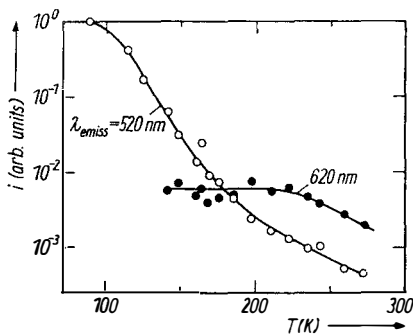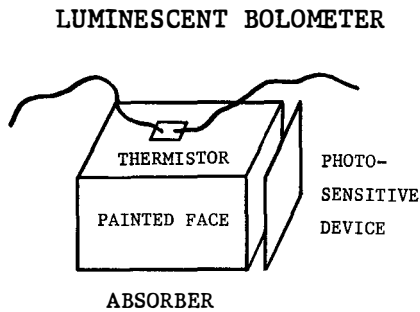
LUMINESCENT BOLOMETER

Fig. 15 (left) - Temperature dependence of the light yield of $MoPbO_4$ (lead molybdate) at two different wavelengths. The green component (520 nm) increases by four orders of magnitude between room and LN_2 temperature. From [85].

Fig. 16 (right) - Rough scheme of the proposed luminescent bolometer. From [37].

5   CONCLUSION AND COMMENTS

Detector developments for low energy neutrinos and dark matter have become a very active field in modern physics. The number of groups implied in such a program is quickly increasing, and unexpected breakthroughs in the near future should not be discounted. Cryogenic detectors are by now the most exciting subject, as unprecedented sensitivity and energy resolution may hopefully be reached.

Low temperature devices are expected to provide, not only a better calorimetric performance, but also a new approach to particle identification by looking simultaneously at thermal and ionization pulses. This kind of measurements would be impossible at room temperature, due to the comparatively high specific heats. Such a new window to event characterization would by itself justify the present effort in cryogenic detectors.

It is also worth noticing that the discovery of high T_c superconductors allows for the preparation of hybrid superconductor-semiconductor electronic devices [86], working in the range $4\ K\ <\ T\ <\ 70\ K$. In this way it may be possible to take advantage of the best qualities of both superconductive and semiconductor materials.

References

[1] See, for instance, Proceedings of the Moriond Workshop on Massive Neutrinos, January 1986, Ed. Frontières.

[2] M. Doi, T. Kotani and E. Takasugi, Prog. Theor. Phys. Suppl. 83 (1985).

[3] See, for instance:

E. Schatzman in the Proceedings of the Moriond Workshop on "New and Exotic Phenomena", January 1987, Ed. Frontieres.

A.J. Baltz and J. Weneser, Comments on Nuclear and Particle Physics XVIII, 227 (1988).

[4] See, for instance, T. Kirsten in [1].

[5] S.P. Mikheyev and A.Yu. Smirnov, Sov. J. Nucl. Phys. 42, 913 (1985).

S. Bertolini, in Proceedings of the $XXIV$ Int. Conf. on High Energy Physics, Munich August 1988, Ed. Springer-Verlag.

[6] J. Faulkner and R.L. Gilliland, Ap. J. 294, 954 (1985). 9 D.N. Spergel and W.H. Press, Ap. J. 299, 663 (1985).

W.H. Press and D.N. Spergel, Ap. J. 296, 679 (1985).

[7] R. Davis, Proceedings of "Neutrino 88", Boston June 1988, Ed. World scientific Pub.

[8] M.B. Voloshin, M.I. Vysotsky and L. Okun, Sov. Phys. JETP 64, 446 (1986).

[9] See, for instance, J. Bahcall et al., Rev. Mod. Phys. 54, 767 (1982).

[10] L. Gonzalez-Mestres and D. Perret-Gallix, these Proceedings.

[11] S. Raby and G. West, Phys. Lett. B194, 457 (1987).

[12] E. Carlson and L.J. Hall, preprint UCB-PTH-89/10, LBL-27202 (1989).

H. Harari, Phys. Lett. B216, 413 (1989).

G. Raffelt, in Proceedings of Telemark IV , World Scientific Pub. 1987.

[13] R.J.N. Phillips, Surveys in High Energy Physics 6, 1 (1988).

[14] M. Fritschi et al., Phys. Lett. 173B, 485 (1986).

[15] S.R. Elliot, A.A. Hahn and K.K. Moe, Phys. Rev. Lett. 59, 2020 (1987).

[16] F.T. Avignone III, R.L. Brodzinski, H.S. Miley and J.H. Reeves, Proc. APS Div. of Particles and Fields, Salt Lake City 1987, World Scientific Pub.; *Ibid.*, Science 235, 534 (1987).

[17] See, for instance, D.O. Caldwell in Procedings of the IX Workshop on Grand Unification, Aix-les-Bains April 1988, Ed. World Scientific Pub.

[18] M. Alston-Garnjost et al., Phys. Rev. Lett. 60, 1928 (1988).

[19] E. Bellotti et al., Nuovo Cimento 95A, 1 (1986).

E. Bellotti et al., Proceedings Telemark IV , World Scientific Pub. 1987.

[20] P. Fisher et al., Proceedings of "Neutrino 88", Boston 1988, Ed. World Scientific Pub.

[21] R. Davis et al., Phys. Rev. Lett. 20, 1205 (1968).

[22] Y. Totsuka, in Proceedings of the *XXIV* International Conference on High Energy Physics, Munich August 1988, Ed. Springer-Verlag, and references therein.

[23] G.T. Ewand et al., Report SNO-87-12, Queen's University, Kingston 1987.

[24] "ICARUS I - An optimized, real time detector of solar neutrinos", ICARUS Collaboration proposal 1988.
See also M. Baldo-Ceolin in the Proceedings of the Moriond Workshop on Massive Neutrinos, January 1986.

[25] BOREX Letter of intent, A.T.T. Bell-Argonne-Drexel-Hawai-MIT-Milan-Pavia Collaboration (1988).

[26] A.I. Abazov et al., SAGE Collaboration (USA-USSR).

[27] R.S. Raghavan, Phys. Rev. Lett. 37, 259 (1976).

[28] See, for instance, N. Booth and A.G. Payne, Oxford preprint (1988).

[29] N. Booth and A. de Bellefon, private communications.

[30] D. Jalabert, Rapport de Stage, ISN Grenoble 1989.

[31] L. Gonzalez-Mestres and D. Perret-Gallix, Proceedings of the "Rencontre sur la Masse Cachée dans l'Univers et la Matière Noire", Annecy July 1987, Ed. Annales de Physique (France).

[32] See, for instance, J.C. Lund et al. in [33].

[33] "Low Temperature Detectors for Neutrinos and Dark Matter - II", Ed. L. Gonzalez-Mestres and D. Perret-Gallix, Frontieres 1988.

[34] See, for instance, N. Booth et al. in [35]

[35] "Low Temperature Detectors for Neutrinos and Dark Matter", Ed. K. Pretzl, N. Schmitz and L. Stodolsky, Springer Verlag 1987.

[36] L. Gonzalez-Mestres and D. Perret-Gallix in [33].

[37] J.P. Chaminade et al., in Proceedings of the Moriond Workshop on "Tests of Fundamental Laws of Nature", January 1989, Ed. Frontieres.

[38] T. Hoshina and S. Kuboniwa, J. Phys. Soc. Japan 32, 771 (1972).

[39] Y. Tsujimoto et al., J. Lumin. 9, 475 (1975).

[40] A.K. Drukier and L. Stodolsky, Phys. Rev. D30, 2295 (1984).

[41] See, for instance, P. de Bernardis in [33].

[42] S.H. Moseley, J.C. Mather and D. Mc Cammon, J. Appl. Phys. 56, 1257 (1984).

[43] N.Coron et al., Nature 314, 75 (1985).

[44] D. Mc Cammon et al., Proc. 18th Conference on Low Temp. Phys., Kyoto 1987, Jap. J. Appl. Phys. 26, Suppl. 26-3.

[45] A. Alessandrello, D.V. Camin, E. Fiorini and A. Giuliani, Phys. Lett. 202, 611 (1988).

[46] H.H. Stroke et al., IEEE Trans. on Nucl. Sc. 33, 56 (1986).

[47] M. Buhler and E. Umlauf, Europhys. Lett. 5, 297 (1988).

[48] E. Fiorini, in [35]

[49] M.W. Goodman and E. Witten, Phys. Rev. D31, 3059 (1985).

[50] See, for instance, B.Cabrera in "Superconductive Particle Detectors", Ed. A. Barone, World Scientific Pub. 1987.

[51] D. Twerenbold and W. Rothmund, A. Zehnder in "Superconductive Particle Detectors".

[52] Th. Peterreins, F. Probst, F. von Feilitzsch, and H. Kraus, in "Superconductive Particle Detectors".

[53] P. Gare et al., ESA preprint (1988).

[54] F. Cardone and F. Celani, in [33].

[55] Th. Peterreins, F. Probst, F. von Feilitzsch and H. Kraus, in [33].

[56] H. Bernas et al., Phys. Lett. 37, 359 (1967).

[57] M. Le Gros et al., Vancouver and Landover 1989.

[58] A. Kotlicki et al. in [35]; A. de Bellefon et al. in [33]; J. Boniface et al., in [33].

[59] For a review of recent results and possible uses, see: L. Gonzalez-Mestres and D. Perret-Gallix, in [33].

[60] M. Franck et al., MPI Muenchen 1989.

[61] J. Boniface, L. Gonzalez-Mestres and D. Perret-Gallix, in Proceedings of the Moriond Workshop on "Tests of Fundamental Laws in Nature", January 1989, Ed. Frontières.

[62] Rapport de la Jeune Equipe "Neutrino-Indium" du CNRS (ENS Paris, LPC Collège de France, Ecole Polytechnique, DPhPE Saclay, IP Strasbourg, LAPP Annecy), January 1987.

358

[63] R.H. Davis, Int. J. Thermophys. 7, 609 (1986).

[64] P. Andreo, J. Garcia-Esteve and A.F. Pacheco, in [35].

[65] C. Valette, G. Waysand, Orsay report (1976).

[66] F. von Feilitzsch et al. in [35].

[67] EXTRAMET, Zone Industrielle, Annemasse (Haute-Savoie), France.

[68] E.G. Lierke and G. Griesshammer, Ultrasonics October 1967, p. 224.

[69] ECKART-WERKE, 8510 Fuerth, Fed. Rep. of Germany.

[70] HEUBACH, 3394 Langelsheim, Fed. Rep. of Germany.

[71] L. Gonzalez-Mestres and D. Perret-Gallix, Proceedings of Underground Physics 85, Ed. Il Nuovo Cimento (1986).

[72] R. Lanou, H. J. Maris and G. Seidel, in [35].

[73] G. Pickett, in [33].

[74] T.O. Niinikoski, in preparation and Proceedings of the "Rencontre sur la Masse Cachée dans l'Univers et la Matière Noire", Annecy July 8-10, 1987 (Annales de Physique, France).

[75] D. Robbes, in [33].

[76] S.M. Sze, "Physics of Semiconductor Devices", John Wiley and Sons 1981.

[77] B. Jacquier, in [33].

[78] J. Lindhard et al., K. Dan. Vidensk. Selsk. May.-Fys. Medd. 33, 10 (1963); 36, 10 (1968).

[79] See, for instance, D.M. Ritson, Techniques of High Energy Physics, Interscience Pub. 1961, and references therein.

[80] L. Gonzalez-Mestres and D. Perret-Gallix, Nucl. Instr. Meth. A279, 382 (1989).

[81] F. Rogemond, Thesis Lyon 1976.

[82] B. Jacquier, private communication.

[83] J. Mares, B. Jacquier, C. Pedrini and G. Boulon, Rev. Phys. Appl. 22, 145 (1987).

[84] R. Stucki, Diplomarbeit, Physikalisches Institut Bern 1989.

[85] Hj. Bernhardt, Phys. Stat. Sol. (a) 91, 643 (1985).
    W. Van Loo and D.J. Wolterink, Phys. Lett. 47A, 83 (1974).

[86] T. van Duzer, Cryogenics 28, 527 (1988).

Conventional Techniques for Dark Matter Detection

G.Gerbier

DPhPE, CEN Saclay, France

Abstract : Direct dark matter searches with conventional techniques have yielded their first results. Experiments using Germanium detectors have already eliminated Dirac neutrinos of masses greater than 11 Gev/c^2. Here, we describe a new experiment using Silicon, that is sensitive to lower masses particles like cosmions. Emphasis is placed on the energy calibration, an essential step to measure the rates as a function of energy. The results of this calibration, obtained for kinetic energies between 5 and 14 keV, agree well with the LSS theory. We also describe the Saclay project to construct a low pressure Hydrogen TPC (Time Projection Chamber). This detector would be sensitive to cosmions with spin dependent interactions .

Introduction

Current wisdom in astrophysics requires the presence of non radiating matter (dark matter) in the universe. Baryonic matter forming faint astronomical objects ("brown" dwarfs, black holes...) could probably account for most of the observational data (rotation curves of galaxies, velocity distributions in clusters and super clusters). However, the inflation scenario of the evolution of the primordial universe and galaxy formation models lead to the conclusion that baryonic matter is not enough. Other non baryonic particles, so called Weakly Interacting Massive Particles (WIMP's), with a mass above a few GeV, and interaction cross section in the 10^{-36}-10^{-40} cm^2 range, are needed to close the universe and to allow for galaxy formation. These particles could be directly detected in laboratory through their elastic scattering with nuclei [1]. However the expected recoil energies are small (keV range), the expected rates of interactions are low (few events/kg/keV/day, see details in section 1), so low energy threshold and low background detectors are needed.

The detectors which are being currently developed for this purpose can be divided roughly into 2 categories:

- conventional ionisation non-cryogenic detectors,
- cryogenic detectors.

While detectors of the first type detect energy quanta in the eV (electron-hole pairs in semiconductors) to 10 eV range (electron-ion pairs in gazeous detectors) those in the second one detect quanta of much lower energy (10^{-5} eV for the phonons in a bolometer, for example). The second type has therefore a much higher potential energy resolution and lower threshold but, so far, the required resolution has not been achieved for massive detectors (i.e. higher than a few grams) .

The present paper concentrates on 2 experiments involving the first type of detectors; one is based on Silicon and the other uses hydrogenous gas.

Semi-conductors have been developed for many years and high purity Silicon and Germanium crystals can be easily obtained; Germanium detectors have already been used to search for dark matter particles [2,3]. In section 2, a new experiment with Silicon involving a collaboration between UC Santa Barbara, Lawrence Berkeley Laboratory , UC Berkeley and Saclay will be briefly described with emphasis on the energy calibration of the detectors. Preliminary results on silicon detector calibration achieved by the Saclay group will be presented.

On the other hand, gazeous detectors could also be used as dark matter detectors, either in calorimetric mode at atmospheric or high pressure [4] or in tracking mode at low pressure [5,6]; low pressure is necessary in order that the recoiling nucleus have a sizeable range in the gas. This provides in principle the direction of the track, a beautiful signature of the galactic origin of the interacting particle. The Saclay project [5] of low pressure hydrogen Time Projection Chamber (TPC) will be briefly presented in section 3.

1 Expected kinematics and event rates

The hypothesis that dark matter particles are gravitationally trapped in the galaxy leads to the conclusion that, like the earth, they have velocities of about 300 km/s. Then, the mean kinetic energy E_r received by a nucleus of mass M_n in an elastic collision with a dark matter particle of mass M_x is:

$$E_r \approx 2 \, keV \, M_n \left(\frac{M_x}{M_x + M_n}\right)^2 \quad (1)$$

The energy distribution is roughly exponential [7].

Expected event rate depend on the local density of dark matter particles, generally estimated to be of order 0.4 GeV/cm^3 [8], on their mean velocity of 300 km/s and on their interaction cross section. Expected cross sections on the basis of astrophysical arguments are of the order of 10^{-38} cm^2 [1]. However, in the case of spin independent interactions (vector couplings), effective cross sections on nuclei may be enhanced by a factor of order Z^2 [1]; this is the case for heavy Dirac neutrinos for example. In the case of spin dependent interactions (axial-vector couplings), e.g. photinos, the cross section is proportional to $J(J+1)$ where J is the spin of the nucleus, which is zero for most of the natural even Z even A nuclei, in particular for the abundant isotopes of Silicon and Germanium.

Other candidates include the so called cosmions, particles invented to solve the solar neutrino puzzle [9]. The characteristics of these particles are strongly constrained in order for the mechanism of cooling of the solar core to work: their mass would fall in the 4-10 GeV range and the effective cross section averaged over the various nuclei of the Sun of the order 10^{-36} cm^2. Cosmions are obviously more readily accessible to observation/elimination as their cross sections are 2 orders of magnitude higher than previous candidates.

However, what is important for laboratory detection is the actual cross section for a specific nucleus. Actual cross sections on various nuclei depend very much on the characteristics of the interaction which is considered: coherence effect, spin and isospin nature of the coupling, magnetic coupling... So expected rates have to be evaluated in the framework of specific models and not just in terms of vector/axial-vector couplings [10]. For example, in the case of the Raby and West magnino model [12], expected rates with a Silicon target are of the order of 200 events /kg/day and 8 events /kg/day on Hydrogen while they are respectively 0 and 200 events /kg/day in the case of a simple axial vector coupling.

The experiments presented in the following are designed for the detection of cosmions.

2 Semiconductors

Semiconductor Germanium detectors as dark matter particles detectors have already put limits on cross sections and masses of WIMPs[2,3].

The original aim of the UCSB/LBL Germanium experiment was the search for double beta decay. The detector consisted of 8 crystals of 900 g each installed in the underground site of Oroville Dam (California); 2 of the 8 crystals were modified to measure energies down to a few keV, the expected energy deposited in dark matter particle interactions (see section 1). Passive shielding,

active NaI anticoincidence counters and careful choice of low radioactivity materials reduced the background level to 3 counts/keV/kg/day in the 4-20 keV region. Most of this residual background is due to activity inside the Ge itself and comes from beta decay of tritium, a spallation product from cosmic ray interactions with the Ge nuclei.

Fig. 1 shows the exclusion plot for the mass and interaction cross sections of WIMPs obtained by this experiment [3]. Dirac neutrinos with masses above 11 GeV/c^2 have been excluded, but the cosmions are not eliminated because of their low mass.
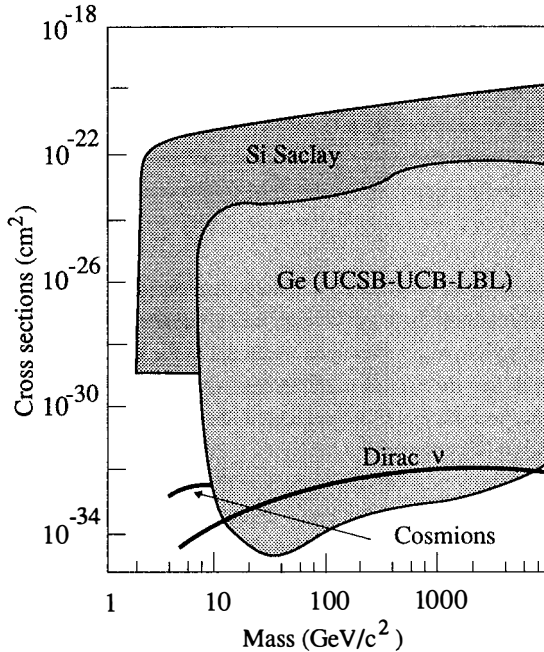
Figure 1: Exclusion plot for the mass and interaction cross section of WIMP's from the UCSB/LBL/UCB Ge experiment [3] and Si Saclay experiment [15] .

- **UCSB/UCB/LBL/Saclay silicon experiment**

In order to investigate the 4-10 GeV/c^2 cosmion mass range, silicon has been found to be better adapted than Ge [11]. The 2 main reasons are that:

- its lower mass is better matched to the expected cosmion mass range, which means higher recoil energies (see formula 1),
- Si has a higher ionisation efficiency than Ge.

Four Silicon crystals of 15 g each have already been installed in place of 2 Ge cristals. No special care has been taken in the choice of these crystals and the background level measured in a

recent engineering run is high : 20 counts/keV/kg/day. Even so, the rate is lower than that expected from cosmions. Fig. 2 shows the rate as a function of measured energy in a typical cosmion model, the Raby West magnino model [11,12]. This model and probably others could be excluded soon, for all masses between 4 and 10 GeV/c^2.
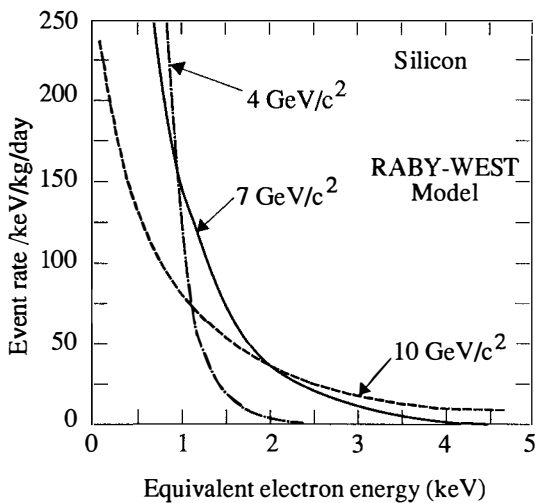

Figure 2: Expected event rate in a silicon detector from the Raby West model [12] for 3 masses of cosmions as a function of the equivalent electron energy, that is, the ionisation energy actually measured in a silicon detector calibrated with X rays.

These conclusions depend crucially on the knowledge of the response of the detectors to nuclear recoils in the keV range; semi conductors are commonly used as X ray detectors and can be easily calibrated with known X ray sources. In dark matter searches, the signal is provided by the recoil of the (Si,Ge) nucleus against the WIMP, which has been shown to be less efficient to produce electron hole pairs than a photo-electron of the same kinetic energy. Fig. 3 shows the relative ionisation (nucleus/electron) α as a function of the kinetic energy of the particle. Data [13] have been obtained down to 20 keV and agree reasonably well with the predictions from a statistical model by Linhard et al. (LSS theory [14]); under 20 keV, this ratio α is predicted to decrease even more with the energy; these predictions were used in Fig. 2 to convert the kinetic energy of the silicon recoil into the ionisation energy actually oberved in the Si detector (equivalent electron energy) down to 0.6 keV. However, no calibration data existed in the region of interest between around a few kev and 20 keV kinetic energy.

Preliminary results concerning this measurement down to 5 keV kinetic energy will be described in the following.
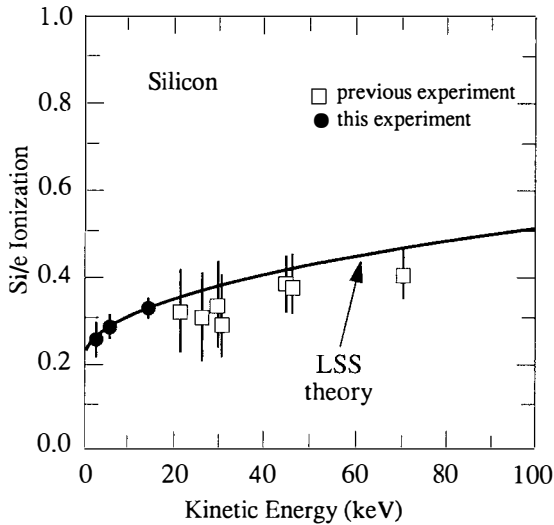
Figure 3: Ratio between the ionisation produced by a Si recoil and the ionisation produced by an electron of the same kinetic energy as a function of the kinetic energy. The data are from Sattler [13], the LSS theory refers to predictions by Lindhard et al. [14]

- **Method of calibration**

To obtain the response of silicon detector to nuclear recoils below 20 keV, we have used the same method as Sattler [13], namely the elastic scattering of neutrons off a silicon nucleus. Among known particles, neutrons are indeed the closest to the WIMP's, by their mass and charge, but have strong cross sections, which is indeed an advantage for calibration.

Neutrons were produced by the following (p,n) reaction:

$$p + {}^7Li \rightarrow {}^7Be + n$$
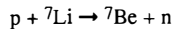
The threshold of the reaction is at E_p=1.850 MeV. Protons are provided by a Van de Graaf machine at Bruyères Le Chatel (CEA, France) with a tunable energy up to 4 MeV and an energy resolution of a few keV. The ^7Li target is made by evaporation on a Tantalum support. Neutrons are produced at all angles relative to the incident proton beam; at a given angle, the neutron energy is fixed by the kinematics of the production reaction. The machine can be operated in a continuous mode or in pulsed mode (frequency 2.5 Mhz). The advantage of the pulsed beam will appear in the following.

Two methods can be used to perform the calibration:

— measuring all the recoils occurring inside the crystal; the spectrum is expected to be a flat distribution with an end point corresponding to the maximum recoil energy given by:

$$E_{max} = 4 \frac{M_{Si}M_n}{(M_{Si}+M_n)^2} E_n \quad (2)$$

where M_{Si} is the mass of the Si nucleus, M_n is the mass of the neutron and E_n the energy the energy of the incident neutron. This method used by Sattler is not very accurate because the expected sharp drop at the end of the spectrum is washed out by the resolutions of the detector and of the incident neutron energy.

— selecting only the recoils produced by neutrons scattered at a given angle; this requires the detection of the scattered neutron with reasonable efficiency. A big advantage of this method, in conjunction with the use of the pulsation of the beam, is that the requirement of a double time coincidence between the beam, the silicon signal and the scattered neutron counter allows a good background rejection. This is the method we have used.

- Calibration results

The incident proton energy was 1980 keV; the neutrons produced at angle 0 ° relative to the proton beam had a mean energy of 200 keV with a dispersion of about 6 keV. With a target thickness of 140 $\mu g/cm^2$, and an incident proton beam intensity of 5 μamps, typical fluxes of 2 10^7 neutrons/sec/sr have been obtained.

The silicon crystal that we used for this calibration was provided by the LBL group; it is 6 mm diameter, 3 mm thickness and mounted in a cryostat cooled to liquid nitrogen temperature. The mounting was done in such a way as to reduce as much as possible the amount of material surrounding the crystal in order to minimize the indirect component of neutrons scattering before reaching the silicon. The drawback of this mounting was a degraded energy resolution (380 ev FWHM) compared to the state of the art (100 eV FWHM).

The scattered neutron counter (named S1 afterwards) consisted of a block of NE110 plastic scintillator viewed by 2 photomultiplier tubes XP 2020, operated in coincidence. A typical efficiency of 70 % was measured at 100 keV. A parrafin collimator was used to shield the counter against direct neutrons from the target.

Calibration of the silicon / peak sensing ADC chain was done with the 59.6 and 13.9 keV X-ray lines from a source of Americium. The energy resolution of the silicon diode was measured to be about 170 eV (sigma).

The trigger requires a coincidence between the silicon signal and the S1 counter; relative times of these signals to the beam pulsation (when available) were recorded together with the amplitude of the silicon detector signal and the data from a neutron monitoring counter.

Three calibration points have been obtained; they correspond to silicon recoil energies of 13.5, 6.9 and 5.0 keV obtained by measuring the scattered neutron at angles 90°, 60°, 50° respectively, relative to the incident proton direction. Unfortunately, due to problems with the Van de Graaf machine, the pulsed beam was not available for the 2 last calibration points at 6.9 and 5.0 keV.

For the first point (13.5 keV), Fig. 4 shows the distribution of the time difference between the beam pulsation and the S1 signal; shown in shaded is the expected background contribution due to accidental coincidences between the Si and the S1 counter. For the in-time neutron triggers, this time represents the total time of flight of the neutron from the target to the neutron counter after scattering on a silicon nucleus; the neutron peak at 160 ns corresponds to the expected time of flight of scattered neutrons. The thin first peak, a few ns after the beam pulse is due to gamma rays produced by the protons stopping in the Tantalum support of the target.

Fig. 5 shows the pulse height distribution of the Silicon signal corresponding to the neutron peak of Fig. 4; the expected contribution from accidentals, shown in the shaded histogram is indeed low. After background substraction, the signal distribution has been fitted to a gaussian shape, from which we deduced a mean energy of 4.4 keV, and a width (sigma) of 0.9 keV. The mean recoil energy of the silicon nucleus has been deduced from the incident energy of the proton, the neutron production kinematics and the scattering angle of the neutron; corrections due to the dispersion of the incident proton energy and to the thickness of the target have been applied, and lead to a mean recoil energy of 13.5 keV. This estimation is confirmed by the neutron time of flight measured in Fig. 4. The same calculations have been done for the two other points.

Previously cited corrections also contribute to the dispersion of the recoil energy of the Si nuclei and to the width of the measured signal. After taking into account these corrections and also the effect of the size of the detectors and the intrinsic detector resolution, we estimated the expected width of the signal to be around 0.5 keV which is definitely lower than the observed one. Systematic effects like secondary scattering of neutrons in the various shieldings, and material in the path of the neutron (cryostat) have been investigated by computer simulation and found to be negligible.

This preliminary analysis suggests that there may be large fluctuations in the way the energy is deposited by the recoiling Si nucleus inside the crystal. This needs further investigation in subsequent runs. The LSS theory does not provide any reliable calculation of this dispersion at such small recoil energies.

As already mentioned above, the pulsed beam was not available in a later run where we studied the 6.9 and 5.0 keV points, so we could not apply the time of flight selection to the data. Fig. 6 and 7 show the pulse height distributions for the two runs at angles 50° and 60°. Also shown are the expected background distributions due to accidentals, normalised to the signal distribution well above the expected signal energies. A clear peak can be observed in the 6.9 keV run from which we deduced a mean ionisation energy of 1.9 keV and a width again larger than expected. Data are of inferior quality for the last run because of the high accidental background and the proximity of the electronic noise which starts creeping up at 0.6 keV. Taking into account the expected width of the distribution from the previous runs, we estimated a mean ionisation energy of 1.2 keV, with a systematic uncertainty of 0.2 keV.

The 3 calibration points shown on Fig. 3 agree well with the LSS predictions; this justifies the calculation shown on Fig. 2 down to an equivalent electron energy of 1.2 keV.
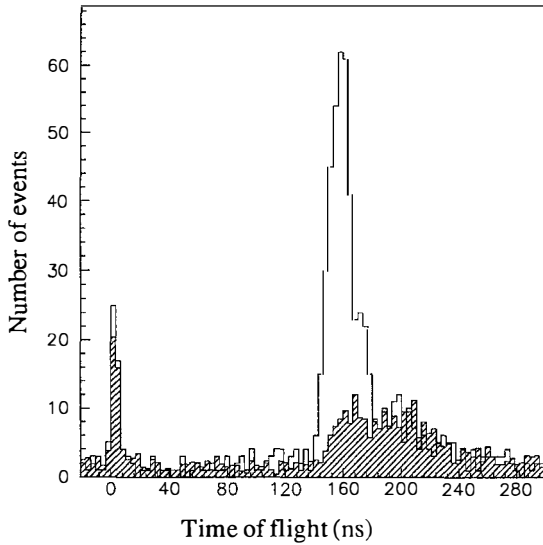
Figure 4; Neutron scattering angle = 90°, E_r=13.5 keV. Distribution of S1 neutron counter times relative to the beam pulse: the full histogram is for the good in-time neutron triggers; the shaded histogram shows the expected contribution from coincidences between uncorrelated counts in Si and S1 . Interpretation of the peaks is explained in the text.
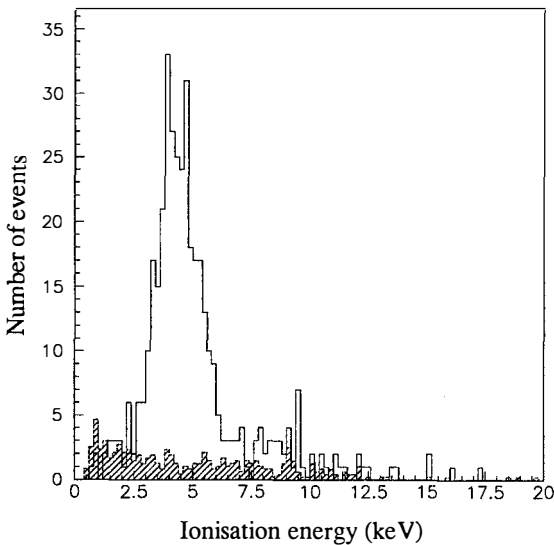

Figure 5: Neutron scattering angle = 90°, E_r=13.5 keV. Distribution of the pulse height of the signals seen in the Si cristal after selection of the neutron events inside the neutron time of flight window on Fig . 4. Shaded histogram shows the contribution from the background.
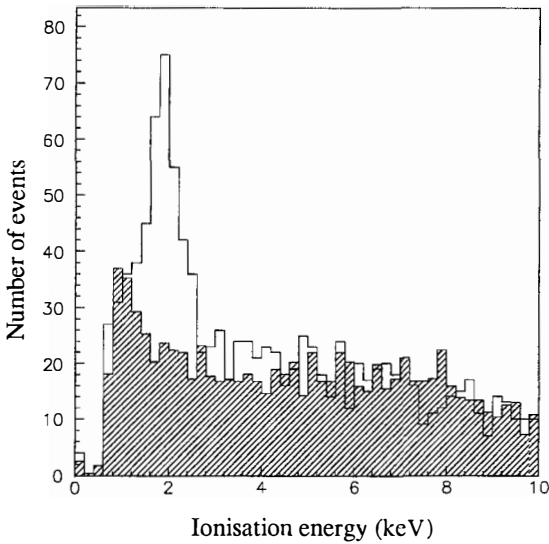
Figure 6: Neutron scattering angle = 60 °; Er=6.6 keV. Distribution of the pulse height of the signals seen in the Si cristal; no time of flight selection was made in this run as the beam pulsation was not available.
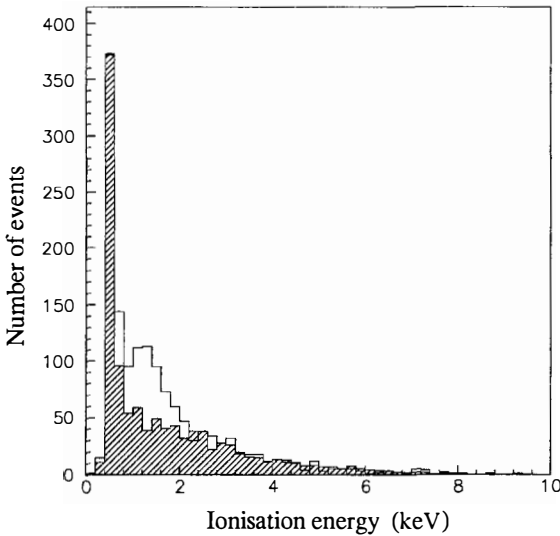

Figure 7 : Neutron scattering angle = 50 °; Er=5.0 keV. Distribution of the pulse height of the signals seen in the Si cristal; no time of flight selection was made in this run as the beam pulsation was not available.

3 TPC project

What is going to be sketched in the following is more extensively described in the reference 5.

The use of protons rather than heavy nuclei as the target offers some theoretical advantages. This is especially the case for cosmions interacting on the nuclei of the Sun. An experiment using hydrogen that was sensitive to such particles could rule out the cosmion hypothesis independent of assumptions about their cross section on heavy nuclei.

For cosmion scattering on hydrogen, the total rate is near 0.2 events/g/day. The density of H_2 at atmospheric pressure is 90 g/m^3, but, for the background reasons discussed below, it may be advantageous to work at low pressure (0.02 atm) where the H_2 density is 2 g/m^3. Hence, cosmions can be studied with low-pressure counters [16] in the form of a time-projection-chamber (TPC) of a few m^3. It would, however, require a considerable effort to construct a TPC sensitive to photinos, which have cross sections at least two orders of magnitude smaller.

The background will come from Compton scatters of gamma rays due to the ambient radioactivity. In the keV range, the lowest rate achieved for this process is of order 10^{-3} counts /g/keV/day in the germanium diode detectors described in the previous section. For proportional chambers, the lowest rates are near 10 counts /g/keV/day in the 1 cm^3 counters used in radiochemical solar neutrino experiments [17]. Fortunately, the use of a low pressure TPC placed in a 0.1 Tesla magnetic field might eliminate much of the Compton background since Compton electrons will spiral in tight orbits while recoil protons of the same energy will have a much straighter trajectory. The range for a 1 keV proton in 0.02 atm H_2 is roughly 1cm.

In addition, the galactic origin of the recoil protons can be established because their direction is preferentially opposite the direction of the movement of the solar-system through the galaxy [18]. The recoil direction can be determined in a TPC from the ionization pattern since, in the keV range, specific ionization falls with decreasing energy [19].

Work now in progress at Saclay (and also at San Diego [6]) should determine if proton recoil with keV energies can be seen in a low pressure TPC and if it is possible to achieve sufficiently low background.

Conclusion

The technique of calibration we have used for Silicon is very well adapted and provides clean results when the pulsed neutron beam is available. This technique can actually be used with the same efficency for the calibration of any dark matter detector using heavy nuclei.

Experimental calibration points obtained between 5 kev and 14 keV recoil energies agree well with the LSS theory. The results at 5 keV will be checked in a future run in order to reduce the uncertainty, and lower energies will be investigated.

When associated with these calibration result, the preliminary measurements of background levels in Silicon crystals at Oroville Dam tend to eliminate the cosmions of the Raby and West model for masses down to 4 GeV/c^2. Final measurements will be done with very low activity crystals; to

370

reduce the tritium background, these crystals will be shielded from cosmic rays from their fabrication to their actual installation underground.

Cosmions with only spin dependent interactions could be studied with a Time Projection Chamber filled with low pressure hydrogenous gas. Tests of feasibility are under way.

References

1. M.W. Goodman and E. Witten , Phys. Rev. D31 (1985) 3059

2. S.P. Ahlen et al., Phys. Lett. B195 (1987) 603

3. D.O. Caldwell et al., Phys. Rev. Lett. 61 (1988) 520

4. V.Pomanski, private communication.

5. J. Rich and M. Spiro, Saclay Report DPhPE 88-04 (1988)

6. G. Masek, communication at the Particle Astrophysics Workshop , Berkeley 1988

7. J. Rich, in Dark Matter (Moriond, 1988), edited by J. Audouze (éditions Frontières)

8. D.N. Schramm, Nucl. Phys. B252 (1985) 53
   J. Silk, in Dark Matter (Moriond, 1988), edited by J. Audouze (éditions Frontières)

9. J. Faulkner and R.L. Gilliland, Astrophys. J. 299 (1985) 994
   D.N. Spergel and W.H. Press, Astrophys. J. 294 (1985) 663
   W.H. Press and D.N. Spergel, Astrophys. J. 296 (1985) 679
   R.L. Gilliland et al., Astrophys. J. 306 (1986) 703

10. C. Tao, F. Martin, J. Kaplan, private communication, paper in preparation.

11. B. Sadoulet et al., Astrophys. J. 324 (1988) L75

12. S. Raby and G.B. West, Nucl. Phys. B292 (1987) 793; Phys. Lett. B194 (1987) 557; Phys. Lett. B200 (1988) 547

13. A.R. Sattler, Phys. Rev. 138 6A (1965) 1815

14. J. Lindhard, M. Scharff and H.E. Schiott, Kgl. Dan. Vidensk. Selsk. Mat.-Fys. Medd. 33 (1963) 14; J. Lindhard, V. Nielsen, M. Scharff and P.V. Thomsen, loc. cit. 33 (1963) 10

15. J.Rich, R. Rocchia and M. Spiro, Phys. Lett. B194 (1987) 173

16. A. Breskin, Nucl. Inst. and Meth.196 (1982) 11

17. T. Kirsten in '86 Massive Neutrinos in Astrophysics and in Particle Physics', ed O.Fackler and J.Tran Than Van (Editions Frontières, 1986)

18. D.N. Spergel, Phys. Rev. D37 (1988) 1353

19. V.V. Verbinski and R. Giovanini, NIM 114 (1974) 205

IMPLICATIONS OF A SUB-MILLISECOND
PULSAR IN SN1987A[*]

Arnon Dar

Department of Physics and Space Research Institute,

Technion-Israel Institute of Technology, Haifa 32000, Israel.

ABSTRACT

The neutrino burst from SN1987A, that was detected by the KAMIOKANDE
II and the IMB underground water Cerenkov detectors on Feb. 23, 1987 also con-
tained evidence for pulsed emission of neutrinos after the first ~ 400 milliseconds
with a period identical to that of the sub-millisecond optical pulsar in SN1987A
that was discovered on Jan. 18, 1989. Implications of the optical and neutrino
observaions for astrophysics, nuclear physics and particle physics are pointed out.
In particular, the optical observations impliy a soft nuclear equation of state at
supernuclear densities while the neutrino pulsation implies that the mass of the
electron neutrino is less than 0.05 eV, its electric charge is less than $3 \times 10^{-20}e$ and
it can have a magnetic moment between $10^{-12}\mu_B$ and $10^{-10}\mu_B$ which can solve
the solar neutrino problem.

A SUB-MILLISECOND OPTICAL PULSAR IN SN1987A?

On Feb. 10, 1989 Middleditch et al.[1] reported the discovery of an optical pulsar in SN1987A with a period of $P = 0.50796772$ ms (barycentric). Detection was made with the Cerro Tololo 4-m telescope on Jan. 18 using a silicon photodiode with a sampling rate of 5 kHz. The frequency of the pulsar during the 7-hr observation between Jan. 18.1-18.3 UT was tracked by dividing the data into 15 independent half hour runs. The statistical significance during these runs ranged from 11 to 37 standard deviations. The frequency exhibited a sinusoidal modulation; the 15 frequency measurements were within 5% (rms) of a sine function with a central value of $f = 1968.629$ Hz (barycentric), amplitude $\Delta f = 1.5 \times 10^{-3}$ Hz and a period of 8-hr. The optical pulsation has not been detected by subsequent observations of SN1987A neither by the same group nor by other groups. But the spectacular pulsation (11 to 37 s.d. effect) in each of the 15 half-our runs and the fact that no pulsation was observed when the telescope was pointed at other objects strongly suggest that a half-millisecond pulsar is embeded inside SN1987A and that the conditions near the neutron star are changing rapidly. What are the implications of these optical observations ?

ASTRONOMICAL AND ASTROPHYSICAL IMPLICATIONS

1) THE RADIUS OF THE NEUTRON STAR : An upper bound on the radius R of the neutron star can be easily obtained as follows. The breakup angular velocity for a rotating neutron star is the Keplerian angular velocity Ω_K at the equator, since a faster rotation will produce a centrifugal force at the equator greater than the gravitational binding force there and cause mass ejection from the equator. Consequently

$$\Omega_K = (GM/R^3)^{1/2} \geq \Omega = 2\pi/P = 1.239 \times 10^4 \text{ rad/sec} , \qquad (1)$$

and

$$R \leq 10.6 \times (M/M_\odot)^{1/3} \text{ km.} \tag{2}$$

The precise value of the radius (the shape) of the neutrom star is dificult to deduce. It depends on the mass, the angular momentum and the equation of state of the neutron star which are not well known. Moreover, rapidly rotating configurations in general relativity are technically difficult to construct. In addition, no simple stability criteria are known. Published computations (see e.g. Friedman et al.[2]) confined themselves to uniformly rotating neutron stars and nuclear equation of states that employ only hadronic degrees of freedom. Only the very soft nuclear equation of states admit stable solutions with angular velocity $\Omega = 1.239 \times 10^4$ rad/sec . The corresponding masses are around $1.4 M_\odot$ which are consistent with measurements of neutron star masses in binary systems[3], and the radii are $R = 8 \pm 1$ km . It will be very interesting to see whether lattice QCD and/or high energy heavy ion collisions will yield such soft nuclear equation of states at supernuclear densities.

2) THE MAGNETIC FIELD NEAR THE NEUTRON STAR: From the observation of the bolometric light curve (UV to IR) of SN1987A with the 111.3-day exponential decline characteristic of the radioactive decay $^{56}Ni \rightarrow ^{56}Co \rightarrow ^{56}Fe$ of $\approx 0.07 M_\odot$ ^{56}Ni that has not slowed down yet[4], one may conclude that the emission of magnetic dipole radiation by the pulsar must be smaller than 3×10^{37} ergs/sec . Consequently[3]

$$\dot{E}_{EM} \sim B^2 R^6 \Omega^4 \sin^2\alpha/6c^3 \leq 3 \times 10^{37} \text{ erg/sec} , \tag{3}$$

where B is the magnetic field at the surface of the neutron star, R is its radius,

and α is the angle between the dipole moment and the axis of rotation. Thus for $R = 8 \pm 1$ km one obtains $B \leq 6 \times 10^9/\sin^2\alpha$ Gauss .

3) A NEUTRON STAR WITH A COMPANION?: If the sinusoidal fequency modulation of the pulsar with an amplitude of $\Delta f \approx 1.5 \times 10^{-3}$ Hz and an 8 hr period is a Doppler shift due to the orbital motion of the pulsar (mass M) which is induced by a companion star (mass m) then Kepler laws for a circular orbit yield the simple relation

$$m \sin i = (P_{orb}/2\pi G)^{1/3} c(\Delta f/f)(M + m)^{2/3} . \tag{4}$$

where i is the inclination angle of the orbital plane to the line of sight. A nearly circular orbit is suggested by the fact that the frequency modulation is sinusoidal within 5% accuracy, i.e. the eccentricity of the elliptical orbit satisfies $\epsilon \leq 0.05/2 = 0.025$. Thus the companion mass is probably $\sim 10^{-3}M_\odot$ unless we are observing the system from very near the orbital axis.

The distance between the pulsar and the companion can also be estimated from Kepler's law

$$D = (G[M + m])^{1/3}(P_{orb}/2\pi)^{2/3} \approx 1.5 \times 10^{11}(M/1.4M_\odot)^{1/3} \text{ cm} . \tag{5}$$

This distance is much smaller than the estimated radius of Sanduleak -69^0202 which is thought to be the progenitor of SN1987A. Furthermore, the fragmentation of a rapidly rotating core, which was invoked to explain the time gap in the neutrino events that were detected by KAMIOKANDE II[5], cannot produce a nearly circular orbit with a radius much larger than that of the rotating core.

A SUB-MILLISECOND NEUTRINO PULSAR IN SN1987A?

Is there evidence for the formation of a half-millisecond pulsar in the supernova explosion SN1987A from the neutrino observations of the explosiom on Feb. 23, 1987 with the KAMIOKANDE II (KII) detector and the IMB detector[6]?

Standard supernova (SN) theory[3] does not lead to neutrino pulsation following gravitational collapse. Moreover, rotation is not stable neither during the hydrodynamical phase of core-collapse, which spins up the core, nor later when a significant gravitational mass is radiated away by neutrino emission. However, it is not inconceiveable that after the fast hydrodynamical phase, which according to recent two-dimensional hydrodynamic calculations[7] of gravitational collapse of fastly rotating cores may last as much as 200-ms, accretion onto the protoneutron star which rotates with breakup velocity and radiates neutrinos, stabilizes the rotation. Moreover, since neutrino emission by gravitational collapse is still a virgin field, both observationally and theoretically, it may be worthwhile to search for periodicity in the neutrino burst inspite of theoretical reservations.

If neutrino emission from a gravitational stellar collapse is pulsed, should we expect neutrino pulsation to have a period similiar to that of the optical pulsar two years later? This question is addressed next before we present our search for periodicity in the neutrino burst from SN1987A on Feb. 23, 1987.

In all cases where timing observations have been carried out over intervals of a year or longer, it has been found[8] that pulsar periods are gradually lengthening, with typical derivatives $\dot{P}$ around 10^{-15}. An upper limit on the secular change of the pulsar period in SN1987A can be estimated from the 8-hr sinusoidal modulation of the optical period: The rms deviation from the sinusoidal modulation during 8-hr was 5%. Consequently,

$$\dot{P} = P^2\dot{f} \leq P^2 \times 0.05 \times \left(1.5 \times 10^{-3}/8\right) \approx 6.7 \times 10^{-16} . \tag{6}$$

With such a secular change the relative change in the period between the neutrino detection by the KII and IMB detectors and the optical detection of the pulsar 694 days ($\approx 6 \times 10^7$ sec) later could have been $\Delta P/P \leq 8 \times 10^{-5}$. However, if the magnetic dipole radiation is the dominant spin-down mechanism then $\dot{E}_{EM} = \dot{E}_{rot} = I\Omega\dot{\Omega} \leq 3 \times 10^{37}$ erg/sec , where $I \sim 1.4 \times 10^{45}$ erg/sec is the moment of inertia of the pulsar and $\Omega = 2\pi/P$ is its angular velocity. Hence

$$\dot{P} \leq \dot{E}_{EM}P^3/4\pi^2 I \approx 7.1 \times 10^{-20} , \tag{7}$$

and $\Delta P/P \leq 8.4 \times 10^{-9}$. Such a small change has no visible effect on our results below.

The Doppler shifts in P due to the rotation of Earth around the sun and the spining of Earth are significantly larger: On Feb. 23.316 UT, 1987 the projected velocity of Earth in the direction to SN1987A was $v_p \approx 0.69$ km/sec at KAMIOKA and $v_p \approx 0.91$ km/sec at the IMB detector. The Doppler effect would have shift the barycentric period P of the pulsar by $\Delta P \approx -(v_p/c)P \approx -2.3 \times 10^{-6}P$ at KAMIOKA, and by $\approx -3 \times 10^{-6}P$ at IMB, respectively, on Feb. 23.316 UT, 1987.

General relativistic effects may produce a significant shift between the neutrino period and the optical period two years later. Even if the rotation of the neutron star has not practically changed since its birth the neutrinos and the photons two years later experience a different gravitational potential which produces the following gravitational shift:

$$\Delta P/P = \Delta\Phi/c^2 , \tag{8}$$

where $\Delta\Phi$ is the difference in the gravitational potential felt by them when they are

emitted. The difference in the gravitational potential at the surface of the neutron star during the neutrino emission after core collapse and two years later when the ejecta of the explosion have expanded to quite a large distance can be estimated from published calculations of density profiles of the expanding shell following core collapse[9]. It yields $10^{-5} < \Delta P/P < 10^{-4}$. (The exact value cannot be estimated reliably.) Note that the gravitational shift yields a longer neutrino period than the optical period two years later while energy losses lengthen the pulsar period. But, according to our estimates the energy losses of the pulsar are quite insignificant. Therefore, we expect a neutrino period which is slightly larger than the optical period that was found two years later. How to search for such neutrino period?

Because only the relative arrival times of the neutrinos from SN1987A that were detected by the KAMIOKANDE II detector (KII) on Feb. 23, 1987 were measured with sufficient accuracy, and because one does not expect the neutrino events during the first few hundreds milliseconds to have already the periodicity of the optical pulsar, I adopted the following strategy: I computed the arrival phases of the neutrinos which were detected by KII after the first 400-ms by folding their arrival times, relative to the last event with a periodicity P_ν , i.e., I divided the arrival times of the neutrinos in the detector relative to the last event, $\Delta_{li} \equiv t_l - t_i$, by the period P_ν and subtracted the nearest integer:

$$r_i = \Delta_{li}/P_\nu - N(\Delta_{li}/P_\nu) . \tag{9}$$

From the phases r_i I calculated their mean values $\bar{r}$ and the mean square deviation

$$s \equiv \Sigma_i(r_i - \bar{r})^2/n , \tag{10}$$

where the summation extends from 1 to n. If the neutrinos arrived with a peri-

odicity P_ν, their phases peak around 0 (and around 1/2 if neutrinos are emitted from two opposing magnetic poles and they both intersect the line of sight during a single period). If they arrive randomly then their phases are uniformly distributed between -1/2 and +1/2, their m.s.d. for large n tends to 1/12 and the probability that $s \leq x$ for $x \ll 1$ is given to a very good approximation by

$$P_n(s \leq x) \approx (x\pi n)^{n/2}/(n/2)! . \qquad (11)$$

Fig.1 presents plots of s as function of P_ν around $P_\nu \sim P$. Fig.1 shows that s has a deep minimum at $P_\nu = 0.50797653$ ms , i.e. when $(P_\nu - P)/P \approx 1.7 \times 10^{-5}$. In Table 1 I listed the times of the KAMIOKANDE and IMB events and their phases r_i, for that period. These phases are also plotted in Fig.2 Table 1 and Fig. 2 show that for $P_\nu = 0.50797653$ ms the KII and IMB events after the first 400 ms are peaked around r=0, while they are uniformly distributed for $P_\nu = P$. At the minimum $s = 4.86 \times 10^{-3}$ for KII and $s = 1.2 \times 10^{-2}$ for IMB, respectfully. The chance probabilities that such values of s are produced by a uniform distribution are less than 10^{-5} and 2×10^{-3} , respectfully. The probability that such values of s will be found within $\Delta P/P \leq 2 \times 10^{-5}$ is less than 10^{-3}. Therefor we conclude that the neutrino events from SN1987A that were detected by KAMIOKANDE II after the first 400-ms from the begining of the burst suggest that neutrino emission was pulsed with a periodicity $P_\nu = 0.50797653$ ms , similiar to that of the optical pulsar in SN1987A.

We note that previous searches[10] of periodicity in the neutrino burst from SN1987A have not looked for sub-millisecond periods, employed neutrino arival times which were rounded to 0.1-ms, required that even the first events (in the first 400-ms) had the same periodicity and consequently failed to discover the

0.50797653-ms neutrino periodicity. If for instance, one uses in Eq. 4 the period P instead of P_ν, one obtains a broad distribution which is not peaked around r=0, as shown for comparison in Fig. 2b.

It is difficult to conceive mechanisms which yields pulsed emission of neutrinos from supernovae explosions but it is not inconceivable. For instance, pulsars are believed to be rotating neutron stars with a magnetic dipole moment oriented at a non zero angle α to the rotation axis[1] . If the electron neutrino has a small anomalous magnetic moment in the range $10^{-12}\mu_B \le \mu_\nu \le 10^{-10}\mu_B$, where μ_B is the Bohr magneton, which is below the laboratory and the astrophysical upper limits[11], then it may account[12] for the suppressed counting rate in the solar neutrino experiment and its apparent anticorrelation with the sun spot number[13]. Such a magnetic moment may result in the emission of neutrinos which arrive at Earth as left handed "detectable" neutrinos mainly from the magnetic poles (in a narrow cone along the magnetic lines) and to the arrival at Earth of mainly right handed neutrinos from all other directions of emission where the magnetic field of the neutron star has a large component perpendicular to the direction of motion of the neutrino[14]. Thus, the emission of left handed detectable neutrinos may have the same periodicity and the same phase as the optical light emission (synchrotron radiation from electrons accelerated along the magnetic lines at the magnetic poles?). and most of the energy of a supernova explosion may be carried away by "invisible" wrong-helicity neutrinos.

Other mechanisms for pulsed emission of neutrinos are discussed in Ref. 9 and references quoted therein. However, most of the proposed mechanisms do not produce stable periodicity right after the begining of neutrino emission, they do not predict that the neutrino emission cone and the light emission cone are along

the same axis (necessary if both are observed from Earth) and they require rather large magnetic fields ($\geq 10^{14}$ *Gauss*) whereas the magnetic field near the pulsar in SN1987A is probably less than 10^9 gauss!

Let me conclude with some interesting consequences suggested by the optical and neutrino observationsfor patricle physics:

IMPLICATIONS FOR PARTICLE PHYSICS

1) REVISED BOUNDS ON PARTICLE PROPERTIES: Estimates of the gravitational binding energy released by neutrino emission in the SN1987A explosion were based on the assumption that the neutrino emission was isotropic. But, the gravitational collapse and neutrino emission could have been highly nonisotropic due to angular momentum[5] and magnetic field effects. For instance, the c.m. energy in neutrino-matter collisions is significantly smaller for neutrinos that move along the rotation axis then that for neutrinos moving perpendicular to it due to the high rotational velocity of the neutron star, yielding a smaller neutrino opacity along the rotation axis, i.e., stronger emission along the rotation axis. Consequently, estimates of the energy released by SN1987A, which were based on the KII, IMB and Baksan measurements and assumed isotropic emissin, are unreliable and limits on particle properties which were based on those energy estimates must be revised. However, limits on particle properties which were derived from the time length of the neutrino burst are valid.

2) A NEW BOUND ON THE MASS OF THE ELECTRON NEUTRINO: The flight time of massive neutrinos from a supernova explosion at a distance D to Earth in the limit $m_\nu c^2 \ll E_\nu$ is given by

$$t = (D/c)(1 + (m_\nu c^2/E_\nu)^2/2) . \tag{12}$$

The resulting dispersion in arrival times of massive neutrinos of different energies can be used to measure the neutrino mass if one makes assumptions on the emission times[15]. Various authors have assumed a smoothly varying function of time for the neutrino luminosity of SN1987A and deduced[16] a conservative upper bound $m_{\nu_e} < 15\ eV$. However, if the neutrinos that were detected in the KII detector were emitted in short pulses and have arrived within $\pm .1P \sim \pm 50\ \mu s$, without an apparent energy-time correlation as can be seen from Fig. 1, then a similar analysis yields $m_\nu < 0.050\ eV$.

3) A NEW BOUND ON THE ELECTRIC CHARGE OF THE ELECTRON NEUTRINO: If neutrinos have an electric charge q they are deflected by galactic and intergalactic magnetic fields and their path lengths and flight times from SN1987A to Earth depend on their energy. If they have a Boltzman energy distribution with temperature T(MeV) and if δt is the dispersion in their arrival times after a flight in perpendicular magnetic fields $B(\mu G)$ along a path D(10 kpc) then

$$q/e < 3 \times 10^{-12}(\delta t/t)^{1/2}T/BD .\qquad (13)$$

Assuming galactic magnetic fields $B \sim 1\mu G$ over ~ 10 kpc path, Barbiellini and Cocconi[17] derived from the energy spread and the dispersion in arrival times of 11 neutrinos from SN 1987A that $q < 2 \times 10^{-17}e$. If their time dispersion is $\delta t \sim \sqrt{S}P \sim 34\ \mu s$ then Eq. 11 yields the limit $q < 3 \times 10^{-20}e$.

CONCLUSION

Verification of the reported discovery of a sub-millisecond optical pulsar in SN1987A by future optical observations is highly desireable. Verification of neutrino pulsation from gravitational collapse require neutrino observations of future nearby supernovae explosions. But if "detectable" neutrinos from gravitational

stellar collapse are emitted primarily in narrow cones then, unfortunately, the chances of detecting neutrinos from stellar collapse are not very bright.

Acknowledgements

The author is very grateful to Prof. Yoji Totsuka and Prof. J. van der Velde for kindly sending him the precise values of the arrival times of the neutrinos on Feb. 23, 1987 in the KAMIOKANDE II detector and the IMB detector, respectively, and to Professors H. Harari, T. Mazeh, M. Moshe, S. Nussinov and G. Shaviv for useful suggestions. The observation of a possible periodicity in the IMB and KII events with a period identical to that of the optical pulsar in SN1987A was made independently also by the IMB collaboration, by A. De Rujula, by M. Fukugita, and by S. Nussinov.

REFERENCES

1. J. Middleditch et al., IAU circular No. 4735, 10 February, 1989.

2. J.L. Friedman et al., Ap. J. 304, 115(1986) and references therein.

3. See for instance S.L. Shapiro and S.A. Teukolsky, "Black Holes, White Dwarfs and Neutron Stars", John Wiley and Sons. Inc. 1983.

4. R.M. Catchpole and P.A. Whitelock, to be published.

5. K. Hirata et al., Phys. Rev. Lett. 58, 1490(1987).

6. R.M. Bionta et al., Phys. Rev. Lett. 58, 1494(1987).

7. H.T. Janka and R. Monchmeyer, Max Planck Institute Preprint MPA 414, November 1988.

8. See e.g. J.H. Taylor and D.R. Stinebring, Ann. Rev. Astron. Astrophys. 24, 285(1986) and references therein.

9. See for instance J.R. Wilson et al., Ann. N.Y. Acad. Sci., 470, 267(1986).

10. See for instance M. Harwit et. al., Nature 328, 503(1987).

11. See for instance M. Fukugita and S. Yazaki, Phys. Rev. D and references therein.

12. M.B. Voloshin et al., Sov. J. Nucl. Phys. 44, 440(1986); L.B. Okun et al., Sov. J. Nucl. Phys. 44, 546(1986).

13. R. Davis Jr., Proc. 7th Workshop On Grand Unification, ICOBAN 86, Toyama Japan (April 1986), P. 267.

14. A. Dar, to be published.

15. G.I. Zatsepin, JETP Lett. 8, 205(1986).

384

16. See e.g. J.N. Bahcall and S.L. Glashow, Nature, 326, 476(1987); J.N. Bahcall
    and D. Spergel, 200, 366(1988) and references therein.

17. G. Barbiellini and G. Cocconi, Nature 329, 21(1987).

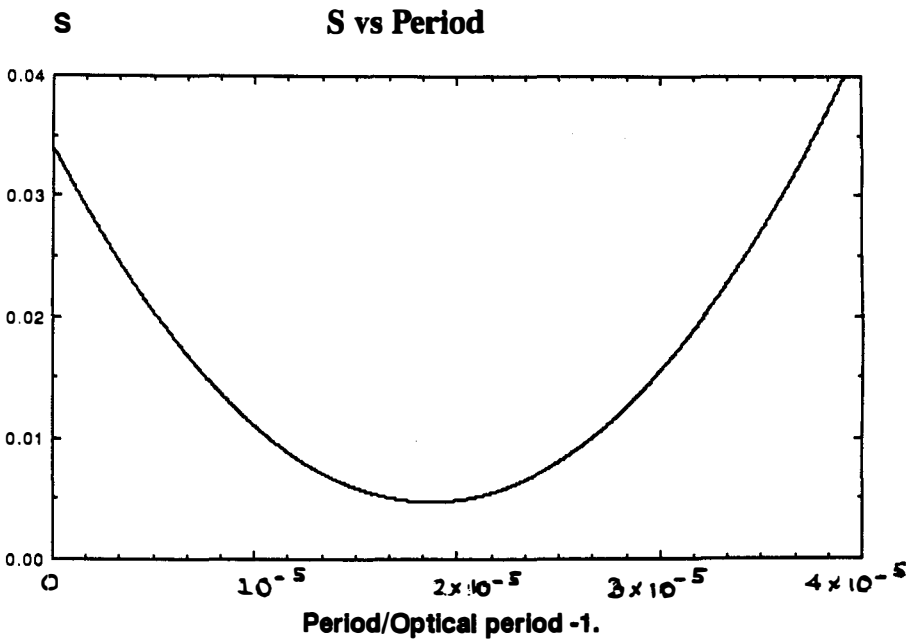**S**   **S vs Period**

Period/Optical period -1.

Fig 1a

1) The mean standard deviation s of the phases of the KII events from the
   average phase, after the first 400ms, (a) around the minimum of s as function
   of the relative deviation of the neutrino period from the optical period (b)
   beyond the minimum of s as function of the neutrino period.

S   **S vs Period**

$P = 10^{-5}$

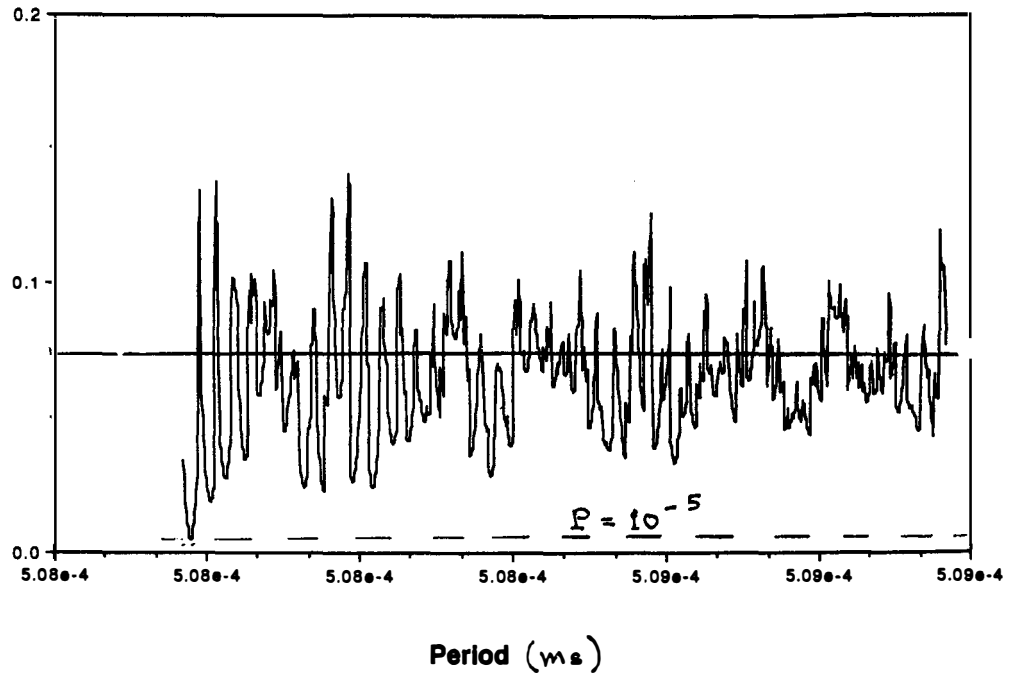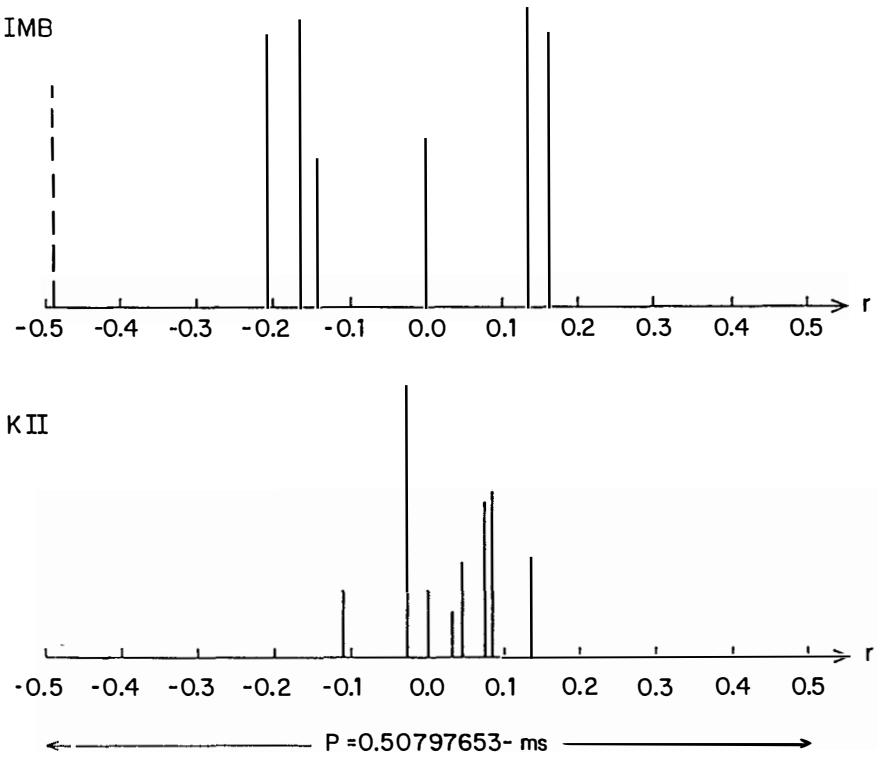**Period** (ms)

Fig 1b

IMB

KII

P =0.50797653- ms

Fig. 2a

2) The phases of the neutrinos events from the supernova explosion SN1987A relative to the last event as detected by KAMIOKAMDE II and IMB on Feb. 23, 1987: (a) The phases as calculated with the period $P_\nu = 0.50797653$ ms .
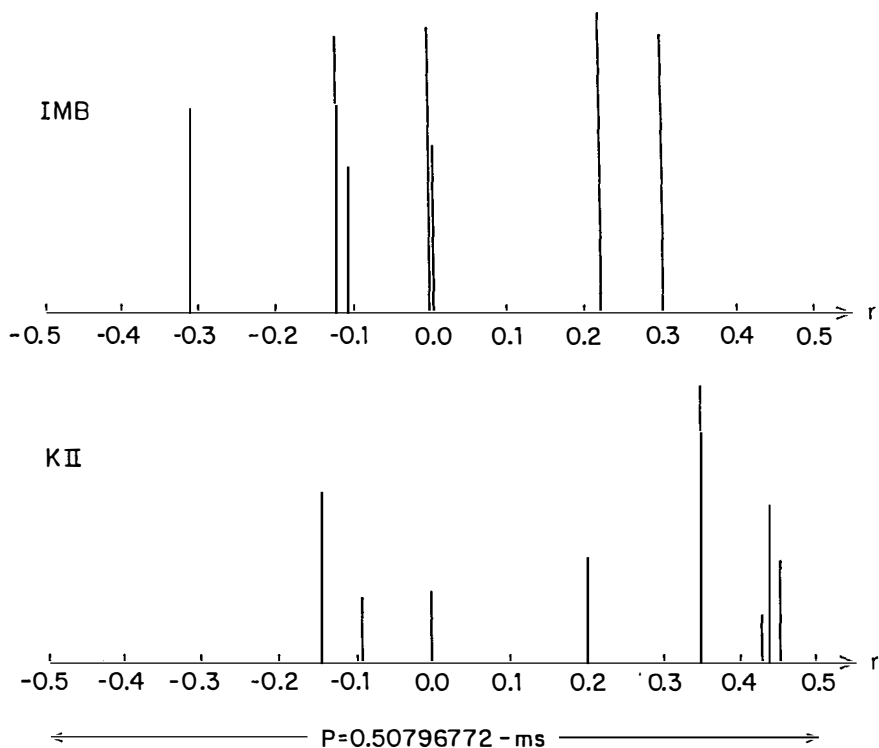
Fig. 2 b

(b) The phases as calculated with the barycentric period $P = 0.50796772$ *ms* of the optical pulsar in SN1987A on Jan. 1989. The lengths of the lines are proportional to the observed energies of the events.

Event	t_i(sec)	$\|N_i\|$	r_i	P_{ν} =0.50797653 - ms
KAMIOKANDE				
1	0			
2	0.10679086			
3	0.30241038			
4	0.32325402			
5	0.50692330	23489	+0.044	
6	0.68523072	23138	+0.029	
7	1.54018224	21455	-0.024	
8	1.72757060	21086	+0.084	$P \leq 10^{-5}$
9	1.91450924	20718	+0.078	
10	9.21879824	6339	-0.108	
11	10.4322318	3950	+0.133	
12	12.4388068	0	0.000	
IMB				
1	0			
2	0.4112	10178	-0.168	
3	0.6496	9709	-0.481	
4	1.1405	8742	+0.136	
5	1.5616	7913	+0.161	$P \leq 2 \times 10^{-3}$
6	2.6834	5705	-0.209	
7	5.0099	1125	-0.145	
8	5.5813	0	0.000	

$$P = P_{KII}P_{IMB} \leq 2 \times 10^{-8}$$

TABLE 1: The arrival times of the neutrinos from SN1987 that were detected by the KAMIOKANDE II and IMB detectors on February 23, 1987 and their phases relative to the last event in each detector as calculated with the Doppler shifted period of the optical pulsar had it been seen from Earth on that day.

ON SOLAR NEUTRINOS AND SN1987A

Miriam Leurer

The Randall Laboratory of Physics

University of Michigan

Ann Arbor, MI 48109-1120

ABSTRACT

Large magnetic moments or transition moments of the neutrino have been suggested as explanations for the solar neutrino puzzle. These scenarios have the attractive feature of incorporating an anticorrelation of the solar neutrino flux with sun spot activity. Recently it has been claimed that the 1987 supernova results put a severe bound on the neutrino magnetic moment, allowing only values that are too small to account for the solar flux depletion. Here we show that this bound does not apply to the magnetic transition moment of Majorana neutrinos.

The flux of solar neutrinos, measured in Davis's experiment, is about a quarter of the central value of the theoretical prediction. On the average, Davis and his collaborators saw 2.1 ± 0.3 SNU (1 SNU=10^{-36} captures per atom per second) while Bahcall and Ulrich [1] predict 7.9 ± 2.6 SNU. This is the so called "solar neutrino puzzle". In addition, there is an indication that the fluctuations in the flux are anticorrelated with sun spot activity (see figure 1). The sun spot number has an 11 year cycle and, during the period Davis ran his experiment, sun activity reached two minima, at which times the measured neutrino flux was above average, and one maximum, at which time the flux was below average. At the last period of minimal activity, Davis et al. observed 4.2 ± 0.7 SNU – about twice the average, or half of the theoretically predicted flux. This result was confirmed by Kamiokande which started to measure solar neutrinos at that time. The observed flux at Kamioka was also about half of the corresponding theoretical prediction.

In the following I will concentrate on solutions to the solar neutrino puzzle that incorporate anticorrelation with sun spot activity. All these solutions predict a significant reduction of the flux in the next period of maximal activity, which will be in 1990-1992, in both Davis and Kamiokande experiments.

The number of sun spots is related to the strength of the magnetic fields in the convective zone, which is the outer region of the sun, and occupies the last $(1 - 2) \cdot 100,000$ km of the solar radius. The magnetic fields there could reach 1-10 kilogauss at times of maximal activity. Neutrinos are produced in the core of the sun and pass through the convective zone on their way to the detectors on earth. If neutrinos had some peculiar magnetic properties, their interactions with the strong magnetic fields present at time of maximal activity, could render them undetectable, but at times of minimal activity they would pass almost unscathed. (Note that if the theoretical and experimental errors are taken into account, then the fluxes measured at Homestake and at Kamioka in the 1987-88 period of minimal activity, are almost in the theoretically predicted regime). Voloshin, Vysotsky and Okun (VVO) have suggested [2] a large magnetic moment for the neutrino. However, after the observation of the neutrino pulse from SN1987a [3], it was pointed out by many authors [4] that the magnetic moment could not be as large as required by the VVO scenario. Here I wish to advertise another

solution to the solar neutrino puzzle, which also incorporates anticorrelation with sun spot activity. This solution, suggested by Lim and Marciano [5] and independently by Akhmedov [6] (LMA) assumes Majorana neutrinos with large magnetic transition moments. My purpose is to show that the observation of the supernova pulse does not put any bounds on the LMA magnetic transition moment [7]. In the following I will describe the VVO and LMA scenarios in more detail. Then I will discuss the supernova neutrino pulse and the implications of its observation to each of these two proposals for solving the solar neutrino puzzle.

According to VVO, the neutrinos are of Dirac type. One should add to the standard model right-handed neutrinos and also assume the existence of some new interaction which induces, via radiative corrections, a large magnetic moment for the neutrino [8]:

$$\mathcal{L} = \mu \bar{\nu}_R \sigma_{\alpha\beta} \nu_L F^{\alpha\beta} + \text{h.c.}$$

The left-handed neutrino, produced in the core of the sun, when passing through strong magnetic fields in the convective zone, will spin-precess and convert into a sterile, undetectable right-handed neutrino. Unfortunately, the precession of the neutrinos is somewhat suppressed by matter effects. When a neutrino passes through matter, it undergoes coherent forward scattering via weak interactions which sum up to an effective potential [9]. In the case of the Dirac neutrino, only the left-handed component interacts weakly and gains such an effective potential, and consequently the two neutrino states, which are degenerate in vacuum, split in matter. The hamiltonian describing the left and right handed neutrino states is:

$$H(\nu_L, \nu_R) = k + \frac{m^2}{2E} + \begin{pmatrix} V & \mu B \\ \mu B & 0 \end{pmatrix}$$

where k, E and m are the momentum, energy and mass of the neutrino and B is the magnetic field. $V = \frac{G_F}{\sqrt{2}}(2N_e - N_n)$ where N_e and N_n are the number densities of electrons and neutrons respectively. The magnetic moment interaction μB produces the desirable precession of the left-handed to the right-handed neutrino, but V will quench the precession if $| V | \geq | \mu B |$. This disturbing effect of matter will however decay through the convective zone as the density of matter will drop with increasing radius, and spin precession will occur at times of maximal activity if the magnetic moment is

$\approx 10^{-11}\mu_B$ (where μ_B is the Bohr magneton). Larger values for μ are not allowed by astrophysical [10] and cosmological [11] considerations.

According to the less known LMA scenario, the neutrinos are of Majorana type. No new, right-handed neutrinos are added to the standard model. It is assumed that the neutrinos have large magnetic transition moments (magnetic moments for Majorana neutrinos are forbidden by CPT), so that a left-handed electron neutrino produced in the core of the sun, when passing at times of maximal activity through the convective zone, flips to a right-handed muon (or tau) *anti*neutrino. Although $(\bar{\nu}_\mu)_R$ is not sterile, it may not be detected in either Davis's experiment or in Kamiokande; hence the flux suppression at times of maximal activity.

Matter effects are helpful in this case. The Hamiltonian is:

$$H((\nu_e)_L, (\bar{\nu}_\mu)_R) =$$

$$k + \frac{1}{4E}(m_{\nu_e}^2 + m_{\nu_\mu}^2) + \frac{1}{2}(V_{\nu_e} + V_{\bar{\nu}_\mu}) + \frac{1}{2}\left(\begin{array}{cc} \Delta V - \frac{\Delta m^2}{2E} & 2\mu B \\ 2\mu B & \frac{\Delta m^2}{2E} - \Delta V \end{array}\right)$$

where $\Delta V = V_{\nu_e} - V_{\bar{\nu}_\mu} = \frac{G_F}{\sqrt{2}}2(N_e - N_n)$, and we assume that $\Delta m^2 > 0$ (namely, we assume that in vacuum the muon neutrino is heavier than the electron neutrino). ΔV gradually drops as the distance from the sun center grows, and it finally vanishes at the solar radius. Suppose that in the core of the sun $\Delta V > \Delta m^2/(2E)$ and consider a time of minimum sun spot activity, when the magnetic moment interaction is practically turned off. The electron neutrino, which is produced in the core, is the heavier of the two eigenstates, but as it emerges out of the sun it is the lighter of the eigenstates. Level crossing has occured at the point were $\Delta V = \Delta m^2/(2E)$. When the magnetic moment interaction is turned on, such level crossing will be avoided, as is the usual case in quantum mechanics for energy levels that are mixed by some perturbation. If the transition through the resonance point (where $\Delta V = \Delta m^2/(2E)$) is adiabatic, the original neutrino will follow the development of the heavier eigenstate and will emerge from the star as a right-handed muon antineutrino. This resonance mechanism for converting the original ν_e to the undetectable $\bar{\nu}_\mu$ is similar to the MSW [12] mechanism (where ν_e is converted to ν_μ), except that in the case described here the mixing of the two eigenstates which avoids the level crossing and is responsible for the conversion of the neutrino is due to the magnetic moment interaction, while in the MSW case, mixing

is provided by the neutrino mass matrix.

The magnetic moment interaction plays a role only when $| 2\mu B | \geq | \Delta V - \Delta m^2/(2E) |$; that is only around the resonance point. The resonance should therefore occur at the convective zone, since the flux is anticorrelated with the magnetic fields in this region. In addition, the resonance should be adiabatic (or partially adiabatic) at times of maximal activity. The condition on the location of the resonance fixes Δm^2 and the adiabaticity fixes the magnetic transition moment μ. Taking into account astrophysical bounds on μ, one finds: $\Delta m^2 \approx 10^{-8}\text{eV}^2$ and $\mu \approx 10^{-11}\mu_B$.

The two solutions to the solar neutrino puzzle described above differ in their predictions for the Gallium experiment [6]. The first predicts the same time variation for the solar neutrino flux in the Ga detector as in the Cl detector – spin precession will occur in the convective zone independently of the energy of the neutrino and the eleven year cycle of sun spot number will be seen in the Ga experiment as well. In the case of the LMA solution, however, the resonance point depends on the energy. Since the average energy of the detected neutrino in the Ga experiment is lower – the resonance will occur deeper in the sun. If ν_e will be rotated into $\bar{\nu}_\mu$, it will be the effect of the magnetic fields in this deeper region. These fields do not change in time (on the time scale relevant to the experiment). The only possible time dependence of the neutrino flux could be from our rotation around the sun. At different seasons of the year, the solar neutrinos that reach terrestrial detectors, traverse different regions of the sun and experience the effect of possibly different magnetic fields. Getting rid of such seasonal effects by integrating the flux over the year, we conclude that, according to LMA, the *yearly* flux in the Gallium experiment should be time independent.

We now turn to the supernova neutrinos and their implications for the VVO and LMA models. We first describe the theoretical prediction for the supernova neutrino pulse in the standard model (where neutrinos are massless and have no magnetic moments or transition moments)[13]. Neutrinos and antineutrinos are pair produced in the supernova core, where the temperature reaches 100 MeV or more, through the annihilation processes $e^+e^- \rightarrow \nu_i\bar{\nu}_i$, $i = e, \mu$ or τ (electron neutrinos are also produced in the neutronization process $p + e^- \rightarrow n + \nu_e$). The density in the core is so high that all six neutrinos and antineutrinos are trapped by weak scattering. The frequent scattering

with the surrounding material also forces the ν's and $\bar{\nu}$'s into thermal equilibrium with their neighbourhood. Neutrinos will therefore slowly drift out of the core keeping all the while in thermal equilibrium with the material around them, until they reach the "neutrino sphere". Beyond this sphere, the density is lower than $\approx$ few$\cdot 10^{11}$ gr/cm^3 and neutrinos do not scatter anymore. The only matter effect from now on is the usual coherent forward scattering, amounting to an effective potential, depending on N_e and N_n. Roughly, these thermal neutrinos will carry away about 90% of the collapse energy, and the energy flux is equally distributed [14] among the six neutrino and antineutrino species. The electron neutrinos and antineutrinos are trapped for a little longer than μ and τ neutrinos due to their charged current interaction with electrons. Consequently, the ν_e sphere is at somewhat bigger radius and lower temperature than the ν_μ and ν_τ sphere. It is estimated that the average ν_e energy is half the average of ν_μ or ν_τ energy and that the number of emitted ν_e's is twice the number of emitted ν_μ's or ν_τ's. Of the neutrinos emitted by SN1987a we, on earth, could only expect to see the $\bar{\nu}_e$ pulse. Its predicted characteristics are its duration, spectrum and intensity. The duration should be about 10 seconds, reflecting the long time the neutrinos needed to drift out of the core. The spectrum is expected to be concentrated around a few MeV, reflecting the temperature of the electron neutrino sphere, where the neutrinos have last exchanged energy with matter. The intensity should correspond to about 15% of the collapse energy. Within the theoretical errors and statistical limitations, all these features were indeed seen.

Suppose now that, in order to solve the solar neutrino problem, we assume that the electron neutrino is of Dirac type and has a magnetic moment. Then a new, quicker way for cooling opens up for the supernova [4]. Left-handed neutrinos and right-handed antineutrinos will be pair produced in the core through electron-positron pair annihilation, as in the standard model. But instead of going through the slow drifting to the neutrino sphere, the $(\nu_e)_L$'s and $(\bar{\nu}_e)_R$'s will scatter electromagnetically on an electron or a proton, (see figure 2), flip their helicity, become sterile, and escape from the core as free noninteracting particles. Unless the magnetic moment is smaller than $10^{-12}\mu_B$, the supernova core will be drained of its neutrinos within 2 seconds or less. As the observed neutrino pulse from SN1987a lasted about 10 seconds, one concludes that $\mu \leq 10^{-12}\mu_B$. The magnetic moment solution to the solar neutrino

puzzle requires $\mu \approx 10^{-11} \mu_B$ and is therefore excluded.

A large magnetic moment of Dirac electron neutrino could also lead to distortions in the average energy and total intensity of the detectable $(\bar{\nu}_e)_R$ pulse. This, however, is still a controversial subject [15]. We should also mention that ref. [16] discusses, in the framework of a specific model, a way around the above supernova bound on the neutrino magnetic moment.

Consider now the case of LMA Majorana neutrinos with a flavour changing magnetic transition moment. In the supernova core all six neutrinos and antineutrinos are pair produced in the electron-positron annihilation process. The magnetic transition moment interaction will induce electromagnetic scattering of e.g., $(\nu_e)_L$ on charged particles (see figure 3). The left-handed electron neutrino will flip its helicity and flavour and become a right-handed muon antineutrino. However, in contrast to the VVO case, here the flipped neutrino is not sterile. $(\bar{\nu}_\mu)_R$ interacts weakly and is trapped in the core. Moreover, $(\bar{\nu}_\mu)_R$ is directly produced in the e^+e^- annihilation process and the magnetic transition moment may therefore be thought of as merely an additional interaction that keeps $(\nu_e)_L$ and $(\bar{\nu}_\mu)_R$ in thermal equilibrium. We do not expect μ of the order of $10^{-11} \mu_B$ to lead to any drastic changes in the neutrino pulses that emerge from the neutrino spheres. Out of the neutrino sphere, resonance flippings of neutrino flavours (similar to the process described above for the the solar neutrinos) may interchange $(\bar{\nu}_e)_R$'s with $(\nu_\mu)_L$'s. As these two pulses are expected to be very similar, only mild modification of the detectable $(\bar{\nu}_e)_R$ pulse could result. Such a modification could not be identified with present theoretical uncertainties and the low statistics of Kamiokande and IMB detectors. We conclude that the the solution to the solar neutrino puzzle suggested by Lim, Marciano and Akhmedov is consistent with the observation of the supernova neutrinos [17].

In summary, we described here two solutions to the solar neutrino puzzle which incorporate correlation with sun spot activity. The first, suggested by Voloshin, Vysotsky and Okun, assumes that the neutrinos are of Dirac type and have a large magnetic moment. The second solution, by Lim, Marciano and Akhmedov, proposes that neutrinos are of Majorana type and have a magnetic transition moment. A crucial test for the two solutions will be the neutrino flux in Davis and Kamiokande experiments in 1990-

1992. Both models predict significant suppression of the flux in this period. The models differ however in their predictions for the Ga experiment. According to VVO, the flux measured in Gallium should exhibit anticorrelation with sun spot activity, while LMA predict that the yearly flux will not change in time. The observation of the neutrino pulse from SN1987a provides us with still another test for these models. The VVO solution seems to be in serious trouble while the LMA scenario is consistent with this observation.

References

[1] J. N. Bahcall and R. K. Ulrich, Rev. Mod. Phys. 60 (1988) 297.

[2] M. B. Voloshin and M. I. Vysotsky ITEP Report No.1, 1986; L. B. Okun, Yad. Fiz. 44 (1986) 847 [Sov. J. Nucl. Phys. 44 (1986) 546]; L. B. Okun, M. B. Voloshin and M. I. Vysotsky, *ibid.* 91 (1986) 754 [44 (1986) 440]; Zh. Exp. Theor. Fiz. 91 (1986) 754 [Sov. Phys. JETP 64 (1986) 446].

[3] Kamiokande II Collab., Phys. Rev. Lett. 58 (1987) 1490; IMB Collab., Phys. Rev. Lett. 58 (1987) 1497.

[4] S. Nussinov and Y. Rephaeli, Phys. Rev. D36 (1987) 2278; I. Goldman, Y. Aharonov, G. Alexander and S. Nussinov, Phys. Rev. Lett. 60 (1988) 1789; J.M. Lattimer and J. Cooperstein, Phys. Rev. Lett. 61 (1988) 23; R. Barbieri and R.N. Mohapatra, Phys. Rev. Lett. 61 (1988) 27; D. Notzold, Phys. Rev. D38 (1988) 1658.

[5] C. S. Lim and W. J. Marciano, Phys. Rev. D37 (1988) 1368.

[6] E. Kh. Akhmedov, preprint IAE-4568/1 (1988).

[7] M. Leurer and J. Liu, Phys. Lett. 219 (1989) 304.

[8] Several models for nonstandard interactions which could produce such large magnetic moment were suggested, see e.g., M. Fukugita and T. Yanagida, Phys. Rev. Lett. 58 (1987) 1807.

[9] L. Wolfenstein, Phys. Rev. D17 (1978) 2369.

[10] P. Sutherland et al. Phys. Rev. D13 (1976) 2700; M. A. B. Beg,

[11] J. Morgan, Phys. Lett. 102B (1981) 247.

[12] P. Mikheyev and A. Yu. Smirnov, Nuovo Cimento C9 (1986) 17.

[13] *see e.g.* J. R. Wilson et al., Ann. NY Acad. Sci. 470 (1986) 267; R. Mayle, J. R. Wilson and D. N. Schramm, Fermilab 86/81-A (1986); A. Burrows and J. M. Lattimer, Ast. J. 307 (1986) 178.

[14] A. Burrows and T. L. Mazurek, Nature 301 (1983) 315.

[15] M. B. Voloshin, Phys. Lett. 209B (1988) 360; L. B. Okun, ITEP-88-079.

[16] R. Barbieri, R. N. Mohapatra and T. Yanagida, Univ. of Maryland preprint, UM PP # 88-232.

[17] For further discussion of LMA resonances in the supernova and implications for the prompt neutrino burst, see ref. [7].
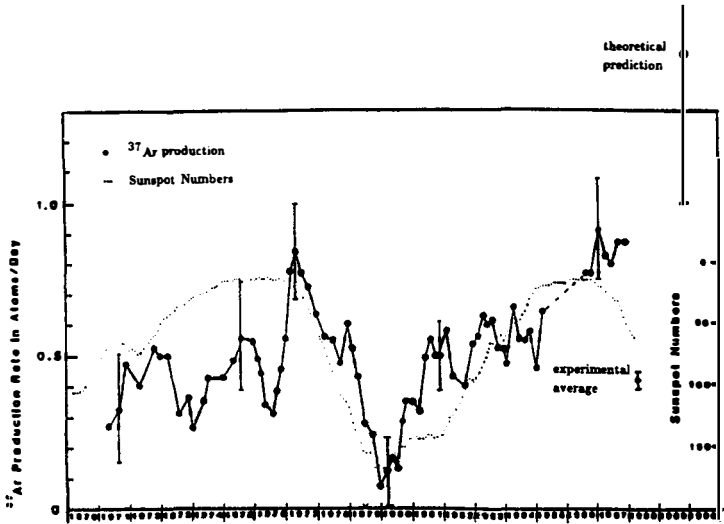
Fig. 1

Figure 1: Comparison of the measured solar neutrino flux with sun spot activity during the last 18 years. The points of the flux correspond to averages over five Argon extractions. Note the number of sunspots (scale on the left) grows *downwards*.
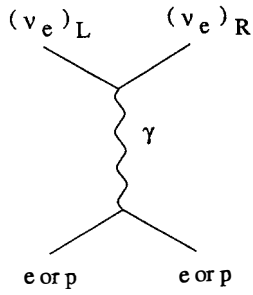
Fig. 2. The VVO case. A left-handed electron neutrino scatters electromagnetically
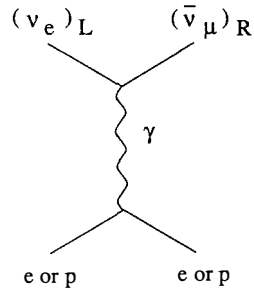on an electron or a proton and flips its helicity.

$(\nu_e)_L$ $(\bar{\nu}_\mu)_R$

γ

e or p   e or p

Fig. 3. The LMA case. A left-handed electron neutrino scatters electromagnetically on a charged particle and flips its helicity and its flavour.

VI. GENERAL DISCUSSION

SOME QUESTIONS ON LARGE-SCALE MOTIONS

R. B. Partridge

Haverford College
Haverford, Pa 19041, U.S.A.

ABSTRACT

As a non-expert, I ask several questions about large-scale motions in the Universe. Most await definitive answers, in particular the scale and the sources of these motions.

I have been asked by Colin Norman to review large-scale motions. I have chosen to discuss large-scale motions in cosmology rather than large-scale motions in skiing, not because I know more about the former than the latter, but because ignorance of the former is probably easier to get away with in this company.

So I propose in the space allotted to ask five questions about large-scale motion in the Universe, and to supply approximately two answers. Allons-y!

1.) How reliable is the dipole moment of the cosmic microwave background radiation? Very reliable, at T_1 = 3.31 ± 0.08 mK in the direction α = $11^h.2$ ± $0^h.04$, δ = − 7° ± 0.5° (for the data, see my earlier remarks here). The conventional and widely-held view is that this dipole is produced by the motion of the observer (or, in this case, the solar system). In principle, the dipole moment could be due to anisotropic expansion, but in that case, the quadrupole moment would be far larger than the limits I discuss elsewhere in this volume. Nor is the dipole due to the radio emission of local radio sources (Partridge and Lahav, 1988). The Doppler explanation survives. The solar motion with respect to matter at large distances is thus known very precisely.

2.) How certain is the solar motion in the local group? It is thought to be ∼ 300 Km/sec, but neither the amplitude nor the direction is known as well as the corresponding figures for the microwave dipole (see, for instance, Yahil et al, 1977). Thus the uncertainty in the velocity of the local group v_{LG} arises almost entirely from uncertainty in the solar motion relative to the center of mass of the local group. This point must be borne in mind when comparing other measured dipole distributions to the microwave dipole (as in papers by Meiksin and Davis, 1986; Yahil et al, 1986; Lahav et al, 1988; Strauss and Davis, 1988). Clearly, it is best to omit the uncertain correction needed to obtain v_{LG}, and to compare solar motions directly.

3.) What causes v_{LG}? Almost certainly gravity.

4.) On what scale is the motion coherent? The work of Rubin et al (1976), Collins et al (1986) and more recently the 7 Samuri (e.g., Lynden-Bell et al, 1988) among others, has shown that the scale is large, perhaps as large as 100 Mpc. Given the limited range of our measurements, can we be sure there are not even large-scale motions? The resolution of this point is linked to the last of my five questions:--

5.) What is the scale of the lump or lumps responsible for the gravitational acceleration? Is v_{LG} explained by the mass we can see and measure within our catalogs, be they optical or ir? Technically, one asks whether the dipole amplitude and direction have converged within a distance corresponding to $v = H_0 d \approx 4000$ Km/sec (see Colin Norman's contribution here). Are known superclusters (e.g., Hydra-Centaurus) enough, or is an additional mass needed, the Great Attractor, the " . . . point to which all masses from all parts are drawn[*]," to quote from Dante's Divine Comedy? Time and, especially, deeper and more systematic observations will tell.

References

Collins, C. B., Joseph, R. D., and Robertson, N. A. 1986, *Nature*, 320, 506.

Lahav, O., Rowan-Robinson, M., and Lynden-Bell, D. 1988, *Mon. Not. Roy. Astr. Soc.*, 234, 677.

Lynden-Bell, D., Faber, S. M., Burstein, D., Davies, R. L., Dressler, A., Terlevich, R. J., and Wegner, G. 1988, *Ap. J.*, 326, 19.

Meiksin, A., and Davis, M. 1986, *Astron. J.* 91, 191-198.

Partridge, R. B. and Lahav, O. 1988, *Mon. Not. Roy. Astr. Soc.*, 235, 1p.

Rubin, V. C., Thonnard, N., Ford, Jr., W. K., and Roberts, M. S. 1976, *A. J.*, 81, 719.

Strauss, M. A., and Davis, M. 1988, in *IAU Symposium 130, Large Scale Structure of the Universe*, ed. J. Audouze, M.-C. Pelleton and A. Szalay, Kluwer Acad. Publ. Co., Dordrecht, Netherlands.

Yahil, A., Tammann, G. A., and Sandage, A. 1977, *Ap. J.*, 217, 903.

Yahil, A., Walker, D., and Rowan-Robinson, M. 1986, *Astrophys. J. Lett.* 301, L1-L5.

*Inferno, canto 34, " . . . quand'io mi volsi, tu passasti il punto al qual si traggon d'ogni parte i pesi."

AUTHOR INDEX

LIST OF PARTICIPANTS

Charles ALCOCK	Livermore, USA
Jean AUDOUZE	Paris, France
Georges BIGOT	Marseille, France
François BOUCHET	Paris, France
Bernard BURKE	Cambridge, USA
Alberto CAPPI	Bologna, Italy
Noël CORON	Verrières, France
Philippe CRANE	Garching, Germany
Valérie de LAPPARENT	Paris, France
Pierre de MARCILLAC	Paris, France
David EICHLER	Beer Sheba, Israel
Gilles GERBIER	Saclay, France
Luis GONZALEZ-MESTRES	Annecy, France
Bruno GUIDERDONI	Paris, France
Daniel KUNTH	Paris, France
Jes MADSEN	Aarhus, Denmark
Kei-Ichi MAEDA	Tokyo, Japan
Sophie MAUROGORDATO	Meudon, France
Colin NORMAN	Baltimore, USA
Ornella PANTANO	Trieste, Italy
R.B. PARTRIDGE	Haverford, USA

. . .

Jim PEEBLES	Princeton, USA
Denis PERRET-GALLIX	Annecy, France
Hubert REEVES	Saclay, Paris
Michael ROWAN-ROBINSON	London, UK
Brigitte ROCCA-VOLMERANGE	Paris, France
Robert ROOD	Charlottesville, USA
Bernard SADOULET	Berkeley, USA
Katsuhiko SATO	Tokyo, Japan
David SCHRAMM	Chicago, USA
Peter SHAVER	Garching, Germany
Joseph SILK	Berkeley, USA
Joan SOLA-PERACAULA	Bellaterra, Spain
Rolf STABELL	Oslo, Norway
Gary STEIGMAN	Colombus, USA
Roland TRIAY	Marseille, France
Sylvie VAUCLAIR	Toulouse, France
Amri WANDEL	Rehovot, Israel